CRANFIELD INSTITUTE OF TECHNOLOGY
SCHOOL OF MECHANICAL ENGINEERING
DEPARTMENT OF FLUID ENGINEERING AND INSTRUMENTATION

PH D THESIS

ACADEMIC YEAR 1989-1990

L. M. FERNANDO

JET MIXING OF WATER IN CRUDE OIL PIPELINES

SUPERVISOR:- DR. C. P. LENN

FEBRUARY 1990

VOLUME CONTAINS CLEAR OVERLAYS

OVERLAYS HAVE BEEN SCANNED SEPERATELY AND THEN AGAIN OVER THE RELEVANT PAGE

TO CHITRANI, NATASHA AND MARK,

AND TO

MY PARENTS

ACKNOWLEDGEMENTS

The author wishes to express his grateful thanks to the following people:-

Dr. C. P. Lenn	-	for the supervison and for giving encouragement throughout the course of the work.
Prof. R. C. Baker	-	for being my second supervisor and for devising this project originally.
Dr. J. Hemp and Dr. J. Heritage	-	for their support in theoretical aspects.
Mr. R. Dunn Mr. C. Evans	-	for the technical assistance in the laboratories.
Mr. B. Hunt and his collegues	-	for carrying out valuable photographic services.
Mr. G. Oddie	-	for proof reading and commenting on the thesis.

Finally, I would like to thank my wife, Chitrani, daughter Natasha and son, Mark for having to put up with my long hours of work, my parents for funding my first degree that lead to this work, and Department of Fluid Engineering and Instrumentation for providing me a studentship to carry out this project and its members of staff and students for assisting and supporting me in many ways.

ABSTRACT

The jet mixing of water in crude oil pipelines by single nozzle and multi-nozzle mixers was studied by dividing the mixing domain into to three regions, the penetration, near field and farfield regions. At the penetration region the quantitative experimental data were aided by a flow visualisation study in an attempt to to form fundamental semi-empirical correlations to estimate the entrainment rate of stratified water from the bottom and the Sauter mean diameter (d_{32}) of the entrained water droplets for a single nozzle jet mixer.

The flow field diagnostics into the near field region, defined as the region where high level of swirl and mixing is occuring, were conducted theoretically using computational fluid dynamic code "Phoenics" and experimentally through LDA measurements and flow visualisation. The entrainment rate found in penetration region was treated as a source term for theoretical analysis.

Experimental analysis of this region was conducted in single phase flow for two mixer nozzles i) Single nozzle mixer and ii). Existing multi-nozzle mixer. Experimental results have revealed that the swirl velocities decay faster for higher velocity ratios and their dependence on Reynolds number (in the range 27600 to 48400) is weak. Higher velocity ratios would generate and dissipate higher levels of energy, therefore break up water droplets to smaller sizes and increase the eddy viscosity. The dispersion strength due to swirl decays faster and the gravity settling begins earlier.

As the flow reaches downstream, approximately four diameters, the distribution of velocities (mean and RMS) flattens out and their magnitude begins to close up for the two mixers, when their momentum ratios are equal. It was also shown that the swirl velocities (at axis) die away, approximately at the same axial point for both of the nozzles. The multi-nozzle mixer is shown to be better in two characteristics; i). The mixing is faster and ii) The jet energy is more evenly distributed in the vicinity of the injection cross section, hence improving the quality of the droplet size distribution.

Besides providing information to aid understanding of the complex flow in the mixer zone, the experimental data is believed to be of sufficient quality and quantity to improve the present simple modelling procedures as well as to be used as test cases for assessment of the predictive accuracy of more elaborate computational models.

Comparision with computational results (of low velocity ratios) shows the agreement with swirl velocities is reasonable, but not always acceptable for mean axial velocities. However, the computational model predicts the near field jet trajectory reasonably well. The flow visualisation of dispersion of passive contaminant agrees qualitatively with the contours of the passive contaminant.

In the far field region, where the swirl has decayed, the flow behaves two dimensionally. Therefore, an exact solution was obtained for two dimensional water conservation equation. The boundary conditions were specified by using sticking probability constants. A relationship was obtained to specify eddy viscosity through turbulent kinetic energy. The turbulent kinetic energy and swirl decay were estimated from LDA experimental data. This solution can be used to study the developing characteristics of water concentration profiles along the far field region of the pipeline.

LIST OF FIGURES

3.3.1 Breakup of entrained water as it penetrates the oil/water interface to oil
(A) V_j=5.8 m/s; (B) V_j=7.3 m/s; (C) V_j=6.0 m/s; (D) V_j=7.3m/s

3.3.2 Breakup of entrained water as it penetrates the oil/water interface to oil

3.4.1 Oil/water interface without(A) and with(B) the penetrating oil jet

3.5.1 Streak lines, in the water layer, of the entraining water

3.6.1 Breakup of entrained water as it penetrates the oil/water interface to oil (at relatively low penetrating velocities
(A) V_j = 1.0 m/s; (B) V_j = 1.4 m/s

3.6.2 Breakup of entrained water as it penetrates the oil water interface to oil
(A) V_j= 3.2m/s; (B) V_j= 1.6m/s; (C) V_j=2.9m/s; (D) V_j= 2.1m/s

3.7.1 Oil jet, A) with and B) without the stratified water

3.7.2 Breakup of oil jet in water

3.8.1 Penetration of oil jet through the stratified water as the water layer height is consecutively decreased

3.8.2 Penetration of oil jet through stratified water as its velocities is consecutively increased

3.9.1 Penetration of oil jet through a water layer, stratified in oil

3.10.1 Calibration for jet velocity

3.10.2 System response to the opening of the solenoid valve

3.10.3 System response to the opening of the solenoid valve at point (2)

3.11.1 Composite overlay of jet outlines from video frames
jet velocity = 3.7 m/s

3.11.2 Composite overlay of jet outlines from video frames
jet velocity = 8.1 m/s and 5.8 m/s

3.11.3 Composite overlay of jet outline from video frames
jet velocity = 5.2 m/s

3.12 Structure and stages of breakup and entrainment process

3.13.1 Apparatus used for measurement of properties

3.13.2 Instruments and the rig arrangement

3.13.4 High speed video (spin physics 2000) in use

4.1.1 Breakup of disturbance wave by undercutting

4.1.2 Breakup of disturbance wave by rolling

4.1.3 Mechanism of the shearing off of roll-wave

4.1.4 Wave region of the interface in pipe flow

4.1.5 Schematic diagram of droplet pool entrainment

4.2.1 (A) Volume distribution data, (B) Number distribution data, (C) Cumulative distribution of all drops, (D) Cumulative volume distribution

4.3.1 Measurement of angle Φ of equation 4.4.2 at t = 0.0 sec
h = 17.4 mm

4.3.2 Measurement of angle Φ of equation 4.4.2 at t = 0.6 sec
h = 17.4 mm, V_j = 6.0 m/s

4.3.3 Measurement of angle Φ of equation 4.4.2 at t = 0.8 sec
h = 18.4 mm, V_j = 6.8 m/s

4.4.1 Ultrasonic transducer arrangement

4.4.2 Calculation of interface area

4.4.3 The echo produced by the ultra-sonic transducer due to the water/oil interface, allows measurement of the interface height

4.4.4 Echoes produced by two ultra-sonic transducers allows measurement of the interface drop rate

4.4.5 A grid was positioned to scale the measuring plane

4.4.6 A grid was tilted to 30 degrees to horizontal to measure the depth of view

4.4.7 Optomax V video interface image analyser in use

4.5.1 Interface area against water height

4.5.2 Interface drop at position 1 and 3
V_j = 7.6 m/s, h = 18 mm (at t=0.0 sec)

4.5.3 Entrainment against jet velocity
h = 16.4 mm, σ = 0.033 N/m, $\mu_{oil} = 1.15 \times 10^{-3}$ Nsm^{-2}

4.5.4 Entrainment against interfacial surface tension
V_j = 5.8 m/s, h = 16.4 mm, $\mu_{oil} = 1.15 \times 10^{-3}$ Nsm^{-2}

4.5.5 Entrainment against height
V_j = 5.8 m/s, σ = 0.033 Nm^{-1}, $\mu_{oil} = 1.15 \times 10^{-3}$ Nsm^{-2}

4.5.6 Entrainment against height
V_j = 5.8 m/s, σ = 0.013 Nm^{-1}, $\mu_{oil} = 1.15 \times 10^{-3}$ Nsm^{-2}

LIST OF TABLES

NOTATION

English letter symbols

A = area

a = liquid thickness

b = depth

C = concentration of tracer mass per mixture mass (or C given by the transformation equation 8.14)

C_1 = turbulent model constant

C_2 = turbulent model constant

C1 = concentration of tracer volume per mixture volume (PHOENICS variable)

C_D = turbulent model constant

C_μ = turbulent model constant

C_d = droplet drag coefficient

C_f = skin friction coefficient

c = concentration of tracer mass per mixture volume

D = diameter of the pipe

D_f = diffusion coefficient

d = diameter of the drop

d_{ave} = average diameter of the droplet

d_j = diameter of the jet orifice

d_{max} = maximum diameter of the droplets

d_{32} = Sauter mean diameter

e = energy of one eddy

E = spectral energy density

E_w = entrainment rate of water

ENUT = turbulent kinematic viscosity (PHOENICS variable)

f = friction factor

f_o = oscillator frequency

f_d = Doppler frequency

G_K = turbulent production term (= generation of turbulent kinetic energy)

g = gravitational acceleration

H = Hydraulic diameter of the channel

H_ℓ = liquid jet length

h = height of the water layer

k = wave number $=2\pi/\lambda$

k = turbulent kinetic energy

K = pressure loss coefficient

K_v = Von Karman constant

K_n = n-th order modified Bessel function of the second kind

L = distance for ν_t to decay 50% of its initial value

L_1 = intact surface length

L_2 = intact core length

LDA = Laser Doppler Anemometry

L_p = length scale as prescribed by Prandtl/Kolomogrov formula

ℓ = length scale of energy containing eddies

ℓ_m = mixing length

ln = natural log (ie: Log to the base 'e')

MMD = mass mean diameter $\approx$ 1.2 SMD

M_r = ratio of jet to pipe momentum

m = mass flow rate

N = number of sampling points

P, p = pressure

Pe = Peclet Number = (Re)(Pr)

Pr = Prandtl Number

Q = pipe flow rate

R = radius of the pipe

Re = Reynolds number = $(\rho v_j d_j/\mu)$, ρ, μ are related to continuous phase unless specified

Res = residual

Rh = roughness

RMS = root mean square

R_t = turbulent Re number

R_v = velocity ratio

r = radius of an eddy

S_Φ = source term related to variable 'Φ'

Sc = Schmidt number

SMD = Sauter mean diameter

s = number of focused squares

t = time

U, V = mean velocity

u^*, U^* = friction velocity

u, v, w = RMS (root mean square) velocity

u_i, u_j, u_k = fluctuating (turbulent) velocity component

u', v', w' = fluctuating (turbulent) velocity component

V_f = cumulative volume fraction

We = Weber number = $(\rho_c v_j^2 d_j/\sigma)$

W = relative velocity of water droplets in oil

X = nondimensional wave length = $(\rho_2 v_j^2/\sigma k)$

ΔX = characteristic length in turbulent energy dissipation

x, y, z = rectangular coordinates

x, r, θ = cylindrical coordinates

Z = Ohnesorge number = $(\mu/\sqrt{(\rho_1 \sigma d_j)})$

Greek letter symbols

β, β_1, β_2 = jet divergence angles

ϵ = energy dissipation per unit mass per unit time

δ = boundary layer thickness

δ_f = fringe separation

λ = wave length

λ_o = length scale of smallest eddies

λ_i = interfacial friction coefficient

λ_d = air only friction coefficient

μ = molecular dynamic viscosity

μ_t = eddy dynamic viscosity

μ_{eff} = effective viscosity

ν = molecular kinematic viscosity

ν_t = eddy kinematic viscosity

π = 3.14159

Φ_i = general conserved property for phase 'i'

ρ = density

ρ_a = ambient density

σ = surface tension (or interfacial surface tension)

σ_d = standard deviation

σ_Φ = Schmidt number of species 'Φ'

σ_t = Prandtl number

Γ = exchange coefficient

τ = shear stress

ω = growth rate

supercripts

$\overline{}$ = root mean square

$\tilde{}$ = vector

subscripts

b = bottom

f,ℓ,1 = liquid

w = water

c = continious

cr = critical

j = jet

a,g,2 = air, gas

T = total

t = turbulent

S = static

R = reservoir

r = radial component

p = pipe

oil = oil

n = value at a node adjacent to the wall

x = axial component

θ = tangential component

CONTENTS

PART 3 FLOW FIELD ANALYSIS OF JET MIXER NOZZLES IN PIPE CROSS FLOW, USING LDA MEASUREMENTS - Single phase flow study

---

Chapter 7 Experimental work

PART 4 INTERRELATIONSHIPS AND IMPLICATIONS OF THE ABOVE THREE PARTS, GENERAL DISCUSSION AND CONCLUSIONS

TEXT

CHAPTER 1.0 INTRODUCTION

1.1 General introduction to jet mixing in crude oil pipelines

1.1.1 Problem definition

When a crude oil shipment is unloaded, a substantial proportion of water and other contaminants on board are likely to come off during pumping. Therefore the economic importance of accurately determining the water content of crude oil transfers is becoming increasingly significant. Accurate sampling from a flowing pipeline requires that the water is well mixed, therefore the sample drawn is representative. Particularly under conditions of low flowrates the free water may settle out, but their exact distribution is not properly known along the pipeline circuitry. Thus it must be ensured that the flowing stream at the sampling point is completely homogenised, before sampling. If the pipeline velocity is adequate, the homogeneity of the cross section may be assured by natural turbulence. Where natural turbulence is insufficient, the distribution can be improved by using an appropriate mixer. The chosen mixer should satisfy three main functions They are:-

1. Destratification of settled out water layer.
2. Breakup of large water globules into small droplets.
3. Distribution of the water droplets uniformly across the pipe cross section.

At present, the draft ISO/DIS 3171 (1985) sets out the required conditions for dispersions and the distribution of water drops at a point in a pipeline, for representative sampling.

1.1.2 Mixer types available

Mixers may be divided into two main families. Static mixers are those in which no energy is supplied to the mixer except for that which is imparted by the flowing fluid, whilst dynamic mixers are supplied with some external source of energy. These families may be further

sub-divided, leading to the following main classes:-

a). Fixed static mixers:- the proprietary "Kenics" mixers is the best known example of this class, but an orifice plate has also been used in this way and so has a series of several pipe bends in succession. The fixed static mixer is subject to very serious limitations, since the energy consumed by it is proportional to the square of the pipe velocity. If the mixer is designed for a low flow rate, to suit the begining and end of a typical crude oil transfer (Hayward et al, 1981) then the system would impose unacceptably high pressure drops at normal and high flow rates.

b). Variable static mixers:- an example of this class is the partially closed butterfly valve. Unfortunately the potential of this type of device does not appear to have been realised yet, since it would seem that the only variable static mixer that had been tested by Boyle (Hayward, 1981), did not appear to give good mixing

c). Mechanical mixer:- mixers of this type are commonly used in the process industries. This type of mixer would present a major installation problem on existing pipelines, and a significant maintenance problem on all pipelines. In addition, there is the disadvantage that it provides a permanent obstruction in the line which causes a significant energy loss on those occasions when it is not needed to run the mixer, for example, when high density oil is being unloaded.

d). Jet mixers:- In these, a portion of the flowing oil is sucked out of the pipeline and pumped back into the pipline as one or more jets of high velocity (figs. 1.2 and 1.3). The jet mixer appears to be the only system of mixing which is free of serious limitations mentioned above, neverthless they also possess impressive list of advantages.

1.1.3 Advantages of jet mixers

1). The power input to the mixer can be varied independently of the flowrate in the pipeline. By this means the mixer can be made to

operate efficiently at all pipe velocities. At low velocities where mixing is most needed the power input can be high enough to give efficient mixing, and at high velocities or with high density oil, where mixing may not be needed at all, the jet can be shut off thus saving energy.

2). The jet nozzle provides negligible blockage in the pipe and consequently negligible energy loss at high pipeline velocities. If the nozzles are made easily retractable, as they can be, the jet mixer installation need not be an obstacle to pigging the pipeline.

3). A jet mixer system can easily be installed on an existing pipeline without shutting it down by welding bosses on the outside of the line and hot-tapping.

4). The only mechanical working part of a jet mixing system is the pump, and since these are installed outside the pipeline there is no problem of maintenance while the pipeline is in operation.

1.1.4 Principle of jet mixing of water in oil for representative sampling

A portion of the flowing oil is withdrawn from the line and pumped back through a jet or jets (fig. 1.2) configured to cause the maximum amount of turbulence within the pipeline. By selectively positioning the pump suction point either upstream or downstream (fig. 1.2) of the jets mixing zone the pumped fluid can either be mainly separated water or low concentration water in oil.

When oil (ie. oil/low concentration water mix) is the injected fluid, which is more common, it is usually jetted through the layer of separated water at the bottom of the pipe in order to lift and disperse it across the pipe. However, when separated water (or oil/high concentration water mix) is injected it will break up as it enters the pipeline through the jet, dispersing across the cross section of the pipeline.

The basic principle of the jet mixer is different from any other mixing system. Instead of generalised turbulence and shear of the whole fluid mass, the jet energy is concentrated locally to the breakup the slugs of water, thus requiring less energy to distribute. This is achieved by locating the area of maximum energy addition at the point where the concentration of water is highest (eg. the bottom of a horizontal pipe). As the droplets are broken up, they are simultaneously redistributed.

1.2 The process 'Mixing' in the context of representative sampling of water in oil

Mixing depends to a great extent on the definition of the term "mixture", we shall use mixing to mean any blending into one mass and mixture to mean "a complex of two or more ingredients which do not bear a fixed proportion to one another and which, however thoroughly commingled, are conceived as retaining a separate existence". Therefore in any specific case our mixture will depend on the scale of our view. If our scale of view is very large, then even the very coarse mixture would be satisfactory and the molecular diffusion would mean little in this process. For a mixture of finer scale, dispersion would not do alone, but requires fine scale mixing by the smallest of eddies in the turbulence in conjunction with molecular processes.

In general, mixing is a combination of three diffusional processes, namely molecular, eddy and bulk diffusion. The "molecular diffusion" is caused by relative molecular motion. The turbulent process breaks up fluid elements to some limiting point. Since energy is required for this breakup, the limiting scale should be associated with the smallest of the energy containing eddies. However, because of the macroscopic nature of turbulence, the ultimate level of breakup is nowhere near molecular size. Therefore these are motions of large groups of molecules which give rise to the material transport called "eddy diffusion" or dispersion.

Kolmogorov, Landau and Lifshitz (Brodkey, 1978) eloquently summarized

the role of energy in turbulent mixing. They pointed out that there is a distribution of different eddy sizes in turbulent flows. Eddy size is defined as the distance over which there is an appreciable change in velocity. The largest eddies are the same order of magnitude in size as the apparatus carrying the flow, and they contain most of the kinetic energy. Energy in the turbulence continually cascades from the largest to the smallest eddies where it dissipates as heat. The smallest eddies have a Reynold's number of the order of one and a size of order of,

$$\lambda_o \simeq (\nu^3/\epsilon)^{0.25} \qquad (1.1)$$

Where ν is the kinematic viscosity of the fluid and ϵ is the energy dissipation per unit mass per unit time. At the λ_0 scale mixing occurs by a complex interaction between turbulence and molecular diffusion. Equation (1.1) shows that increasing the rate of energy dissipation reduces λ_0, resulting in more rapid turbulent dispersion. From this idea it is possible to show that mixing is favoured by high velocities. Non-molecular and noneddy diffusion processes are called "bulk diffusion". This is usually an axial (or secondary swirl flow) convection.

Generally all of the above mentioned three diffusional processes occur simultaneously in turbulent flows of liquid-liquid miscible systems. Miscible means that when mixing, they retain their separate existence only at molecular level. Two main aspects of mixing depend on the degree to which the material has been spread out (dispersed) by the turbulent action (scale of segregation) and the approach to uniformity by the action of molecular diffusion (intensity of segregation). In the case of immiscible liquid-liquid systems mixing by "molecular diffusion" process is impossible. But in a mixture of finer scale of droplets of colloid sizes ($< 10^{-6}$ m), this process would be replaced by a process called "Brownian diffusion".

It should be noted, in applictions of jet mixing of water in crude oil, the danger of over dispersion of the water. This would produce very small water droplets in the form of a stable emulsion which makes

subsequent analysis and separation very difficult. Therefore droplet formation of colloidal range should be avoided and mixing for the purpose of representative sampling should be better confined to eddy and bulk diffusion processes. But presently, due to erroneous design procedures jet mixing has often produced stable emulsions. The mixing required for this purpose may be defined as the condition, when the water is distributed over the cross-section of the pipe in such a way that its concentration is the same at every point, and the dispersion of the water in the oil is of such a degree that the water droplets formed are sufficiently small as to have no effect on the sampling accuracy. The distribution of water across a pipe can be characterized by an rms velocity profile, since it is related to eddy diffusion. The maximum water droplet size, when there is no other technique available, is usually estimated from the Hinze (1955) formula, which is briefly discribed in the paragraph below.

In order to understand a given transport process without a good droplet size estimate, one could use order of magnitude arguments or undertake an experimental effort. Order of magnitude arguments derive a critical Weber number for a breakup of a droplet to occur. Based on this, Hinze (1955) obtained an expression for the maximum drop diameter, stable against breakup as:-

$$d_{max}(\rho_c/\sigma)^{3/5}\epsilon^{2/5} = constant = 0.725 \qquad (1.2)$$

Where d_{max} is the maximum drop diameter, ρ_c is the density of the continuous phase, σ is the interfacial tension, ϵ is the energy dissipation per unit mass per unit time.

1.3 Introduction to previous investigations

None of the investigations were associated with jet mixing of water in crude oil (or immiscible liquid) pipelines. Therefore this section was further divided and was reviewed under the following sub-heading:-

i). Water dispersion in crude oil pipelines

ii). Jet mixing of miscible liquids in pipe cross flow

1.3.1 Water dispersion in crude oil pipelines

The annex A of ISO/DIS 3171 (1985) sets out minimum required conditions for representative sampling. It uses calculation procedures based on a simplified theory to give some indication of the dispersion of water-in-oil. This analysis assumes fully developed velocity and concentration profiles. Therefore sections taken too close to a mixing element (where swirl effects may be present) or section taken too far downstream (where settling may dominate) may not be properly described by this analysis. The degree of dispersion in horizontal pipe was estimated by the formula:-

$$c_1/c_2 = exp(-W/D_f D) \qquad (1.3)$$

where c_1/c_2 is the ratio of water concentration at top(c_1) to that at the bottom(c_2). W is the settling velocity of water, D_f is the eddy diffusivity and D is the pipe diameter. The ISO/DIS 3171 recommends a c_1/c_2 ratio of 0.9 to 1.0 for representative sampling. The derivation of this formula was based on a simplifed theory given by Prandtl, who assumed the concentration and velocity profiles to be fully developed. His dispersion equation under these conditions became:-

$$-c(1-c)W = D_f \, dc/dy \qquad (1.4)$$

Since the particle eddy diffusivity is characterising the pipe turbulence, it was correlated to the eddy diffusivity of the suspending fluid. Therefore particle eddy diffusivity (D_f) was given by:-

$$D_f = \varepsilon R u^* \qquad (1.5)$$

Where R is the radius of the pipe and u^* is the pipe friction velocity. Assumming a value of 0.36 for ε and relating u^* to the Fanning friction factor and the mean flow velocity (V) in the pipe the following relationship was obtained:-

$$D_f/D = 6.313\times10^{-3}\nu^{0.125}\ V^{0.875}\ D^{-0.125} \qquad (1.6)$$

Where ν is the kinematic viscosity of the crude oil. In this analysis the average droplet size correlated from Hinze's formula (eq. 1.2) was assumed to be small enough to ensure that the droplets obey Stokes' law for their terminal velocity under gravity. Therefore the settling velocity was given by:-

$$W = \frac{g}{18}\ \frac{(\rho_w-\rho_{oil})d^2_{ave}}{\rho\nu} \qquad (1.7)$$

Where g is the gravitational acceleration, ρ_w, ρ_{oil} are the density of water and crude oil respectively. d_{ave} is the average diameter of the water droplets given by:-

$$d_{ave} = 0.3625(\sigma/\rho)^{0.6}\epsilon^{-0.4} \qquad (1.8)$$

Where ϵ is the energy dissipation rate in the flow, the water droplet surface tension, σ, was taken as 0.025 N/m. The energy dissipation rate, ϵ, was related to the pressure drop (ΔP) by the relation:-

$$\epsilon = \Delta PQ/\rho q = \Delta PV/\rho\Delta X$$

Where Q and V are the volumetric flow rate and velocity. The q and ΔX are the volume and characteristic length of the liquid subjected to the dissipation action respectively. Since the pressure gradient of a long straight unobstructed pipe is $\Delta P/\Delta X = 2f\rho V^2/D$, the energy dissipation rate(ϵ) for a pipe flow reduces to:-

$$\epsilon = 2fV^3/D \qquad (1.9)$$

Where V is the pipe flow velocity, f is the friction factor.

Karabelas (1978) has used an approach similar to the above, but using rather more precise physics. According to Baker (1985 and 1987), neither of these methods can adequately estimate the dispersion of

water in pipeline sampling situations where violent mixing is still occuring and the concentration profile has not reached a steady state. Segev (1984) has found the three dimensional concentration profile of the dispersed phase in a circular pipe by numerically solving the diffusion-convection equation, given below for a fully developed turbulent velocity profile in a gravitational field.

$$\partial c/\partial t + U.\nabla c = V\nabla.\epsilon_t \nabla c - \nabla.(Wc) \qquad (1.10)$$

He has also obtained a closed-form expression (exact solution), for a situation where concentration profile is fully developed. Karabelas (1978) has shown experimentally that the measured size distribution of water droplets in fully developed flow can be represented by the Rosin-Rammler equation given by:-

$$V' = exp[-2.996(d/d_{max})^n] \qquad (1.11)$$

Where V' is the cummulative volume fraction of particles with diameter greater than d, and n=1.5.

Equation 1.9 was substituted into the Hinze (=equation 1.2) formula, for maximum droplet diameter, to obtain the relationship below, which was subsequently substituted to Karabelas' Rosin -Rammler equation to give a droplet size distribution.

$$d_{max}/D = [0.725/(2f)^{0.4}]We^{-0.6} \qquad (1.12)$$

or

$$d_{max}/D = 1.52(Re)^{0.1}\ (We)^{-0.6}$$

$$(since\ f=0.079Re^{-0.25})$$

All other parameters in Segev's analysis such as diffusivity, settling velocity etc., were evaluated from relations given in ISO/DIS 3171 (1985).

Baker (1988) developed Segev's model to obtain the concentration of water in a downstream of pipe fittings, where the velocity profile is undeveloped. He assumed that a "bend like" secondary flow will be

found downstream of various pipe fittings. Thus, he described the inlet to a region of severe mixing with an idealised pipe bend secondary flow and a solid body rotation, and the former was assumed to decay in a distance similar to that for a bend. In order to account for the high turbulence levels in a mixing region, he obtained the turbulent dispersion coefficient by multiplying the value of fully developed flow by a factor, and also introduced a factor to represent the decay of the turbulence downstream.

He made use of an expression for the decay of turbulence behind a gauze by Batchelor (1953) to obtain the decay of turbulent viscosity downstream of a plane where high turbulence has been created (eg. flow discharging from a smaller to larger pipe) as:-

$$\nu_t = 0.4\, u^* R \, \frac{(V_{jet}/V^2)}{(z/L+1) + z/L(z/L+1)} \qquad (1.13)$$

Where V, V_{jet} are mean velocities of the larger and smaller pipes respectively, L is the distance required for ν_t to decay to fifty percent of its initial value. The "Bend-like" secondary flow patterns were obtained by using the following expressions:-

$$V_r = (c'/r).J_1(kr)Cos\ \theta \qquad (1.14)$$

$$V_\theta = (c'/r).J_1(kr)Sin\ \theta - c'kJ_0(kr)Sin\ \theta \qquad (1.15)$$

where kR =3.83 and R is the pipe radius, J_0 and J_1 are Bessel functions. To account for the decay, the secondary flow was multiplied by exp(-0.22.z/D), where z is the axial distance. For the "swirl-like" secondary patterns a solid body rotation was assumed:-

$$V_r = 0 \qquad (1.16)$$

$$V_\theta = v_{\theta o}(r/R) \quad for \quad r \neq R \qquad (1.17)$$

$$V_\theta = 0 \quad for \quad r = R \qquad (1.18)$$

Since the decay of swirling flow is slow, the decay factor was taken as exp(-z/20D).

There is a certain amount of empirical data available for static mixers. Some of these have been published by manufacturers, for example by Cathie (1981) and Chen et al (1978), but there are some independent test reports by Novak et al (1985), Hartung and Hiby (1972) and Christy and Macleod (1985).

Chemineer Ltd., manufacturers of Kenics static mixer, adopts a design calculation method as follows (Cathie et al, 1981). For the prediction of the Sauter mean droplet size, SMD from a known mean fluid velocity in pipe axial direction (V), they give:-

$$\frac{SMD}{D} = 1.14(We)^{-0.75}\left[\frac{\mu_d}{\mu_c}\right]^{0.18} \qquad (1.19)$$

The Weber number (We) was related to continuous phase fluid properties and given by $We = \rho V^2 D/\sigma$. Where D is internal pipe diameter, ρ_c is the continuous phase density, σ is the interfacial surface tension, and μ_d and μ_c are the dynamic viscosity of the disperse and continuous components respectively. This is an empirical relationship based on the manufacturers own experimental data.

The prediction for pressure drop across the Kenics mixer was based on the Reynolds number and pressure drop across empty pipes. The expression for pressure drop is:-

$$\Delta P = K_{ot}(Re)^{0.1}\Delta P_o$$

Where K_{0t} is a function of pipe size, and ΔP is the pressure drop across the mixing section. This relationship was empirically derived by the manufacturer. The pressure drop, ΔP_o, for empty pipes is given by:-

$\Delta P_o = f(L/D)\rho(U^2/2)$ where f is the friction factor.

Another static mixer manufacturer, Sulzer Bros. Ltd., uses a design calculation method (Novak et al, 1985, Streiff, 1979, Underhill et al, 1981) as follows. The Sauter mean diameter of the droplets is given

by:-

$$SMD = 0.21 d_h (We)^{-0.5} (Re)^{0.15} \qquad (1.21)$$

Where d_h is the hydraulic diameter of the Sulzer mixing element cannels, and the Weber and Reynolds numbers refer to this diameter and continuous phase fluid properties. The pressure drop in a Sulzer mixer was given by:-

$$\Delta P = f_s (\rho/2)(L/d_h) V^2 \qquad (1.22)$$

Where f_s is a friction factor which depends on the disperser geometry and L is the length of the mixing section.

The only supplier of jet mixer nozzles, Jiskoot Ltd., adopt a design method which is unclear (Baker, 1987 and Hayes, 1987). Consequently, their prediction method is not quoted here.

1.3.2 Jet mixing of miscible liquids in pipe cross flows

The scope of the theoretical work was limited. The analytical approaches used mainly integral methods which required empirical values for some of the parameters and concentrated only on single jet mixers. Fitgerald et al (1979) obtained, from experimental analysis, momentum ratios for optimum mixing of passive contaminants. Stoy et al (1973) carried out experimental and simple one dimensional analytical studies to obtain the distance to the impinging point on the opposite wall. Maruyama et al (1976) experimentally correlated impinging point on the opposite wall. Edwards et al (1985) assumed that the global vorticity declines as inverse time and the concentration fluctuation declines by a constant fraction at each global rotation. Then they obtain an order of magnitude argument for the concentration fluctuations of a passive contaminant at a downstream section. None of the work was associated with mixing of immiscible liquids.

1.4 Scope of this study

It is known from previous single phase studies of jets in (unconfined) cross flow, that they are very difficult to model. Over the years, the trend in the modelling of jets in crossflows has moved from those based mainly on empirical findings, which were therefore limited in their range of applicability, to numerical models of a more general nature. However, although numerical models show a great deal of promise for universality, they are still in their infancy and none of them has yet been applied or indeed capable of predicting the whole range of turbulent jets in cross flow to a reasonable degree of accuracy. Fairly good prediction has been obtained in relatively few cases. Between the two extremes lie integral methods which have been widely applied to jet flow problems; but these are semi-empirical in nature and require many assumptions which limit their range of validity.

When it comes to jets in confined cross flow in two component flows, as in the case of present study, difficulties in predictibility increases many fold. In addition, the problems of this nature are not available in open literature. The concept of jet mixing of water in oil pipelines is still in its infancy, therefore frequent changes in the design of nozzle geometries can be expected. Therefore the research into this problem should begin at the most fundamental level and then explore to find methods to extend them to more complicated forms. As a whole, the study should improve the understanding of jet mixers. However predictive techniques can be found only through idealization and simplification.

The study in this thesis mainly divides into four parts as follows:-

i). Penetration of a single oil jet through a stratified water layer- two component flow study.

ii). Dispersion of broken up stratified water layer in a pipe flow- numerical model.

iii) Flow field analysis of jet mixer nozzles in pipe cross flow by using Laser Doppler Anemometry (LDA) measurement-Single phase experimental study.

iv). Inter relationships and implications of above three parts, and general discussion and conclusions.

Part i) is a study of a liquid jet penetrating through another stratified liquid layer. A flow visualisation study is used to observe and understand the basic mechanism and structure of the process. A simple physical model would be developed to clarify the salient features associated with entrainment. Correlations will be attempted for entrainment and water drop sizes (ie: SMD) from the experimental data.

Part ii) is a numerical study that uses a general purpose computational fluid dynamics code, Phoenics. Here, the results obtained in part i) are coupled into a Homogeneous and into a Two-fluid model, to explore an area that had not been approached before. This will also give an insight into the flow field and the water concentration distribution, which Baker (1988) has indicated to be of value. The entrainment rate formulated in part i) now behaves as a source of water at the jetting point, for the mass conservation equation of water.

Part iii):- characteristics of the flow field are important in determining the water droplet breakup and mixing capabilities of jet mixer, but the flow field information, even for relatively simple flow through pipe components, is scarce. At present designers have to rely on very crude models and subsequent experimental analysis (for one particular situation) based on trial and error. Therefore, as an initial step towards improving the understanding of the flow field developed by these jet mixers, a single phase experimental study is conducted in chapter 7.0, through LDA measurement and flow visualisation. The single phase study is justified as the water concentration is relatively very low and hence the effect due to

presence of water on continuous phase is not considerable. Flow field information is measured, using LDA, for two types of jet mixers firstly for the relatively simple single jet nozzle mixer and secondly for a multi-nozzle mixer. The studies in parts i) and ii) are conducted for the single jet nozzle mixer. Here, the two mixer types are compared to determine whether any relationships between the two exist. These results will also allow validation of any future numerical computational model.

Part iv):- To put this problem in perspective, the mixing domain can be divided into three regions, penetration, near field and farfield (fig. 1.4). The region, where the jet (or jets) penetrates the stratified water layer, is defined as the penetration region. The downstream region, where severe mixing is occuring, is defined as near field. And lastly, the region, where the flow behaves two-dimensionally without swirl, is defined as the far field. To simulate the far field, an exact solution for the two dimensional water mass conservation equation is obtained in chapter 8.0. The wall boundary conditions are specified by using sticking probability constants. And then a simple (low level) model for multi-nozzle is also formulated and programmed.

In chapter 9.0 we compare experimental results of chapter 7.0 with the numerical results. Lastly, the general discussions and conclusions of the whole study are brought together in chapter 10.0.

PART 1

PENETRATION

OF A

SINGLE OIL JET

THROUGH A

STRATIFIED WATER LAYER

CHAPTER 2.0 LITERATURE REVIEW OF BACKGROUND CONSIDERATIONS

The mechanisms of two immiscible fluid interactions are varied and complex, and depends upon numerous factors whose influences have not yet been fully quantified. Previous relevant work involving high shear rates, such as in jet atomisation, has only been investigated for gas/liquid two phase flows, the only exception being the studies by Hinze (1955) for droplet breakup. Hence, updating the present understanding of the roles of various significant factors as well as their degree of influence in gas/liquid and, where possible in liquid/liquid immiscible flows are a pre-requisite to research in this study. Before any complicated problems are discussed, the breakup of a single drop moving in another medium will be considered.

2.1). Breakup of a drop

When a liquid drop is in relative motion with respect to a surrounding immiscible medium, pressure and shear forces are set up on its surface due to the hydrodynamic (or aerodynamic) drag. These forces are opposed by the internal forces arising from surface tension and viscosity. Following a change in the droplet shape, the pressure distribution around it will also change such that a new equilibrium state is reached. However, droplet distortion beyond a certain limit results in its disintegration because the internal forces can no longer contain the external pressure force. If the surface tension force is still too small, further sub-division will take place until the drop becomes so small that its surface tension is large enough to resist any further deformation of the drop.

The modes by which the breakup occurs depend on the conditions of experimentation. The large free-falling drop in still air, or the somewhat smaller drop in a steady stream of air was first considered by Lenard (1921) and by Hochschwender (1919). They allowed water drops to fall into a free upward current of air and noted that some of the drops were blown inside out. Fig. 2.7 shows this phenomenon, which can be described as follows: At the critical velocity of breakup, the drop passes through stages of increasing flattening, formation of a torus

(a roughly circular rim with an attached film, shaped like a hollow bag), increasing bag size, bursting of the film to produce a shower of very fine droplets. Another mode of breakup very different from the previous one was first observed by Lane (1951), who subjected a drop to a transient pulse of air. In this case it was deformed in the opposite direction and presented a convex surface to the flow.

The deformation of moving drops has been analysed further by Hinze (1955). He considered the balance between the normal continuous phase forces and the liquid surface tension forces and, in addition, analysed mathematically the effect of liquid viscosity on the splitting of drops. He reached the conclusion that a drop will split if the ratio of continuous phase resistance pressure, represented by the expression $\rho_c V^2$, to the surface tension pressure, represented by 'σ/d'is greater than a certain critical value. This ratio is known as the Weber number and depends on the properties of the continious phase. It appears from Hinze's analysis that the critical Weber number for two immiscible liquids is about 1.18. However, the critical Weber number and the critical velocity at which the spliting of a drop may occur, depend also on disperse phase liquid viscosity. Disperse phase viscosity will delay and dampens the tendency for deformation.

In a subsequent treatment, Hinze (1955) outlines the different ways a liquid globule may disintegrate depending upon the flow pattern around it (fig. 2.8). These are:-

a). The flattening of the globule, forming an oblate ellipsoid in the initial stage. This may be distorted into a form, which after stretching, breaks up into many small droplets.

b). The globule becomes more and more elongated, forming a prolate ellipsoid and ultimately results in the formation of a long cylindrical thread (cigar- shaped defomation) that bursts into droplets.

c). The surface of the globule may be deformed locally, forming bulges and protuberances, and ultimately parts of the globule may become

bodily separated (bulgy deformation).

Hinze, also proposed (1955) that the critical Weber number for high viscosity liquids can be obtained from its corresponding value for low viscosity liquids by multiplying the latter by a factor function of the disperse phase viscosity group '$\mu_d/d\sigma\rho_d$' that is:

$$(We_{cr})_{\mu} = (We_{cr})_{\mu=0}(1 + f[\mu_d/(d\sigma\rho_d)]^{1/2}) \qquad (2.1.1)$$

Where $(We_{cr})_{\mu}$ = critical Weber number for high viscosity liquid (dispersed).

and $(We_{cr})_{\mu=0}$ = critical Weber number for low viscosity liquid (dispersed).

The foregoing material implies a gross relative motion between the drop and its surroundings. Such a difference might not always exist or be definable. In such cases one may surmise that the parameters of the local turbulence might be more important and controlling, and that the large-scale motions will have little effect on the process. Kolmogoroff (1949) and Hinze (1955) took this view and further assumed that since the breakup was to be considered local, the principles of local isotropic turbulence would be valid. Assuming also that a constant critical Weber number still applies, the following expression was obtained:

$$d_{max} = C(\sigma/\rho_c)^{3/5}\epsilon^{-2/5} \qquad (2.1.2)$$

Experimental data on drop breakup in an isotropic field are non-existent, so direct verification of the equation is not possible. Some indirect support is given in Shinnar (1961) and Vermeulen et al (1955). Sleicher (1972) investigating droplet (order of 5mm in diameter) breakup in pipe of 37mm diameter has shown that the above equation is not valid for a pipe flow. The breakup occurs in the vicinity of the wall, where the conditions are the furthest from the approximate isotropic condition at the centreline. The breakup in the pipe system is probably the result of a balance between surface forces, velocity fluctuations, pressure fluctuations, and the steep

velocity gradient. In cases where the ratio of droplet diameter to pipe diameter is very small then Hinze's approach is more appropriate.

2.2). Jet breakup

The mechanisms of jet breakup discussed here are the results of steady injection of liquid through a single hole nozzle into a quiescent gas. These are required in order to provide a basis for understanding the more complex process involved in this study. They are reviewed since, liquid jet breakup has been more extensively examined in gas media rather than immiscible liquid media due to their vast commercial applications.

The general approach followed is to divide the jet breakup phenomena of interest into various breakup regimes (fig. 2.1). These regimes reflect the difference in the appearence of the jet as the operating conditions are changed. The existing theory is found to offer a reasonably complete description of the breakup mechanisms of low speed jets. For high-speed liquid jets however, the initial state of the jet appears to be progressively more important and less understood. It should be also pointed out that the breakup due to only fluid dynamic instablities are only considered here. There are also other causes of breakup such as superheating, electrostatic charge, acoustical excitation and chemical reactions.

If all other parameters are kept constant the jet velocity would become a convenient quantity to introduce various regimes. Grant and Middleman (1966) reviewed the behaviour of low speed jets and reported results in the form of a breakup curve which describes the unbroken length of the jet, L, as a function of the jet velocity 'V_j'. Once a jet is formed (point C, fig. 2.1) the jet breakup length at first increases linearly with increasing jet velocity. Thereafter it reaches a maximum (point E) and then decreases, these first two breakup regimes are reasonably well understood, and are called the Rayleigh (CD) and first wind-induced breakup (EF) regimes. A feature of breakup in these two regimes is that drops are effectively pinched off from the end of the jet. (figs. 2.4A and B).

In Rayleigh's jet breakup regime, the jet breaks up many jet diameters downstream of the nozzle and forms drops whose diameters exceed that of the jet. it is due to the growth of axisymmetric oscilations of the jet surface that are induced by surface tension. In the first wind-induced breakup regime the breakup occurs many jet diameters downstream of the nozzle, and yields drops whose diameters are of the order of the jet diameter. In this case, the surface tension effect is augmented by the relative motion of the ambient gas and the jet.

Reitz et al (1985) identified the difficulties in interpreting these published results, as being due to a lack of consistent terminology in the field and insufficient charaterization of the injection system and the nozzle geometry. Indeed many authors do not even distinguish between the two- wind induced regimes. He therefore, conducted a review into jet breakup with a view to updating and solving some of these difficulties. As he pointed out, for higher velocity jets beyond the point F (fig. 2.1) there remains some confusion over the true shape of the breakup curve. The definition and measurement of the intact length becomes increasingly difficult as 'V_j' is increased, as pointed out also by Grant and Middleman (1966). At sufficiently high velocities, the jet surface is disrupted prior to the breakup of the jet core and use of only one breakup length is no longer a complete measure of the jet stability. This two breakup lengths are defined as the intact-surface, L_1 , and the intact-core length,L_2. In the second wind-induced and atomization regimes the disruption starts at the jet surface and eventually reaches the jet axis so that at least two lengths (L_1 and L_2) are necessary to identify the gross features of the breakup.

In the atomization regime the intact-surface length is zero (but the intact-core length is not necessarily zero). The term atomization has been used in a variety of different contexts. This regime is of interest in many fuel injection applications. For breakup in the second wind-induced regime (curve FG or FH, fig. 2.1), both the intact surface length and the intact-core length are finite and drops are formed with sizes also much smaller than the nozzle diameter (fig.

2.4D). Attempts have been made by various authors to offer criteria with which to demonstrate breakup regimes. For example, Miesse (1955) correlated breakup regime data and presented the results in a form suggested by Ohnesorge (1936) as shown in fig. 2.2.

The effect of ambient gas density on jet breakup regimes was discussed by Ranz (1956) who argued that the Weber number should be a controlling parameter. He offered the criterion We=13 (based on continious phase density) for the onset of atomization. However, it should be noted that this definition of the term atomization differs from the above. He does not refer to the state of the jet itself but instead refers to the process of disintegration of already formed droplets during their flight within a spray. He argued that the criteria for the formation and subsequent further breakup of the droplets should be the same. This is because the inertial stresses developed by the surrounding gas exceed the surface tension stresses opposing the deformation sufficiently and the liquid drop (or ligament in the formation process) will sub-divide into smaller units. But a Weber number correlation by itself is still incomplete since now the liquid viscosity is not accounted for, Thus completely satisfactory correlations for the regime boundaries are not yet available. Indeed many authors do not even distinguish between the two-wind induced regimes.

The breakup of low speed jets has been studied analytically by examining the stability of the liquid surface to perturbations with the use of first order linear theory. This ultimately leads to a dispersion equation (Reitz et al, 1985). This equation relates the growth rate ω, of an initial perturbation of infinitesimal amplitude, η_o, to its wavelength λ (or wave number ,k $=2\pi/\lambda$).

$$\beta_1^2 + 2Zk^2d_j^2F_1\beta_1 = kd_j(1 - k^2d_j^2)F_2 + We_2k^2d_j^2F_3 \qquad (2.2.1)$$

where $\beta_1 = \omega(\rho_d d_j^2/\sigma)^{1/2}$; $Z = \mu_d/(\rho_d \sigma d_j)^{1/2}$; $We_2 = \rho_a V_j^2/\sigma$ and F's are dimensionless ratios of Bessel functions and wave numbers. Reitz et al (1985) has illustrated these complicated ratios, they are not quoted here since equation 2.2.1 would only be used to distinguish the

important parameters and regimes theoretically. 'k' is the wave number, the subscript 'j' refers to the jet and the subscript 'd' refers to the disperse phase, in this case the jet liquid.

Rayleigh (1878) made substantial contributions to the understanding of the stability of low-speed jets. He obtained a dispersion equation for the growth of axisymmetric surface disturbances by simply equating the potential and kinetic energies of an inviscid jet. With the hypothesis that the disturbance with the maximum growth rate would lead to the destruction of the jet, he also obtained an expression for the droplet size, assuming that it would be of the order of the wavelength of this disturbance. His equation for the growth rate, was:-

$$\omega^2 = [\sigma k/(\rho_d d_j^2)][1 - k^2 d_j^2](I_1(kd_j)/I_2(kd_j)) \qquad (2.2.2)$$

which is the equation 2.2.1 (Reitz et al, 1985) above when Z=0 and We =0. Where Z= Ohnesorge number = $\mu_d/(\rho_d \sigma d)^{1/2}$. This wave growth curve were found experimentally by vibrating low speed jets at various frequencies and measuring the growth rate of axisymmetric surface oscillations.

The theoretical influence of the liquid viscosity is found by retaining the term involving Z in equation 2.2.1. Therefore for large Z (high liquid viscosity) the maximum wave growth rate is:

$$\omega = [1/(2\sqrt{2})][\sigma/(\rho_d d_j)]^{1/2}[1/(1+3Z)] \text{ at } k = 1/[d_j\sqrt{(Z+2)}] \qquad (2.2.3)$$

where 'kd' has been assumed to be small and the Bessel functions and their arguments have been replaced by their asymptotic values. This relationship was first obtained by Weber (1931). His analysis predicts that the jet breakup yields droplets many nozzle diameters downstream of the nozzle. The drop diameters are larger than that of the jet and a photograph typical of jet breakup in this regime is shown in fig. 2.4A. In this regime jet breakup is due to the destabilizing combinations of surface tension and interia forces on the jet. To estimate the droplet size Rayleigh assumed that all of the liquid

enclosed within the wave forms the volume of the newly created drop when the surface amplitude equals the jet radius.

The second term on the right-hand side of equation 2.2.1 becomes important when the jet velocity (for example) is increased. In this case (first wind-induced breakup regime) the inertial effects of the surrounding air can no longer be neglected and the Weber number 'We_c' becomes a controlling parameter in the dispersion equation. Therefore, the breakup is due to the destabilizing influence of surface tension as well as the aerodynamic interaction between the liquid and gas. Weber (1931) showed that the effect of the environment on the jet is to enhance the growth rate of disturbance, leading to an earlier breakup of the jet. He obtained the result:

$$\omega^2 + 3\nu_d k^2 \omega = [\sigma/(2\rho_d d_j)][1-k^2 d_j^2]k^2 d_j^2 + (\rho_c/\rho_d)[V_j k^3 d_j^3/(2d_j^2)][K_0(kd_j)/K_1(kd_j)] \qquad (2.2.4)$$

Where K_n is the n^{th} order modified Bessel function of the second kind. This equation is the same as equation 2.2.1 (Reitz, 1985) in the limit $kd_j << 1$. The influence of the initial state of the jet in this regime is discussed by Phinnry (1972) who proposed that liquid turbulence also enhances the jet breakup process. He noted that even in the absence of aerodynamical effects, the jet breakup length L is reduced once a critical value of the jet Reynold's number is reached. Furthermore, this critical Reynold's number is of the same order as that for transition to turbulence in the nozzle.

The present study in this report is more closely related to the other two regimes which are the second wind-induced breakup and atomization regimes. With further increase in We_c in equation 2.2.4 predicts (Reitz et al, 1985) that the maximum wave growth rate occurs at progressively larger wavenumber (ie: shorter wave lengths). An inspection of equation 2.2.4 shows (Reitz et al, 1985) that the first term on the right hand side changes sign at kd =1, after which the surface tension forces oppose the breakup process. Jet breakup is now due the unstable growth of short wavelength surface waves (kd > 1)

which are induced by the relative motion between the jet and the ambient gas. Analysis of equation 2.2.4 showed (Stirling et al, 1975) that the maximum wave growth rate occurs at kd =1 when We_c = 12 for inviscid jets. This estimate was made using the numerical results of Sterling and Sleicher (1975). The estimate also agrees well with the experimentally obtained criterion of Ranz (1956), We =13, for the onset of short wavelength waves. An expression for the growth rate of short wavelength surface waves was presented by Levich (1962) and Levich and Krylov (1969) who examined equation 2.2.1 in the limit kd_j >>1 and deduced, neglecting the liquid viscosity, that

$$\omega^2 = (\rho_c k^2 V_j^2 - \sigma k^2)/\rho_d \qquad (2.2.5)$$

Equation 2.2.5 shows that the dispersion relation equation 2.2.1 becomes independent of the jet radius in this limit and implies the existence of unstable waves when $k<\rho_c V_j^2/\sigma$. Consequently, for kd_j >>1, jet curvature effects are unimportant. The influence of the liquid viscosity is seen by retaining the second term on the left side of equation 2.2.1. This produces results identical to that of Taylor (1940) who performed an analysis of the unstable growth of two-dimensional planar surface due to the relative motion between a liquid and a gas. He considered the limit kd_j >>1 and, assuming $\rho_c << \rho_d$ (since continuous phase is air), he found that the wave growth rate is:-

$$\omega/kV_j = 2(\rho_d/\rho_c)^{1/2} \times g(\Gamma, X) \qquad (2.2.6)$$

The function g is a correction to the results of Levich (1962) which now accounts for the effects of the liquid viscosity. It is shown as a function of the new parameter:-

$$\Gamma = (\rho_d/\rho_c)[\sigma^2/(\mu_d^2 V_j^2)] = (\rho_d/\rho_c)(Re_d/We_d)^2 \qquad (2.2.7)$$

and the nondimensional wavelength $X = \rho_d V_j^2/\sigma k$ from Taylor's work (fig. 2.3). Taylor (1940) also estimated the intact core length, L_2, by computing the rate at which droplets remove mass from the liquid core. Here the droplet sizes were assumed to be proportional to the unstable surface wave wavelengths. This analysis has given:-

$$L_z = B_1 d_j (\rho_d/\rho_c)^{1/2}/f(\Gamma) \qquad (2.2.8)$$

Where B_1 is a constant of order of unity. The function $f(\Gamma)$ corresponds to the maximum wave growth rate (fig. 2.3).

In the atomizing regime the breakup appears to commence almost at the nozzle exit. Though numerous theories have been postulated concerning the mechanisms involved in this regime, a complete and tested theory is not yet available, and also in many instances the various writers do not agree. Much of the disagreement is attributed to two facts: a). the mechanism by which atomization is accomplished is quite different for different conditions and (b) atomization may and usually does, take place in successive stages involving more than one single mechanism. There is general agreement, however, on one point, namely that the atomization of liquid is an extremely complicated process.

Reitz and Bracco (1979) examined previously proposed theories for atomization in detail. For example, DeJuhasz (1931) and Schwietzer (1932) proposed that liquid turbulence causes atomization. But if pipe turbulence was the only mechanism, turbulent jets (ie: from the nozzles with large length to diameter ratios (Rumsheiht et al, 1962)) would have been the most unstable flows. Similarly, cavitation phenomena were proposed by Berwerk(1983) to lead to atomization. But jets were found to atomize even when the cavitation free nozzles (Wu et al, 1983) were used. In fact, an evaluation of other proposed atomization mechanisms has revealed that none of the theories taken alone, is able to explain the results fully. These theories include proposals that the atomization is caused by:-

i). Aerodynamic surface wave growth (Castleman, 1932), then the results would be independent of the nozzle geometry.

ii). Rearrangement of the jet velocity profile (Rupe, 1962), then high viscosity jets would be the most unstable.

iii). Liquid supply pressure osillations (Giffen et al, 1953).

iv). Wall boundary-layer velocity profile relaxation (Shakadov, 1970), then atomization would have been independent of the gas density.

However, the aerodynamic surface wavegrowth theory was found to predict many of the trends in tests with a given nozzle. Ranz (1956) argued that the spreading angle of the atomizing jet could be predicted by comparing the radial velocity of the fastest growing of the unstable surface waves with the axial injection velocity:-

$$\tan(\Theta/2) = V_j/U_j = 4\pi(\rho_c/\rho_d)^{\frac{1}{2}}f(\Gamma)/A \qquad (2.2.9)$$

where the proportionality constant A is obtained from experiments, U_j and V_j are radial and axial jet velocities.

Other aspects that still remain unresolved, besides the influence of the nozzle (ie. not predicted by the stability theory), are the size and size distribution of the unstable wave at the moment of breakup and also the time between successive ruptures. Away from the nozzle exit, as the generating surface regresses towards the axis of the jet, there are questions as to what gas velocity is seen by the liquid surface. The velocity of the entrained gas certainly approaches that of the liquid surface. Thus the breakup process should be coupled with the two-phase flow field that exists between the presumed intact-core and the unperturbed outer gas. As the relative velocity between the liquid and gas decreases inside the jet, larger drops or ligaments or blobs should be formed just as larger drops are found when the injection velocity is decreased. An additional factor to be considered is coalescence of the liquid fragments which can be expected where locally large values of the liquid volume fraction exist.

2.3). Atomizing systems

Commercial users require atomizers that will disintegrate and disperse a liquid over the maximum area for the least cost. The three types of atomizers in general use are; pressure, centrifugal and pneumatic.

Pressure atomizers and the atomizing jet discussed above refer to the same system. The swirl-type or centrifugal nozzle atomises by imparting swirling or spinning motion to the liquid before it is sprayed. These units produce a conical spray pattern with a hollow cone. In the present study two types of atomization occur, pressure type atomization of kerosene in the water layer and sheet type atomization of water as soon as the jet peneterates the water layer. Therefore the above mentioned systems are briefly reviewed here in order to provide background and a feeling to the extent of the problem, and reviewed again in some detail in section 4.1. Pneumatic atomization uses the action of a high velocity gas stream on a liquid jet to produce the desired liquid breakup. The mechanisms of all the above mentioned units are extremely complex and do not lend themselves to complete theoretical treatment. Hence semi-empirical correlations were obtained through dimensional analysis.

In a series of papers Fraser et al (1956, 1962, 1963 and 1963) have made a comprehensive photographic investigation of different aspects of atomization (when the continuous phase is a gas) from liquid sheet to spining cups. They give an insight into the manner of disintegration of a liquid sheet. Through high speed flash photography they observed perforations in liquid sheets. These perforations remain circular until they coalesce forming long threads, quickly becoming unstable and breaking up into drops. Fig. 2.6 shows this and an idealization of the breakup process given by Dombrowski and John (1963) in a theoretical analysis. They have extended the inviscid uniform-thickness solution for aerodynamic instability made by Squire (1953) and by Hagerty and Shea (1955) to the viscous-fluid case in which thinning of the film could be specified. They applied a force balance to the disturbed film and considered the effects of pressure, surface tension, inertial forces, and viscous forces and obtained:-

$$Gr + \alpha^2 Gr.Re + 2s\alpha^2(1/We - 1/\alpha) = 0 \qquad (2.3.1)$$

$$Gr = \beta h'/V;\ Re = h'V\rho_d/\mu_d;\ We = h'V^2\rho_a/\sigma$$

where $\alpha = 2\pi h'/\lambda = kh'$. β is defined as the amplitude growth factor.

s is the ratio of gas to liquid densities, h' is the liquid sheet thickness and V is the mean relative air wave velocity defined by:-

$$V^2 = \tfrac{1}{2}(V_1^2 + V_2^2) \qquad (2.3.2)$$

The first term in the equation (eq. 2.3.1) stems from the inertial force, or the rate at which the momemtum of the liquid element changes. The second term is associated with the viscous forces, and is zero for zero viscosity (ie. Re → ∞); the first part of the third term is a result of surface tension forces and would be zero for zero surface tension (ie. We → ∞) and the last part of the third term results from the force caused by the air pressure. Solutions for the equation 2.3.1 were obtained by taking, $d(Gr)/d\alpha = 0$ for maximum growth and one of the following four conditions:-

a). Inviscid uniform thickness (h) and Re → ∞ (ie; Squire and Hagerty)

b). Viscous effects considered with zero surface tension (ie; We → ∞) and attenuating sheet, in which thickness was assumed to decrease in proportion to the time of transit of the fluid element from the nozzle.

c). $(3We)^3/s(4Re)^2$ is less than or greater than two.

To translate these results into a drop size, it is assumed that, at some distance from the nozzle, the waves separate into ligaments, which are initially '$\lambda/2$' in width. These then contract into cylinders which by continuity, $d_L^2 = 4h'/k$.

where d_L is as indicated in fig. 2.6. It is further assumed that these ligaments breakup, according to Weber's modification of Rayleigh's jet-breakup theory (eq^n. 2.2.3), hence (see Dombrowski and John, 1963)

$$d^3 = (3\pi/\sqrt{2})d_L^3(1 + 3\mu_d/\sqrt{(\sigma\rho_d d_L)})^{\frac{1}{2}} \qquad (2.3.3)$$

Brodkey (1978) has identified this to be a reasonable beginning for a description of the breakup process of sheets. Further refinement of the theory and more extensive data would be necessary for more satisfactory predictions.

One shortcoming of these theories is that they predict a uniform single - particle size, while in reality a complete distribution of sizes is obtained. The first order analysis used by these previous workers was extended to second order analysis by Clark et al (1972) to calculate the breakup lengths of attenuating sheets. Their results compared reasonably well with experimental values.

Castleman (1932) proposed the so-called "ligament theory" for the atomization regime. He analysed high velocity distribution of the liquid jets (in gas environment) and included in his investigation some high speed photograpic observations made by other workers. Castleman described the process of jet disintegration as " a portion of the large mass of liquid is caught up by the air and, being anchored at the other end, is drawn out into a fine ligament. This ligament is quickly cut off by the rapid growth of a dent in its surface, and the detached mass, being small, is quickly drawn up into a spherical drop". Castleman's theory, therefore, considers that the most important factor in the process of atomization is the effect of the relative motion between the outer jet layer and the air, which, combined with air friction, causes the irregularities in the previously smooth liquid surface and the production of the unstable ligaments. As the air velocity increases, the size of the ligaments decreases, their life period becomes shorter, and upon their collapse much smaller drops occur in accordance with Rayleigh's theory.

Castleman claimed that the drop sizes approach a limiting value of the order of several microns, below which the drop diameter may not fall, however great the relative velocity. Subsequently, this was found to be consistent with the experimental findings of Fraser, Dombrowski and Routley (1963).

2.4 Jet breakup in another immiscible liquid

The dispersion of one liquid into another immiscible liquid is widely used in many industrial processes such as liquid-liquid extraction, direct contact heat transfer, and emulsification. Although, the dispersion in actual equipment is influenced by the complex flow and subsequent shear fields, only the very basic phenomena, such as breakup of a liquid column in near stationary liquid, is properly understood at present.

Previous work on immiscible systems has only been focused on relatively low velocites of the order less than 0.1 m/s (Kitamura et al, 1986). Out of these, the analytical treatments, for example by Tomotika (1935), were confined to extremely low velocites. Tomotika, using stability analysis, gave a reasonable theoretical explanation for Taylor's experimental work (Taylor, 1934) on breakage of a cylinderical thread resting in another liquid. Rumsheiht and Manson (1962) confirmed that the wavelength and growth rates of the disturbances for stationary liquid threads have good agreement with Tomotika's limiting solution, where the surrounding liquid was highly viscous.

Kitamura and Takahashi (1986) conducted experiments on a jet, having jet velocities upto the order of 0.1 m/s, injected into another immiscible liquid. Their photographic analysis has indicated that the continious phase turbulence has very little effect on jet stability. They have also shown that the drop size is an increasing function of μ_c/μ_d.

Meister and Scheele (1969) improved the drop formation model (of low velocity laminar jets) of Tomotika (1935), by analysing the dependence of surface velocity on the distance from the nozzle, and by introducing a complicated criterion for wave splitting. They reported that their analysis showed better agreement with experimental results than previous analysis. Their experimental results on laminar cylindrical jets have shown that the drop size is an increasing function of continuous phase viscosity.

In reality jet breakup of a liquid injected into another liquid, however, differs from those near zero relative velocities and those of a stationary column in four-roller apparatus (Taylor, 1934). In higher injection velocities the drag due to surrounding air has been shown to be playing an important role in liquid/air systems, therefore, in liquid-liquid systems the effect of the hydrodynamic resistance of the continous phase liquid on jet stability must also be considered

Another important type of liquid/liquid (immiscible) dispersion are performed in mixing vessels. Vermeulen et al (1955) measured droplet sizes in stirred liquid-liquid systems and obtained the following correlation:-

$$\frac{N^{3/2} D\, d\, \rho_c^{1/2}\, \mu_d^{1/4}}{\sigma\, \mu_c^{1/4}} = \text{constant}$$

Where D is the diameter of the agitator and N is its speed in revolution per second. The d is the droplet Sauter mean diameter. Later Shinnar (1961) attempted a theoretical concept of local isotropy to these systems and shown that the above equation agrees with this concept.

CHAPTER 3.0 FLOW VISUALISATION AND THE THEORETICAL MODEL

3.1 Flow visualisation

No previous experimental studies on the atomisation of a liquid due to the penetration of another liquid jet have been found. Therefore, the aim of the flow visualisation was to observe and understand visually the basic mechanism and structure of the process. Since these liquids undergo processes that are chaotic as well as involving very fast changes, the measurements are difficult. Therefore, another purpose of this investigation was to provide a supporting framework for the experimental study in Chapter 4.0.

Two methods of photographic visualisation were employed;

a). High speed flash still photographs were taken of the jet about 1 second after the initial injection, to look at the steady state.

b). Visualisation by high speed framing video, to look at the transient effects.

To observe the region of penetration through the stratified water layer by the oil jet, it was first assumed that the near region of the injection point is unaffected by the pipe axial cross flow due to the high jet to pipe velocity ratio. Previous works by Kitamura and Takahasi (1986), researching on low velocity jets, indicated that the continous phase turbulence has very little effect on the jet stability. Since the study involves two component immiscible liquid phases, it is also necessary that the jet should be injected in a confined space. Therefore the spray chamber was designed with out the pipe cross flow, but was formed from a pipe section.

The spray chamber (figs. 3.13.2) was made of perspex throughout with a perspex pipe section of 134mm in length and 140mm in internal diameter and two flat perspex sheets were bolted to the front and back ends. The front plate is easily removable to allow access to the inside of the spray chamber. The jet penetrates radially to the chamber from the

bottom of the pipe wall and the injected fluid leaves it from the top via a 15 mm outlet. A schematic diagram of this arrangement is shown in figure 3.1.4. The jet is energised by a pressurised reservoir containing kerosene (or appropriate oil), and activated by operating a normally closed solenoid valve. The reservoir pressure was maintained to a required level by regulating the high pressure nitrogen gas, supplied by the gas cylinder. The injection nozzle was designed so that it could be interchangeably mounted into a holder on the perspex pipe. The nozzle was drilled and reamed to 2 mm. The length to diameter ratio, L/d (=2.5), of the nozzle was designed so as to be similar to the nozzles of the present Jiskoot jet mixing systems.

The reservoir pressure was monitored from the output of a fast reponse Kistler piezoresistive pressure transducer type 4043A5 operated by a charge amplifier (type 4601). The transducer's natural frequency was larger than 30 KHz. A digital storage oscilloscope (type Gould 4050) triggered by a sequencer delay generator (type 2, by Bowen Electronic Ltd., Dorset, U.K.) records the output response from the transducer. The hard copies of the oscilloscope traces were obtained from a digital plotter unit that followed instructions from a BBC micro computer via a IEEE 488 interface unit.

3.1.1 Photographic system

1). The high speed video, Spin Physics SP 2000, was capable of framing 2000 frames per second. The system is shown in fig. 3.13.4.

2). The high speed flash used for the static photographs was Pulse Photonics double Argon spark source which can be triggered by a 5 volt pulse or short circuit. This light source discharges 2.5 Joules in 0.3 micro-seconds. The flash occurrence was controlled by sending a 5 volts pulse from the sequencer delay generator. The sequencer delay generator has times adjustable from 1 to 999 seconds and fitted with a 4 MHz crystal oscillator with temperature stabilty of 5 parts per million at 25^{o} C and jitter 250 nano seconds. The spark source, the test/observation chamber and the camera were arranged as shown in fig. 3.1.3. A translucent screen was hung between the spark source and test

chamber to disperse the flash light evenly.

3). The actions that are triggered by the push button of the delay unit, may therefore be tabulated in chronological order as follows.

i). Camera shutter is opened to a pre-set period by short circuiting, via the normally open relay at junction 3 (in delay generator). The camera shutter can be opened by short circuiting the terminals at the camera release socket.

ii). Then the solenoid valve is opened to activate the jet by closing the normally open relay at junction 2 for a pre-set period.

iii). The flash unit responds to a 5V pulse that is produced at junction 4 and fires to a set time, after the jet is activated.

iv). Relay at junction 3 returns to its normally open position at the end of the period and the camera shutter closes accordingly.

A characteristic trace of any sensor, at any time during the injection, can be obtained from the digital storage scope by replacing the camera and flash units from junction 3 and 4 with input signals to the scope via the side panel 15 way D type connector to 'enable arm'.

4). Photographs were taken by a Yashica FR1 aperture priority SLR camera fitted with a Tamron high speed Macro 35-80mm, f/2.8-3.8 lens. The images were recorded, unless specified, on 400 ASA 35mm film. The aperture was set in the range 5.6 - 8.0.

3.1.2 Calibration of the system for jet velocity

The aim of the calibration is to obtain a relationship between reservoir pressure under static situations and the jet velocity when the solenoid valve is opened, for a limited period. One may do this by

recording the time taken to collect certain amount of injected fluid. But first it is necessary to monitor the system response to the opening of the solenoid valve.

Pressure at point 1 was monitored for about 10 seconds from the time of opening of the solenoid valve, and then the pressure at point 2 was monitored similarly. Typical plots of these results are shown in figs. 3.10.2 and 3.10.3. These plots indicate that the impulsive pressure wave dies out very quickly as soon the solenoid opens and then, although there is a quasi-decrease in static pressure, the difference in static pressure between points 1 and 2 is almost a constant. Therefore if the pressure loss coefficient from the reservoir to the pipe is 'K' and the reservoir and pipe cross sectional areas are 'A_R' and 'A_P', the total pressure difference between point 1 and 2 can be written as:-

$$\Delta P_T = \tfrac{1}{2}\rho K V_P^2 \qquad (3.1.1)$$

Where V_P is the velocity in the pipe section. But ΔP_T can be also related to static pressure difference (ΔP_S) between point 1 and 2 as:-

$$(P_2-P_1)_t=(P_2-P_1)_s + \tfrac{1}{2}\rho V_2^2 - \tfrac{1}{2}\rho V_1^2$$

$$\Delta P_T = \Delta P_S + \tfrac{1}{2}\rho(A_P V_P/A_R)^2 - \tfrac{1}{2}\rho V_P^2$$

$$= \tfrac{1}{2}\rho K V_P^2$$

$$\text{Therefore, } \Delta P_S = \tfrac{1}{2}\rho K' V_P^2 \qquad (3.1.2)$$

$$\text{where } K' = [(A_P/A_R)^2 - 1 + K)$$

Since it was shown that ΔP_S attains a constant value very quickly with respect to time, the velocity through the pipe (V_p) can be assumed to become a constant in a negligible time. Hence the jet velocity is a constant for times bigger than 0.1 seconds. It is also possible to use equation 3.1.2 to obtain the velocity of the jet. But this requires proper calibration of the pressure transducer and measurement of the coefficient of discharge of the jet nozzle. Therefore the system was directly calibrated, as mentioned before, by collecting the injected

oil for a period of 10 seconds for various water layer heights of 0mm to 20mm and various Kerosene mixtures. These relationships are shown in fig. 3.10.1. The relationship is seen to follow a square law, for example, when the oil was pure kerosene:-

Voltmeter reading/volts = $21.7 \times 10^{-4} (V_j / ms^{-1})^2$, for velocities > 5 m/s.

3.1.3 Measurment of fluid properties

To measure the influence of fluid property variation it is necessary to use liquids that have a range of values for the property that is being tested, with constant values for the other properties. Therefore it is necessary to use appropriate solvents in the base liquids to achieve this end. Further these solvents should also satisfy the following:-

i) The solvents should be only soluble in one of the base liquids.

ii). The solvents should not react with any one of the base liquids to produce end products.

iii). The solution so obtained, should be transparent to enable photographic analysis.

iv). As mentioned before, the solvent should change only one property of the base liquid, keeping others approximately constant.

After a few investigations, the following methods were adopted and the properties of these solutions are tabulated.

i). Various percentages of Base oil by volume were dissolved in kerosene to obtain wide ranges of kinematic viscosities and then Ethanol (99-100% v/v from BDH Ltd.) was dissolved in water (Water purified from BDH Ltd.) to obtain constant interfacial surface tension with respect to these oil solutions. The densities of these solutions are approximately constant.

ii). Various percentages of Ethanol by volume were dissolved in water to obtain a wide range of interfacial surface tension with kerosene. The densities and viscosities of these solutions were approximately constant.

Kinematic viscosity was measured to ASTM D 445-53T standard, using glass capillary Ubbelohde kinematic viscometers, immersed in a constant temperature water bath. Interfacial tension was measured by using a Leconte du Nouy's platinum ring apparatus. Measurements of densities were made by using a density bottle and hydrometers.

i). Solutions of Base oil and Kerosene were made to give wide ranges of kinematic viscosities				
Immiscible Liquid System	Kinematic viscosity of oil sol^{n} at 20°C/cSt	Dynamic viscosity of oil sol^{n} at 20°C/Nsm^{-2}	Density ratio water sol^{n} to oil sol^{n}	Interfacial surface tension /Nm^{-1}
Pure Kerosene and 15% Ethanol	1.48	1.15×10^{-3}	1.23	0.023
10% Base oil and 11.5% Ethanol	1.9	1.53×10^{-3}	1.22	0.0235
20% Base oil and 8.2% Ethanol	2.41	1.95×10^{-3}	1.22	0.023
30% Base oil and Pure water	3.102	2.53×10^{-3}	1.22	0.023

ii). Solutions of ethanol and water were made to give wide ranges of interfacial surface tension with kerosene.

Immiscible Liquid System	Kinematic viscosity of oil sol^{n} at 20°C/cSt	Dynamic viscosity of oil sol^{n} at 20°C/Nsm^{-2}	Density ratio water sol^{n} to oil sol^{n}	Interfacial surface tension /Nm^{-1}
Pure kerosene and Pure water	1.48	1.15×10^{-3}	1.25	0.033
Pure kerosene and 8.2% Ethanol	1.48	1.15×10^{-3}	1.23	0.0298
Pure kerosene and 11.5% Ethanol	1.48	1.15×10^{-3}	1.24	0.0263
Pure kerosene and 15% Ethanol	1.48	1.15×10^{-3}	1.23	0.023
Pure kerosene and 0.1% Decon 90	1.48	1.15×10^{-3}	1.25	0.017
Pure kerosene and 0.2% Decon 90	1.48	1.15×10^{-3}	1.25	0.013

** Decon 90 = from BDH (Cat. No. 56002) surfactant especially suitable for biological and radio active work.

30% Base oil and Pure water	3.102	2.53×10^{-3}	1.22	0.023
30% Base oil and 15% Ethanol	3.102	2.53×10^{-3}	1.21	0.015

3.1.4 Observations and discussion

1. There are two different distinct regions in figures 3.1.1 and 3.12. Region 1, where the oil jet is submerged in water and the region 2, where the oil jet penetrates the water layer. In both of these regions atomisation occurs. In the first region the kerosene jet breaks up into kerosene droplets. This may occur by several mechanisms depending on the injection conditions. Figures. 3.2.1 to 3.2.3, show how a kerosene jet submerged in water, region 1, would break up as its velocity is increased. This appears to form the same regimes as liquid jet breakup in air, ie. Rayleigh, first wind induced, second wind induced and atomisation. This terminology is now changed to Rayleigh, first-induced, second-induced and atomisation for this study, to avoid confusion due to the term 'wind'. Figures 3.2.1 and 3.2.2 indicate that a sinuously wavy jet breakup can be expected when the selected velocity is in between the velocities represented by these figures. These low velocity regimes are very sensitive to changes therefore, and are very difficult to achieve in this system. Such sinuously wavy jets are formed by merging of drops with the jet, because the terminal velocity of the drop formed from the jet is opposite to the jet velocity in the system. These sinuous waves were also observed when dispersed phase was more viscous than continuous phase, by Kitamura and Takahashi (1986). Second-induced and atomisation occurs approximately, for velocities greater than 4 m/s for pure water/ kerosene system. The regimes of interest in the present study, are second induced and atomisation.

2. The breakup of oil jet in water is in the atomisation regime, when the atomisation starts as soon as it penetrate the water layer. These droplet sizes indicate (fig. 3.2.3) that they are too small to be formed by shear wave jet instability, that is due to boundary layer instability (performing the calculations by Lin et al, 1987). Therefore it appears that the continuous phase viscosity (μ_w) is not important in this atomisation (ie. atomisation of oil jet in water) process.

3. Figures. 3.3.1 and 3.3.2 show the breakup behaviour of the

penetration region of the oil. They seem to indicate that the penetrated water reaches its ultimate drop sizes through several stages of the breakup mechanisms. Dombrowski and Johns (1963) idealized the breakup process of a fan nozzle spray as shown in fig. 2.6. This idealization process assumed that at some distance from the nozzle the waves separate into ligaments which are initially $\lambda/2$ in width. These contract into, cylinder ligaments and break up according to Rayleigh's jet breakup theory. Careful observation of low speed jets in figure 3.6.1 and 3.6.2 show that there is some agreement with the idealised model. But, since the jet speeds are low, curvature of the water sheath may have some effect on its breakup. At higher jet speeds a ideal model of this nature is shown not to be sufficient. The irregular dynamic pressures on oil jet surface deform the thin water layer locally and initially protuberances occur on the outer surface of the layer, then they elongate to finger like ligament (or 'ciger' shaped) due to the couette flow type shear (Hinze, 1955) in the oil boundary layer. They breakup into chunky droplets (fig. 3.11.3), which subsequently breakup into smaller droplets on their travel in the turbulent flow field.

4. These finger like ligaments are only visible from the outer side of the annular water sheet due to the chaotic flow conditions on the other inner side as well as the similar refractive indices of water and kerosene. Therefore, air was injected through the water layer into an air environment, in order to visualise the structure of the inner side (ie. oil jet side, noting also the differences due to the compressibility effect of air) of these ligaments. They indicated a similar structure to that which Mullinger and Chiger (1974) had observed in their photographic studies of twin fluid atomizers; long thread like ligaments which break down into droplets. These ligaments have different sizes of undulations. Careful observation of figures 3.3.1 and 3.3.2, obtained when oil was injected, show similar ligaments with different sized undulations. Under simple Couette type shear, droplets would breakup into sizes of the same order of magnitude as the thickness of the entrained water layer. A ligament as well as its undulations are formed under the high dynamic pressure fluctuations in the turbulent oil jet and breaks up

into relatively smaller droplets. Therefore, this mechanism can not be considered purely as a simple Couette type shear breakup.

5. As the jet penetrates the interface to region 2 (fig. 3.12),it consists of atomised oil droplets in water surround by an annular water sheet and also a portion of the unbroken kerosene jet core. The outer surface of the annular water sheet would now create an oil boundary layer around it. As the jet proceeds downstream, the water sheet breaks up into droplets exposing the inner atomised oil core to the outer continious oil phase. The entrainment of oil towards the jet causes a transition from oil droplets in water to water droplets in oil (more precisely two component water drops). Further downstream this transition would be completed to form a jet of water droplets in oil.

6. The penetrating jet hardly disturbs the surrounding water/oil interface. The interface stays almost optically flat and horizontal during this period, unless the interface height is not too thin (less than around 8mm). To verify this, 40 gauge copper wire was placed horizontally on the back perspex plate of the chamber. The camera and this wire were ajusted in order to obtain a reflection of this wire at the interface (fig. 3.4.1). Figures 3.4.1A and B show this with and without the penetrating jet respectively, demonstrating the placid nature of the interface. These figures also show a fairly clean straight water layer edge. Therefore the level drop at a point is representative of the jet entrainment of water for a given water layer height.

7. Entrainment stream lines were also observed by suspending plastic beads (<0.2 mm) in the stratified water layer and then illuminating a sheet of light across the jet plane. The light source was from a slide projector with a slit (2mm wide) cut out of a blanked off slide. This produced an approximately 5mm wide sheet of light at the viewing section. Photographs (fig. 3.5.1) were taken at 1/8 second shutter speed. These entrainment lines appeared to be fairly smooth and were directed towards the axis of the jet without any complicated flow patterns such as recirculation zones. This also clarifies the reasons

for the placidness of the stratified layer indicated in no. 6 above.

Therefore, from no. 6 and 7 we can conclude that the features of the entrainment process are local to the jet interface.

8. Drops were observed to be spherical except for very, low velocities and for large water layer heights 'h', in these cases relatively large droplets were produced. These cases are out of the range of interest of the present study, since they are to be avoided in practice.

9. If the entrainment of water is measured from a similar method to that mentioned above in no. 6, then this should be done before any droplets deposit back to the stratified layer. For all the jet velocities (ie. between the 3 to 10m/s) investigated, none of the droplets fall back in time periods of less than 1 second.

10. Figures 3.7.1A and B, show a comparison of a two component jet (water drops in kerosene) with a single phase jet. In the case of single phase jet, waxoline blue was mixed into kerosene to provide a better contrast. Both of these jets produced a similar global structure with approximately equal jet divergent angles. Similar comparison was also made in figures. 3.7.3A and B with kerosene jet breaking up in water. Again there was no considerable difference in global structure.

11. Consecutive figures 3.8.1 to 3.8.3 illustrate the variation in structure when the water level height is decreased and the velocity of the jet is increased, respectively.

12. The video frames showed the rapidity with which the emerging (liquid) jet approaches to its steady developed state confguration. This is demonstrated in figure 3.11.3 which is a composite overlay of the jet outlines from individual frames of the transient video photographs which allows one to visualize the initial development of the jet. The region behind the head of the jet quickly assumes the final jet divergence angle which then remains unaltered as the injection continues. The pixels of the video screen are sometimes of

the same order of magnitude as the droplet sizes, therefore the droplet size distribution or the water level drop cannot be accurately measured from the video photographs.

13. Due to high concentration of indistinguishable water drops closer to the centre of the jet, this area is opaque to light. This would disable optical measuring methods such as a light scattering technique. Hence, measurements are only possible in the regions, where individual droplets are clearly visible, ie. at the edges of the jet and away from the darker core.

14. If the drop sizes are to be measured in the proximity of the injection point, this should be done before the falling droplets disrupt the view of the near field.

15. The gauge pressure change inside the spray chamber was less than 1.0 KPa (0.14 PSI) during the injection period, for injection velocities less than 10 m/s.

16. The techniques mentioned in no. 6 above and photographic analysis of the edges of the jet may be adopted to measure entrainment and drop sizes respectively. These measurements can only be estimations. In the drop measurement experiment height 'h' higher than 15mm should be avoided, because they generally produce high water entrainment levels and relatively large droplets (ie. the high concentration of water). Therefore, the congestion of droplets would make the manual counting extremely difficult and inaccurate.

3.2 Theoretical model for entrainment

3.2.1 Single jet

The main aim of this analysis is to clarify the salient features associated with entrainment, so that a semi-empirical correlation can be formed with the data from experimental study in chapter 4.0.

Assumptions:-

a). The penetrating jet is approximated to a hypothetical rough cylinder (fig. 3.2.4) having a surface roughness equivalent to the wave (unstable wave length) amplitude at the interface.

Previous work (Briffa et al, 1966, Akoi et al, 1980, Sinai et al, 1987, Hanratty et al, 1957, Eilis et al, 1959, Spalding, 1981) in two phase (ie. gas/liquid) stratified flow considered that the flow over a wavy interface is similar to that of a turbulent flow over a rough flat plate with the roughness equal to wave amplitude. Typical studies in this regard can be seen in Hanratty et al (1957), Ellis et al (1959) and in a series of papers by Akai et al(1977, 1980 ,1981). The measured gas velocity profile over the wavy interface has indicated that they are similar to the turbulent flow over rough flat plates. Akai et al (1981) has also theoretically analised turbulent transport mechanisms in horizontal stratified two phase flow by considering the interfacial waves to have a flow seperation effect similar to a rough surface in a single-phase flow. These predictions were found to be in good agreement with the experimental data. Sinai's (1987) predictions of the stresses on a pool interface, from the theory of a boundary layer on a flat plate is also surprisingly favourable.

More relevant to the present study is the work on entrainment of air into a completely broken up flat liquid spray by Briffa and Dombrowski (1966). They assumed a plate, having a skin friction independent of its roughness, at the centre of the flat spray.

b). The water layer height 'h' is less than the length of the unbroken jet core length 'L_2'. Photograpic observations show this to be the

case for the water layer heights 'h' that are of interest (ie. for less than 5% stratified water) in this study.

c). At the jet orifice outlet the velocity profile of the jet is fully developed and turbulent.

d). Inside the unbroken jet core the velocity is taken to be equal to jet orifice velocity V_j.

e). The dissipation of energy as heat in the control volume considered is negligible (fig. 3.2.5).

f). Roughness (Rh) was taken as the effective interfacial area (on a plane perpendicular to velocity) of protuberance per unit width. Then it can be shown 'Rh/y = C', where C is the tangent of the spreading angle (ref. Ranz, 1985 and also see eq. 3.2.26), and y is the distance measured along the jet axis.

g). The whole water boundary layer penetrates the interface as entrained water. This observed to be a good approximation from the photograpic analysis. To estimate the rate of air entrainment by a plunging water jet, Ervine et al (1980) make use of the air laminar boundary layer thickness on the surface of the jet. He assumed a laminar boundary layer thickness equivalent to that of flow over a finite flat plate.

h). Gravity effects are negligible compared to jet momentum transfer.

i). An exact analysis of the momentum transfer from the broken up oil jet edges to the surrounding water requires a detailed knowledge of the nature of the flow fields around each drop and of the manner of the flow fields effect the movement of the drops. Briffa and Dombrowski (1966) assumed the velocity distribution over their hypothetical plate (see assumption a).) to be that of turbulent flow past a flat solid surface, given by Prandtl's mixing length theory:-

$$(\tau/\rho_a)^{1/2} \ln y/B = -v + \text{constant}$$

where τ = shear stress

B = constant

y = distance normal to the flow

V = mean velocity

ρ_a = density of air

From this velocity profile, they obtained an average velocity, appropriate to the jet cross section and then the jet momentum. They used a friction factor given by Schlichting (1979) and also assumed that it is independent of the surface roughness. In the present analysis, in addition to assumption (a), the water boundary layer velocity profile is taken to be that of a rough turbulent flat plate as:

$$U = V_j\left\{1 - \left[\frac{r}{\delta}\right]^{1/n}\right\} \qquad (3.2.1)$$

where δ = boundary layer thickness

n = a function of the roughness = $3/C_\tau^{1/2}$ (Blevins, 1984)

C_τ = skin friction

U = mean velocity

V_j = jet velocity

The jet curvature effect can be considered to be insignificant, since $\delta << d$ (see appendix A4.1). The boundary layer flow on the rough interface is assumed to be turbulent. This is also justified, because for example, when V_j, h, ρ_w, μ_w are 10 m/s, 1 mm, 1000 kg/m^3 and 10^{-3} Nsm^{-2} respectively, the Reynolds number is 10^4.

j). Viscous stresses are much smaller than the corresponding turbulent shear stresses.

k). The pressure gradient outside the boundary layer parallel to the cylinder axis is zero.

1). Properties of the stratified water are fixed and therefore, do not change. This means only oils with different properties are used.

There is no exact theory for turbulent wall bounded (eg. flat plate) flow, although there are many elegant computer solutions of the boundary layer equations using various empirical models for the turbulent eddy viscosity. A widely accepted result is simply an integral analysis. The aim of this analysis is to gauge the importance of each individual parameter. Therefore, this analysis will make the format of the ultimate relationship, the semi-empirical correlation, less complex without affecting the purpose. Hence, consider first the control volume shown in figure 3.2.5, two dimensionally. The continuity equation and momentum equation in 'y' and 'r' directions are;-

$$\frac{\partial U}{\partial y} + \frac{\partial V}{\partial r} = 0 \qquad (3.2.2)$$

$$U\frac{\partial U}{\partial y} + V\frac{\partial U}{\partial r} = -\frac{1}{\rho}\frac{\partial P}{\partial y} + \nu\frac{\partial^2 U}{\partial y^2} + \nu\frac{\partial^2 U}{\partial r^2} - \frac{\partial \overline{u'v'}}{\partial r} - \frac{\partial \overline{u'^2}}{\partial y} \qquad (3.2.3)$$

$$\frac{1}{\rho}\frac{\partial P}{\partial r} = -\frac{\partial \overline{v'^2}}{\partial r} \qquad (3.2.4)$$

Where U, V are mean velocities in the 'y' and 'r' direction, P is the mean pressure, and u', v' denote the fluctuating components of the velocities, and $\bar{u}$, and $\bar{v}$, are their root mean square values. Integrating the equation 3.2.4 with respect to 'r' gives:-

$$p = -\rho\overline{v'^2} + p_\infty \qquad (3.2.5)$$

Where P_∞ is the pressure outside boundary layer. Substituting this to equation 3.2.3 and also accounting for the assumption j), the equation 3.2.3 reduces to:-

$$U\frac{\partial U}{\partial y} + V\frac{\partial U}{\partial r} = -\frac{1}{\rho}\frac{\partial P_\infty}{\partial y} - \frac{\partial \overline{u'v'}}{\partial r} - \frac{\partial(\overline{u'^2} - \overline{v'^2})}{\partial y} \qquad (3.2.6)$$

The pressure gradient in the above equation is zero (assumption k)) and the last term is smaller than the other remaining terms (Rajaratnam, 1976, p4) and therefore, can be neglected. For convenience, if the turbulent shear stress ($-\rho\overline{uv}$) is denoted by τ, then the momentum equation in 'y' direction becomes:-

$$\rho U \frac{\partial U}{\partial y} + \rho v \frac{\partial U}{\partial r} = \frac{\partial \tau}{\partial r} \qquad (3.2.7)$$

Integrating the above equation with respect to 'r' between r=o and , we have:-

$$\rho \int_A U \frac{\partial U}{\partial y}\, dr + \rho \int_B V \frac{\partial U}{\partial r}\, dr = \int \frac{\partial \tau}{\partial r}\, dr \qquad (3.2.8)$$

Letting: $A = \rho \int U \frac{\partial U}{\partial y}\, dr = \frac{1}{2} \int \frac{\partial(\rho U^2)dr}{\partial y} = \frac{1}{2} \frac{d(\int \rho U^2 dr)}{dy}$ *(by Liebnitz rule)*

And: $B = \rho \int V \frac{\partial U}{\partial r}\, dr = \left[\rho UV\right]_0^{\infty} - \rho \int U \frac{\partial V}{\partial r}\, dr = \rho \int U \frac{\partial V}{\partial y}\, dr$

$$= \frac{1}{2} \frac{d(\int \rho U^2 dr)}{dy} \text{ (from continuity)}$$

Substituting 'A' and 'B' to 3.2.8 gives:-

$$\tau_w = \text{wall shear stress} = d(\int \rho U^2 dr)/dy \qquad (3.2.9)$$

$$= d(\int_0^{\delta} \rho U^2 dr)/dy, \text{ since } d\int_{\delta}^{\infty} \rho U^2 dr/dy = 0$$

This indicates that the increase in total momentum flux per unit length and unit width in 'y' direction is equal to the momentum flux from the wall ($=\tau_w$). The boundary conditions are:-

At $r = 0 \rightarrow U = V_j$ and $V = 0$

$r \rightarrow \infty \quad U = 0$ and $V = 0$

These boundary conditions with the governing flow equation can be

easily reduced (although the sign of the velocity is opposite to that of conventional boundary layer on a flat plate) to the Blasius equation of boundary layer flow on a flat plate. These boundary conditions with the assumption i) could be solved for parameters such as skin friction coefficient (C_τ) with the same value as that for flow over a finite flat plate (White, 1986).

Integrating equation 3.2.9 with respect to 'y' between y=o and h gives the momentum flux per unit width at y= h as:-
where 'h' is the interface height.

$$\int_0^h \tau_w \, dy = \left[\int_0^\delta \rho_w U^2 dr\right]_0^\delta = \int_0^\delta \rho_w U_{y=h}^2 dr \qquad (3.2.11)$$

$$= \int_0^\delta \rho_w V_j^2 \left\{1 - \left[\frac{r}{\delta}\right]^{1/n}\right\} dr \quad \textit{(from assumption i)}$$

$$= \int_0^\delta \rho_w V_j^2 \left\{1 - 2\left[\frac{r}{\delta}\right]^{1/n} + \left[\frac{r}{\delta}\right]^{2/n}\right\} dr$$

$$= \rho_w V_j^2 \left[r - 2\frac{n}{\delta^{1/n}}\frac{r^{(n+1)/n}}{n+1} + \frac{n}{\delta^{2/n}}\frac{r^{(n+2)/n}}{n+2}\right]_0^\delta$$

$$= \rho_w V_j^2 \left[\delta - 2\frac{n\delta}{n+1} + \frac{n\delta}{n+2}\right]$$

$$= \rho_w V_j^2 \left[\frac{n^2 + 3n^2 + 2 - 2n^2 - 4n + n^2 + n}{(n+1)(n+2)}\right]\delta$$

$$= \frac{2\rho_w V_j^2 \delta}{(n+1)(n+2)} \qquad (3.2.12)$$

If the mass flow entrainment rate is given by 'E_w', then:-

E_w/z = mass entrainment rate per unit width.
where z = width of the plate

Therefore, $$\frac{E_w}{z} = \int_0^\delta \rho_w U_{y=h} dr = \int_0^\delta \rho_w V_j \left\{1 - \left[\frac{r}{\delta}\right]^{1/n}\right\} dr$$

$$= \rho_w V_j \left[r - \frac{n}{\delta^{1/n}}\frac{r^{(n+1)/n}}{n+1}\right]_0^\delta$$

$$= \rho_w V_j \left[\delta - \frac{n\delta}{n+1} \right]$$

$$= \frac{\rho_w V_j \delta}{(n+1)} \qquad (3.2.13)$$

From equations 3.2.12 and 3.2.13:-

$$\int_0^h \tau_w \, dy = \frac{2V_j E_w}{z(n+2)} \qquad (3.2.14)$$

Therefore,

$$\frac{E_w}{z} = \frac{(n+2)}{2V_j} \int_0^h \tau_w \, dy \qquad (3.2.15)$$

$$= \frac{1}{4} \rho_w V_j \left[2 + \frac{3}{C_T^{1/2}} \right] \int_0^h C_T dy \qquad (3.2.16)$$

(since $n = 3/C_T^{1/2}$, Blevins, 1984 and $\tau_w = \frac{1}{2}\rho_w V_j^2 C_T$)

m). Approximation of shear stress at the interface

i). Wall shear stress due to turbulent boundary layer on a smooth flat plate.

Skin friction (C_T) = $0.027/(V_j y/\nu)^{1/7}$ (White, 1986; ie: n=7) (3.2.17)

$$\tau_w = \tfrac{1}{2}\rho_w V_j^2 C_T = \frac{0.027 \, \rho_w \, V_j^2}{2(V_j y/\nu)^{1/7}} \qquad (3.2.18)$$

From equation 3.2.14

$$2V_j E_w/9z = \int_0^h \tau_w dy = [(0.027/2)\rho_w V_j^2/(V_j/\nu)^{1/7} \times (7/6) y^{6/7}]_0^h$$

Therefore, $E_w/z = [(0.027 \times 9 \times 7/(4 \times 6)][\rho_w^6 V_j^6 h^6 \mu]^{1/7}$

If we approximate 'z' to πd_j (ie: circumference of the cylinder), where d_j = diameter of the cylinder

$$E_w = 0.0709 \pi d_j (\rho_w^6 V_j^6 h^6 \mu)^{1/7} \qquad (3.2.19)$$

$$= \frac{0.223 d_j (\rho_w^6 V_j^6 h^6 \mu)^{1/7}}{} \qquad (3.2.20)$$

ii). Wall shear stress due to turbulent boundary layer on a rough plate.

The shear stress 'τ_W' was calculated from the skin friction coefficient (C_τ) for turbulent boundary layer on a a rough flat plate.

$$C_\tau = 1/[3.48 + 0.707 \ln(y/Rh)]^{2.5} \qquad (Blevins, 1984)$$

$$= [\ln (137.3\ y/Rh)^{0.707}]^{-2.5}, \qquad \text{where Rh = Cy = roughness}$$

The constants 3.476 and 0.707 of C_τ correspond to rough flat plate, and therefore, cannot be expected to be the same for this situation. For generality, we replace these constants with A and n_1, so that C_τ now becomes:-

$$C_\tau = [\ln (A/C)^{n_1}]^{-2.5} \qquad (3.2.21)$$

Equation 3.2.21 indicate that C_τ = constant between y = 0 and h

Therefore, shear stress $\tau_W = \frac{1}{2}\rho_w V_j^2 C_\tau \qquad (3.2.22)$

Approximating $z = \pi d_j$ equation 3.2.16 becomes:-

$$E_w = (\text{entrainment of water}) = \tfrac{1}{2}\rho_w V_j \pi d_j h (2C_\tau + 3C_\tau^{1/2}) \qquad (3.2.23)$$

The value of y/Rh is in the order of 5 or more, therefore $2C_\tau << 3C_\tau^{1/2}$ (assuming same order of magnitude for A and n_1 as in flow over rough plate).

$$\text{And also the jet mass flow rate} = m_j$$
$$= (\pi/4) d_j^2 \rho_{oil} V_j$$

Therefore, equation 3.2.23 becomes,

$$\frac{E_w}{m_j} = \frac{h}{d_j}\frac{\rho_w}{\rho_{oil}}\left[\,3C_T^{1/2}\right] \qquad (3.2.24)$$

Substituting 3.2.24 to 3.2.21 gives:-

$$\frac{E_w}{m_j} = \frac{h}{d_j}\frac{\rho_w}{\rho_{oil}}\left\{3\left[\,ln\left[\frac{A}{C}\right]^{n_1}\,\right]^{-1.25}\right\} \qquad (3.2.25)$$

==========

Ranz (1958) argued that the spreading angle of the atomizing jet in air could be predicted by considering the radial velocity of the fastest growing of the unstable surface waves with the axial injection velocity and showed that;

$$\tan \beta/2 = V/V_j = (1/A)(1/K_m)(\omega_m/V_j) \qquad (3.2.26)$$

Where tan $\beta/2$ = C , in equation 3.2.25 (see figure below), and

V = radial velocity

K_m= unstable surface wave number

ω_m= maximum wave growth rate

A = constant

λ_m= unstable surface wave length

Multiplying numerator and denominator by time 't', then the equation becomes:-

$$\tan \beta/2 = (1/A)(1/K_m)(\omega_m t/y) \qquad (3.2.27)$$

$\omega_m t \propto$ *Number of drops produce after time 't'.*

$\propto N$ *(say)*

Therefore

$$\tan \beta/2 = (1/A')(d.N/y) = (1/A')(Rh/y) \qquad (3.2.28)$$

(since $1/K_m \propto d$*, therefore* $dN \propto Rh$*)*

This shows that the value 'Rh/y' is constant for a particular jetting

condition.

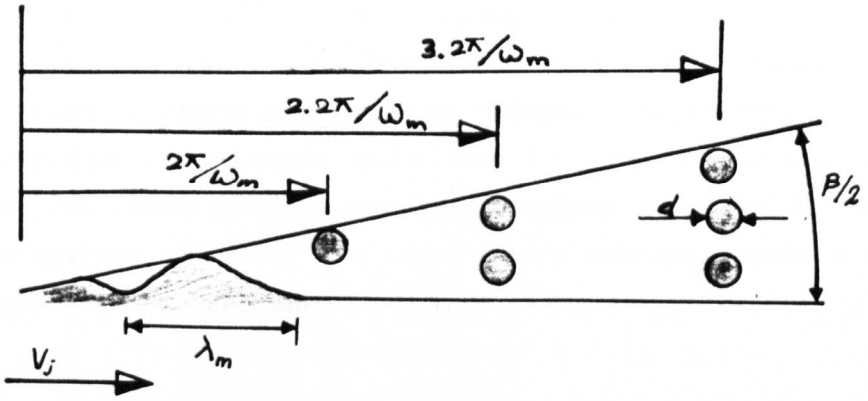

Therefore from dimensional analysis 'y/Rh' can be written as:-

$$y/Rh = f(We,\ Re,\ \mu_{oil}/\mu_{w},\ \rho_{water}/\rho_{oil}) \qquad (3.2.29)$$

The dynamic viscosity of water (μ_{water}), as mentioned in section 3.1 before, and also the diameter of the jet orifice is insignificant for the atomisation process. Therefore equation 3.2.29 should reduce to :-

$$y/Rh = f((We/Re)_{oil},\ \rho_{water}/\rho_{oil}) \qquad (3.2.30)$$

Then the expression for entrainment rate, from equations 3.2.25, 3.2.28 and 3.2.30, becomes:-

$$\frac{E_w}{m_j} = \underbrace{\left[\frac{h}{d_j}\right]\left[\frac{\rho_w}{\rho_{oil}}\right]}_{\text{part 1}} \underbrace{\left\{3\left[n_1\ ln\ f\left[\frac{We_{oil}}{Re_{oil}},\frac{\rho_{oil}}{\rho_{water}}\right]\right]^{-1.25}\right\}}_{\text{part 2}} \qquad (3.2.31)$$

Above equation indicates clearly the problem in two folds. Part 1 provides the relationship if the oil/water interface has a fixed roughness (such as on a rough cylinder) on the outer surface of the oil jet. But oil/water jet interface structure is a function of the jetting conditions, hence the equivalent roughness should also change accordingly. The effect on entrainment due to these changes in the structure is indicated in part 2 and, as one would expect the 'Re' and 'We' numbers characterise these changes. The surface roughness would be expected to decrease with the jet velocity since i) the high velocities would produce smaller atomized droplets ii) and Taylor's investigation has (ie:- for air/ liquid systems) shown a tendency for the jet angle to decrease with increasing jet velocity.

4.0 Experimental study

4.1 Literature review

4.1.1 Atomization of liquid sheets

In this section analytical studies of the breakup of a liquid sheet in another fluid (having relatively high velocity), are reviewed. These studies only involved air as the second high velocity fluid due to its vast commercial application as the atomizing fluid.

An almost complete theoretical description for droplet size has been attempted by Dombrowski and John (1963) as demonstrated in section 1.1.1. They idealised the breakup process in their analysis, but found further refinement of the theory was necessary for satisfactory predictions.

Liquid atomization in a high velocity gas stream was investigated analytically by Mayer (1961). He analysed the growth of capillary waves produced by the high velocity gas flowing across a liquid surface and postulated the following mechanism of atomization. *"When the wind induced wave of length 'λ' has grown to an amplitude comparable with 'λ', the crest of the wave is eroded as a ligament from which droplets of size proportional to 'λ' are formed".* Drawing upon the theoretical results of Jeffrey's (1925), Mayer proposed the following expression for the mean drop diameter obtained under primary atomization.

$$d_{mean} \propto \frac{\mu_\ell^{2/3} (\sigma_\ell \rho_\ell)^{1/3}}{\rho_g^{2/3} \nu_g^{2/3}} \qquad (4.1.1)$$

where d, μ, σ, ρ and ν are number mean drop diameter, dynamic viscosity, surface tension, density and kinematic viscosity, and subscripts ℓ and g are related to liquid and gas respectively. It should be noted that when the analysis of Mayer is applied to a liquid jet (or sheet), some modification of the theory may be required. This is due to the fact that the jet (or sheet) is finite in size and hence

other internal wave (and instability) effects need to be considered.

In an effort towards a better understanding of the influence of the factors involved in the mechanism of disintegration of liquid sheets useful photographic studies have been carried out by Fraser (1957). However, the most important advances in this area are due to Dombrowski and his colleagues (Fraser et al, 1963; Dombrowski et al, 1963; Clark et al 1972, 1974 and Rizk et al, 1977). Their photographic evidence suggests that the interaction with the surrounding air creates waves in the thin liquid sheet which causes the sheet to break down into ligaments and then into drops.

Rizk and Lefebvre (1975) studied the influence of initial liquid film thickness on spray characteristics. They used two specially designed airblast atomizers that were constructed to produce a flat liquid sheet across the centre line of a two dimensional air duct, with the liquid sheet exposed on both sides to high velocity air. From analysis of the process involved, and from correlation of the experimental data, it was found that high values of liquid viscosity and liquid flow rate results in thicker films. It was also observed that thinner liquid films produced better atomization, according to the relationship SMD $\propto a^{0.4}$ (where 'a' is liquid film thickness and SMD is the Sauter mean diameter). This is an interesting result, since if other parameters are held constant, liquid film thickness is directly proportional to nozzle size.

Previous workers had noted a similar relationship. For example, the analysis of York, Stubbs and Tek (1953), Hagerty and Shea (1955) and Dombrowski and Johns (1977), all suggest that mean drop diameter is roughly proportional to the square root of the film thickness. In addition, the photographic studies of film disintegration carried out by Frazer, Dombrowski and Routley (1963) show that, for a sheet breaking down through the formation of unstable ligaments, the diameter of the latter depends mainly on the sheet thickness.

Rizk and Lefebvre (1975) also examined the mechanism of sheet disruption and drop formation using very high-speed flash photography

of 0.2 microsecond duration, which also provided their drop size distribution data. They found that the drop size closely obeyed the Rosin-Rammler and the upper limit distribution functions. A large variety of liquids and solutions, covering a very wide range of density, surface tension and viscosity were used to examine the individual influences of these parameters. They confirmed the process of ligament formation and established that thicker liquid sheets result in thicker ligaments which, in turn, disintegrate in to larger drops. They also found that the thickness of sheet depends on both the air and the liquid properties. High values of liquid viscosity and/or liquid flow rate results in thicker films, while variations in the surface tension appeared to have no effect on the thickness of the sheet. They observed, however, that sheet of low surface tension liquids disintegrated more readily by the action of the airflow and the resulting ligaments were shorter. On the other hand, sheets of high viscosity liquids produced long thick threads.

In areas of air blast atomization, Nukiyama and Tanasawa (1938-40) conducted the first major airblast atomization study using a plain jet atomizer. They obtained drop-size data for several different liquids by collecting the spray samples on glass slides coated with oil. Their mean drop size data was correlated by the following empirical equation:-

$$SMD = 0.0585 \left[\frac{\sigma_\ell}{\rho_\ell V_r^2}\right]^{0.5} + 53 \left[\frac{\mu_\ell^2}{\sigma_\ell \rho_\ell}\right]^{0.225} \left[\frac{Q_\ell}{Q_g}\right]^{1.5} \qquad (4.1.4)$$

where SMD is the Sauter mean diameter and, Q_ℓ and Q_g are liquid and gas volume flow rate respectively and subscript 'r' indicates a relative value. It is worth noting that their correlation, proposed over forty years ago expresses mean drop size as the sum of two separate terms. The first term is dominated by relative air velocity, and the second term by viscosity of the disperse phase. More recently Lefebvre and co-workers (Rizk et al, 1975; El-Shanawany et al, 1980; Lorenzeto et al, 1977) and Jasuja (1981 and 1982) have confirmed the validity of this basic type of SMD equation for air blast atomizers.

A detailed study of the effects of air and liquid properties upon the performance of plain jet airblast atomizers and liquid jet injected into a high velocity cross-flowing air stream were undertaken by Hussein (1983). Using a light scattering technique, he obtained a mean drop size and proposed the following equation:-

$$SMD = A\left[\frac{\sigma}{V_a^2}\right]^{n_1} d_j^{n_2}\left[1+\frac{m_\ell}{m_a}\right]^{n_3} + B\left[\frac{\mu_\ell^2}{\sigma\,\rho_\ell}\right]^{0.45} d_j^{0.55}\left[1+\frac{m_\ell}{m_a}\right]^{n_4} \qquad (4.1.5)$$

It was also shown when the experiment was conducted for the low-viscosity disperse phase liquids (mainly water), for liquid jet injected into cross flow, the second term of the above equation vanishes, indicating SMD is now independent of this term.

4.1.2 Entrainment

Entrainment of a liquid by another fluid arises in a wide range of situations in the process, oil and power-generation industries and is often associated with heat and mass transfer in two-phase gas/liquid flows. Therefore, most of the past studies on entrainment of a liquid by another immiscible fluid were related to gas/liquid flows.

The only direct study on water entrainment by oil flow was conducted by Tsahalis (1977). He developed a theoretical model based on an experimentally derived critical Re number for the onset of entrainment of water films at the bottom of a horizontal crude oil pipelines. This critical Re number had a value of 50 for most of the operating conditions. This theoretical model assumed a linear velocity distribution within the water film and also assumed that it is very close to the velocity that would be achieved if the thin layer was occupied by the flowing oil above.

Understanding and describing general laminar and turbulent transport at a plane surface can be difficult enough but one manifestation of fluid/fluid immiscible coupling at the interface adds another dimension to the level of complexity due to the occurence of

interfacial waves. The process at the interface is unsteady not only because of turbulent fluctuations but also because of the interfacial waves. Therefore, one of the prime objectives in modelling entrainment is the prediction of interfacial shear 'τ' and other interfacial parameters. Other than characterizing the flow above the interface to correspond to that over an aerodynamically rough surface (Briffa et al, 1966, Akoi et al, 1980, Sinai et al, 1987, Hanratty et al, 1957, Ellis et al, 1959), the interfacial shear is generally predicted by purely empirical correlations. For example Wallis (1969) presented a correlation for annular pipe flow in which the interfacial friction coefficient was calculated from:-

$$\lambda_i = \lambda_d(1 + 360\, h^*/D) \qquad (4.1.9)$$

where

λ_i = Interfacial friction coefficient

λ_d = Air only friction coefficient

D = Diameter of the pipe

h^* = Liquid film thickness

Similar correlations for interfacial friction were proposed by Whalley and Hewitt (1978), Asali et al (1985) and Robert and Hartley (1961). Gilchrist and Naim (1987) obtained an expression for the effective interfacial friction coefficient (for a liquid film flowing on a flat plate) as a function of the air Reynolds number, the liquid Reynolds number and a viscosity parameter.

$$(\lambda_i - 0.02) = 8.6483 \left[Re_f . \mu_r^{1.597} . Re_g^{-1.2338}\right]^{0.6156} - 4.5\text{x } 10^{-3} \qquad (4.1.10)$$

where Re_f = liquid Reynolds number based on film thickness

Re_g = gas Reynolds number

Suzanne, Gayral and Masbernat (1978) correlated the interfacial shear stress to air Reynolds number as:-

$$\tau/\rho_\ell g h_\ell = 0.015 \left[Re_g * 10^{-3}\right]^3 \qquad (4.1.11)$$

where τ = interfacial shear stress
g = gravitational constant
h_ℓ = mean depth of liquid phase
Re_g = gas phase Reynolds number
ρ_ℓ = density of liquid

Duns and Ros (1963) expressed the effective interfacial roughness by two dimensionless groups. They are Weber number and a viscosity number given by:-

We = Weber number = $(\rho V^2 E_i)/\sigma$
Vis = Viscosity number = $\mu_\ell/(\rho_\ell \sigma E_i)$

where ρ, μ, σ, E_i are liquid density, liquid viscosity, interfacial surface tension and interfacial roughness respectively. Then the effective interfacial roughness was given by:-

if $We.Vis < 0.005$ $\quad E_i = 34\, C_1\sigma/\rho_g V^{C_2}$
if $We.Vis > 0.005$ $\quad E_i = 170\, C_1\sigma(we.Vis)^{0.3}/(\rho_g V)^{C_2}$

where C_1 and C_2 are constants determined from experimental data.

Sometimes the interfacial shear related to annular flow was also calculated from Colebrook-White equation for rough pipes, given as:-

$$f^{-0.5} = -4\, log\,(Rh_i/3.71D + 1.26/Ref^{0.5}) \qquad (4.1.14)$$

where Rh_i = roughness of the pipe inner surface
D = pipe diameter
Re = Reynolds number of gas
f = friction factor

In gas/liquid flows two important entrainment mechanisms were identified

i). Wave entrainment due to highly turbulent gas flows such as in annular flow and

ii). Pool entrainment from a liquid pool by gas flow in boiling and bubbling.

At present there is no satisfactory general theoretical approach to either of these mechanisms although some limited problems have been considered. Therefore analytical descriptions are normally provided from empirical correlations. Hewitt et al (1970) has given good account of these experimental observations and related empirical correlations for wave entrainment. Hewitt et al (1970) cautioned that the correlations quoted for entrainment should be considered only with reference to the measurement technique used. In particular, care should be taken in using data which was obtained using sampling or isokinetic probe techniques. It is often assumed that a measurement of local entrainment mass flux at the axis of the pipe can be multiplied by the area of gas core to give the total entrainment flow. This assumes, of course, that the droplet mass flux is uniform across the gas core.

Flow visualisation studies have shown that the wave entrainment of the liquid formed along the wall of the pipe is determined by long wavelength intefacial waves. These waves are termed disturbance or roll waves, and are sources of droplet entrainment in annular flow. The breakdown of this disturbance wave was found to be spectacular and exceedingly complex. Though a number of possible mechanisms by which the breakdown occurs (fig 4.1.1 and 4.1.2) were identified, at the present stage there is no definite evidence to favour any particular one. Results in the cases of upwards flow show (Hewett et al, 1970) that entrainment passes through a minimum with increasing air flow rate, when the air-water flows in an annulus or in pipes. Similar results were also obtained for horizontal annular parallel flows. Wicks and Dikler (1972) have attempted to correlate the data for entrained droplet flowrate by means of Martinelli parameter 'X' and shown the results correlate fairly closely for high liquid flowrates by the equation:-

$$X = 0.069\ R^{0.39}$$

where, the entrainment parameter 'R' is given by:-

'R' = $(Bm_e V_\ell / V_g\ (dp/dz)$

m_e = the flow rate of the entrained liquid

dp/dz = friction pressure gradient for the gas flowing along the pipe

B = constant

Truong Quang Minh and Huyghe (1965) and Paleev and Filippovich (Hewett et al, 1970) plotted their results as the fraction of liquid flow which is in the film '(1-E)' against $\rho_g v_g^2$ and $\rho_g/\rho_\ell(\mu_\ell v_g/\sigma)^2$ respectively.

Akegawa et al (1985) determined experimentally the rates of entrainment and deposition of liquid droplets in gas flows. They attempted to introduce some physical aspects of the breakup mechanism by correlating their data to geometrical characteristics of the liquid film. The droplet entrainment rate was correlated to a disturbance wave and a corresponding equation was derived with arbitrary constants as follows. The constants were determined from the experimental data.

$$W_c = 4.57*10^{-7} h^*\ V_{go}\rho$$

$$W_c = 2.93*10^{-5}\ (Re_f x10^{-2})^{3.5}\ (Re_g x10^{-5})^{5.5}$$

where

W_c = droplet entrainment rate and the subscripts f and g relate to fluid and gas respectively.

h^* = liquid film thickness

V_{go} = gas velocity

ρ_ℓ = liquid density

Ishii and Katoaka (1983) attributed the droplet entrainment mechanism the to shearing of roll waves (fig 4.1.5) and the force balance on the ligament which is about to be torn off, given by

$$\pi d\sigma = (\pi/4)d^2 C_d\ \rho_g\ v_g\ /2$$

$$We = 8/C_d$$

A detailed model of droplet sizes in annular flow was developed from these assumptions. The drag coefficient (C_d) and the interfacial shear at the interface was related as:

$$C_d \rho v_g / 2 = 4\, a_{iw} \tau / a_i \qquad (4.1.21)$$

a_{iw} = wave area per unit volume
a_i = effective interfacial area per unit volume

Then critical Weber number for the droplet entrainment from wave crests was obtained as:-

$$We(d_{vm}) = K\, Re_f^{1/6} Re_g^{2/3} (\rho_g/\rho_f)(\mu_g/\mu_f)^{2/3} \qquad (4.1.22)$$

where d_{vm} = volume median diameter

This expression indicated the significant dependance of the critical Weber number on the gas flow. The constant 'K' was obtained by correlation with experimental data.

Recently the importance of the second type of entrainment, the pool entrainment, has been recognized in generator performance and safety analyses of nuclear reactor systems. In the field of chemical engineering, pool entrainment has been studied in relation to the efficiency of the gas/liquid contacting equipment (eg. plate extractor columns, etc.) and fluidized beds. However, most of the analyses were described by empirical correlations, therefore their applicability is limited. A correlation for pool entrainment, for the case of air jet penetrating through a pool of water, was attempted by Ishii and Katoka (1975) from a simple physical model. The simple model assumes that the droplet entrainment occurrs due to the drag force on the liquid ligament (varicose shape) that is lifted (fig. 4.1.5) from the interface. The drag force was determined from the drag coefficient of a spherical particle in the wake regime (ie. $C_d = 10.67/Re_d^{0.5}$).

These theoretical arguments developed an order of magnitude expression for entrainment. The proportionality constant of this expression was determined from experimental data to give,

$$E_w = 0.3975(dJ_g(\sigma/g\Delta\rho)^{1/2})^{1.5} \qquad (4.1.23)$$

where

E_w = rate of entrainment

$J_g = V_g\ (\sigma_g\Delta\rho/\rho_g)^{1/2}$

Kumagai and Endoh (1982) investigated experimentally the effects of kinematic viscosity and surface tension on gas entrainment rate for a liquid jet impinging on a horizontal interface of an identical liquid. They used a bubble trap to collect the air bubbles coming from oblique plunging liquid jets and thus obtained the air entrainment. The plots obtained for gas entrainment against liquid jet velocity divided into four distinct regions (fig 4.1.8) as follows i). initial entrainment reigon ii). low jet velocity region iii). transition region iv). high jet velocity region. The influences of kinematic viscosity in region iv). and surface tension in all four regions were found to be negligible.

The experiments for entrainment by Kazumon Fanatsu, Yung-Chien Hsu and Takemi Kamogawa (1988) for a liquid jet plunging vertically into a receiving identical liquid were based on an over flow method and results were found to be different to those of Kumagai and Endoh (1982). They identified this discrepency to be due to the different behaviour of the air bubbles under the liquid surface due to the jet configuration. Kazumon, Fanatsu et al divided the entrainment into two distinct regions, and their experimental data indicates entrainment to be a function of $\rho_w(v^2 + 2gh)$, H and d, and an accuracy of 10% for the correlation:-

$$C_{\ell}H_{\ell}^{-0.3}d_j^{-1.76} = 0.00215\ \rho_w^{0.61}\ (v_g^2 + 2gH)^{0.61} \qquad (4.1.24)$$

for the first region. And an accuracy of 27% for the correlation:-

$$G_{\ell}H_{\ell}^{-0.3}d_j^{-2.8} = 0.000577\rho_w(v_g^2 + 2gH_{\ell}) \qquad (4.1.25)$$

for the second region.

where G_{ℓ} = gas entrainment rate

H_{ℓ} = liquid jet length

v_j = liquid jet velocity based on diameter of the nozzle

ρ_w = water density

From the basis of the above review, the following main conclusions can be drawn. The complex mechanisms occuring at the interface do not lend themselves to proper well defined theoretical treament. The analyses are mainly conducted through empirical correlations, hence have almost no physical basis and differ from one to the other and have limited ranges of applicability. At present, therefore, a huge source of information for the interface between gas/liquid exist but, the full theoretical predictions of shear or entrainment at the interface are nowhere near completion. However, some theoretical studies in this direction, that is on the behaviour of surface shear flow, have been investigated by Miles (1957, 1959 and 1961) and more recently by Hooper (1985 and 1989) and Hooper et al (1987).

4.2 Mathematical expressions for drop size distribution

When comparing the fineness of different sprays it is useful to introduce some 'mean droplet size' while giving an indication of the degree of atomisation, still has a physical significance. The introduction of a mean droplet size is equivalent to the replacement of the actual spray, composed of droplets of different sizes, by a ficticious spray in which all droplets are of the same size, equal to the mean droplet size. This fictitious spray may, however, still posses certain features of the actual spray that are important from the point of view of the process concerned.

In practice the sizes of the drops found in sprays covers a broad range due to the process of atomization, collision and coalescence between drops (O'Rouke, 1980), secondary breakup of drops and

evaporation. A distribution function is usually employed to represent the various sizes. Drops are counted (eg. from photographs, as in the present study) and divided in groups according to their diameter. Let N be the number of drops with diameter in the range d-Δd/2 and d+Δd/2 and let 'd' range from 0 to ∞ or, in practice, to some upper value. Therefore, the drop size distribution functions f_N and f_V related to total number and volume, can be constructed as:

$$\int f_N d(d) = \int dN \qquad (4.2.1)$$

$$\int f_V d(d) = \int dV = (\pi/6)d^3 dN \qquad (4.2.2)$$

The total number 'N' and total volume 'V' of all the drops sampled can be calculated by integration over the drop diameter as

$$N = \int_0^\infty f_N d(d) \qquad (4.2.3)$$

and

$$V = \int_0^\infty f_V d(d) \qquad (4.2.4)$$

The normalised distribution function are defined as:-

$$\int f_N^* d(d) = \int (f_N/N)\, d(d) \qquad (4.2.5)$$

and

$$\int f_V^* d(d) = \int (f_V/V)\, d(d) \qquad (4.2.6)$$

and give the number and volume fraction contributed by drops with diameters between d-d(d)/2 and d+d(d)/2. In many applications it is found convenient to express the drop size distribution function in cumulative forms:-

$$N^* = \int_0^D f_N^* \, d(d) \qquad (4.2.7)$$

representing the cumulative number fraction of drops smaller than D, and

$$V^* = \int_0^D f_V^* \, d(d) \qquad (4.2.8)$$

the cumulative volume fraction of drops smaller than 'D'

Drop mean diameter '$\bar{d}_{pq}$' describing the quality of atomisation can be written in the general form as:-

$$\bar{d}_{pq} = \left\{ \left[\int_0^\infty f_N^* \, d^p \, d(d) \right] \Big/ \left[\int_0^\infty f_N^* d^q \, d(d) \right] \right\}^{1/p-q} \qquad (4.2.9)$$

when p=3 and q=2 gives the Sauter mean diameter, which is total volume of drops to total surface area. Seven different mean diameters have been defined (Giffen et al, 1953) as follows:-

p	q	*Name of mean diameter*
1	0	*Diameter - Number*
2	0	*Surface - Number*
3	0	*Volume - Number*
2	1	*Surface - Diameter*
3	1	*Volume - Diameter*
3	2	*Volume - Surface (≡ Sauter)*
4	3	*Mean diameter over volume*

The most common of these is the volume to surface area mean, d_{32}, the Sauter mean diameter, which is used in mass transfer work where the surface area governs the resistance and volume determines the concentration. This mean diameter gives a value which is nearer the size of the bigger droplets of the actual spray (fig. 4.2.1), because the volume increase as the third power of the diameter and the surface area as the second power, thus the smaller droplets make a relative

smaller contribution to the Sauter mean diameter.

In addition to mean diameter, drop median diameters have also been defined. Among them, the two most commonly used are the number median diameter '$d_{No.s}$' and volume median diameter '$d_{Vo.s}$'. Drops have diameter smaller than '$d_{No.s}$' and drops smaller than $d_{Vo.s}$' make up half the total number and half the total volume of the drops respectively:-

$$\int_{o}^{d_{No.s}} f_N^* \, d(d) = \tfrac{1}{2} \qquad (4.2.10)$$

$$\int_{o}^{d_{Vo.s}} f_V^* \, d(d) = \tfrac{1}{2} \qquad (4.2.11)$$

These drop median diameters are convenient to use because their values can be evaluated immediately from the cumulative distributions.

In order to facilitate the use of distribution plots, various analytical relationships have been used to represent both frequency and cumulative particle size distributions. These functions are both analytical and empirical, and are called normal, log normal, error function, Cauchy, exponential, Rosin-Rammler, Nukiyama-Tanasawa, Tate-Marshall, etc.). Since no one has a complete understanding of particle production, and no single distribution function can represent all particle size data, it is necessary to approach the problem by testing each of the various distributions.

4.3 Use of dimensional analysis for correlation of atomised data

As pointed out earlier, the mechanism of atomisation, which determines droplet size, is a complex function of independent variables which can be divided into three main groups.

i) The geometry of the atomiser and injecting space

ii) Dynamic condition of the flow

iii) Forces of the physical properties of the injecting fluid and continuous phase liquid

To apply dimensional analysis to a particular problem, it is first necessary to write down all the physical quantities involved. The present study concentrates on the penetration region, when a liquid is penetrating through another liquid into a static environment (ie; assuming the axial pipe flow would not effect this region). Hence the above groups can be interpreted and their related independant variables can be allocated as follows. In the first group, we include the atomizer geometry and diameter of the injecting space. For the group (ii) it is necessary to include jet velocity, diameter of the jet orifice and height of the stratified water. Diameter of the jet orifice and height of the stratified water are included because they control the surface area of the entrained water sheet for a given volume of injecting liquid (oil), and so might be expected to influence the breakup of the sheet. The spray angle (β) may also be included since it has been found that this is important for certain types of atomizers. For example, in swirl atomizers it gives a measure of the ratio of the tangential and axial component of jet velocity, and in plain atomizers the spray angle may be regarded as an indication of the amount of turbulence in the jet and of the radial velocity component. It may later be found that the effect of turbulence may be represented by some other variables or group of variables.

In III) the group of variables that effects atomisation are the physical properties of the liquids, we would include the density, the viscosity and the interfacial surface tension. The effect of gravity is regarded as negligible.

The above are the only variables involving the viscosity forces, surface tension forces and hydrodynamic forces that come into play during the atomisation process. The final product we are concerned with would be represented as a mean droplet size.

Since the atomisation process is a function of all the above variables, it is possible to say that they are related to a function 'f' such as:-

$$f(d,\ d_j,\ V_j,\ \rho_w,\ \rho_{oil},\ \mu_w,\ \mu_{oil},\ \sigma,\ \beta,\ h,\ \textit{atomizer geometry}) \qquad (4.3.1)$$

The dependancy on the injecting space is not taken into account, since the mechanisms taking place are local to the injecting jet (as shown in chapter 3.0). Hinze (1946) explained that with turbulent flow in the issuing liquid the main forces taking part in the atomisation process are:-

i) The dynamical turbulent forces within the liquid
ii) The forces due to surface tension
iii) The air (or hydrodynamic) forces normal to the liquid surface.
iv) The forces due to the viscosity of the liquid

He recommended the use of three independent dimensionless products, when the continuous phase is air:-

$$\rho_a V^2 d_j/\sigma,\ \sigma\rho_l d_j/\mu^2_l,\ \rho_l/\rho_a$$

Beside the forces mentioned above, he pointed out the scale of turbulence of the breaking up liquid is also very important, and suggested that this could be measured, for example in swirl atomizers, by the thickness of the jet. Therefore in our analysis, it is also required to include another dimensionless quantity 'h/d_j' which also controls the thickness of the water sheet. Since the continuous phase in this study is oil (ie: for the water sheet breakup) and water properties are constant in the experimental analysis, it is also necessary to include viscosity ratio for generality.

If we now return back to equation 4.3.1, and say the atomiser geometry is fixed, then the 'π' theorem says that the above variables can be reduced to 7 dimensionless groups. The entraining water layer

thickness is determined by the water layer height 'h', therefore it is the characteristic length. Now applying the 'π' theorem to above variables, it is possible to find the function 'F' such as:-

$$F(d/h,\ h/d_j,\ hV_j\rho_w/\mu_w,\ hV_j^2\rho_w/\sigma,\ \rho_{oil}/\rho_w,\ \mu_{oil}/\mu_w,\ \beta) \qquad (4.3.2)$$

Since we wish to examine the droplet size, 'd' in terms of the other variables, we may re-write this as

$$d/h = \Psi(hV_j\rho_w/\mu_w,\ hV_j^2\rho_w/\sigma,\ h/d_j,\ \rho_{oil}/\rho_w,\ \mu_{oil}/\mu_w,\ \beta) \qquad (4.3.3)$$

where Ψ is another functional symbol.

Also the above dimensional groups may be combined to obtain another form

$$d/h = \Phi\ (\rho_wV_j^2h/\sigma,\ \sigma\rho_wh/\mu_w^2,\ h/d_j,\ \rho_{oil}/\rho_w,\ \mu_{oil}/\mu_w,\ \beta) \qquad (4.3.4$$

If we follow the Hinze's approach, mentioned above, then we would arrive at equation 4.3.5 below. This form is the same as equation 4.3.4, but without the independent variable 'β'.

$$d/h = \Phi\ (h/d_j,\ \rho_wV_j^2h/\sigma,\ \sigma\rho_wh/\mu_w^2,\ \rho_{oil}/\rho_w,\ \mu_{oil}/\mu_w) \qquad (4.3.5)$$

4.4 Experimental Procedures and analysis

The experimental arrangements are the same as in the flow visualisation study in Chapter 3.0 except an ultrasonic method was used to measure the interface level. It was decided to change the stratified water layer after every injection, to inject only fresh oil and to use oil in the test chamber that is less than approximately 20 injections old. Experience, from initial experiments, suggested that these conditions need to be satisfied for the consistency of the results. After every injection, the inside walls of the area surrounding the water layer were cleaned by inserting a brush (No. 5) into the spray chamber. Before the beginning of the experiment, the test chamber was levelled and trapped air between the test chamber and

high pressure oil reservoir was bled out by operating the system without the stratified water layer, at twice the maximum operational pressure. The temperature of the completely enclosed room was stabilised (using a thermostatically controlled blow heater) to (21±1°C). Under this condition the liquid temperatures were approximately (20±1.5°C).

4.4.1 Entrainment measurments:-

The logical approach adopted here for the measurement of entrainment was as discussed in section 3.1.3, statement number 7. The placid nature of the interface during the jet injection allows ultrasonic level sensors to pickup the interface drop. Therefore, 8 MHz ultrasonic transducer probes were arranged as shown in fig. 4.4.1 to penetrate the perspex wall and flush mount with the wall surface. The transducers were mounted on bosses glued to the outer surface of the pipe wall. This was prepared by drilling 10 mm diameter holes through bosses and the wall of the pipe and cutting a groove around the inner surface of the hole and placing a rubber 'O' ring, having a inner diameter somewhat smaller than the transducer in the groove. Then the transducer was pushed through the hole to a firm fit.

Ultrasonic transducers were excited by pulses of spikes produced by a spike generator type 150B by Par Scientific Instruments. The ultrasonic bursts are echoed back from the interface to the transducer and these reflected echoes were monitored on a osciloscope screen. Therefore, for example in fig. 4.4.4, each echo represents height of the interface at positions 1 and 3. Here, the probes see the interface in two different heights due to curvature of the wall in position 1. This effect is conveniently used to measure the interface drop at position 1 and 3 simultaniously.

During the jet injection, the echoes would move towards left corresponding to the interface drops in these positions. For one experimental situation the interfacial drop is measured in two positions simultaniously, that is either position 1 and 3 or 2 and 3. Since the probes at position 2 and 3 are in the same horizontal plane,

a different approach needed to be adopted to distinguish the echoes corresponding to these positions. In this case signal from the spike generator was passed through two parallel bridge rectifier circuits and then to the transducers, the returning signals from the transducers were fed into two different channels of the oscilloscope. This method does degrade the magnitude of the echo to a certain extent without significantly effecting the measurability. The spikes produced by the generator were very sharp with peaks very close to zero, about 0.1 division from the zero for a time scale 2 μs (fig. 4.4.3).

The interface height 'h' was calculated by measuring the horizontal time scale given by transducer '3', from the peak of the firing spike to the receiving echo. For example, if this measurement is 6 divisions, when the time scale of the osciloscope is set to 2 μs, then the height (h) of interface is given by:-

$$h = 1482 \times 2 \times 10^{-6} \times 6/2 = 8.9 \times 10^{-3} m = 8.9 \text{ mm} \qquad (4.4.1)$$

where speed of sound in distilled water = 1482 m/s at 20°C (Kaye and Laby, 1973)

Since the osciloscope can be read to 0.1 of a division the height can be measured to an accuracy of 0.15 mm. Measurements under dynamic conditions (ie. during jet injections) the oscilloscope was set to storage mode and the time scale was set to 0.2 μs. Therefore the change in level drop can be measured to 0.015 mm. The enabling and storing of the oscillosope was triggered by sending a 5 volts pulse from the sequencer delay generator via the 9 pin connector. The sequencer delay generator was pre-set to the time at which the interface drop needs measuring.

Preliminary experiments were conducted to observe the behaviour of the level drop against time, for several jet velocities. The plots for position 1 and 3 are shown (fig. 4.5.2) to produce similar shapes relative to each other for all velocities tested. This indicates that this characteristic shape is a function of the vessel geometry. By computing the gradient of the least square fit of the plot, from interface drop against time a mean value was obtained for the

interface drop rate for the times t= 0.4,0.5,0.6,0.7 and 0.8 seconds, the differences in this mean value corresponding to postions 2 and 3 were shown to be insignificant. Therefore, it was decided only to average interface drop levels at position 1 and 3 for one particular duration. The values were averaged again by repeating the experiment for another three times and then the mean value of these average values corresponding to different durations (eg. 0.4, 0.5, 0.6, 0.7, 0.8 secs.) were calculated from the gradient of the least square fit. Hence, an example of the procedure performed to obtain one experimental reading can be presented in a chart as follows:-

		1	position 1		
			position 3		
	0.4 sec.	2	position 1	average	
			position 3	drop	
		3	position 1	(0.4s)	
			position 3		
		4	position 1		mean gradient
			position 3		
μ = 1.15x10^{-3} Ns/m^2	0.5 sec.			0.5s	of least
			compute		square
h = 16.4mm	0.6 sec.		average	0.6s	fit
			drop		
σ = 0.033 Nm^{-1}	0.7 sec.		AS ABOVE	0.7s	
			correspond		
V_j= 7.6 m/s	0.8 sec.		to	0.8s	

This procedure was repeated, after systematically changing each of the parameters whilst keeping the remaining constant, so that a relationship between interface drop rate and, μ,σ,h and V_j could be developed. Therefore 20 tests were performed to obtain one experimental point. To transform interface drop rate to entrainment rate, the interface area needs to be found. A relationship for surface area can be found from geometrical and surface properties as follows:-

From figure 4.4.2:-

Curvature length 'L_2' = $r(180-\gamma-\psi)/\pi$ (4.4.2)

$$L_1 = (R \sin\gamma) - r \cos(90-\gamma-\psi) \quad (4.4.3)$$

Therefore, surface area = $2(L_1 + L_2)$x depth (4.4.4)

When $y = r$; $\Theta = 90^\circ$ (see appendix A.4)

$$r = \{2\sigma/g(\rho_{water} - \rho_{oil})\}^{1/2} \quad (4.4.5)$$

and $$\cos\gamma = \{R + r + r \sin(90-\gamma-\psi) - h\}/R$$

$$= \{R + r[1 + \cos(\gamma+\psi)] - h\}/R \quad (4.4.6)$$

The value 'γ' needs to be found by trial and error.

The angle 'ψ' (fig. 4.4.2) was measured on photographic prints obtained from high speed photography, of the interaction between the interface and wall. These measurements indicate that this angle is approximately $95\pm4^\circ$ for the conditions t=0.4 seconds and 0.8 seconds, and also for all of the test conditions (fig. 4.3.1 to 4.3.3). Since this curvature at wall/interface interaction is not contributing significantly to the interface area, the average value of 95° was taken as the value of 'ψ'.

Using equations 4.4.2 to 4.4.6 surface area corresponding to each interfacial height was calculated by trial and error. A set of interface areas obtained from this method is plotted in fig. 4.5.1. For the trail and error analysis the initial approximation was taken as $\gamma = 180^\circ$. When the jet is under operation, the interface area is also reduced corresponding to the reduction in interface height with time. Therefore, the effective interface area should correspond to a value between those at t=0.4 and 0.8 seconds. Hence the average level drop was found from the least squares method, then the interface area was calculated corresponding to the level height at $\bar{x}$ (ie. t= 0.6 sec., since $\bar{x}$ =0.6 sec.). A sample calculation is given in Appendix A.4, to show the stages of the calculations performed to find

entrainment 'E_w'.

4.4.2 Drop size measurement

First the front viewing perspex window was removed by unbolting the butterfly nuts and a plastic screen having 1 mm square grid was set firmly at the plane of the jet, across the section (fig. 4.4.5) and the front panel was bolted back into place. The grid was pre-marked to indicate the centre of circular plane. Oil (ie. the test liquid) was poured from the top hole and a photograph was taken without the injecting jet. This procedure was carried out in order to scale the jet plane, meaning the remaining experiments were performed without ajusting the rig setup (including the camera). To improve the resolution, relatively low speed films of 100 ASA were used and the lens aperture was set between 2.8 and 4.0 according to the transparency of the oil. Another advantage of the low speed film is the relatively small depth of field making droplet rejection easier during drop sizing. The camera was mounted 60 mm from the rig front face and its lens was a Tamron high speed macro 35-80 mm, 1:2.8-3.8. The distance guide number of the lens was set to 80 mm and the f number to 2.8 and the jet penetration region through the water was recorded on slide photographic film. This arrangement needed force processing of the film to another additional one minute (one stop), when the lighting, as before, was by back illuminated spark source with a light diffusing screen in between the spark source and test chamber. The depth of the field of view was determined experimentally by arranging a similar grid (as mentioned above) at a 30° angle to horizontal as shown in fig. 4.4.6. Then the camera was focused to a straight wire set at the vertical plane of the jet orifice. Hence, counting the number of focused grid squares in the north/south direction and simple trignometry gives us the depth of the field of view as $s.\cos 30^\circ$ mm, where s = number of focused 1 mm squares. This value was around 6 mm.

For each jetting condition, five photographs were taken at t=0.6 seconds on 100 ASA slide film. For low extremes of the experimental

range the jet has just reached the top wall at t=0.6 sec. and at the other extremes the jet has reached the top and has returned back just about ¼ of the pipe (test chamber) height. Since the core of the jet is opaque to light, droplets were analysed at the edges of the jet. The system used for drop sizing was 'Optomax V' video interactive image analyser (fig. 4.4.7), which under normal operating conditions can analyse dilutly distributed particles automatically. But the capabilities of this system are not sufficient to identify the individual drops in the jets, because of congestion in the overlapping images. Therefore all photographs were analysed using the manual mode. The Optomax V image analysis system consist of a IBM compatible computer central processing unit with image display and a miroscope fitted with monochrome camera. Optomax V demonstrates a high spatial resolution of 704 x 560 pixels coupled with 256 grey level detection. A grey level value corresponds to the intensity at each point in the array, which can range between 0=black and 255=white. The system used produced about 30 times magnification from the slide to the TV monitor. The manually obtained data was first fed into the computer data base and then processed and stored in a floppy disc.

The operational principle of the direct photographic measurement of the drop sizes is to produce a two dimensional image on the film from the projection of drops falling on the focussing plane. Away from the focussing plane, the image becomes less and less clear and, finally not visible, In the region of dense spray, where the distance between drops is small, overlapped images often result. Therefore it is necessary to define a criterion for the acceptance of a drop in the process of drop size counting. Counting droplet samples is not possible very close to the horizontal interface. Therefore, they were taken from regimes ± 30 mm from the centre of the pipe section and as the first criterion well defined droplet regions were selected rather than individual droplets, where the droplets are clearly distingusiable from the others. The droplets in those regions were individually sized. Drops with wide blurred boundaries were considered as out of focus and rejected. Sometimes the relatively bigger ones escape or are thrown out by the jet and normally appear in the photograpic slide as isolated drops sitting far away from the jet edge

by themselves. These drops can also cause erronous counting and so, were considered unacceptable and rejected.

For each condition about 100 drops per sample were counted (from the five photographic slides) at the edge of the jet, in the region mentioned above (this automatically excludes the water droplets that have already reached the top and are returning). The relations for the mean sizes, 'd_{32}', Volume mean diameter, Area mean diameter and Length mean diameter, were programmed into the computer and executed subsequently. In this application an atomization quality may be ascertained by the amount of large drops existing in the jet stream. Since the surface area governs the resistance and volume determines concentration and the 'd_{32}' also gives a value which is nearer the size of the bigger droplets of the actual spray (fig. 4.2.1), it is reasonable to accept that this diameter as the one expressing the purpose of this application. In the calculations, this diameter was related to water layer interface height at t=0.6 seconds. A sample calculation is given in Appendix A.4. Previous experience suggests (Yule-1988, and Wu, 1983) that when the smallest drop counted is in the order of 1/5 th or less of the d_{32}, as in the present experiment, the samples of 100 are enough to determine 'd_{32}'.

4.4.3 Experimental uncertainties

The systematic uncertainities related to fluid properties, interface height measurement and velocity measurements are common to both entrainment experiments as well as drop size measurement experiments. Therefore these are estimated first as follows:—

i). Fluid property measurement

a). Kinematic viscosity:- kinematic viscosity was measured in accordance with ASTM D445-53T standard, using Ubbelohde Viscometers. Most of the uncertainty in viscosity occurs due to variation in temperature. Therefore, the variation in viscosity of water due to $20\pm1{\cdot}5^{o}C$ is calculated. Since other liquids used in the experiment

also have similar trends, estimates of the uncertainity was taken for all liquids as that of water. The error that may incur during the measurement is given by:-

$\delta\nu/\nu = \delta t/t$ since $\nu = Ct$, where C is viscosity meter constant

Therefore, the total relative uncertainity, that is including the error due to temperature variation, is given by:-

$\delta\nu/\nu$ = due to time measurement + due to variation in temperature
$\delta\nu$, due to variation of $\pm 1.5^{o}C$ in temperature can be approximated to 0.022 cSt (Kaye et al, 1973, p36).

$$\delta\nu/\nu = \{(0.5/(60 \times 8))^2 + (0.022/1.002)^2\}^{\frac{1}{2}}$$
$$= \underline{0.03}$$

b). Density:- again the uncertainity estimated for water will be taken to be true for all other liquids.

$\delta\rho/\rho$ = due to hydrometer reading + due to variation in temperature
$\delta\rho$ due to variation of $\pm 1.5^{o}C$ in temperature can be approximated to 0.195 kg/m^3 (Kaye et al, 1973, p29).
Smallest possible hydrometer reading is 0.1/50.

$$\delta\rho/\rho = \{(0.02)^2 + (0.195/998.2)^2\}^{\frac{1}{2}}$$
$$= \underline{0.002}$$

c). Interfacial tension:-

$\delta\sigma/\sigma$ = due to reading the apparatus + due to variation in temperature

Uncertainity due to temperature was approximated to that of surface tension of water against air.

Hence, $\delta\sigma$ due to temperature variation of $\pm 1.5^{o}C$ is obtained from Kaye et al, 1973, p43.

$$\delta\sigma/\sigma = \{(0.00025/0.033)^2 + (0.225/73)^2\}^{\frac{1}{2}}$$
$$= \underline{0.008}$$

ii). Interface height

Interface height can be measured to ±0.15mm (as shown in section 4.4.1).

δh = error due to height measurement + error incurred by taking 'h' as a constant throughout the experiment

$= (\delta h/h)_{measurement} + (\delta h/h)_{experiment}$

Therefore, $(\delta h/h)_{measurement} = 0.15/16.4 = \underline{0.01}$

In this experiment, during a jetting situation, the interface height is not a constant and always decreases with the entrainment of water. Therefore, during an experiment there is an error due to a change in entrainment from one point of the variable to the other. This error is negligible for experiments against μ and σ, since the entrainment seemed to be almost a constant. This effect does not apply for experiment against 'h'. In the experiment against 'V_j' the maximum of the error ($(\delta h)_{experiment}$) for this test= ±0.4 (see appendix A4.4).

Therefore, total ($\delta h/h$) for the experiment against velocity = ±0.03

iv). Velocity measurement

$$\text{Velocity of the jet } (V_j) = \frac{\text{collected oil volume } (V_c)}{(\pi/4)d_j^2.T_c}$$

where T_c is the time taken to collect the volume of oil (V_c)

Therefore, $\delta V_j/V_j = ((\delta V_c/V_c)^2 + (\delta T_c/T_c)^2 + 2(\delta d_j/d_j)^2)^{1/2}$

'δV_c' was estimated by collecting 30 samples of oil, each of 10 seconds, for one fixed jet condition (V_j= 5.8 m/s) and the standard deviation of these samples were calculated to be = 4.32 ml.

Hence, $\delta V_c/V_c = 2\sigma/V_c = 8.65/188 = 0.046$ (ie: for 95% confidence level) and the other two are very small relative to this.

v). Other errors in entrainment measurement

a) Uncertainities in the interface area calculation (X_A)

Surface area = (L_2+L_1). depth (see fig. 4.4.2)

$$X_A = \left\{\left[\frac{\delta(L_1+L_2)}{L_1}\right]^2 + \left[\frac{\delta b}{b}\right]^2\right\}^{1/2} \qquad (4.4.7)$$

Since $\delta b = 0.05mm$ and $b = 134mm$

$$\delta b/b = 3.73\times10^{-3} \qquad (4.4.8)$$

$$\frac{\delta(L_1+L_2)}{(L_1+L_2)} = \left[\frac{1}{(L_1+L_2)}\right]\left\{L_1^2\left[\frac{\delta L_1}{L_1}\right]^2 + L_2^2\left[\frac{\delta L_2}{L_2}\right]^2\right\}^{1/2} \qquad (4.4.9)$$

$L_1 = (R\,Sin\gamma) - r\,Cos(90-\gamma-\psi)$ *(from equation 4.4.3)*

Differentiating the above with respect to L_1 gives:-

$$\delta L_1 = Sin\gamma\,\delta R + R\,Cos\gamma\,\delta\gamma - Cos\,(90-\gamma-\psi)\delta r + r\,Sin(90-\gamma\psi)(-\delta\gamma-\delta\psi) \qquad (4.4.10)$$

$r^2 = (2\sigma/g(\rho_2-\rho_1))$ *(from equation 4.4.5)*

Differentiating with respect to 'r' gives:-

$$\frac{2\,\delta r}{r^2} = \left\{\left[\frac{\delta\sigma}{\sigma}\right] + \left[\frac{1}{(\rho_2-\rho_1)}\right]^2\left[(\delta\rho_2)^2 + (\delta\rho_1)^2\right]\right\}^{1/2} \qquad (4.4.11)$$

$L_2 = r(\pi-\gamma-\psi)$, *(from equation 4.4.2). Differentiating this with respect to* L_2 *gives:-*

$$\frac{\delta L_2}{L_2} = \left\{\left[\frac{\delta r}{r}\right] + \left[\frac{1}{(\gamma+\psi)}\right]\left[\gamma^2\left[\frac{\delta\gamma}{\gamma}\right] + \psi^2\left[\frac{\delta\psi}{\psi}\right]\right]\right\} \qquad (4.4.12)$$

$Cos\gamma = (R + r[1+Cos(\gamma+\psi)] - h)/R$ *(from equation 4.4.6)*

$R\,Cos\gamma = (R + r\,Cos(\gamma+\psi) - h)$

Differentiating with respect to R gives:-

$$Cos\gamma\ \delta R - RSin\gamma\ \delta\gamma = \delta R + \delta r + Cos(\gamma+\psi)\delta r - r[Sin(\gamma+\psi)][\delta\gamma+\delta\psi] - \delta h \qquad (4.4.13)$$

Hence,

$$\delta\gamma[rSin(\gamma+\psi) - RSin\gamma] = \delta R(1-Cos\gamma) + \delta r[1+Cos(\gamma+\psi)] - \delta\psi x rSin(\gamma+\psi) - \delta h \qquad (4.4.14)$$

Since, R = 70mm , $\gamma = 40^{o}$ (approximately), r = 5.8mm, $\psi = 95^{o}$, h = 15mm, the above equation 4.4.14 becomes:-

$$\delta\gamma[-40.9] = \delta R(0.23) + \delta r(0.29) - 4.10\delta\psi - \delta h \qquad (4.4.15)$$

$$\delta\gamma = 5.6x10^{-3}\delta R + 7.1x10^{-3}\delta r - 0.1x10^{-3}\delta\psi - 0.024\delta h$$

Substituting $\delta R = \pm 0.5$mm, $\delta\psi = \pm(5/180)x\pi$, $\delta h = \pm 0.15$mm gives

$$\delta\gamma = \pm 2.81x10^{-3} \pm 7.1x10^{-3}\delta r \pm 8.73x10^{-3} \pm 3.6x10^{-3}$$
$$= 6.82x10^{-3} + 7.1x10^{-3}\delta r \qquad (4.4.16)$$

$$\frac{2\,\delta r}{r^2} = \left\{\left[\frac{\delta\sigma}{\sigma}\right] + \left[\frac{1}{(\rho_2-\rho_1)}\right]^2 \left[(\delta\rho_2)^2 + (\delta\rho_1)^2\right]\right\}^{\frac{1}{2}} \quad (from\ equation\ 4.4.11)$$

$$= \{0.06x10^{-3} + (1/200^2)[4 + 4\ ]\}^{\frac{1}{2}}$$
$$= \underline{0.0162}$$

Hence, $\delta r/r = 0.047$ (4.4.17)

Hence, $\delta r = \underline{0.27}$ (4.4.18)

Therefore, from equation 4.4.16, $\delta\gamma = \underline{0.009}$ (4.4.19)

From equation 4.4.12:-

$$\delta L_2/L_2 = \{0.22x10^{-3} + [1/(2.36)^2][8.1x10^{-5}+7.6x10^{-3}]\}^{\frac{1}{2}}$$
$$= 0.059$$
$$\delta L_2 = \underline{0.34}$$

From equation 4.4.10:-

$$\delta L_1 = 0.643\ \delta R + 53.6\ \delta\gamma - 0.707\delta r - 0.707(\delta\gamma+\delta\psi)$$
$$= \pm 0.321\ \pm 0.48\ \pm 0.19\ \pm 0.068 \qquad (4.4.22)$$
$$\delta L_1/L_1 = 1.06/30 = \underline{0.035}$$

From equation 4.4.9:-

$$\delta(L_1+L_2)/(L_1+L_2) = (1/35)\{(1.06)^2 + (0.34)^2\}^{\frac{1}{2}}$$
$$= (1/35)\{1.12 + 0.116\}^{\frac{1}{2}}$$
$$= \underline{0.032}$$

From equation 4.4.7:-

$$X_A = \{(0.032)^2 + (0.5/134)^2\}^{\frac{1}{2}}$$
$$= \underline{0.032}$$

b). Random uncertainity of the interface drop measurement

Averages of the interface drops at position 1 and 3 were recorded for 30 injections for one jetting condition (ie. V_j= 5.8m/s, μ = 1.15×10^{-3}, σ = 0.033 Nm^{-1}) and at t = 0.6 seconds. The standard deviation of these were = 0.044 mm. Since we are sampling 4 times for one jetting condition, a 95% confidence level of this uncertainity would be $2\sigma/\sqrt{4}$ = 0.044 mm

Hence, the percentage uncertainity = 0.044x100/(4.296x0.375)
= 2.7%

c) Uncertainity due to limited number of interface level measurement (X_p)

No specific tests were carried out to quantify this error, but steps were taken to reduce this to minimum by plotting the level drop against time and taking the gradient (between 0.4 to 0.8 seconds) of the plot as the level drop rate.

iv). Other errors in drop sizing

1). There is an uncertainty due to fact that the interface level height is a function of time, hence is not a constant when it is supposed to be:- this error was minimised by introducing averaging techniques (see appendix A4.4).

2). Uncertainty due to overlapping of droplet on the 2-D photographic

frame:- this error was kept to a minimum by counting droplets at the edge of the jet.

3). Uncertainty due to the measurement of drop sizes been made only at the edge of the jet.:- no test were done to quantify this error.

4). Uncertainty due to person to person bias on drop sizing:- no test was conducted to quantify this bias due to personal judgement, previous work has sometimes quoted values as high as 10%. By defining strict criteria for counting and rejection, and also selecting well defined sampling locations this error can be reduced to a minimum.

5). Uncertainty due to depth of the field of view:- on the 2-D photograph of the calibration grid, no size variations of the grid squares were shown on the sampling region. Therefore, any significant error due to a depth of field of ±3 mm cannot be expected.

4.4.4 Results and Analysis

4.4.4.1 Entrainment measurement

1). Experimental measurements of entrainment (E_w) against jet velocity, interfacial height, viscosity and interfacial surface tension were plotted in figures 4.5.3 to 4.5.10.

2). When the oil jet/water interface was considered rough, due to local atomised droplets, the relationship for the entrainment became (from analysis in chapter 3.0):-

$$E_w/m_j = (h/d_j)(\rho_w/\rho_{oil})[3C_T^{1/2}]$$

We have also shown in chapter 3.0 that (y/Rh) = f(We/Re) for constant density ratios. Where 'f' is a functional symbol.

$$C_T = \left[n_1 \ln f\left[\frac{We_{oil}}{Re_{oil}}\right]\right]^{-2.5}$$

The function f is related to entrainment very weakly. Therefore the value n_1, although shows (from log-log plot) to be of the order of 0.7, is very difficult to determine precisely, unless the experiments are conducted in wider range. Therefore n_1 was taken as 0.707, as in flow over rough plate, and then the experimental data was correlated to the form:-

$$\frac{E_w}{m_j} = \left[\frac{h}{d_j}\right]\left[\frac{\rho_w}{\rho_{oil}}\right]\left\{ ln\left[8.18\ x10^5\ \frac{We_{oil}}{Re_{oil}}\right]^{0.294}\right\}^{-1.25}$$

4.4.4.2 Drop Size Measurement

1). Experimental measurements of SMD (d_{32}) against jet velocity, interfacial height, viscosity and interfacial surface tension were plotted in figures 4.6.9 to 4.6.13 respectively.

2). It is impossible develop a correlation, accounting for all individual variables seperately, when the scatter of experimental results is large and the experimental ranges are restricted due to the methods used and the complexity of the system. Therefore, we first make use of dimensional analysis conducted in section 4.3 to obtain the relevant dimensionless groups. Then the results in figures 4.6.9 to 4.6.13 were approximated to a correlation of the form:-

$$\frac{SMD}{d_j} = \frac{133.6}{We_{oil}}\left[\frac{h}{d_j}\right]\left[\frac{\mu_{oil}}{\mu_w}\right]^{0.31}$$

4.4.5 Discussion

4.4.5.1 Entrainment of stratified water

1). The jet 'Re' number in this experiment varied from 3530 to 14243 and the penetrating kerosene jet can be considered to be in the atomizing regime.

2). Experimental measurements of entrainment (E_w) against jet velocity, interfacial height, viscosity and interfacial surface tension were plotted and compared with theoretical results in figures 4.5.3 to 4.5.10.

3). The simple model based on water boundary layer entrainment due to the penetration of a smooth cylinder through the stratified layer, yields results that are of the same order of magnitude as the experimental values (figs. 4.5.3 to 4.5.10), when the skin friction coefficient '$[0.026/(Vy/\nu)^{1/7}]$' was based on that of the turbulent boundary layer on a flat plate. The model predicts the entrainment from the relationship:-

$$E_w = 0.223(d_j \rho_w^6 V_j^6 h^6 \mu_w)^{1/7}$$

4). However considering the oil jet/water interface as rough, due to local atomised droplets, would be more justifiable. Therefore, the skin friction coefficient was based on boundary layer flow on a rough plate $\{C_T = [\ \ln(A\ y/Rh)^{-2.5}]^{n_1}\}$. Then the relationship for the entrainment correlates (from analysis in chapter 3.0 and experimental data) to an equation of the form:-

$$\frac{E_w}{m_j} = \underbrace{\left[\frac{h}{d_j}\right]\left[\frac{\rho_w}{\rho_{oil}}\right]}_{(1)} \underbrace{\left\{ \ln\left[8.18 \times 10^5 \frac{We_{oil}}{Re_{oil}}\right]^{0.294}\right\}^{-1.25}}_{(2)}$$

This approach, that is a correlation based on a simple theory, has the advantage of showing the salient features among many other factors

which influence this entrainment process.

5). The above equation indicates clearly the problem in twofolds. Part 1 provides the relationship if the oil/water jet interface has fixed roughness, such as on a rough cylinder. But oil/water jet interface structure is a function of jetting conditions hence the equivalent roughness should also change accordingly. The effect on entrainment due to these changes in the structure is indicated in part 2, and the Re and We numbers characterise these changes.

6). The theoretical model (fig. 4.5.9) suggests that if the interface is smooth and solid then the entrainment is independent of oil viscosity. Taylor's theoretical analysis as well as experimental analysis by others (Ranz, 1958) show that the jet divergence angle very slowly decreases with disperse phase viscosity (in this case oil) first before it becomes constant. That means the effective value of 'y/Rh' increases to decrease the skin friction at the interface.

7). Effects of oil viscosity and interfacial tension are not dominant in this entrainment process.

8). For the ranges of parameters tested, the water/oil interface maintained its horizontal, undisturbed placid nature throughout. Therefore, one may argue that the curvature or end effects (ie. due to front and back panels) are not considerable. They are accountable when the demand associated with entrainment is in excess of the availability of stratified water. In these situations the whole interface would tend to pull upwards with the jet at the penetration region and the placidness of the interface breaks down. This occurs when the height of the interface is thin (less than 7mm in this experiment, for higher velocities). Under real situations, this entrainment mechanism becomes steady, when the demand associated with jet entrainment rate is balanced by the upstream water supply.

9). The role of density ratio, (water to oil), on entrainment and water droplet sizes was not investigated, since this density ratio varies very little in the real situation, their effects can be

disregarded.

4.4.5.2 Water droplet breakup

1). Experimental measurements of SMD (d_{32}) against jet velocity, interfacial height, viscosity and interfacial surface tension are plotted in figures 4.6.9 to 4.6.13 respectively.

2). The jet 'Re' number in this experiment varied from 3530 to 14243 and the penetrating kerosene jet can be considered to be in the atomizing regime.

3). The following changes, resulted in an increase in droplet diameter (d_{32}):-

i). a decrease in jet velocity
ii). an increase in viscosity of oil
iii) an increase in interfacial surface tension
iv). an increase in stratified water layer height

4). The droplet sizes generate a positively skewed Gaussian distribution.

5). Experimental results, with the aid of dimensional analysis, were approximated to a correlation of the form:-

$$\frac{SMD}{d_j} = \frac{133.6}{We_{oil}} \left[\frac{h}{d_j}\right] \left[\frac{\mu_{oil}}{\mu_w}\right]^{0.31}$$

6). Further increases in velocity (ie. above the maximum value tested) would create much smaller droplets and the photographic frames become cloudy, so that the manual counting with the aid of Optomax V becomes impossible and beyond the capabilities of the experimental technique.

7). Experiments of entrainment and drop sizing both have the weakness that they have been conducted in limited ranges.

PART 2

DISPERSION OF BROKEN UP STRATIFIED WATER LAYER IN A PIPE CROSS FLOW

– COMPUTATIONAL STUDY –

Part 2 Dispersion of the broken up stratified water layer in a pipe cross flow - Computational studies

The scope of this part is to utilize techniques of computational fluid dynamics, an area which is not been exploited to the full extent for these applications. Before attempting to construct a detailed numerical algorithm for these applications it would be useful initially to model the problem in an existing numerical code. We have chosen a commercially available flow simulation code, PHOENICS, for this purpose. The users of similar codes use the mathematical algorithms of that particular package as a tool for their simulations, but they should have a good understanding of flow models as well as an overall idea of the mathematical basis. The mathematical basis of PHOENICS is very well presented in Patankar(1980). In chapter 5.0, the flow modelling techniques for single and two phase flows and previous simulation of complex elliptic flows, using a similar mathematical basis to PHOENICS, are reviewed. Modelling of the present problem and comparision with the much scarcer experimental data are carried out in chapter 6.0.

CHAPTER 5.0 REVIEW AND MODELLING TECHNIQUES

5.1 Introduction

Consider first the subject of classical fluid-dynamics, the irrotational flow, in which the absence of viscosity and appropriateness of boundary conditions cause the velocity field to obey the Laplace equation for the velocity potential. Solutions of such an equation are useful, and often used, but their validity depends upon whether indeed the effects of viscosity are negligibly small in practice. Sometimes they are and sometimes they are not. Now considering the molecular viscosity of the fluid, it is also possible to solve the relevant differential equation by using a suitable numerical procedure. Yet, it is necessary to decide, on the basis of general knowledge of the problem, whether allowance should additionally be made for the occurrence of turbulence. If turbulence is probable, the turbulence simulating features such as turbulence models, should be used.

As Bradshaw (1986) points out there is no one turbulence model that can cover all the range of engineering flows and for the time being, we have to accept the need to change the empirical input, or even the method, when we change from one flow to another or even one part of a given flow to another. The responsibility for the choices rests with the user of the calculation method, who therefore needs as much background in the subject as the developer does.

What has been said about the simulation of turbulence is even more apposite to that of two-phase flows, in which the interphase transfer of mass, momentum and energy exert large effects by mechanisms, which have still not been adequately reduced to scientific order.

In the present application the flow is two-phase and most certainly turbulent. Therefore, first we set our attention to problems that may encounter in finite difference flow simulation techniques (the method Phoenics uses) and then discuss briefly the turbulent and two-phase models in sections 5.1.2 and 5.1.3.

5.1.1 Finite difference formulation

There exists a number of methods of devising finite difference approximations, included in these are Taylor series expansions, polynomial fitting and the macro-integral/control volume technique. The actual choice to be adopted depends on the features to be desired in the finite difference equations, more particularly whether or not the finite difference equations are to be conservative in the sense of Roache (1976). Put simply a finite difference scheme is conservative if it exactly satisfies (to within machine round off) the same conservation law which was used to derive the corresponding partial difference equation for all mesh spacings. Control volume analysis automatically ensures 'conservation' and experiences of other researchers have (Jones et al, 1979) indicated that these conservative schemes do generally give more accurate results and for elliptic flow calculations, their use appears to be essential.

The governing conservation equations satisfying the present problem should permit upstream influence by flow reversal, by pressure perturbation and by viscous or turbulent stress gradients and hence should be elliptic in nature, therefore should be solved iteratively by successive downstream sweeps. The main difficulties in the solution of elliptic equations is the presence of inaccuracy due to false diffusion and numerical instabilities. The advantage of discretization by implicit method is that they are unconditionally stable for almost all the complicated non-linear equations of real life, whereas the explicit methods needs restrictions on excessively large length step and therefore is conditionally stable (the finite difference equations are said to be stable if perturbations do not grow in a time like direction).

The method is called implicit when the finite difference equation has not one but three unknowns with variables at the new time, as a result a set of coupled equations for the variables at the old time is obtained. The coefficient matrix of the coupled algebraic equation in the implicit method is 'tridiagonal' so the equation can be solved by

the tridiagonal matrix algorithm, Therefore, implicit methods are generally preferred for routine solution techniques.

It was shown that introducing convection and diffusion by a conventional difference technique (eg. upwind) causes an error in the $U\partial U/\partial x$ term in the momentum equation, proportional to $\partial^2 U/\partial x^2$. Because $\partial^2 U/\partial x^2$ appears in the exact equation multiplied by the viscosity, an error proportional to $\partial^2 U/\partial x^2$ represents an additional 'pseudo-viscosity'. Similar arguments apply to the $V\partial U/\partial y$ term in the momentum equation, and to corresponding terms in the other transport equations. In the worst case, where the streamlines cross the coordinate mesh at an angle of 45 degrees (Patanker, 1980), the pseudo-viscosity term is larger than the real viscosity term if the Reynolds number based on mesh size and through-flow velocity exceeds two.

Many ingenious attempts have been made to secure stability and reasonable accuracy in elliptic solutions while keeping an acceptably large mesh Reynolds number (sometimes known as mesh Peclet Number), but no generally accepted technique has yet been found. Fortunately, the problem is less severe in turbulent flows than in laminar flows at high Reynolds number, because the effective Reynolds number of the turbulent flow is based on the eddy viscosity rather than the molecular viscosity.

5.1.2 Turbulence modelling

1). General turbulence concepts:- Turbulence is the most complicated kind of fluid motion making even its precise definition difficult. A fluid motion is described as turbulent if it is rotational, intermittent, highly disordered, diffusive and dissipative. It is also three dimensional and a nonlinear phenomenon. The main charactertic of turbulence is the transfer of energy to smaller spatial scales across a continuous wave-number spectrum. A useful concept for discussing the main mechanisms of turbulence is that of an eddy. An

eddy can be thought of as a typical turbulence pattern, covering a range of wave lengths, large and small eddies coexisting in the same volume of fluid. The eddies can be considered as a tangle of vortex elements (or lines) that are stretched in a preferred direction by mean flow and in a random direction by one another. This mechanism, the so-called "vortex stretcthing" ultimately leads to the breaking down of large eddies into smaller ones. This process takes the form of an "energy cascade". Since eddies of comparable size can only exchange energy with one another, the kinetic energy from the mean motion is extracted from the largest eddies. This energy is then transferred to neighbouring eddies of smaller scales continuing to smaller and smaller scales. The smallest scale being reached when the eddies lose energy by the direct action of viscous stresses which finally convert it into internal thermal energy on the smallest-sized eddies.

It is important to note that viscosity does not play any role in the stretching process nor does it determine the amount of dissipated energy, it only determines the smallest scales at which the dissipation take place. It is the large eddies (comparable with the linear dimension of the flow domain), characterizing the large-scale motion, that determines the rate of energy that can be passed on to smaller scales and be finally dissipated. The larger eddies are thus mainly responsible for the transport of momentum and heat and hence need to be properly simulated in a turbulence model. Because of direct interaction with the main flow, the large scale motion depends strongly on the boundary conditions of the problem under consideration.

An increase in Reynolds number increases the width of the spectrum (ie; the difference between the largest eddies, associated with low frequency fluctuation, and the smallest eddies, associated with high frequency fluctuation). This suggests that at high Reynolds numbers the turbulent motion can be well approximated by a three level procedure, namely, a mean motion, a large-scale motion and a small-scale motion.

When the Reynolds number is high enough the large scale and small scale motion are sufficiently far apart in the spectrum for the direction sensitivity of the small scale motion (due to mean flow) to be lost entirely and the small-scale motion is isotropic. This phenomenon namely, the small scale motion being isotropic while the large-scale motion is not, is called local isotropy and is an important concept in turbulence modelling.

2). The idea and the purpose of the turbulent model:- The practical need for simulation of turbulent flows are enormous, but there is no existing or forseen computer system with large enough memory or speed to allow the resolution of the small-scale effects of turbulence. Therefore "turbulence models" have been invented. These consist of sets of differential equations and associated algebraic equations and constants, solution of which in conjunction with those of the Navier-Stokes equation, closely simulate the behaviour of real turbulent fluids.

The first move towards a model of turbulence can be attributed to Boussinesq (1877). He suggested that the effective turbulent shear stress, arising from the cross correlation of fluctuating velocity, could be replaced by the product of the mean velocity gradient and quantity termed the "turbulent viscosity" (μ_t). Unlike μ, the molecular viscosity, μ_t is not a property of the fluid, being largely determined by the structure of the turbulence at the point in question. But this proposal does not itself constitute a model since there remains the task of expressing the turbulent viscosity in terms of known or calculable quantities. Only then is the model said to be closed.

3). Existing turbulence models:- Modelling of turbulence has been attempted by five methods as follows.

i). Analytical turbulence theories:- they are normally developed in Fourier (wave number or frequency) space. These theories are known to be very complicated and have not yet been applied to complex engineering problems.

ii). Sub-grid scale closure models:- computers of today are too small and too slow to resolve the small scale turbulence motion. However, the computer capacity is sufficient to solve the time dependent equation for large-scale turbulent motion, the small scale turbulence that cannot be resolved with the chosen numerical grid must then be approximated by a model. This kind of turbulence model is therefore called sub-grid-scale model. Since the small-scale turbulence is much less problem dependent than the large-scale turbulence the details of the model are much less influential for the overall flow behaviour. These methods, although promising still require too much computational time to be useful for engineering applications.

iii). Direct numerical simulation:- this method attempts to simulate directly all the dynamically important scales of large Reynolds number turbulent flows. It is based on the hypothesis that direct simulation may be carried out by artifically decreasing the Reynolds number to the point where the important scales can be simulated accurately on existing computers, and that a sufficient number of large scales remain unchanged by any change in Reynolds number. This method still requires too much computational time.

iv). Turbulence transport models:- these are the basis of the engineering approach, where attempts are concentrated on seeking simplified models of the terms governing the transport of momentum heat etc.. These models are similar to the analytical theories in that they both treat dynamical quantities as satistically-averaged fields, but they simulate gross features of turbulence, while analytical theories pay attention to interactions betweeen the various scales of motion.

v). Two-fluid models of turbulence:- the "fragmentariness" of turbulent flows is neglected by the convectional (single-fluid) models of turbulence. It can be allowed for by the use of a multi-fluid model which permits different (arbitrarily distinguished) fluids to exist and interact in the same space. Thus, when the model is applied to a

turbulent jet, two-phase theory is applied to the flow of a single thermodynamic phase. The "two fluids" are

a). Injected fluid possessing vorticity.

b). Surrounding irrotational fluid

vi). Vortex dynamics method:- this is a concept based on the realization that the turbulent flows consist of structures which are created and destroyed and it is their interaction that produces the transport of mass, momentum and energy. Therefore, these structures are simulated with discrete vortices and are solved to obtain the mean flow while the effects of diffusion and decay (ie. viscous effects) of vorticity are incorporated by a ramdon walk component and exponential ageing for each vortex.

We will now discuss below in detail the turbulence transport models because they have been under intensive development and are essentially the current standard practice and will also be used in this study. It must be realized that the available transport models pay no respect to the actual physical modes they purport to represent. It is therefore hardly surprising that the actual physics of turbulence is nowhere to be seen in the transport models, simply because no one can see how mathematics can be employed to represent them in the models. However, it is also true that the engineering community has been often fortuitous in obtaining very useful results by using transport models, results that would have required much more time and experimental cost to obtain in their absence. Therefore, if cautiously exercised and interpreted, these turbulence models would be valuable tools in research and design, despite their physical deficiencies.

The turbulence transport models can be classified in several ways. The one most often used is that arranged in the order of the mean flow equations:-

i). Zero equation models
ii). One equation models
iii) Two equation models
iv). Stress equation models

Most of the models classes i). to iii). use Boussinesq eddy viscosity model (sometimes called gradient diffusion models), where diffusion flux of $\overline{u_i u_j}$ have been expressed by simple gradient diffusion. Local isotropy is assumed so that the dissipation is the same for all three normal components. Other models which do not use the eddy viscosity assumption (class iv.), obtain the Reynolds stress from a differential equation.

There are large differences between the simplest and the most advanced eddy-vicosity models. For example the use of a constant eddy viscosity (diffusivity) tuned to suit the problem has little to do with any changes in local turbulence structure, whence it cannot in general discribe correctly the details of main flow field. The simplest models for determining the distribution of ν_t over the flow field relates ν_t directly to the mean velocity distribution (eg. the local gradient). These models implicitly assume that the turbulence is dissipated where it is generated, which means that there is no transport of turbulence in the flow field. In cases where the state of turbulence at a point is influenced significantly by the turbulence generation somewhere else in the flow, for example grid turbulence, the turbulence that is generated by the wake directly behined the grid and is then transported downstream by the mean motion. These simple models would yield zero eddy viscosity because the mean velocity is uniform in the downstream region. Therefore in order to account for the transport of turbulence, models have been developed which employ transport equations for quantities characterizing the turbulence. Therefore the turbulence models are classfied according to the number of transport equations used.

i). Zero equation model:- this uses only the partial differential equation for the mean flow field and no transport equations for turbulence quantities, and is also called "mean field" closure. The classes ii) to iv) are called "transport equation" closures.

The most basic form of this model is to consider the turbulent viscosity as a constant. This is popular when a crude representation

of the flow field is required, for example, to initialise the flow field for a simulation using a more elegant model.

The concept of a constant eddy viscosity diffusity has its (Rodi, 1979) greatest importance in depth average calculation (eg. in open channels) where only horizontal transport is considered. In this case depth mean values ν_t and σ_Φ (Prandtl/Schmidt Number of species 'Φ') are used to relate the depth-averaged momentum and heat fluxes to the gradient of the depth-averaged velocities and temperatures (or concentration). This model has found its widest application in the so-called diffusion methods which assume the velocity field to be known and solve only the depth averaged temperature/concentration equation. When the turbulence is mainly bed generated as channel flow, the depth-mean diffusity for horizontal transport is resonably well correlated with the friction velocity 'U^*' and the water depth 'h' by $\nu_t = CU^*h$ where the empirical constant 'C' is geometry dependent

A more realistic first turbulence model proposed by the Prandtl's mixing length hypothesis, is still among the most widely used models. It employs the eddy viscosity concept which relates the turbulent transport terms to the local gradient of mean flow quantities. For example, for thin shear layers:-

$$-\overline{u'v'} = \nu_t(\partial U/\partial y) \qquad (5.1.1)$$

where ν_t = *eddy* kinematic *viscosity*

As the concept eddy viscosity was concevied by presuming an analogy between the molecular motion and the turbulent motion. The turbulent eddies were thought of as lumps of fluid which, like molecules, collide and exchange momentum. The molecular viscosity is proportional to the average velocity and mean free path of the molecules. Hence, the eddy viscosity is considered proportional to velocity characterizing the fluctuating motion and to a typical length of this motion which Prandtl called "mixing length".

Accordingly Prandtl (1925) proposed a mixing length hypothesis to obtain an algebraic relation for μ_t. The hypothesis is that the

turbulent viscosity is equal to the local product of the density, of the magnitude of the mean rate of strain and of the square of a characteristic length scale of the turbulent motion ($C.\rho \ell_m^2 |\partial U/\partial y|$). We call this length scale the mixing length (ℓ_m). The mixing length must be presented algebraically; but, in boundary-layer flows, whether near to or remote from walls, a few simple rules usually serve for its prescription. Prandtl went on to propose that ℓ_m was proportional to the distance from the nearest wall. This is an additional feature that some might regard as essential to Prandtl's hypothesis; but it will be useful to us to recognise that it is not, one can calculate ℓ_m in any way one pleases. Usually ℓ_m is related to the width of the shear zone(b) as ℓ_m=Const. b.

The relation, $C.\rho \ell_m^2 \partial U/\partial y$, involves a single unknown parameter, the mixing length 'ℓ_m' whose distribution over the flow field has to be prescribed with the aid of empirical information. C is a constant. The mixing length model has been used, in the past, for free shear layer and wall boundary layers.

It should be emphasized here that another model that is frequently used in free jet flow applications , as given below, is a simplified version of this.

ν_t = 0.01*flow width * velocity difference

ii). One equation model:- The one equation model requires the solution of an equation for the turbulent kinetic energy (k) and , as a result, allows for its transport. The turbulent kinetic energy equation can be derived from the Navier- Stokes equation. A differential model for μ_t was proposed by Prandtl (1945), where the determination of μ_t entails the solution of a differential equation for at least one property of the turbulence. Since the turbulent viscosity is essentially a property of the turbulent motion it would seem appropriate that velocity and length-scale of the turbulence should be used in determine μ_t. Prandtl suggested that a more representative velocity scale would be the square root of the turbulence kinetic energy denoted by the symbol k. The formula for μ_t thus becomes μ_t =

$\rho\sqrt{k}L_p$. In this model the length scale (L_p) was still prescribed algebraically but the kinetic energy of turbulence was determined from the solution of a differential equation expressing the processes by which k is transported. Kolomogrov (1942) proposed a similar turbulent model where $\mu_t = \rho k/f$, this makes $L_p=k^{\frac{1}{2}}/f$. Therefore the $\mu_t = \rho k^{\frac{1}{2}} L_p$ is sometimes known as Prandtl/Kolomogrov formula.

iii). Two-equation model:- There are a number of situations of practical interest where a suitable value of length scale cannot be found from a simple algebraic expression. For example, the case of the merging of mixing zones from one cross-sectional plane. Near the point of injection, each jet is unware of the others, and the local width of a single jets mixing zone is the length scale. Further downstream, the several mixing zones have grown to the point where they merge, more or less abruptly. Clearly, the local flows in one of the middle jets cannot instantly respond to the presence of all of these other jets in a linear way, as would be implied by taking ℓ_m as proportional to the new mixing zone width. Therefore, in attempts to eliminate the need for specifying the turbulence length scale as a function of position throughout the flow, a second differential equation, which in effect gives ℓ (length scale), has been used. In general, one looks for the second equation of a quantity that is a combination of k and ℓ, $Z=k^{\alpha}\ell^{\beta}$. It has the form (Launder, 1979):-

$$\rho\frac{DZ}{Dt} = \frac{\partial}{\partial y}\left\{\frac{\mu_t}{\sigma_Z}\frac{\partial Z}{\partial y}\right\} + Z\left\{\frac{C_1\mu_t}{k}\left[\frac{\partial U}{\partial y}\right]^2 - \frac{C_2\rho^2 k}{\mu_t}\right\} + S_Z \qquad (5.1.2)$$

Here σ_Z is a Prandtl number (or Schmidt number) for the diffusion of 'Z'. S_Z is a secondary source term which appears in some models, and C_1 and C_2 are constants.

If the length scale was taken as the scale of energy containing eddy ($\ell = C_D k^{3/2}/\epsilon$), then the Z can be taken as energy dissipation rate ϵ ($\epsilon=C_D k^{3/2}/\ell$). In this case $\alpha = 3/2$ and $\beta=-1$ and the model known as k-ϵ turbulent model, which has been favoured by more workers than any other. Hence, the two equations, when isotropic turbulence is assumed, becomes:-

$$\frac{Dk}{Dt} = -\frac{1}{\rho}\frac{\partial}{\partial x_k}\left[\frac{\mu_t}{\sigma_k}\frac{\partial k}{\partial x_k}\right] + \frac{\mu_t}{\rho}\left[\frac{\partial U_i}{\partial x_k} + \frac{\partial U_k}{\partial x_i}\right]\frac{\partial U_i}{\partial x_k} - \epsilon \qquad (5.1.3)$$

$$\frac{D\epsilon}{Dt} = \frac{1}{\rho}\frac{\partial}{\partial x_k}\left[\frac{\mu_t}{\sigma_k}\frac{\partial \epsilon}{\partial x_k}\right] + \frac{C_1\mu_t}{\rho}\frac{\epsilon}{k}\left[\frac{\partial U_i}{\partial x_k} + \frac{\partial U_k}{\partial x_i}\right]\frac{\partial U_i}{\partial x_k} - \frac{C_2\epsilon^2}{k} \qquad (5.1.4)$$

$$\mu_t = \frac{C_\mu \rho k^2}{\epsilon} \qquad (where\ C_\mu = C_D C_v,\ \mu_t = C_v k^{1/2} \ell) \qquad (5.1.5)$$

The constants in these equations have been found to take the following values

$C_D = 1.0$, $C_\mu = 0.09$, $C_1 = 1.44$, $C_2 = 1.92$, $\sigma_k = 1.0$, $\sigma_k = 1.3$

values of C_μ and C_2 were deduced from experimental data on the decay of turbulence behind a fine wire screen, and C_1 was estimated from near-wall turbulence. Therefore final tuning of all C's and σ's were done by computer optimisation (Lauder et al, 1974).

However, these constants may need to be changed in order to accommodate the effects such as curvature, low Re number and near wall etc.

iv). Stress equation models (multi-equation models)

a). Reynolds stress models:- The main practical limitation of classes i) to iii) is the assumption of isotropic eddy viscosity. The same values of ν_t are taken for different $\overline{u_i u_j}$ terms. In order to account for the different development of the individual stresses, transport equation for $\overline{u_i u_j}$ have been introduced. In this model one needs to solve the equation for the turbulence energy dissipation rate ϵ, in addition to those for $\overline{u_i u_j}$ for the length scale. Models employing transport equations for $\overline{u_i u_j}$ are called second order closure models, since second order correlations are treated directly. Because of the complexity and the large amount of computational effort required, the model has not been widely used.

b. Algebraic stress models:- In Reynolds stress models, there are differential transport equation for each component of $\overline{u_i u_j}$ in addition

to 'ϵ' equation. To reduce the computational effort, Rodi (1979) proposed an algebraic relation for calculating the Reynolds stress. The convection and diffusion terms in the transport equation of $\overline{u_i u_j}$ are replaced by model approximations, reducing the equations to algebraic equations, having k and ϵ terms. Thus the k and ϵ equations have to be added in order to complete the turbulence model. Therefore the algebraic expressions together with k and ϵ equations form this model.

k-ϵ modelling

i) Theory:- The effective viscosity hypothesis connects the stresses to the mean velocity gradients (for incompressible flow) through the relation:-

$$\rho\overline{u_i u_j} = \tau_{eff} = \frac{2}{3}\rho k\delta_{ij} - \mu_{eff}\left\{\frac{\partial U_i}{\partial x_j} + \frac{\partial U_j}{\partial x_i}\right\} \qquad (5.1.6)$$

when i=j $\rho\overline{u_i u_i}$ = normal stress

i≠j $\rho\overline{u_i u_i}$ = Reynolds stresses and the above equation (5.1.6) reduces to original Boussinesq's turbulent-viscosity concept. In the past, isotropic turbulence has generally been assumed and the same μ_{eff} has been used for each of the components of this equation .

k is defined as $k = \frac{1}{2}\overline{u_i u_i}$ (5.1.7)

and

ϵ is defined as $\epsilon = \frac{\mu}{\rho}\left\{\frac{\partial u_i}{\partial x_j}\frac{\partial u_i}{\partial x_j}\right\}$ (5.1.8)

from Prandtl/Kolomgrov formula and taking length scale = scale of energy containing eddies.

$$\mu_{eff} = C_\mu \rho\, k^2/\epsilon. \qquad (5.1.9)$$

The values of k and ϵ are obtained by solving the k and ϵ transport equation. The transport equation for 'k' is:-

$$\underset{(A)}{\frac{\partial k}{\partial t}\bar{\rho} + \frac{\partial}{\partial x_j}\overline{\rho U_i k}} = \underset{(B)}{-\rho\overline{u_i u_j}\frac{\partial U_i}{\partial x_j}} - \underset{(C)}{\frac{\partial}{\partial x_j}\left[\frac{1}{2}\overline{\rho u_j u_i u_j} - \mu\frac{\partial k}{\partial x_j} + \overline{P' u_j}\right]} + \underset{(D)}{\mu\left[\overline{\frac{\partial u_i}{\partial x_j}}\right]^2} \qquad (5.1.10)$$

In this equation term (A) denotes the change along an averaged stream lines while term (B) is the production of turbulent kinetic energy; its definition implies that it is a positive term. Term (C) represents the transport of k due to turbulent and viscous actions. The last term (D) is the dissipation of k due to viscosity action. By analogy to the laminar transport of k, its turbulent transport is modelled as:-

$$\frac{1}{2}\bar{\rho}\,\overline{u_i u_i u_j} - \mu\frac{\partial k}{\partial x_i} + \overline{P' u_i} = -\frac{\mu_{eff}}{\sigma_k}\frac{\partial k}{\partial x_i} \qquad (5.1.11)$$

Thus, finally, the modelled kinetic energy equation for the steady state stands as:-

$$\frac{\partial(\rho U_i k)}{\partial x_i} = \frac{\partial}{\partial x_i}\left[\frac{\mu_{eff}}{\sigma_k}\frac{\partial k}{\partial x_i}\right] - \rho\overline{u_i u_i}\frac{\partial U_i}{\partial x_i} - \rho\epsilon \qquad (5.1.12)$$

where $\rho\overline{u_i u_j}\dfrac{\partial U_i}{\partial x_j} = \mu_{eff}\left[\dfrac{\partial U_i}{\partial x_j} + \dfrac{\partial U_i}{\partial x_i}\right]\dfrac{\partial U_i}{\partial x_j} - \rho\epsilon$ *(from equation 5.1.6)*

After some mathematical manipulation (Launder, 1974 and Khalil, 1982), the transport equation for ϵ is given as:-

$$\frac{D\epsilon}{Dt} = -2\nu\left[\overline{\frac{\partial u_i}{\partial x_\ell}\frac{\partial u_j}{\partial x_\ell}} + \overline{\frac{\partial u_\ell}{\partial x_i}\frac{\partial u_\ell}{\partial x_j}}\right]\frac{\partial U_i}{\partial x_j} - 2\nu\overline{\frac{\partial u_i}{\partial x_\ell}\frac{\partial u_j}{\partial x_\ell}\frac{\partial u_i}{\partial x_j}} - 2\nu\left[\overline{u_i\frac{\partial u_i}{\partial x_\ell}}\right]\frac{\partial^2 U_i}{\partial x_j \partial x_\ell} - 2\left[\overline{\nu\frac{\partial^2 u_j}{\partial x_j \partial x_\ell}}\right]^2$$

$$- \frac{\partial}{\partial x_j}\left[u_{j\epsilon} + \frac{\nu}{\rho}\overline{\frac{\partial P}{\partial x_\ell}\frac{\partial u_j}{\partial x_\ell}} - \nu\frac{\partial \epsilon}{\partial x_j}\right] \qquad (5.1.13)$$

The net rate of change of ϵ for a fluid element is equal to the net imbalance due to the following interactions (given by Khalil, 1982).

i). Generation due to vortex stretching by mean flow.

ii). Generation due to vortex streching by turbulence.

iii) Secondary generation by mean flow.

iv). Destruction of ϵ due to tendency of viscosity to smear out velocity variation.

v). Diffusive transport arising from velocity and pressure fluctuations and from molecular diffusion.

The final modelled form of the ϵ equation according to Jones et al (1973) is expressed for steady state as:-

$$\frac{\partial(\rho\epsilon U_i)}{\partial x_i} = \frac{\partial}{\partial x_i}\left\{\frac{\mu_{eff}}{\sigma_\epsilon}\frac{\partial\epsilon}{\partial x_j}\right\} - \frac{\rho\epsilon}{k}(C_1 G_K + C_2\epsilon) \qquad (5.1.14)$$

In the above equation $G_K = \overline{u_i u_i}(\partial U_i/\partial x_j)$ and C_μ , C_1 and C_2 are the constants of the turbulence model. C_μ was obtained from equilibrium flows, C_1 from turbulence decay behind grids and C_2 from computer optmization. Launder et al (1974) after extensive examination of free turbulent flows, recommended that the constants should take the following values:-

$$C_\mu = 0.09,\ C_1 = 1.44,\ C_2 = 1.92,\ \sigma_k = 1.0,\ \sigma_\epsilon = 1.22$$

For axisymmetric jets it was found necessary to modify two of the constants; continued efforts have failed to devise any single set of constants that will predict their behavior as well as that of the plane free shear flows and the plane or axisymmetric wall flows. The following recommendation has therefore been made by Launder (1974):-

$$C_\mu = 0.09 - 0.04f' \qquad (5.1.15)$$

$$C_2 = 1.92 - 0.0667f' \qquad (5.1.16)$$

$$\text{where } f' = \left|\frac{y}{2\Delta U}\left\{\frac{\partial U_{c1}}{\partial x_1} - \left|\frac{\partial U_{c1}}{\partial x_1}\right|\right\}\right|^{0.2} \qquad (5.1.17)$$

Here reference is made to U_{C_1} the velocity at, and in the direction of the symmetry axis of the flow; Y is the radial width of the mixing region, and ΔU is the axial-direction velocity difference across the width of this region. This recommendation is especially tailored to fit the experimental data for axisymmetric jets and little universality can truly be claimed for it.

However, Rodi (1972) has found that a further modification of the constants (C_μ, C_1 and C_2) is required in turbulent flows where velocity gradients are so weak that the rate of turbulence-energy generation is appreciably less than the energy dissipation rate. It also needs to be emphasised that the great majority of flows of interest to mechanical engineers are ones adjacent to, and often enclosed by, rigid surfaces. The presence of a wall enforces steep velocity gradients; consequently the level of turbulence-energy production is always large; the first set of turbulence model constants are therefore nearly always applicable. But ad hoc corrections to the model or to the "constants" said to be necessary in order to procure agreement with experiments are as follows:-

i). Boundary layer on convex and concave wall.

ii). Strongly swirling and recirculating flows

iii) Axi-symmetric jets in stagnant surroundings

iv). Three dimensional wall jets

v). Gravity-stratified flows

vi). Flow involving chemical reaction

v). Two-phase flows

ii). Boundary and initial conditions

The following general conditions and rules are prescribed and observed when specifying boundary conditions (Gosman, 1987).

i). No slip at wall

ii). Conditions applying at surface or axes of symmetry

iii) Precise knowledge of the condition prevailing at outflow boundaries is often unnecessary if the Reynolds number is not too small ($>10^2$) and the velocity vector is nearly normal to the boundary and everywhere outwards directed. These conditions are usually sufficient to allow the outflow condition to be approximated by simple gradient assumption with minimal effect upstream (see also Patankar, 1980). If this requirement is not satisfied then detailed specification of the outflow condition is needed.

iv). The boundary conditions at inflow surfaces are influential, although this need not apply with equal weight to all variables.

v). In the case of unsteady flows the temporal variation of the inflow conditions, where occurring, also require specification.

a).Specification of inflow turbulence quantities:- One of the obvious answers would be to locate the inflow boundary where the flow structure is especially simple, or the effects of the uncertainties are acceptably small in the downstream region of interest. These two methods can be employed, thus for example, the inlet duct could be shaped as a smooth nozzle aimed at giving a low turbulence plug flow at inlet, or as a long straight duct giving a fully developed exit flow. There are obviously applications for which the full measurement of inlet turbulence condition cannot be avoided. The following are the more obvious alternative ways of arriving at 'ϵ' .

i). By direct measurement, entailing determination of local instantaneous velocity gradients. This appears never to have been done, presumably because of the difficulties involved.

ii). Indirectly, by experimental determination of the balancing terms in ϵ containing a transport equation like that of k which, it should be noted, should be in its unmodelled form. It has dual drawbacks of involving effect and uncertainty of the pressure-containing ones to LDA, which necessitates estimating them.

iii). Approximately, through measurement or estimation of the length

scale (ℓ, length scale of energy containing eddies) which, together with k allows ϵ to be obtained from equation $\ell=C_D k^{3/2}/\epsilon$ or similar. This has been by far the most popular approach, with ℓ being invariably estimated rather than measured. The following values were found from experimental meaurements of fully developed flow and are the most common prescription at present.

$$k_{in} = 0.00325\ w_{in}^2$$
$$\epsilon_{in} = 0.164\ k_{in}^{1.5}/\ell_m \qquad (5.1.18)$$
$$\ell_m = 0.09*\text{height} \quad (\text{note:- } 0.164\ell = \ell_m).$$

Where the subscript 'in' indicates the inlet condition.

b). Specification of solid boundary condition:- This region close to the wall where the shear stress τ is uniform, the length scale increases linearly with distance from the wall. Now, using the differential equation governing the variable ϵ, the logarithmic law of the wall, $\mu_t=C_\mu \rho k^{1/2}/\ell$ and also because the length scale ℓ is proportional to the distance from the wall , an algebraic relation (Launder, 1974) between the constants can be found as:-

$$\frac{n^2}{\sigma_t} + \frac{C_1 C_\mu^{1/2}}{K^2} - \frac{C_2 C_\mu^{1/2}}{K^2} = 0 \quad \textit{where K= Von Karman's constant} \qquad (5.1.19)$$

Closer to solid walls the local Re number of turbulence ($\equiv k^{1/2}\ell/\nu$, where $\ell=k^{3/2}/\epsilon$) is so small that viscous effects dominate over turbulent ones. There are two methods of accounting for these regions in numerical methods for computing turbulent flows the wall-function methods and the low Re number modelling method.

The wall function method :- This method is the one which has been most widely used. The first feature to make sure of when using the wall function method is that the first grid is sufficiently remote from wall, for $(k^{1/2}\ell/\nu)_{grid}$ to be much greater than unity, so much greater in fact that the viscous effects are entirely overwhelmed by the turbulent ones.

The flux of momentum to the wall is then supposed to obey the

relation:-

$$\frac{U_n \quad C_\mu^{1/4} k_n^{1/2}}{(\tau/\rho)_{wall}} = \frac{1}{K} \ln\left\{ E\, y_n \frac{(C_\mu^{1/4} k_n)^{1/2}}{\nu} \right\} \qquad (5.1.20)$$

E = a function of the wall roughness, approximately equal to 9.0 for a smooth wall. And subscript 'n' refers to the value at a node adjacent to the wall.

The value of k for the grid point, is supposed to be known. It should be calculated from the regular balance equation of the finite-difference grid, diffusion of energy to the wall being set equal to zero (in the absence of better information). When calculating this value of k, it is necessary to assign a value for the average energy dissipation rate over the control volume. This is to be deduced from the assumption that:-

$$\int_0^{y,n} \epsilon dy = C_\mu \frac{k^{3/2}_n}{K} \ln\left\{ \frac{E y_n (C_\mu^{1/4} k_n)^{1/2}}{\nu} \right\} \qquad (5.1.21)$$

The rationale for these recommendations comprise the following main points:-

a) The wall function reproduces identically the full implications of the "logarithmic velocity profile" when a uniform shear stress prevails in the first grid layer, and the generation and dissipation of energy are in balance there.

b). The appearance of the logarithmic function (in equation 5.1.21) results from the necessity to presume ϵ to be proportional to $k^{3/2}/y$, coupled with a further modelling of the wall function on the constant shear stress situation.

Extra empirical information can be inserted by way of wall functions (for example, roughness and mass transfer through the wall). When the 'wall' is slightly flexible as in the interface between two immiscible

liquids further influences are present which can, perhaps, be expressed by way of the formulae. However, there is much research to be done in this branch of turbulence-model theory.

The low Re number modelling method:- several authors have sought to devise turbulence model equations which are valid throughout the laminar, semi-laminar and fully turbulent regions. Extra terms are included in the k and ϵ equation to account for laminar diffusive transport and destruction. And the following constants were set to vary as:-

$$C_\mu = C_{\mu\infty}\ exp[-2.5/(1 + R_t/50] \qquad (5.1.22)$$

$C_2 = C_{2\infty}$ exp[1.0 - 0.3 exp-R_t] where R_t denotes the turbulence Re number and $C_{\mu\infty}$ and $C_{2\infty}$ are the values assumed by C_μ and C_2 in a fully turbulent region.

4). Extension to flows with non-isotropic effective transport coefficients;-

This extension to the k-ϵ model would form an equivalent algebraic stress model.

5.1.3 Modelling multi-phase flows

The knowledge of the properties of turbulent flows is an essential task, but as pointed out before, the randomness of the turbulent motion of a fluid remains to be solved. In the case of multi-phase flows the difficulty of the problem increases many fold. For example, homogeneously dispersed fine particles in a turbulent field, have many complicated relationships between each other. There exists not only the response of the particles to the turbulent motion of the fluid but also the reaction of the particle collective on the turbulence in the fluid, this effect naturally increases with higher particle concentration. If the particles are small enough, so that their inertial response-time can be neglected they will follow completely the fluid fluctuations but the energy which they consume will cause a

damping effect on the turbulence. On the other hand if the particles are big enough they themselves will function like disturbing cells from which new turbulent vorticies will be produced. These are some of the mechanisms in dispersed multi-phase flows, but the complexities of general multi-phase situations are enormous. Therefore this modelling review is mainly concentrated on dispersed multi phase flows as this is more relevant to the present study.

Although the present application comes under the two-component category two phase flow and two-component flow imply, a flow that consists of same chemical substance and a flow that does not. Yet the mathematics which describe these flows are identical especially in the case of dispersed flows. Therefore, it does not really matter which definition is chosen, the treatment would be the same.

Methods of multi-phase flow analysis can be classified in the ascending order of sophistication as follows (see also fig. 5.1.1):-

1). Correlations

2). Analytical models-these studies have followed two methods of approaches:-
   i). Treating the dynamics of single particles and then extending to a multiple particle system.
   ii). Modifying the continuum mechanics of single phase fluids in such a way in order to account for the presence of particles.

Therefore they can be divided as follows, where a) and b.2) below take up the approach in ii) and b.1) the approach in i).

a). Homogeneous models

b). Separated flow models
   b.1) Only the continuous phase is a continuum, discrete formulation for dispersed phase, 'Lumped models'.
   b.2) Both phases in interpenetrating continuum.

1). Correlations

Correlations of experimental data in terms of chosen variables are convenient ways of obtaining design equations with a minimum of analytical work. The crudest correlations are mere mathematical exercises, while more advanced techniques use dimensional analysis or the grouping of several variables together on a logical basis.

2). Analytical models

a). *Homogeneous models:-* Homogeneous flow theory provides the simplest technique analysing two-component flows. Suitable average properties are determined and the mixture is treated as a pseudofluid that obeys the usual equations of single-component flow. That is, this model assumes that each component flows at the same velocities with pseudo properties. Therefore, the analysis implies that the phases are in dynamic and thermodynamic equilibrium and all of the standard methods of fluid mechanics in single phases can then be applied. In general the applicability of these models is limited to high mass flux situation where the relative velocity is a small fraction of the individual component velocities. This analysis is also sometimes known as local homogeneous flow (LHF) analysis.

b). Separated flow models

These models are divided into two major approaches of analysis. In general form, continous phase is considered as a continuum and treat the particle dispersion either in the frame work of an Eulerian reference system or the particles are tracked through the flow field using a Langrangian reference system. In the Eulerian approach, the discrete particles are considered as a continuous field or a set of continuous fields, depending on whether the particles are monosized, or not. This is also known as the interpenetrating continuum approach. In the Langrangian approach, the dispersed phase is divided into representative groups (by size) whose motion and transport are tracked through the flow field to obtain trajectories, and these are sometimes known as 'lumped' models. The interpenetrating continuum approach is

now becoming more popular among researchers due to its adaptability to complex dispersed flows, compared to the relativly cumbersome tracking approach.

b.1). Lumped models:- In general seperated flow models treat the continuous phase as a continuum and discrete formations are used for the dispersed phase. Discrete formation involves dividing the dispersed phase into representative groups (by size) whose motion and transport are tracked through the flow field using a Langrangian reference system and then extend to multiple particle systems Typical values of these representative groups are in the order of 1000-5000. The analysis divides into to two types a). deterministic seperated flow (DSF) analysis where the dispersed phase and turbulence interactions are ignored b). stochastic seperated flow (SSF) analysis, where the effects of dispersed phase and turbulence interaction are considered.

b.2). Interpenetrating continuum approach:- These models examine the common features of dispersed two-phase flows from a continuum -mechanical approach. The approach is based on the view that it is sufficient to described each material as a continuum, occupying the same region in space. This new 'material' consists of two interactive materials called phases (or components). The two-phase material is often called the mixture. In analogy with continuum mechanics, we shall have to specify how the mixture interacts with itself.

Drew (1983) instructs researchers who do not subscribe to this view and treats the mechanics of the two materials, plus the dynamics of the interface as fundamental, and uses derived results and or measurements to gain the understanding needed for their particular application, to consider the approaches to gas dynamics. Most scientists believe that a gas is a collection of many molecules that move, vibrate and interact in a complex but describable way. In spite of the knowledge of the 'correctness' of this model, many scientists and engineers use a continuum model for gas dynamics. For example, flow around an airfoil is a problem in continuum gas dynamics and the computers are not big enough to treat it as a problem in molecular

dynamics.

Indeed the concept of interpenetrating continua is natural in mixtures where the dipersion occurs on the molecular level and Fick's idea of diffusion is valid. Several influential books on general two phase flow that use this approach are i). Fluid Dynamics of Multi Phase Systems by Soo (1967), ii). One Dimensional Two Phase Flow by Wallis (1969) iii). Flowing Gas-Solid Suspensions by Boothroyd (1971). Wallis' approach was strongly influenced by gas-liquid flows and dealt with the basic concept of interpenetrating continua. Soo's work was largely based on particle/fluid flows. He assumed interpenetrability from the start, and included forces in the momentum equation known from experiments or inferred from calculations. Boothroyd was interested in particle-gas flows, and contributed to ideas on turbulence and drag reduction.

We give below the general assumptions given by Abou-Arab for the derivation of the general governing equations (1987), for turbulent two phase flows.

i). Both phases behave macroscopically as a continuum, but only the carrier fluid behaves microscopically as a continuum.

ii). The dispersed phase consists of particles or dropets spherical in shape and uniform in size. But this may be extended to a nonuniform size distribution in a later stage.

iii). The volume fraction of dispersed phase is such that no collisions occur between the particles or droplets. This assumption renders the equations valid only for dilute suspensions.

iv). Neither the suspended matter nor the carrier fluid undergoes any phase changes. He suggested the extension to phase changes is a simple task.

v). The bouyancy force is mainly due to the density difference between the phases.

vi). The deposition (if it exists) is entirely due to fluid turbulence.

vii). The roughness effect is ruled out by considering the wall to be smooth.

This approach mainly divides into two methods i). the more general approach, the two fluid-model and ii) drift flux model.

b.2.1). *The two-fluid model*:- the two fluid model is the most general form of the seperated flow models. Partial differential equations for conservation of mass, momentum and energy are written for each phase (component). Constitutive relationships are needed for the fluid properties and to specify interaction between the two phases (components). While the two fluid model may be appealing from a fundamentalist view-point, the complexity of formulation, specification of the interfacial conditions, and computer storage and costs, make the full two-fluid model inconvenient to use. According to Ishii (1975) the two-fluid model is most appropriate if the two phases are weakly coupled.

b.2.2). *Drift flux model*:- if the motion of the two phases (components) are strongly coupled, as is usually the case with dispersed flows a major simplification to the two fluid model can be made. Instead of writing two momentum conservation equation (one for each phase), a single momentum equation can be written (eg. coupling the two equations with drop drag force) for the mixture as a whole, resulting in the drift-flux model. The relative velocity between the phases is specified through constitutive relations, or algebraic relationships. Most of the troublesome interfacial equations in the two-fluid model are eliminated in this approach.

5.2 Background and Review

5.2.1 Computer simulation of water in oil

Segev (1984) solved the three dimensional concentration profile of the dispersed phase (water droplets) in a circular pipe by numerically solving the diffusion-convection equation in fully developed pipe flow field. His approach is related to Homogeneous models. But he included a source term in his diffusion equation to account for the relative velocity between the water droplet and oil. Hence his diffusion-convection equation became (see section 1.3 for more details):-

$$\frac{\partial c}{\partial t} + U.\nabla c = V.\epsilon\nabla c - \nabla.(Wc)$$

He assumed that the relative velocity is equal to the droplet settling velocity in the Stokes flow regime, given by:-

$$W = \frac{g}{18}\left\{\frac{\rho_p - \rho}{\mu}\right\}d^2$$

He also obtained a closed-form solution, for a situation where the concentration profile is fully developed.

Baker (1985, 1988) developed the Segev's model to obtain concentration of water downstream of a mixing pipe section, where the velocity profile is undeveloped. He assumed that a "bend like" secondary flow will be found downstream of various pipe fittings. Therefore, he described inlet to a region of severe mixing with an idealised pipe bend secondary flow and a solid body rotation, and the former was assumed to decay in a distance similar to that for a bend. In order to account for the high turbulence levels in a mixing region, he obtained the turbulent dispersion coefficient by multiplying the value of fully developed flow by a factor, and also introduced a factor to represent the decay of the turbulence downstream.

Baker (1985 and 1988) also made use of an expression for the decay of turbulence behind a gauze by Batchelor (1953) to obtain the decay of turbulent viscosity downstream of a plane where high turbulence has been created (eg. flow discharging from a smaller to larger pipe) as:-

$$\nu_t = 0.4.U^*R[(U_{jet/U})^2/(z/L+1)+z/L(z/L+1)]$$

Where U, U_{jet} are mean velocity of the larger and smaller pipes respectively, L is the distance required for ν_t to decay to fifty percent of its initial value. The "Bend-like" secondary flow patterns were obtained by using the following expressions:-

$$V_r = (c'/r).J_1(kr)\text{Cos }\theta$$
$$V_\theta = (c'/r).J_1(kr)\text{Sin }\theta - c'kJ_0(kr)\text{Sin }\theta$$

where kR =3.83 and R is the pipe radius, J_0 and J_1 are Bessel functions. To account for the decay, the secondary flow was multiplied by exp(-0.22.z/D). This factor was empirically obtained to conform to previous experimental data. For the "swirl- like" secondary patterns a solid body rotation was assumed:-

$$V_r = 0$$
$$V_\theta = v_{\theta o}(r/R) \quad \text{for} \quad r \neq R$$
$$V_\theta = 0 \quad \text{for} \quad r=R$$

Since the decay of swirling flow is slow, the decay factor was taken as exp(-z/20D).

Rodi's (1979) has given values of σ_t (Schmidt Number) as:-

0.9 for near-wall flows
0.5 for plane jets and mixing layer
0.7 for round jets.

Therefore, with reference to these values Baker (1985) has chosen a value of σ_t=0.5 regions where severe mixing is been taking place.

5.2.2 Multi-phase flow simulations

The approach attempted in this study, is related to interpenetrating continuum method. Therefore we would place the emphasis on the models that were used and published by previous researchers as given below. Their work is summarised in the table that follows.

i). Deposition and entrainment in pipe flow of a suspension by Soo and Tung (1972).

ii). Numerical prediction of the fully developed two-phase (air-solids) flow in a pipe by Militger (1986).

iii). The modelling of tangential and axial agitators in chemical reactors by Pericleous and Patel (1987).

iv). Mathematical simulation of hydrocyclone by Pericleous (1987).

v). Mathematical calculations of two-phase turbulent round jet by Danon, Wolfshtein and Hetsroni (1977)

Abou-Arab (1987) and Drew (1983) have given a general description of the treatment of these models in turbulent flow fields.

Ref. No. of Previous work	i	ii	iii	iv	v
Flow field	fully developed turbulent	simul. by k-ϵ model	const. vis. model= 100 lam.vis	mixing length model	one eqn. model
Continuous phase	liquid	liquid	liquid		liquid
Disperse phase	solid;range 0.7 mm	solid;range dia.>250μm	bubles;range 0.5to 500μm	solid;range 1 to 15μm	particles
Loading		6%		10%	
Sc. number					
Turbulent const. C_μ, C_1,C_2,σ_k		0.9, 1.44, 1.92, 1.0, 1.3			
Convergence criterion			continuity error be< 0.1% of a typical vol. flow		
Two-phase model	modified homogeneous model	two-fluid model with source term for interphase slip	homogeneous model with algebraic slip approach	homogeneous model with algebraic slip approach	interpen-etrating continuum approach
Remarks	identifies a sticking probability, considers lift force		soln. was not checked for grid independence		

The above table shows, the published data and information in these references are far from complete.

5.2.3 Jet mixing of miscible liquids in pipe cross flow

Much of the published work on jets in cross-flow has centred on the unconfined problems. The theoretical work of these problems have mainly involved application of integral methods which suffer from two drawbacks, firstly an entrainment function must be specified, and secondly the jet cross section is usually assumed to be circular. The extension of these methods to predict the present problem is, however, unlikely to be profitable. Patanker et al (1977) have used a finite difference scheme together with a two-equation turbulence model to solve an unconfined problem and obtained good agreement with experimental data for velocity ratios from 2 to 10.

For confined crossflow, the experimental data are much scarcer. Stoy and Ben-Haim (1973) made measurements of jet trajectories for a single blockage ratio in 2-D flows. The closest study to the present problem was published in papers by Maruyama et al (1981, 1983). Their experimental work was directed towards optimisation of jet mixing of air in circular pipe cross flow. Even here the data is by no means plentiful, they do, however, provide some basis for comparision and assessment of theoretical predictions. Computation of a round turbulent jet discharging into a confined 2-D channel cross flow was conducted by Jones et al 1979), Tatchall (1975) and Kawashima et al (1983). Tatchell and Karwashma et al were concerned only with very low velocity ratios and Jones et al (1979) obtained good qualitaive agreement with experimental data.

The scope of previous theoretical work was limited. The analytical approaches mainly used integral methods which required empirical values for some of the parameters. None of the work was associated with jet mixing of immiscible liquids.

5.2.4 Complex elliptic nature previous flow simulations by volume control differencing

reference	turbulent model	convergence criteria	no. of sweep to converge	grid	application
Sampath and Ganesan (1987)	k-ε	the sum of the continuity residual for the CVs was less than 0.1%		25*10*9	gas-turbine combustor
Pericleous and Patel(1987)	uniform eddy vis. based on jet width	change in variable <.001 & total continuity residual <0.1% of vol. flow	400	30*50	agitators in chemical reactors
Pericleous (1987)	mixing length		500	30*25	hydro-cyclone
Shah and Markatos (1987)	k-ε		260 time steps	22*22 *22	internal combustion engine
Pantanker, et al (1977)	k-ε	the change in each local vel. is <0.1% of main stream velo.	80	10*15 *15	jet in cross flow
Jones and McGuirk (1979)	k-ε		100	20*15 *15	jet in confined cross flow

5.2.4 Cont.					
Green and Whitelaw turbine (1984)	k-ϵ		700	10*20 *30	gas-combustor
Jan Jeen Seppen (1982)	fixed eddy viscosity (from measured values)			12*11 *12	internal combustion engine

All of the above researchers used the "wall function method" for the treatment near the wall.

5.3 Introduction to Phoenics computer code

5.3.1 The Mathematical Basis of Phoenics

Phoenics solves discretised versions of the partial differential equations governing the balances of mass, momentum, energy and of scalar quantities such as chemical-species concentration and indeed of any entity which can be expressed in terms of:-

i) Time dependence
ii). Diffusion
iii) Convection and
iv). Source terms

Phoenics embodies a finite difference formulation of the differential equations and is an acronym for Parabolic, Hyperbolic or Elliptic Numerical Integration Code Series. In order to obtain the finite difference equations, the conservation equations are generally discretized by i) integration over elementary control volumes for each

grid node in the computational domain or ii) interpolation between grid nodes using Taylor series expansion (or polynomial fitting). Phoenics uses the former approach, which is sometimes called the finite-volume formulation (or macro-integral approach) and is very popular among complex flow problems. The finite difference equations are derived by use of the 'staggered' grid arrangement and with a hybrid implicit scheme. Staggered grid arrangement (as shown below) is such that the velocities are stored at locations on the wall of the cells and temperature pressure and concentration etc. are evaluated for the location like W, P, N and E (or the values of velocities u, v, and w are stored at location midway between the nodes). Within each cell the fluid property values are regarded as constant. The accuracy of the procedure will depend on the number and therefore the size of the cells used. The finite difference algorithm is based on the well known SIMPLE (Semi-Implicit Method for Pressure Linked Equation) algorithm. It handles elliptic problems parabolically at each slab (cross section X-Y plane) and then marches forwards and backwards iteratively until all the boundary conditions are satisfied. Therefore the whole numerical procedure can be summarised as follows:-

Velocity convention- staggered grid method

Finite difference method- finite volume/macro integral approach

Gradient for convection and diffusion- through 'hybrid' differencing as default, but upwind differencing is also available as a option. The 'Hybrid scheme' which is a combination of the so- called central and upwind differencing schemes where central diference is used when $Pe \leq 2$ *and upwind difference for convection, neglecting diffusion, is used when* $Pe \geq 2$*. The rationale behind this method is given in Patankar et al (1980).*

Solution method- SIMPLEST algorithm, stands for SIMPLE shortened.

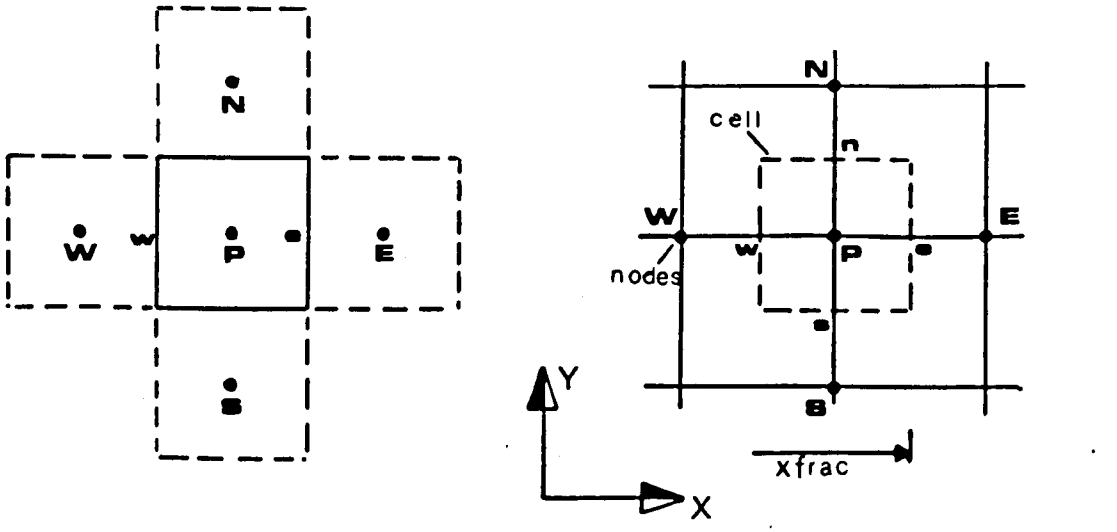

The resulting algebraic equations representing conservation of matter, momentum energy and species in each cell are then of the form:-

$$a_p\Phi_p = \Sigma a_i\Phi_i + b \qquad i = N, S, H, L \qquad (5.1.23)$$

where a_i are the coefficients, b is a representaive source for Φ and the subscipts P, N, S, H, L, T represents the control, North, South, High, Low and Old grid node locations.

The computation proceed to convergence via a series of continuity satisfying velocity fields. Though a method for a nonlinear unsteady problem is claimed to be noniterative, it is , in fact, accepting that the solution at the end of one iteration is sometimes used to obtain the steady state solution at the end of many time steps . Such time steps are truly iterations and sometimes known as false time steps.

A method of monitoring convergence is to examine how perfectly the discretization equations are satisfied by the current value of the dependent variables. Therefore at each grid point a residual 'Res' can be calculated from:-

$$Res = \Sigma\, a_{nb}\,\Phi_{nb} + b - a_p\Phi_p \qquad (5.1.24)$$

When the discretization equation is satisfied 'Res' will be zero. Incidentally the quantity 'b' in the pressure correction equation,

which is the residual of the continuity equation, can be used as one of the indicators of the convergence of the iterative process.

5.3.2 The solution procedure:- The linkage between the velocity components and pressure is handled by estimating the pressure distribution first and the momentum equations are solved to obtain a preliminary velocity field. This in general does not satisfy the continuity equation. Therefore, in the next stage, appropriate corrections to the pressure field are computed such that the resulting corrections to the velocity field will bring the latter into conformity with the continuity equation. The governing equations are non-linear and coupled. Thus, the values depend on the values of the variables themselves. This is handled by iteration; the coefficients are continually recalculated until the resulting values of the variables cease to change. Usually the equations (elliptic) are solved slab-by-slab by means of a slab-wise linear solver which proceeds as follows (a slab is a two dimensional section, for example a cross section of a pipe):-

a). Treat off-slab values (H, L, T) as known(T ≡ grid node at previous time), reducing the equations (Cham, 1986) to:-

$$a_p\Phi_p = a_n\Phi_n + a_s\Phi_s + a_e\Phi_e + a_t\Phi_t + b' \qquad (5.1.25)$$

where $b' = b + a_h\Phi_h^* + a_l\Phi_l^* + a_t\Phi_t^*$

Φ^* = the value which they possessed before the updating sweep

b). Postulate the existence of the subsidiary equation set:-

$\Phi_p = N\Phi_n + E\Phi_e + B$ and derive equations for N, E, and B by, algebraic substituion, in terms of a_n, a_e, a_w, b, Φ_{nw} and Φ_{se}.

c). Compute values of N, E, and B from these equations by recurrence starting in the south west corner.

d). Compute values of Φ_p starting in north-east corner.

e). Repeat the process until convergence.

Iteration is needed because the B's contain Φ's for the north-west and south-east neighbours of point P.

The sequence of operations are as follows (fig. 5.2.1) and appropriate equations are given in Patankar (1980, p126):-

a). Guess the pressure field P^*.

b). Solve the momentum equation to obtain U^*, V^*, W^*.

c). Solve the P'(pressure correction) equation and calculate $P=P^* + P'$

d). Calculate U, V, W, from their starred values using the velocity correction formulas.

e). Solve the discretization equation for other Φ's if they influence the flow field.

f). Treat the corrected pressure P as a new guessed P^* and return to step 'b' and repeat the whole procedure until convergence.

5.3.3 Code structure

Phoenics has a three-part structure (see fig. A5.1 in Appendix) namely satellite for data input, Earth for the main numerial computation and 'Photon' a graphics package for post processing.

In 'SIMPLE' algorithm, the number of iterations needed to reach a fixed level of convergence is said to be proportional to number of grid points 'N'.

More generally, the initial input data can be set in satellite by use of its own language called 'PIL', the file so created is known as Q1. A empty Fortran sub-program called 'SATLIT' may be filled with the user's own fortran coding when his requirements fall far out of general situations. The 'Earth' program receives a formulated file (DF10) of data settings written by the satellite. 'EARTH' is in two parts, open and closed. The open part, in which the Fortran coding can be incorporated or modified by the user, contains all that he needs to concern himself with, especialy the mechanisms of the fluids. The closed part sets up the finite difference equations according to the fundamental balance laws and solves them. In other words it can be

regarded as a mere logic box, a slave which works out meticulously the mathematical consequences of assumptions which its master commands it to make and deals with the mathematics of numerical integration in accordance with the solution procedures 'Simplest' algorithm (Cham Ltd., 1986).

By contrast, the open part deals with the less certain components of a flow-simulation calculation for example the representations of interface friction and various models of turbulence. This open portion is called 'GROUND' is a set of Fortran subroutines (empty subroutines the user fills with his own coding) which are called from within 'EARTH' at times in the solution cycles (see fig. A5.2 in Appendix). These subroutines concern themselves with modification to boundary conditions, fluid properties, sources of mass, momentum and energy, convergence and print-out control, and indeed whatever aspect of the flow-simulation process the user wishes to control.

Turbulent model constants in Phoenics:- one thing that should be noted is that in Phoenics code the turbulent constants are related to mixing length scales rather than to turbulent scales where ($0.1643\ell=\ell_m$).

Since $\mu_t = 0.09k^{1/2}\ell = 0.09k^{1/2}\ell_m/0.1643$

$= 0.5478k^{1/2}\ell_m$

Therefore, $C_\mu = 0.5478$

$C_1 = 1.44$, $C_2 = 1.92$

$\sigma_K = 1.0$, $\sigma_\epsilon = 1.22$

$\ell = k^{3/2}/\epsilon = \ell_m/0.1643$

E = function of wall roughness = 9.0 (assumed smooth)

Hence, $\ell_m = 0.1643\ k^{3/2}/\epsilon$

Therefore, C_D was given as 0.1643.

Von Karman constant 'K' = 0.435

CHAPTER 6.0 MODELLING A SINGLE JET MIXER IN A PIPE CROSS FLOW

6.1 Theory - Penetration Region and Near Field

6.1.1 General

The governing differential equations for mass, momentum, energy, species concentration are all elliptic in nature and can be written in the same general form. For single phase flow this equation is:-

$$\frac{\partial(\rho\Phi)}{\partial t} + \mathrm{div}(\rho V\Phi - \Gamma_\Phi \mathrm{grad}\ \Phi) = S_\Phi \qquad (6.1.1)$$

where Φ is the dependent variable, Γ_Φ is the appropriate exchange coefficient for the variable Φ and S_Φ is the source term which includes both the sources of Φ and any other terms which cannot find a place on the left-hand side of the above equation.

According to ISO standard 3171 the critical parameters for determining suitability for sampling of water in oil are a). concentration ratio (C_t/C_b) top to bottom is greater than 0.9 and b). a critical maximum droplet size. Therefore, it is best to identify the dispersion by the concentration and the maximum size of the drop. The C_t/C_b can be easily obtained from the computations. The entrainment flux of water and droplet sizes at the penetration region were approximated from the correlations derived in part 1, chapter 4.0 (equation 4.4.25). These features were programmed into the Phoenics subroutine 'GROUND'.

No	Equation	Φ	Γ	S_Φ
1	Continuity	1	0	0
2.	x-momentum	U	μ	$-\frac{\partial p}{\partial x}+\frac{\partial}{\partial x}\left\{\mu\frac{\partial U}{\partial x}\right\}+\frac{1}{r}\frac{\partial}{\partial r}\left\{r\mu\frac{\partial V}{\partial x}\right\}+\frac{1}{r}\frac{\partial}{\partial\theta}\left\{\mu\frac{\partial W}{\partial x}\right\}$
3.	r-momentum	V	μ	$-\frac{\partial p}{\partial r}+\frac{\partial}{\partial x}\left\{\mu\frac{\partial U}{\partial x}\right\}+\frac{1}{r}\frac{\partial}{\partial r}\left\{r\mu\frac{\partial V}{\partial r}\right\}+\frac{\rho W^2}{r}$ $+\frac{1}{r}\frac{\partial}{\partial\theta}\left\{\mu\left\{\frac{\partial W}{\partial r}-\frac{W}{r}\right\}\right\}-\frac{2\mu}{r}\left\{\frac{1}{r}\frac{\partial W}{\partial\theta}+\frac{V}{r}\right\}$
4.	θ-momentum	W	μ	$-\frac{1}{r}\frac{\partial p}{\partial\theta}+\frac{\partial}{\partial x}\left\{\mu\frac{\partial U}{r\partial\theta}\right\}+\frac{1}{r}\frac{\partial}{\partial r}\left\{\mu r\left\{\frac{1}{r}\frac{\partial V}{\partial\theta}-\frac{W}{r}\right\}\right\}$ $-\frac{\rho VW}{r}+\frac{1}{r}\frac{\partial}{\partial\theta}\left\{\mu\left\{\frac{\partial W}{r\partial\theta}+\frac{2V}{r}\right\}\right\}+\frac{\mu}{r}\left\{\frac{\partial W}{\partial r}+\frac{1}{r}\frac{\partial V}{\partial\theta}-\frac{W}{r}\right\}$
5.	Turbulence energy	k	$\left\{\frac{\mu}{\sigma_k}\right\}$	$G_k-\epsilon\rho$
6.	Energy dissipation rate	ϵ	$\left\{\frac{\mu}{\sigma_g}\right\}$	$(C_1G_k-C_2\rho\epsilon)\frac{\epsilon}{k}$
7.	Concentration	c	$\left\{\frac{\mu}{\sigma_c}\right\}$	$-\nabla.(w_{rel}.c)$ (for two-fluid model)

** Note:-here μ is refered to effective dynamic viscosity in the above table.

6.1.2 Two-component computational models

6.1.2.1 Homogeneous model:- We start with a simplest two-component model, a Homogeneous model, where the following assumptions are made:-

i). The transport between phases(components) are fast in comparision to the development of the flow field as a whole ie. all phases have the same velocity.

ii). Thermodynamic equilibrium is attained

iii). The droplet size distribution is ignored

iv). The exchange coefficients are related to one mean drop size.

In turbulent sprays, the application of this assumption is sometimes questionable. The homogeneous model of Komiayama et al (Khalil, 1982) was concerned with the effects of droplets on fuel and air mixing. They suggested, on the whole above model assumptions are most appropriate when i). The droplet size is small, and ii). The densities of phases are nearly equal. Simply, the dispersed water phase is treated as a passive contaminant in a Homogeneous model.

In addition to the above assumptions, it was assumed the densities of the two components are close enough and that the intensity of agitation was sufficient to render buoyancy effects negligible. This means the Froude number, ratio of interia to gravitational forces, is large. Also entrainment due to secondary flow is not considered, and may well be negligible for the velocity ratios that were modelled.

Therefore the modelling details can be summarised as follows:-

a). The flow field:-

Radius of pipe	70 mm
Water layer height	10mm
Turbulent model	k-ϵ model

Model constants $C_D = 1$, $C_\mu = 0.9$, $C_1 = 1.44$ $C_2 = 1.92$ $\sigma_\epsilon = 1.22$
$\sigma_K = 1.0$, $K = 0.435$

Boundary conditions:-

i). Wall — Wall function method
Distance to first grid node 'y_p' is selected such $y_p u^*/\nu = y^* = 35$ (since $30 < y^* < 100$ is a requirement)

ii). At inlet — fully turbulent flow field with $k_{in} = 0.00325\ w_{in}^2$ and $\epsilon_{in} = 0.164 k_{in}^{1.5}/\ell_m$ and uniform velocity U=V=0. 1/7 power law axial(W) velocity. To calculate axial velocity distribution from average axial velocity a subroutine was coded in GROUND. - see appendix A6)

iii).At outlet — set to a fixed gauge pressure of 0.0.

iv). At axis of symmetry — along axis of symmetry the gradient in tangential direction of all the variables are equal to zero. Also the stream function is a constant.

b) Water droplet dispersion:-

Boundary conditions

i) At wall - no flux $\partial c/\partial r = 0$ ie: α (sticking probability)=0

ii) At jet inlet - water concentration source was approximated from the experimental correlation obtained in chapter 4

iii) At pipe inlet water concentration is zero

Sc number 0.5 Rodi(1979), Baker(1988) and Syed(1981)

c) Fluid properties:-

i). Densities:-

water = 1000 kg/m^3

oil = 800 kg/m^3

ii). interfacial surface tension = 0.023 N/m

iii). Dynamic viscosity:-

oil = 1.15 x10^{-3} Ns/m^2

water = 1.002 x10^{-3} Ns/m^2

Incorporation of sticking probability in the homogeneous model:- For homogeneous models, since there is no relative velocity, Soo's (1972 and 1982) boundary conditions cannot be used. Therefore, some other means need to be devised to provide a net transport at the wall to represent a deposition or an entrainment. Here, we do not use the complicated deposition theory at the boundary layer, but we will make use of the Soo's sticking probability concept. First the domain is solved for all variables except for water concentration (c). Segev (1984) included a source term in his diffusion equation to account for the relative velocity between the water droplet and oil as given below (see also equation 1.10).

$$\frac{\partial c}{\partial t} + U.\nabla c = \nabla.D_f\nabla c - \nabla.(Wc)$$

When the slip velocity 'W' is a constant the above relation becomes:-

$$\frac{\partial c}{\partial t} + (U + W).\nabla c = \nabla D_f\nabla c \qquad (6.1.2)$$

The slip velocity is now added to the first flow field and the domain is solved only for (c), corresponding to a newly formed flow field compatible with equation 6.1.2. As for the boundary conditions, an outlet flux of '$\alpha V c \rho_w$' was set to the walls of the pipe, where V is the radial velocity towards the wall, c is the concentration of water and α is the sticking probability.

Computational grid:- Setting up the grid is one of the tasks that seems simple, however with a developing elliptic flow this requires some experimenting. The criteria used for the grid setting was a balance between coarse grid for minimum computer time and a satisfactory convergence flow field for analysis. After trying several combinations of radial, tangential and axial grids, a 20*16*60 layout was found to be satisfactory. The jet inflow orifice was located at cell number 8 and 9 of the axial direction and the pipe length was set to approximately 25 diameters. The grids are more finely divided near the walls, where the gradients are steepest, and at the centre. But the first grid at the wall was set to ensure that the requirement of the wall function boundary condition method is satisfied. At the centre it is important to set a very fine grid, otherwise the flow would behave as though a false obstruction similar to a solid cylinder (due to cylinderical coordinate grid layout) was placed along the axis. Flow was considered to be symmetrical about the x=0 plane, therefore the computational domain was taken as one half of the pipe.

Convergence criteria:- When the sum of the continuity residual for all the control volume is less than 0.5% of total flow rate and the maximum continuity residual for any control volume was less than 0.004% of the total flow rate.

6.1.2.2 Two fluid model, Interpentrating continuum approach:-

Where there are several phases present the general equation (for single phase) 6.1.1 becomes:-

$$\frac{\partial(R_i\rho_i\Phi_i)}{\partial t} + \mathrm{div}(R_i\rho_i V_i\Phi_i - R_i\Gamma_{\Phi i}\,\mathrm{grad}\,\Phi_i) = R_i S_{\Phi i} \qquad (6.1.3)$$

where Φ_i = general conserved property for phase 'i'

R_i = volume fraction of phase 'i'

ρ_i = density of phase 'i'

V_i = velocity vector

$\Gamma_{\Phi i}$= exchange coefficient for Φ_i

$S_{\Phi i}$= source of Φ_i per unit phase volume

The following main assumptions were made in this two fluid model.

i). The two-component flow, flowing in horizontal pipe, is steady.

ii). The continous phase, oil, is Newtonian.

iii). The dispersed phase is composed of uniform diameter water droplets flowing as a dilute phase. Thus, the droplet flow is assumed to be inviscid and free from collisions. Particle rotation, electrostatic forces and friction between the pipe wall and the droplets are neglected.

iv). The continuous phase (oil) and droplets share a common pressure and interact only through viscous drag.

In most models one of the basic assumptions is that the mixture is dilute. The boundary between the dense and dilute suspensions is not clearly established. According to Crowe (1982) a qualitative limit is given by the ratio between the aerodynamic response time (time required for a particle released from rest to achieve 63% of the velocity of the free stream) and the time between collisions. For dilute suspensions this ratio must be smaller than one. In the present investigation it seems to be appropriate to consider the suspension as dilute.

One of the most controversial areas in the study of dilute suspensions is the effect of the presence of the disperse phase on the turbulent and velocity fields of the continuous phase. Soo, Ihrig and El Kouh (1960) found that for loadings of up to 6% (or 0.06) with particles of diameter below 250μm the stream turbulence is not significantly affected by the presence of the solid phase. Kada and Hanratty (1960) found that for dilute suspensions of solids in water only with relatively high concentrations and high slip velocities did the presence of the solid phase affect the diffusion rate. Genchev and Karpuzov (1980) developed a turbulence model that predicts a decrease of up to 20% in the tubulent effective viscosity of the dust laden gas as compared with the clean gas. That experimental evidence presented

by Tsuji, Morikawa and Shiomi (1984) confirms the effect of loading and particle size on turbulence quantities. As a consequence of the change in the turbulent diffusion the fluid momentum equation is affected and thus the resulting velocity field. Nevertheless, it was decided that in this first study the effects of disperse phase on the turbulent kinetic energy and its rate of dissipation would not be incorporated.

In the present model besides neglecting the effect of the presence of thedisperse phase on the turbulence quantities, the friction between the water droplets and wall is assumed to be negligible and the coupling of the momentum equation is limited to the interphase viscous drag term. This keeps the complexity of the model to the minimum capable of giving two-phase flow predictions and also shows more clearly where the shortcomings of the model are in order to guide future modelling improvements.

Since the flows are considered to be steady equation 6.1.3 becomes

$$\mathrm{div}(R_i\rho_i V_i\Phi_i - R_i\Gamma_{\Phi i}\,\mathrm{grad}\,\Phi_i) = R_i S_{\Phi i} \qquad (6.1.4)$$

Note:-since the 2nd phase (component) water is in droplet form there would be droplet diffusion in the domain, so when we consider the equation 6.1.4 in mass conservation of oil and water, an extra gradient diffusion term ($\mathrm{div}\Gamma_{\Phi i}\ \mathrm{grad}R_i$) is incorporated in the right hand side.

The water (droplet) flow was assumed to be inviscid and free from particle collisions. Particle rotation, eletrostatic forces and friction between the wall and the particles are also neglected. Further, the droplet sizes are considered to consist of one drop diameter equal to the SMD.

The drag force on each droplet is "F" = $C_d A_p \tfrac{1}{2}\rho_1 |V1-V2|(V1-V2)$
and by Newton's third law the reaction on the fluid is -F

$$A_p = \tfrac{1}{4}\pi d^2$$

and

$$C_d = 24/Re \quad \text{if } Re \leq 2 \text{ laminar}$$
$$= 17.0\ Re^{-0.48} \quad \text{if } 2 < Re \leq 2000$$
$$= 0.44 \quad \text{if } 2000 < Re \text{ turbulent}$$

(Clift et al, 1978)

$$Re = \rho_1 V_{slip}\, d/\mu_1 \text{ and } V_{slip} = |V1-V2|$$

The two liquids are coupled via the drag force on the droplets. This model at the present state does not permit any transport of liquid through the wall (ie:- sticking probability= 0). A sticking probability for the water can be physically modelled by assuming the pipe wall to be fractionally porous to water droplets reaching there under gravity.

Exchange coefficients and source terms for the conservation and transport equation 6.1.4 were set as follows:-

Conservation of	variable Φ	Diffusion coe. ($\Gamma_{\Phi i}$)	Inter-phase source(I)	Within phase source ($S_{\Phi i}$)
Mass				
oil	1	$\mu_{eff}/0.5$	0	0
water	1	$\mu_{eff}/0.5$	0	0
Momentum				
oil	U1, V1, W1	μ_{eff}	drag force	pressure gradient
water	U2, V2, W2	0	drag force	pressure gradient and gravity (neg. bouyancy force)
Turbulence				
	k	μ_{eff}/σ_k	0	$G_k - \rho\epsilon$
	ϵ	$\mu_{eff}/\sigma_\epsilon$	0	$(C_1 G_k - C_2 \rho\epsilon)\epsilon/k$
Where bouyancy force = $(\rho_2 - \rho_1)g$				

6.2 Analysis, and Comparision with Existing Experimental Data

6.2.1 General

The inlet velocity distribution of the main pipe flow was calculated in accordance with $^1/_7$ a power law. The average velocity (WIN) is specified in the Q1 file (Appendix A6.1). A subroutine was coded in GROUND to calculate the velocity distribution across the pipe, according to the 1/7 power law.

The water source at the injection point was calculated in accordance with the correlation developed in chapter 4.0 (equation 4.4.25). A subroutine was programmed (Appendix A6.2) in SATLIT in order to evaluate the water source.

Post processing of the results, where necessary, was carried out using the graphic package 'PHOTON'. To obtain contours of total velocities on planes $\theta=0$ and π, another new variable given by $(V^2 + W^2)$ was coded in GROUND (Appendix A6.2)

6.2.2 Comparision with Existing Experimental Data

As we have mentioned in section 5.2.3 the experimental data for a single jet in a confined pipe cross flow is scarcer. Even the experimental results of the few existing ones cannot be directly related to output data such as mean velocity of the computational results. Therefore the only possible comparision of experimental data can be made is for the jet trajectory. Maruyama et al (1981) conducted experiments in single phase for confined air jets in pipe cross flow and measured the impinging distance of jet on the opposite wall for several velocity ratios. Fitzgerald et al (1979) experimentally determined the velocity ratios for optimum jet mixing and showed that for optimum jet mixing (ie; in single phases) the jet trajectory should bend over to coincide with the pipe axis. They conducted their experiments in water flows.

Hence, the experiment of Maruyama et al (1981) was computationally

simulated for two jet ratios and the jet trajectories are compared in figures 6.1.1 to 6.1.6 . The experiments of Fitzgerald et al (1979) were simulated for one velocity ratio and then the jet trajectories are compared in figures 6.2.1 to 6.2.3.

6.2.3 Homogeneous Models

Computational predictions were performed for two conditions as follows:-

i). Velocity ratio=11, equivalent diameter of the jet=4.2mm, average velocity of the main pipe= 0.95 m/s, pipe diameter = 140mm. Distributions of concentration for this simulation are shown in contour form in figure 6.3.1.

ii). Velocity ratio= 11, equivalent diameter of the jet= 6.7mm, average velocity of main pipe= 0.95 m/s, pipe diameter= 140mm. Distributions of concentration for this simulation are shown in contour form in figure 6.4.1.

6.2.4 Interpentrating Continuum Approach

Two-fluid flow computations were performed for the following conditions:—

Average pipe velocity= 0.95 m/s, velocity ratio= 11, equivalent diameter of the jet=4.2mm, pipe diameter= 140mm.

The droplet size (SMD) was calculated in accordance with the equation 4.4.26 in chapter 4.0. Subroutines were incorporated in GROUND (Appendix A6.5) to evaluate the drop size, viscous drag and gravitational force (negative bouyancy force) on water droplets.

Water volume fraction contours obtained from this two-fluid model were presented in figure 6.5.1.

6.3 Discussion

1.0 We have chosen k-ϵ model for turbulent flow simulation since it is traditionally the most commonly used model for the calculation of complex flows and implies generality for its governing equations. Previous complex flow simulations have indicated this model to be providing the best compromise between accuracy and computational cost.

2.0 Some convergence difficulties were encounted for the k-ϵ model therefore relatively heavy under-relaxation factors were used for these variables. To fulfil the convergence criteria around 1000-1200 sweeps were needed. When the convergence criteria are satisfied the monitored values of the variables set to critical grid points do not change appreciably.

3.0 It is encouraging to see that the computed results indicate the correct trends. The little experimental data available for jets in pipe cross-flow, are found in Maruyama et al(1981) and Fitzgerald et al (1979). These data can only be used to compare the computational results qualitatively for the penetration character of the jet trajectory. They seem to agree reasonably well for the chosen coarse grid.

4.0 Detailed experimental data coupled with fine grid spacing would be needed for the quantitative validation of these models. On the other hand taking into account the inaccuracies that may be induced from two phase effects and due to incomplete understanding and other non-universalities in the turbulent models, the computational cost that would be inccurred by using a finer grid spacing may not be worthwhile and therefore, at this stage the models can only serve as an initial predictive tool for these applications.

5.0 The k-ϵ model required about 1000 to 1200 sweeps for convergence. Use of a constant turbulent eddy viscosity model would reduce this to about 300 sweeps for the same convergence criteria. Therefore an algebraic eddy viscosity or mixing length may be carefully modelled for this particular problem in order to reduce computational costs.

6.0 Water droplet concentration contours obtained from Homogeneous and Two-fluid models indicate that uniformity of water concentration at a downstream point can be achieved by changing jetting conditions such as increasing the diameter of the jet orifice and the velocity ratio.

7.0 In practice the required condition for sampling water in crude for horizontal pipes is the concentration ratio of water between top and bottom larger is than 0.9. But examination of these contour plots indicates that this rule for the uniform dispersion of water can be in error. Because, sometimes the constant water concentration contours run from top to bottom, yet having different high concentrations on either sides of the vertical diameter.

8.0 In the Two-fluid model, the number of solved equations becomes almost twice that of the Homogeneous model, hence increasing the cost of computation by a factor of two. But the Two-fluid model makes the simulation more physically real. Simulations indicate the water concentrations obtained from homogeneous model tend to become uniform faster than the two-fluid model.

9.0 Above a velocity ratio of 20, obtaining convergence becomes difficult. Setting a finer grid did not improve this situation. When the eddy viscosity was set to a constant (ie. 100 x dynamic vicosity), convergence was possible even for velocity ratio of 30.

10.0 Experimental data, describing the flow field thoroughly, is needed to validate the numerical model. Therefore further numerical work was conducted in chapter 9.0. And their results were compared and discussed against the experimental data presented in chapter 7.0.

PART 3

FLOW FIELD ANALYSIS

OF

JET MIXER NOZZLES

IN

PIPE CROSS FLOW

-SINGLE PHASE FLOW STUDY-

7.0 THE SINGLE PHASE EXPERIMENTAL STUDY

7.1 Purpose and Scope of the Experimental Work

Characteristics of the flow field are important in determining the water droplet breakup and mixing capabilities of jet mixers, but the flow field information, even for relatively simple flow through pipe components, is scarce. At present, designers have to rely on very crude models and on subsequent experimental analysis (for one particular situation) based on trial and error. Therefore, as an initial step towards improving the understanding the flow field developed by these jet mixers, their capability of mixing a passive contaminant, a somewhat simpler flow situation (single phase, one component), is considered. This approach can be justified on the grounds that the disperse phase water, being low concentration and small in droplet size, does not have a significant effect on the flow field of the continious phase.

The purpose of these experiments, now conducted in a single component flow situation, can be divided into threefold and, as a whole, are designed to improve the fundamental understanding of mixing occuring due to turbulence and swirl flow in jet mixers. Firstly, a thorough description of the flow field of a fluid injected into the same fluid in a pipe cross-flow was desired, as no such measurments are reported in the literature. Secondly, as there is considerable incentive to predict mixer performance from numerical models due to high cost of full-scale trials and the difficulty of generalising experimental data it was intended to use this body of data to test the computational study of single nozzle and to compare the two nozzle types, and in addition to provide experimental data to assess numerical models of the future. Thirdly, we attempt to establish the manner and rate of decay for swirl, and then to empirically correlate multi- nozzle mixer data, to be useful in practical applications.

These experiments were conducted in a single phase and single component, and for convenience the water was chosen as the test fluid. This work consisted of the measurement of the axial and tangential

components of mean and RMS (turbulent) velocity together with flow visualisation at downstream pipe sections from the jetmixers. The experimental rig was made up of a primary and a secondary (injection) closed water circuits. And two types of scaled up jetmixer nozzles:-

i). Single nozzle (figs. 7.13.4 and A7.1 in Appendix))

ii). Multiple nozzle (figs. 7.13.4 and A7.1 in Appendix), that are in use today were chosen for the investigation.

Forward scatter Laser Doppler Anemometry was used for the velocity measurement because of its non-intrusive character and its accuracy. Fluorescein Sodium dye water solution was excited by ultra violet light to visualise flow at any plane of the pipe cross-section.

7.2 Description of the test circuit

7.2.1 Main Circuit

The main water circuit was constructed as shown in fig. 7.1. The fibre glass tanks were made of 4 feet square panels, and contained about 1200 gallons (5.45 m^3). To avoid dust particles entering the water the tank was covered with a plastic sheet. A thermometer capable of measuring the temperature to within 0.5° C was hung inside the tank. The tank receives water through a float valve and hence maintains a constant water level. Two thermostatically controlled heater elements, each rated at 2 kw, protrude from the side wall into tank to maintain the water temperature to a reasonable range. Most of the pipes of the circuit were constructed from 3" ABS except for the test section. Water from the tank was pumped out by a 1.5 kw self priming centrifugal pump by Worthington and Simpson, type 50WB100, and was delivered to a Tee junction via a gate valve.

At the Tee-junction the flow divides into bypass and main branches. The bypass flow passes through a ball valve and returns to the water tank. The other branch connects to a flow straightner via a ball valve. Then the straightener was connected to the test section after

2.5 metres of straight pipe length. The downstream end of the test section was first reduced to 2" bore after passing through 90 degree elbow, and then fitted to a turbine flowmeter unit.

The flowmeter unit consists of a tubine meter, with an unobstructed 10 pipe diameters upstream and 5 pipe diameters downstream, and a flow straightner at the upstream end of the unit. The turbine meter is by Foxboro 81A (size code $^{3}/_{4}$). Finally, the flow returns to the tank via a gate value. The main function of the gate valve is regulation of flow pressure in the primary circuit. The flow rate may be regulated by throttling ball values upstream to Tee-junction. The 'K' (=48800 pulses per meter^{3}) factor of the turbine flow meter unit was pre-checked with a reference flow meter in the department.

7.2.2 Test section and mixer nozzles

The test section was made of extruded perspex piping of 90mm outside diameter with 5mm thick walls and 2 metres long. Stub flanges/backing plates are glued to each end (fig. 7.2.1). Hence, loosening flange bolts from the fixed piping at each end will allow rotation of the perspex pipe about its own axis. The downstream flange of this pipe section was bolted to a glass 'Y' piece by Corning (cat. ref. PY3A). The straight outlet branch was blanked off from perspex sheet to allow upstream visual observations of the test section.

The other branch was fitted to the pipe returning to the tank. The jet nozzle holder was pre-fabricated and glued to the pipe (fig. 7.2.2) near the upstream end. The jet nozzles were designed so that they could be interchangeably mounted into the holder. A slot in the base of the multi-nozzle mixer nozzle engages into a pin on the holder to ensure that the jet injection plane is perpendicular to pipe axis.

The inside wall of the perspex pipe section was easily cleaned from time to time by removing the perspex sheet from the blanked off end of the 'Y' piece and inserting a flexi-hose with ball of cotton wool at its head. The jet multi-nozzle (figs. 7.14.4 and A7.1 in Appendix)) was scaled in accordance with the drawing no. C16922 of Jiskoot

Autocontrol Ltd. (Presently, Jiskoot Autocontrol Ltd. is the sole manufacturer of mixing nozzles for crude oil pipe line conditioning). This mixer has 8 jet nozzles arranged as shown in fig. A7.1 in Appendix A7.

A single nozzle was designed such that the nozzle area was equal to the total nozzle area of the multi nozzle. Thus, when both nozzles have the same velocity ratio their momentum ratio is also be the same. Mixers were constructed from brass throughout and their nozzle holes were reamered to the appropriate sizes.

7.2.3 Injection circuit

A schematic diagram of the injection circuit is shown in fig. 7.1. The injection circuit was constructed from 1.5" galvanised pipe. The high injection head (max. 100 psi) to the flowrate was achieved from Worthington and Simpson Multi-Line pump type WMV. Pump delivery was connected to a Tee- junction, as in the main circuit, to allow for bypass flow. The injecting water in the other branch of the 'Tee', was first passed through a valve and then via a turbine flowmeter, The turbine meter, Foxboro type 81A series-size code 314, was arranged as in the primary circuit flowmeter unit. The 'K' factor of the flow meter is 1005.18×10^3 pulses per cubic meter.

A few diameters downstream from the flow meter, the piping was tapped by a Bourdon type pressure gauge. Then, from this point to the nozzle assembly the rigid galvanised piping was replaced by 1.5 metre long reinforced flexi-tubing. A 400mm length of the flexi-tubing at the nozzle assembly end was arranged to ensure that it was straight and approximately perpendicular to pipe wall.

7.3 The velocity measurement

The velocity of the flow field downstream of the mixing unit was measured using Laser Doppler Anemometry. Axial and tangential velocities were measured, for both jet mixers, along three diameters (fig. 7.3) of each pipe section, that is 1, 2, 3, 4, 5 and 6 diameters

downstream of the mixing unit, for one velocity ratio and one flow Reynolds number.

Measurements were also made for another two ratios for the single nozzle mixer. Low velocity ratios were especially measured to compare with the numerical predictions since the computational study (in chapter 5.0) demonstrated difficulties in achieving proper convergence for high velocity ratios when the k-ϵ tubulence model was used. In order to establish the swirl decay rate of the multi-nozzle mixer, tangential velocity was measured along the pipe axis starting from 1 diameter downstream with subsequent increments of 0.25 diameters until 4 diameters downstream. These measurements were then repeated for another two ratios and for another higher Reynolds number.

The programme of these measurements is given in table 7.1 and the purposes of these measurements are explained in detail in section 7.5.1.7. Velocity components were also measured, without the mixers being activated, as a check for fully developed pipe flow and integrity of the measuring system.

7.4 The flow visualisation

Ultraviolet radiation was used in conjunction with the photographic process to provide a visible interpretation of an invisible state by inducing "fluorescence" (visible light), which can in turn be photographed. Fluorescence means a luminescence stimulated by radiation, not continuing for more than about 10^{-8} seconds (Hansell 1968) after the stimulating radiation is cut off. The invisible ulraviolet radiation begins at wavelength 4000 A° and extends to 140 A°. The conventional optical material (including perspex) absorbs radiation (Hensell, 1968) of wavelength shorter than about 3500 A°. Therefore, this work was restricted to the use of the 4000-3500 A° band. The substance, Fluorescein Sodium is able to absorb short wave radiation (3500 to about 3800 A°) and to emit in turn radiation of longer wavelength which is in the visible range, therefore it glows. Hence, the techinque involves injection of Fluorescein Sodium water solution (0.5g/litre) through the jet mixers, and this tracer was

excited at pipe cross sections 1, 2, 3, 4 and 6 diameters downstream by a sheet of ultra violet light.

Instantaneous and long exposure photographs of the the excited fluorescein were taken. For the long exposure photographs, a vertical sheet of light across the pipe section was produced as follows; Two slide projectors (note: projector light sources do provide a fair amount of ultra violet light) were illuminated on each side of the pipe about 300mm from the pipe axis. An empty photographic slide was covered to block the beam except for 2mm vertical slit across it and then fed into each projector. Consequently, when this silt beam focused onto the wall of the pipe through the matching box, approximately 3-4 mm thick sheet of light penetrates from the other end. The expansion of the sheet thickness from one outside pipe wall to the other is not considerable.

For the instantaneous photographs, a zoom flash unit (note: electronic flash units provide a fair amount of ultra violet light), type Braun Vario Zoom 340 SCA, capable of illuminating an object at 34 metres, was used. Between short distances the zoom flash beam is approximately parallel. Flash speeds less than 1/10000 seconds are recommended by the manufacturer for close ranges, therefore, are capable of freezing any instantaneous movement of the fluid in the test section.

The face of the zoom flash was covered with tape, so as to illuminate a 3mm vertical slit of light across it. Then a half circle perspex piece was constructed (fig. 7.7) from perspex pipe (90mm inner diameter). The face of the of the perspex piece was covered with black tape, leaving a long 3mm vertical slit across the centre. As the outer diameter of the test pipe and the corresponding inner diameter of the perspex piece were equal, the perspex piece could be conveniently clipped on to the test section concerned.

The zoom flash was arranged to be about 300mm from the pipe axis on the same side of pipe as the clipped-on piece so that the two slits, on the perspex piece and the zoom flash, lined up. The slide projector (fig. 7.4), on the other side with slides prepared as before, served

two purposes; it helps to line up the zoom flash and the 'clipping on device' and it also provides a sheet of light to pre-focus the camera.

One of the problems associated with continous injection of fluorescein dye is contamination of water storage tank rather quickly . Therefore, a system was devised, as shown in fig. 7.4(A), to control the operation of jet injection to limited periods and other operations in an ordered sequence.

First, the jet pressure was noted on a Bourdon gauge (fig. 7.1), and the pressure difference (at the proximity of the injection point) between the jet (secondary circuit) and primary circuit (proximity of the injection plane) was plotted against velocity. Then the jet supply was transformed to a different circuit to inject the fluorescein solution (fig. 7.4). The fluorescein solution was stored in a pressurised reservoir, and was delivered to the jet nozzle via a solenoid valve. The jet was activated by energising the solenoid valve at preset times, programmed in a sequencer delay generator. The system was calibrated as follows; the reservior was pressurised when it was filled with fresh tap water. Then two reservior pressures (with respect to primary pressure), when jet is activated and deactivated, were noted down. By repeating this for pressure ranges of interest and comparing with the first plot, a graph of reservior pressure for jet deactivated conditions against jet velocity was drawn. Hence, reservoir static pressure can now be pre-set in order to achieve a required jet velocity. Yiashica SLR camera mounted with 70-100mm zoom lens was arranged at the blanked off end of the 'Y' piece. The photographs were taken about 2.5 seconds after the jet was activated since the jet can be considered to be fully developed during this time in the test region concerned. The pictures were recorded on 100 ASA Fujica colour slide film and force processed to another additional one minute.

7.5 Experimental procedures

7.5.1 Laser Doppler Anemometry

7.5.1.1 Introduction

Basically a Laser Doppler Anemometry (LDA) system consisted of two laser beams, that interact at a point to form a interferance fringe pattern. Therefore, when a dust particle following the flow passes through these fringes an oscillation (simplisticly stated) of scattered light from bright to dark occurs, the frequency of this oscillation is proportional to the speed of the fluid in the direction perpendicular to the fringes.

The LDA system, Dantec type LDA 04, contained a 15mw He-Ne laser (wave length 632.8nm), Beam spliter, Bragg cell, frequency shifter and a focusing lens (focal length 300mm) to produce the intersecting beams, and a counter/processor to process the data provided by the photomultiplier. The photomultimplier (focal length 150mm) situated on the other side of pipe picks up a forward scattered light, which now has a frequency shift due to the Doppler effect, and converts it to frequency modulated current bursts. During the experiments, natural dust particles in the water were used as seeding. In subsequent sections we examine in some detail the significance of these components, methods of signal processing used, the alignment procedures, the methods of calibration and allowance for refractive index effects, the procedure followed when taking mearsurements and a summary of errors involved. A more detailed description of the LDA method is given in books by Durst et al (1976), lecture notes by Adrian (1977) and lecture notes of DANTEC course (1988).

The Bragg cell shifts the frequency of one of the beams by 40 MHz in order to make the fringe pattern a moving one. This lessens the effects of various error inducing phenomenae such as low velocity of particle and particle crossing the intersection volume at shallow angles to the fringes it also removes the possibility of sign ambiguity where there is flow reversal.

7.5.1.2 Signal processing

A frequency of 40 MHz (f_o) is too high for the signal processor. To overcome this difficulty the signal from the photomultiplier (F_{pm}) which is a combination of the 40 MHz and the Doppler frequency (f_d) is mixed with a signal from a local oscillator($F_{lo}=40 \pm f_s$). The output from the mixer, the frequency difference $F_{lo}-F_{pm}$, is then fed to the signal processor. This signal (output from the mixer) is a combination of Doppler frequency and 'f_s'. The 'f_s', known as the real frequency shift, is set by user controls of the frequency shifter unit.

A typical Doppler signal consists of a low frequency component related to the particle transit time across the measurement volume, and a high frequency component equal to the fringe crossing frequency and noise. The velocity information is contained in the fringe crossing frequency. Therefore the signal was processed, by the counter/ processor, to extract the fringe crossing frequency. The counter/ processor determines the Doppler frequency from individual signal bursts by counting a number of zero crossings in the signal. First, the electronic filter isolates the flow signal and removes most of the noise and the low frequency envelope of the burst, leaving ideally a symmetrical (about the zero level) burst containing the Doppler signal.

The problem of remaining noise on the signal is overcome by building hysteresis into the system, such that after a zero crossing the signal must cross two Schmitt triggers set at 100mv and 50mv before another zero crossing may be detected. Only those cycles in the Doppler burst which cross both Schmitt triggers give rise to a pulse. Then the cycle were further validated by an operation called a combined mode. This mode of validation was selected since it was said to be more suited to measurements in which the particle arrival rate at the measurements control volume fluctuates.

The signals that are accepted give rise to a validation rate as a fraction of the data of bursts considered. Allowance is made for the fact that there is a bias towards particles with higher velocity by

using the inverse averaging method. These values are then transferred to an Apple computer (via the Buffer interface unit) which calculates the mean and standard deviation of the data collected. During the experiments, the counter was optimized by adjusting the high and low pass filters to cover the expected Doppler frequency range (including frequency shift), the comp. accuracy of the counter processor unit was set to 30%.

7.5.1.3 The alignment procedure

The laser and photomultiplier unit were both placed on a horizontal table face lying under the test pipe section, so that they face each other on each side of the pipe section. The table was mounted on screw thread traversing system that can be moved up or down on a vertical plane and in two directions, parallel and perpendicular to pipe axis, on a horizontal plane. Then the traversing system was mounted on a free standing table which had ajustable legs. Now, if the two laser beams are in a vertical plane and travel into the pipe to intersect at a horizontal diameter, the knowledge of the beam intersecting point is poor or has to be establish with difficulty due to the lensing effect of the pipe. In order to relieve this difficulty, a perspex matching box was made in two parts which could be presssed together into place around the pipe at a chosen section.

The surfaces that would be pressed together were carefully prepared to allow easy movement and rotation of the box with respect to the pipe. First, a layer of silicone sealent by Dow Corning was applied (fig. 7.7) to the appropriate surfaces and a strip of thin gauge Acetate sheet was placed on it. Then after applying a thin layer of silicon grease for the joining surfaces to be water tight, the box was loosely mounted at the required postion. When the sealent was dry, the box was rotated about the pipe axis until its side walls were vertical and then tightened into place. When the box is filled with water, it almost remove the distortion due to the different refractive indices involved. A few drops of clear detergent were added to the water in the box to stop formation of air bubbles at the inner wall of the box and outer wall of the perspex pipe.

A considerable amount of time was spent on the alignment of the system. The legs of the freestanding table were first ajusted to make the table top horizontal in direction perpendicular to the pipe and parallel to the direction of the pipe axis. This was conducted by means of a spirit level to within ± 0.1°. The laser baseplate screws were finely adjusted so that it was horizontal in the cross-pipe direction and parallel in the direction of the pipe axis. Then the laser beam tube was also checked to see whether it is horizontal. The laser beams were positioned in the horizontal plane by rotating about its axis (this should be done when the frequency shifter unit is swithed on).

The laser was traversed until the beams intersected on the outside of the vertical box wall and the freestanding table was rotated on vertical axis until the returning and outgoing laser beams coincided. Then the laser beams were traversed inwards until the beams intersected on the outside the pipe wall and the table top was traversed vertically until the returning and the outgoing beams coincided. Finally, as a check on the possibility of 'twist' about the beams axis the laser was traversed much further into pipe (so that the laser beams passed through the nearest pipe wall by about 10mm apart each other) and using piece of paper with a straight edge, spots of returning and outgoing beams on the outer wall of the box were checked. They were found to be on a straight line, indicating that the beams were in the same plane.

By moving the laser towards and back from the pipe, it was also observed that the two spots of the returning beam intersected at point on the outer vertical wall of the box. For axial velocity, measurements were made when the beams are in this horizontal plane. Tangential velocities were made by simply rotating beams by 90 degrees to vertical position.

The importance of having the beams aligned in a direction perpendicular to the pipe axis when measuring the tangential velocity is considerable. If the plane of the beams were misaligned by 1 degree then there is an addition to the tangential velocity readings of

around 0.008 m/s when the axial velocty is 0.5 m/s. If mistakes were made, the error would be of one sign, shifting the zero point of the tangential velocity distribution and would therefore be obvious, especially at downstream sections , if it is significant.

A check on this error was also made by measuring the tangential velocity of the fully developed pipe flow (ie when the mixer is deactivated). There is no significant effect on the axial velocity measurements due to slight misalignment.

7.5.1.4 Calibration of fringe seperation, and alterations in the point of intersection and LDA constants due to refraction

The velocity that is being measured is given by the product of fringe separation (δ_f) and Doppler frequency (f_d). The fringe separation is a function of wavelength, λ, and beam intersection angle (2θ) as

$$\delta_f = \frac{\lambda}{2\sin\theta}$$

Therefore δ_f can be calibrated by measuring the beam intersecting angle (2θ). The angle was measured by traversing the aligned laser light right through the pipe so that the beams' intersection was positioned on the far side of the perpex box and placing a vertical screen about 1.5 metres away from it. The distance from the spot where the beams intersected and the screen was measured with a tape measure and the distance between the spots where the beams hit the screen was also measured. The inaccuracy is not only due to the tape measure but also to the fact that the spots caused by the beams hitting the screen were of finite size. This measurement results in a value for θ of 5.45° and value for δ_f of $3.33\mu m$ to an accuracy of 1%, based upon the value for λ of 632.8nm. These measurements refer to the values in air. There is no need in general to change the value of δ_f when the beams meet in the water because although $\sin\theta$ changes by the ratio of the refractive indices, the wavelength of the light λ changes similarly, these effects cancel out. We now turn to the effects of refraction at the pipe walls on the linearity of the traverse and upon the

calibration factor.

In the case of the measurement of the axial velocity on the horizontal diameter it is clear that the position of the beams' intersection is a linear function of the position of the traversing table. The beams always intersect at the same angle and so the calibration constant δ_f does not change across a traverse.

In the case of the measurements of the tangential velocity however, adjustments seem to be needed owing to the refraction at the wall of the pipe. It was shown by Halsey (1986) and Peacock (1984), that these required alteration are in fact well within the precision bounds of the tangential velocity measurements, therefore they can be ignored.

7.5.1.5 The measurement procedure

The table (fig. 7.6) was traversed until the beams intersected at the near inner wall of the pipe. To establish the point of measurement the diameter inside the pipe should be scaled with respect to traversing distance of the laser. In order to do this a 'mm' scale, capable of measuring to ± 0.5 mm, was glued onto the moving part and a stationary arm was mounted on the freestanding static frame with the aid of magnetic clamps. For example, when the table was traversed on a horizontal plane, with the beams on horizontal plane, from the near inner wall to far inner wall, the arm indicated a 59 mm (average) movement on the scale which is equivalent to 79.6 mm movement of the intersecting point inside the pipe. When the beams were on a vertical plane the corresponding movement was 58.5 mm (average) on the scale. The measuring points were set according to this scale, first a measurement was made at 2.5mm, then 5mm and 5mm intervals upto 55mm. When this is reached the point at the far inner wall was noted and another measurement was made 2.5mm into the pipe.

The errors in positioning the laser for measurements consisted of the errors in positioning the beam intersection on the wall of the pipe at the start of a traverse (about ±0.25×1.34=0.335 mm) plus half the beamwise length of the spot(±0.35mm= beam diameter) making an error of

± 0.5 mm.

The photomultiplier was positioned approximately symmetrically between the beams and angled at about 10° to the plane of beams in order to obtain a strong signal. The adaptor ring between the photomultiplier optics was set loose, therefore this section always positioned to the vertical (as recommended by the manufacturer). The system was optimised by increasing the voltage applied to the laser, precise focusing of the photomultiplier to the measuring volume and selecting high and low pass filters to suit.

The required frequency shift was approximated by estimating the Doppler frequency from expected mean velocity. The Doppler frequency satisfies the relationship given by $V = \delta_f f_d$.

For instance, when velocity, V = 0.4 m/s, f_d is approximately equal to 120 kHz. Very near the jet nozzle sometimes high values of 900 kHz required as the frequency shift in order to obtain a good symetrical distribution. The flow signal seems to be satisfactory if the validation rate is higher than 25%, but normally, it was higher as 40%. Sampling numbers of 2000 and 2500 were taken for axial and tangential velocity measurements respectively. But around 1 diameter downstream, sampling points high as 4000 were required.

During the experiment, the primary circuit water pressure was set around 20 psi (138 kPa) to avoid cavitation at the injection nozzle. First, the measurements were made on a horizontal diameter, that is perpendicular to the injection axis (or in the case of multi-nozzle, to its stem). When measurements along the offset diameter were required, the retaining flange bolts at each end of test pipe were loosened and the test pipe was rotated about its axis until the diameter concerned was horizontal and the alignment procedure was repeated so that the this diameter was in-line with laser beam.

When making a measurement, the upper and lower bounds of the expected velocities need to be specified, then the computer eliminates those measurements lying outside these bounds to calculate the mean and

standard deviation. Then all data lying outside the range of the new ($\mu \pm 2\sigma_d$) were rejected and mean and standarded deviation computed again. The bounds used were then reset using a mixture of trial and error iterations until the bounds used coincided with the values $\mu \pm 2\sigma_d$ as calculated from the measurement made using those bounds.

7.5.1.6 Assessment of Errors

Errors involved in the measurements can be divided into systematic and random errors. The word accuracy is normally refered to systematic error whereas the word precision is related to all random errors. Tabulated below are the systematic followed by random errors, also briefly described are their sources.

Measurement	Error	Brief description
1 Systematic errors		
1.1 Volume flow rate	± 0.5%	Recommended by manufacturer of turbine meter.
1.2 Jet velocity		due to construction limitations. This error is relatively insignificant.
1.3 Reynolds no.	4%	$\delta Re/Re \triangleq \mp(\delta\nu/\nu + \delta v/v)$ $\delta\nu/\nu = 0.035$(due to temperature change during experiment, 19.5—21°C, and temperature measurement error)
1.4 Velocity measurement		
i) Calibration	± 1%	$\delta(\delta_f)/\delta_f \rightarrow$ distance measurement error during calibration.
ii) Location from wall	±0.5mm	half beam diameter+distance measurement error on scale.
iii) Alignment	±0.25°	

7.5.1.6 Cont.

2. Random error		
2.1 Mean velocity	<8%	Yanta (1973) has shown, this error to be dependent on flow conditions such as $\frac{2}{N^{0.5}} \frac{u}{U} * 100\ \%$ error correspond to one of the worst cases, u'=0.1m/s, N=2500 & V_θ=0.05 m/s, was 8%.
2.2 turbulent velocity (RMS)	5%	Yanta (1973) has shown, this error is independent of flow conditions, and equal to 2/(√2N)*100% for 95% confidance.

7.6 Results and analysis

First, the detail of the programme of measurements in table 7.1 and the flow visualisation is explained. Then the results are analysed. The results were plotted, where necessary, against diameter across the pipe, and the rest are presented in a tabulated manner. Photographs of flow visualisation of dispersion of passive contaminant at pipe cross section are also presented.

1. *In Experiments A, B* and *C*, measurements were made in three diameters at cross sections 1, 2, 3, 4 and 6 diameters downstream with a view to understanding the general flow field produced by the multi-nozzle mixers. The velocity ratio was 57 and the Reynolds number of the main flow was set at 27600 (related to upstream). The results, plotted in fig. 7.9.1 to 7.9.18, show how fast the secondary flow decays to almost nothing (less than 5% of the initial injection velocity) at 3 diameters downstream. The turbulent fluctuation decays

to a flat profile at about 3 diameters and stays flat at 6 diameters. In this region, between 3 and 6 diameters, the turbulent fluctuations have shown local isotropy (when the tangential component was assumed to be equal to radial component) within the accuracy of the measurements.

2. *In experiments E, I, M* and O the tangential velocity at the pipe axis was measured in order to develop a simple correlation for its decay, when the velocity ratios were 36, 57 & 70 and Reynolds number was 27600 (related to upstream). The results, plotted in log-linear scales (fig. 7.11), showed a linear relationship. When these relationships were extended towards upstream points, they appear to intersect at a common point. The relationship of velocity ratio 36 at Reynolds number 48400 shows the Reynolds number is weakly related to swirl decay. The experimental data, when the Reynolds number was 27600, was correlated to an equation of the form:-

$$\ln\left[\frac{V_\theta}{1.83*U_x}\right] = -2.73*10^{-3}\left[R_v^{1.66}\right]\left[\frac{x}{D} - 1.625\right] \qquad (7.1)$$

where U_x is the average downstream axial velocity, R_v is the jet to pipe velocity ratio and x is the axial distance from the injection plane.

The experimental results of Chilton et al (1930), Ger et al (1974), Morgan et al (1976), Revill et al (1982) and Fitzgerald et al (1979) indicated that the behaviour of jets injected into pipes is a function of momentum ratio (M_r) rather than being a function of V_r and (d/D) separately. Forney (1985) indicated that the behaviour of jets is independent of the dimensionless quantity d/D, when its value is small. Therefore it is quite evident the above equation needs to be transformed to represent momentum ratio rather than velocity ratio, as below:-

$$\ln\left[\frac{V_\theta}{1.83\ U_x}\right] = -0.363\left[M_r^{0.83}\right]\left[\frac{x}{D} - 1.625\right] \qquad (7.2)$$

3. The equation generally used to obtain turbulent kinematic viscosity

of the fully developed turbulent pipe flow is given as $\nu_t = 0.4\ U^*R$ (ISO/DIS 3171 and Baker, 1988). In fully developed pipe flow the u/U^* against radial distance is almost linear (Laufer, 1954 and Lawn, 1971). Therefore an average value for u^2 was calculated (appendix A6.9) by using the 1/7 power law for the velocity distribution and approximating the u/U^* to a linear distribution. This average value was $u^2 = 2.496\ U^{*2}$. Hence,

$$u = 1.58\ U^* \qquad (7.3)$$

Substituting into the above equation gives, $\nu_t = 0.25\ uR$. This equation illustrates an energy model similar to $\mu_t \propto k^{1/2}\ell$. Launder et al (1979, p82) has indicated that the energy models suffice to discribe μ_t for developing flows. Hence we assume this model for ν_t to be true for this developing pipe flows, behaving two dimensionally.

Experiments F, G, J and K (in addition to A, B andC), were conducted in order to establish the decay of average kinetic energy at downstream cross sections. We have seen before that the kinetic energy shape up to a flat profile around 3 diameters downstream. Therefore, the average kinetic energy corresponding to a cross section (ie, 3 diameters onwards) was taken as its arithmetic average of the measurements across the horizontal diameter. The turbulent kinetic energy may be evaluated, assuming isotropic turbulence, from the axial component of the RMS velocity ($\overline{u}'$). The average $\overline{u}'^2$ was correlated to an equation of the form:-

$$\frac{(u^2 - u_o^2)_{ave}}{U_x^2} = 8.16 * \exp\left\{-5.05 * R_V^{-0.250}\left[\frac{x}{D}\right]^{0.65}\right\}$$

where u is turbulent RMS (axial) velocity, u_o is the corresponding value of downstream fully developed value. The value u_o was estimated from equation 7.3 and U^* (friction velocity) was related to downstream velocity.

Edwards et al (1985) conducted experiments into turbulent mixing in tubes with transverse jets. And Bredenthal et al (1986) conducted experiments into turbulent mixing in ducts with transverse multiple

jets. They found the RMS concentration fluctuation (c') of passive contaminants is a function of momentum ratio and independent of the small diameter ratio (d/D). We know that the RMS concentration fluctuation (c') is directly related corresponding velocity component. Therefore it is evident, also due to the findings of others given in number 2 above, the equation above should be transformed to represent momentum ratio (M_r).

$$\frac{(u^2 - u_o^2)_{ave}}{U_x^2} = 8.16 * \exp\left\{-2.88 \times M_r^{-0.125} \left[\frac{x}{D}\right]^{0.65}\right\} \qquad (7.5)$$

After 4 diameters, the flow behaviour can be taken as 2 dimensional, and so, a 2 dimensional diffusion equation has been solved in chapter 8.0, to predict the behaviour of water droplets after 4 diameters. In order to do this we should make allowance for the decay of eddy viscosity (since this is directly related to eddy diffusivity). Therefore, one purpose of these experiments was to find a relationship to make an allowance for eddy viscosity decay, starting from 4 diameters downstream until the flow becomes fully developed pipe flow.

4. *The experiments P, Q & R* were carried out in order to understand the general flow field produced by the single mixer nozzle and also to compare the single and multi-nozzle mixers. And then, in addition to these, *experiments T, V and W* were carried out to provide quantitative information for the assessment of computational models. *The experiment V* was carried out to compare the two mixer nozzles for the higher velocity ratio (70).

5. The single nozzle mixer having the same velocity and momentum ratio as the multi-nozzle mixer, shows similar qualitative trends such as rapid decay of secondary swirl and flat RMS profiles beyond 4 diameters downstream. Therefore, in order to establish the manner of the decay of secondary swirl, experiments E, I and M were repeated in *O, S and U* for the single nozzle mixer.

6. Basically, the flow visualisation work was carried out to provide

a supporting frame work for the study, and in addition it was also hoped to compare mixing patterns, obtained from flow visualisation, with the concentration contours of numerical models, in order to check models' predictions qualitatively.

7.7 Discussion

1. The long exposure flow visualisation studies of the single nozzle have shown a symmetric horseshoe vortex system (a pair of symmetric counter-rotating vortices) in the cross section normal to the main pipe. As the velocity ratio was increased, the vortex system, at a cross section, moved towards the wall opposing the injection wall. This vortex system also gradually move towards the opposite wall along the pipe flow, illustrating the jet trajectory.

2. Flow visualisation studies of the multi-nozzle have illustrated a complicated system of vortices across the sections near to the injection point. Flow patterns obtained from multi-nozzle mixer are shown in figs. 7.13.6.

3. The injection of the jet obstructs the pipe flow in the same way to that of flow impinging on a rigid circular cylinder, But the boundaries of the jet are compliant and entraining, and the flow is confined between pipe walls therefore, interaction of the two flows may led to periodic shedding of vortices behind the jet similar, but of a more complicated form to those of a Von Karman-Bernard street. This is one of the reasons why the flow patterns of the instantaneous photographs near downstream of the single nozzle mixer were not exactly symetrical.

4. As the injected fluid enters the cross flow, it undergoes a process that rapidly transfers mean kinetic energy to turbulence energy which eventually dissipates as heat. This transfer process is relatively more pronounced on the multi-nozzle mixer, therefore, the mixing rate is faster and more intense near the nozzle. Hence, the multi-nozzle mixer initially demonstrates a higher decay of secondary swirl energy than the single nozzle. One of the reasons for this higher decay rate can be attributed to the way individual jets roll up first, as shown by the visualisation study, to form high velocity gradients (fig. 7.13.6) due to their opposing velocity vector at their borders.

5. These jet mixing processes produce two mixing scales, near the

injection point the scale is that of the jet and far downstream the scale is related to the pipe. The mixing process of the multiple nozzle, is dominant very near the injection point, therefore it is reasonable to assume the jet scales are more relevant for the initial mixing process.

6. The volume flowrate was calculated using the trapezium rule across the velocity profile, when the jet mixer was deactivated. When this volume flow rate was compared with the flow meter, they were within 3%. The turbulent RMS velocities were also compared with the experimental results of Laufer (1954) and Lawn (1971) shown in fig. 7.12. They were also in reasonable agreement.

7. Mixing patterns of the flow visualisation can be used to assess the qualitatively the dispersion of passive contaminant predicted by computational models.

8. Present design calculations, by Jiskoot (Baker, 1987), assume that the injected jets completely dissipate as soon as they impinge on the top wall, the experimental measurements demonstrate that this is not the case. The jet impingement on the wall occured, for velocity ratios 36 and 56, at less than 0.5 diameters downstream, yet turbulent intensities of the order of one were measured at one diameter downstream. Therefore, the assumption, made by the existing calculation method, is not justifed.

9. As the flow reaches downstream, approximately 4 diameters, the distribution of velocities (mean and RMS) flattens out and their magnitudes begin to close up for the two mixers (for vel. ratios 36, 57 and 70), indicating that the flows are now almost independent of their different origins. When velocity ratios are 57 and 70 the average difference in RMS velocity for single and multi-nozzle is approximately 7% at 6 diameters downstream. And their magnitudes are about 3 times higher than the corresponding fully developed pipe flow values.

10. Secondary swirl flow, as mentioned earlier, plays an important

role by dispersing the water droplets in a cross-pipe direction whilst turbulent (eddy) viscosity diffuses them. Therefore, as the secondary swirl flow dies out the gravity settling begins to become dominant and the flow field behaviour becomes two dimensional. When the velocity ratio is 57, the secondary swirl flow decays quite fast and becomes proportionally very small at 3 diameters downstream. Hence the sampling probe ideally needs to be installed fairly close to the mixer, that is before the gravity settling has commenced.

11. Interestingly, the tangential velocities at the axis of pipe decay faster for higher velocity ratios. This indicates higher velocity ratios would break up droplets to smaller sizes and increase the eddy viscosity by generating and dissipating energy, but dispersion strength decays faster and the gravity settling begins earlier. Therefore, an increase in velocity ratio would improve the distribution quality by reducing standard deviation of the droplets size distribution, but has to trade-off with downstream dispersion strength. On the other hand, higher velocity ratios would break up the droplets to smaller sizes therefore, the swirl dispersion strength required to suspend them is much less to than for the larger drops. The optimum balance of these effects can be identified from the model developed in Chapter 8.0.

12. Axial and tangential turbulent velocities (RMS) are generally different, but further downstream, about 3 diameters onwards, they become close to equal (for velocity ratios 36, 57 and 70). In most situations we do consider fully developed pipe flow as isotropic, although this is not truly the case. Therefore, the assumption of isotropy is justified for these mixers from the vicinity of 3 diameters downstream.

13. The average turbulent (axial) kinetic energy across the diameter was correlated to an equation (Re no= 27600) of the form:-

$$\frac{(u^2 - u_o^2)_{ave}}{U_x^2} = 8.16 * \exp\left\{-2.88 \times M_r^{-0.125} \left[\frac{x}{D}\right]^{0.65}\right\}$$

where u is average turbulent RMS velocity at a cross section and u_o is the corresponding value of downstream fully developed pipe flow. This equation with the procedure given in section 7.6 will be used to estimate the value of the decaying turbulent diffusion coefficient in Chapter 8.0.

14. The relationship, on log-linear scale, of tangential velocity at the pipe axis against axial distance (figs. 7.11.1 and 7.11.2) is linear. This can be expected since, in general, swirling pipe flows were shown to decay exponentially (Kuroda et al, 1986). They have also illustrated that the swirl decay is independent of Reynolds number, when the Reynolds number is greater than 5000. Furthermore, the linear relationships shown in fig. 7.11.1 and 7.11.2 appear to intersect at the same upstream point (when some upstream points closer to the nozzle are appropriately rejected). These linear relationships (Re no= 27600) of the multi-nozzle were correlated to a common equation of the form-

$$\ln\left[\frac{V_\theta}{1.83\ U_x}\right] = 0.363\left[M_r^{0.83}\right]\left[\frac{x}{D} - 1.625\right]$$

where V_θ is the tangential mean velocity at the pipe axis.

15. When the velocity ratio was 36 the Reynolds number was changed (ie by varing the velocity) from 27600 to 48400 a relatively weak change in swirl decay was demonstrated.

16. The angular velocity vector of the multi-nozzle mixer at the axis is in the direction opposite to the main flow, however, swirl velocity of the single mixer is in the direction of the main flow and their magnitudes are also different very near the mixers. Therefore a direct comparision of individual velocities or RMS values is not possible. But swirl velocities, at the pipe axis, of both mixers die away approximately at the same cross-section.

17. Eventually, we may conclude that the multi-nozzle is superior in performance in two characteristics; i). Mixing is faster and the RMS

distribution flattens out closer to the mixer, indicating a well mixed cross-section. ii). Jet energy is more evenly distributed at the injection cross section, hence improving the quality of the droplet distribution (and entrainment, if applicable).

As the flow reaches downstream, approximately 4 diameters, the distribution of both mean and RMS velocities flattens out and their magnitudes for both nozzles begins to close up for the two mixers indicating that the flows are now almost independent of their different origins.

The LDA experimental data besides providing information to aid understanding of the complex flow in the mixer zone, is believed to be of sufficient quality and quantity to use as test cases for assessment of the predictive accuracy of the computational models.

18. The long exposure flow visualisation studies of the single nozzle (figs. 7.13.1 to 7.13.5) have shown a symmetric horseshoe vortex system (a pair of symmetric counter-rotating vortices) in the cross section normal to the main pipe. As the velocity ratio was increased, the vortex system, at a cross section, moved towards the wall opposing the injection wall. This vortex system also gradually move towards the opposite wall along the pipe flow, illustrating the jet trajectory.

19. Flow visualisation studies of the multi-nozzle have illustrated a complicated system of vortices across the sections near to the injection point. Flow patterns obtained from multi-nozzle mixer are shown in figs. 7.13.6. The multi-nozzle mixer initially demostrates a higher decay of secondary swirl energy than the single nozzle. One of the reasons for this higher decay rate can be attributed to the way individual jet roll up first, as shown by the visualisation study to form high velocity gradients (fig. 7.13.6) due to their opposing velocity at their borders

20. The injection of the jet obstructs the pipe flow in the same way to that of flow impinging on a rigid circular cylinder, But the boundaries of the jet are compliant and entraining, and the flow is

confined between pipe walls therefore, interaction of the two flows may led to periodic shedding of vortices behind the jet similar, but of a more complicated form to those of a Von Karman-Bernard street. This is one of the reasons why the flow patterns of the instantaneous photographs near downstream of the single nozzle mixer were not exactly symetrical.

21. The photographs obtained for the dispersion of the passive contaminants agrees qualitatively well with the concentration contours of the numerical simulation performed in chapter 9.0 (overlaid transparency on fig. 7.13.1). As the velocity ratio increases there is a gradual tendancy to degrade the qualitative agreement, specially at the top wall.

22. These mixing patterns of the flow visualisation, can be used to assess qualitatively the dispersion of a passive contaminant, predicted by a computational models. Use of yellowish-green Ar laser beam (since its diameter is relatively very small) for this visualisation technique would provide better definition, improving the quality of the assessment.

PART 4

INTER–RELATIONSHIPS

AND

IMPLICATIONS OF ABOVE THREE PARTS,

AND

DISCUSSION AND CONCLUSIONS

8.0 AN EXACT SOLUTION OF THE WATER DROPLET MASS CONSERVATION EQUATION AND PREDICTION OF DISPERSION QUALITY AT A DOWNSTREAM SECTION

8.1 Introduction

The main purpose of this chapter is to obtain an exact solution for the water conservation equation adopted by Segev (1984) and Baker (1988). They solved this equation numerically for three dimensional pipe flow, when the velocity profile is fully developed. From the experimental study in chapter 7, it was demonstrated that the complicated flow pattern created by swirl decays very fast to nothing, thus from here onwards the flow would behave two dimensionally. Therefore, this character may be idealised to a two dimensional situation to reduce the flow complexities and costs of evaluation drastically. We will define this region as the far field. In the far field, for example in horizontal flow, the water droplets would settle under gravity which would be opposed by the diffusional mass transfer of water droplets.

Secondly, a two-dimensional exact solution for the elliptic water conservation equation is combined with other experimental information obtained in chapter 7.0 in an attempt to form a low level model for multi-nozzle systems. In the formation of this low level model, the following main function of jet mixers are considered and briefly discussed,

i). Destratification of settled out water

ii). Breakup of large globules into smaller droplets, so that the sampler probe mouth would not impose any restrictions to isokinetic sampling

iii). Distribution of water droplets uniformly across the pipe cross-section so that the sample taken is representative.

The ISO/DIS 3171 standard recommends the concentration ratio, top to

bottom should be higher than 0.9 for the sample to be acceptable. Therefore, to ensure that the above three functions are met, the designers should be first able to predict performance of mixers and modify, if necessary, their parameters.

At present, there are no satisfactory design calculation methods, due to the complexity of the problem and limitations of existing knowledge. The predictions have been performed using crude theoretical models, usually having no proper justification.

8.2 The proposed model philosophy

The following design guide lines are proposed for the three main functions to ensure that the jet mixers were capable of satisfying the objectives efficiently. Although the whole system can be optimised by trial and error to satisfy all three functions, only two criteria (drop size and concentration distribution) are modelled here.

8.2.1 Destratification of settled out water

There is little existing knowledge or information on this subject. The destratification of water due to the penetration of a single jet was conducted in chapter 3.0 and 4.0. A similar approach, assuming the entrainment is purely due to penetration of the water boundary layer formed around the jet and then modelling appropriately to suit, may be used.

The secondary swirl flow, produced by the injecting jets impinging on the pipe wall, may also entrain water from the stratified water layer. Tsahalis (1977) has found a critical Reynolds number(=50), based on water layer height, for the onset of entrainment. He has conducted his experiments in fully developed pipe flow. Although we may assume this theory to be true for a critical Reynolds number based on secondary swirl flow, a direct relationship between this critical Reynold's number and the entrainment rate is not possible.

8.2.2 Droplet breakup

The flow visualisation study (chapter 7) demonstrated how rapidly the jet flow mixes with the pipe flow. Mixing is observed to be almost complete at 0.5 diameters for velocity ratios smaller than would normally be encountered in real situations. Therefore we assume the near field mixing scales of the multi-nozzle mixer, to be related to jet scales. The experimental evidence has shown (1986)that the multiple jets behave as individual free jets before they merge. Therefore in order to obtain an average turbulent intensity, the jet geometry at the injection cross section was idealised as shown in fig. 8.2. The turbulent kinetic energy was weighted across the area, assuming it corresponds to fully developed pipe in the back ground (fig. 8.2) and to the value at half radius in the jet cone.

8.2.3 Dispersion of droplets and their concentration distributions at downstream (far field)

Mixing can occur across the pipe cross-section only if the injecting jets penetrate to the opposite wall. This velocity ratio was determined, using the formula given by Pratt-Baines (1967)

$$y_p/d_j = 2.05\, R_v^{0.72}\, (x/d_j)^{0.28} \qquad (8.1)$$

where y_p is the penetration distance, R_v is the ratio of the jet inlet velocity to line velocity, d_j is the nozzle diameter and x is distance in the axial direction. The rationale for this argument is given in Sugiyama et al (1986). They have shown that the jet trajectory obtained for unconfined jets in cross flow approximates quite well for a jet in confined cross flow, until the jet reaches the upper wall. The duct to jet diameter ratios of their experiments were approximately equal to 10.

The secondary swirl flow decays very quickly, as we have seen in chapter 7, and is negligeble at about 3 diameters downstream. Therefore, from 3 diameters downstream the behaviour of the flow field can be considered as two dimensional. When the velocity ratio was

chosen for the jet to reach the opposite wall, the flow can be taken as well mixed to the point where the secondary swirl is just dominant over gravity settling. From this point gravity settling gradually begins to become dominant. Therefore the solution of the two dimensional water conservation equation can be used in this region, defined before as the far field, to obtain the quality of distribution. The solution that has been arrived at can deal with dispersion due to gravity settling and the diffusion of droplets, but, being two dimensional, secondary swirl flow effects can not be considered. Therefore it is necessary to define a sharp cut-off point where the dispersion by secondary swirl flow and diffusion changes over to dispersion by gravity settling and diffusion.

The cut-off point was defined as the location where the secondary swirl flow, approximated to the tangential velocity at the axis, is just enough to lift a droplet from the bottom to the top. Further upstream from this point the secondary swirl flow gradually becomes dominant. On the other hand the gravity effects become dominant further downstream. Since the swirl decay rate is fast for the range of velocity ratios in use, the change over from the dominance of secondary swirl to gravity effects would not be expected to cover a significant axial distance.

8.3 The theory of the proposed model

8.3.1 Droplet breakup

Hinze (1955) has indicated that the critical Weber number, based on turbulent RMS velocity (v), for droplet breakup in an emulsion is equal to a constant (=1.18).
Therefore,

$$\frac{\rho v^2 d_{max}}{\sigma} = 1.18 \qquad (8.2)$$

Therefore

$$d_{max} = \frac{1.18\,\sigma}{\rho_c v^2} \qquad (8.3)$$

where $v^2 = (RMS)^2$

We attempt to obtain an average v^2, weighted by the area, by idealising the jet geometry in the injection plane as shown in fig. 8.2.

The average value of v^2 at a distance 'x' from the injection point of a free jet was assumed to be characterised by the corresponding value at half radius. Half radius is defined as the distance from the jet centre line, when the velocity becomes half of the velocity at centre line.

For a free jet the turbulent intensity at half radius $v/V = 0.4$ (Schetz, 1980, p25, fig. 9). Which makes $v = 0.4\ V = 0.2\ V_c$, where V_c is the centre line velocity. The velocity profile for an axisymmetric jet is given by:-

$$\begin{aligned} V_j &= V_c[1 + 2(x/d_j)\tan(\theta/2)] \qquad (8.4)\\ &= V_c[1 + 0.25(x/d_j)], \quad \text{since } \theta = 14^\circ\\ &\triangleq 0.25(x/d_j)\ V_c \quad \text{for } d_j \ll x \end{aligned}$$

Therefore, $V_c = 4\ V_j(d_j/x)$ (8.5)

Substituting 8.5 to 8.4 gives:

$$v = 0.8\ d_j V_j/x$$

$$v^2 = 0.64\ (V_j d_j/x)^2$$

To obtain an average (weighted by area) for v^2 for one jet cone, v^2 was related to '$\bar{x}$' (centroid=2R/3), therefore:-

$$v^2 \text{ at } \bar{x} = 1.44\ V_j^2(d_j/R)^2$$

Where 'R' is the radius. The total projected area of N_j jet cones is $0.125\ N_j\ R^2$ (since jet width at x=R is 0.25R). The area of the pipe cross section is πR^2

The remaining (back ground) $\bar{v}^2$ was related to the fully developed pipe flow value, that is:-

$$v \triangleq 1.58\, V(f/2)^{1/2} \quad \text{(Laufer, 1954 and Appendix A6.9)}$$

$$v^2 = 0.31\, V^2 f; \quad \text{where } f = 0.079\, Re^{-0.25}$$

Therefore the average 'v^2' at
the jet injection cross section * πR^2 = $1.44\ 0.125R^2V_j^2N_j(d_j/R)^2 + (\pi R^2 - 0.125N_jR^2)\ 0.31\ f\ V_j^2$

$$= 1.26R^2V_j^2(d_j/R)^2 + 0.702\ f\ R^2V^2 \quad \text{for } N_j=7$$

Therefore average v^2, weighted by area

$$= \frac{1.26R^2V_j^2(d_j/R)^2 + 0.702\ f\ R^2V^2}{\pi R^2}$$

$$= \frac{1.26V^2(d_j/R)^2 + 0.702\ f\ V^2}{\pi}$$

8.3.2 Concentration distribution downstream

8.3.2.1 Solution to Segev's water conservation equation

A two-dimensional exact solution to Segev's conservation equation (Segev, 1984) was sought. When droplets are passing through a two dimensional flow field in a channel, their behaviour can be characterised by the two combined mechanisms of turbulent diffusion and gravitational settling. The relative contribution of each individual mechanism depends upon the parameter '$\ell W/D_f$', where 'ℓ' is the height of the channel, 'W' is the settling velocity of a particle and 'D_f' is the diffusion coefficient. When this parameter is small the droplet's behaviour is solely due to turbulent diffusion.

The annex A of ISO/DIS 3171 sets out the minimum required conditions for representative sampling of water in crude oil by specifying the uniformity of droplet dispersion. They estimate the uniformity of dispersion in horizontal pipe by the formula

$$\frac{c_1}{c_2} = \exp\left[\frac{-W}{D_f D}\right] \qquad (8.6)$$

The derivation of this formula was based on a simplified theory given by Prandtl, who assumed the concentration and velocity profiles to be fully developed. His dispersion equation under these conditions became:-

$$-c(1-c)W = \frac{dc}{dy} \qquad (8.7)$$

There had been many investigations to obtain exact solutions for aerosol behaviour in ducts due to the individual mechanism of diffusion or sedimentation. Investigations into simultaneous diffusion and sedimentation are scarce. The following researchers made use of various methods with various assumptions, one being zero concentration at the wall, in their analysis. They assumed that the particles are removed instantly from air (continuous phase) as they touch the wall.

Taulbee et al (1979) considered aerosol loss to the wall of a narrow parallel plate channel through which aerosol is passing with simultaneous consideration of diffusion and sedimentation. The solution they obtained, using Laplace transforms, for mean concentration variations along the channel has shown that the loss due to the combined mechanism is significantly smaller than algebraic sum of the loss due to two independent mechanisms.

Ingham (1977) determined the bulk mean concentration of aerosol particles in a flow in a parallel plate channel with simultaneous settling and diffusion, when the settling is relatively larger than diffusion. He adopted a different solution procedure, using a series, to that of Taulbee (1979).

Goldberg (1978) has given a method of solution for the combined mechanism, diffusion and settling, when the continuous fluid is at rest. Ingham (1984) considered the problem of simultaneous diffusion of aerosols in a short cylindrical pipe, taking into account the fluid

flow entrance effects into the pipe. They obtained solutions for mean concentration across the pipe, since this is directly related to the aerosol loss to the wall. All these workers used different solution methods which changed also with different situations, but they all assumed zero concentration at the wall.

Here we solve Segev's (1984) conservation equation for the combined mechanism with non-uniform initial concentration and having Soo's (1972 and 1982) boundary conditions for the walls. These boundary conditions are completely new to the work mentioned above, and incorporate a sticking probability (at walls) for the water droplets at the walls. The sticking probability describes the probability of a droplet to deposit (ie. become lost from the system) at the wall. This parameter ranges from $\alpha=0$ when no deposition occurs (ie complete re-entrainment of all particles that have reached the wall) to $\alpha=1$ when all particles drifting to wall stick or settle. These conditions were obtained by balancing the mass conservation at the wall, therefore are more representative than assuming zero concentration at the wall.

The general equation describing conservation of a scalar (eg. 'c') is given by:-

$$\frac{\partial c}{\partial t} + \nabla.U'c = \nabla.D_f\nabla c \qquad (8.8)$$

where U' is the convective velocity of the scalar. In the case of droplet flow, U' is the velocity of droplets.

Let $U' = U + W$

where U = velocity of the flow field of the media

W = relative velocity of the droplets and fluid

Substituting to the above equation gives:-

$$\frac{\partial c}{\partial t} + \nabla.(U+ W)c = \nabla.D_f\nabla c \qquad (8.9)$$

$$\frac{\partial c}{\partial t} + U.\nabla c + c\nabla.U + \nabla.(Wc) = \nabla.D_f\nabla c \qquad (8.10)$$

but if the flow field media (eg. oil) is incompressible, from continuity:-

$$\nabla.U = 0 \qquad (8.11)$$

Therefore

$$\frac{\partial c}{\partial t} + U.\nabla c = \nabla.D_f\nabla c - \nabla.(Wc)$$

$$\frac{\partial c}{\partial t} + U.\nabla c = \nabla.D_f\nabla c - W.\nabla c - c\nabla W \qquad (8.12)$$

The following assumptions were made for the two dimensional solution of the above equation.

a). The velocity profile is fully developed. Therefore the main (axial) flow velocity is taken as a constant U_a.

b). The axial diffusion is negligible compared to the axial convection along the pipe.

c). The transverse diffusion is constant.

d). The droplets have achieved their terminal velocities, and relative velocity is only due to gravitational force and $\nabla.W=0$, and

e). The flow is continuous and steady.

Therefore equation 8.12 becomes:-

$$U_a\frac{\partial c}{\partial x} + W_x\frac{\partial c}{\partial x} + W_y\frac{\partial c}{\partial y} = D_f\frac{\partial^2 c}{\partial y^2}$$

Let $(U_a + W_x) = U$ and $W_y = -W$

$$U\frac{\partial c}{\partial x} - W\frac{\partial c}{\partial y} = D_f\frac{\partial^2 c}{\partial y^2} \qquad (8.13)$$

where U is the absolute axial velocity and W is the settling velocity of the droplets.

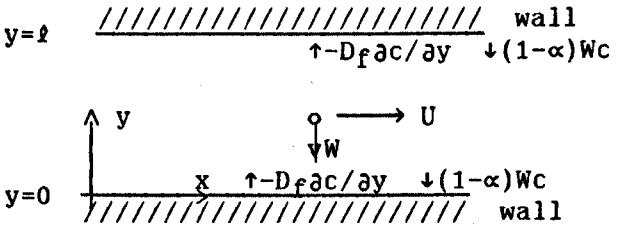

We seek a transformation in the form:-

$$c(x,y) = C(x,y)f(x,y) \qquad (8.14)$$

to reduce the equation 8.13 to:-

$$U\frac{\partial C}{\partial x} = D_f\frac{\partial^2 C}{\partial y^2} \qquad (8.15)$$

Substituting equation 8.14 to 8.13 gives:-

$$U\left\{f\frac{\partial C}{\partial x} + C\frac{\partial f}{\partial x}\right\} - W\left\{f\frac{\partial C}{\partial y} + C\frac{\partial f}{\partial y}\right\} = D_f\left\{f\frac{\partial^2 C}{\partial y^2} + 2\frac{\partial f}{\partial y}.\frac{\partial C}{\partial y} + C\frac{\partial^2 f}{\partial y^2}\right\} \qquad (8.16)$$

Since there are no terms having 'C' and '$\partial C/\partial y$' in equation 8.15, the terms having these on the left hand side of equation 8.16 should equate to those on the right hand side. Hence,

$$\text{'C'} \Rightarrow \quad U\frac{\partial f}{\partial x} - W\frac{\partial f}{\partial y} = D_f\frac{\partial^2 f}{\partial y^2} \qquad (8.17)$$

$$\text{'}\frac{\partial C}{\partial y}\text{'} \Rightarrow \quad -Wf = 2D_f\frac{\partial f}{\partial y} \qquad (8.18)$$

Equation 8.18 can also be written as:-

$$-\frac{W}{2D_f}\frac{\partial y}{} = \frac{\partial f}{f} \tag{8.19}$$

Integrating equation 8.19 gives:-

$$\ln f = -\frac{Wy}{2D_f} + g(x) \tag{8.20}$$

$$f = \exp\left[-\frac{Wy}{2D_f} + g(x)\right] \tag{8.21}$$

Substituting 8.21 to 8.17 gives:-

$$Ufg'(x) + Wf\frac{W}{2D_f} = D_f\frac{W}{2D_f}.\frac{W}{2D_f}f \tag{8.22}$$

$$g'(x) = -\frac{W^2}{4D_fU} \tag{8.23}$$

$$g(x) = -\frac{W^2x}{4D_fU} \tag{8.24}$$

$$f(x) = \exp\left\{-\frac{Wy}{2D_f} - \frac{W^2x}{4D_fU}\right\} \tag{8.25}$$

Therefore there exists a transformation that would transform equation 8.13 to 8.15.

Evaluation of differential equation 8.15

Solution to the equation 8.15 were attempted by considering four types of boundary conditions:-

a). c=0 at top wall; $0.0<\alpha<1.0$ at bottom wall

b). $\alpha=0$ at top wall; $\alpha=0.5$ at bottom wall

c). $\alpha=0$ at top and bottom walls

For the first instance, initial concentration was taken as a constant. ie at x=0, $c=c_o$. The analysis given below would not change when c_o is a function of 'y'.

a). y=0, c=0; y=ℓ, 0.0<α<1.0

In this problem the y=0 coordinate was set at the top wall. Therefore the 'f' function becomes

$$f(x,y) = \exp(Wy/2D_f - W^2x/4D_f)$$

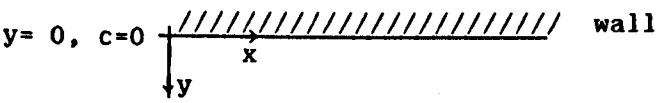

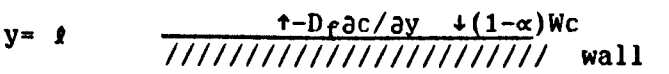

$c = 0 \Rightarrow C = 0$ at $y = 0$ and $(\partial C/\partial y) = hC$ at $y=\ell$ (8.27)

Soo's (1972 and 1982) boundary conditions for the bottom wall are given by:-

$$D_f\frac{\partial c}{\partial y} = (1-\alpha)Wc \qquad (8.29)$$

substituting $c(x,y) = C(x,y).f(x,y)$ gives

$$fD_f\frac{\partial C}{\partial y} + D_f f.\frac{W}{2D_f} = (1-\alpha)WfC \qquad (8.31)$$

$$\frac{\partial C}{\partial y} + \frac{CW}{2D_f} = (1-\alpha)\frac{W}{D_f}C \qquad (8.32)$$

$$\frac{\partial C}{\partial y} = (0.5-\alpha)\frac{W}{D_f}C \qquad (8.33)$$

$$\text{Let } h = (0.5-\alpha)\frac{W}{D_f} \qquad (8.34)$$

Now we have to evaluate,

$$U\frac{\partial C}{\partial x} = D_f\frac{\partial^2 C}{\partial y^2} \qquad (8.35)$$

With boundary conditions

$$\frac{\partial C}{\partial y} - hC = 0 \quad \text{at } y = \ell, \quad C = c_o \text{ at } y = 0 \text{and} \qquad (8.36)$$

$$C(0,y) = c_o \exp\left[\frac{-Wy}{2D_f}\right], \text{ where } c_o = \text{initial concentration} = \text{constant}$$

The expression,

$$\exp\left[\frac{-D_f\alpha_n^2 x}{U}\right] A\cos\alpha_n y + B\sin\alpha_n y \qquad (8.37)$$

satisfy the conditions 8.35 and 8.36 if,

$A = 0$ and

$\tan\alpha_n\ell = \alpha_n/h$

Therefore, the expression 8.37 becomes

$$\exp\left[\frac{-D_f\alpha_n^2 x}{U}\right] B\sin\alpha_n y \qquad (8.38)$$

Where α_n are the roots of $\tan\alpha_n\ell = \alpha_n/h$, which was solved by using the Newton-Raphson method, and B is an arbitary constant.

C(0,y) can now be developed in an infinite series as:-

$$C(0,y) = c_o \exp\left[\frac{-Wy}{2D_f}\right] = B_1Y_1 + B_2Y_2 + B_3Y_3 \text{-----} B_nY_n + \text{--} \qquad (8.39)$$

where $Y_n = \sin\alpha_n y$

Therefore the solution can be given as:-

$$C(x,y) = \sum_{n=1}^{\infty} B_n Y_n \exp\left[\frac{-D_f \alpha_n^2}{U}\right] x \qquad (8.40)$$

This is method given in Carslaw and Jaeger (1959) for solution of parabolic partial differential equations.

$$\text{Hence} \quad c(x,y) = f(x,y) \sum_{n=1}^{\infty} B_n Y_n \exp\left[\frac{-D_f \alpha_n^2}{U}\right] x \qquad (8.41)$$

Multiplying 8.39 by $\sin(\alpha_m y)$ and integrating gives the Fourier coefficients from the following expression (equation 8.42).

$$\sum_{n=1}^{\infty} B_n \int_0^{\ell} \sin\alpha_n y \sin\alpha_m y\, dy = \int_0^{\ell} C(0,y) \sin\alpha_m y\, dy$$

$$\int_0^{\ell} C(0,y) \sin\alpha_n y\, dy = 0 \qquad \text{when } m \neq n$$

$$= \frac{B_n\{\ell(\alpha_n^2 + h^2) - h\}}{2(\alpha^2 n + h^2)} \qquad \text{when } m=n, \text{ carrying out similar analysis to A8.1}$$

Hence,

$$B_n = \frac{2(\alpha_n^2 + h^2)}{\{\ell(\alpha_n^2 + h^2) - h\}} \int_0^{\ell} c_o \exp\frac{Wy}{2D_f} \sin\alpha_n y\, dy \qquad (8.42)$$

This expression is evaluated in Appendix A8.2

Therefore the solution is:-

$$c(x,y) = \sum_{n=1}^{\infty} f(x,y)\, A_n \sin\alpha_n y$$

$$= c_o \exp\left[\frac{Wy}{2D_f} - \frac{W^2 x}{4D_f U}\right] \sum_{n=1}^{\infty} B_n \sin\alpha_n y \exp\left\{-\frac{D_f}{U}\left[\alpha_n\right]^2 x\right\} \qquad (8.43)$$

where α_n are the roots of equation 8.29.

==========

b). Sticking probability is $\alpha = 0$ at top and $\alpha = 0.5$ at bottom walls

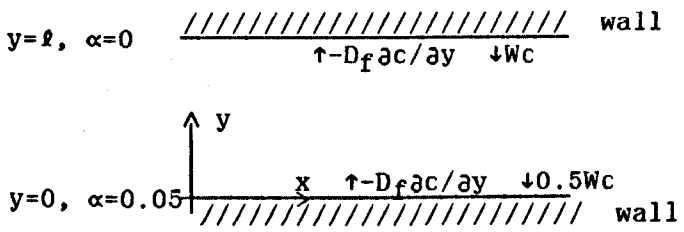

According to above coordinate system, Soo's boundary conditions for both walls are:-

$$-D_f \frac{\partial c}{\partial y} = (1-\alpha)Wc \qquad (8.61)$$

Substituting $c(x,y)=C(x,y).f(x,y)$ to equation 8.61 gives:-

$$C'.f + f'.C = \frac{-(1-\alpha)W.C.f}{D_f} \qquad (8.62)$$

$$f' = \frac{-Wf}{2D_f} \quad \text{(from equation 8.25)} \qquad (8.63)$$

Substituting equation 8.63 into 8.62 gives:-

$$C' = \frac{\partial C}{\partial y} = \frac{-(0.5 - \alpha)WC}{D_f} \qquad (8.64)$$

At top wall $\alpha=0$, hence :-

$$C' = \frac{\partial C}{\partial y} = \frac{-0.5\ WC}{D_f} \qquad (8.65)$$

Let $h = \dfrac{-0.5\ W}{D_f}$

At bottom wall $\alpha=0.5$, hence :-

$$C' = \frac{\partial C}{\partial y} = 0.0 \qquad (8.66)$$

Now we have to evaluate,

$$U\frac{\partial C}{\partial x} = D_f\frac{\partial^2 C}{\partial y^2} \tag{8.67}$$

with boundary conditions

$$\frac{\partial C}{\partial y} - hC = 0 \quad \text{at } y = \ell, \quad \frac{\partial C}{\partial y} = 0.0 \text{ at } y = 0 \text{ and} \tag{8.68}$$

$$C(0,y) = c_o \exp\left[\frac{Wy}{2D_f}\right] \text{ where } c_o = \text{initial concentration} = \text{constant}$$

The expression,

$$\exp\left[\frac{-D_f\alpha_n^2 x}{U}\right]\left[A\cos\alpha_n y + B\sin\alpha_n y\right] \tag{8.69}$$

satisfy the condtions 8.67 and 8.68 if,

$B = 0$ and

$\tan\alpha_n\ell = -h/\alpha_n$

Therefore, the expression 8.69 becomes

$$\exp\left[\frac{-D_f\alpha_n^2 x}{U}\right] A\cos\alpha_n y \tag{8.70}$$

Where α_n are the roots of $\tan\alpha_n\ell = -h/\alpha_n$, which was solved using the Newton-Raphson method.

C(0,y) can be be developed in an infinite series as:-

$$C(0,y) = c_o \exp\left[\frac{Wy}{2D_f}\right] = A_1Y_1 + A_2Y_2 + A_3Y_3 \text{-----} A_nY_n + \text{--} \tag{8.71}$$

where $Y_n = \cos\alpha_n y$

Therefore the solution is:-

$$C(x,y) = \sum_{n=1}^{\infty} A_n Y_n \exp\left[\frac{-D_f \alpha_n^2}{U}\right] x \qquad (8.72)$$

Hence $$c(x,y) = f(x,y) \sum_{n=1}^{\infty} A_n Y_n \exp\left[\frac{-D_f \alpha_n^2}{U}\right] x \qquad (8.73)$$

Multipling 8.71 by Y_m and integrating term by term gives the Fourier coefficients from the following expression:-

$$\int_0^{\ell} C(0,y).Y_m = \Sigma A_n \int_0^{\ell} Y_n Y_m \, dy$$

$$\Sigma A_n \int_0^{\ell} Y_n Y_m \, dy = 0 \qquad m \neq n$$

$$= \frac{A_n\{\ell(\alpha_n^2+h^2)-h\}}{2(\alpha_n^2 + h^2)} \qquad m=n, \text{ see A8.1}$$

$$\text{Therefore } A_n = \frac{2(\alpha_n^2 + h^2)}{\{\ell(\alpha_n^2+h^2)-h\}} \int_0^{\ell} C(0,y).Y_n \, dy \qquad (8.75)$$

This expression is evaluated in Appendix A8.3 and the solution is:-

$$c(x,y) = \sum_{n=0}^{\infty} f(x,y) \, A_n.Y_n \exp\left[\frac{-D_f \alpha_n^2}{U}\right] x, \text{ where } A_n \text{ is given by equation 8.75}$$

$$= c_o \exp\left[\frac{Wy}{2D_f} - \frac{W^2 x}{4D_f u}\right] \sum_{n=0}^{\infty} A_n.Y_n \exp\left[\frac{-D_f \alpha_n^2}{U}\right] x \qquad (8.76)$$

==========

c). Sticking probability is α =0 at top and bottom walls

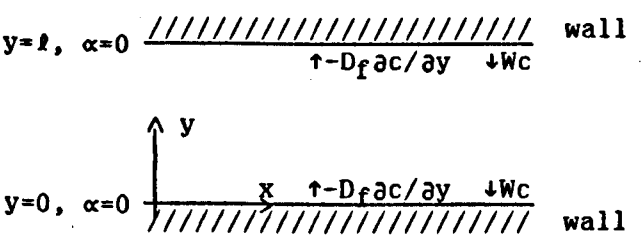

According to above coordinate system, Soo's boundary conditions for

both walls are:-

$$-D_f \frac{\partial c}{\partial y} = (1-\alpha)Wc \qquad (8.77)$$

Substituting $c(x,y)=C(x,y).f(x,y)$ to equation 8.77 gives:-

$$C'.f + f'.C = \frac{-(1-\alpha)W.C.f}{D_f} \qquad (8.78)$$

$$f' = \frac{-Wf}{2D_f} \qquad \text{(from equation 8.25))} \qquad (8.79)$$

Substituting equation 8.79 into 8.78 gives:-

$$C' = \frac{\partial C}{\partial y} = \frac{-(0.5 - \alpha)WC}{D_f}$$

When $\alpha=0$ for both walls:-

$$C' = \frac{\partial C}{\partial y} = \frac{-0.5\ WC}{D_f} \qquad (8.80)$$

Let $h = \dfrac{-0.5\ W}{D_f}$

Now we have to evaluate,

$$U \frac{\partial C}{\partial x} = D_f \frac{\partial^2 C}{\partial y^2} \qquad (8.81)$$

with boundary conditions

$$\frac{\partial C}{\partial y} - hC = 0 \quad \text{at } y = 0 \text{ and } y = \ell \text{ and} \qquad (8.82)$$

$$C(0,y) = c_o \exp\left[\frac{Wy}{2D_f}\right] \text{ where } c_o = \text{initial concentration} = \text{constant}$$

The expression given below,

$$\exp\left[\frac{-D_f\alpha_n^2 x}{U}\right] A\cos\alpha_n y + B\sin\alpha_n y \qquad (8.83)$$

satisfy the conditions given by equations 8.81 and 8.82 if,

$\alpha_n B - hA = 0$ and

$h^2 + \alpha_n^2 = 0$ or

$\sin\alpha_n \ell = 0$

(since $(Bh + A\alpha_n)\sin\alpha_n y + (hA - \alpha_n B)\cos\alpha_n y = 0$)

Therefore, the expression 8.83 becomes

$$\exp\left[\frac{-D_f\alpha_n^2 x}{U}\right] A\,[\cos\alpha_n y + (h/\alpha_n)\sin\alpha_n y]$$

where α_n are the roots of,

$$\sin\alpha_n \ell = 0 \text{ ; ie } \alpha_n = n\pi/\ell \text{ and}$$
$$h^2 + \alpha_n^2 = 0$$

C(0,y) can be be developed in an infinite series as:-

$$C(0,y) = c_o \exp\left[\frac{Wy}{2D_f}\right] = A_0Y_0 + A_1Y_1 + A_2Y_2 + \text{-----}A_nY_n + \text{--} \qquad (8.84)$$

where $Y_n = \cos\alpha_n y + \dfrac{h}{\alpha_n}\sin\alpha_n y$

and Y_o corresponds to Y_n when $\alpha_n^2 + h^2 = 0$

Therefore the solution is:-

$$C(x,y) = \sum_{n=o}^{\infty} A_nY_n \exp\left[\frac{-D_f\alpha_n^2}{U}\right] x \qquad (8.85)$$

Hence $$c(x,y) = f(x,y) \sum_{n=o}^{\infty} A_nY_n \exp\left[\frac{-D_f\alpha_n^2}{U}\right] x \qquad (8.86)$$

Multipling 8.84 by Y_m and integrating term by term gives the Fourier coefficients from the following expression:-

$$\int_0^{\ell} C(0,y).Y_m = \Sigma\, A_n \int_0^{\ell} Y_n\, Y_m\, dy$$

$$\Sigma\, A_n \int_0^{\ell} Y_n\, Y_m\, dy = 0 \qquad m \neq n$$

$$= A_n \ell(\alpha_n^2 + h^2)/2\alpha_n^2 \qquad m=n \Bigg\} \text{ (see appendix A8)}$$

$$\text{Therefore } A_n = \frac{2\alpha_n^2}{\ell(\alpha_n^2 + h^2)} \int_0^{\ell} C(0,y).Y_n\, dy \quad n=1,2,\text{----}\infty \qquad (8.88)$$

this expression is evaluated in Appendix A8.4

The coefficient A_o correspond to roots $\pm ih$ of α_n. Therefore to find A_o, first we multiply equation 8.8.4 by Y_o and then integrate with respect to 'y'.

$$\int_0^{\ell} Y_o C(0,y)dy = \int_0^{\ell} Y_o\, A_o \exp\left[\frac{-Wy}{2D_f}\right] dy \qquad \text{other terms are zero since other roots are real.}$$

$$Y_o = \cos(ihy) + \frac{1}{i}\sin(ihy) = \cos(-ihy) - \frac{1}{i}\sin(-ihy) = \exp(hy)$$

Therefore, the above integral reduces to:-

$$c_o \ell = A_o \int_0^{\ell} \exp\left[\frac{-Wy}{D_f}\right] dy$$

$$A_o = \frac{-c_o \ell W}{D_f \exp[(-W\ell/D_f) - 1]} \qquad (8.89)$$

$$c(x,y) = \sum_{n=o}^{\infty} f(x,y)\, A_n.Y_n \exp\left[\frac{-D_f\alpha_n^2}{U}\right]x, \text{ where } A_n \text{ is given by equations 8.88 and 8.89.}$$

$$= c_o \exp\left[\frac{Wy}{2D_f} - \frac{W^2x}{4D_f u}\right] \sum_{n=o}^{\infty} A_n.Y_n.\left[\frac{-D_f\alpha_n^2}{U}\right]x$$

==========

8.3.2.2 Definition of cut-off point from secondary swirl to gravitation dominated flow

The force balance equation of a droplet (neglecting the diffusional forces) gives:-

$$F_d - mg = mf \tag{8.103}$$

$$C_d \tfrac{1}{2}\rho V_\theta'^2 D d^2 \pi/4 - mg = mf \tag{8.104}$$

$$f = - V_\theta'^2/2D \tag{8.105}$$

V_θ' is the swirl velocity that would just lift a drop from bottom to top of the pipe.

Substituing 8.105 into 8.104

$$V_\theta'^2 \{\tfrac{1}{2}\rho C_d \pi d^2/4 + m/2D\} = mg \tag{8.106}$$

since the flow surrounding droplets are turbulent, C_d was taken as 0.44.

In Chapter 7.0, when the Reynolds number was 27600, we have found:-

$$\ln\left[\frac{V_\theta}{1.83\ V_X}\right] = -\ 0.363(M_r^{0.83})\left[\frac{X}{D} - 1.625\right]$$

In order to obtain a general equation for this study the Reynolds number was also incorporated in the above equation to satisfy the experimental results of Reynolds number =48400. Hence:-

$$\ln\left[\frac{1.04*10^{-5} V_\theta Re^{0.4}}{V_X}\right] = -\ 0.367(M_r^{0.83})\left[\frac{X}{D} - 1.625\right] \tag{8.107}$$

We should emphasise that this alteration was carried out purely to make progress in this problem, but ideally more experimental data is needed to verify the dependence of V_θ on Reynolds number.

By substituting 8.106 into 8.107, we can find 'X_i' the distance where the swirl velocity (V_θ') is just enough to a lift a droplet to the top.

The distance to cut-off point was defined as X_1.

8.3.2.3 The decaying turbulent mass diffusivity

The equation generally used to obtain kinematic viscosity of fully developed turbulent pipe flow is given as $\nu_t = 0.4\ U^*\ R$ (ISO/DIS 3171 and Baker, 1988)

In fully developed pipe flow the u/U^* against radial distance is almost linear (Laufer, 1954 and Lawn, 1971). Therefore an average value for u can be found (appendix A6.9 and section 7.6) as, $u = 1.58U^*$. Substituting to the above gives, $\nu_t = 0.25\ u\ R$. This equation shows an energy model similar to $\mu_t \propto k^{1/2}\ell$. Launder et al (1979, p82) has indicated that the energy models suffice to discribe μ_t for developing flows. Hence we assume this model for ν_t to be true for the developing flows, behaving two dimensionally. As we have correlated a value for u experimentally in chapter 7, an estimate for turbulent diffusivity, 'D_f', can be found (since $D_f = \nu_t . Sc$).

8.3.2.4 Sticking probability, 'α'

A review for a value of 'α' was conducted in Fernando et al (1987). The review has indicated the complexity of the phenomena of droplet deposition and entrainment and has been found difficult to describe even by statistical approaches. Tsahalis (1977) has found a critical Reynolds number (=50), based on water layer height for the onset of entrainment in fully developed pipe flow. Beal's (1978) approach was encouraging. He found that the sticking probability for particle deposition on the wall of the pipe was a function of a dimensionless stopping distance. If this correlation can be demonstrated to be applicable to water droplets in oil then a very useful method of evaluating 'α' would result. But at present α has to be prescribed through experimental effort.

8.3.2.5 Droplet settling (slip) velocity

The droplet settling velocity was assumed to be small enough to ensure that they have reached their terminal settling velocities under gravity and obey Stoke's law. Therefore, to obtain the slip velocity for the droplets obeying Stoke's law, the expression used by ISO/DIS 3171, Segev (1984) and Baker (1988) was used. This expression is given below:-

$$W = (g/18)[(\rho_d-\rho)/\rho]d_{ave}^2/\nu$$

where $d_{ave} = (d_{max}/2)$, ρ is the density of oil, ρ_d is the density of water droplet and ν is the kinematic viscosity of the oil.

8.3.2.6 Program structure

The program was menu driven, and was structured (fig. 8.3) to be executed interactively. Therefore input parameters, such as diameter, pipe velocity , densities, viscosities etc. can be modified easily until a suitable concentration distribution at a downstream section is achieved.

8.4 Discussion

1). By substituting X=x/L; Y=y/ℓ and $c^*=c/c_o$ to equation 8.13 gives:-

$$\frac{U}{L}\frac{\partial c^*}{\partial X} - \frac{W}{\ell}\frac{\partial c^*}{\partial Y} = \frac{D_f}{\ell^2}\frac{\partial^2 c^*}{\partial Y^2}$$

$$\frac{U\ell^2}{LD_f}\frac{\partial c^*}{\partial X} - \frac{W\ell}{D_f}\frac{\partial c^*}{\partial Y} = \frac{\partial^2 c^*}{\partial Y^2}$$

This shows that for long distances downstream the equation reduces to

$$-\frac{W\ell}{D_f}\frac{\partial c^*}{\partial Y} = \frac{\partial^2 c^*}{\partial Y^2} \qquad \left(\text{since } \frac{U\ell^2}{LD_f} \ll 1\right)$$

In other words the concentration profiles have reached fully developed status.

The above equation indicates, that when $W\ell/D_f \gg 1$, the dispersion is dominated by convection process on the other hand if $W\ell/D_f \ll 1$ the dispersion is dominated by the droplet diffusion process. To obtain uniform distribution of water droplet concentration from top to bottom, the settling convection process should be smaller than the diffusion process, ie $W\ell/D_f \ll 1$. By substituting the appropriate relationships given before for $W\ell/D_f$, We find that:-

$$\frac{WH}{D_f} \propto \frac{(\rho_d - \rho)\sigma^2}{\nu\rho^3[(d_j/H)^2 + 1.22]\{U^2[\exp(-M_r(x/h)^{0.52})] + \nu^{0.125}U^{0.875}H^{-.125}\}^{1/4}}$$

$\propto$ = proportional

In these applications, normally $d_j/H \ll 1$, (H=ℓ)and so can be neglected, leaving;

$$\frac{WH}{D_f} \propto \frac{(\rho_d - \rho)\sigma^2}{\nu\rho^3[1.22]\{U^2[\exp(-M_r(x/H)^{0.52})] + \nu^{0.125}U^{0.875}H^{-.125}\}^{1/4}}$$

Thus, a better profile at a sampling location could be obtained when the values of oil (continous phase) kinematic viscosity, density, flow

velocity and momentum ratio are higher and when the values of surface tension, channel height (hydraulic diameter of the pipe), difference between droplet and oil densities are lower.

2). This model can be used to study the developing characteristics of water concentration profiles along the pipeline, downstream of the injecting plane, and also to obtain estimations for initial stages of a design. It has shown that different boundary conditions produce different concentration profiles. Baker (1988) has found a value for the sticking probability of 0.5 to be appropriate for his predictions near "Tee" junctions. There were no experimental data available for two component flow mixing systems. But some comparision with experimental data would be useful, particularly to prescribe a value for the sticking probability (α).

3). This model does not incorporate numerical analysis such as a finite difference scheme, and consequently it is less costly and more easy to execute, but these gains had to be traded-off with flexibility. Flexibility of the model may be improved by solving th 2-dimensional conservation equation numerically. For example, general purpose computer package Phoenics can be used for this purpose.

4). The results of the model have shown that the concentration profile changes quite rapidly initially, from uniform concentration and then gradually becomes the fully developed concentration state.

5). Complexities and general limitations are imposed on these models due to several unknown mechanisms that are involved in the process. These limitations and complexties are discussed by Baker (1988). Hence major simplications, as have been applied, have had to be made to make any progress. We have defined a cutoff point where a sharp change over from dispersion by swirl flow to gravitational settling is assumed. And also no allowance has been made upstream of this point, to accommodate deposition (ie through 'α'), if it exists.

This model in its present form does not consider a droplet distribution, but only an average size for all the droplets. This can

be extended to incorporate a size distribution of the form of the Rosin– Rammler equation as done by Segev (1984). The decaying turbulence diffusivity is represented by an arithmetic average between the, initial and the final axial points. When these points become further and further apart, this average value is not a good representation for turbulent diffusivity. In these situations the model needs to be modified by dividing the domain of interest into acceptable distances (elements), over which the diffusion coefficient would be taken as constant and then march forward element by element. Since the initial concentration of the n^{th} element is equal to the final concentration distribution of the $(n-1)^{th}$ element, the final concentration distribution of the $(n-1)^{th}$ element is matched to a polynomial that is a function height 'y'. Hence, the initial concentration distribution, one of the boundary conditions of the nth element, is known as a function of 'y'.

CHAPTER 9.0 COMPARISON OF NUMERICAL AND EXPERIMENTAL RESULTS

9.1 Introduction

As mentioned before, it would be useful to adopt computational fluid dynamics procedures for the design of a mixer nozzle, and for the better definition and understanding of the flow fields produced by them. To be able to apply these procedures with confidence it is essential that the accuracy of the physical model is neither over nor under estimated. In order to contribute to this above task preliminary verification of the numerical models was carried out.

Experimental results (velocity ratio 17) of chapter 7.0 are compared with numerical predictions. The experiments conducted in chapter 7.0, were numerically simulated in 'PHOENICS'. It was hoped that this study would provide additional data and a basis to guide the development and improvement of the method.

Velocities were quantitatively compared with the LDA measurements. Dispersion of passive contaminant was qualitatively tested at selected axial stations by comparing the contour plots obtained from the computer simulation and the photographs in chapter 7.0.

9.2 Theory

Theory used here is same as that in Chapter 5.0 and Chapter 6.0.

9.3 Simulation details

a. Flow domain

Radius of pipe	39.5mm
Diameter (equivalent) of the jet orifice	4.2 mm

b). Flow model

Turbulent model k-ϵ model

Model constants $C_D = 1$, $C_\mu = 0.9$, $C_1=1.44$ $C_2=1.92$ $\sigma_\epsilon=1.22$ $\sigma_k=1.0$ $K=0.435$

Boundary conditions:-

i). Wall — Wall function method. Distance to first grid node 'y_p' is selected such $y_p u^*/\nu=y^*=35$ (since $30<y^*<100$ is a requirement).

ii). At inlet — fully turbulent flow field with $k_{in} = 0.00325W_{in}^2$ and $\epsilon_{in}=0.164k_{in}^{1.5}/\ell_m$. The 1/7 power law for axial(W) velocity and U=V=0 (this was coded in subroutine GROUND- see appendix)

iii).At outlet — set to a fixed gauge pressure of 0.0.

iv). At axis of symmetry — along the axis of symmetry the gradient in the tangential direction of all the variables is equal to zero. Also the stream function is a constant

c) Water droplet dispersion

Boundary conditions:-

i) At wall — no flux $\partial c/\partial r = 0$ ie: α (sticking probability)=0

ii) At jet inlet — passive contaminant source of 0.1 by volume is injected.

iii) At pipe inlet — water concentration is zero

Sc number — 0.5 — Rodi(1979), Baker(1988) and Syed(1981)

d. Fluid properties

i). Density 1000 kg/m^3

ii). Dynamic viscosity 1.002 x 10^{-3} Ns/m^2

e. Computational grid:- After trying several combinations, a layout of 20*16*60 was found to be satisfactory. The jet inflow orifice was located at cell number 10 and 11 of the axial direction and the pipe length was set to 15 diameters. The grids are more finely divided near the wall, where the gradients are steepest, and at the centre. The first grid at the wall was set to ensure the requirements of the wall function boundary conditions method are satisfied (see boundary conditions above). The flow was considered to be symmetrical about the x=0 plane therefore the computational domain was taken as one half of the pipe.

f. Convergence criteria:- when the sum of the continuity residual for all the control volume is less than 0.5% of the total flow rate and the maximum continuity residual for any control volume is less than 0.004% of the total flow rate.

All dimensions were specified in length units "mm". Thus the inaccuracies that can result as a consequence of very small grids are avoided.

9.4 Analysis, and Comparison with Existing Experimental Data

1. Flow visualisations, by injecting fluorescein sodium dissolved in water, of the pipe cross sections were conducted by taking instantaneous and long exposure photographs in chapter 7.0. These long exposure photographs are compared qualitatively with the concentration contours of the numerical solutions.

9.5 Discussion

1. Predictions of tangential mean velocities (fig. 9.2.1 to 9.2.5) agree reasonably with measurements, when the complexity of the flow and existing crude simulations are taken into consideration. The main discrepencies are shown to be in the centre and near the wall. At the centre the tangential (swirl) velocity decreases sharply to zero. The reason for this being the selected coordinate system. In cylindrical coordinates, however finely the centre grids are layed out, it would not allow flow to pass through the centre of the pipe. Therefore the flow would take up zero velocity at this point. To stop spreading this effect too far, the centre grids were set very finely around this point. This situation can be avoided by having a body fitted coordinate system, for example a bipolar coordinate system, for the pipe cross section PHOENICS has just begun to introduce body fitted coordinate facilities to their code. These are still under development. According to Cham Ltd., the developer of the PHOENICS code, the code should be capable of generating body fitted coordinates, for complex geometries in any confined space, in the near future.

The second discrepancy at the wall is due to the fact that the curvature effects are not taken into account in the development of wall functions. Minor modifications to the first grid from the wall, such as improving the fineness, did not make any significant changes in the solution.

2. The vectors at the pipe cross-section show an almost static recirculation region near the top wall. Due to this the predicted tangential velocity of fig. 9.2.5 shows a negative velocity near the upper wall. A check on the same figure for the measured values show a positive values for the tangential velocity for the same region indicating the absence of this recirculating region. This discrepancy can be attributed to artifical (false) obstruction set out at the centre of the pipe by the coordinate system.

In all, several combinations of the grid layout were tried in order to

reduce these discrepancies and ultimately the layout in fig. 9.1 was chosen to be the most reasonable for this coordinate system.

3. The photographs obtained for the dispersion of a passive contaminant agree qualitatively well with the concentration contours of the numerical study (over laid transparency on fig. 7.13.1). As the velocity ratio increases there is a gradual tendency to degrade the qualitative agreement and the effect of the discrepancy at the top wall begins to show.

4. The predictions of mean axial velocity profiles (figs. 9.3.1 to 9.3.5) are not very good. Experimental evidence suggests that near the jet, high velocity gradients exist. The predicted profile tends to be relatively flatter than the experimental results. This may be because of the anisotropy of the turbulence. The k-ϵ models assume isotropic turbulence and specify equal eddy viscosities for all three directions. Therefore, the eddy viscosity in the axial direction is over specified and the flow behavior in that direction is more viscous than the true value.

CHAPTER 10.0 CONCLUSIONS AND SUGGESTIONS FOR FUTURE WORK

The mixing domain was divided to three regions, the penetration, near and far fields, and the investigations were conducted as indicated in chapter 1.0. Complete discussions and conclusions were presented at the end of each appropriate chapter. The main conclusions that can be drawn from this study are summarised below, followed by the suggestions for future work.

10.1 DISCUSSION AND CONCLUSIONS

10.1.1 Part 1 Penetration of single oil jet through a stratified water layer

1. When the oil jet penetrates the stratified water layer two different distinct regions were shown, region 1, where the oil jet is submerged in water and the region 2, where the oil jet penetrates the water/oil interface to oil. In both of these regions atomisation occurs. In the first region the kerosene jet breaks up into kerosene droplets. This may occur by several mechanisms depending on the injection conditions. The droplet sizes of the broken up oil jet indicate that they are too small to be formed by shear wave jet instability, that is due to boundary layer instability. Therefore it appears that the continuous phase (water) viscosity (μ_w) is not important in this atomisation (ie. atomisation of oil jet in water) process.

As the jet penetrates the interface to region 2, it consists of atomised oil droplets in water surrounded by an annular water sheet and also a portion of the unbroken kerosene jet core. The outer surface of the annular water sheet would now create an oil boundary layer around it. As the jet proceeds downstream, the water sheet breaks up into droplets exposing the inner atomised oil core to the outer continuous oil phase. The entrainment of oil towards the jet causes a transition from oil droplets in water to water droplets in oil (more precisely two component water drops). Further downstream

this transition would be completed to form a jet of water droplets in oil.

2. Features of water entrainment to the oil process are local to the jet interface.

3. The entrained water sheath does not strictly breakup due to Kelvin-Helmoltz instability waves at high oil jet velocities (when the oil jet is in the atomization region). At higher jet speeds, the irregular dynamic pressures on the oil jet surface deform the thin water layer locally and initially proturberances occur on the outer surface of the layer, then they elongate to finger like ligaments (or 'cigar' shaped) due to the Couette flow type shear (Hinze, 1955) and combinations of other mechanisms in the oil boundary layer. Then they break up into chunky droplets (more precisely two component water drops), which subsequently break up into smaller droplets on their travel in the turbulent flow field.

4. Using a simple physical model the results (jet Re number 3530 to 14243) of water entrainment, were approximated to a correlation of the form:-

$$\frac{E}{m_j} = \left[\frac{h}{d_j}\right]\left[\frac{\rho_w}{\rho_{oil}}\right]\left\{\ln\left[\frac{8.18\times10^5\ We_{oil}}{Re_{oil}}\right]^{0.294}\right\}^{-1.25}$$

The theoretical and experimental values are in the same order of magnitude, when the water entrainment rate was derived by assuming boundary layer entrainment is due to penetration of a smooth cylinder. In this case entrainment rate is given by:-

$$E_w = 0.223\ d_j\ (\rho_w^6 V_j^6 h^6 \mu_w)^{1/7}$$

5. The SMD experimental results (jet Re number 3530 to 14243), with the aid of dimensional analysis, were approximated to a correlation of the form:-

$$\frac{SMD}{d_j} = \frac{133.6}{We} \left[\frac{h}{d_j}\right] \left[\frac{\mu_{oil}}{\mu_w}\right]^{0.31}$$

Therefore the following changes, resulted in an increase in droplet diameter (d_{32}):-

i). a decrease in jet velocity

ii). an increase in viscosity of oil

iii) an increase in interfacial surface tension

iv). an increase in stratified water layer height

This equation indicates that the SMD is a weak function of oil viscosity. The above equation indicates a critical We number criterion, and so it appears that the measured droplets have assumed their size through secondary breakup, that is on their travel in the turbulent flow field rather than the initial breakup from the water sheath. The droplet size distributions generate a skewed Gaussian distribution

6). The role of density ratio (water to oil), on entrainment and water droplet sizes was not investigated, since this density ratio varies very little in the real situation.

10.1.2 Part 2 Dispersion of broken up stratified water layer in pipe cross flow- *computational study*

The single jet mixer in pipe cross flow was simulated using a commercially available code 'Phoenics'. Appropriate physical conditions were programmed into the code to simulate the problem in an homogeneous and a two fluid models. The entrainment levels formed in part 1 now behave as a source for the water conservation equation.

1. Some convergence difficulties were encounted for the k-ϵ model therefore relatively heavy under-relaxation factors were used for these variables. To fulfil the convergence criteria around 900-1000 sweeps were needed.

2. It is encouraging to see that the computed results indicate the

correct trends. The little experimental data available for jets in pipe cross-flow, are found in Maruyama et al(1981) and Fitzgerald et al (1979). These data can only be used to compare the computational results qualitatively for the penetration character of the jet trajectory. They agreed fairly with the computational results.

3. Detailed experimental data coupled with fine grid spacing would be needed for the quantitative validation of these models. On the other hand taking into account the inaccuracies that may be induced from complex two phase flow effects and due to incomplete understanding and other non-universalities in the turbulent models, the computational cost that would be inccurred by using a finer grid spacing may not worthwhile and therefore, at this stage the models may only serve as an initial predictive tool for these applications.

5. The k-ϵ model required about 900 to 1000 sweeps for convergence. Use of a constant turbulent eddy viscosity model would reduce this to about 200 sweeps for the same convergence criteria. Above a velocity ratio of 20, obtaining convergence with k-ϵ model becomes difficult. Setting a finer grid did not improve this situation. When the eddy viscosity was set to a constant (ie. 100 x dynamic viscosity) convergence was possible even for a velocity ratio of 30. Therefore algebraic eddy viscosity or mixing length may be carefully modelled for this particular problem in order to minimise these difficulties and costs.

6. Water droplet concentration contours obtained from Homgeneous and Two-fluid models indicate that uniformity of water at downstream can be achieved by changing jetting conditions such as increasing diameter of the jet orifice and velocity ratio.

7. In practice the required condition for sampling water in crude for horizontal pipes is for the concentration ratio of water between top and bottom to be larger than 0.9. But examination of these contour plots indicates that this rule for the uniform dispersion of water can be in error. Because, sometimes the constant water concentration contours run from top to bottom, yet having different high

concentrations on either sides of the vertical diameter.

10.1.3 Part 3 Flow field analysis of jet mixer nozzles in pipe cross flow, using LDA measurements- *Single phase flow study*

The purpose of these experiments was to improve the fundamental understanding of mixing occuring due to turbulence and swirl flow in jet mixers. Firstly a thorough description of the flow field of a fluid injected into a pipe cross flow was desired. And then, it was intended to use the body of data to test the finite difference (volume) computational model of the single mixer and to compare the two nozzle types. The conclusions drawn below, are from the experimental measurements corresponding to velocity ratios 36, 57 and 70.

1. As the injected fluid enters the cross flow, it undergoes a process that rapidly transfers mean kinetic energy to turbulence energy which eventualy dissipates as heat. This transfer process is relatively more pronounced on the multi-nozzle mixer, therefore, the mixing rate is faster and more intense near the nozzle. One of the reasons for this higher dissipation rate can be attributed to the way individual jets roll up first to form high velocity gradients due to their opposing velocity vectors at their borders.

2. Mixing patterns of the flow visualisation can be used to assess qualitatively the dispersion of a passive contaminant predicted by computational models. Use of yellowish-green Ar Laser beam for this visualisation technique would provide better definition, improving the quality of the assessment.

3. Present design calculations, by Jiskoot (Baker, 1987), assume that the injected jets completely dissipate as soon as they impinge on the top wall, the experimental measurements demonstrate that this is not the case. The jet impingement on the wall occurred, for velocity ratios 36 and 56, at less than 0.5 diameters downstream, yet turbulent intensities of the order of one were measured at one diameter

downstream. Therefore, the assumption, made by the existing calculation method (used by manufacturers of jet mix nozzles), is not quite justifed.

4. As the flow reaches downstream, approximately 4 diameters, the distribution of velocities (mean and RMS) flattens out and their magnitudes begin to close up for the two mixers, indicating that the flows are now almost independent of their different origins. When velocity ratios are 57 and 70 the average difference in RMS velocity for single and multi-nozzle is approximately 7% at 6 diameters downstream. And their magnitudes are about 3 times higher than the corresponding fully developed pipe flow values.

5. Interestingly, the tangential velocities at the axis of pipe decay faster for higher velocity ratios. This indicates higher velocity ratios would breakup droplets to a smaller sizes and increase the eddy viscosity by generating and dissipating energy, but dispersion strength (due to swirl) decays faster and the gravity settling begins earlier. Therefore, an increase in velocity ratio would improve the size distribution quality of the droplets, but has to trade-off with downstream dispersion strength due to swirl. On the other hand, higher velocity ratios would break up the droplets to smaller sizes therefore, the dispersion strength required to suspend them is much less than for the larger drops. The optimum balance of these effects can be identified from the model developed in Chapter 8.0.

6. Secondary swirl flow, as we may recall, plays an important role by dispersing the water droplets in the cross-pipe direction whilst turbulent (eddy) viscosity diffuses them. Therefore, as the secondary swirl flow dies out the gravity settling begins to become dominant and the flow field behaviour becomes two dimensional. When the velocity ratio is 57, the secondary swirl flow decays quite fast and becomes proportionally very small at 3 diameters downstream. Hence the sampling probe ideally needs to be installed fairly close to the mixer, that is before the gravity settling has commenced.

7. Axial and tangential turbulent velocities (RMS) are generally

different, but further downstream, about 3 diameters onwards, they become close to equal for both nozzles. In most situations we consider fully developed pipe flow as isotropic, although this is not truly the case. Therefore, the assumption of isotropy is justified for these mixers from the vicinity of 3 diameters downstream.

Experiments have also shown that the axial and tangential RMS velocities tend to become closer to equal (hence isotropic) faster for higher velocity ratios than for low velocity ratios.

8. The average turbulent (axial) kinetic energy across the diameter was approximated to an equation (Re no= 27600) of the form:-

$$\frac{(u^2 - u_o{}^2)_{ave}}{U_X{}^2} = 8.16 * \exp\left\{-2.79 * M_r{}^{-0.094}\left[\frac{x}{D}\right]^{0.52}\right\}$$

where u is average turbulent RMS velocity at a cross section and u_o is the corresponding value of fully developed pipe flow (related to downstream flow conditions). This equation was used to estimate the value of the decaying turbulent diffusion coefficient in the form of an energy model.

9. The relationship, on a log-linear scale, of tangential velocity at the pipe axis against axial distance is linear. These linear relationships (Re no= 27600) of multi-nozzle mixer were correlated (when some upstream points closer to the nozzle are appropriately rejected) to a common equation of the form-

$$\ln\left[\frac{V_\theta}{1.83 * U_X}\right] = 0.363\left[M_r{}^{0.83}\right]\left[\frac{x}{D} - 1.625\right]$$

where v_θ is the tangential mean velocity at the pipe axis.

10. When the velocity ratio was 36 the Reynolds number was changed (ie by varing the velocity) from 27600 to 48400, a relatively weak change in swirl decay was demonstrated.

11. The angular velocity vector of a multi-nozzle mixer at its axis

is in the direction opposite to the main flow, however, swirl velocity of the single mixer is in the direction of the main flow and their magnitudes are also different very near the mixers. Therefore a direct comparision of individual velocities is not possible. But the swirl velocities, at the pipe axis, of both mixers die away (to 10% of the pipe axial velocity and lower) approximately at the same cross section.

12. Eventually, we may conclude that the multi-nozzle is superior in performance in two characteristics; i). Mixing is faster and RMS distribution flatten out closer to the mixer, indicating well mixed cross-section. ii). Jet energy is more evenly distributed at the injection cross-section, hence improving the quality of the droplet size distribution (and entrainment, if applicable).

As the flow reaches downstream, approximately 4 diameters, the distribution of both mean and RMS velocities flattens out and their magnitudes for both nozzles begin to close up for the two mixers indicating that flows are now almost independent of their different origins.

The LDA experimental data besides providing information to aid understanding of the complex flow in the mixer zone, is believed to be of sufficient quality and quantity to be used as test cases for the assessment of the predictive accuracy of the computational models.

10.1.4 Part 4 Inter-relationships and implications of above three parts

In this part we have obtained an exact solution for the 2-D water conservation equation. This equation was combined with some of the empirical data of the near field to develop a low level model for a multi-nozzle mixer. The predictions of the finite difference (higher level) model were also compared with LDA experimental results. The following conclusions were drawn from this analysis.

10.1.4.1 Low level model

1. The dimensionalised water concentration equation indicates, when the dimensionless quantity $WH/D_f >> 1$, that the dispersion is dominated by the settling convection process. On the other hand if $W\ell/D_f << 1$ the dispersion is dominated by the droplet diffusion process. To obtain uniform distribution of water droplet concentration from top to bottom, the settling convection process should be smaller than the diffusion process, ie $WH/D_f << 1$. By substituting appropriate relations given before for WH/D_f, We find that:-

$$\frac{WH}{D_f} \propto \frac{(\rho_d - \rho)\sigma^2}{\nu\rho^3[1.22]\{U^2[\exp(-M_r(x/H)^{0.52})]+\nu^{0.125}U^{0.875}H^{-.125}\}^{1/4}}$$

Thus, a better water concentration profile at a sampling location could be obtained when the values of oil continous phase kinematic viscosity and density, flow velocity and momentum ratio are higher and when the values of surface tension, channel height (H = hydraulic diameter of the pipe), difference between droplet and oil densities are lower.

2). The low level model developed from the 2-D exact solution of the water concentration equation can be used to study the developing characteristics of water concentration profiles along the pipeline, and also to obtain estimations for initial stages of a design. It has been shown that different boundary conditions produce different concentration profiles. Baker (1988) has found value of sticking probability 0.5 is more appropriate for his predictions near "Tee" junctions. There were no experimental data available for these two component flow mixing systems. But some comparision with experimental data would be useful, particularly to obtain a value for the sticking probability.

3). To estimate the turbulent diffusivity a kinetic energy model for the flow was developed and given by:-

$\nu_t = 0.25\ u\ R$ where u and R are RMS velocity and pipe radius.

4). This low level model does not incorporate numerical analysis such as a finite difference scheme, and consequently it is relatively less costly and easier to execute, but these gains had to be traded-off with flexibility. Flexibility of the model may be improved by solving th 2- dimensional conservation equation numerically.

5). The results of the model have shown that the concentration profile changes quite rapidly, initially, from uniform concentration and then gradually changes towards the fully developed concentration state.

6). Complexities and general limitations are imposed on these models due to several unknown mechanisms that are involved in the process. These limitations and complexties are discussed by Baker (1988). Hence simplifications, as have been utilised here, have had to be made in order to make any progress. We have defined a cutoff point where a sharp change over from dispersion by swirl flow to gravitational settling is assumed. This may be justified on the grounds of very fast swirl decay. And also no allowance has been made upstream from this point, to accommodate deposition (ie through 'α'), if it exists.

10.1.4.2 Comparision of experimental data with finite difference (higher level) model

1. Predictions of tangential mean velocities (fig. 9.2.1 to 9.2.5) agree reasonably with measurements, when the complexity of the flow and existing basic simulations are taken into consideration. Main discrepancies are shown to be in the centre and near wall. At the centre the tangential (swirl) velocity decreases sharply to zero. The reason for this being the selected coordinate system. In cylindrical coordinates, however finely the centre grids are layed out, it would not allow flow to pass through the centre of the pipe. Therefore the flow would take up zero velocity at this point. To stop spreading this effect too far, the centre grids were set very finely around this point. This situation can be avoided by having a body fitted coordinate system, for example a bipolar coordinate system, for the

pipe cross-section. Cham Ltd., the developer of the PHOENICS code, has just begun to introduce body fitted coordinate facilities to their code. These are still under development. According to them the code should be capable of generating body fitted coordinates, for complex geometries in any confined space, in the near future.

The second discrepancy at the wall is due to the fact that the curvature effects are not taken into account in the development of wall functions. Minor modifications to the first grid from the wall, such as improving the fineness, did not make any significant changes in the solution.

2. The vectors at the pipe cross-section shows an almost static recirculation region near the top wall. Due to this the predicted tangential velocity of fig. 9.2.5 shows a negative velocity near the upper wall. A check on the same figure for the measured values shows a positive value for the tangential velocity for the same region indicating the absence of this recirculating region. This defficiency can be attributed to an artifical (false) obstruction set out at the centre of the pipe by the coordinate system.

3. The photographs obtained for dispersion of passive contaminant agrees qualitatively well with the concentration contours of the numerical study. As the velocity ratio increases there is a gradual tendency to degrade qualitative agreement and the effects of the recirculation (in the numerical model) at the top wall begin to show.

4. The comparision with experimental data was made for a low velocity ratio (17) as the convergence for high velocity ratios with k-ϵ model was not possible. Near the jet injection (> 1 diameter downstream) the velocity gradients in the radial direction are higher for the experimental values than for the predicted values. It was shown in the experimental study 7.0, that the swirl motion for low velocity ratios decays more slowly and the anisotropy of turbulence associated with low velocity ratios is higher. Thus, this discripancy may be because of the anisotropy of the turbulence. The k-ϵ models assume isotropic turbulence and specify equal eddy viscosities for all three

directions. Therefore, the eddy viscosity in the axial direction is over specified and the flow behaviour in that direction is more viscous than the true value.

10.2 Suggestions for future work

Further to this study the most immediate suggestions for the future work are as follows:-

1. Experiments, accomodating wider changes in the dependent variables, are required for the fine tuning of the entrainment and SMD correlations

2. Further work in the form of photographic studies for examining water entrainment due to secondary swirl flow, in order to to identify the entrainment mechanism, would be worthwhile.

3. Use of body fitted coordinates for example a bi-polar system, to improve the finite difference model.

4. This model in its present form did not consider a droplet distribution, but only an average size for all the droplets. This can be extended to incorporate a size distribution.

5. It would be worthwhile to model the eddy viscosity by using a mixing length for this particular problem in order to reduce computational costs and to avoid convergence difficulties in higher velocity ratios. One way of doing this is to divide the flow into two counter rotating voticies for the single jet mixer. Then specify $\mu_t = \rho\lambda^2|(\partial V_\theta/\partial r) - V_\theta/r|$, where V_θ and r correspond to a coordinate system based on the centre of each of the vortices. The mixing length λ has to be prescribed from experimental data.

6. The LDA study should be extended to establish the Re number dependence of swirl decay and to compare the two nozzles at higher velocity ratios (higher than 70).

7. Experiments in chapter 7.0 have shown that there is a tendency for axial and tangential RMS velocities to become closer to equal faster for higher velocity ratios than for low velocity ratios. This needs further investigation. If the main cause, for higher velocity ratios, for secondary entrainment is isotropic turbulence (as the swirl also decays faster), the secondary entrainment could be modelled assuming local isotropy (assuming the water layer is not too thin). This would simplify the analysis of secondary entrainment considerably

8. Experimental data is needed for jet mixers in two component (oil/water) flow in order to specify a suitable value for the sticking probability and to validate models for concentration distributions at pipe cross-sections.

REFERENCES

REFERENCES

Abou-Arab, T. W. "Turbulence Models for Two-Phase Flows." Chapter 30, Encyclopedia of Fluid Mechanics, Edited by Cheremisinoff, vol. 3, 1986.

Adelberg, M. "Breakup rate and penetration of a liquid jet in gas stream." AIAA Journal, 1967(Aug.), 5, pp1408-1415.

Adelberg, M. "Mean drop size resulting from the injection of a liquid jet into a high-speed gas steam." AIAA Journal, 1968(June), pp1143-1147.

Adrian, R. J. and Fingerson, L. M. "Laser anemometry theory, application and techniques.' TSI short course notes.

Akegawa, K., Fuki, T., Ito, J., Hemmano, Y., Horinchi, T., "Horizontal liquid film mist two-phase flow." (2nd report droplet deposition and entrainment rates), Bulletin of JSME 1985(Feb.), 28(236), pp 301-308.

Akai, M., Inoue, A., Aoki, S and Endo, K. "A co-current stratified air-mercury flow with wavy interface." Int. J. Multiphase Flow 6, 1980, pp 173-190.

Akai, M., Inoue, A. and Aoki, S. " The prediction of stratified two-phase flow with a two-equation model of turbulence." Int. J. Multiphase Flow, Vol. 7, 1981, pp21-39.

Akoi, M., Inque, A. and Aoki, S. "Structure of a co-current stratified two phase flow with wavy interface." Theor. Appl. Mech. 25, 1977 pp445-456.

Asali, Hanrantly and Andreussi "Interfacial drag and film height for vertical annular flow." A.I.Ch.E. J., 1985, 31, p895.

Baker, R. C. "Computation method to obtain concentration of water in crude oil downstream of a mixing section." 1985(June), Report No. 18/207/36.

Baker, R. C. "Sampling water-in-oil." Cranfield press, 1987.

Baker, R. C. "Compuational method to assess concentration of water in crude oil downstream of a mixing section." Proc. Instn. Mech. Engrs., Vol. 202, No. A2, 1988.

Baker, R. C. "Private communication with Prof. R. C. Baker" Dept. of Fluid Engineering and Instrumentation, Cranfield Institute of Technology, Cranfield, 1987.

Batchelor, G. K. "The theory of homogeneous turbulence." Cambridge University Press, 1953.

Beal, S. K. "Correlation for the sticking probability and erosion of particles." J. Aerosol Sci., Vol. 9, 1978, pp 455-461.

Beer, J. M. and Chigier, N. A. "Combustion Aerodynamics." 1972, Applied Science Publishers Ltd., London.

Bergwerk, W. "Flow pattern in diesel nozzle spray holes." Proc. Instn. Mech. Engrs., 1983, 105, p406.

Blevins, R. D. "Applied Fluid Dynamics Handbook." 1984, Van Nostrand Reinhold Company.

Bradshaw, P. "Introduction to Numerical Methods and Turbulence Modelling." Lecture notes, Advanced Flow Calculations for Internal Flow and Turbomachinery.", Cranfield, 9^{th}-11^{th} Sept. 1986.

Bredeenthal, R. E., Kwok-On Tong, Wong, G. S., Hamerquist, R. D. and Laundry, P. B. "Turbulent mixing in two-dimensional ducts with transverse jets." AIAA Journal, Vol. 24, No. 11, Nov.' 86 p 1867.

Briffa, E. J. F. and Dombrowski, N., "Entrainment of air into a liquid spray." A.I.Ch.E. J., 1966(July), p708.

Brodkey, R. S. "The phenomena of fluid motions." Addison-Wesley Publishing Company.

Carslaw, H. S. and Jaeger, J. C. "Conduction of Heat in Solids." Oxford, Clarendon Press, 1959.

Castleman, R. A. "Mechanism of Atomization accompanying solid injection." N.A.C.A. Report 440, 1932.

Cathie, N. M. "Static Mixer for Pipeline Sampling" Automatic Sampling and Water Determination for Crude Oils Symposium, Institute of Measurement and Control, Maidstone, Nov., 1981.

Cham Ltd. "The Phoenics user's manual" Cham Report Number TR/100, October 1986.

Cham Ltd. "Lecture Panels for Phoenics Advanced Course." 1987.

Cham Ltd. "Mathematical Basis of Phoenics." Lecture Panels for Phoenics Introdution Courses, Sept. 1986, CHAM TR/121.

Champion, F. C. and Davy, D. "Properties of matter." third edition, 1961, Blackie and Son Ltd.

Chen, S. J. and Libby, D. R. "Gas Liquid and Liquid-Liquid Dispersion in a Kenics Mixer." Proceeding of the AIChE meeting, Miami Beach, USA, 1978.

Cheng, K. C. and Yuen, F. P. "Flow Visualisation Studies on Secondary Flow Patterns in Straight Tubes Downstream of a 180 deg Bend and in Isothermally Heated Horizontal Tubes." Tran. ASME, J. of Heat Transfer, Feb. 1987, Vol.109, pp 49-54.

Chilton, T. H. and Genereaus, R. P. American Institute of Chemical Engineers Transactions, Vol. 25, 1930, pp 102-127.

Christy, J. R. E and Macleod, N "A Study of the Performance of a Static Mixer in Pulsatile Flow." 5th European Conference on Mixing, Wurzburg, Germany, 1985.

Clark, C. J. and Dombrowski, N. "Aerodynamic instability and disintegration of invicid liquid sheets." Pro. R. Soc. Lon. A329, 1972, pp 467-478.

Clift, R Grace, J. R and Weber, M. E "Bubble, Drops and Particles." Academic press 1978.

Crank, J. "The mathematics of diffusion. " Clarendon Press, Oxford, England 1964.

Crowder III, R. S., Daily, J. W. and Humphrey, J. A. C "Numerical Calculation of Paritcle Dispersion in a Turbulent Mixing Layer Flow." J. Pipelines, vol. 4, no. 3, May 1984, pp 159-169.

Danon, Wolfshtein and Hetsroni "Numerical Calculations of Two-Phase Turbulent Round Jet." Int. J. Multiphase Flow, 1977, 3, pp 223-234.

Dantec (short course) "Laser Doppler Anemometry at Cranfield institute of technology, 1988.

Davies, C. N. "The Sedimentation and Diffusion of Small Particles." 1949, Proc. R. Soc., A200, pp 100-113.

Demuren, A. O. "Modelling turbulent jets in cross flow." Encyclopedia of Fluid Mechanics, chapter 17, Edited by Cheremisinoff, vol. 2, 1986, pp 431-436.

DeJuhasz, K. J. "Dispersion of sprays in solid injection oil engines." Trans. A.S.M.E., 1931, 53, p65.

Dombrowski, N. and Hooper, P. C. "A Study of the Sprays Formed by Impinging Jets in Laminar and Turbulent Flow."J. Fluid Mech., 1964, 18, pp392-400.

Dombrowski, N. and John "A photographic investigation into the disintegration of liquid sheets." Phil. Trans. Roy. Soc. London, Ser. A, Maths. and Phys. Sci., 247, pp101-130.

Dombrowski, N. and John "The aerodynamic instability and disintegration of viscous liquid sheets." Chem. Engng. Sci., 1963, 18, pp203-214.

Drew, D. A. "Mathematical Modelling of Two-Phase Flow." Annual Review of Fluid Mechanics, Vol. 15, 1983, Edited by Von Dyke Wehausen and Lumley.

Durst, F., Melling, A. and Whitelaw, J. H. "Principles and practice of Laser- Doppler Anemometry." Academic press 1976.

Dus and Ros "Simultaneous flow of gas and liquid as encounted in well tubing." J. of Pet. Tech., 1963(Oct.), pp1037-1049.

Edwards, A. C., Sherman, W. D. and Breidenthal, R. E., "Turbulent mixing in tubes with transverse injection.", AIChE Journal, Vol. 31, No. 3, March 1985, p 516.

El-Shanawany, M. S. and Lefebvre, A. H. "Airblast atomization- The effect of linear scale on mean drop size." J. Energy, 1980, 4, pp184-189.

Ellis, S. R. and Gay, B. "The parallel flow of two fluid streams; Interfacial shear and fluid-fluid interaction." Trans. Inst. Chem. Engrs., 37, 1959, pp206-213.

Ellul, I. R. and Issa, R. I. "The Prediction of Interspersed Two-Phase Flow Through Pipe Obstructions." 3rd International Conference on Multi-Phase Flow, The Hague, Netherlands 18-20 May 1987, pp 213-222.

Ervine, D. A. McKeogh, E. and Elsamy, E. M. "Effect of turbulence intensity on the rate of air entrainment by plunging water jets." Proc.Insti. of Civil Engrs., part 2, 1980, (June) 69, pp425-445.

Fernando, L. M. and Lenn, C. P. "Review of the literature for 'α' (droplet deposition parameter) and K (droplet coalescence parameters)." Cranfield Institute of Technology, Fluid Engineering and Instrumentation, Report prepared for BP international Ltd., Jan.'87, report no. 18/308/68.

Fernando, L. M. and Lenn, C. P. Jet mixing of water in crude oil pipelins for representative sampling- experimental study." A paper accepted to be presented at the 2nd International symposium on application of analytical techniques to industrial process control, ANATECH'90, 3-5 April 1990, Noordwijkerhout, Netherlands.

Fitzgerald, S. D. and Holley, E. R. 'Jet injection for optimum mixing in pipe flow." Illinois University at Urbana-Champaign Water Resources Centre, Report UILU-WRC-79-0144, Dec.'79.

Flaschel, E., Nguyen, K. T. and Renken, A. "Improvement of Homogeneous Tubular Reactor Operated at Low Reynolds Number." 5th European Conference on Mixing, West Germany, June 1985.

Forney, L. J. "Jet injection for optimum pipeline mixing." Chapter 25, Encyclopedia of Fluid Mechanics, Edited by Cheremisnoff, vol. 2, 1985.

Fraser, R. P., Dombrowski, N. and Routley, J. H. "The Production of Uniform Liquid Sheets from Spinning Cups." Chem. Eng. Sci., Vol. 18 1963, pp315-321, pp323-337, pp339-353.

Fraser, R. P. and Eisenklam, P. "Liquid Atomisation and the Drop size of Sprays." Trans. Inst. Chem. Engrs., London, 1956, vol. 34, pp294-319.

Fraser, R. P., Eisenklam, P., Dombrowski, N. and Hasson, D., "Drop Formation from Rapidly Moving Liquid Sheets." A.I.Ch.E. J. , vol. 8, No. 5, 1962, pp 672-680.

Fraser, P. R., Dombrowski, N. and Routley, J. H. "The atomization of liquid sheet by an impinging air stream." Chem. Engng. Sci., 1963, 18, pp339-353.

Friedlander, S. K. and Topper, L. (editors) "Turbulence-classic papers on statistical theory." 1961, Interscience Publishers, Inc., New York.

Ger, A. M. and Holley, E. R. 'Turbulent jets in crossing pipe flow." Hydraulic Engineering Series Report 30, University of Illinois at Urbana- Champaign, 1974, p 198.

Giffen, E. and Muraszew, A. "The atomisation of liquid fuels." 1953, London, Chapman and Hall Ltd.

Gilchrist and Naom "Co-current flow of air and thin liquid film in a vertical tube." 3rd international conference on multi-phase flow, Hague, Netherlands, 1987(May 18-20).

Goldberg, I. S., Lam, K. Y., Bernstein, B. and Hutchens, J. O. "Solution to the Fokker-Planck equations governing simultaneous diffusion and gravitational settling of aerosol particles from a stationary gas in a horizontal circular tube." J. Aerosol Sci., Vol. 9, pp209-218.

Golitzene, N., Sharp, R. and Badham, L. G. "Spray nozzles for the simulation of cloud conditions in icing tests of engines." N.A.E. Canda, Report No. 14, 1951.

Gosman, A. D. "Application of LDA Measurements to Computational Fluid Mechanics." Second International Conference on Laser Anemometry Advances and Applications, 21st-23rd, Sept. 1987 ,U.K.

Gosman, A. D
Issa, R. I.
Lockwood, F. C
Taylor, A. M. K. P.
and Whitelaw, J. H. "Expermental and Computational Techniques for Dispersed Two-Phase Flows." Dept. of Mechanical Engineering Imperial College of Science and Technology, London, Short Course Lecture Notes, Sept'1989.

Grant, R. P. and Middleman, S. "Newtonian jet stability." A.I.Ch.E. J., 1966, 12, p669.

Green and Whitelaw "Isothermal model of Gas-turbine Combustors." J. Fluid Mech. 183, 126, 1984, pp 399-413.

Hagerty, W. W. and Shea, J. F. J. Appl. Mech., 1955, 22, p509.

Halsey, D. M. "The character of swirl in turbulent pipe flow with reference to its effects on flowmeters.' Ph.D Thesis, Department of Fluid Engineering and Instrmentation, 1986.

Hansell, P. "Ultraviolet and fluorescene recording." Chapter 8, Photography for the scientist, Edited by Charles E. Engel, Academic Press, 1968

Hanratty, T. J. and Engen, J. M. "Interaction between a turbulent air stream and a moving surface." 1957, A.I.Ch.E. J., 3, pp299-304.

Hartung K. H and Hiby, J. W "Comparsion of Turbulence Promotors for In-Line Mixing, IV International Congress of Chemical Equipment Design and Automation, 1972, Prague.

Harvey, D. W. "Drop size distribution resulting from liquid jet injection across a supersonic stream." McDonnell Douglas Astronautics Co., 1977(May), Huntington Beach, California.

Hayes, E. R. "Analysis of the Mixing Requirements for Representative Sampling at the Forties Charlie Fiscal Metering System." Dept. Fluid Engineering and Instrumentaion, Cranfield Institute of Technology, England, Report No 18/211V/72, April 1987.

Hayward, A. T. J. "Improving the accuracy of two phase flow measurement by momentary homogenisation." Proceedings of Flomeko, 1983(Sept.), IMEKO Conferences on flow measurement, Budapest, Hungary.

Hayward, A. T. J. and Jelfts, P. A. M. "Homogenisation by jet mixers with special reference to tanker discharge pipelines." Automatic sampling and water determination for crude oils." Symposium organised by the Kent section of the Institute of Measurement and Control, England, 1981 (Nov.).

Hayward, P. "Minimum hydraulic conditions for automatic sampling 1985(Nov.), Petrole et Technique No. 295, pp 64-68.

Hewett and Hall Taylor "Annular two-phase flow." Pergamon Press, 1st Edition, 1970.

Hinze, J. O. Private reports of the Dutch/Shell Laboratory, Delft, 1946.

Hinze, J. O. "Turbulence." McGraw-Hill series in mechanical engineering, McGraw-Hill Co., 1975.

Hinze, J. O. "Forced deformation of viscous liquid globules." Applied Scientific Research, 1949, A1.

Hinze, J. O. " Funamentals of hydrodynamic mechanism of splitting in dispersion process." A.I.Ch.E. J., 1955, 1, pp289-295.

Hochschwender, Z. Dissertation, 1919, University of Heidelberg, Germany.

Hooper, A. P and Boyd, W. G. C. "Shear-flow instability due to a wall and a viscosity discontinuty at the interface." J. Fluid Mech., Vol. 179, 1987, pp. 201-225.

Hooper, A. P "Long-wave instability at the interface between two viscous fluids; thin layer effects." Phy. Fluids, Vol. 28, 1985, p 1613.

Hooper, A. P. "The Stability of Two Super Imposed Viscous Fluids in a Channel." Phys. Fluids A1, vol. 7, July 1989.

Hussein, G. A. "The Effect of Air/Liquid and Injector Geometry Variables on Performance of a Plain-Jet Air Blast Atomizer." Ph.D Thesis, School of Mechanical Eng. Cranfield Institute of Technology, 1983.

Ingham, D. B. "Diffusion of Aerosols from a Stream Flowing Through a Short Cylindrical Pipe." J. Aerosol Sci., Vol. 15, 1984, No. 5, pp63.

Ishii, M. "Thermo-Fluid Dynamics Theory of Two-Phase Flows." Eyrolles, Paris, 1975.

Ishii, M., Kataoka and Mishima "Generation and size distribution of droplets in annular two-phase flow." Trans. ASME, 1983(June), 105.

Ishii, M. and Zuber, N "Drag Coefficient and Relative Velocity in Bubbly Droplet or Particulate Flows." AIChE Jounal Vol. 25, No. 5, Sept.'79, pp843-855.

ISO/DIS 3171 "Petroleum Liquids-Automatic Pipline Sampling." ISO/DIS 3171, Annex A.

Jasuja, A. K. "Airblast atomization of alternative liquid petrolem fuels under high pressure conditions." Transactions of the ASME Journal of Engineering for Power, 1981(July), 103, pp514-518.

Jasuja, A. K. "Plain-jet airblast atomization of alternative liquid petrolem fuels under high ambient air pressure conditions." ASME paper no.82-GT-32, presented at the Wembley Gas Turbine Conference, 1982(April).

Jeffrey, H. "On the formation of water waves by wind." Proc. Roy. Soc. Sec. A., 1925, 110, pp341-347.

Jiskoot, J. J "Crude Oil Sampling-From Sampling Point to Laboratory Handling." Collected paper from the Symposium Flow Metering and Proving Techniques in the Offshore Oil Industry, Organised by Institute of Measurement and Control in Aberdeen, UK, 11-12 May 1983.

Jiskoot, J. J. " A new approach to pipeline conditioning." Petro-Expo, Houston, Texas, 1985(March).

Jones, W. P. and Launder, B. E. "Prediction of Low Reynolds Number Phenomena with a Two Equation Model of Turbulence." Int. J. Heat and Mass Transfer, 1973, 16, p119.

Jones, W. P. and McGuirk, J. J. "Computation of a round turbulent jet discarging into confined cross-flow." Shear Flows 11, Springer Verlag, New York, 1979, pp 233-245.

Karabelas, A. J. "Vertical distributuion of dilute suspensions in turbulent pipe flow." A.I.Ch.E. J., 1977(July), 23(4).

Karabelas, A. J. "Droplet size spectra generated in turbulent pipe flow of dilute liquid/liquid dispersion." A.I.Ch.E. J., 1978(March), 24(2).

Katoka and Ishii "Mechanistic modelling of pool entrainment phenomenon." Int. J. Heat Mass Transfer, 1984, 27(11), pp1999-2014.

Kawaashima Nakagawa and Iuchi "The Two-Dimentional Pattern of Flow at a right-angle, T-shaped confluence." Int. Chemical Engineering, Oct. 1983, 23, no. 3.

Kaye, G. W. C. and Laby, T. H. " Tables of Physical and Chemical Constants and some mathematical functions. " fifteenth edition, Longman, 1973.

Kazumon, Funatus, Yung-Chien Hsu and Takemi, Kamogawa "Gas holdup and gas entrainment of plunging water jet with constant entrainment guide." The Canadian J. of Chem Eng., 1988(Feb.), 66.

Khalil, E. E. "Modelling of Furnances and Combusters." Abacus press, 1982.

Kim, K. Y. and Marshall, W. R. "Dropsize distribution from pneumatic atomizers." A.I.Ch.E. J., 1971, 17(3), pp575-584.

Kitamura, Y. and Takahashi, T. "Stability of jets in liquid-liquid systems." Chapter 19, Encyclopedia of fluid mechanics, Vol. 2, 1986, Edited by Cheremisinoff.

Kobayashi, T. and Yoda, M. "Modified k-ϵ Model for Turbulent Swirling Flow in a Straight Pipe." JSME International Journal, Vol. 30, No. 259, 1987.

Kolmogoroff 1949, USSR(NS) 66, pp825-828.

Kumagai and Endoh "Effect of kinematic viscosity and surface tension on gas entrainment rate of an impinging liquid jet." J. of Chem. Eng. of Japan, 1982, 15(6).

Kuroda, C. and Ogawa, K. "Turbulent swirling pipe flow." Chapter 20, Encyclopedia of Fluid Mechanics, Vol. 1, 1986 Edited by Cheremisinoff.

Lane, W. R. "Shattering of drops in stream of air." Ind. and Eng. Chem., 1951, 43(6).

Laufer, J. "The Structure of Turbulence in Fully Developed Pipe Flow." 1954, NACA Report 1174, Technical Note 2954.

Launder, B. E. and Spalding, D. G. "Lectures in Mathematical Models of Turbulence." 1979, 3rd Edition, Academic Press Inc. (London) Ltd.

Launder, B. E. and Spalding, D. B "The Numerical Computation of Turbulent Flows." Computer Methods in Applied Mechanics and Engineering, 1974, 3, pp269-289.

Lawn, C. J. "The determination of the rate of dissipation in turbulent pipe flow." J. of Fluid Mechanics (1971), vol. 48, part 3, pp 477-505.

Lee. J. M. "Drop Size Formations in Agitating Systems." Complex Flow Phenomena and Modelling, Encyclopedia of Fluid Mechanics, Vol. 6, 1987, p141.

Lenard, P. Ann. Physik 1921, 65, p629.

Levich, V. G. "Surface tension driven phenomena." Annual review of Fluid Mech., 1969, 1, p293.

Levich, V. G. "Physicochemical Hydrodynamics." 1962, Prentice-Hall, New Jersey.

Liburdy, J. A. "Turbulent Jets." Aerodynamics and Compressible Flows, Encyclopedia of Fluid Mechanics, Vol. 8, 1989, p257.

Lin, S. P. and Kang, D. J. "Atomization of a liquid jet." Phys. Fluids, Vol. 30, No. 7, July 1987.

Lorenzetto, G. E. "Measurement of drop size on a plain-jet airblast atomizer." AIAA J.,1977, 15(7), pp1006-1010.

Mayer, E. "Theory of liquid atomization in high velocity gas stream." ARS Journal, 1961, 31, pp1783-1785.

Maruyama, Suzki and Mizushina "Pipeline mixing between two fluid streams meeting at a 'T'-junction." Int. Chem. Eng., vol. 21, No. 2, April 1981, pp205-212.

Maruyama, T. Mizushina, T and Hayashiguchi, S. "Optimum Conditions for Jet Mixing in Turbulent pipe flow." Int. Chem. Eng., vol. 23, no. 4, Oct.'83, pp707-716.

Meister, B. J. and Scheele, G. F. "Drop formation from cylindrical jets in immiscible liquid systems." AIChE. J., Vol. 15 NO. 5, Sept. 1969, p700.

Miesse, C. C. "Correlation of experimental data on the disintegration of liquid jets." Indust. Engng. Chem., 1955, 47, p1690.

Militzer, J. "Numerical Prediiction of the Fully Developed Two-Phase (air-solid) Flow in a Pipe." Circulating Fluidized Bed Technology, Proceeding of the First International Conference on Circulating Fluidized Beds, Halifax, Nova, Scotia, Canada, 1985, Edited by Prabir Basu, New York, Pergamon, 1986, Sponsored by the Canadian Sociaty for Chemical Engineering.

Miles, J. W. "On the generation of surface waves by shear flows." J. Fluid Mechanics, Vol. 3, 1957

Miles, J. W. "On the genration of surface waves by shear flows." J. Fluid Mechanics, Vol. 6, 1959 and 1961.

Miller, J. S. S "Jet mixing for crude oil pipeline to ensure representative sampling for water content measurement." BP Engineering and technical centre rep. no. 82.20.0159, 1983.

Morgan, W. D., Brinkworth, B. J. and Evans, G. V. "Upstream penetration of an enclosed counterflowing jet." Ind. Eng. Chem., Fundam., Vol. 15, no. 2, 1976, pp 125-127.

Nallasamy, M. "Turbulence Models and Their Application to the Prediction of Internal Flows- A Review." Computers and Fluids, 15, no. 2, 1987, pp151-194

Novak, V. and Reiger, F. "Homogenization Efficiency of Motionless Mixers." 5th European Conference on Mixing, Wurzburg, Germany, 1985.

Nukiyama, S. "Experiments on the atomization of liquid by means of an air stream." Transactions of the Society of Mechanical Engineers, Japan, 1938-40, report 1-6, 4-6.

Mullinger and Chigier "The Design and Performance of Industrial Mixing Multi-jet Twin Fluid Atomizers." J. of Institute of Fuel, Dec. 1974, pp 251-261.

Ohnesorge, W. von, " Formation of drops by nozzles and breakup of liquid jets." Z. Angew. Math. Mech., 1936, 16, p355.

O'Rouke and Bracco "Modelling of drop interaction in thick sprays and comparision with experiments." proceedings of the stratified charge automotive engine conferance, The Institution of Mechanical Engineers, London, England, 1980(Nov.).

Paleev and Filippovich "Phenomena of liquid transfer in two-phase dispersed annular flow." Int. J. Heat mass Transfer, 9, 1089.

Patankar, S. V "Numerical Heat Transfer and Fluid Flow." Series in Computational Methods in Mechanics and Thermal Sciences, Hemisphere Publishing Corporation, 1980.

Patanker, S. V. Basu, D. K. and Alpay, S. A. "Prediction of the Three-Dimentional Velocity Field of a Deflected Turbulent Jet." Trans. ASME. Dec. 1977, PP758.

Peacock, G. " The effect of asymmetric inlet flow on the hydraulic forces in a centrifugal pump." MSc. Thesis School of Mechanical Engineering, Cranfield Institute of Technology, Sept.1984.

Pericleous, K. A. Mathematical Simlation of Hydrocyclones." Appl. Math. Modelling, Aug., 1987, 11.

Pericleous, K. A. and Petel, M. K. "The Modelling of Tangential and Axial Agitator in Chemical Reactor." PCH Phsico Chemical Hydrodynamics, 1987, 8, no. 2, pp 105-123.

Phinney, R. E. "Stability of laminar viscous jet- The influence of the initial disturbance level." A.I.Ch.E. J., 1972, 18, p432.

Pratt, B. D. and Baines, W. D. "Profiles of the Round Turbulent Jets in a Cross Flow." Proc. A.S.C.E., J. Hydraul. Div., 92:53-64.

Radcliffe, A. and Clare, H. "A correlation of the preformance of two airblast atomizers with mixing sections of different size." N.G.T.E. Report no. 144, 1953(Oct.).

Rajaratnam, N. "Turbulent Jets." Developments in Water Science, 1976, Elsevier Scientific Publishing Company

Ranz, W. E. "Some experiments on orifice sprays." Canad. J. Chem. Engng., 1958, 36, p175.

Ranz, W. E. "On sprays and spraying." Dept. Engng. Res., Penn. State University, Bulletin 65, 1956.

Rasmuson, A. and Neretnieks, I. "Exact solution of a model for diffusion in particles and longitudinal dispersion in packed beds." AIChE. J., 26, 686, 1980.

Rayleigh, W. S. "On the instability of jets." Proc. Lond. Math. Soc., 1878, 4, p10.

Reitz, R. D. and Bracco, F. V. "On the dependence of spray angle and other spray parameters on nozzle design and operating conditions." SAE paper 790494, 1979.

Reitz, R. D and Bracco, F. V. "Mechanisim of Breakup of Round Liquid Jets." Encyclopedia of Fluid Mechanics, Edited by Cheremisinoff, vol. 3, 1985.

Revill, B. K. "Jet mixing." Mixing in the Process Industries 5-9 July 1982, University of Bradford, Sponsored by I. Ch. E..

Rizk and Lefebvre "The influence of air/liquid properties on air blast atomization." Trans. ASME, J. Fluids Engng. 1975, 97.

Roberts and Hartly "A correlation of pressure drop data for two-phase annular flow in vertical channels." Queen Mary College, London, Memorandum No. 6, 1961.

Rodi, W "Turbulence models for enviromental problems." Lecture Series on Prediction methods for turbulent flow, Von Karman Institute for Fluid Dynamics, 15-19 January 1979.

Rodi, W. "Turbulence models and their application in hydraulics." Presented by the IAHR-Section on Fundamentals of division 11: Experimental and Mathematical Fluid Dynamics, March 1979.

Rodi, W. "Predictions of Free Turbulent Boundary Layers by Use of a Two- Equation Model of Turbulence." PhD Thesis, 1972, University of London.

Rodi, W. "Examples of Turbulence Models for Incompressible Flows." AIAA Journal, Vol. 20, No. 7, 1982, pp 872-879.

Roache, P. J. "Computational Fluid Dynamics." Hemosa Publishers, Albuquerque, New Mexico, 1976.

Rumsheiht, F. D. J. Colloid Sci., vol. 17, no. 260, 1962.

Rupe, J. H. "On the dynamics characteristics of free liquid jets and partial correlation with orifice geometry." JU.P.L. Tech. Report, No. 32, 1962. p207.

Sampath, J.
Ganesan, V. "Numerical Prediction of Flow and Combustion in Three- Dimensional Gas Turbine Combustors. J. Inst. of Energy, vol. 15, March 1987, pp15-28.

Schetz, I. A. "Injection and mixing in Turbulent Flows." Progress in Astronautics and Aeronautics, vol. 68, 1980 Editor Martin Summerfield, Published by the American Institute of Aeronautics and Astronautics.

Segev, A. "Mechanistic model for estimating water dispersion in crude oil flow" Annual A.I.Ch.E. meeting, 1984(Nov.), San Francisco.

Schweitzer, P. H. "On the formation and dispersion of oil spray." Penn. State University Bulletin, 1932, 40.

Seppen, J. J. "A Study of Flow Phenomena in Internal (piston) Combustion Engines." Ph.d Thesis, Delftr University of Technology, Delft, 1982.

Serag-Eldin, M. A.
Spalding, D. B. "Computation of Three-Dimentioanl Gas Turbine Combustion Chamber Flows." J. Eng. for Power, July 1979, Vol. 101, pp327-336

Shah, P. and
Markatos, N. C. "Computer Simulation of Turbulence in Internal Combustion Engines." International Journal for Numerical Methods in Fluids." 7, 1987, pp927-952.

Shinnar, R. "On the Behaviour of Liquid Dispersions in Mixing Vessels." J. Fluid Mech., 1961, 10, pp259-275.

Shakadov, V. Ya. "Wave formation on the surface a viscous liquid due to tangential stress." Fluid Dynamics, 1970, 5, p473.

Simpson, J. "Industrial turbulent mixing-Turbulence in mixing operation." Turbulence in Mixing Operations a Theory and Application to Mixing and Reaction, Edited by R. S. Brodkey, Academic Press Inc., June 1974.

Sinai, Y. L. "A model of interfacial stress and spray generation by gas flowing over a deep wavy pool." 1987, J. Fluid Mech., 179, pp327-344.

Sleicher, C. A. "Mechanism of stable drop size in turbulent flow." 1972, A.I.Ch.E. J., 8(4).

Soo, S. L., Ihrig Jr, H. K., and El Kouh, A. F. "Experimental Determination of Statitical Properties of Two Phase Turbulent Motion." J. Basic Engng., Transactions ASME, 82D, 1960, pp609-621.

Soo, S. L. "Fluid dynamics of multiphase systems." 1967, Blaisdell Publishing Company.

Soo, S. L. "The boundary conditions of the diffusion equation." Powder Technology, 1982, 32, pp 117-119.

Soo, S. L. and Tung, S. K "Deposition and entrainment in pipe flow of a suspension." Powder Technology, 1972, 6.

Spalding, D. B. "Numerical Computation of Multi-Phase Flows." A Lecture Course, HTS/81/8, Presented at Imperial College, London, 2 - 6th Nov.' 1981.

Squire, H. B. Bri. J. Appl. Phys., 1953, 4, pp167-169.

Stirling, A. M. and Sleicher, C. A. "The instability of capillary jet." J. Fluid Mech., 1975, 68, p477.

Stoy, R. L. and Ben-Haim, Y. "Turbulent Jets in Confined Crossflow." J. of Fluid Eng. Dec. 1973, pp 557.

Streiff, F. A. "Adopted Motionless Mixer Design." 3rd European Conference on Mixing, April 1979.

Sugiyama, Y., Kojima, Y. and Niwa, F. "A Three Dimentional Flow Around a Turbulent Jet Injected Normally into a Confined Cross Flow." Memoirs of the Faculty of Engineering, Nagoya University, Vol. 38, No. 2 (1986)- Research Report.

Suzanne, Cayral and Masbernat "Mean velocity and Reynold's stress in Co-current gas-liquid stratified channel flow." Two-phase momentum, heat and mass transfer vol.2, edited by Durst, Tsiklauri and Afgan, Hemisphere Publishing.

Syed, S. A. "Velocity and Concentration Characteristics and their Cross Correlation for Co-axial jets in a Confined Sudden Expansion Part 11- Predictions." Fluid Mechanics of Combustion Systems Presented at the Fluid Engineering Conference, Boulder, Col.,USA, Published by ASME New York, NY, USA, 1981, pp161-167.

Tatchall, D. G. "Convection Processes in Confined Three Dimensional Boundary Layer." Ph.D. Thesis, University of London, 1975.

Taulbee, D. B. "The effect of diffusion on the settling of aerosol particles in flow in a parallel plate channel." J. Aerosol Sci., Vol. 10, pp. 95 to 102.

Taulbee, D. B. and Carpenter, P. S. "Gravitational deposition of aerosol particles from a developing flow in a horizontal circular tube." J. Aerosol Sci., Vol. 9, 1978, pp513-519.

Taulbee, D. B. "Simultaneous diffusion and sedimentation of aerosols in channel flows." J. Aerosol Sci., 1975, Vol. 6, pp 433-441.

Taylor, G. I. "The Formation of Emulsions in Definable Fields of Flows." Proc. Roy. Soc., A, 1934, A146:501.

Tomotika, S. "Breaking up of a drop of viscous liquid immersed in another viscous fluid which is extending at a uniform rate." Proc. Roy. Soc., 1935, A150:322.

Truong Quang Minh and Huyghe "Some hydrodynamical aspects of annular dispersed regime." Doct. Ing. thesis, Grenoble, 1965.

Tsahalis, T. D. "Condition for the entrainment of settled water in crude oil and product pipelines." 83rd National Meeting of A.I.Ch.E., 1977, March 21-24, Houston, Terxas.

Underhill, K. E. and Wright, C. M. "Inline Static Mixing as a Sample Handling Method Prior to Water Content Determination." Automatic Sampling and Water Determination for Crude Oils Symposium, Maidstone, 1981.

Vermeulen, T. Williams, G. M. and Langlois, G. E. "Interfacial area in liquid-liquid and gas-liquid agitation." Chem. Eng. Progr., Vol. 51 No. 2, 1955, p85F.

Wallis "One dimensional two-phase flow." 1969, McGraw-Hill Book Company.

Weber, C. "On the breakdown of a fluid jet." Z.A.M.P., 1931, 11, p136.

Webb, S. W. "Modelling Techniques for Dispersed Multiphase Flows." Chapter 31, Encyclopedia of Fluid Mechanics, Edited by Cheremisinoff, vol. 3, 1985.

Wen-Hsiung Li "Differential Equations of Hydraulic Transients, Dispersion, and Groundwater Flow." Mathematical Methods in Water Resources, 1977.

Weiss, M. A. and Worsham, C. H. "Atomization in high velocity air streams." Applied Science Research, 1959(April), 29(4).

Whalley and Hewitt "The correlation of liquid entrainment fraction and entrainment rate in annular two-phase flow." AERE-R9187, HTFS-RS237, 1978.

White, F. M. "Fluid Mechanics." 2nd edition, 1986, McGraw-Hill Company.

Wicks and Dukler "Entrainment and pressure drop in cocurrent gas-liquid flow." A.I.Ch.E. J., 6, p463.

Wigg, L. D. "The effect of scale on fine sprays produced by large airblast atomizers." N.G.T.E. Report no. 236, 1959(July).

Wu, K. J. "Atomizing Round Jets." Ph.D. Thesis, Dept. of Mech. and Aero. Engr., Princeton University U.S.A.

Wu, K. J. et al "Measurements of the spray angle of atomizing jets." J. Fluids Engng., 1983, 105, p406.

Yanta, W. J. and Smith, R. A. "Measurements of Turbulent Transport Properties with a Laser Doppler Velocimeter. AIAA paper 73

York, Stubbs and Tek "The mechanism of disintegration of liquid sheets." Trans. ASME, 1953, 75(7), pp1279-1286.

Yule, A. J., Balachandran, W., Boysan, F. and Swithenbank, J. "Atomiser and Spray Technology- Design, Performance, Measurement and Computation." A Short Course Organised in Cooperation with ILASS- Europe at UMIST, UK., 12 - 14th of Dec.'1988.

TABLES

Table 3.1 Specifications of jets in the plates

Figures	h (at t=0) mm	V_j mm/s	Scale, 1mm mm's on plate	Comments
3.1.1	9	3.8	0.9	
3.1.2	9	2.9		
3.2.1	∞	0.5*	4.3	
3.2.2	∞	1.1*	4.3	
3.2.3A	∞	2.3	3.75	
3.2.3B	∞	3.2	3.75	
3.2.3C	∞	4.5	3.75	
3.2.3D	∞	5.5	3.75	
3.3.1A	10	5.8	4.52	$KMnO_4$ was dissolved in
3.3.1B	10	7.3	4.52	water to improve contrast
3.3.1C	10	6.0	3.77	
3.3.1D	10	7.3	3.74	
3.3.2A	10	4.7	3.6	30% Base oil/water
3.3.2B	10	5.5	3.6	30% Base oil/water
3.3.2C	10	6.6	3.6	30% Base oil/water
3.3.2D	10	7.4	3.6	30% Base oil/water
3.4.1A	10	0.0	1.17	
3.4.1B	10	6.2	1.17	
3.5.1A	18	5.3	3.5	
3.5.1B	18	5.3	3.5	
3.6.1A	6	1.0*		30% Base oil/water
3.6.1B	6	1.4*		30% Base oil/water
3.6.2A	6	3.2		30% Base oil/water
3.6.2B	6	1.6*		
3.6.2C	6	2.9		30% Base oil/water
3.6.2D	6	2.1		20% Base oil/water
3.7.1A	6	6.3	0.67	
3.7.1B	0	6.3	0.67	submerged oil jet. Jet was dyed with Waxoline blue
3.7.2A	∞	7.2	0.67	
3.7.2B	∞	7.8	0.67	
3.8.1A	16	6.2	0.67	

Table 3.1 Cont.

3.8.1B	13	6.2	0.67
3.8.1C	11	6.2	0.67
3.8.1D	9	6.2	0.67
3.8.2A	11	3.8	0.67
3.8.2B	11	4.5	0.67
3.8.2C	11	6.2	0.67
3.8.2D	11	7.0	0.67
3.8.3A	11	7.2	0.67
3.8.3B	11	7.5	0.67

* = velocity was approximated

TABLE 7.1 EXPERIMENTAL PROGRAMME

	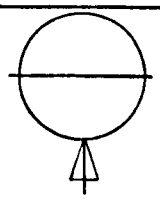	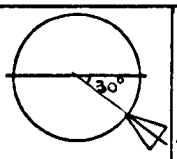	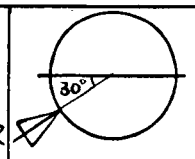	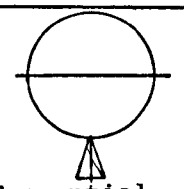 Tangential at axis
Multi-nozzle Vel. Ratio=57 Re No.=27600	(A) D^*=1,2,3,4 & 6 Axial & Tangential	(B) D^*=1,2,3,4 & 6 Axial & Tangential	(C) D^*=1,2,3,4 & 6 Axial & Tangential	(E) D^*=1 to 3 in 0.25 increments &, 3.5 &4
Multi-nozzle Vel. Ratio=36 Re No.=27600	(F) D^*=3,4,5,6 & 8 Axial only	(G) D^*=3,4,5,6 Axial & Tangential		(I) D^*=1 to 3 in 0.25 increments &, 3.5 &4
Multi-nozzle Vel. Ratio=70 Re No.=27600	(J) D^*=3,4,5,6 & 8 Axial only	(K) D^*=3,4,6 Axial & Tangential		(M) D^*=1 to 3 in 0.25 increments &, 3.5 &4
Multi-nozzle Vel. Ratio=57 Re No.=27600	(N) D^*=5 & 8 Axial only			
Multi-nozzle Vel. Ratio=36 Re No.=48400				(O) D^*=2 to 3.25 in 0.25 increments & 4
Single-nozzle Vel. Ratio=57 Re No.=27600	(P) D^*=1,2,3,4 & 6 Axial & Tangential	(Q) D^*=1,2,3,4 & 6 Axial & Tangential	(R) D^*=1,2,3,4 & 6 Axial & Tangential	(S) D^*=1 to 3 in 0.25 increments
Single-nozzle Vel. Ratio=36 Re No.=27600	(T) D^*=1,2,3,4 Tangential only			(U) D^*=1 to 3 in 0.25 increments
Single-nozzle Vel Ratio=70 Re No.=27600	(V) D^*=3,4,6 Axial velo. only			

Table 7.1 Cont.

Single-nozzle Vel Ratio=17 Re No=27600	(W) D^*=1,2,3,4 & 6 Axial & Tangential	(X) D^*=1,2,3,4 & 6 Axial & Tangential	Experimental results of A, B, C, E, I, M, P, Q, R, S, U, W and X were plotted on graphs.
No nozzle tabulated. Fully Develop flow check	(Y) Axial & Tangential		Experimental results of F, G, J, K, N, T and V were D^* = number of diameters downstream

Table 7.2 Multi-nozzle-(exp. F)

Reynolds number = 27600; velocity ratio = 36

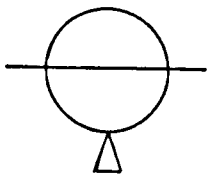

	3 diameters downstream		4 diameters downstream	
position x/dia	axial velocity m/s	axial RMS velocity m/s	axial velocity m/s	axial RMS velocity m/s
0.0	pipe wall			
0.085	0.326	0.101	0.382	0.081
0.171	0.302	0.103	0.361	0.080
0.256	0.311	0.121	0.364	0.083
0.342	0.366	0.132	0.374	0.091
0.427	0.414	0.139	0.394	0.094
0.513	0.434	0.138	0.394	0.095
0.598	0.417	0.138	0.403	0.092
0.684	0.372	0.130	0.389	0.095
0.769	0.345	0.110	0.378	0.083
0.855	0.337	0.100	0.382	0.079
0.94	0.363	0.094	0.397	0.086
1.0	pipe wall			

Table 7.3 Multi-nozzle-(exp. J)

Reynolds number = 27600, velocity ratio = 70

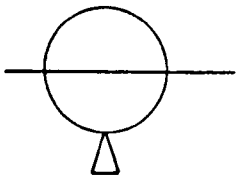

	3 diameters downstream		4 diameters downstream	
position x/dia	axial velocity m/s	axial RMS velocity m/s	axial velocity m/s	axial RMS velocity m/s
0.0	pipe wall			
0.085	0.418	0.166	0.423	0.123
0.171	0.390	0.153	0.411	0.114
0.256	0.362	0.150	0.378	0.111
0.342	0.325	0.133	0.374	0.104
0.427	0.301	0.136	0.359	0.096
0.513	0.330	0.161	0.350	0.095
0.598	0.302	0.135	0.357	0.100
0.684	0.335	0.143	0.380	0.114
0.769	0.353	0.182	0.401	0.117
0.855	0.420	0.197	0.430	0.129
0.94	0.470	0.219	0.448	0.133
1.0	pipe wall			

Table 7.4 Multi-nozzle-(exp. F)

Reynolds number = 27600, Velocity ratio = 36

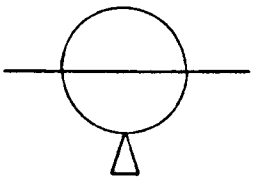

	5 diameters downstream		6 diameters downstream	
position x/dia	axial velocity m/s	axial RMS velocity m/s	axial velocity m/s	axial RMS velocity m/s
0.0	pipe wall			
0.085	0.400	0.066	0.395	0.051
0.171	0.397	0.057	0.400	0.051
0.256	0.390	0.070	0.398	0.052
0.342	0.389	0.076	0.389	0.052
0.427	0.388	0.074	0.393	0.051
0.513	0.400	0.072	0.397	0.051
0.598	0.402	0.069	0.392	0.052
0.684	0.398	0.069	0.407	0.052
0.769	0.394	0.062	0.404	0.054
0.855	0.406	0.071	0.402	0.057
0.940	0.398	0.072	0.377	0.057
1.0	pipe wall			

Table 7.5 Multi- nozzle-(exp. J)

Reynolds number = 27600, Velocity ratio = 70

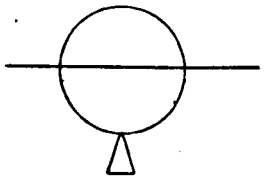

	5 diameters downstream		6 diameters downstream	
position x/dia	axial velocity m/s	axial RMS velocity m/s	axial velocity m/s	axial RMS velocity m/s
0.0	pipe wall			
0.085	0.410	0.093	0.403	0.073
0.171	0.402	0.090	0.402	0.069
0.256	0.393	0.084	0.406	0.069
0.342	0.383	0.085	0.395	0.066
0.427	0.377	0.083	0.390	0.068
0.513	0.376	0.081	0.388	0.070
0.598	0.377	0.081	0.387	0.069
0.684	0.398	0.081	0.396	0.066
0.769	0.407	0.087	0.410	0.072
0.855	0.406	0.093	0.405	0.067
0.940	0.416	0.098	0.400	0.074
1.0	pipe wall			

Table 7.6 Multi-nozzle-(exp. A)

Reynolds number = 27600, Velocity Ratio = 57

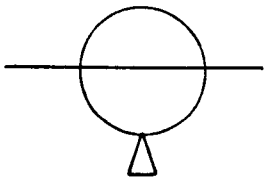

	5 diameters downstream		8 diameters downstream	
position x/dia	axial velocity m/s	axial RMS velocity m/s	axial velocity m/s	axial RMS velocity m/s
0.0	pipe wall			
0.085	0.410	0.083	0.392	0.044
0.171	0.412	0.082	0.405	0.044
0.256	0.418	0.085	0.407	0.045
0.342	0.403	0.067	0.410	0.042
0.427	0.392	0.067	0.411	0.041
0.513	0.404	0.070	0.412	0.041
0.598	0.402	0.077	0.409	0.044
0.684	0.401	0.073	0.407	0.044
0.769	0.407	0.068	0.409	0.047
0.855	0.412	0.080	0.404	0.049
0.940	0.393	0.087	0.381	0.048
1.0	pipe wall			

Table 7.7 Multi-nozzle-(exp. F)

Reynolds number = 27600, Velocity ratio = 36

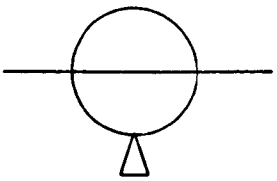

	8 diameters downstream	
position x/dia	axial velocity m/s	axial RMS velocity m/s
0.0	pipe wall	
0.085	0.376	0.039
0.171	0.390	0.035
0.256	0.393	0.036
0.342	0.397	0.036
0.427	0.397	0.033
0.513	0.395	0.034
0.598	0.395	0.034
0.684	0.392	0.034
0.769	0.387	0.038
0.855	0.380	0.042
0.94	0.353	0.045
1.0	pipe wall	

Table 7.8 Multi-nozzle-(exp. J)

Reynolds number = 27600, Velocity ratio = 70

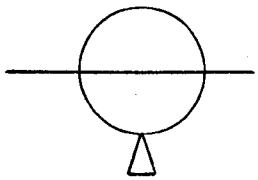

	8 diameters downstream	
position x/dia	axial velocity m/s	axial RMS velocity m/s
0.0	pipe wall	
0.085	0.406	0.059
0.171	0.419	0.053
0.256	0.418	0.048
0.342	0.417	0.048
0.427	0.420	0.048
0.513	0.416	0.048
0.598	0.414	0.048
0.684	0.419	0.051
0.769	0.422	0.048
0.855	0.419	0.053
0.940	0.406	0.059
1.0	pipe flow	

Table 7.9 Multi-nozzle-(exp. G)

Reynolds number = 27600, Velocity ratio = 36

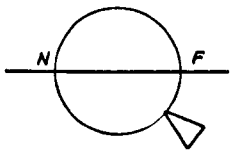

	3 diameters downstream		4 diameters downstream	
position x/dia	axial velocity m/s	axial RMS velocity m/s	axial velocty m/s	axial RMS velocity m/s
0.0	pipe flow			
0.085	0.317	0.159	0.342	0.101
0.171	0.338	0.156	0.360	0.115
0.256	0.395	0.169	0.358	0.118
0.342	0.430	0.152	0.358	0.120
0.427				
0.513	0.461	0.122	0.400	0.150
0.598				
0.684	0.414	0.116	0.395	0.088
0.769	0.390	0.110	0.399	0.074
0.855	0.416	0.100	0.417	0.084
0.940	0.446	0.094	0.432	0.075
1.0	pipe wall			

Table 7.10 Multi-nozzle-(exp. K)

Reynolds number = 27600, Velocity ratio = 70

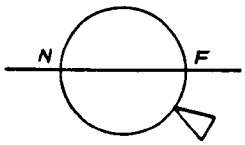

	3 diameters downstream		4 diameters downstream	
positon x/dia	axial velocity m/s	axial RMS velocity m/s	axial velocity m/s	axial RMS velocity m/s
0.0	pipe wall			
0.085	0.420	0.204	0.392	0.122
0.171	0.392	0.206	0.387	0.120
0.256	0.364	0.189	0.350	0.111
0.342	0.303	0.169	0.334	0.090
0.427				
0.513	0.208	0.138	0.342	0.098
0.598				
0.694	0.341	0.142	0.368	0.102
0.769	0.385	0.149	0.400	0.120
0.855	0.406	0.160	0.438	0.132
0.940	0.417	0.168	0.441	0.132
1.0	pipe wall			

Table 7.11 Multi-nozzle-(exp. G and K)

Reynolds number = 27600, 6 diameters downstream

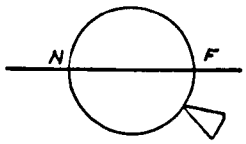

	Velocity ratio = 36		Velocity ratio = 70	
position x/dia.	axial velocity m/s	axial RMS velocity m/s	axial velocity m/s	axial RMS velocity m/s
0.0	pipe wall			
0.085	0.367	0.057	0.378	0.075
0.171	0.373	0.055	0.386	0.076
0.256	0.388	0.058	0.393	0.077
0.342	0.386	0.056	0.394	0.065
0.427				
0.513	0.396	0.053	0.383	0.080
0.598				
0.684	0.411	0.052	0.408	0.078
0.769	0.422	0.049	0.416	0.077
0.855	0.426	0.054	0.431	0.082
0.940	0.421	0.050	0.437	0.086
1.0	pipe wall			

Table 7.12 Multi-nozzle-(exp. G)

Reynolds number = 27600, Velocity ratio = 36

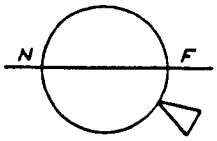

position x/dia.	3 diameters downstream tangential velocity m/s	tangential RMS velocity m/s	6 diameters downstream tangential velocity m/s	tangential RMS velocity m/s
0.0	pipe wall			
0.085	-0.057	0.139	0.013	0.070
0.171	-0.009	0.142	-0.002	0.067
0.256	0.035	0.141	0.004	0.064
0.342	0.073	0.148	0.007	0.066
0.427				
0.513	0.102	0.137	0.017	0.060
0.598				
0.684	0.052	0.107	0.014	0.060
0.769	0.009	0.102	0.014	0.054
0.855	-0.026	0.090	0.010	0.053
0.940	-0.047	0.084	0.009	0.058
1.0	pipe wall			

Table 7.13 Multi-nozzle-(exp. K)

Reynolds number = 27600, Velocity ratio = 70

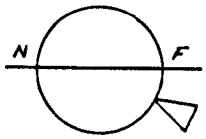

position x/dia.	3 diameters downstream tangential velocity m/s	tangential RMS velocity m/s	4 diameters downstream tangential velocity m/s	tangential RMS velocity m/s
0.0	pipe wall			
0.085	0.052	0.180	0.016	0.127
0.171	0.018	0.185	0.009	0.116
0.256	0.018	0.177	-0.007	0.120
0.342	-0.034	0.161	-0.028	0.103
0.427				
0.513	-0.018	0.141	-0.032	0.105
0.598				
0.684	-0.016	0.141	-0.010	0.119
0.769	0.01	0.144	0.035	0.128
0.855	0.041	0.156	0.038	0.138
0.940	0.095	0.199	0.096	0.146
1.0	pipe wall			

Table 7.14 Multi-nozzle-(exp. K)

Reynolds number = 27600, Velocity ratio = 70

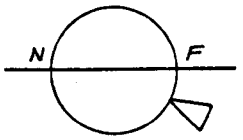

position x/dia.	6 diameters downstream tangential velocity m/s	tangential RMS velocity m/s
0.0	pipe wall	
0.085	-0.038	0.101
0.171	-0.021	0.080
0.256	-0.018	0.076
0.342	-0.007	0.074
0.427		
0.513	0.006	0.077
0.598		
0.684	0.020	0.082
0.769	0.040	0.087
0.855	0.037	0.076
0.940	0.053	0.075
1.0	pipe wall	

Table 7.15 Single-nozzle-(exp. V)

Reynolds number = 27600, Velocity ratio = 70

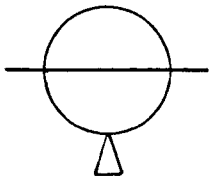

position x/dia.	3 diameters downstream axial velocity m/s	axial RMS velocity m/s	4 diameters downstream axial velocity m/s	axial RMS velocity m/s
0.0	pipe wall			
0.085	0.452	0.216	0.421	0.135
0.171	0.411	0.181	0.409	0.137
0.256	0.322	0.202	0.402	0.122
0.342	0.321	0.146	0.393	0.120
0.427	0.332	0.163	0.382	0.105
0.513	0.312	0.210	0.373	0.114
0.598	0.353	0.182	0.390	0.120
0.684	0.384	0.154	0.401	0.137
0.769	0.391	0.192	0.403	0.123
0.855	0.422	0.221	0.424	0.135
0.940	0.423	0.230	0.420	0.137
1.0	pipe wall			

Table 7.16 Single-nozzle-(exp. V)

Reynolds number = 27600, Velocity ratio = 70

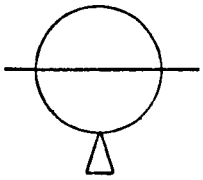

position x/dia.	6 diameters downstream axial velocity m/s	axial RMS velocity m/s
0.0	pipe wall	
0.085	0.381	0.076
0.171	0.383	0.072
0.256	0.392	0.070
0.342	0.401	0.068
0.427	0.404	0.077
0.513	0.394	0.072
0.598	0.413	0.069
0.684	0.401	0.079
0.769	0.395	0.068
0.855	0.382	0.070
0.940	0.376	0.075
1.0	pipe wall	

Table 7.17 Single nozzle-(exp. T)

Reynolds number = 27600, Velocity ratio = 36

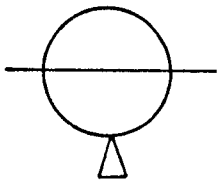

position x/dia.	1 diameters downstream tangential velocity m/s	tangential RMS velocity m/s	2 diameters downstream tangential velocity m/s	tangential RMS velocity m/s
0.0	pipe wall			
0.085	0.380	0.264	0.339	0.191
0.171	0.120	0.172	0.185	0.204
0.256	0.042	0.156	0.003	0.213
0.342	-0.116	0.227	-0.142	0.213
0.427	-0.159	0.240	-0.266	0.170
0.513	-0.142	0.220	-0.337	0.178
0.598	-0.102	0.217	-0.265	0.178
0.684	-0.060	0.199	-0.134	0.171
0.769				
0.855	0.092	0.142	0.143	0.178
0.940	0.217	0.232	0.246	0.191
1.0	pipe wall			

Table 7.18 Single nozzle-(exp. T)

Reynolds number = 27600, Velocity ratio = 36

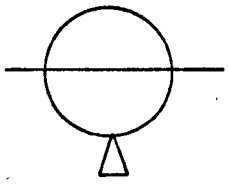

position x/dia.	3 diameters downstream tangential velocity m/s	tangential RMS velocity m/s	4 diameters downstream tangential velocity m/s	tangential RMS velocity m/s
0.0	pipe wall			
0.085	0.160	0.168	0.071	0.125
0.171	0.127	0.166	0.041	0.139
0.256	0.008	0.183	-0.020	0.125
0.342	-0.077	0.179	-0.046	0.122
0.427	-0.163	0.150	-0.067	0.119
0.513	-0.156	0.152	-0.060	0.111
0.598	-0.116	0.141	-0.053	0.117
0.684	-0.068	0.161		
0.769			0.024	0.120
0.855	0.124	0.154		
0.940	0.196	0.137	0.100	0.114
1.0	pipe wall			

FIGURES

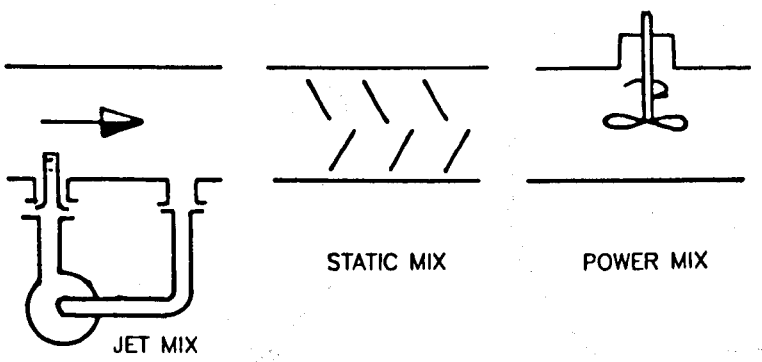

FIGURE 1.1 MIXING SYSTEMS

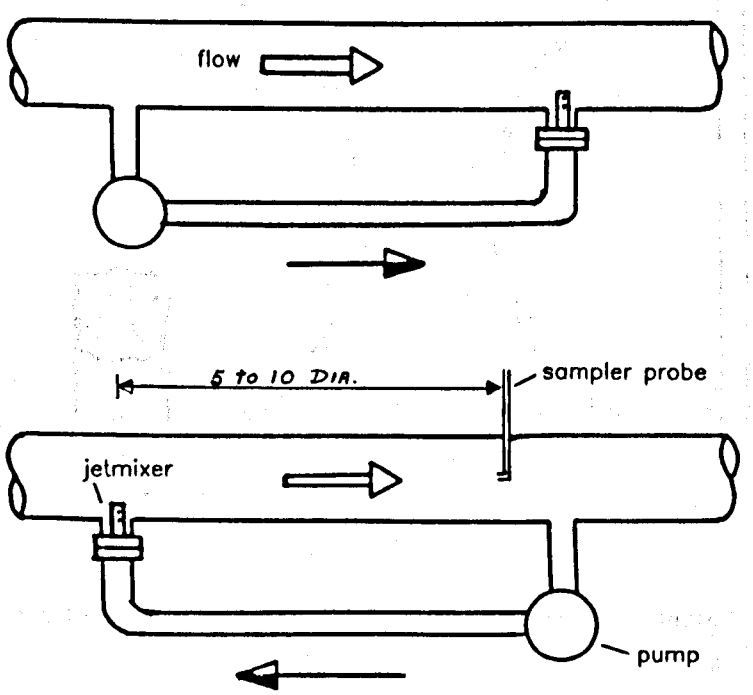

FIGURE 1.2 JET MIX SYSTEMS

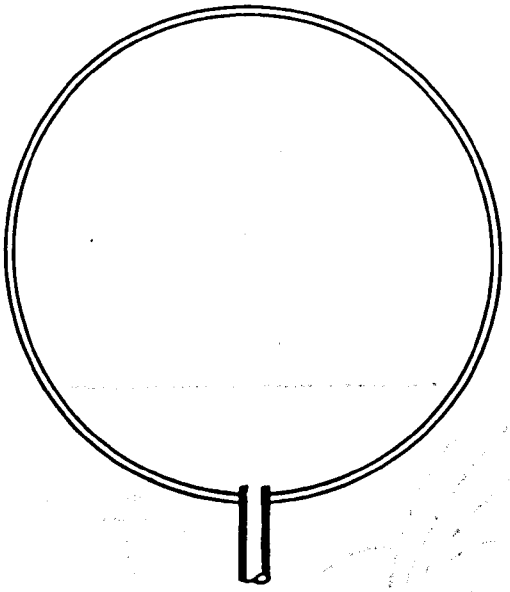

1. SINGLE JISKOOT NOZZLE

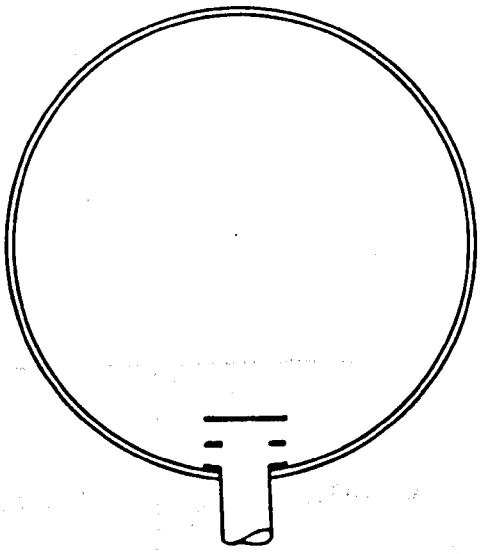

2. MOORE BARRETT AND REDWOOD NOZZLE

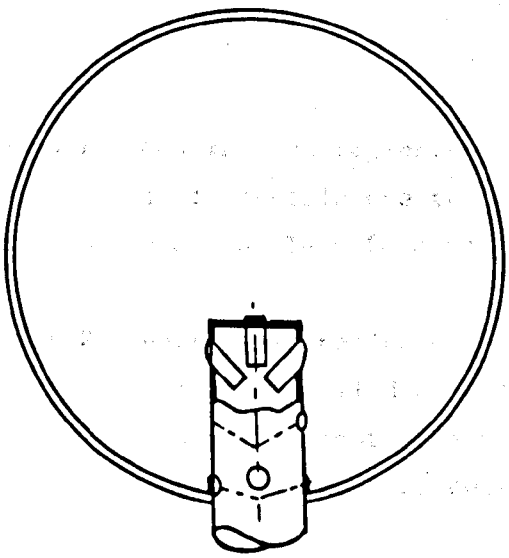

3. MULTI–JET JISKOOT NOZZLE

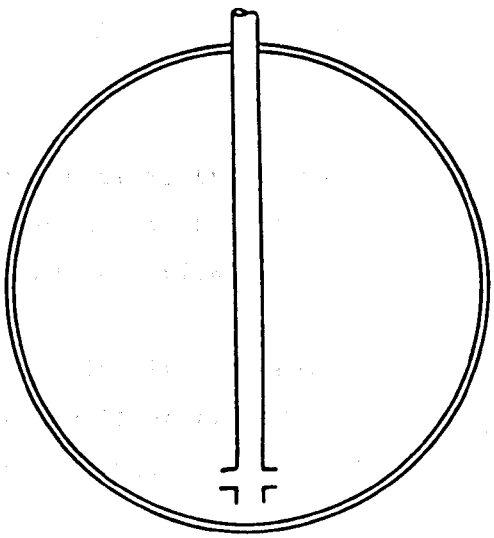

4. REDWOOD NOZZLE

FIGURE 1.3 EXISTING JET MIX NOZZLES

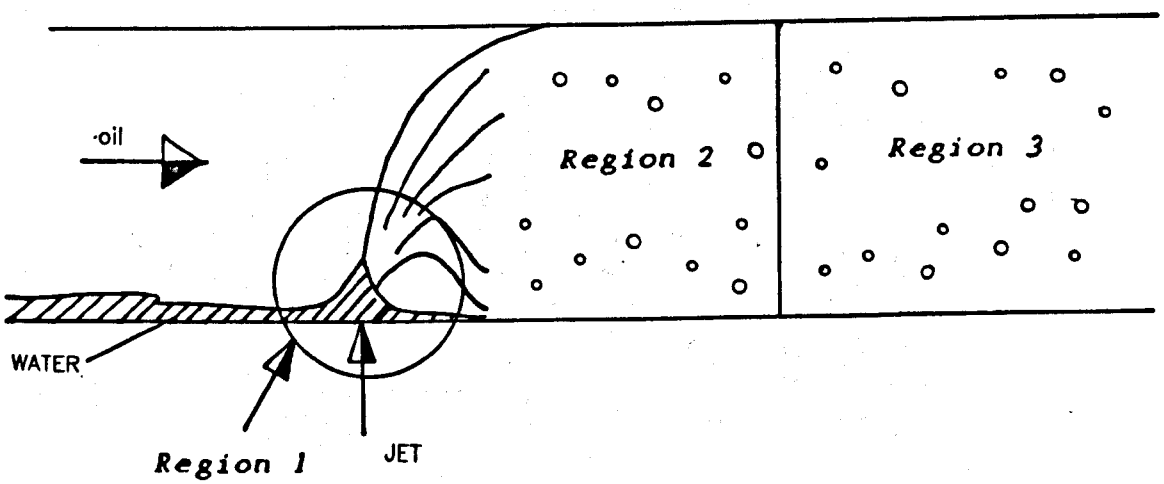

Region 1 = *Penetration region:-* Complete theoretical treatment is impossible due to complex entrainment and breakup process. Therefore analysis is semi-empirical.

Region 2 = *Near field region:-* The secondary flow is dominant. This is modelled numerically, using Phoenics code. And entrainment levels in region '1' acts as a source for the water mass conservation equation.

Region 3 = *Far field region:-* The gravity is dominant. The flow behaves two dimensionally. Therefore, the analysis can be carried out using 2-dimensional exact solutions.

FIG. 1.4 DIVISION OF THE MIXING DOMAIN INTO DIFFERENT REGIONS

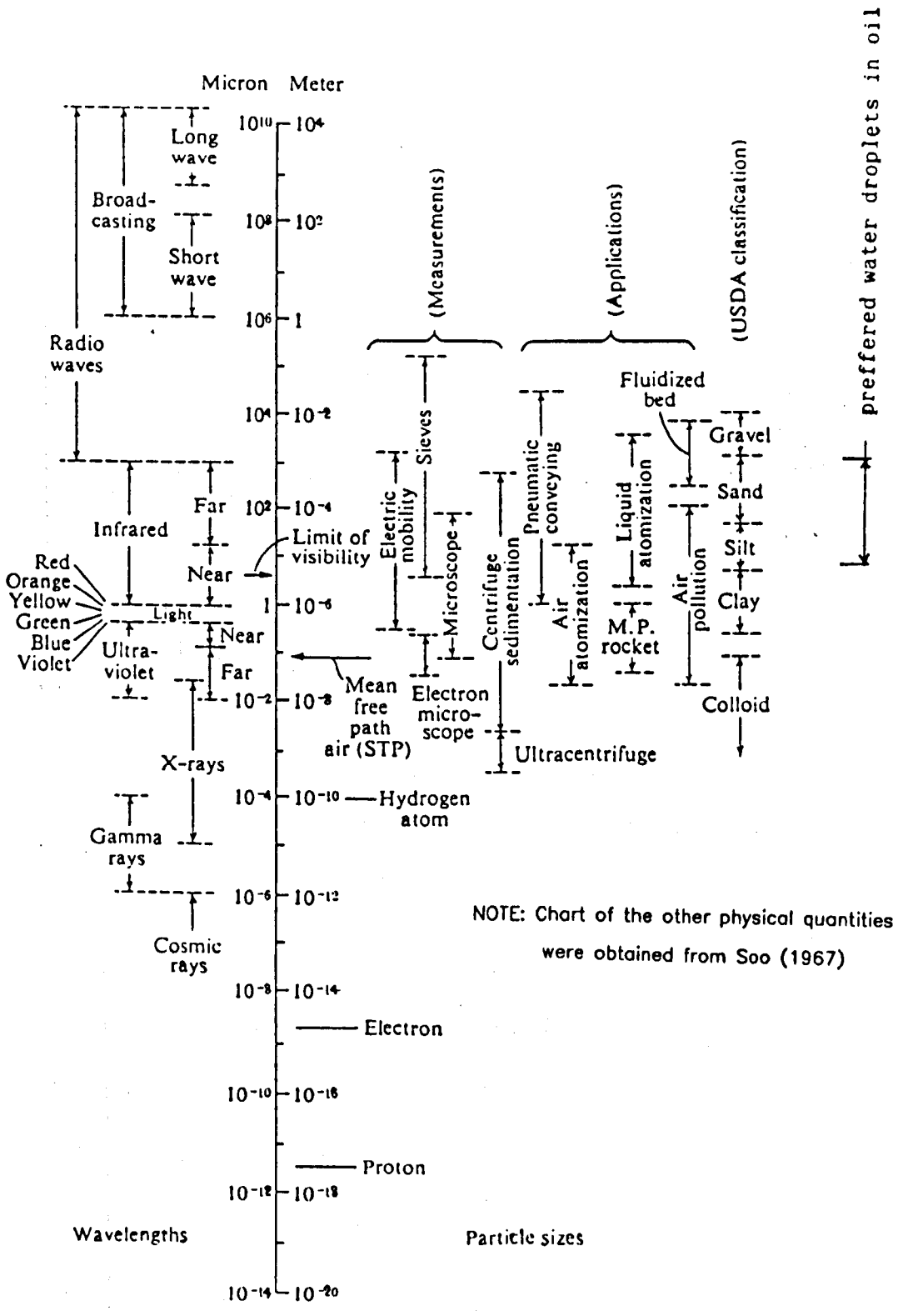

FIGURE 1.5 MAGNITUDE OF THE OIL DROPLET SIZES IN RELATION TO OTHER PHYSICAL QUANTITIES

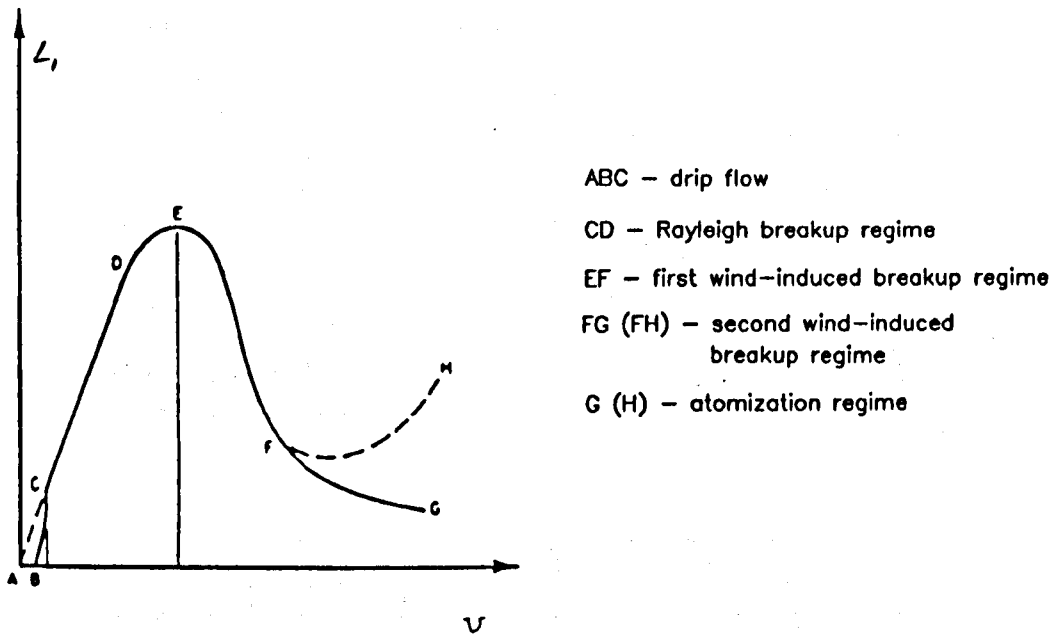

FIGURE 2.1 JET SURFACE BREAKUP LENGTH AS FUNCTION OF JET VELOCITY (REITZ ET AL, 1987)

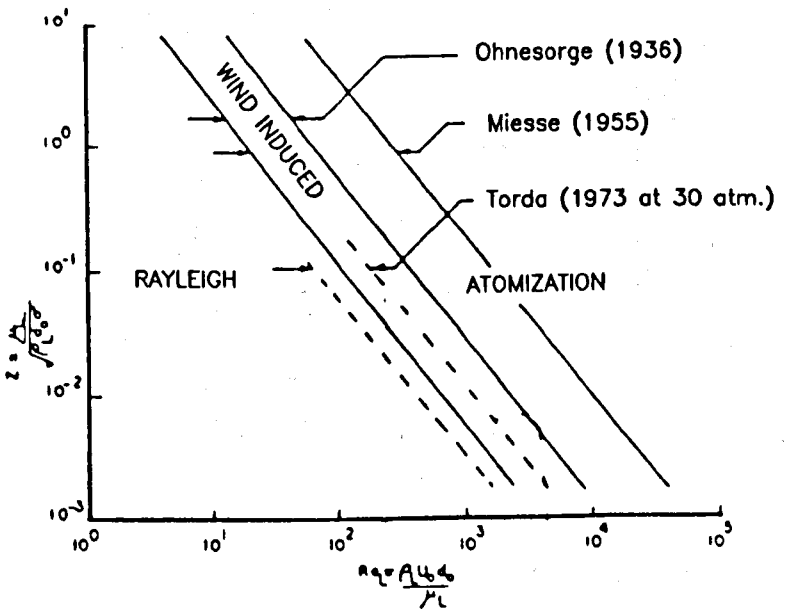

FIGURE 2.2 JET BREAKUP REGIME BOUNDARIES (REITZ ET AL, 1987)

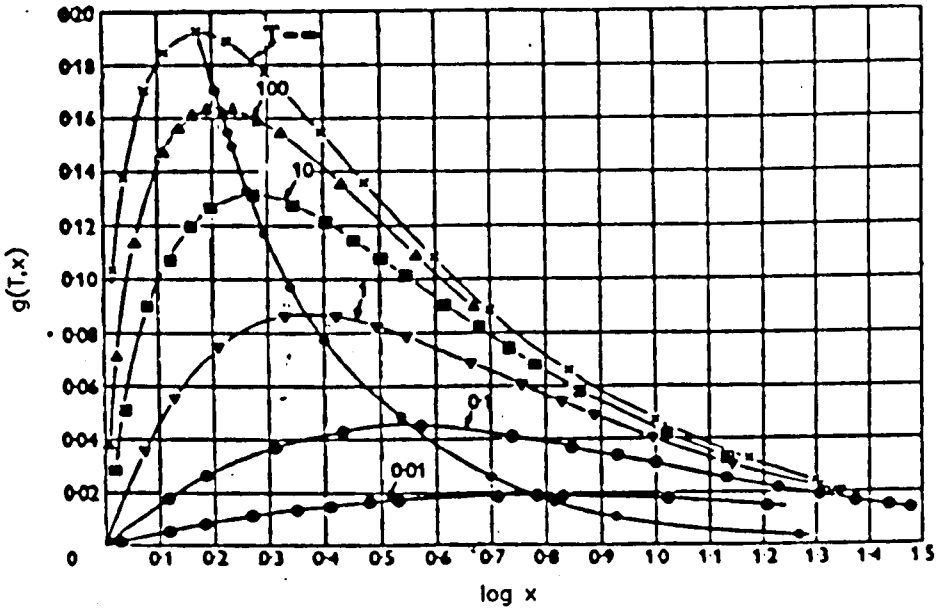

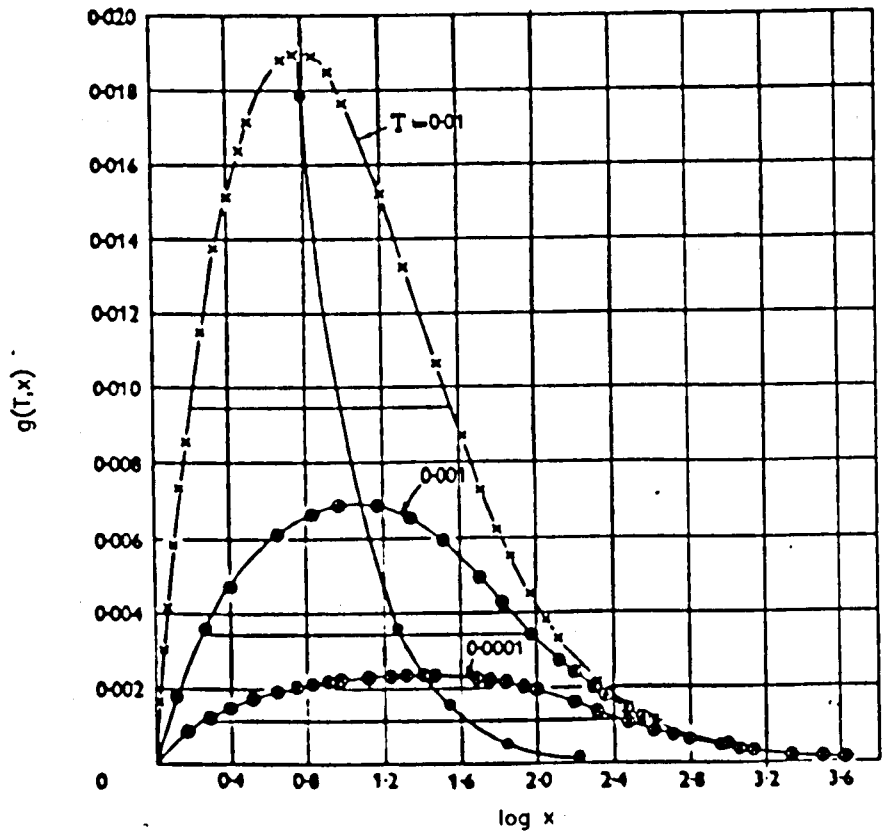

FIGURE 2.3 DISPERSION RELATION FOR THE SECOND WIND-INDUCED JET BREAKUP REGIME (TAYLOR, 1940)

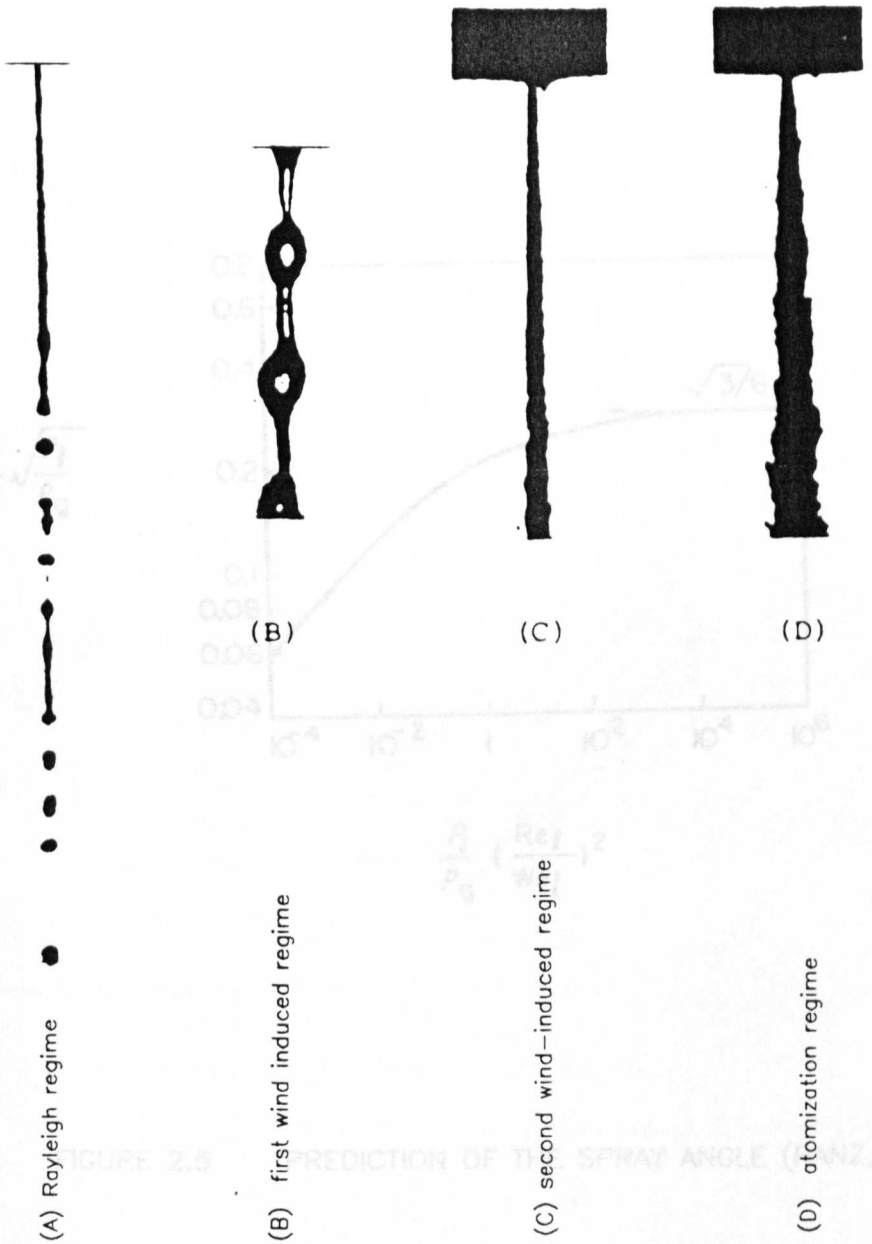

FIGURE 2.4 EXAMPLE OF FOUR JET BREAKUP REGIMES

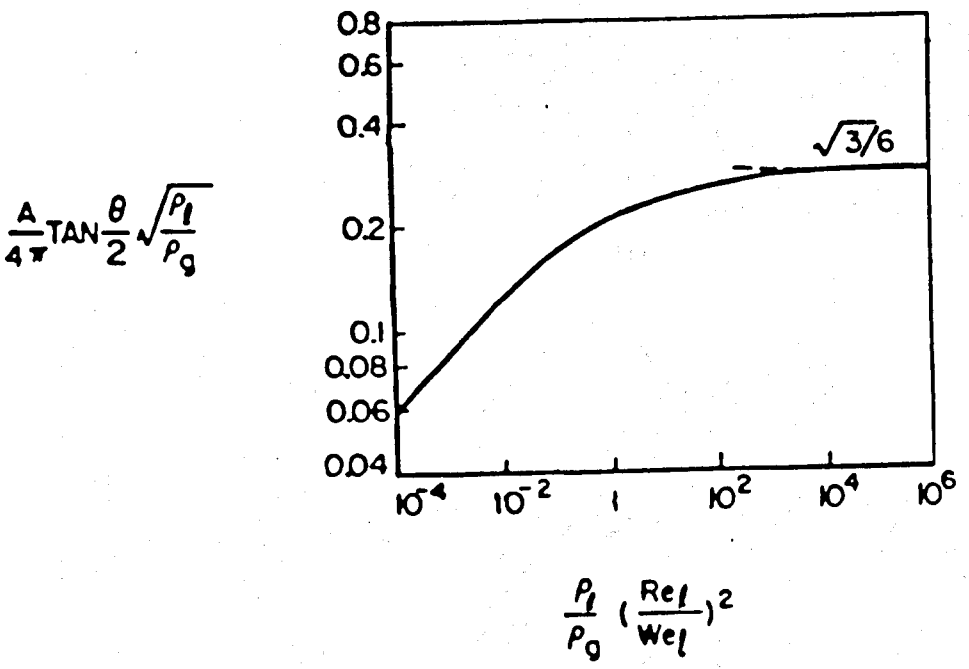

FIGURE 2.5 PREDICTION OF THE SPRAY ANGLE (RANZ, 1956)

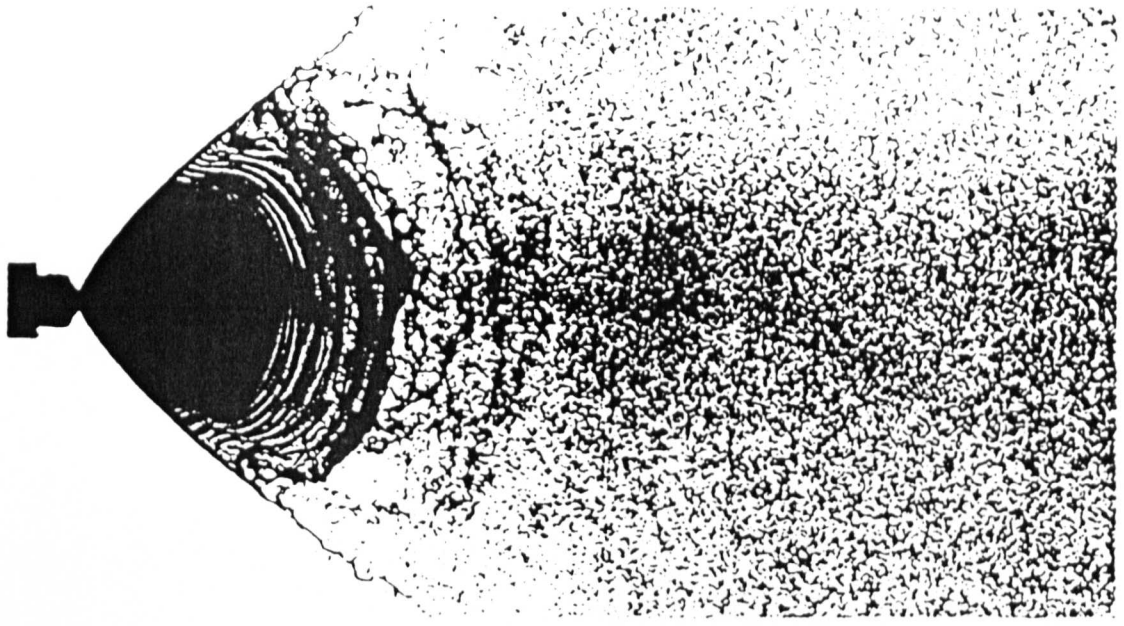

(a)

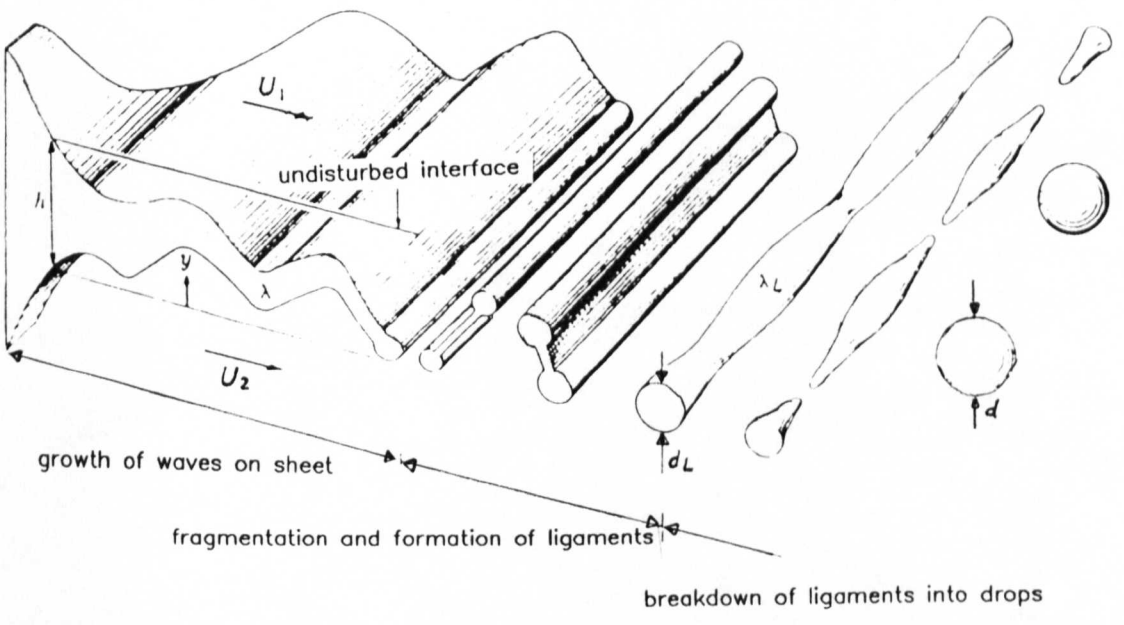

(b)

FIGURE 2.6 (a) FAN–NOZZLE SPRAY, (b) IDEALIZATION OF BREAKUP PROCESS (Dombrowski, 1963)

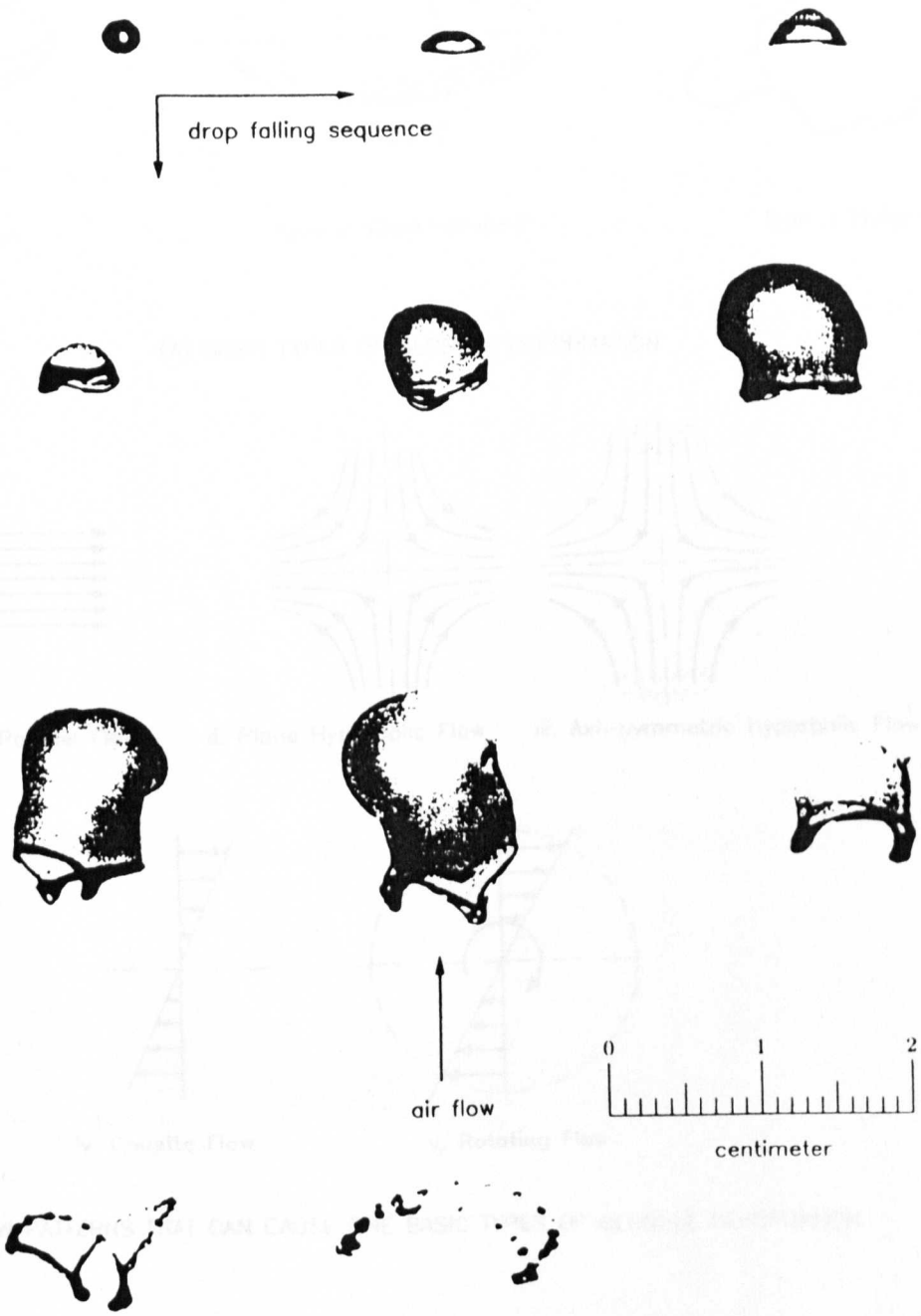

FIGURE 2.7 STAGES OF BREAKUP OF DROP OF WATER; AIR VELO. 24 M/SEC. (BRODKEY, 1963)

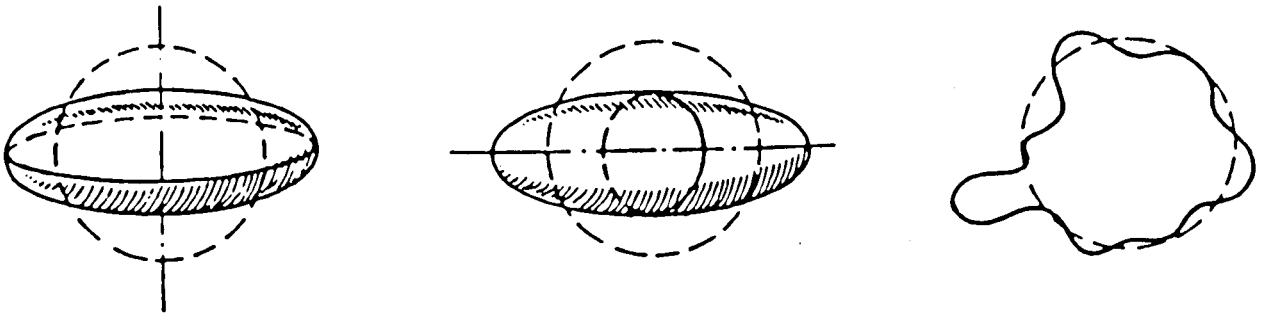

(A) BASIC TYPES OF GLOBULE DEFORMATION

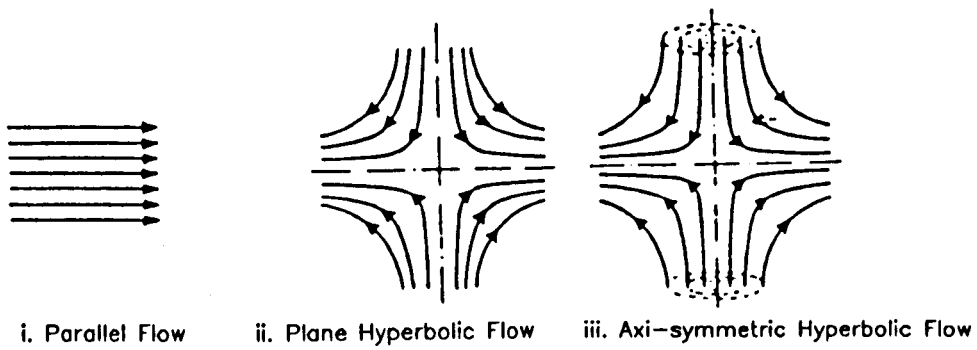

(B) FLOW PATTERNS THAT CAN CAUSE ONE BASIC TYPES OF GLOBULE DEFORMATION

FIGURE 2.8 CONDITIONS FOR BREAKUP AND TYPES OF DEFORMATION (HINZE, 1955)

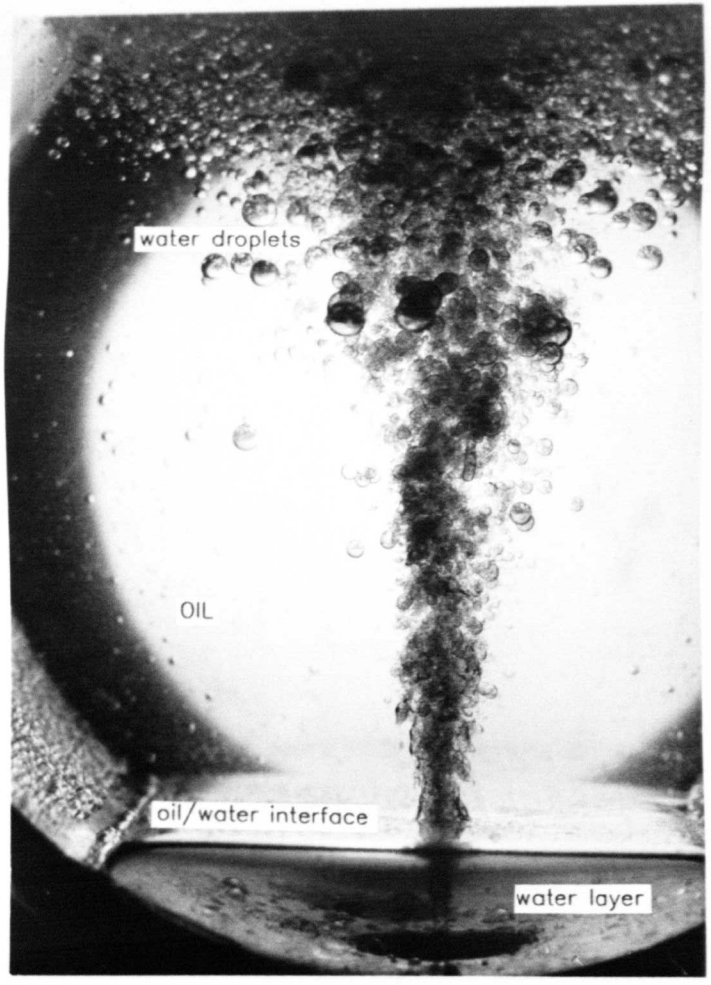

FIGURE 3.1.1 PENETRATION OF AN OIL JET THROUGH A WATER LAYER, STRATIFIED IN OIL

h= 9mm, V_j= 3.8m/s

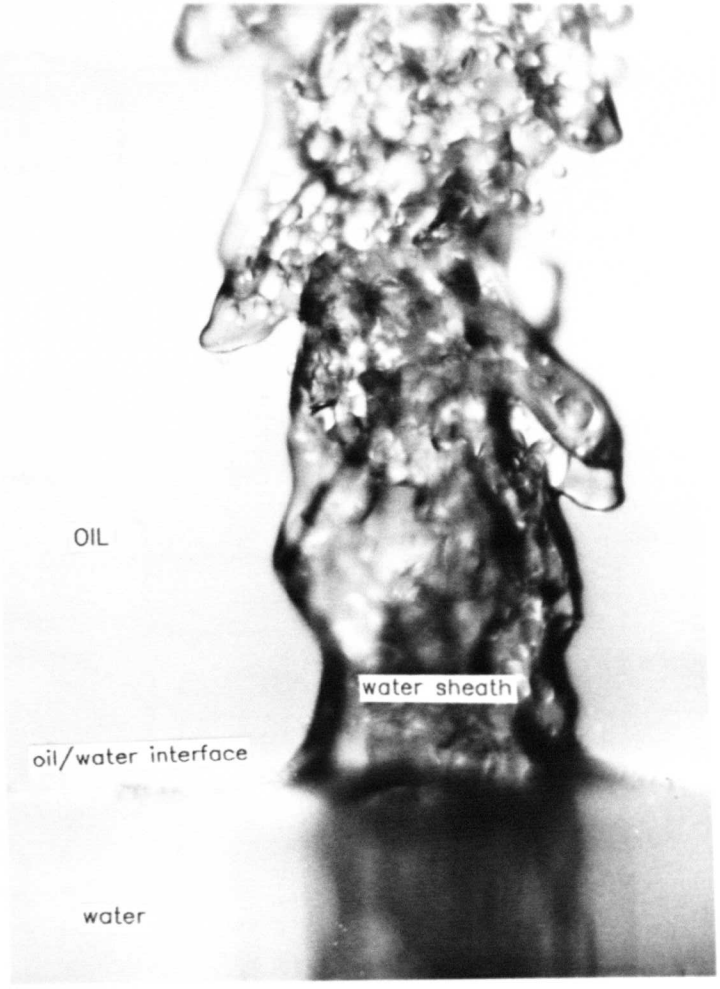

FIGURE 3.1.2 THE ENLARGED VIEW OF THE REGION, WHERE THE OIL JET PENETRATES THE OIL/WATER INTERFACE

h= 9mm, V_j= 2.9m/s

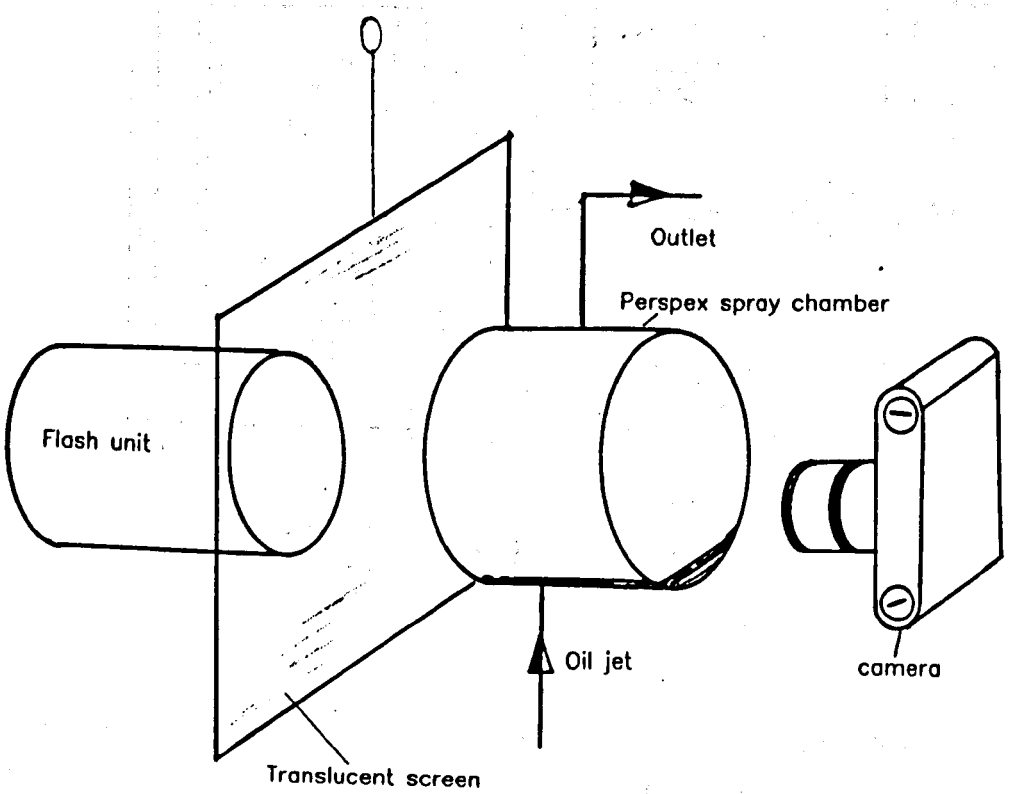

FIGURE 3.1.3 THE ARRANGEMENT OF THE FLASH, TEST CHAMBER AND CAMERA

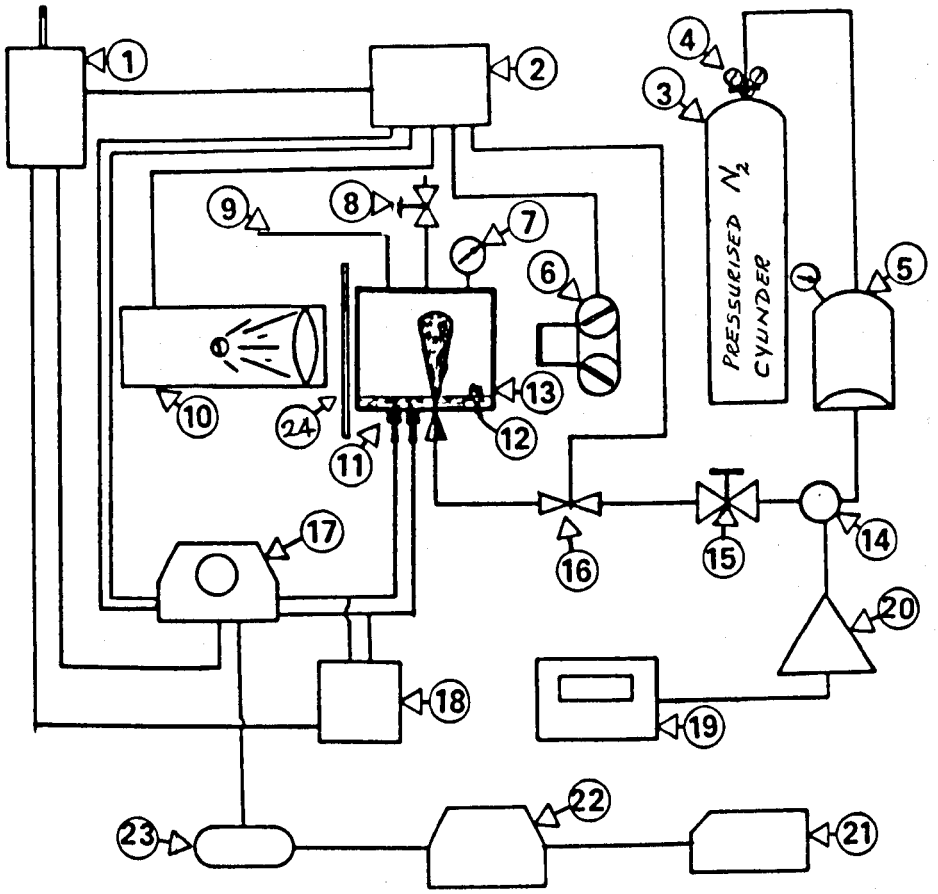

1 = Voltage stabilizer
2 = *Sequencer delay generator*
4 = *Pressure regulator*
5 = *Oil reservoir*
6 = *SLR Camera*
7 = *Pressure gauge*
8 = *Manual value*
9 = *Outlet pipe*
10 = *Atgon spark source*
11 = *Ultra-sonic transducer*
12 = *Water layer*
13 = *Spray camber containing oil*
14 = *Kistler piezoresistive pressure transducer*
15 = *Manual value*
16 = *Solenoid value*
17 = *Digital storage scope*
18 = *Spike generator*
19 = *Voltmeter*
20 = *Charge amplifier*
21 = *Plotter*
22 = *BBC micro computer*
23 = *IEEE 488 interface*
24 = Translucent screen

FIGURE 3.1.4 THE SCHEMATIC DIAGRAM

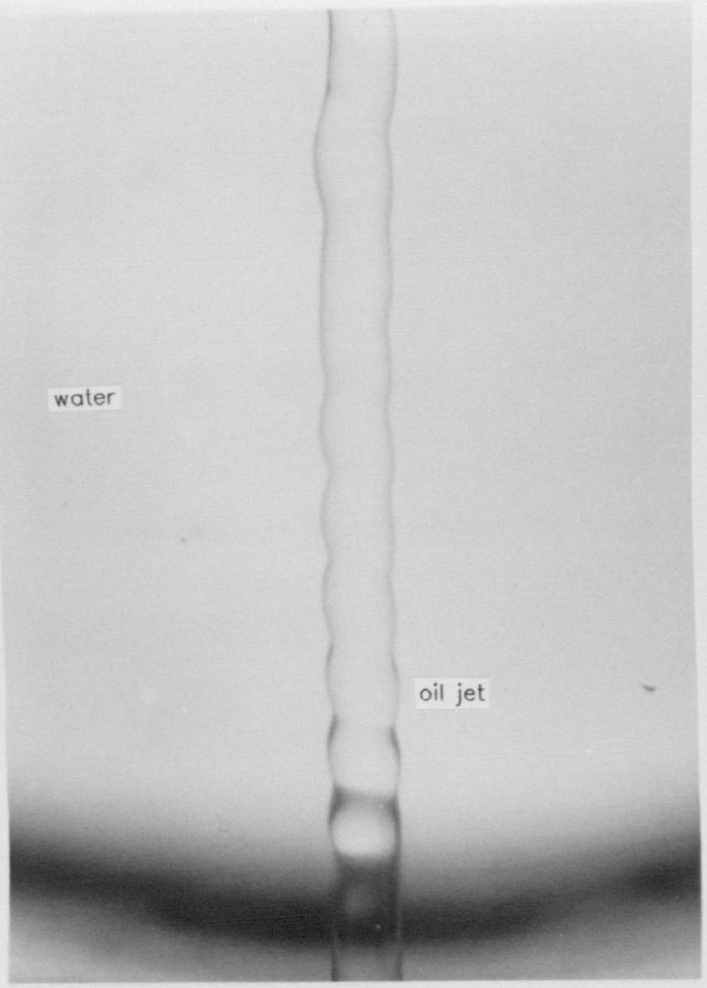

FIGURE 3.2.1 INITIAL INSTABILITIES OF THE OIL JET, PENETRATING WATER

V_j= 0.5m/s

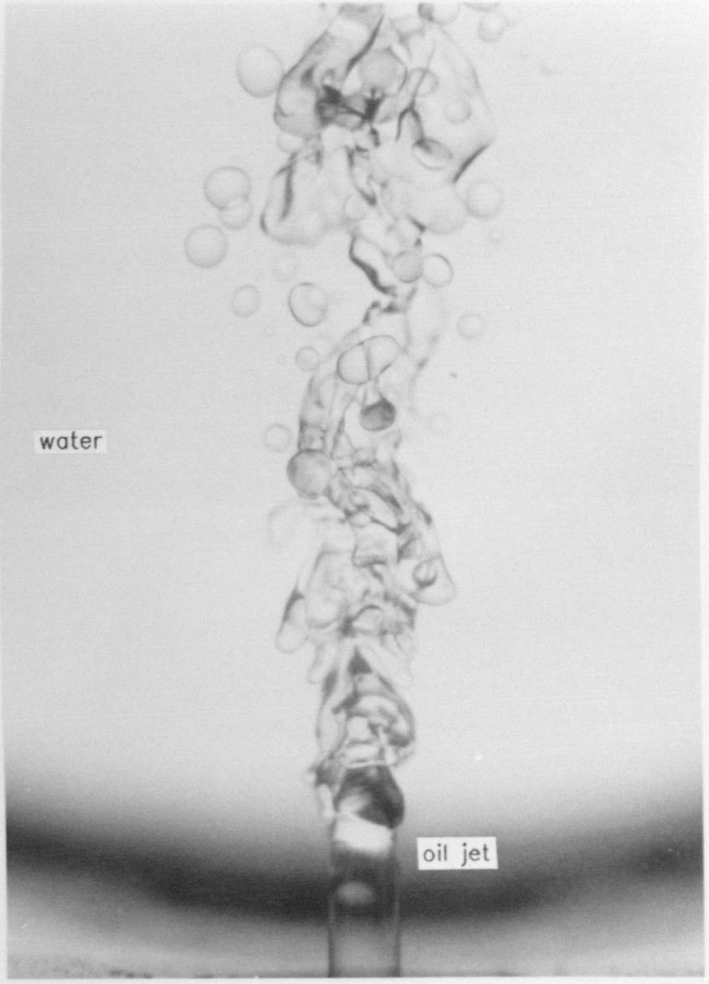

FIGURE 3.2.2 BREAKUP OF AN OIL JET, PENETRATING WATER

V_j= 1.1m/s

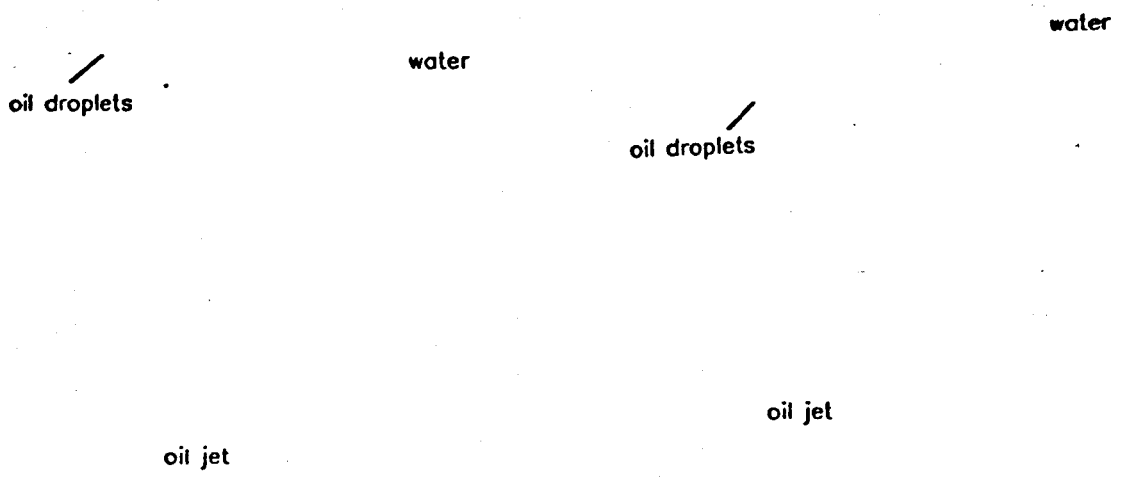
water
oil droplets
water
oil droplets
oil jet
oil jet
water
water
oil droplets
oil jet
oil jet

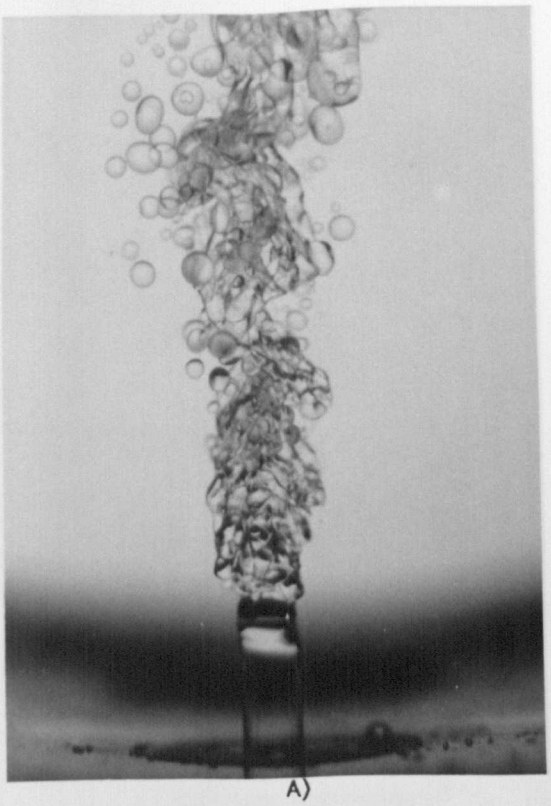

A)

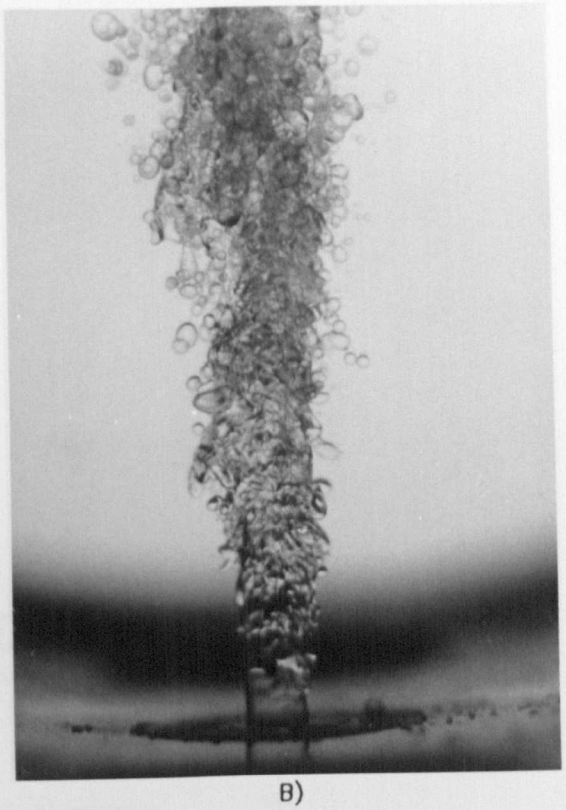

B)

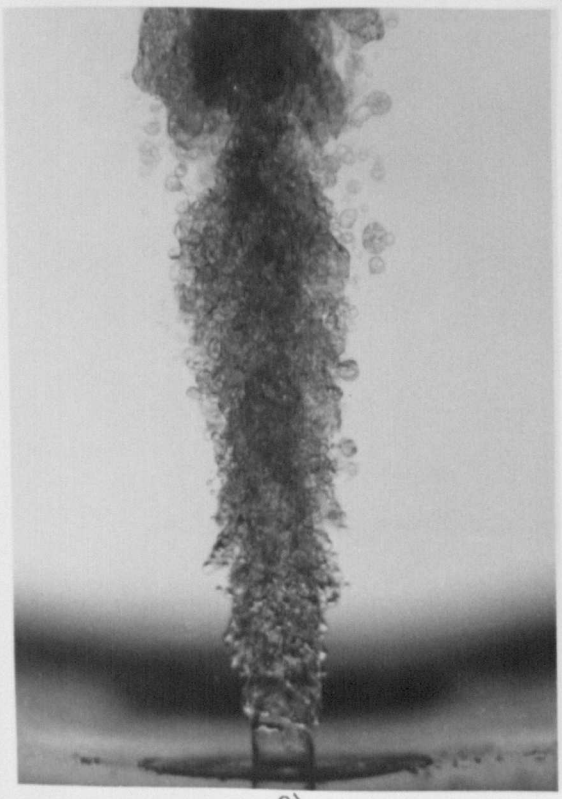

C)

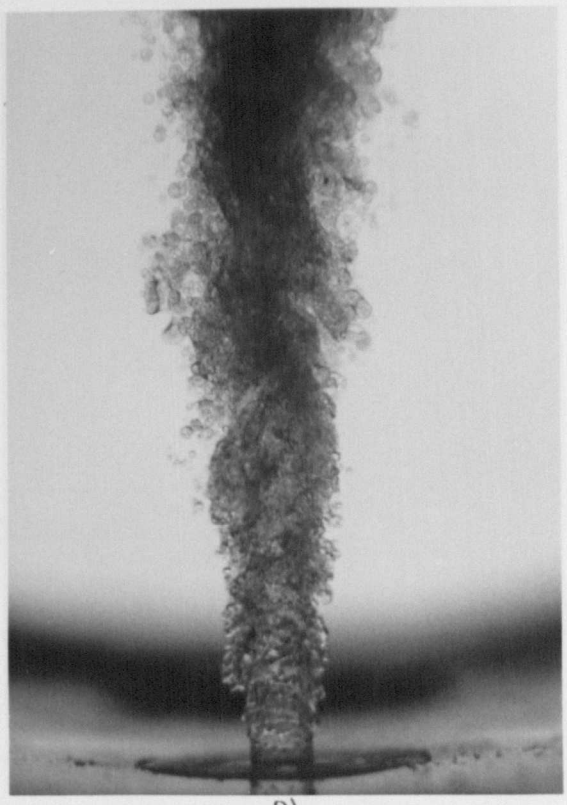

D)

FIGURE 3.2.3 BREAKUP PATTERNS OF AN OIL JET, PENETRATING WATER, AS ITS VELOCITY IS CONSECUTIVELY INCREASED (SEE TABLE 3.1 FOR MORE DETAILS)

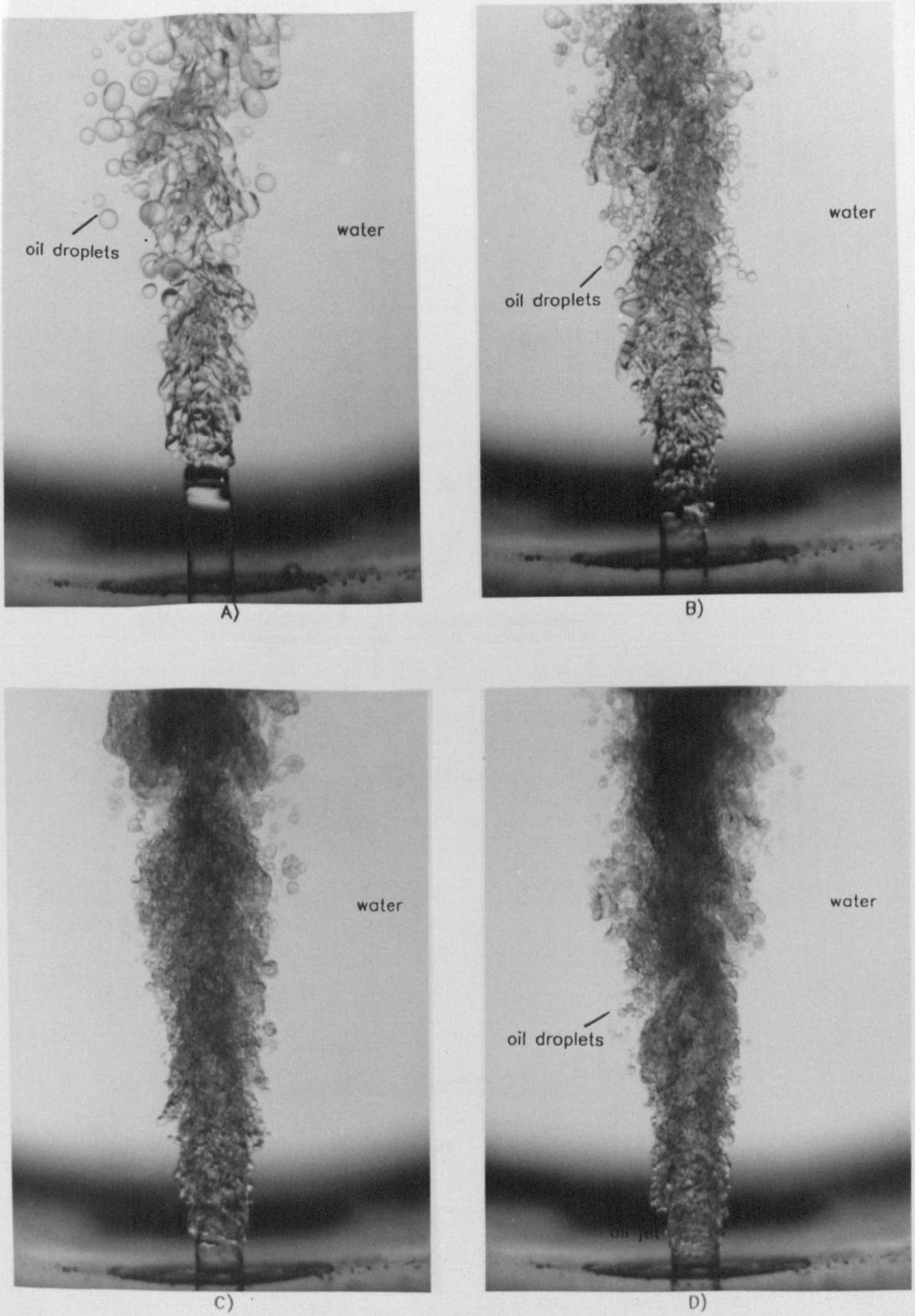

FIGURE 3.2.3 BREAKUP PATTERNS OF AN OIL JET, PENETRATING WATER, AS ITS VELOCITY IS CONSECUTIVELY INCREASED (SEE TABLE 3.1 FOR MORE DETAILS)

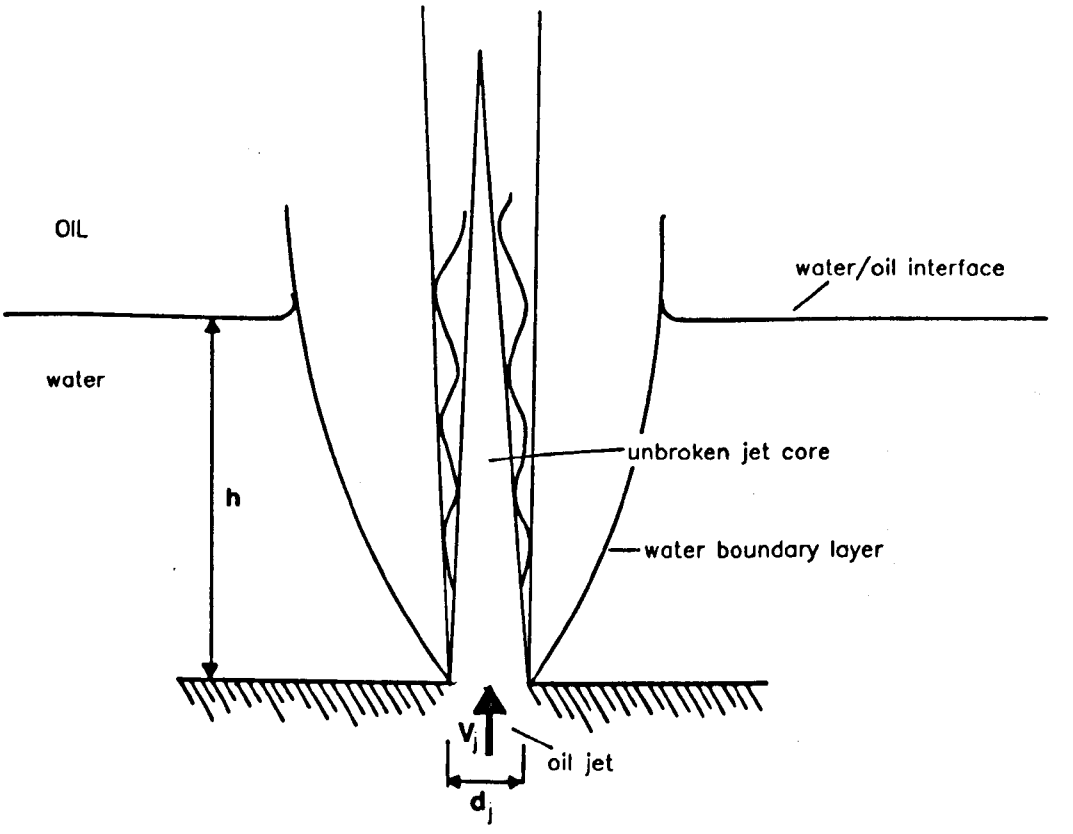

FIGURE 3.2.4 PENETRATION OF OIL JET THROUGH WATER

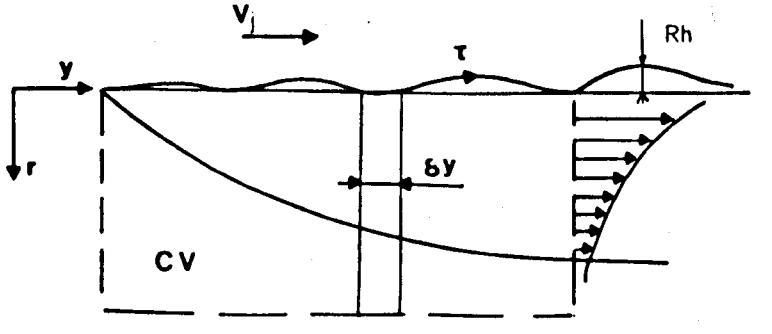

FIGURE 3.2.5 CONTROL VOLUME OF THE BOUNDARY LAYER FOR INTEGRAL ANALYSIS


OIL
oil/water interface
water
water droplets
oil/water interface
OIL
oil/water interface
water
water droplets
oil/water interface

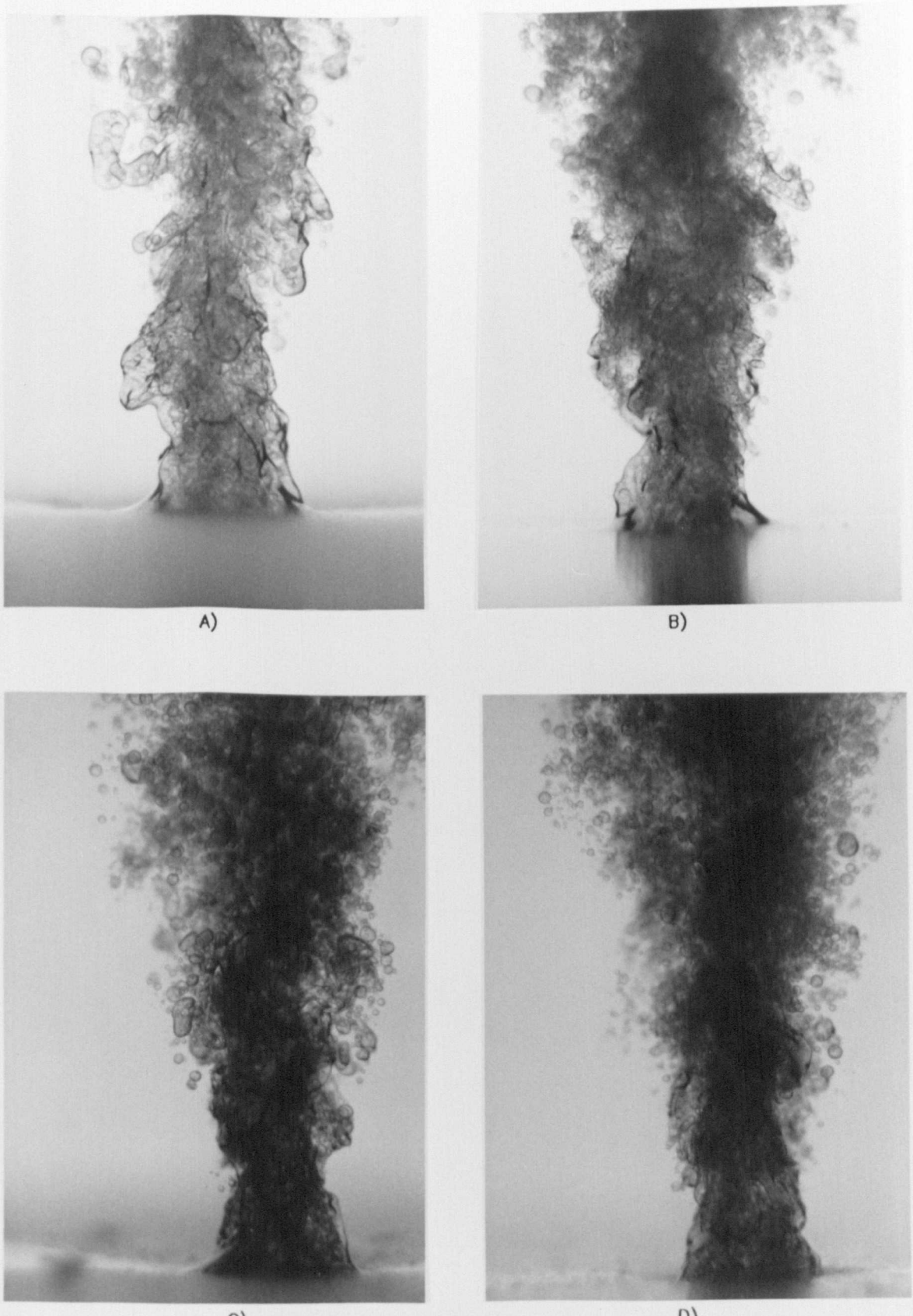

FIGURE 3.3.1 BREAKUP OF ENTRAINED WATER AS IT PENETRATES THE OIL/WATER INTERFACE TO OIL
(SEE TABLE 3.1 FOR MORE DETAILS)

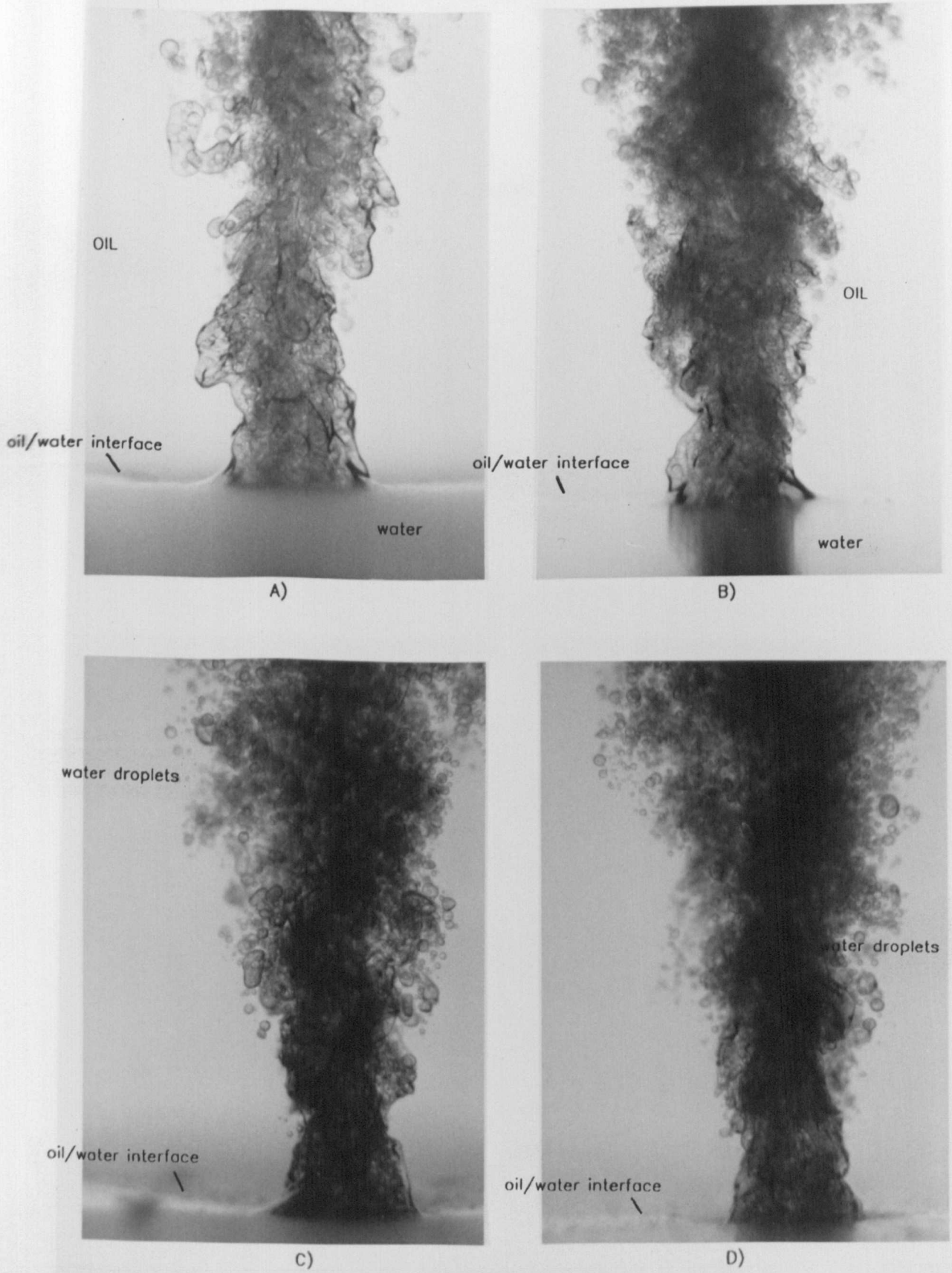

FIGURE 3.3.1 BREAKUP OF ENTRAINED WATER AS IT PENETRATES THE OIL/WATER INTERFACE TO OIL
(SEE TABLE 3.1 FOR MORE DETAILS)

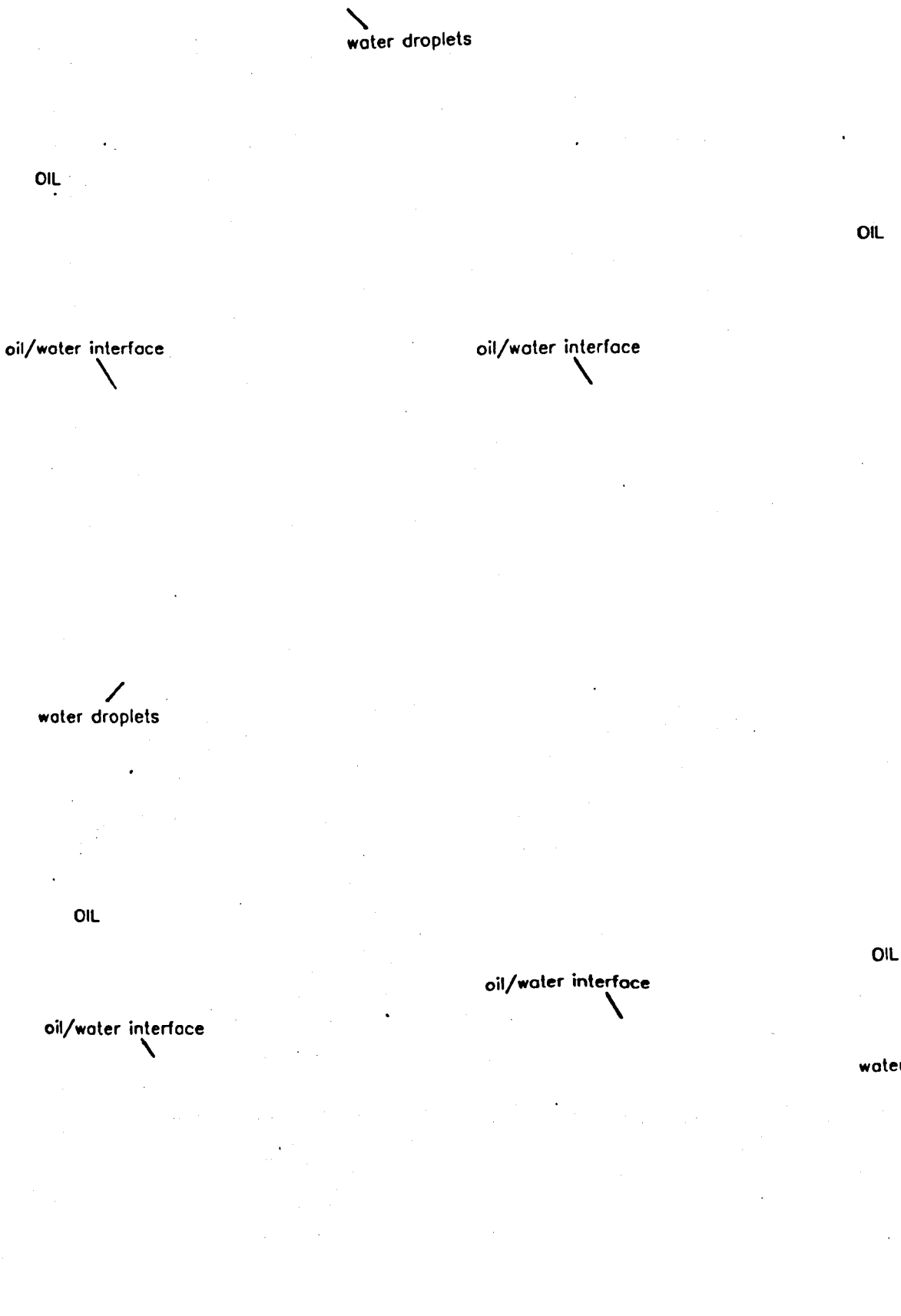
water droplets
OIL
OIL
oil/water interface
oil/water interface
water droplets
OIL
OIL
oil/water interface
oil/water interface
water

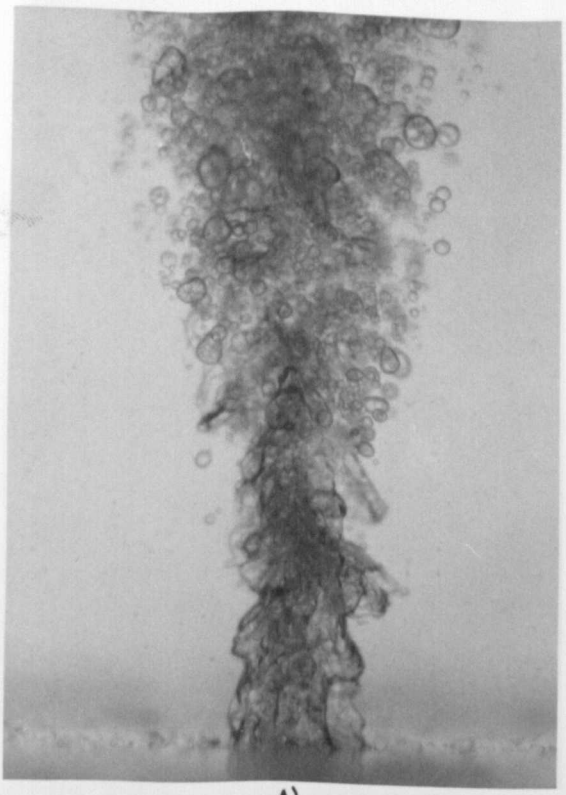

A)

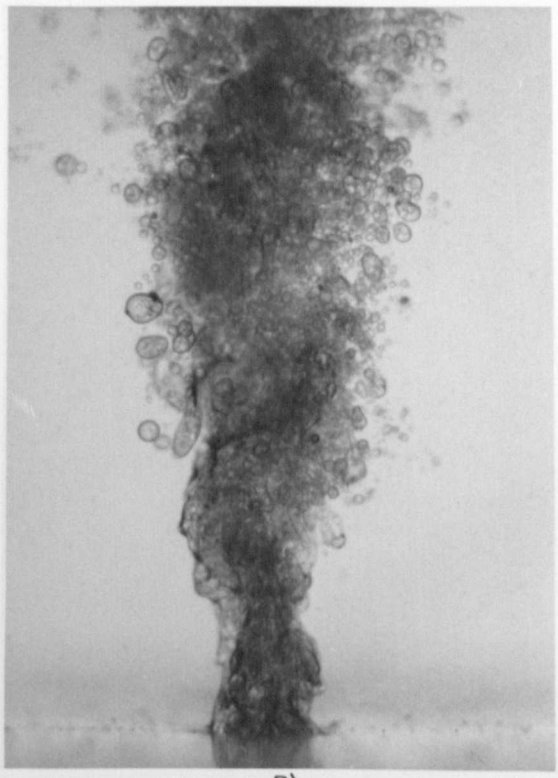

B)

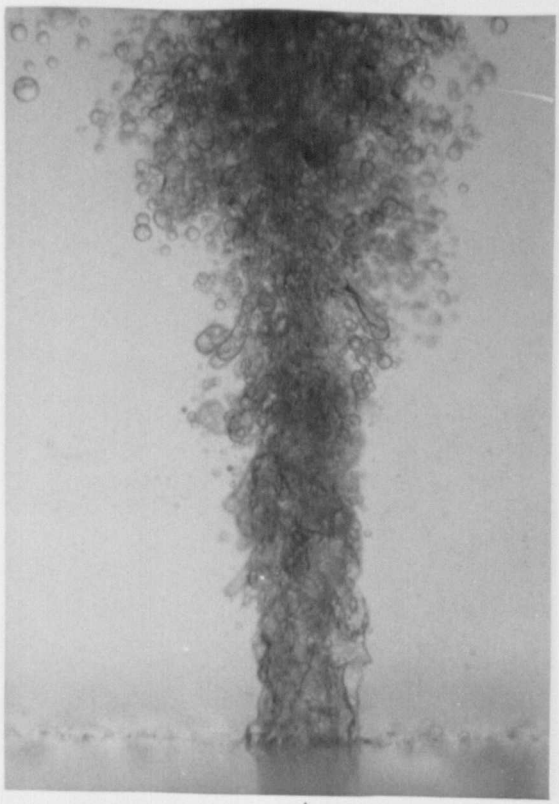

C)

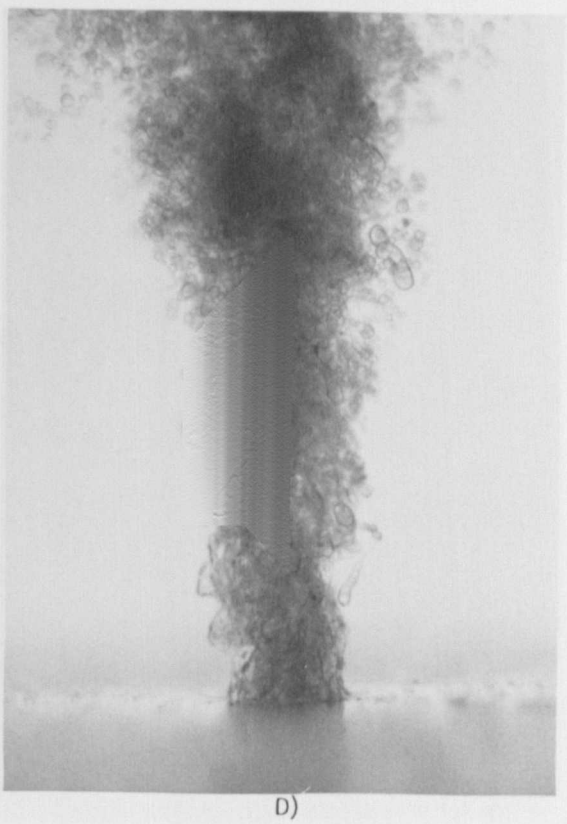

D)

FIGURE 3.3.2 BREAKUP OF ENTRAINED WATER AS IT PENETRATES THE OIL/WATER INTERFACE TO OIL System:– 30% Base oil/pure water

(SEE TABLE 3.1 FOR MORE DETAILS)

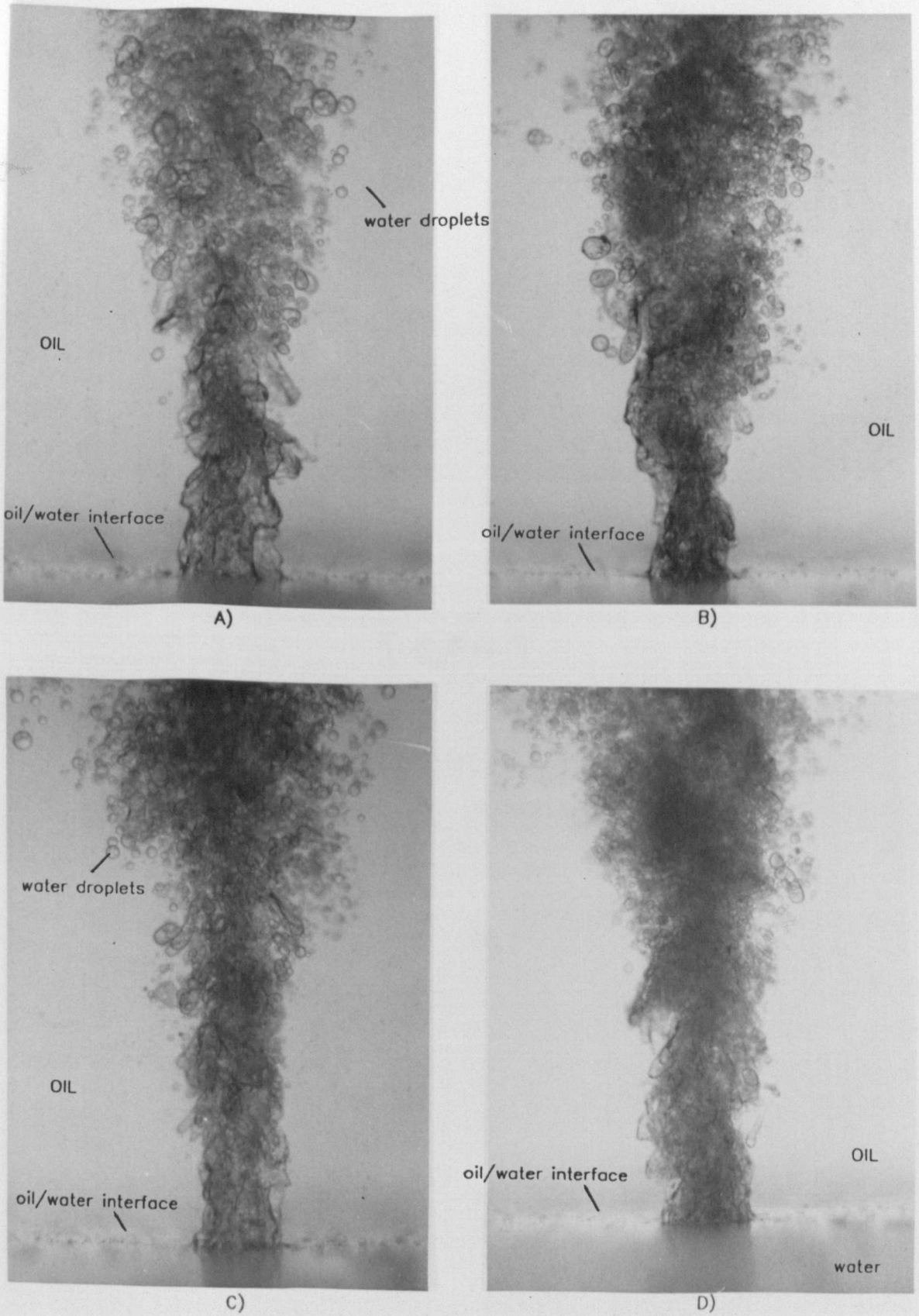

FIGURE 3.3.2 BREAKUP OF ENTRAINED WATER AS IT PENETRATES THE OIL/WATER INTERFACE TO OIL System:- 30% Base oil/pure water

(SEE TABLE 3.1 FOR MORE DETAILS)

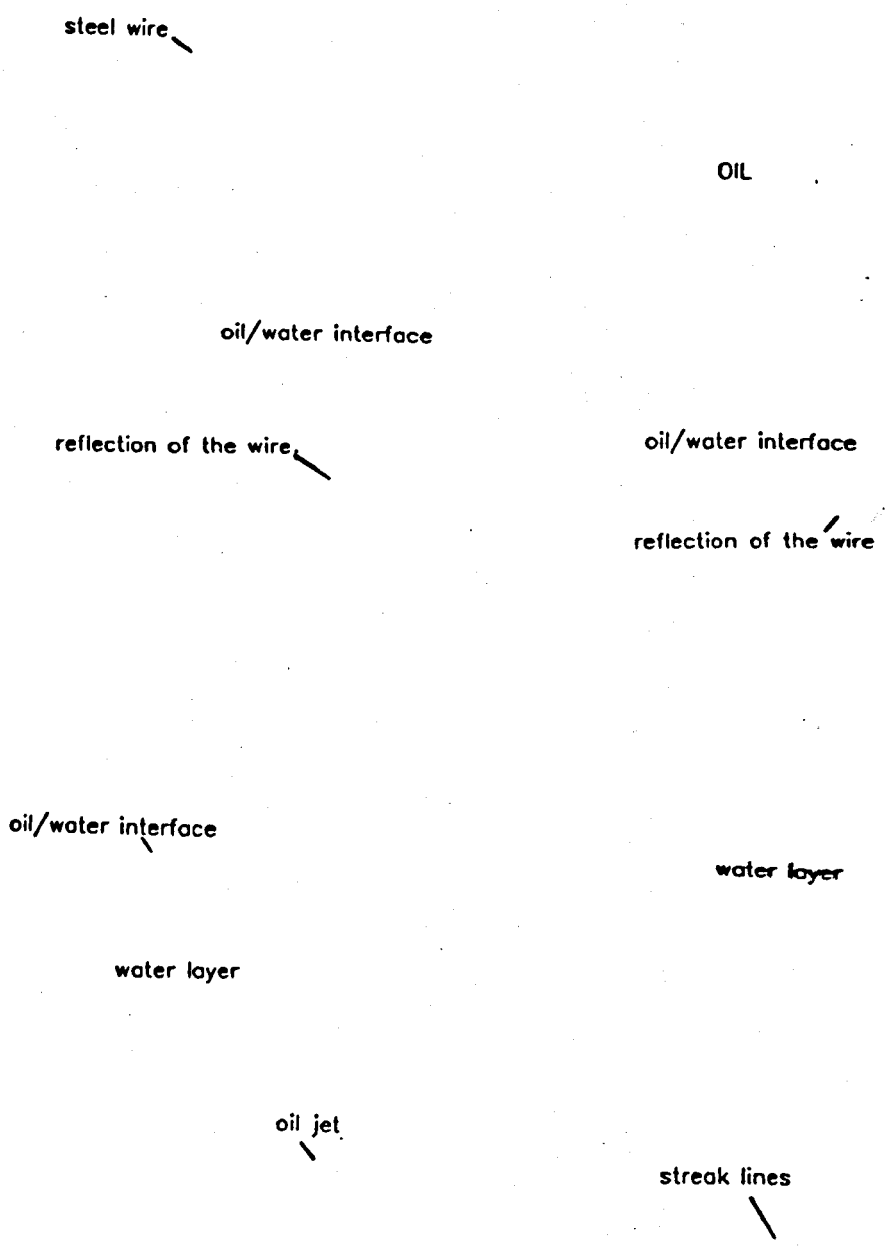
steel wire
OIL
oil/water interface
reflection of the wire
oil/water interface
reflection of the wire
oil/water interface
water layer
water layer
oil jet
oil jet
streak lines

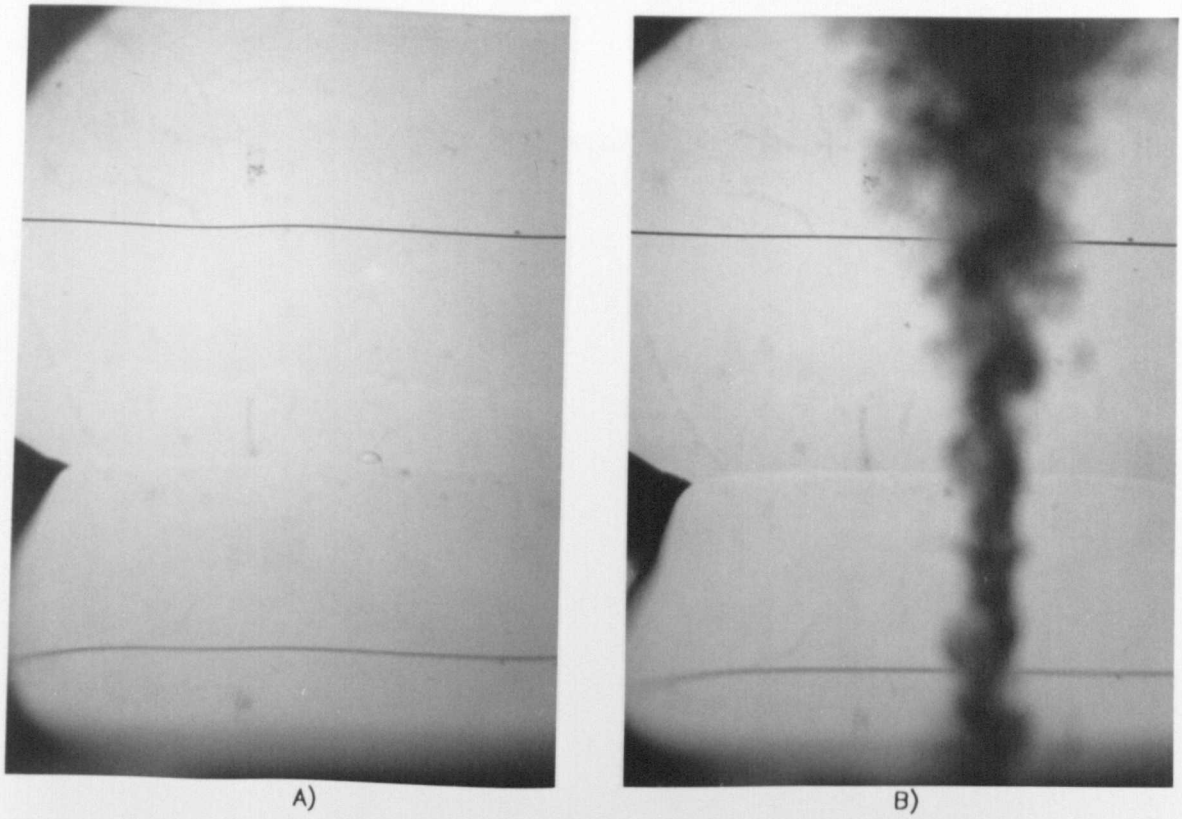

A) B)

FIGURE 3.4.1 OIL/WATER INTERFACE WITHOUT(A) AND WITH(B) THE PENETRATING OIL JET

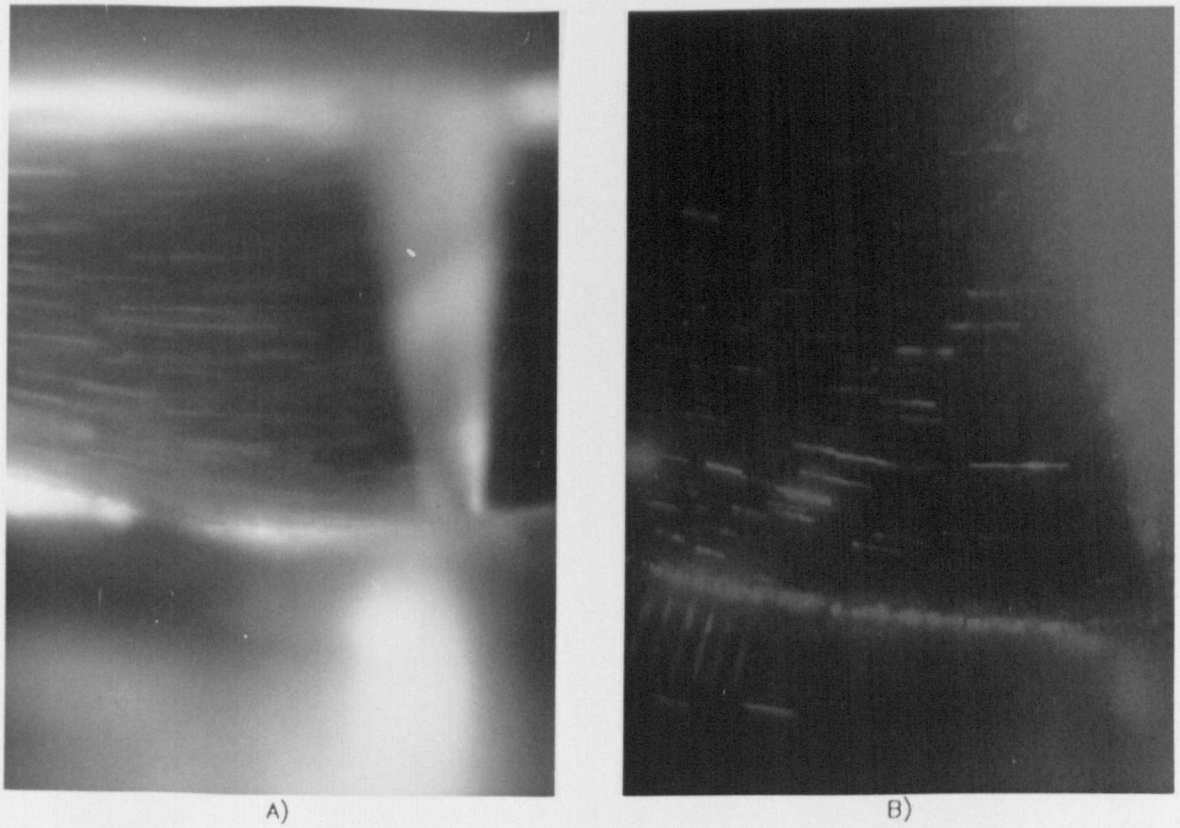

A) B)

FIGURE 3.5.1 STREAK LINES, IN THE WATER LAYER, OF THE ENTRAINING WATER

A). ILLUMINATED BY TUNGSTEN-HALOGEN SHEET LIGHT SOURCE

B). ILLUMINATED BY HE-NE LASER SHEET SOURCE

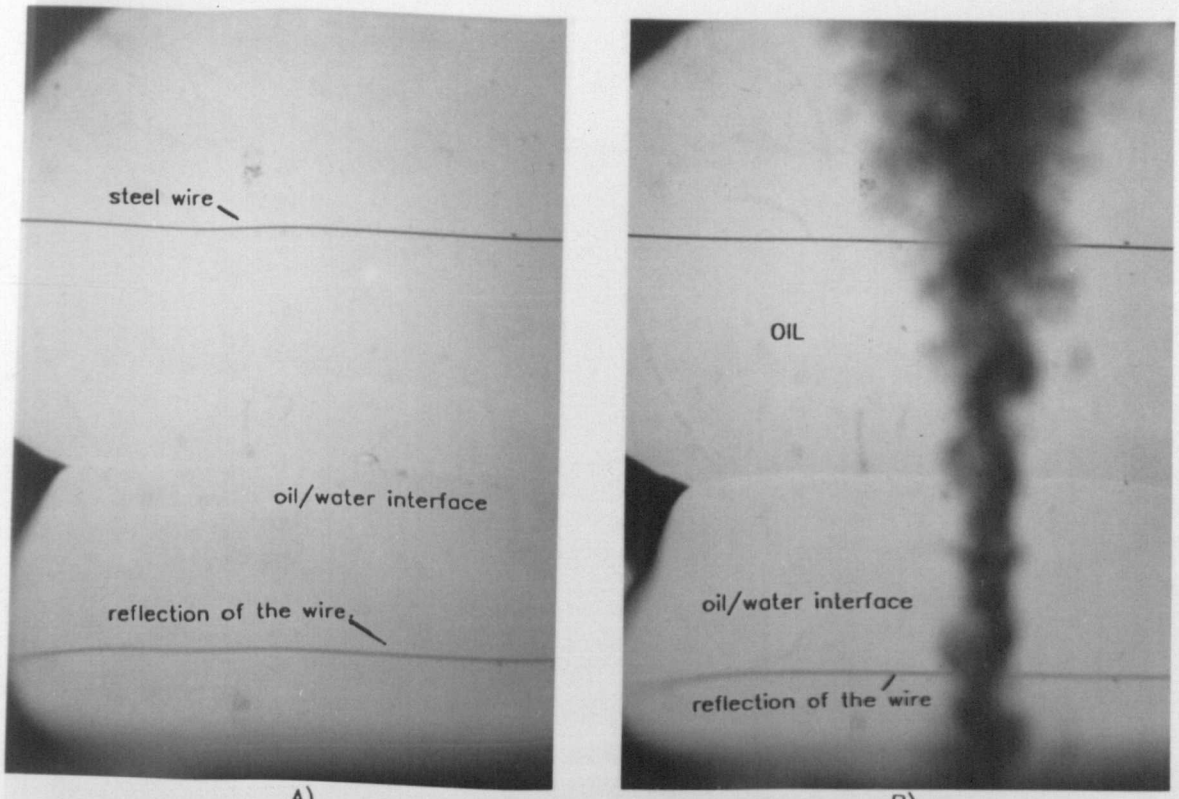

FIGURE 3.4.1 OIL/WATER INTERFACE WITHOUT(A) AND WITH(B) THE PENETRATING OIL JET

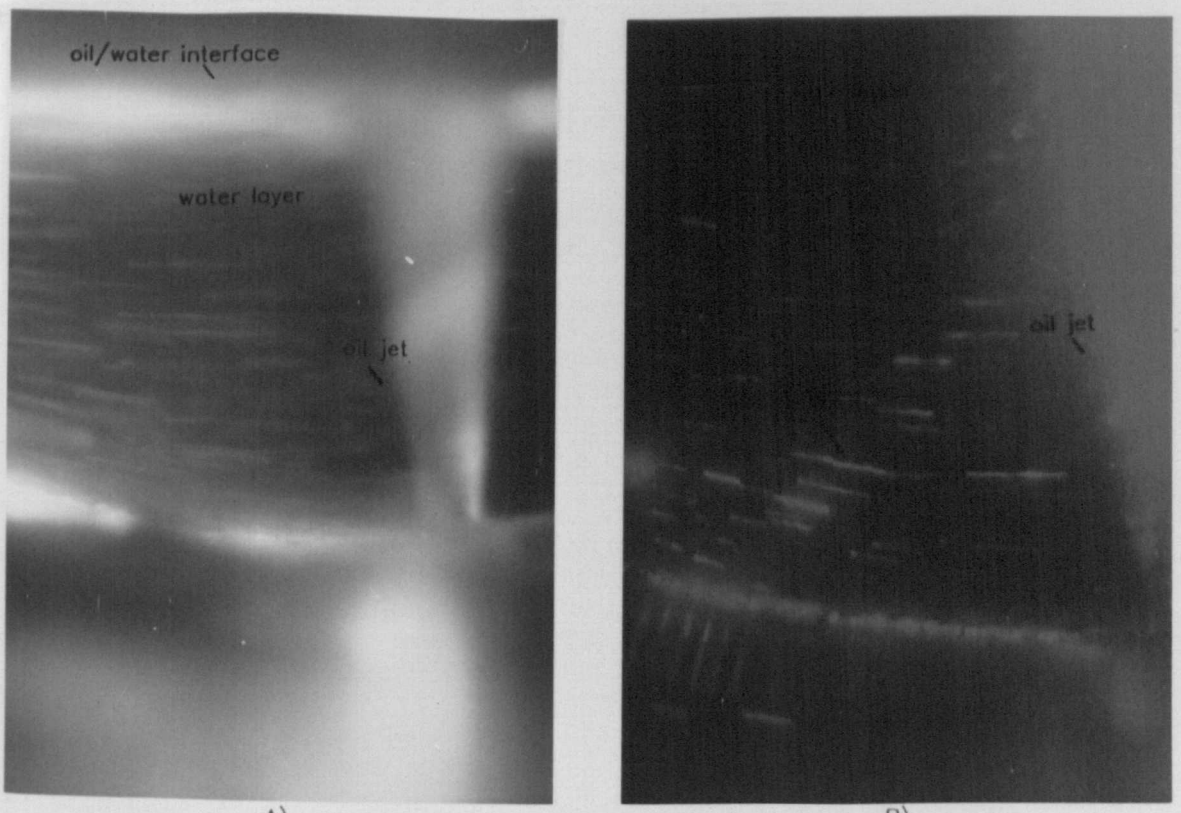

FIGURE 3.5.1 STREAK LINES, IN THE WATER LAYER, OF THE ENTRAINING WATER

A). ILLUMINATED BY TUNGSTEN-HALOGEN SHEET LIGHT SOURCE

B). ILLUMINATED BY HE-NE LASER SHEET SOURCE

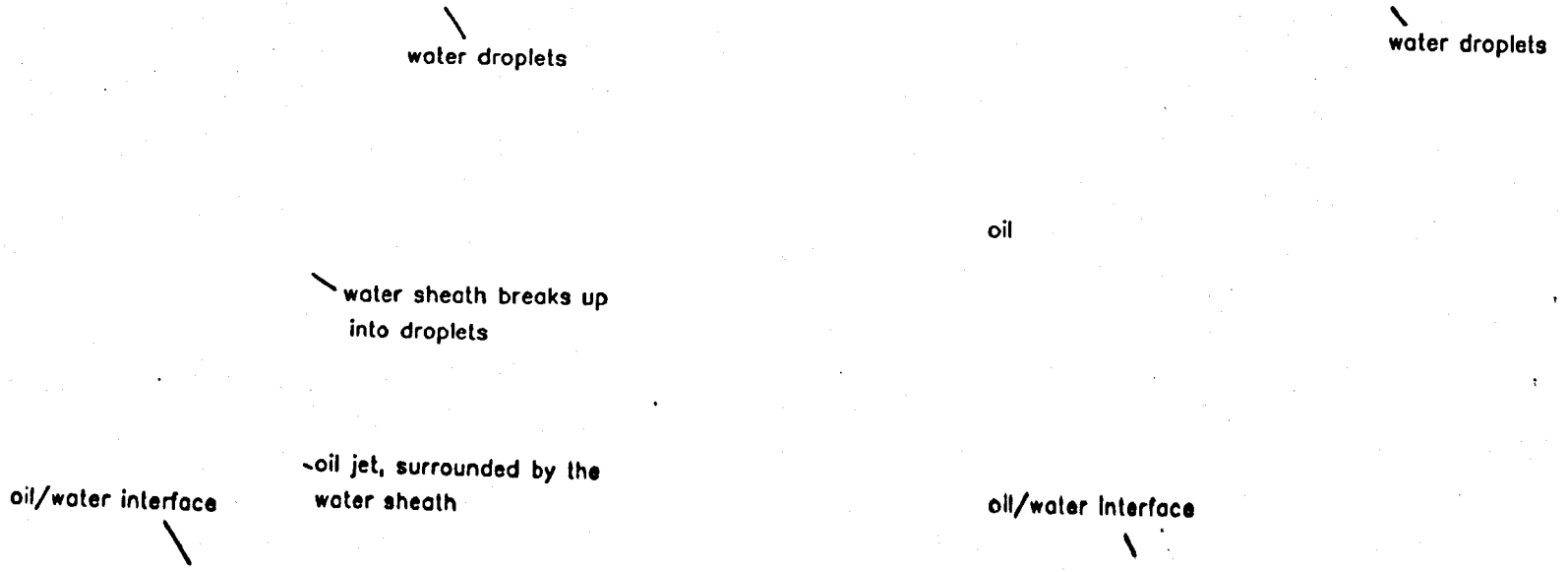
water droplets
water droplets
oil
water sheath breaks up into droplets
oil jet, surrounded by the water sheath
oil/water interface
oil/water interface

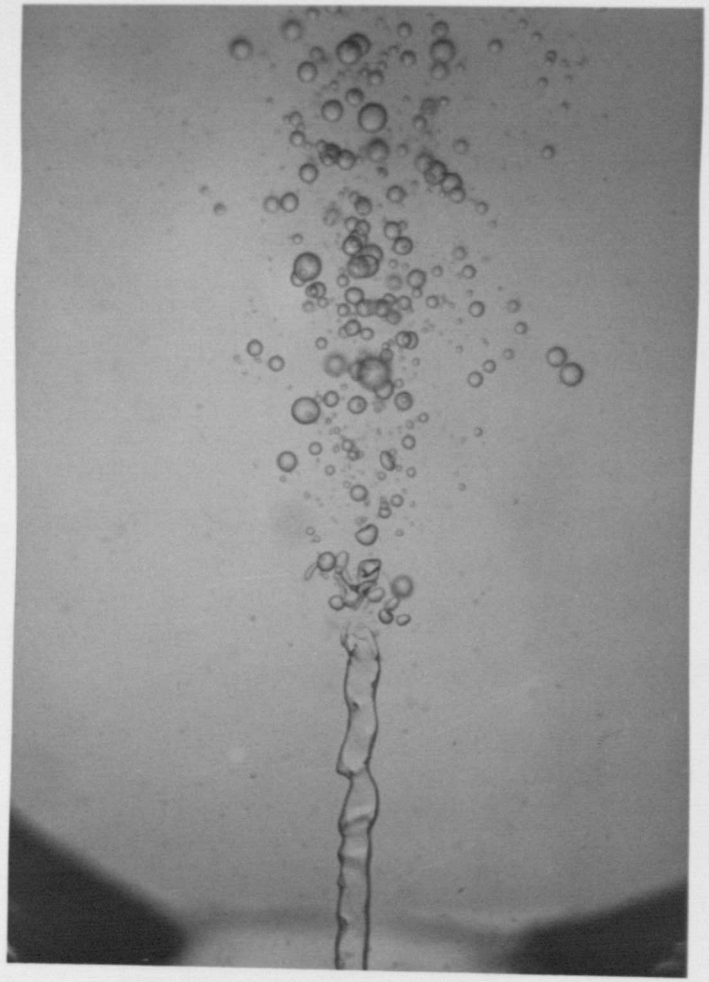

(A)

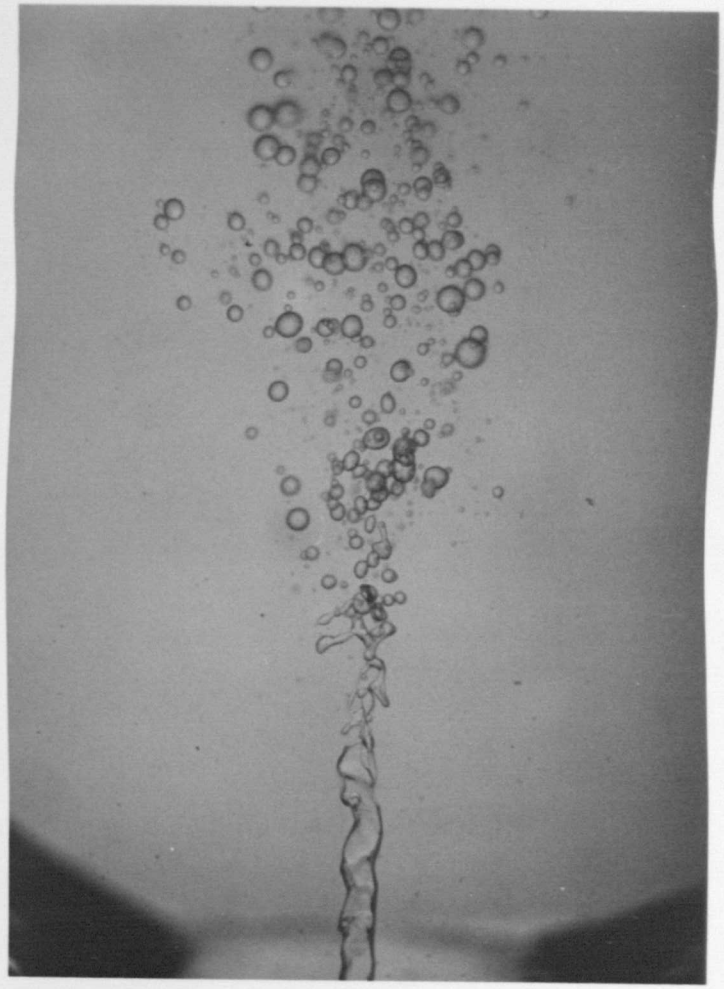

(B)

FIGURE 3.6.1 BREAKUP OF ENTRAINED WATER AS IT PENETRATES THE OIL/WATER INTERFACE TO OIL (AT RELATIVELY LOW PENETRATING VELOCITIES) (SEE TABLE 3.1 FOR MORE DETAILS)

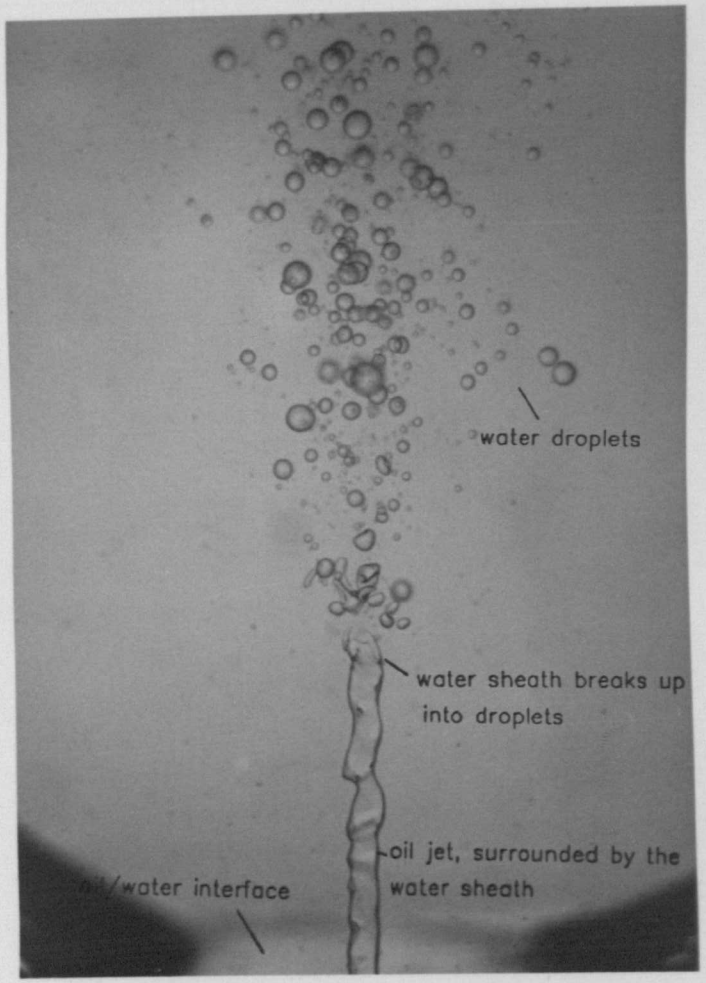

(A)

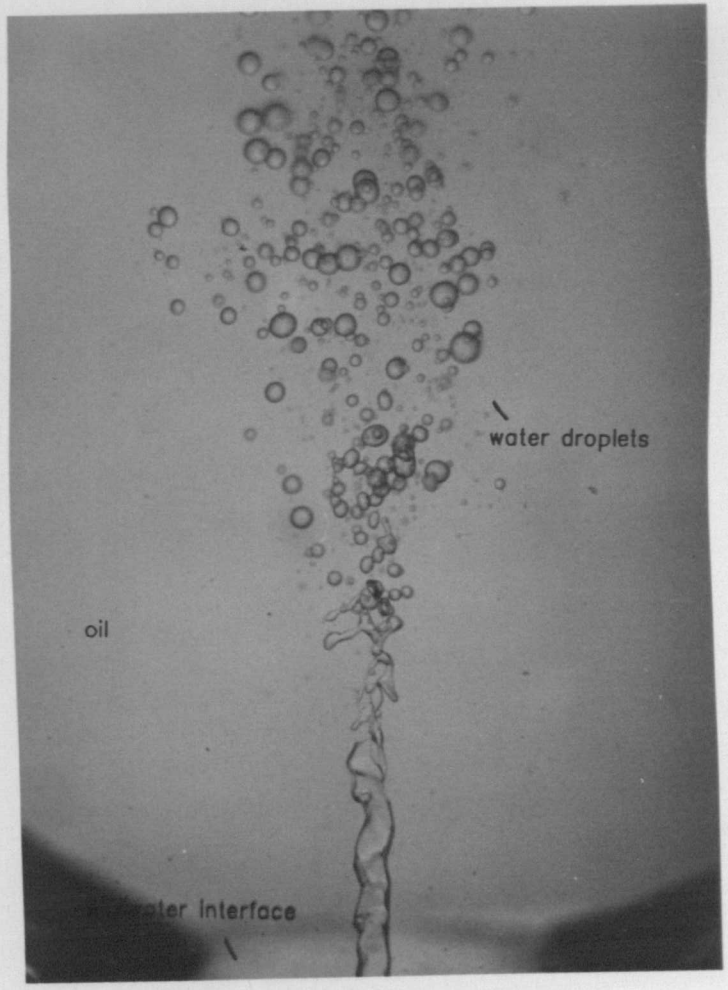

(B)

FIGURE 3.6.1 BREAKUP OF ENTRAINED WATER AS IT PENETRATES THE OIL/WATER INTERFACE TO OIL (AT RELATIVELY LOW PENETRATING VELOCITIES) (SEE TABLE 3.1 FOR MORE DETAILS)

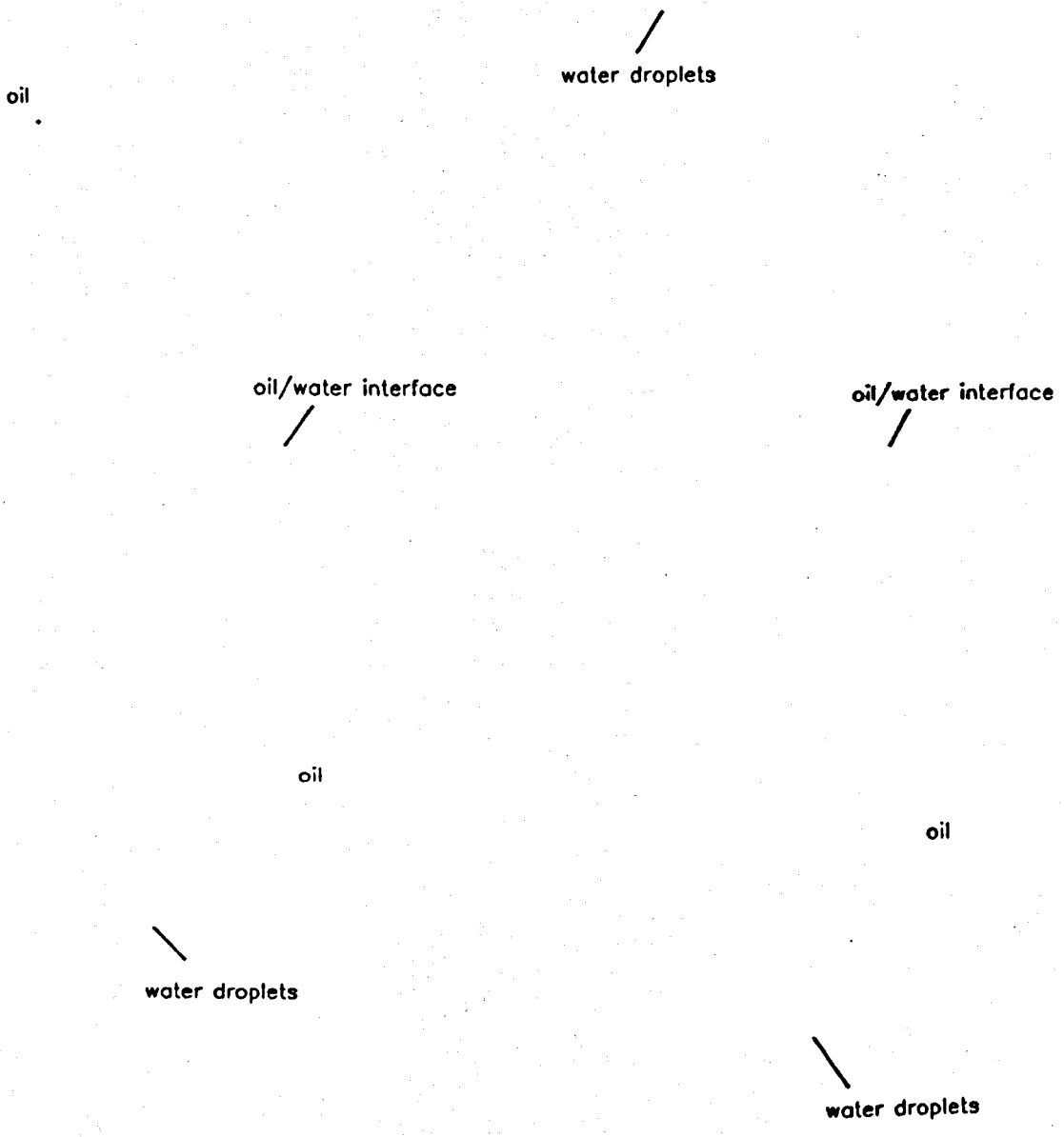
water droplets
oil
oil/water interface
oil/water interface
oil
oil
water droplets
water droplets

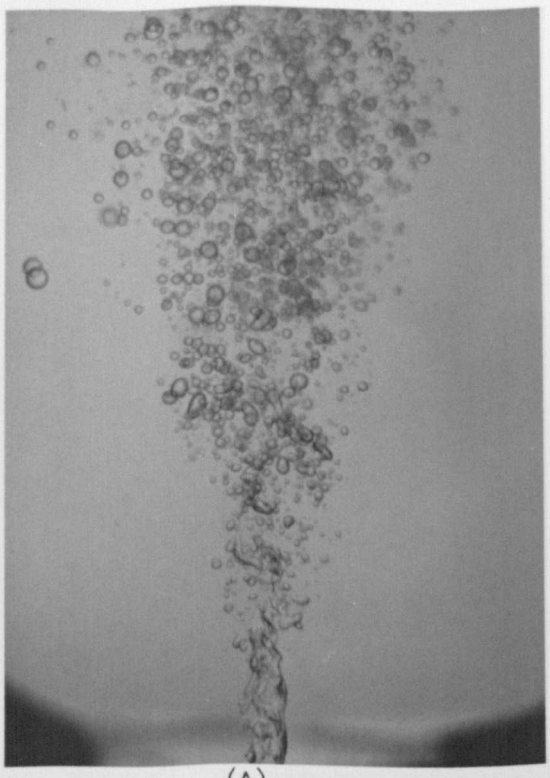

(A)

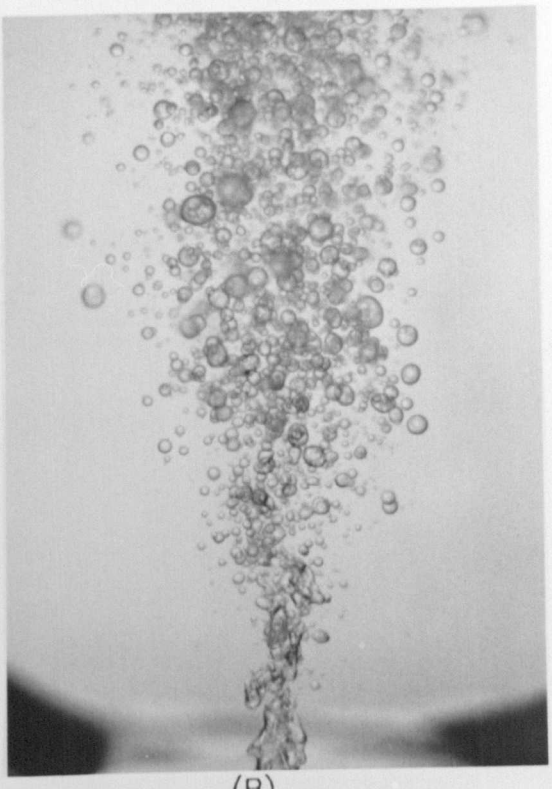

(B)

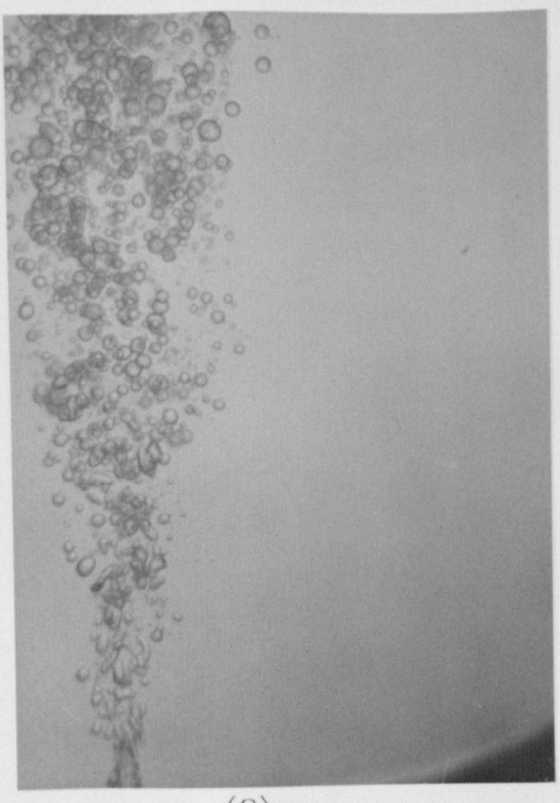

(C)

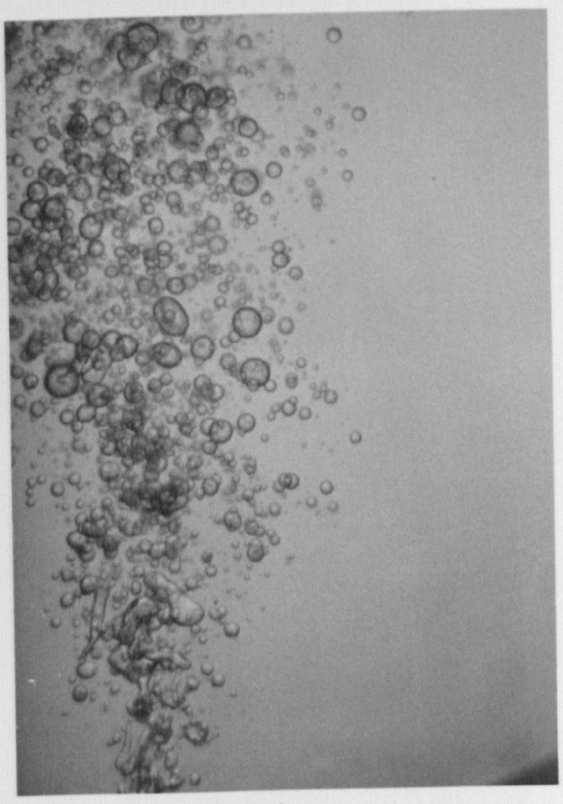

(D)

FIGURE 3.6.2 BREAKUP OF ENTRAINED WATER AS IT PENETRATES THE OIL/WATER INTERFACE TO OIL (AT RELATIVELY LOW PENETRATING VELOCITIES) (SEE TABLE 3.1 FOR MORE DETAILS)

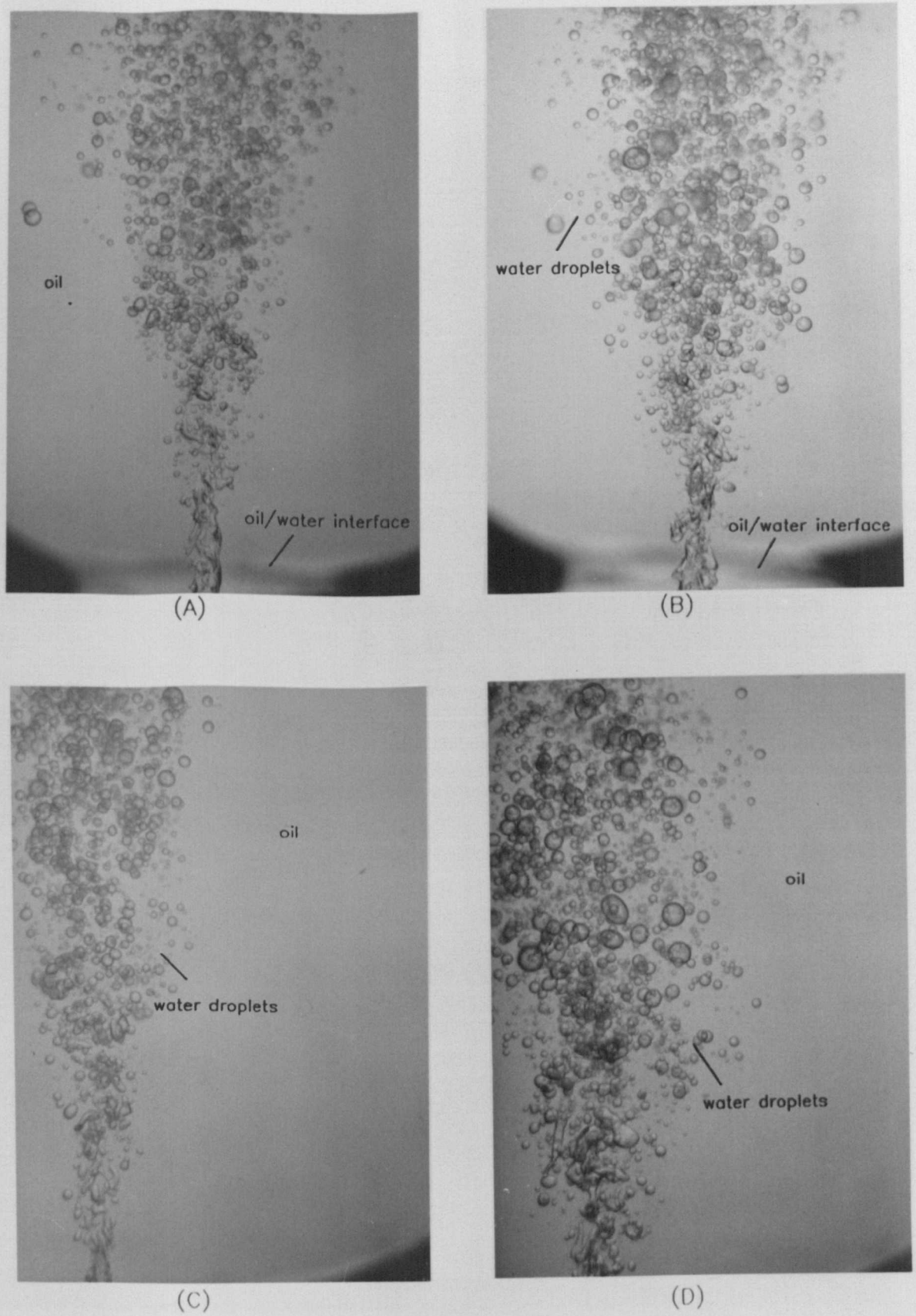

FIGURE 3.6.2 BREAKUP OF ENTRAINED WATER AS IT PENETRATES THE OIL/WATER INTERFACE TO OIL (AT RELATIVELY LOW PENETRATING VELOCITIES) (SEE TABLE 3.1 FOR MORE DETAILS)

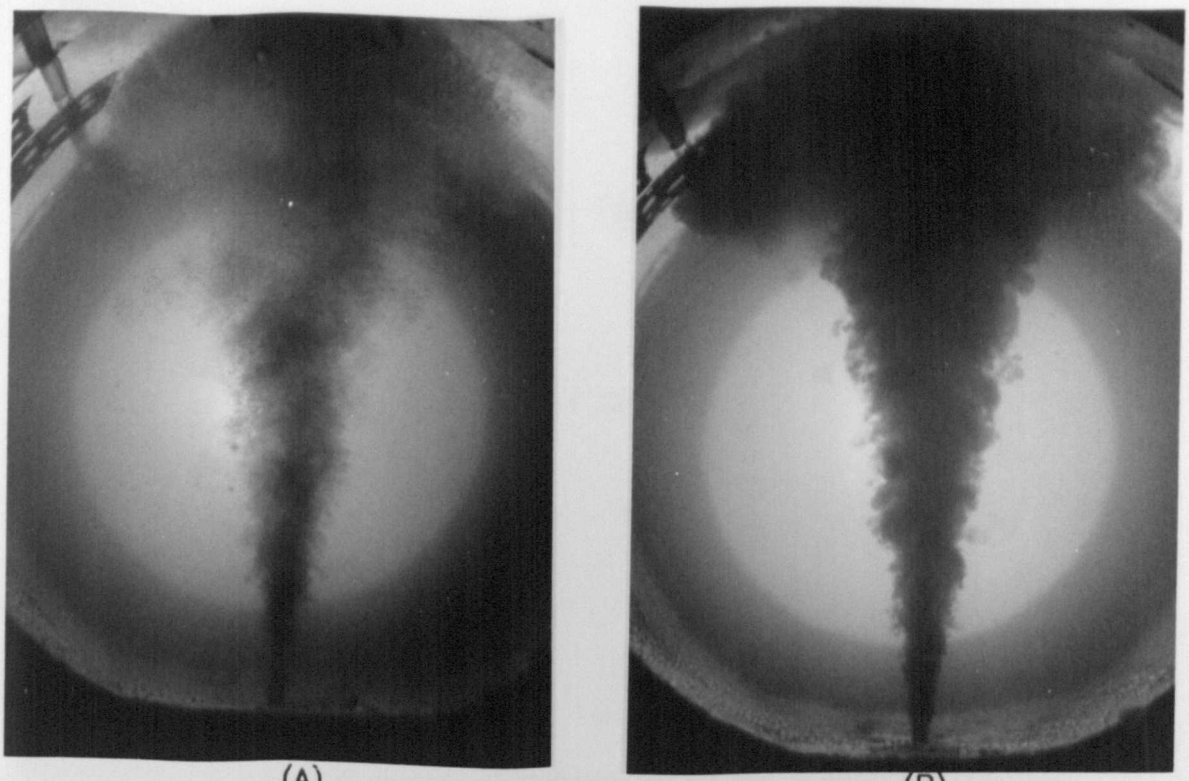

FIG. 3.7.1 OIL JET, A). WITH AND B). WITHOUT THE STRATIFIED WATER
(SEE TABLE 3.1 FOR MORE DETAILS)

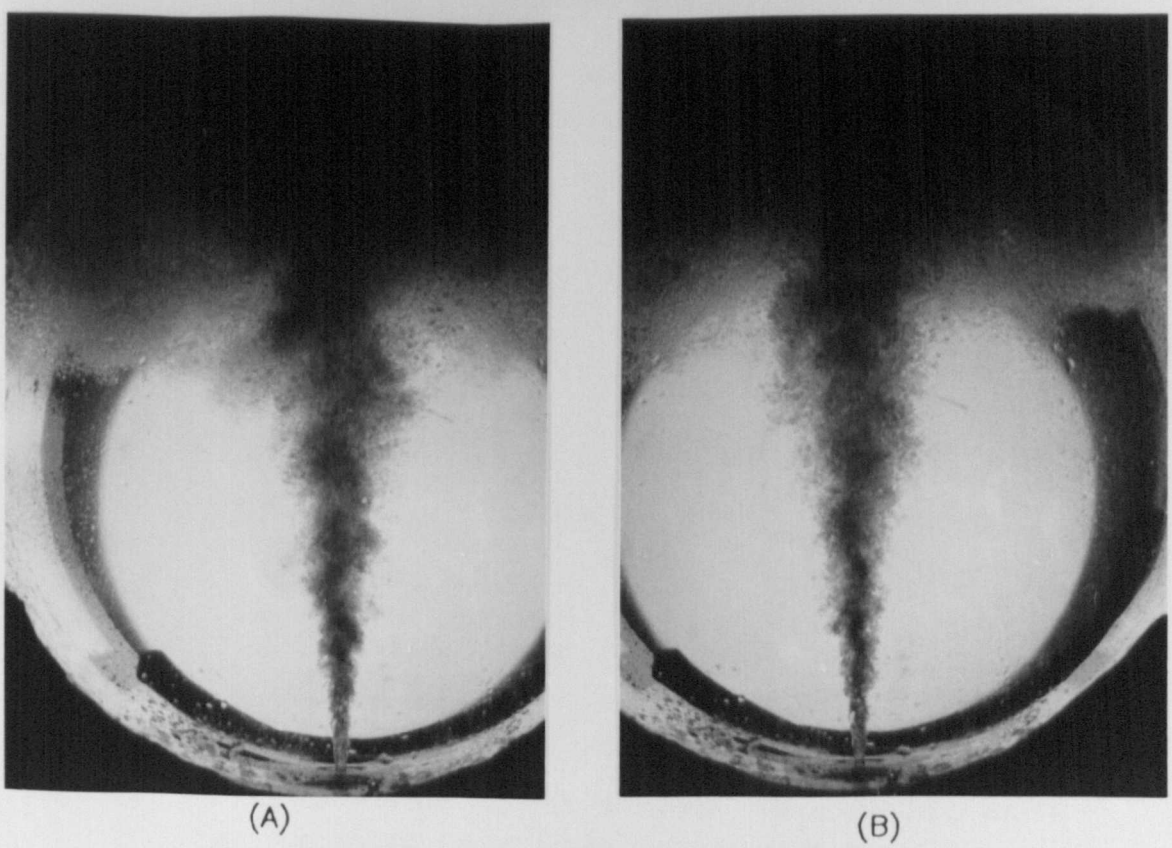

FIG. 3.7.2 BREAKUP OF OIL JET IN WATER
(SEE TABLE 3.1 FOR MORE DETAILS)

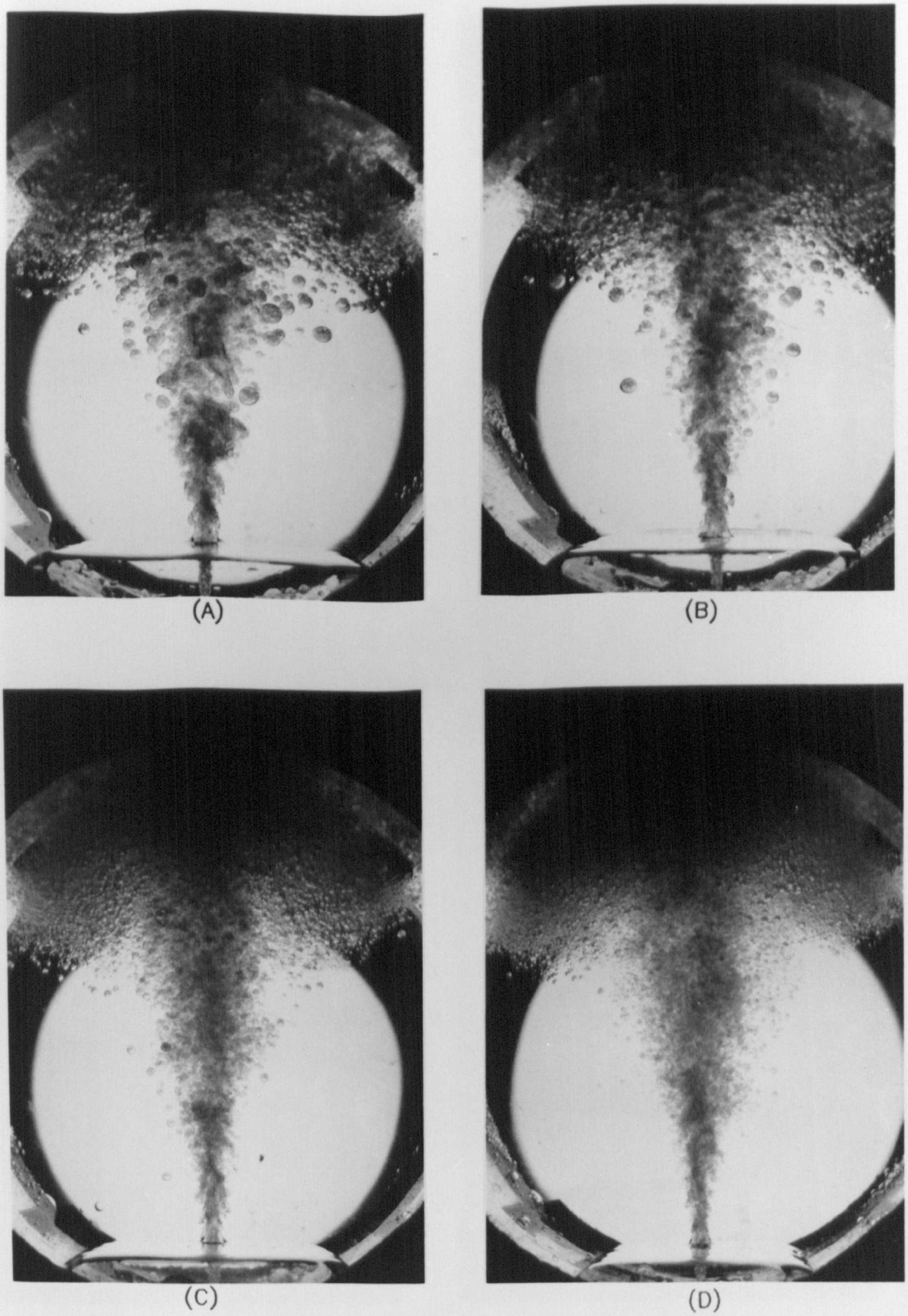

FIG. 3.8.1 PENETRATION OF OIL JET THROUGH THE STRATIFIED WATER AS THE WATER LAYER HEIGHT IS CONSECUTIVELY DECREASED (SEE TABLE 3.1 FOR MORE DETAILS)

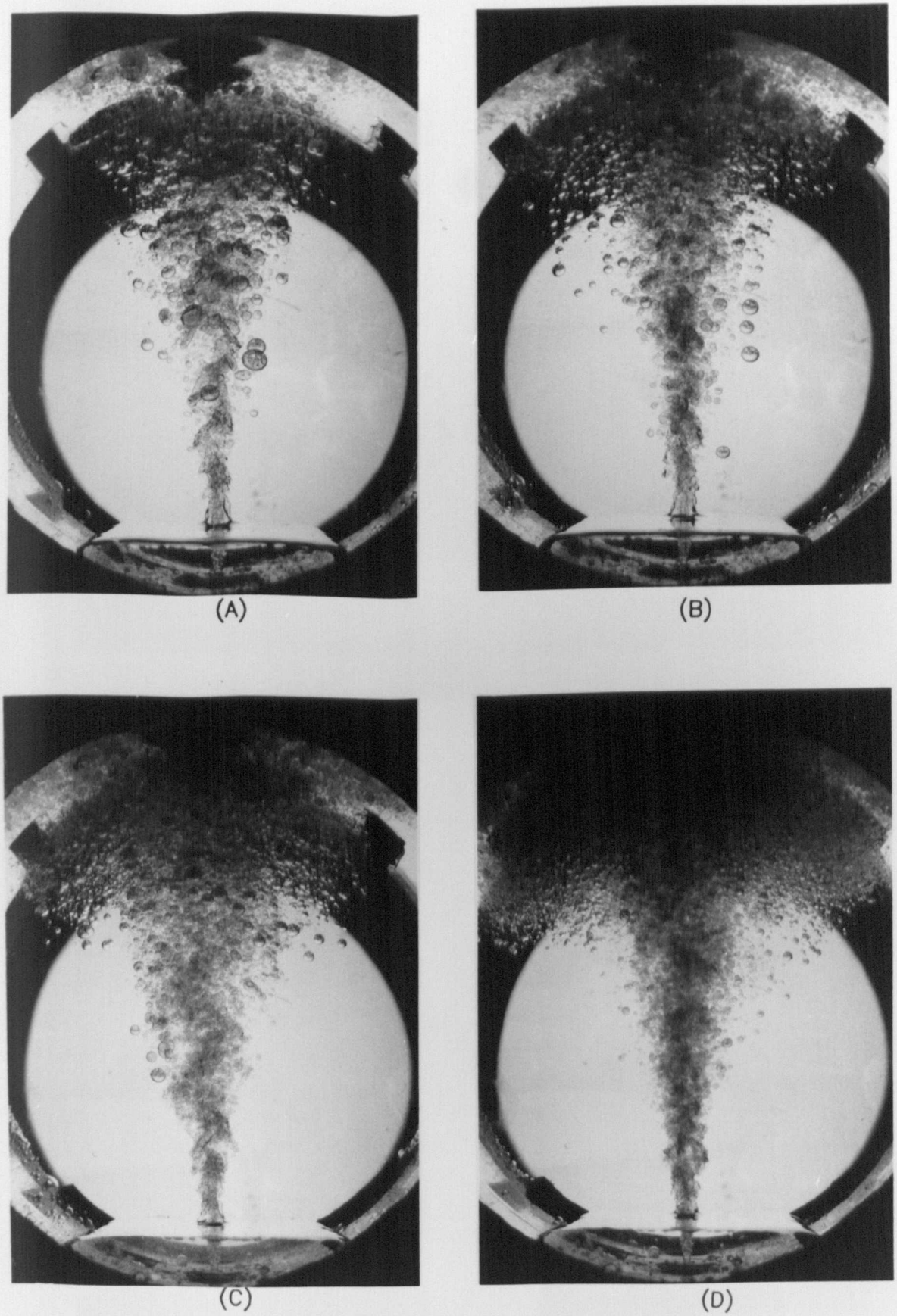

FIG. 3.8.2 PENETRATION OF OIL JET THROUGH STRATIFIED WATER AS ITS VELOCITY IS CONSECUTIVELY INCREASED (SEE TABLE 3.1 FOR MORE DETAILS)

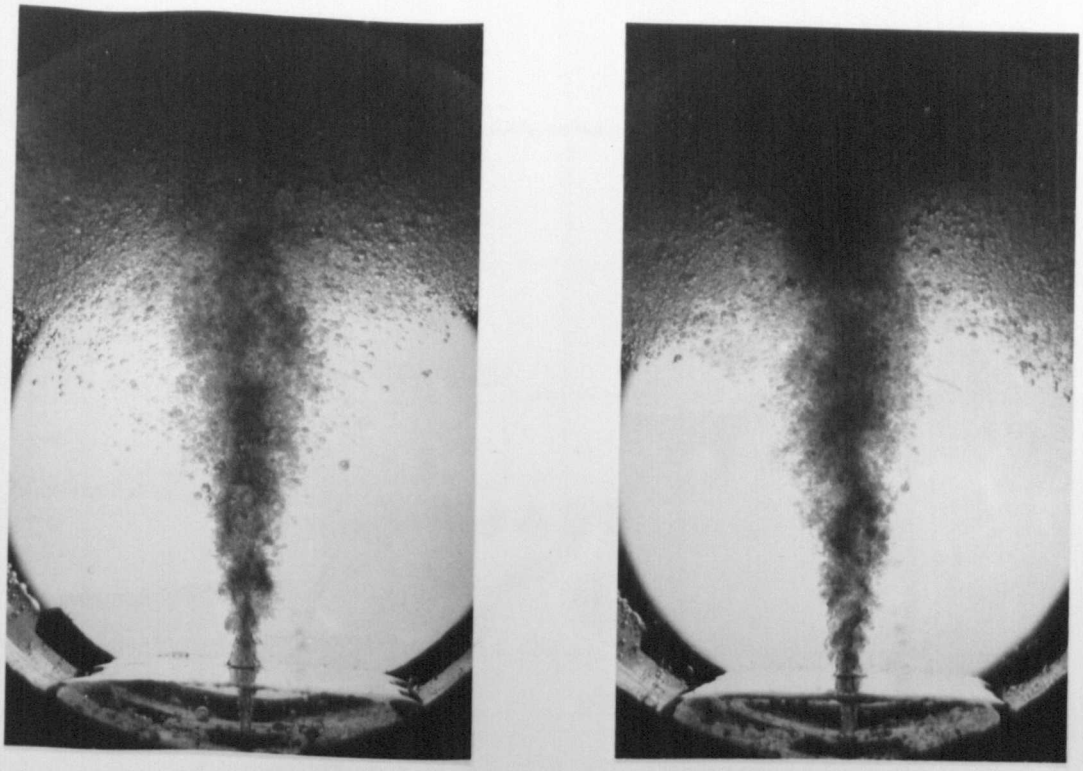

FIG. 3.8.3 CONTINUATION OF FIG. 3.8.2

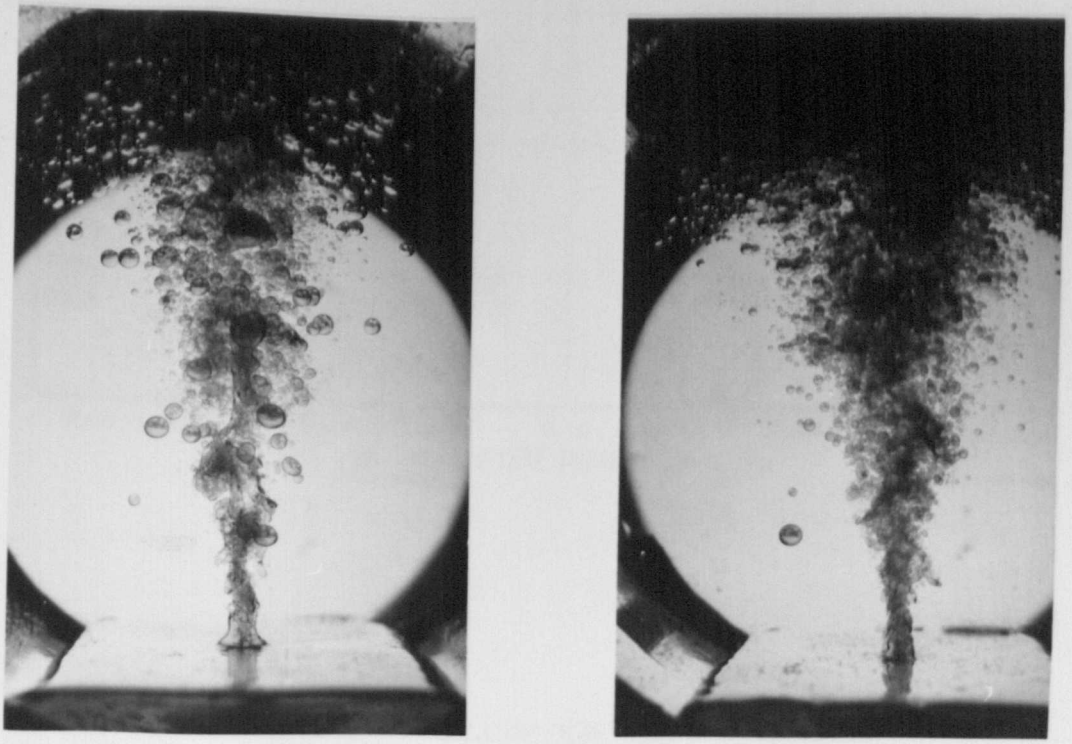

FIG. 3.9.1 PENETRATION OF OIL JET THROUGH A WATER LAYER, STRATIFIED IN OIL

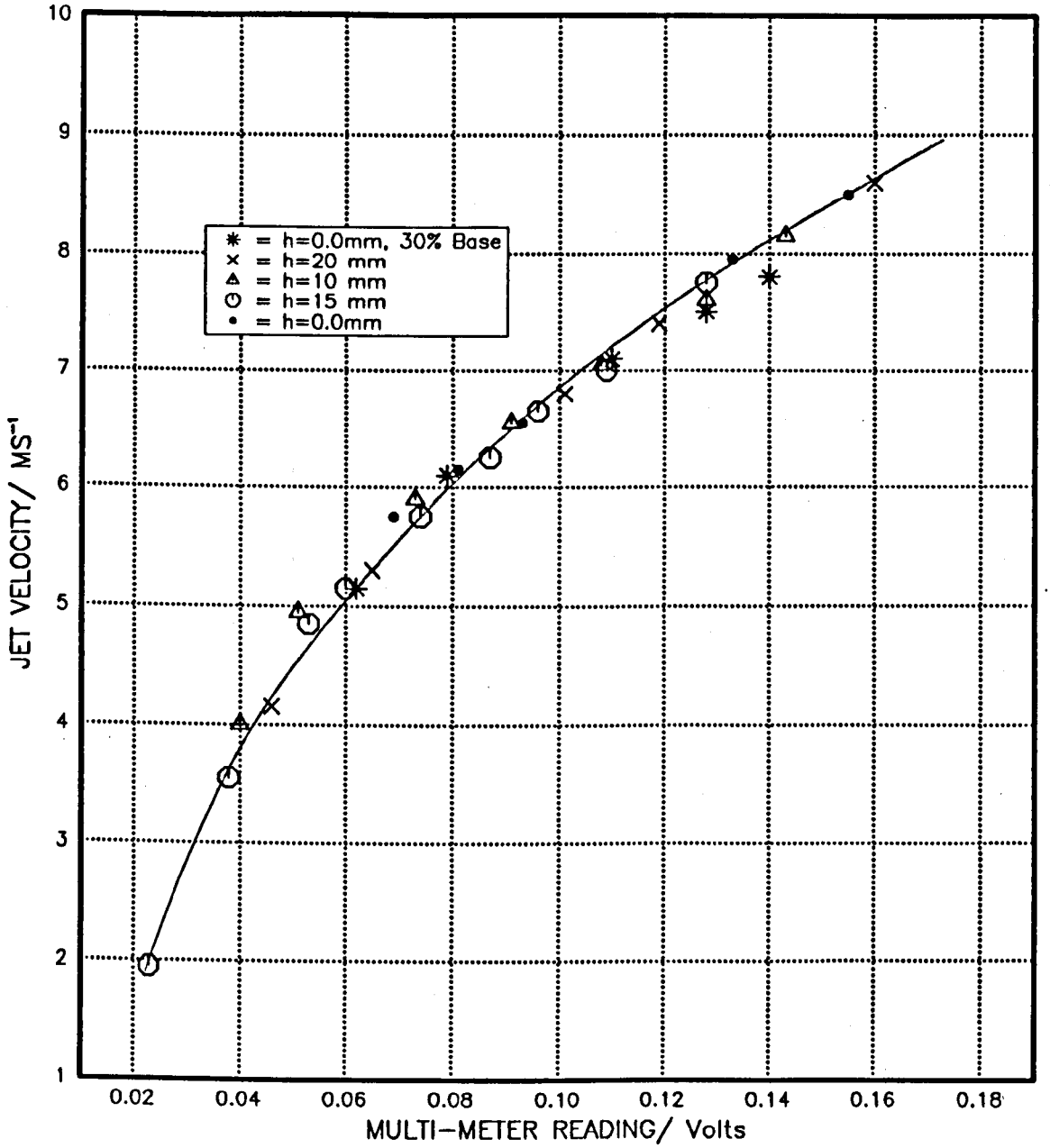

FIGURE 3.10.1 CALIBRATION FOR JET VELOCITY

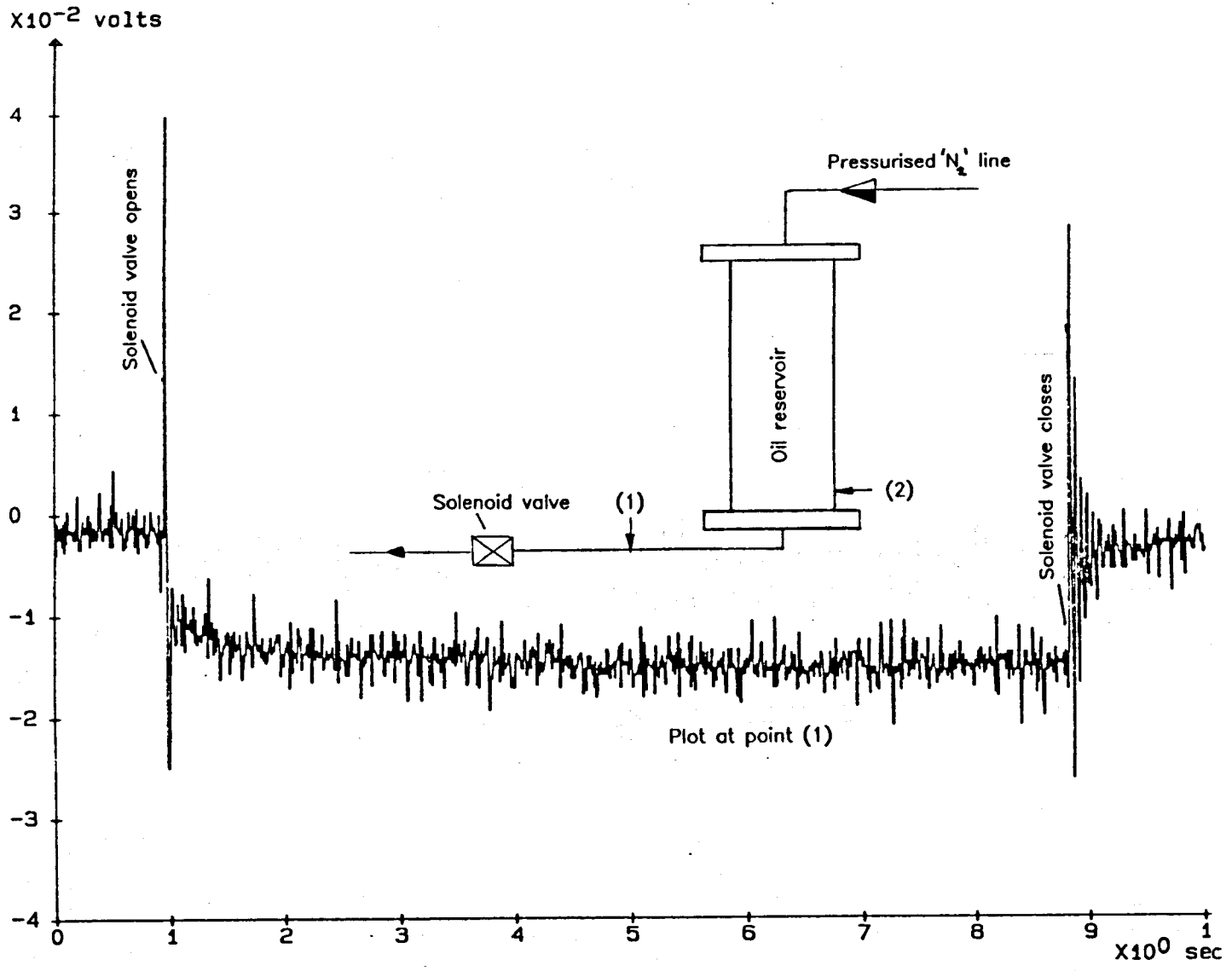

FIGURE 3.10.2 SYSTEM RESPONSE TO THE OPENING OF THE SOLENOID VALVE

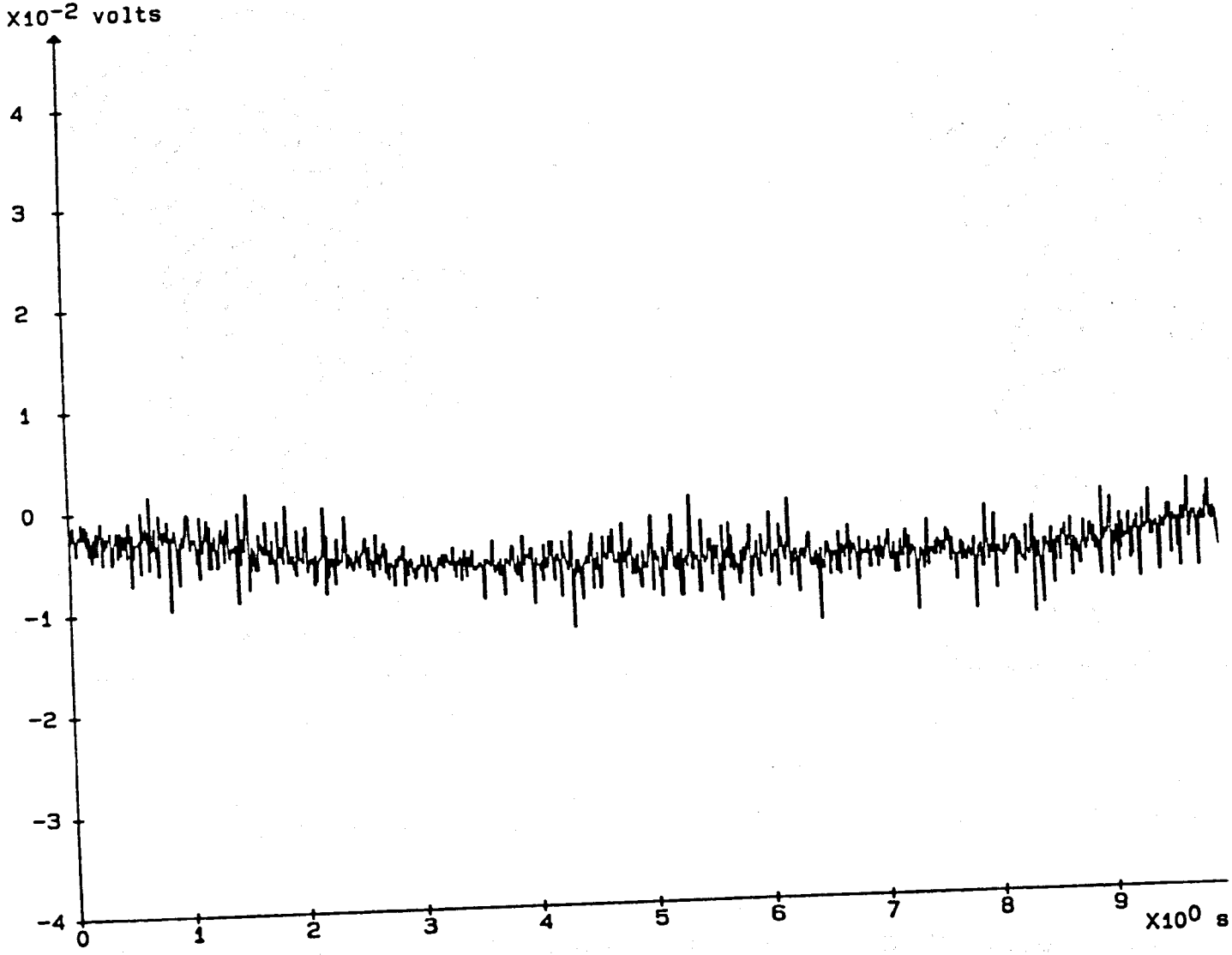

FIGURE 3.10.3 SYSTEM RESPONSE TO OPENING OF THE SOLENOID VALVE AT POINT (2)

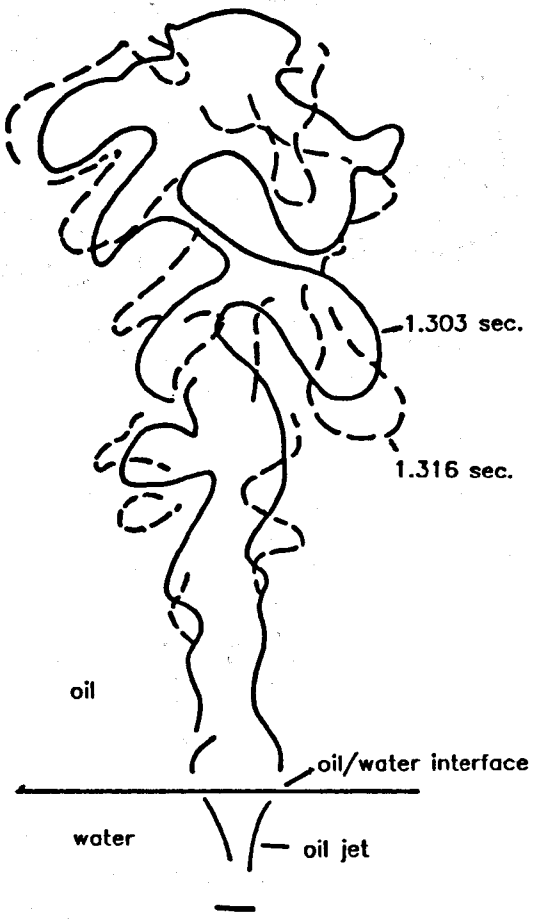

Scale = 1:10/7; Jet velocity = 3.7 m/s

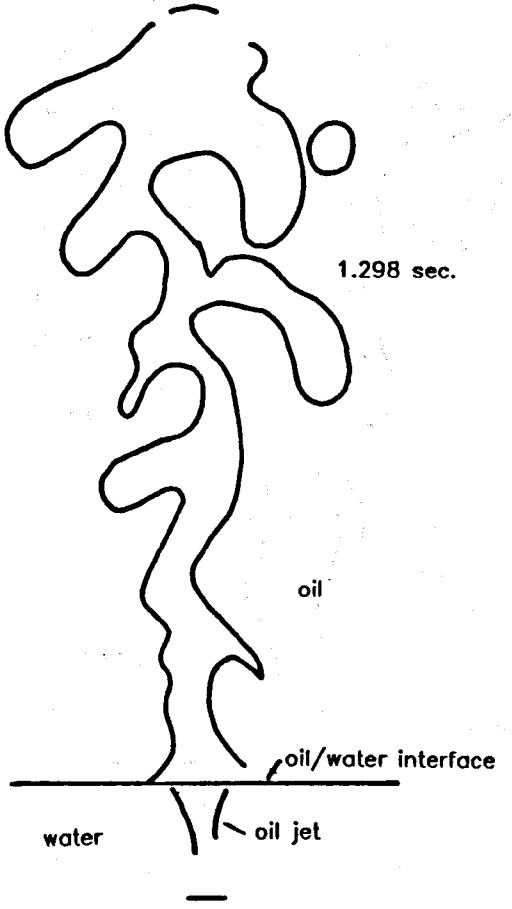

Scale = 1:10/7; Jet velocity = 3.7 m/s

FIGURE 3.11.1 COMPOSITE OVERLAY OF JET OUTLINES FROM VIDEO FRAMES

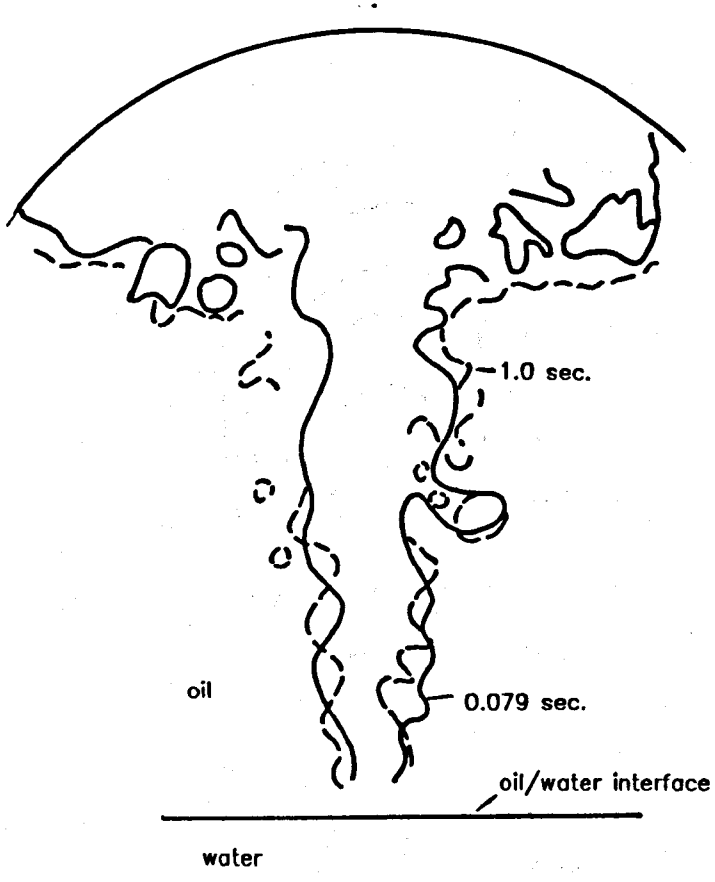

Scale 1:10/7 Jet velocity = 8.1 m/s

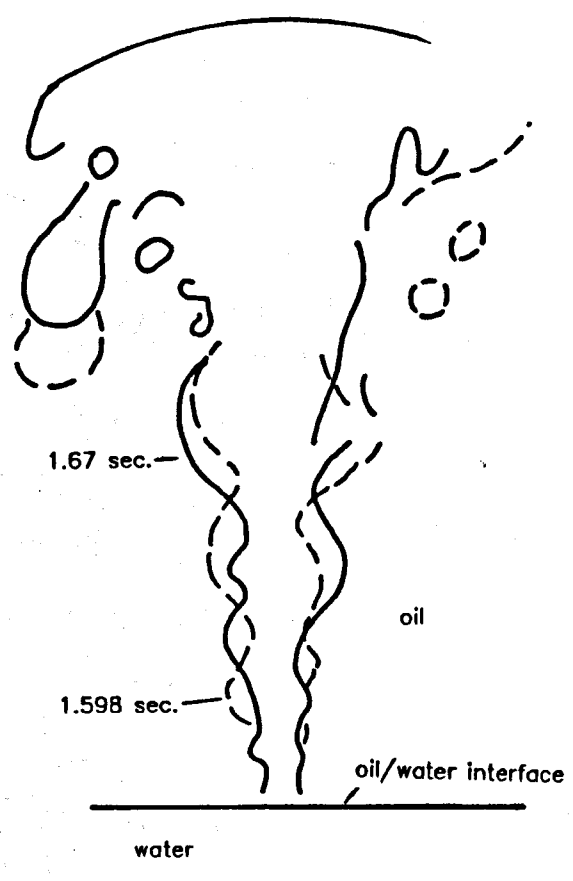

Scale 1:10/7 Jet velocity = 5.8 m/s

FIGURE 3.11.2 COMPOSITE OVERLAY OF JET OUTLINES FROM VIDEO FRAMES

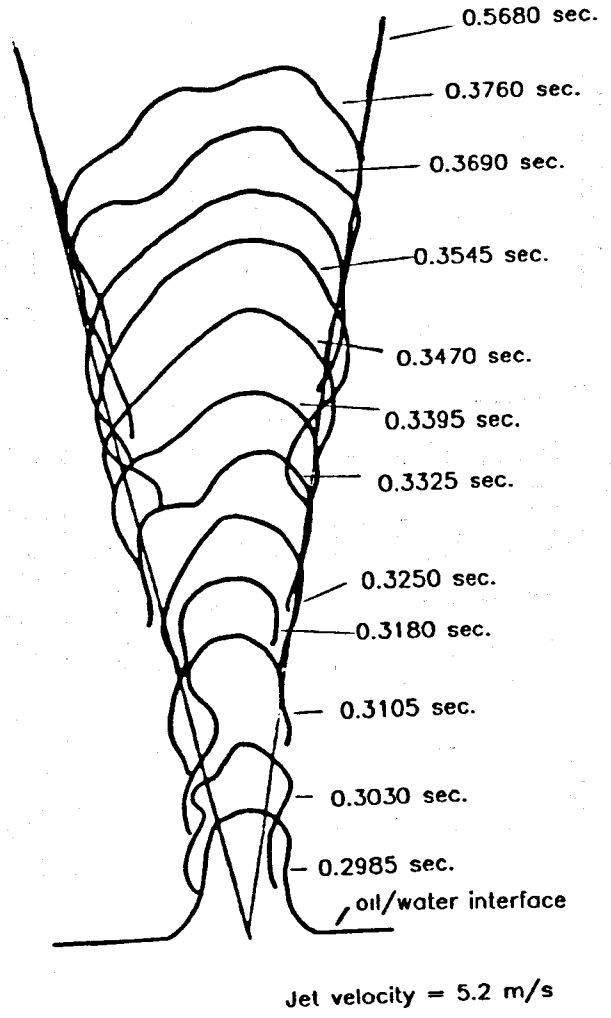

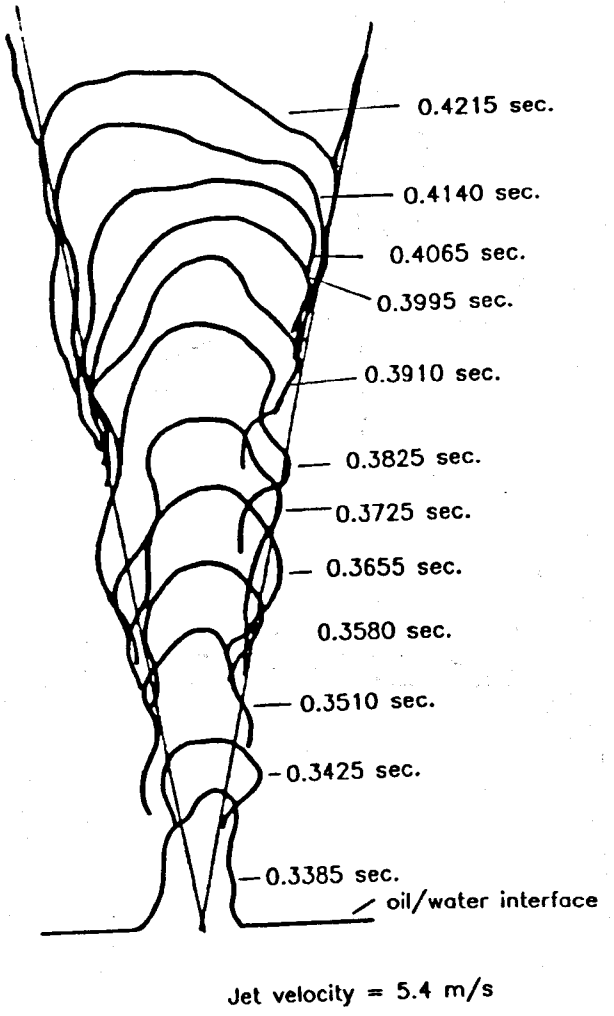

FIGURE 3.11.3 COMPOSITE OVERLAY OF JET OUTLINES FROM VIDEO FRAMES

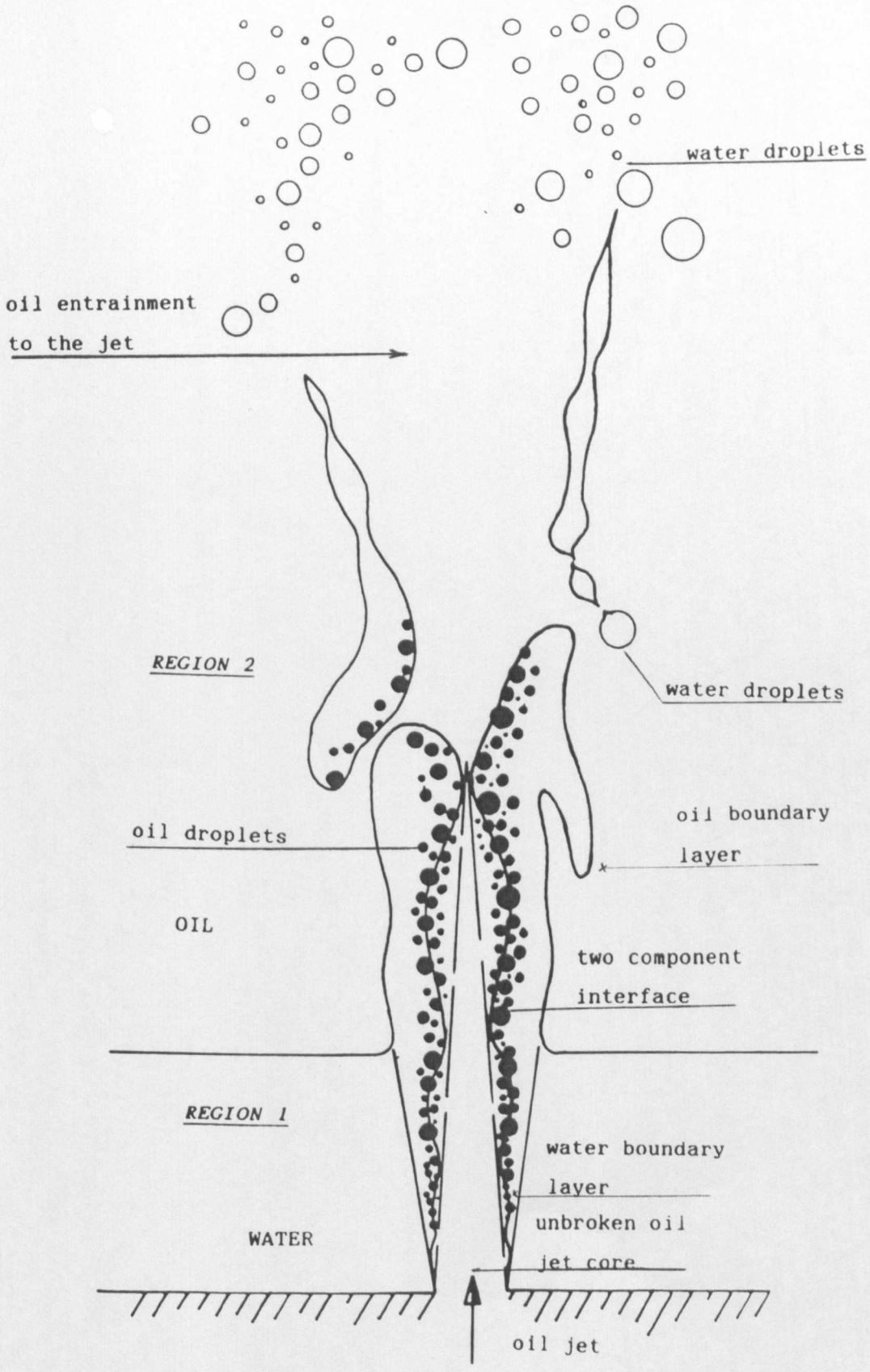

FIGURE 3.12 STRUCTURE AND STAGES OF BREAKUP AND ENTRAINMENT PROCESS

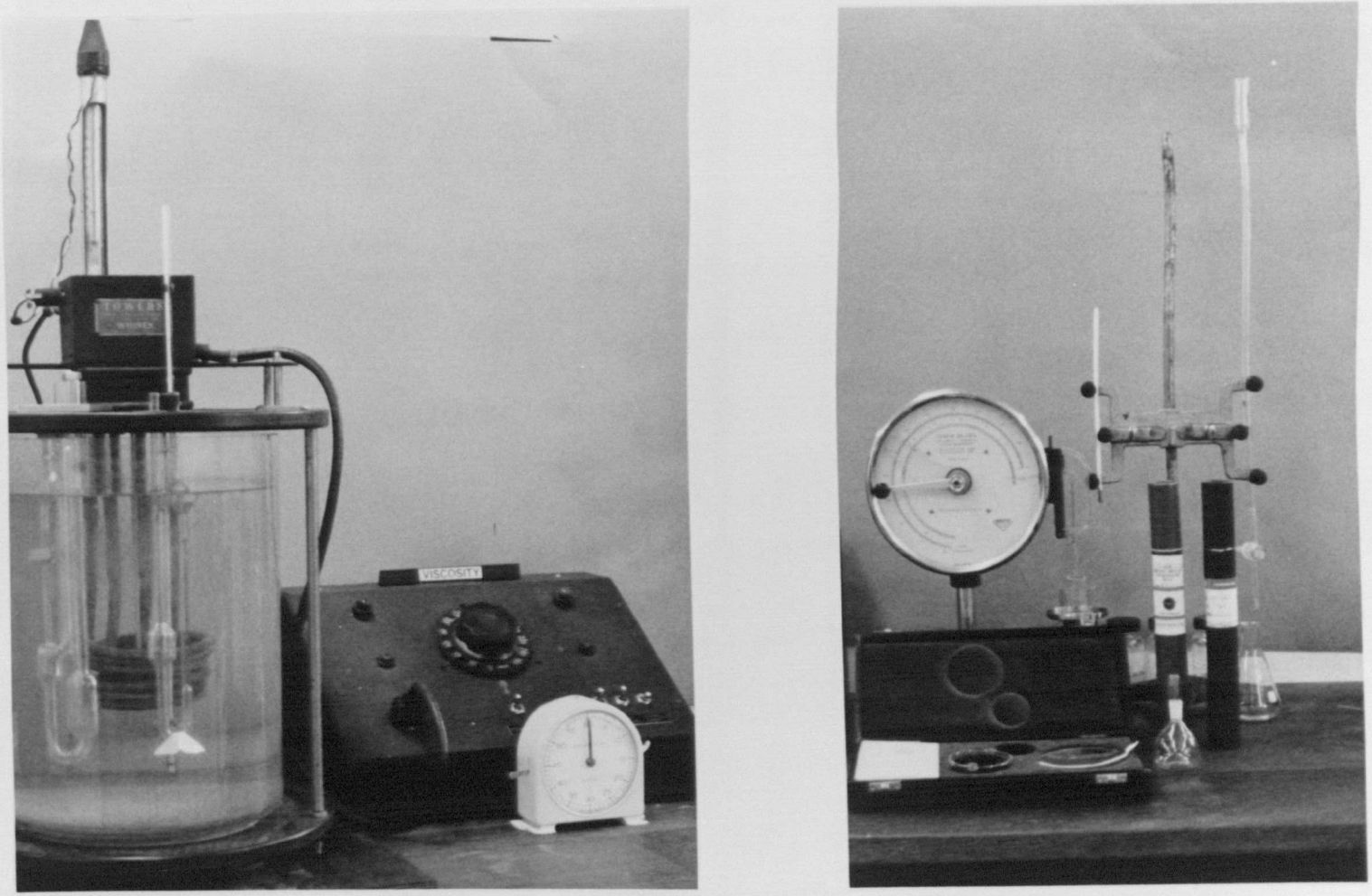

FIGURE 3.13.1 APPARATUS USED FOR MEASUREMENT OF PROPERTIES

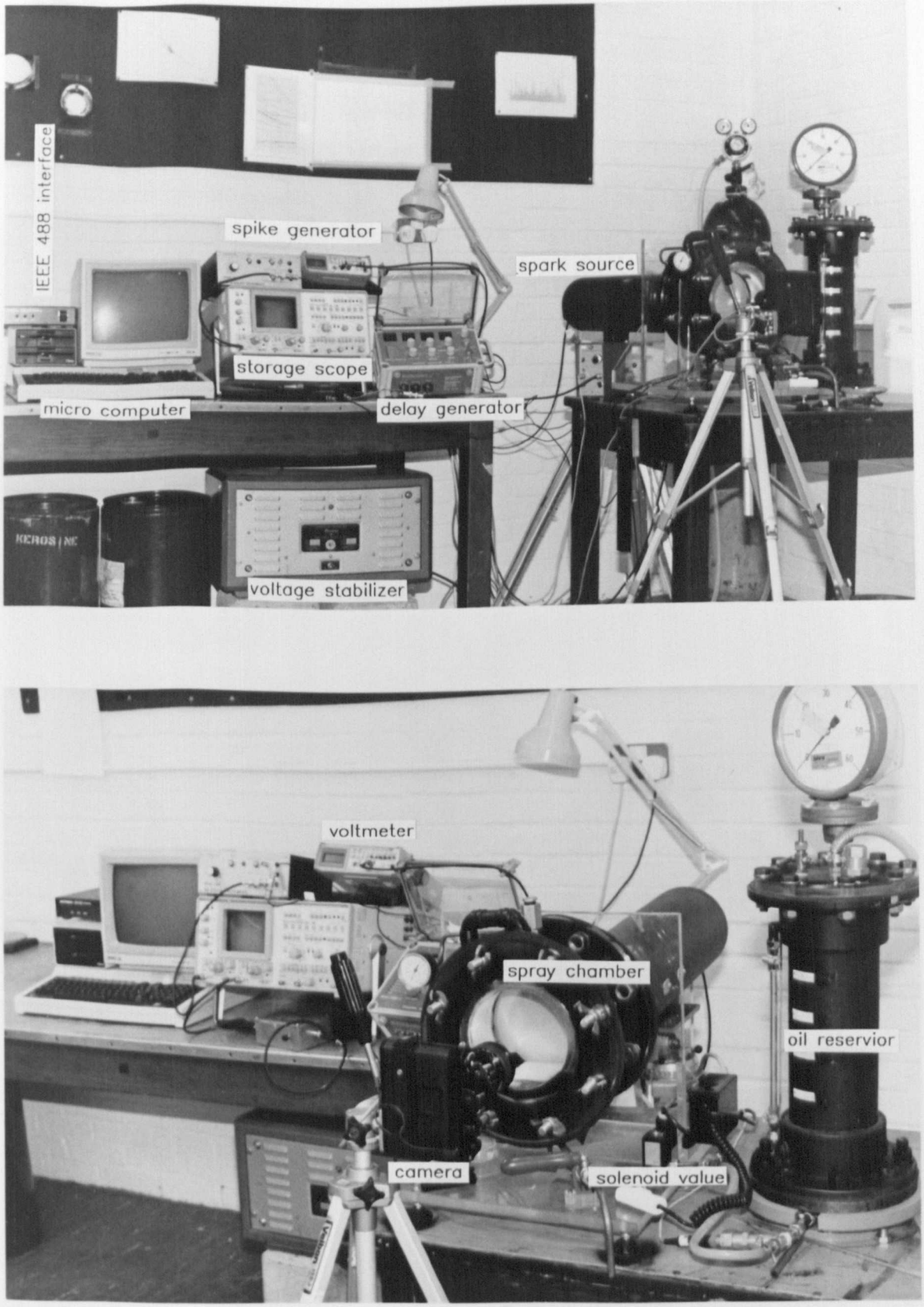

FIGURE 3.13.2 INSTRUMENTS AND THE RIG ARRANGEMENT

FIGURE 3.13.4 HIGH SPEED VIDEO (SPIN PHYSICS 2000) IN USE

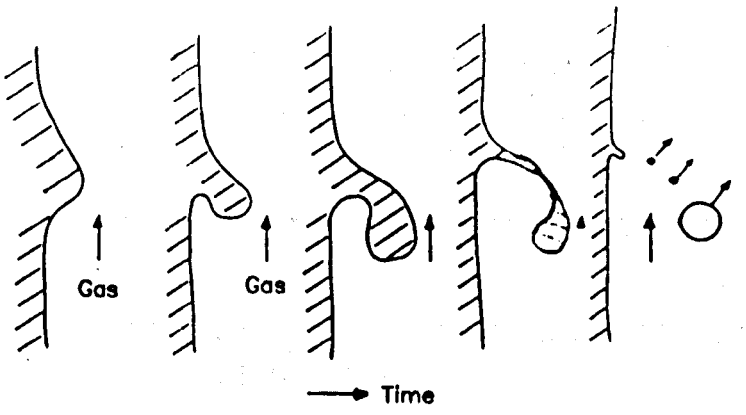

FIGURE 4.1.1 BREAKDOWN OF DISTURBANCE WAVE BY UNDERCUTTING (HEWITT ET AL, 1970)

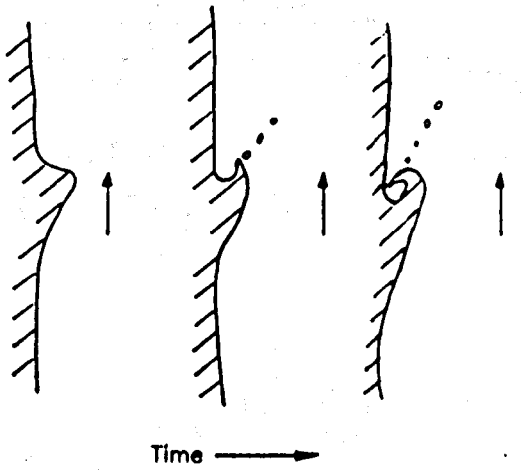

FIGURE 4.1.2 BREAKDOWN OF DISTURBANCE WAVE BY ROLLING (HEWITT ET AL, 1970)

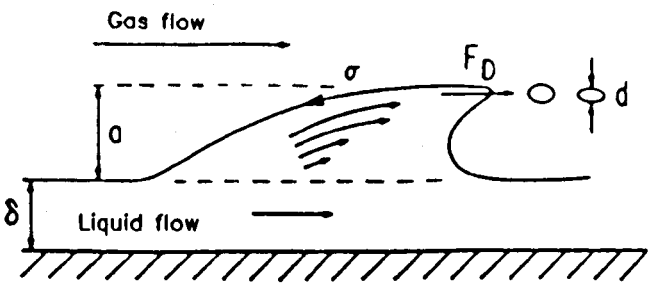

FIGURE 4.1.3 MECHANISM OF THE SHEARING OFF OF ROLL-WAVE (ISHII ET AL, 1983)

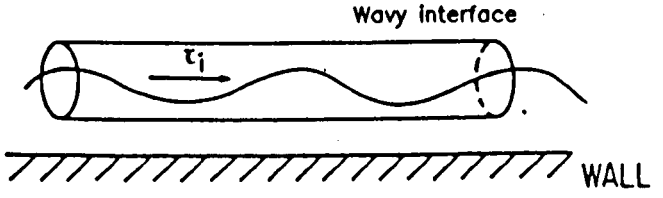

FIGURE 4.1.4 WAVE REGION OF THE INTERFACE IN PIPE FLOW (ISHII ET AL, 1983)

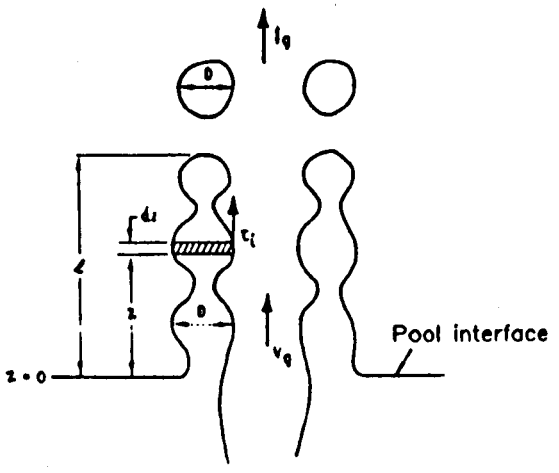

FIGURE 4.1.5 SCHEMATIC DIAGRAM OF DROPLET POOL ENTRAINMENT (KATOKA ET AL, 1984)

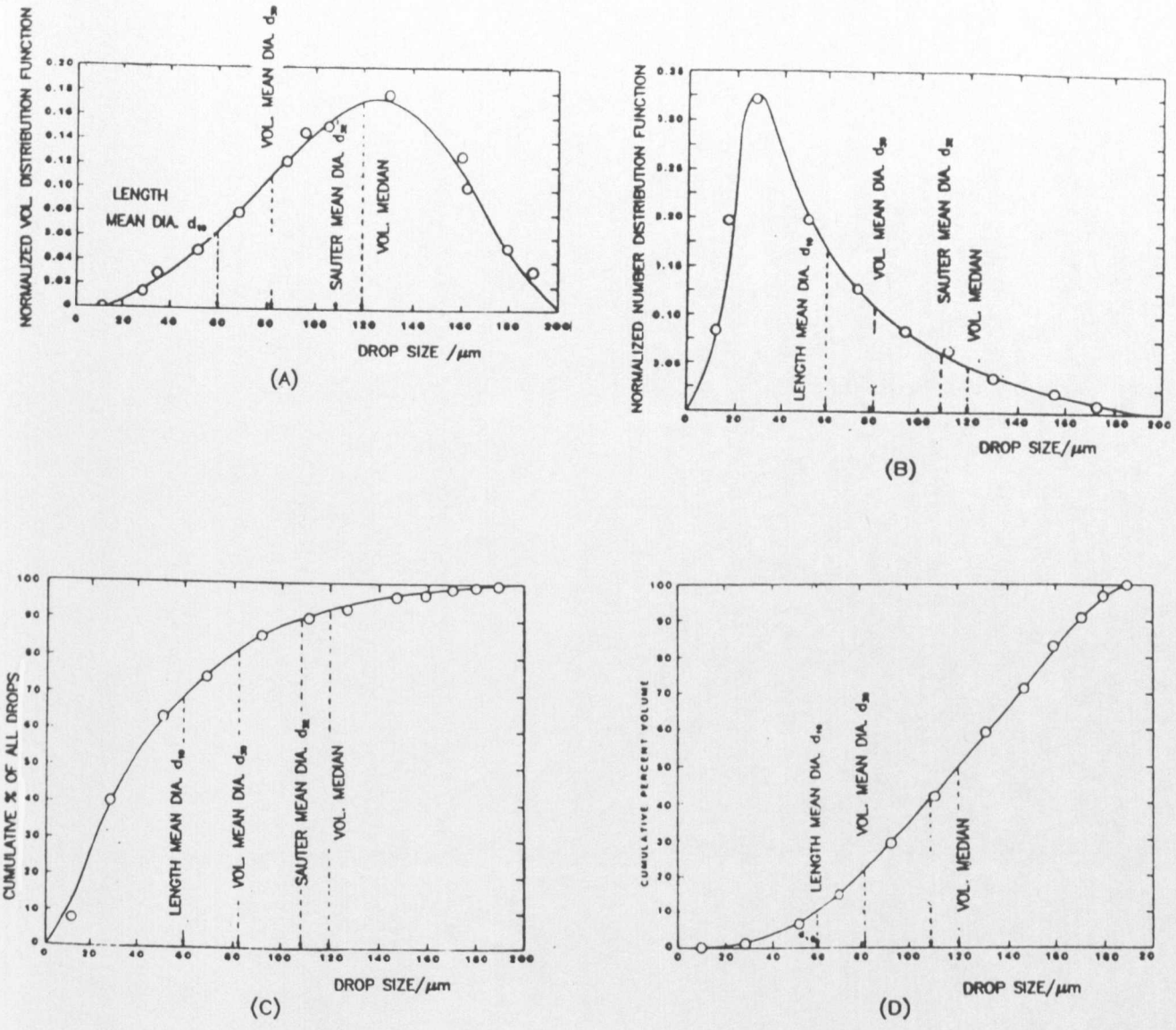

FIGURE 4.2.1 (A) VOLUME DISTRIBUTION DATA, (B) NUMBER DISTRIBUTION DATA (C) CUMULATIVE DISTRIBUTION OF ALL DROPS, (D) CUMULATIVE VOLUME DISTRIBUTION

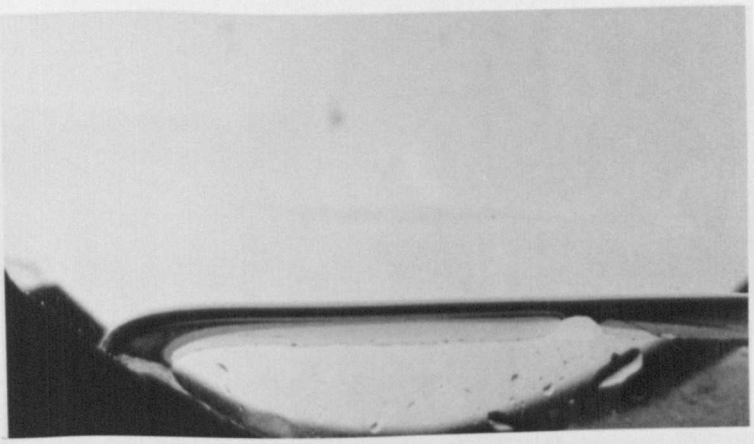

FIGURE 4.3.1 MEASUREMENT OF ANGLE φ OF EQUATION 4.4.2
AT t = 0.0 sec; Liquid:– Pure Water/Pure Kerosene
h = 17.4 mm

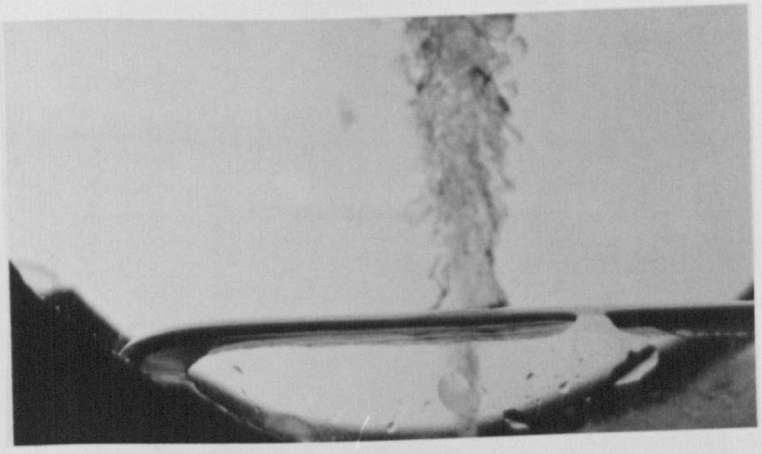

FIGURE 4.3.2 MEASUREMENT OF ANGLE φ OF EQUATION 4.4.2
AT t = 0.4 sec.; Liquid:– Pure Water/Pure Kerosene
h = 17.4 mm (t=0.0 sec.); V_j = 6.0 m/s

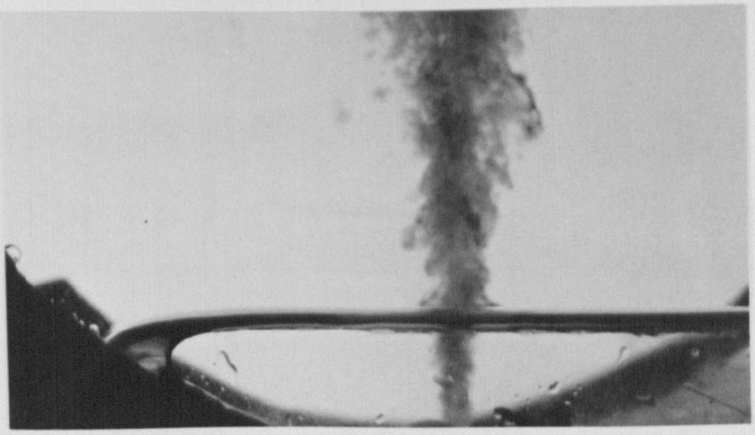

FIGURE 4.3.3 MEASUREMENT OF ANGLE φ OF EQUATION 4.4.2
AT t = 0.8 sec.; Liquid:– Pure Water/Pure Kerosene
h = 18.4 mm (t=0.0 sec.); V_j = 6.8 m/s

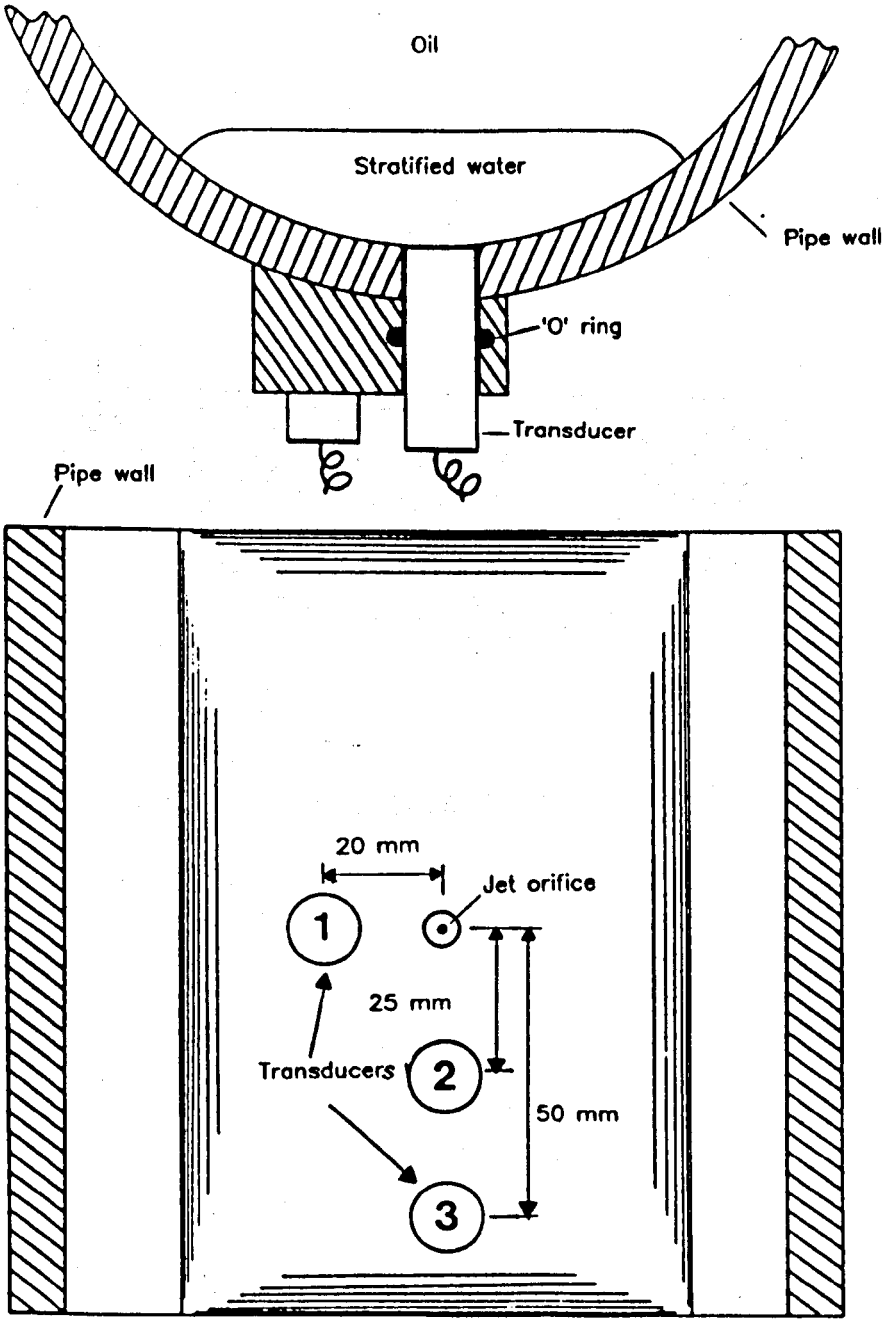

FIGURE 4.4.1 ULTRASONIC TRANSDUCER ARRANGEMENT

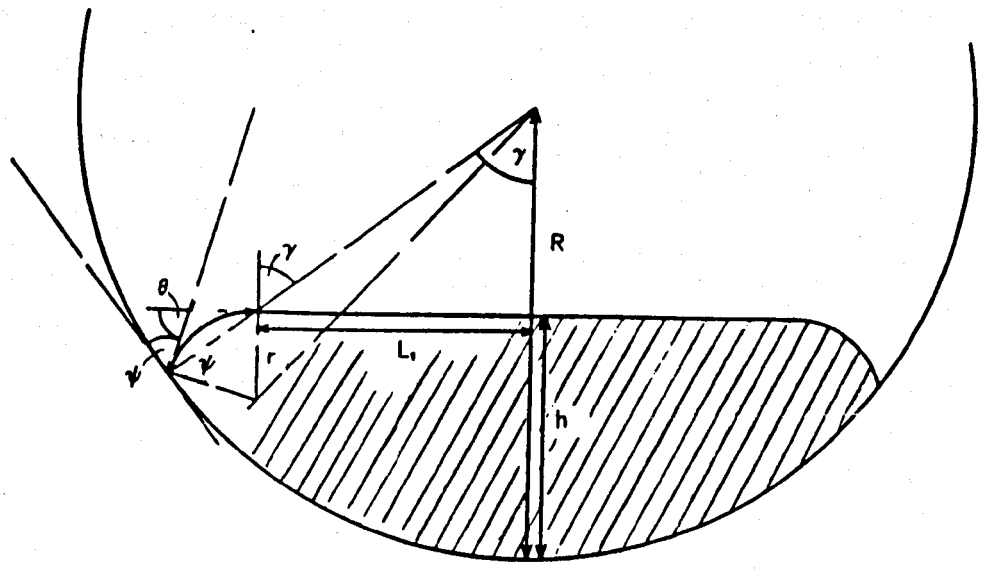

FIGURE 4.4.2 CALCULATION OF INTERFACE AREA

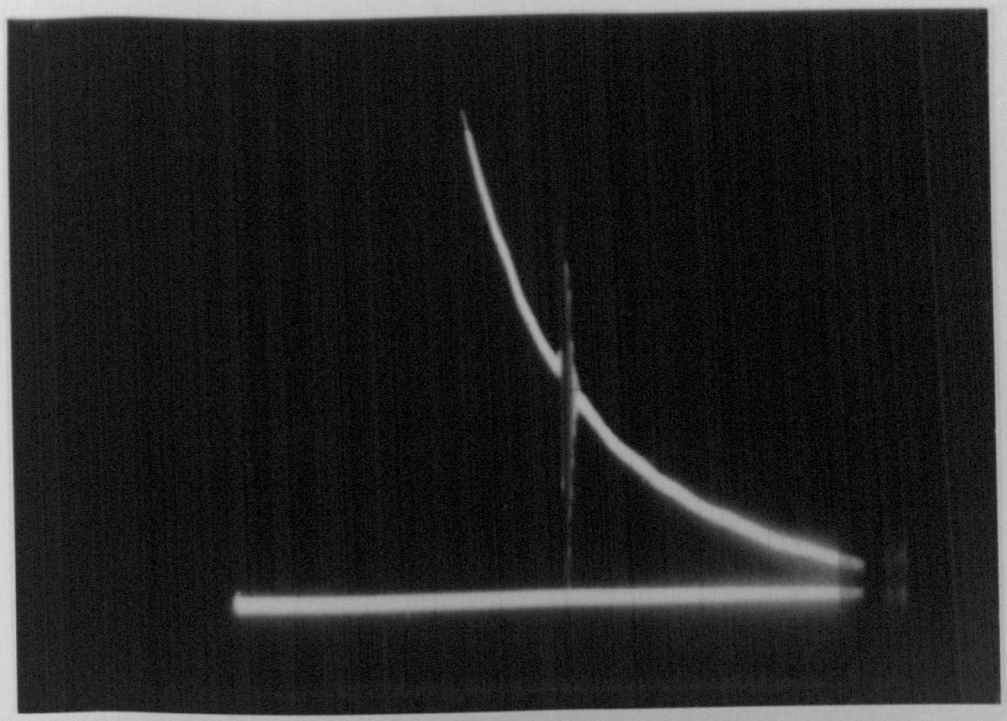

FIGURE 4.4.3 THE ECHO PRODUCED BY THE ULTRA-SONIC TRANSDUCER DUE TO THE WATER/OIL INTERFACE, ALLOWS MEASUREMENT OF THE INTERFACE HEIGHT

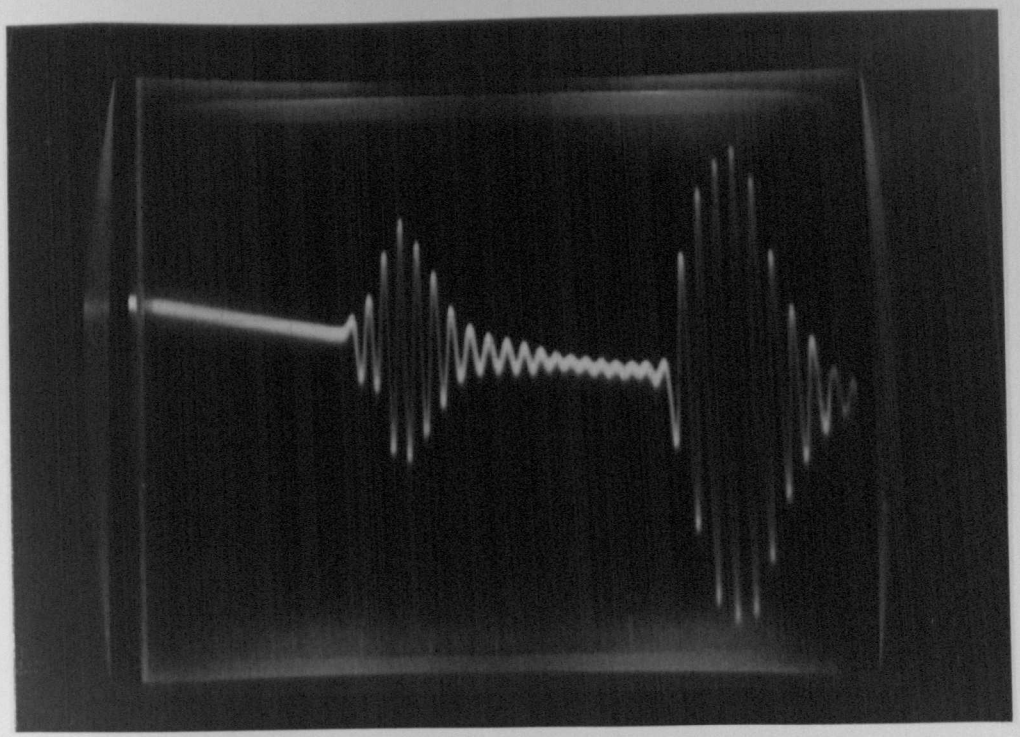

FIGURE 4.4.4 ECHOES PRODUCED BY TWO ULTRA-SONIC TRANSDUCERS ALLOW MEASUREMENT OF THE INTERFACE DROP RATE

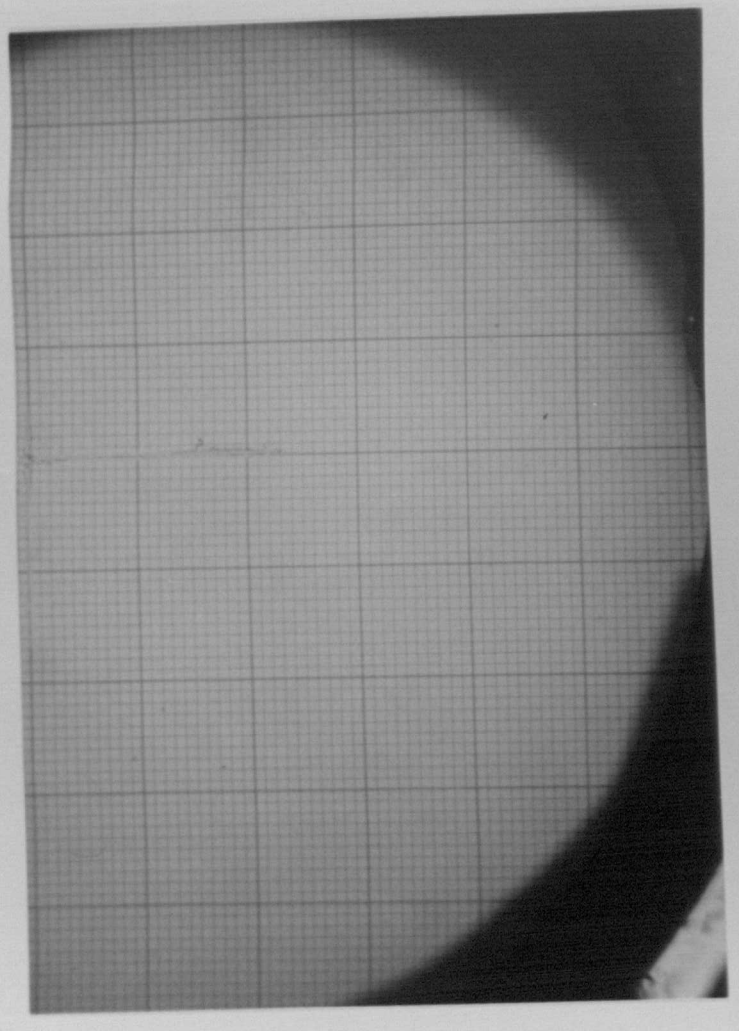

FIGURE 4.4.5 A GRID WAS POSITIONED TO SCALE THE MEASURING PLANE

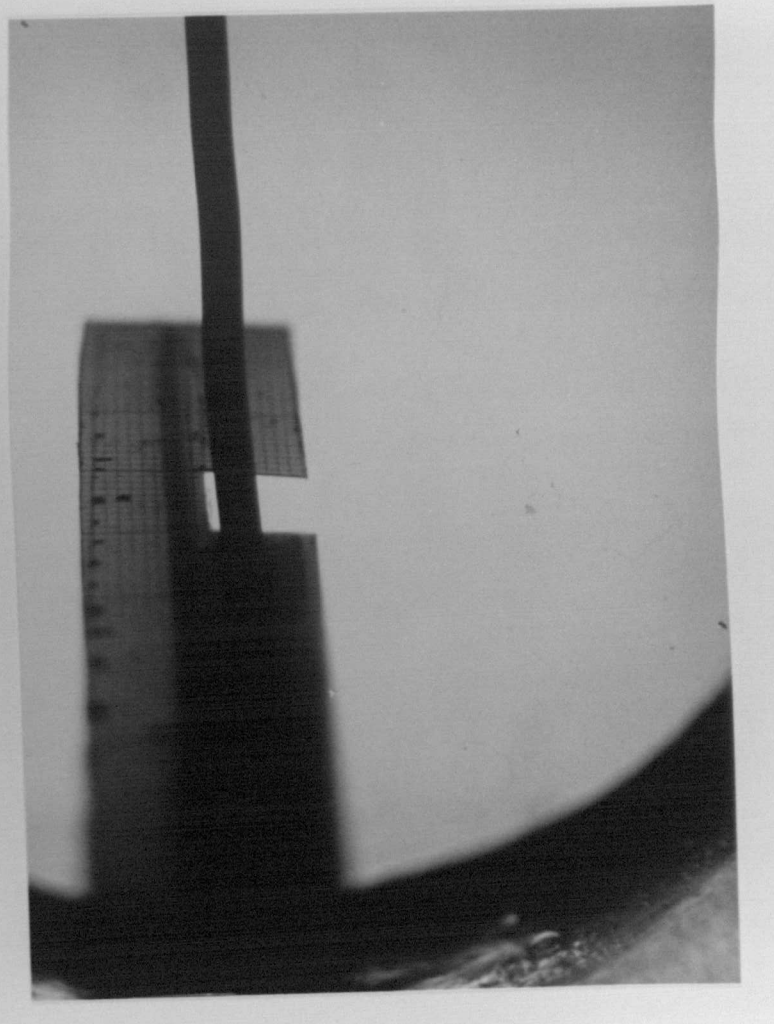

FIGURE 4.4.6 A GRID WAS TILTED TO 30 DEGREES TO HORIZONTAL TO MEASURE THE DEPTH OF VIEW

high resolution monitor

TV camera

data processing software

central processing unit

microscope

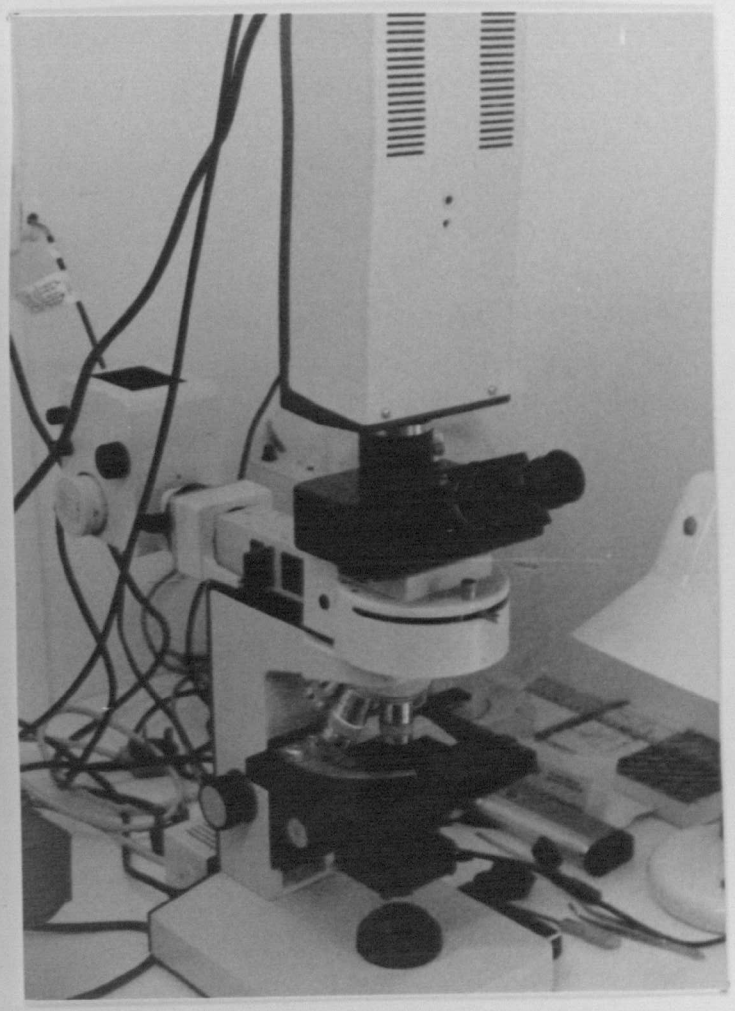

FIGURE 4.4.7 OPTOMAX V VIDEO INTERACTIVE IMAGE ANALYSER IN USE

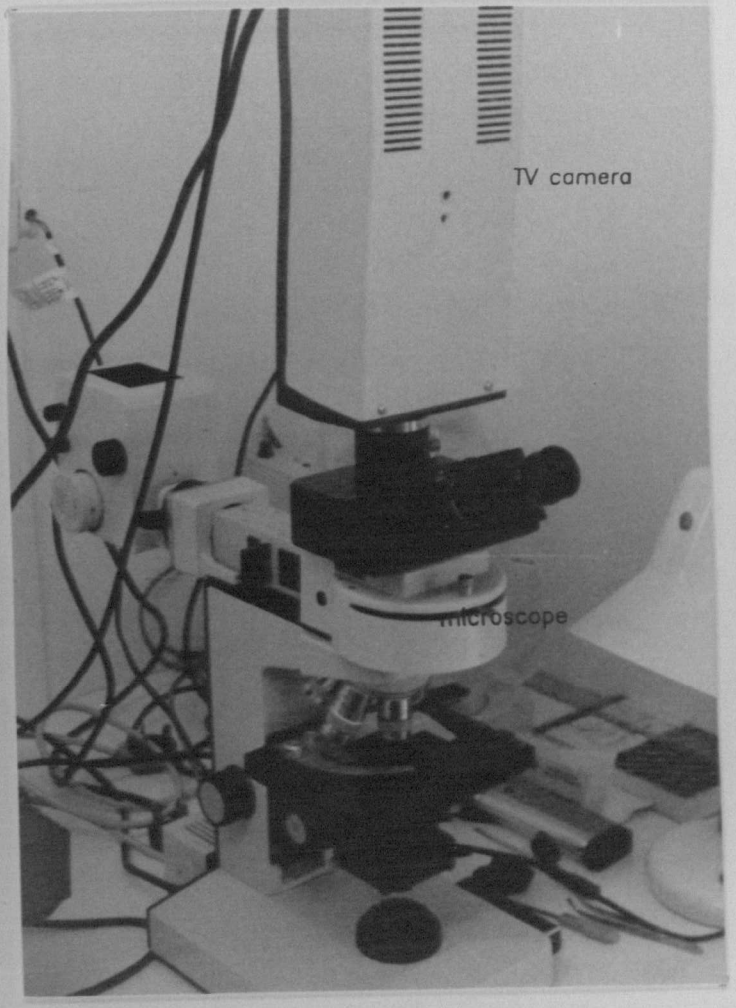

FIGURE 4.4.7 OPTOMAX V VIDEO INTERACTIVE IMAGE ANALYSER IN USE

FIG. 4.5.1 INTERFACE AREA AGAINST WATER HEIGHT
ψ (SEE FIG. 4.4.2) = 95°

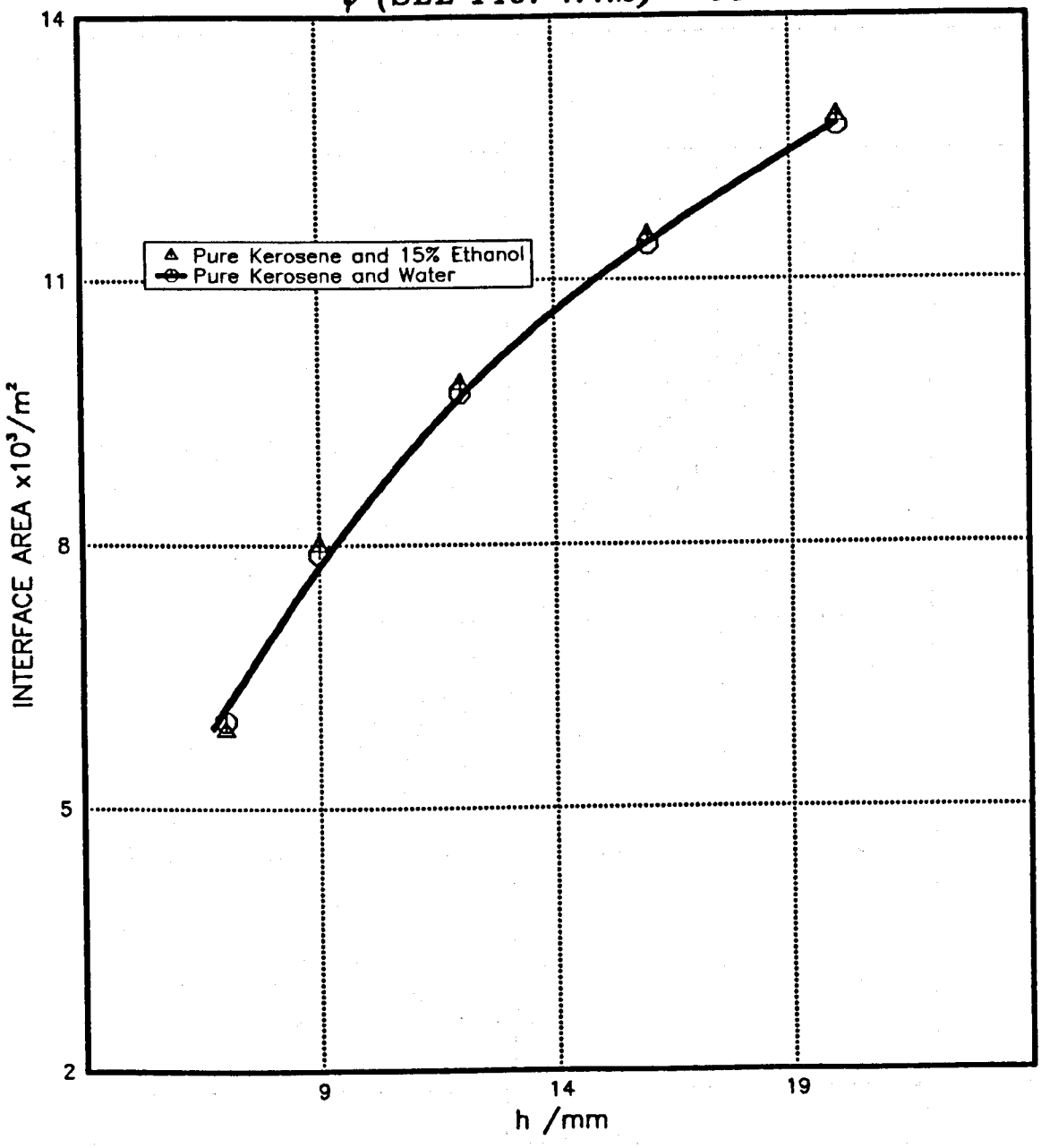

FIG. 4.5.2 INTERFACE DROP AT POSITION 1 AND 3

V_j = 7.6 ms^{-1}; h = 18mm (ie. at t=0.0 sec.)

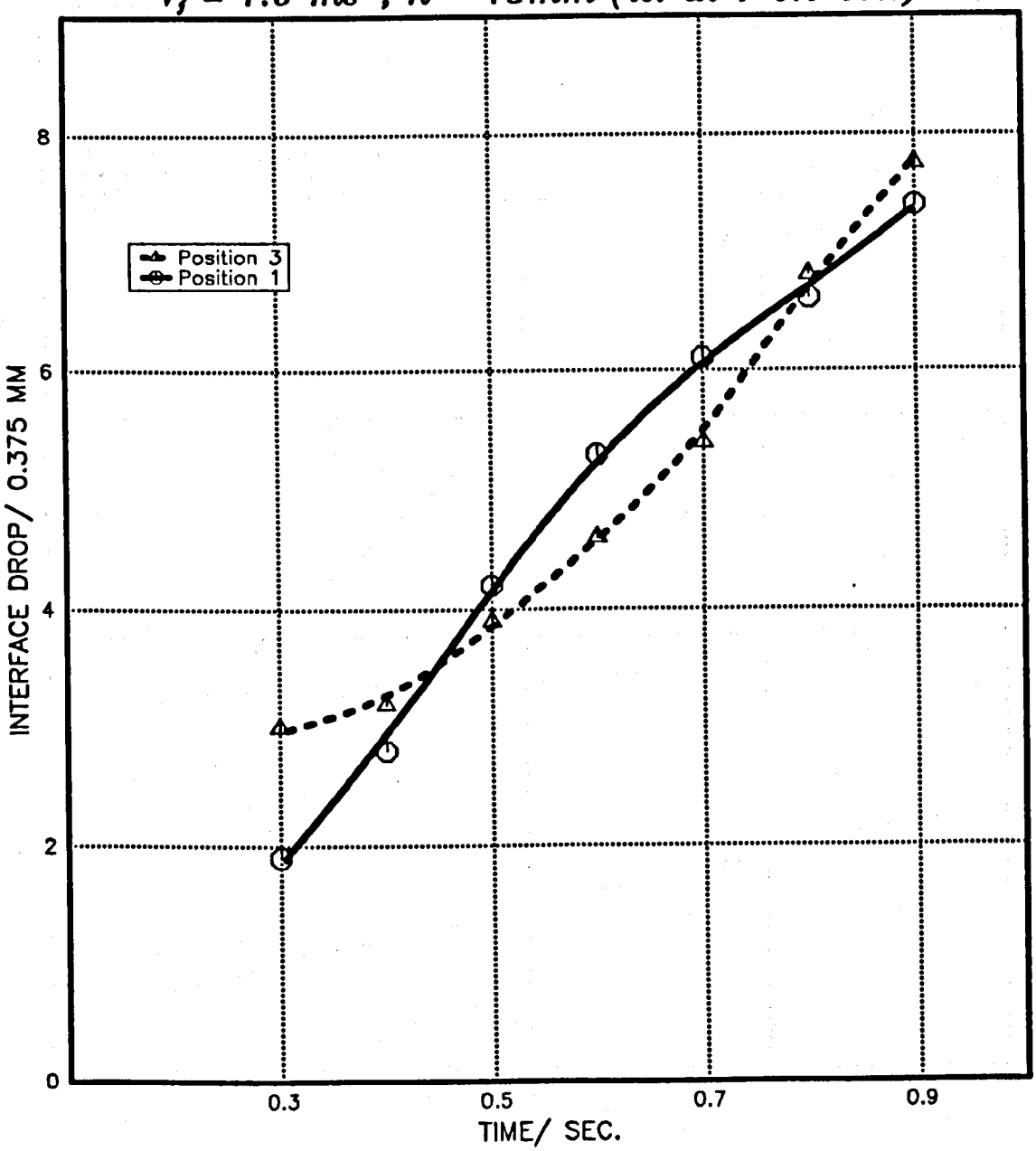

FIG. 4.5.3 ENTRAINMENT AGAINST JET VELOCITY

h =16.4mm; σ =0.033Nm^{-1}; μ =1.15 $\times 10^{-3}$ Nsm^{-2}

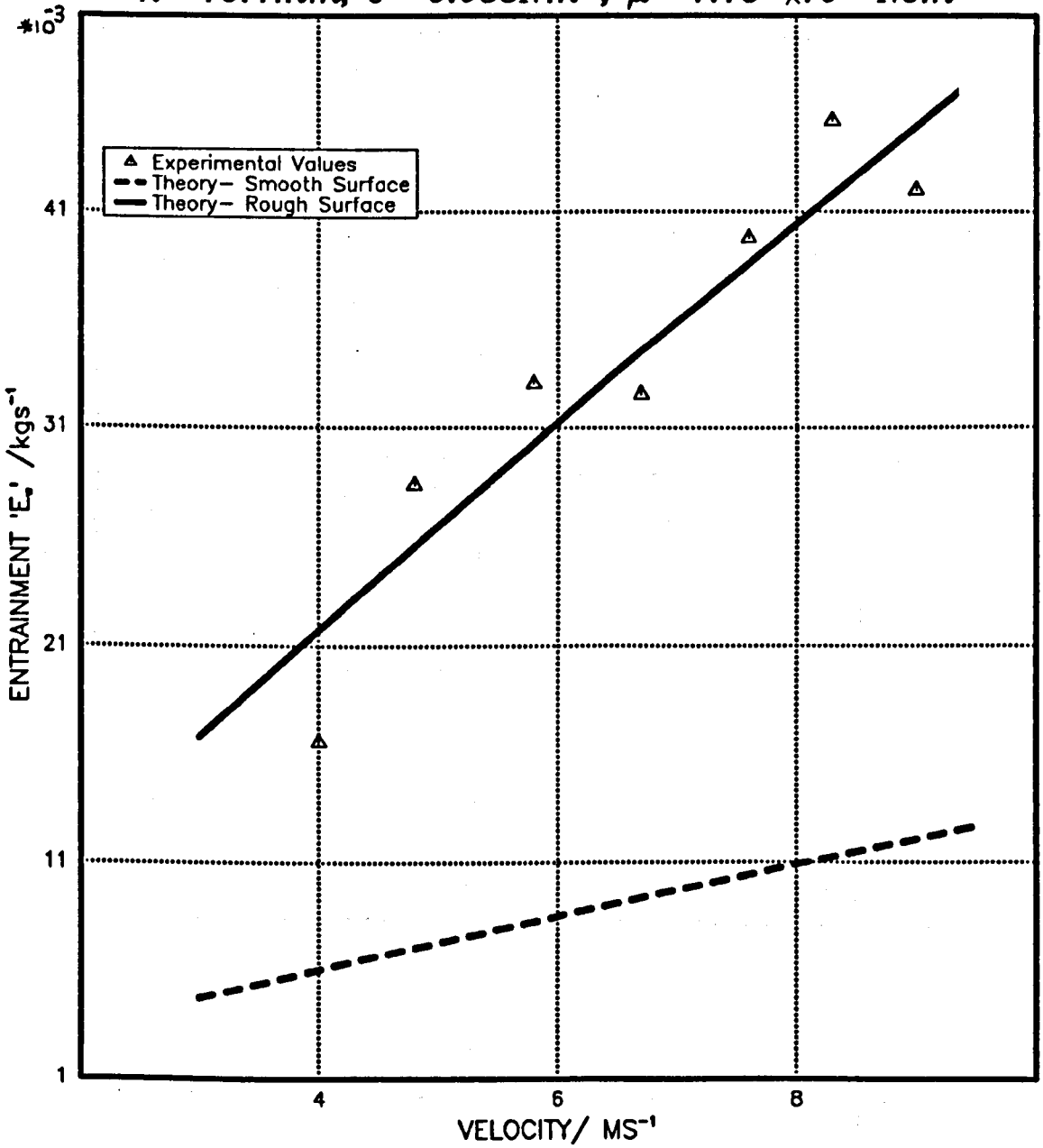

FIG. 4.5.4 ENTRAINMENT AGAINST INTERFACIAL TENSION

V_j =5.8 ms^{-1}; h =16.4 mm; μ =1.15 $\times 10^{-3}$ Nsm^{-2}

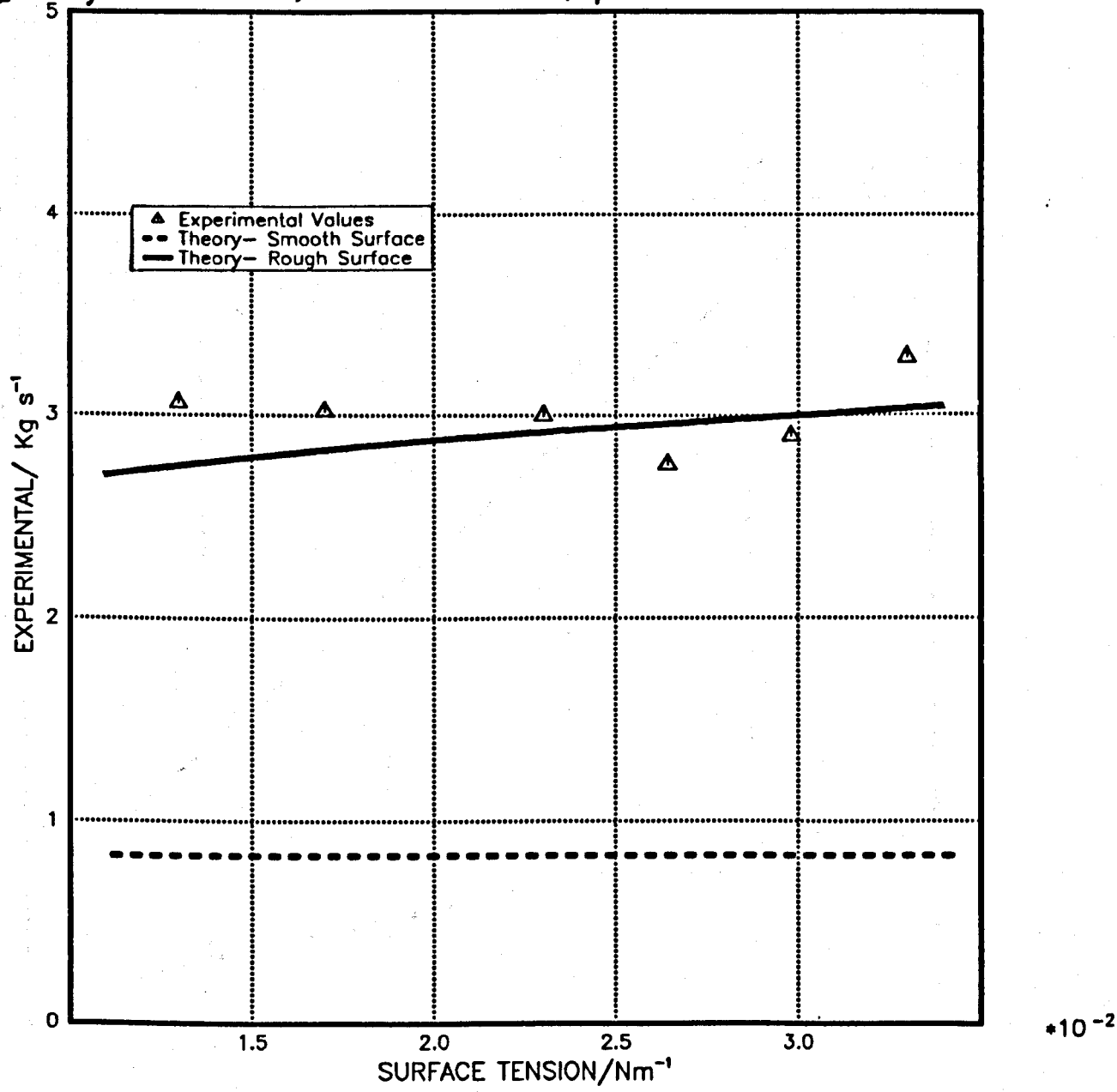

*10 $^{-3}$ *FIG. 4.5.5 ENTRAINMENT AGAINST HEIGHT*

$V_j = 5.8\ ms^{-1}$; $\sigma = 0.033\ Nm^{-1}$; $\mu_{eu} = 1.15 \times 10^{-3}\ Nsm^{-2}$

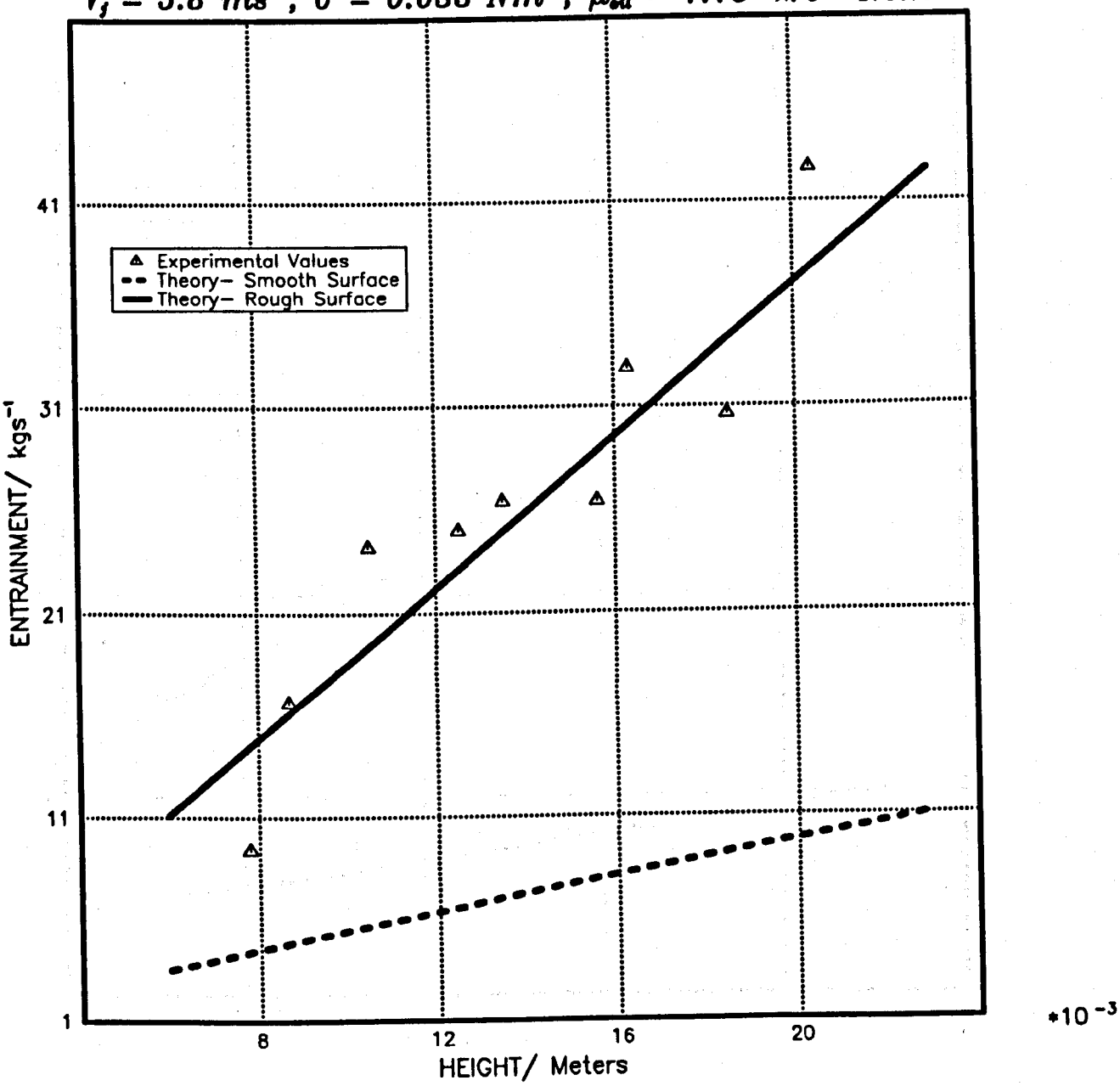

FIG. 4.5.6 ENTRAINMENT AGAINST HEIGHT

V_j= 5.8 ms^{-1}; σ = 0.013 Nm^{-1}; μ = 1.15 $\times 10^{-3}$ Nsm^{-2}

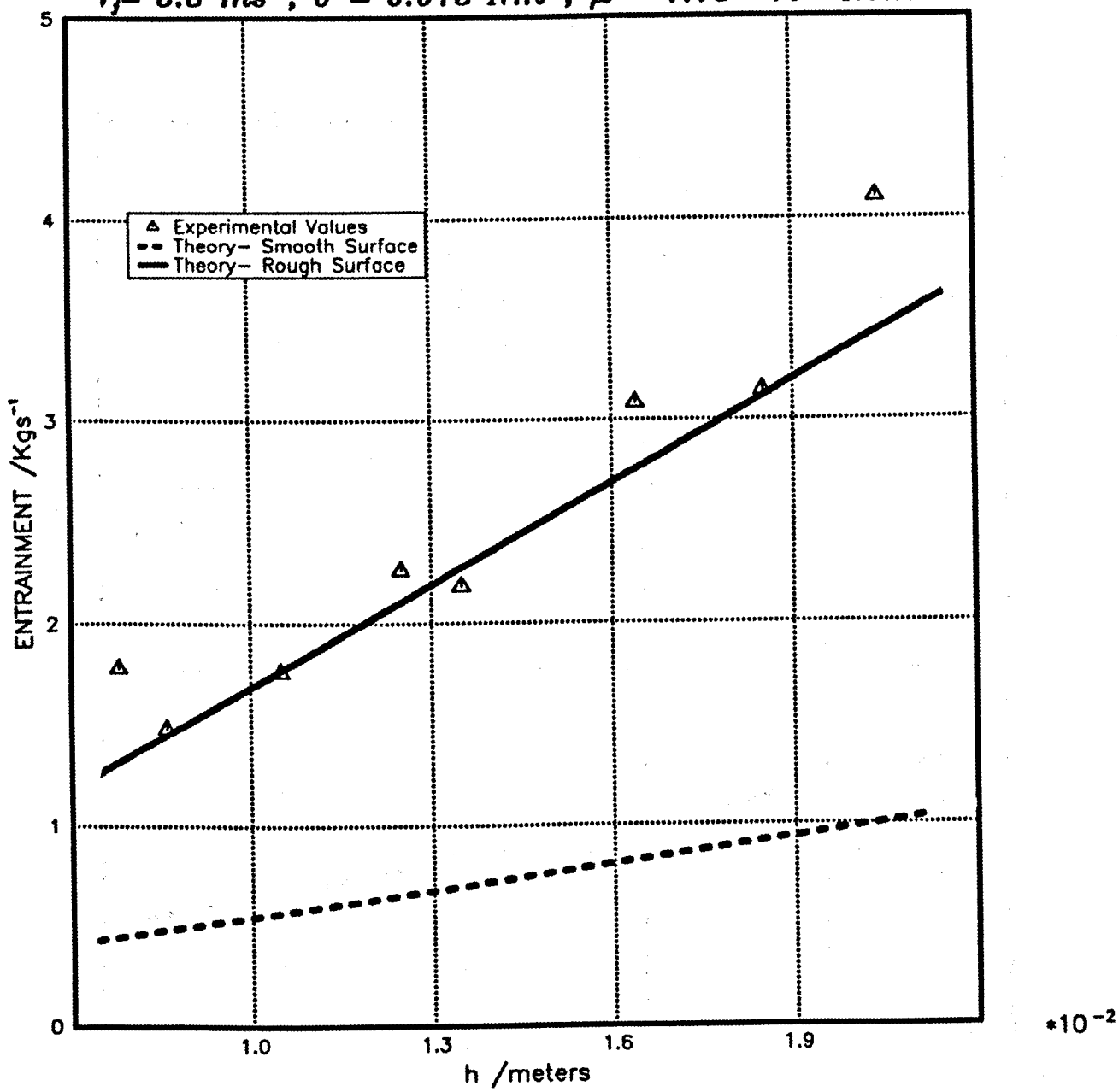

FIG. 4.5.7 ENTRAINMENT AGAINST HEIGHT

V_f= 9.0 ms^{-1}; σ = 0.033Nm^{-1}; μ = 1.15 $\times 10^{-3}$ Nsm^{-2}

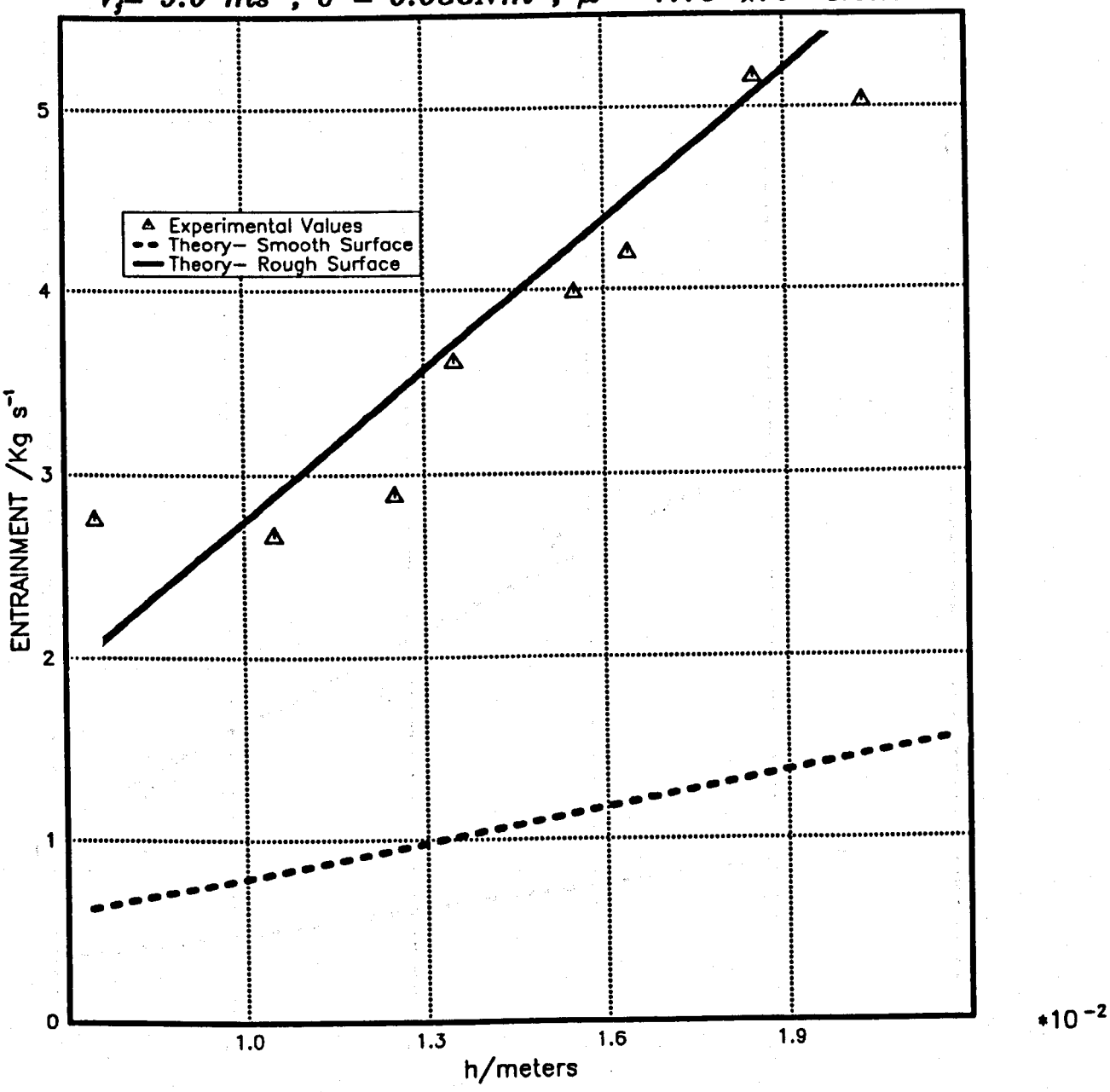

FIG. 4.5.8 ENTRAINMENT AGAINST HEIGHT

$V_i = 5.8\ ms^{-1}$; $\sigma = 0.023\ Nm^{-1}$; $\mu = 2.53 \times 10^{-3}\ Nsm^{-2}$

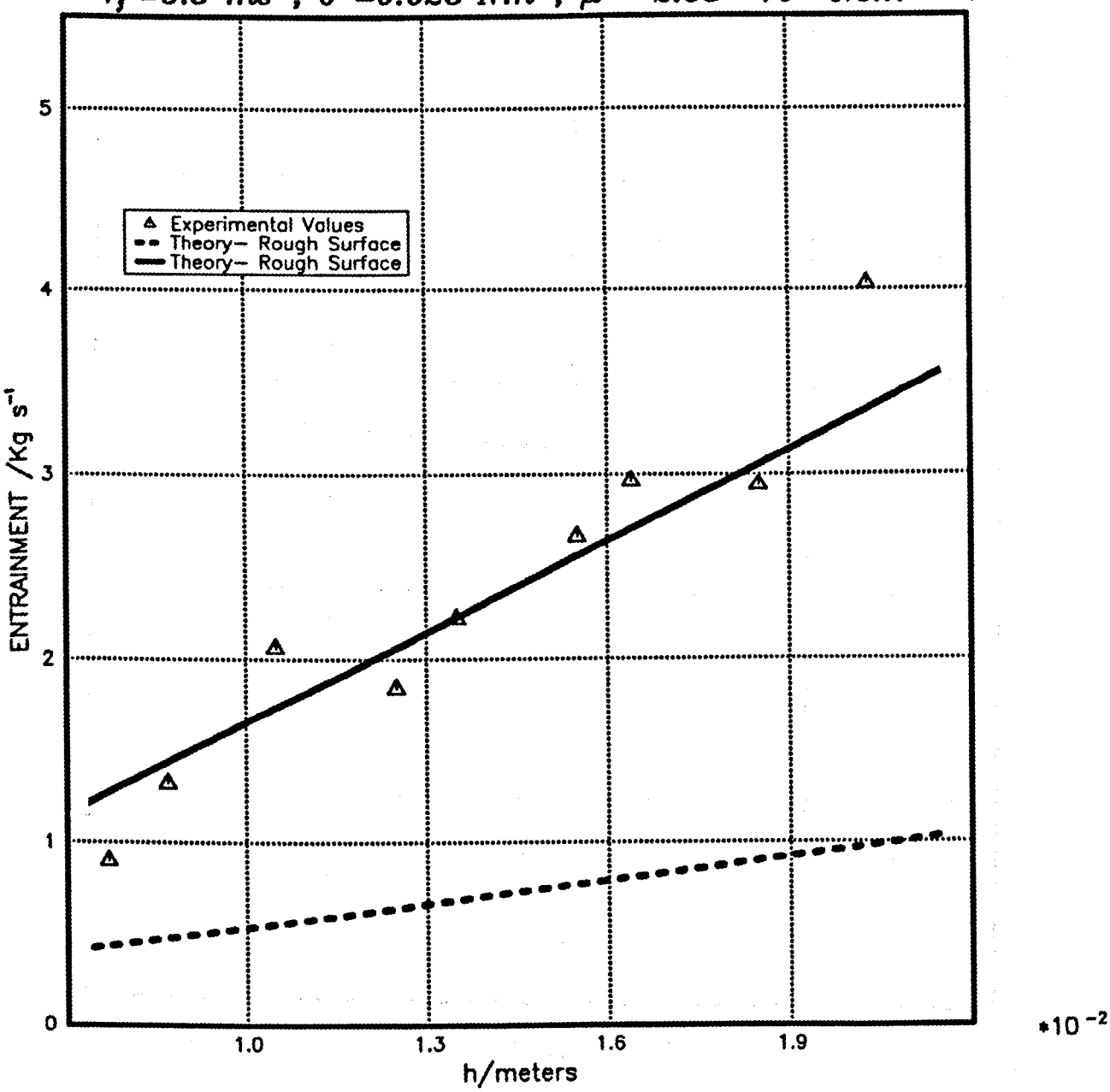

FIG. 4.5.9 ENTRAINMENT AGAINST OIL VISCOSITY

V_j =5.8 ms^{-1}; h = 16.4mm; σ = 0.023 Nm^{-1}

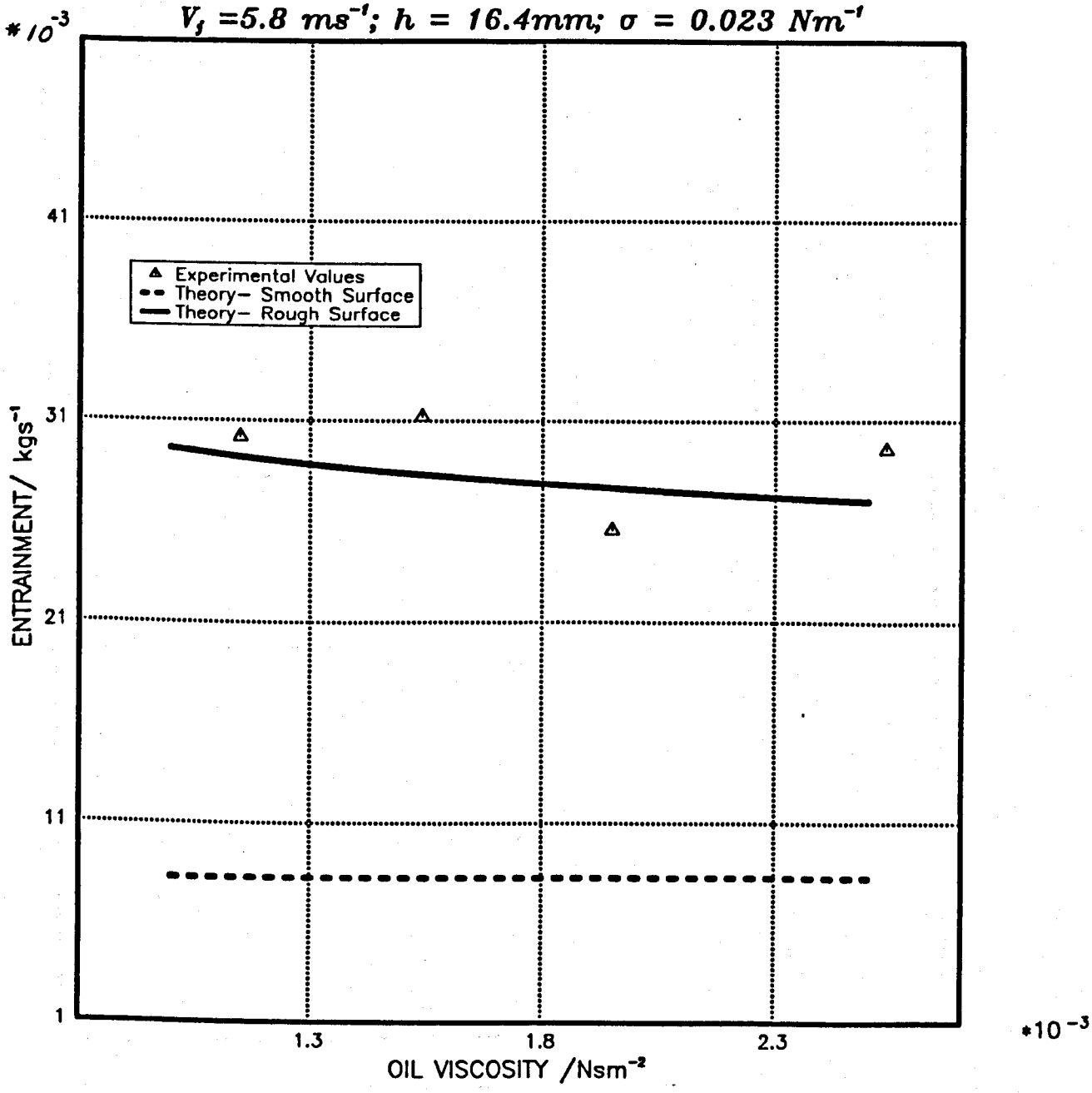

FIG. 4.5.10 COMPARISION OF EXPERIMENTAL AND PREDICTED VALUES OF ENTRAINMENT

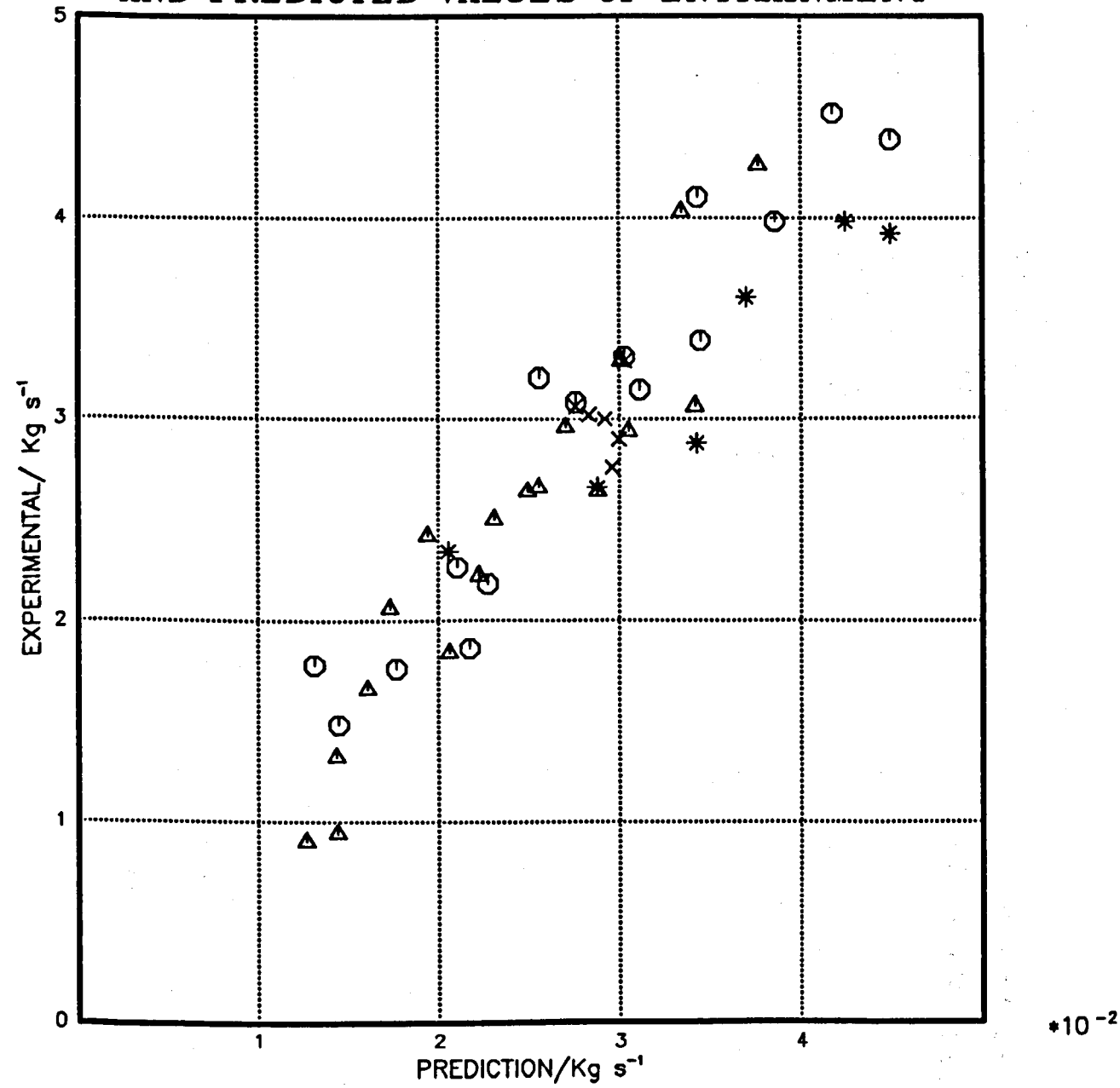

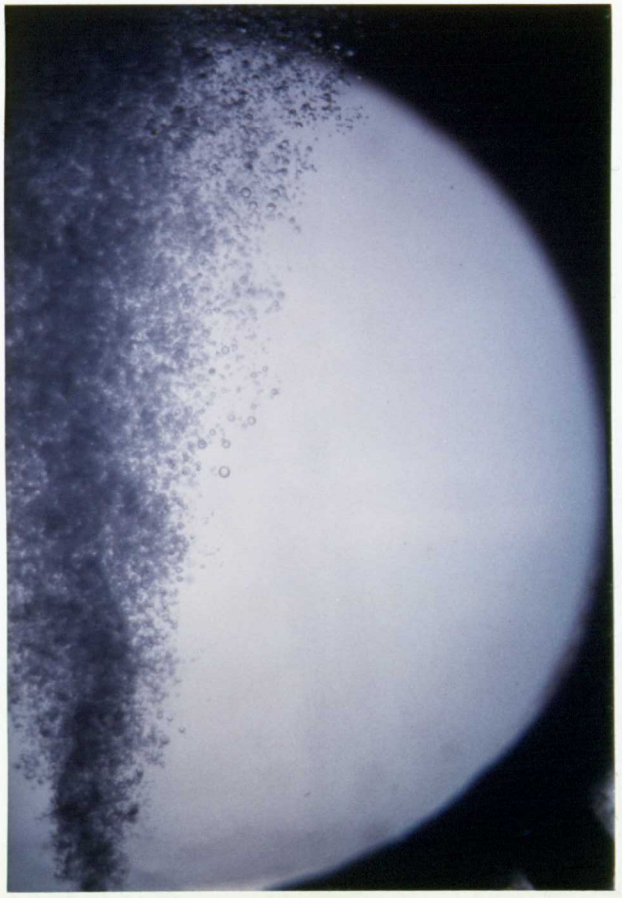

FIGURE 4.6.1 V_l = 5.8m/s, h = 8.8mm,
μ_{oil} = 1.15 x10^{-3} Nsm^{-2}, σ = 0.017 N/m

FIGURE 4.6.2 V_l = 5.8m/s, h= 8.8mm,
μ_{oil} = 1.15 x10^{-3} Nsm^{-2}, σ = 0.0298 N/m

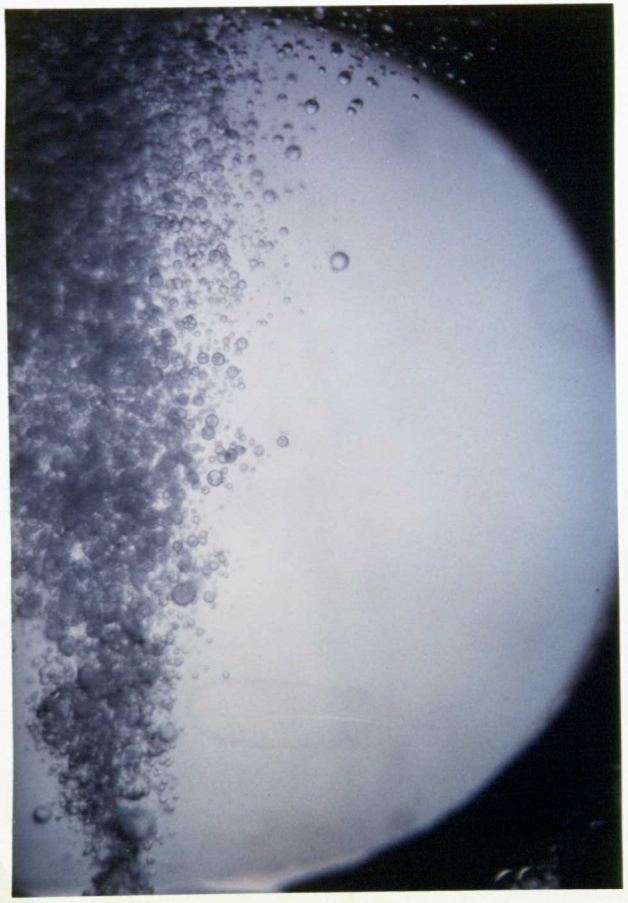

FIGURE 4.6.3 V_j = 4.4, h = 8.8mm,
μ_{oil} = 1.15 x10^{-3} Nsm^{-2}, σ = 0.033 N/m

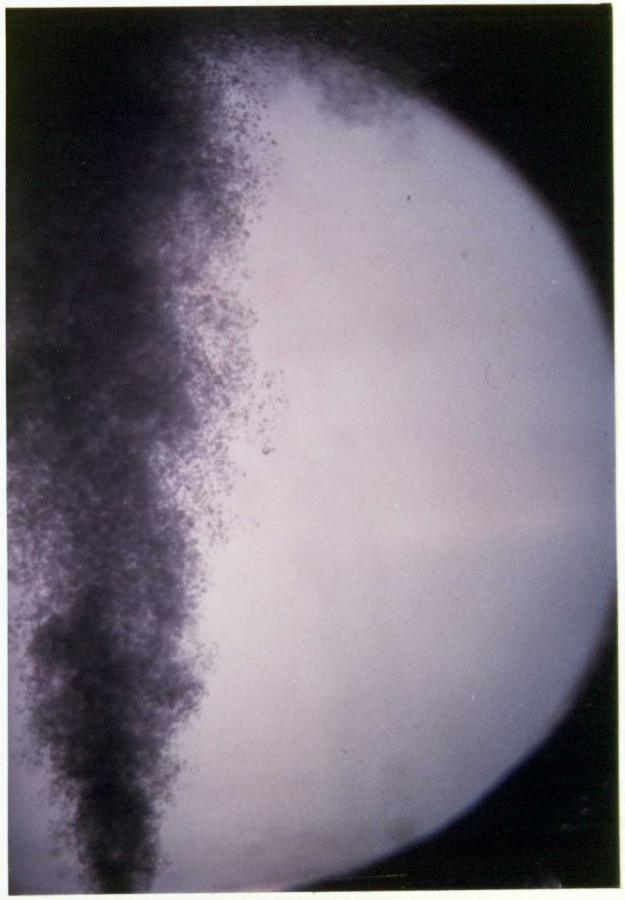

FIGURE 4.6.4 V_j = 8.9 m/s, h = 8.8mm,
μ_{oil} = 1.15 x10^{-3} Nsm^{-2}, σ = 0.033 N/m

FIGURE 4.6.5 V_j = 5.8 m/s, h = 8.8mm,
μ_{tol} = 1.15 x10^{-3} Nsm^{-2}, σ = 0.023 N/m

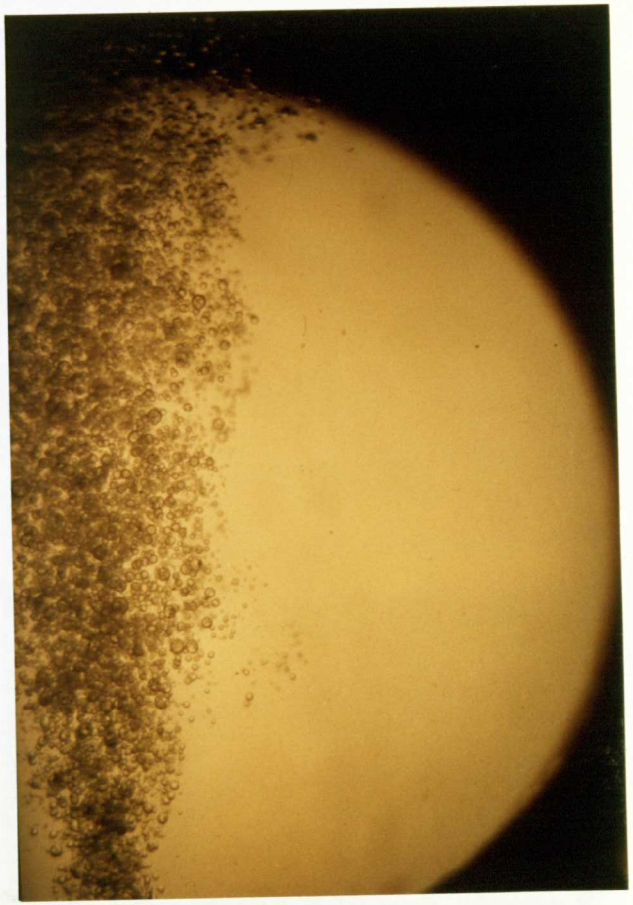

FIGURE 4.6.6 V_j = 5.8m/s, h = 8.8mm,
μ_{oil} = 2.53 x10^{-3} Nsm^{-2}, σ = 0.023 N/m

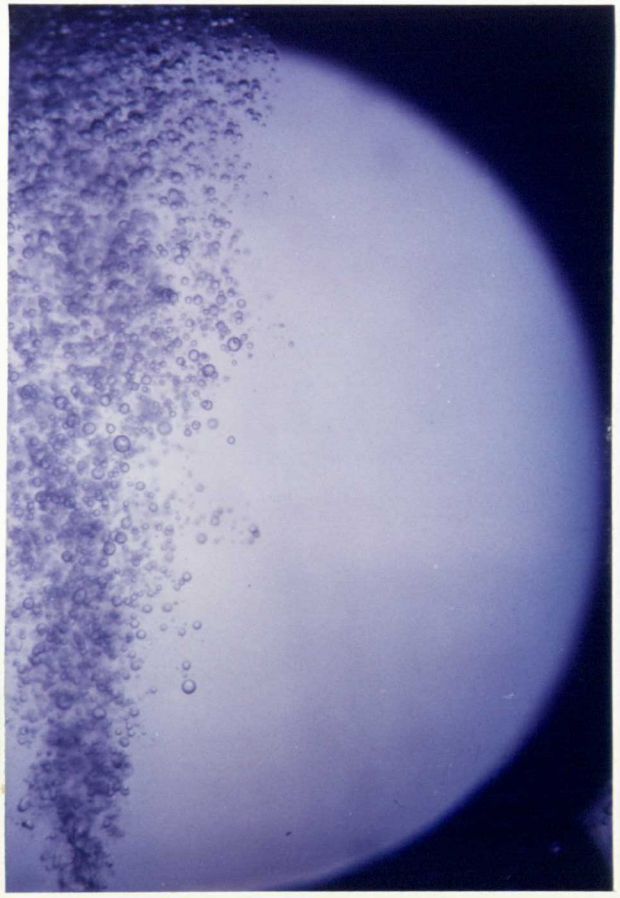

FIGURE 4.6.7 V_j = 5.8 m/s, h = 7.9 mm,
μ_{oil} = 1.15 x 10^{-3} Nsm^{-2}, σ = 0.033 N/m

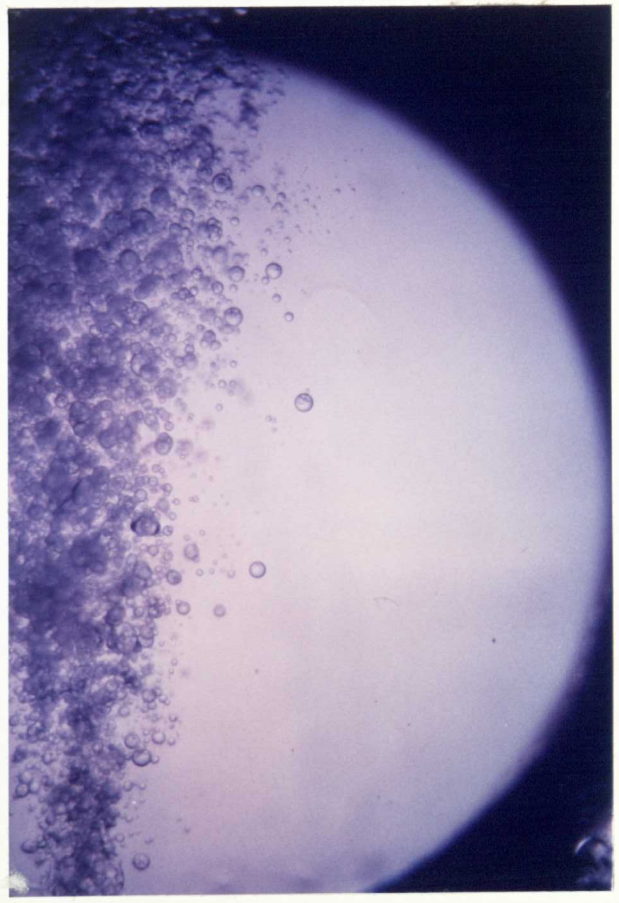

FIGURE 4.6.8 V_j = 5.8 m/s, h = 12.5mm,
μ_{oil} = 1.15 x10^{-3} Nsm^{-2}, σ = 0.033 N/m

FIG. 4.6.9 SMD AGAINST JET VELOCITY

h =8.8mm; σ =0.033Nm^{-1}; μ_{oil} =1.15 ×10^{-3} Nsm^{-2}

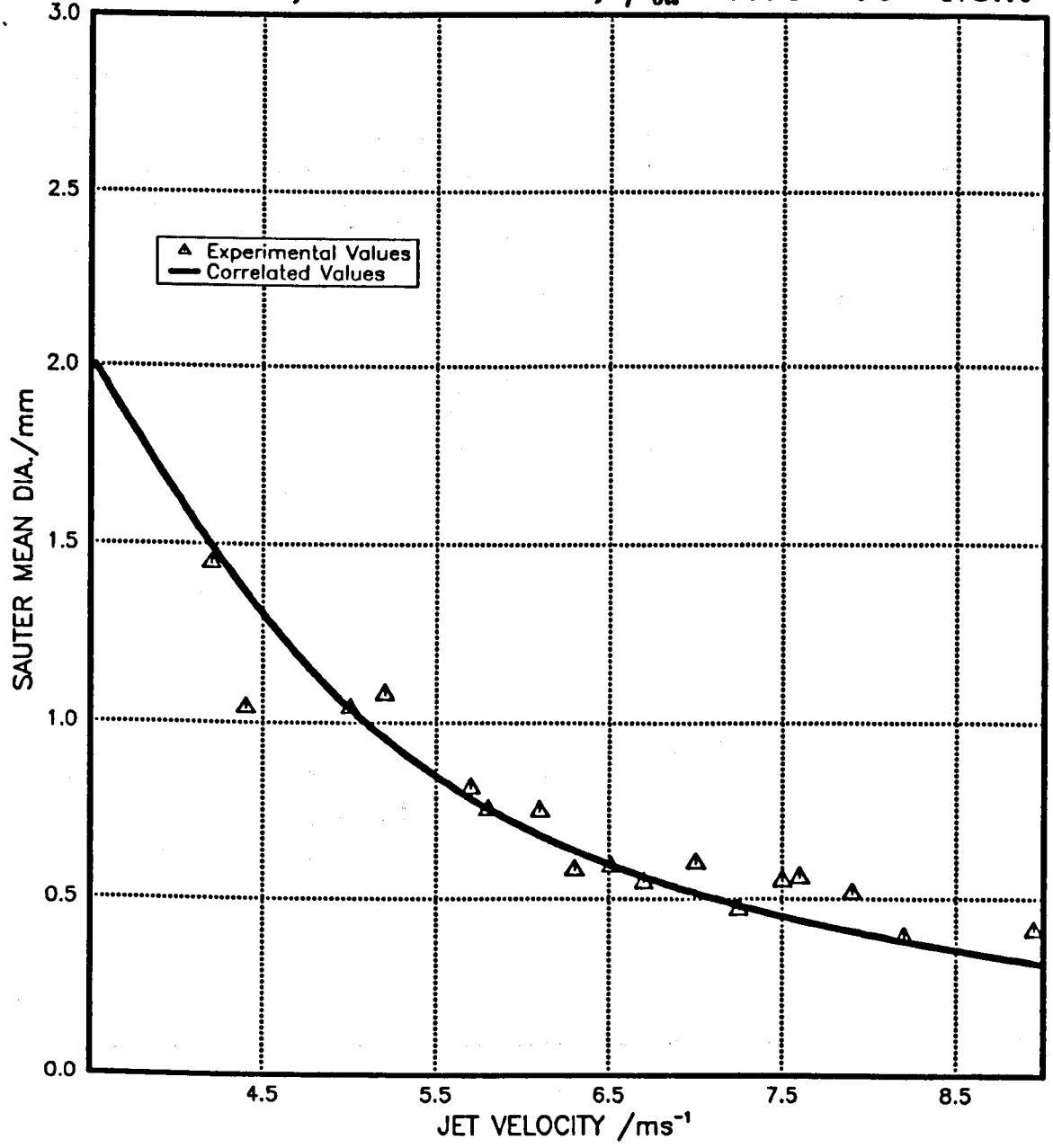

FIG. 4.6.10 SMD AGAINST HEIGHT (h)

$V_j = 5.8\ ms^{-1}$; $\mu_{oil} = 1.15 \times 10^{-3}\ Nsm^{-2}$

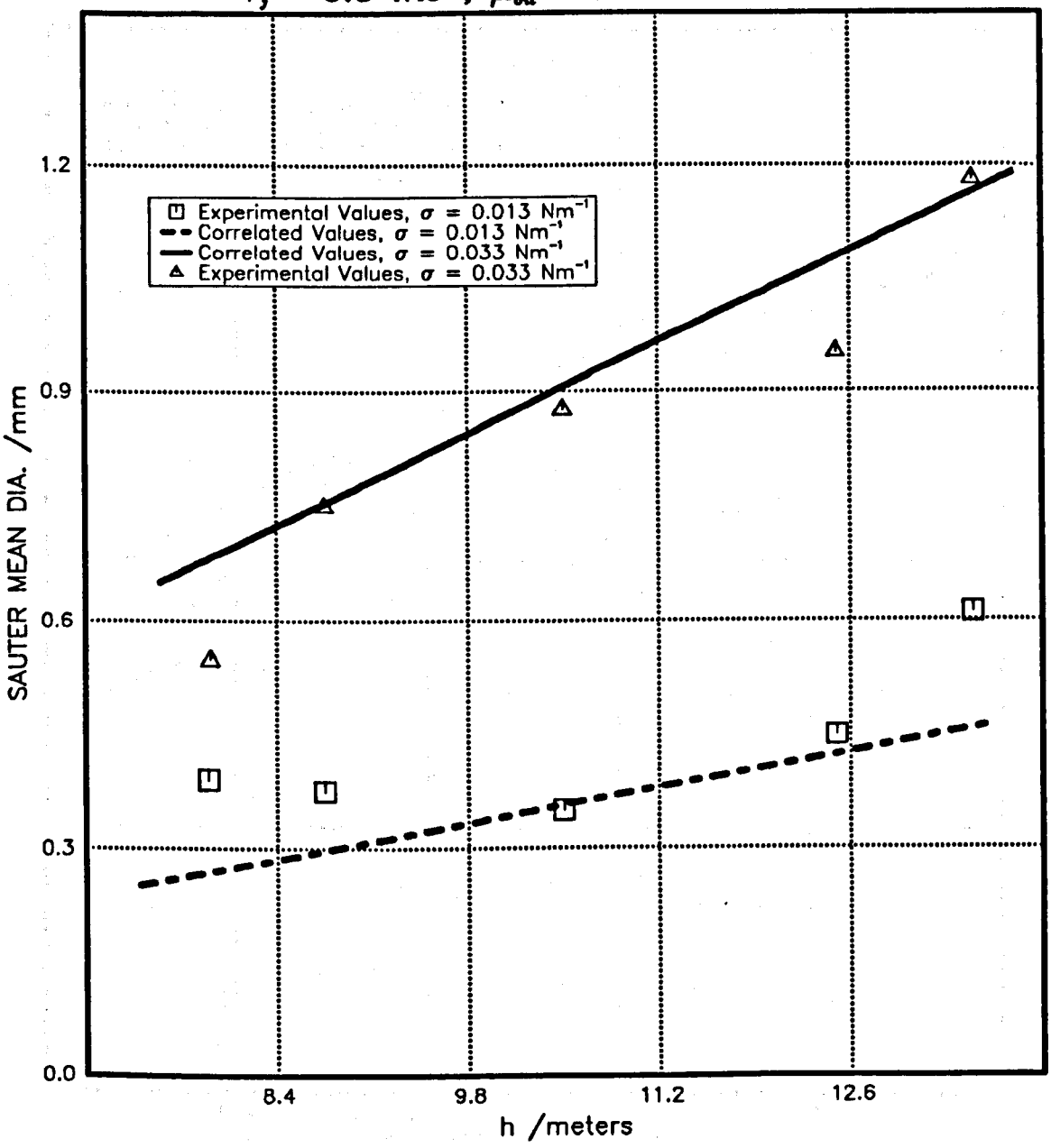

FIG. 4.6.11 SMD AGAINST OIL VISCOSITY (μ_{oil})
V_j = 5.8 ms^{-1}; σ = 0.023 Nm^{-1}

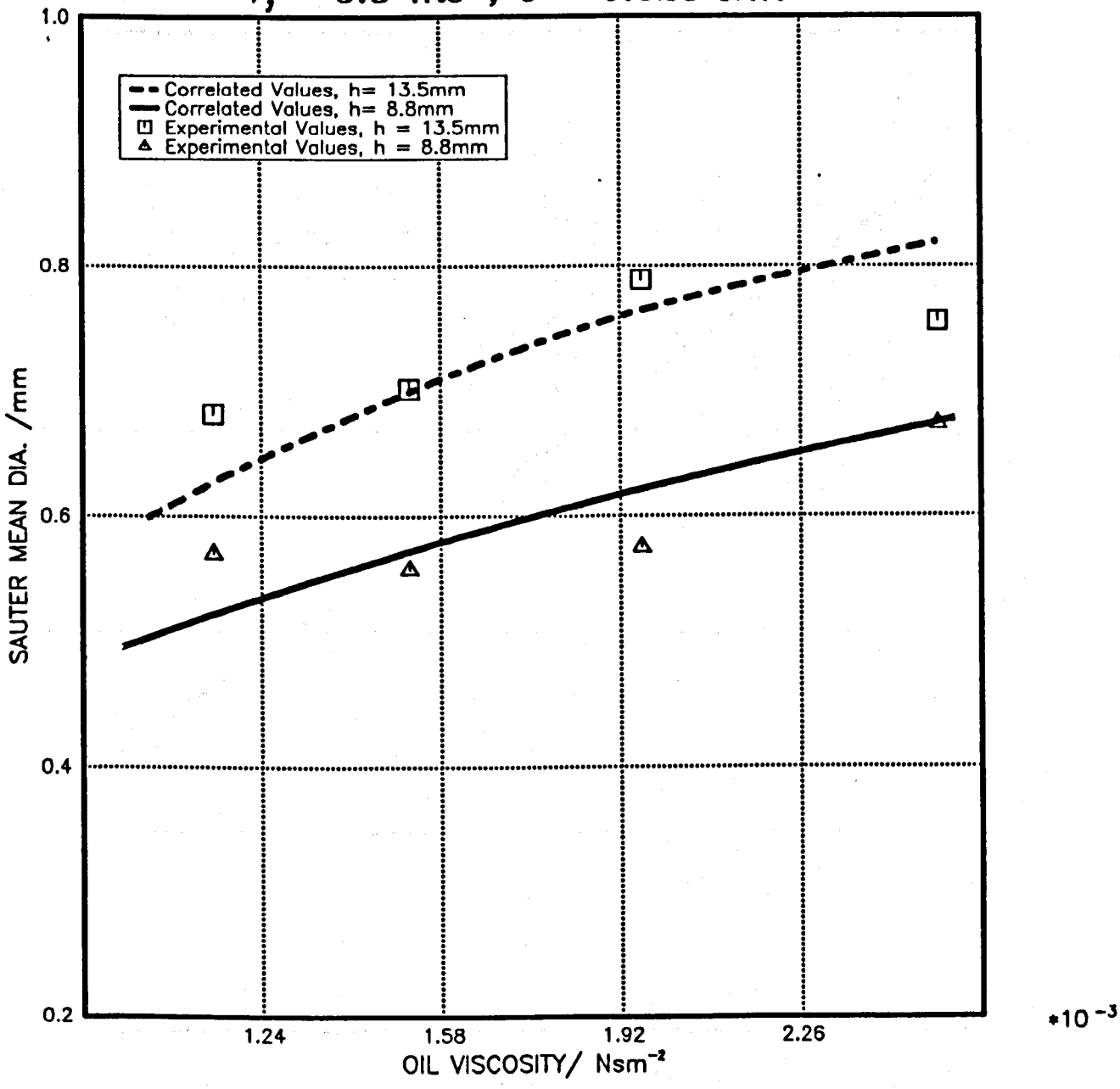

FIG. 4.6.12 SMD AGAINST INTERFACIAL TENSION (σ)

h = 8.8mm; V_j = 5.8ms^{-1}; μ_{oil} =1.15 ×10^{-3} Nsm^{-2}

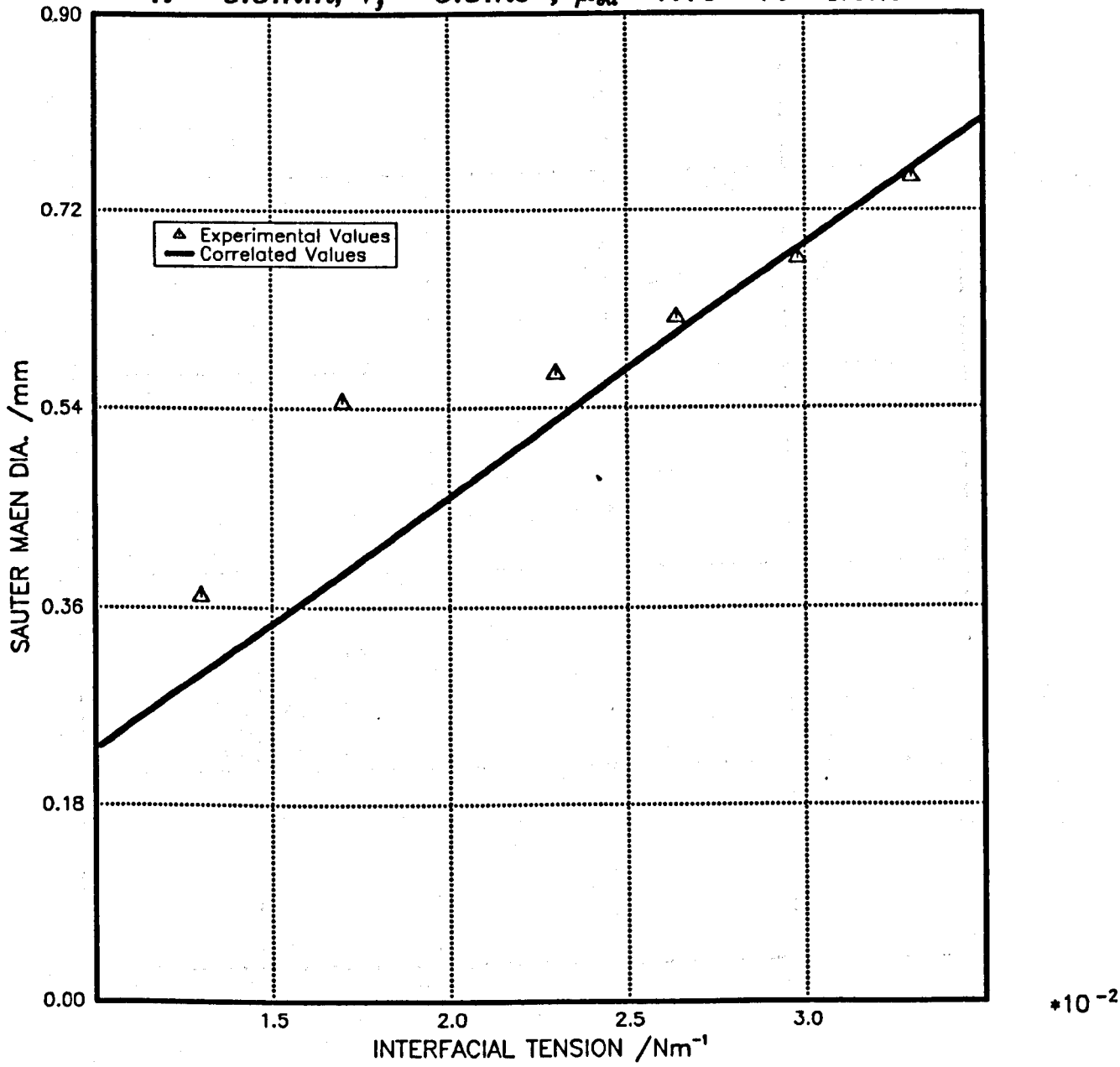

FIG. 4.6.13 ***COMPARISION OF EXPERIMENTAL AND PREDICTED VALUES OF SMD***

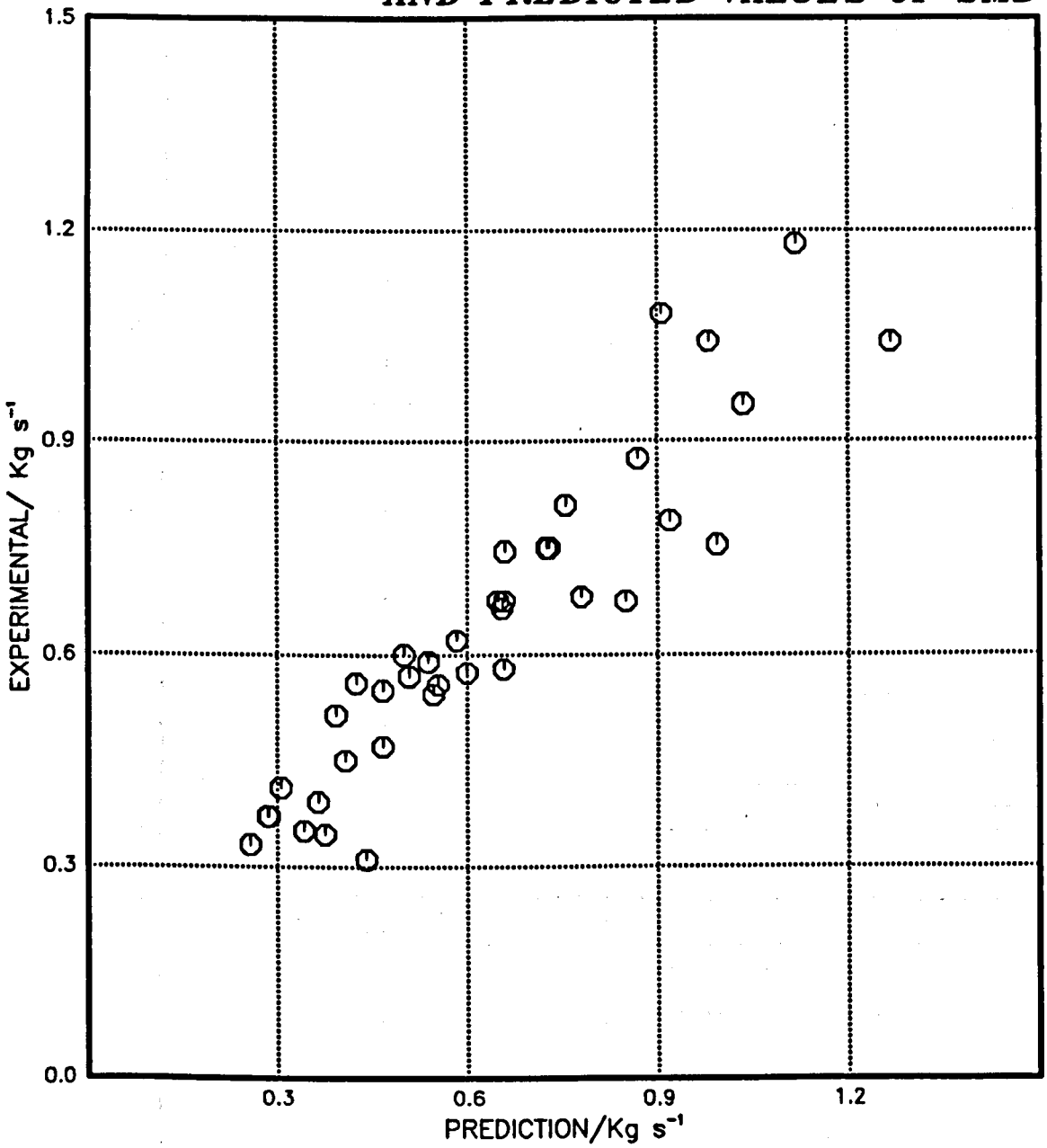

FIG. 4.5.14 DROPLET SIZE DISTRIBUTION

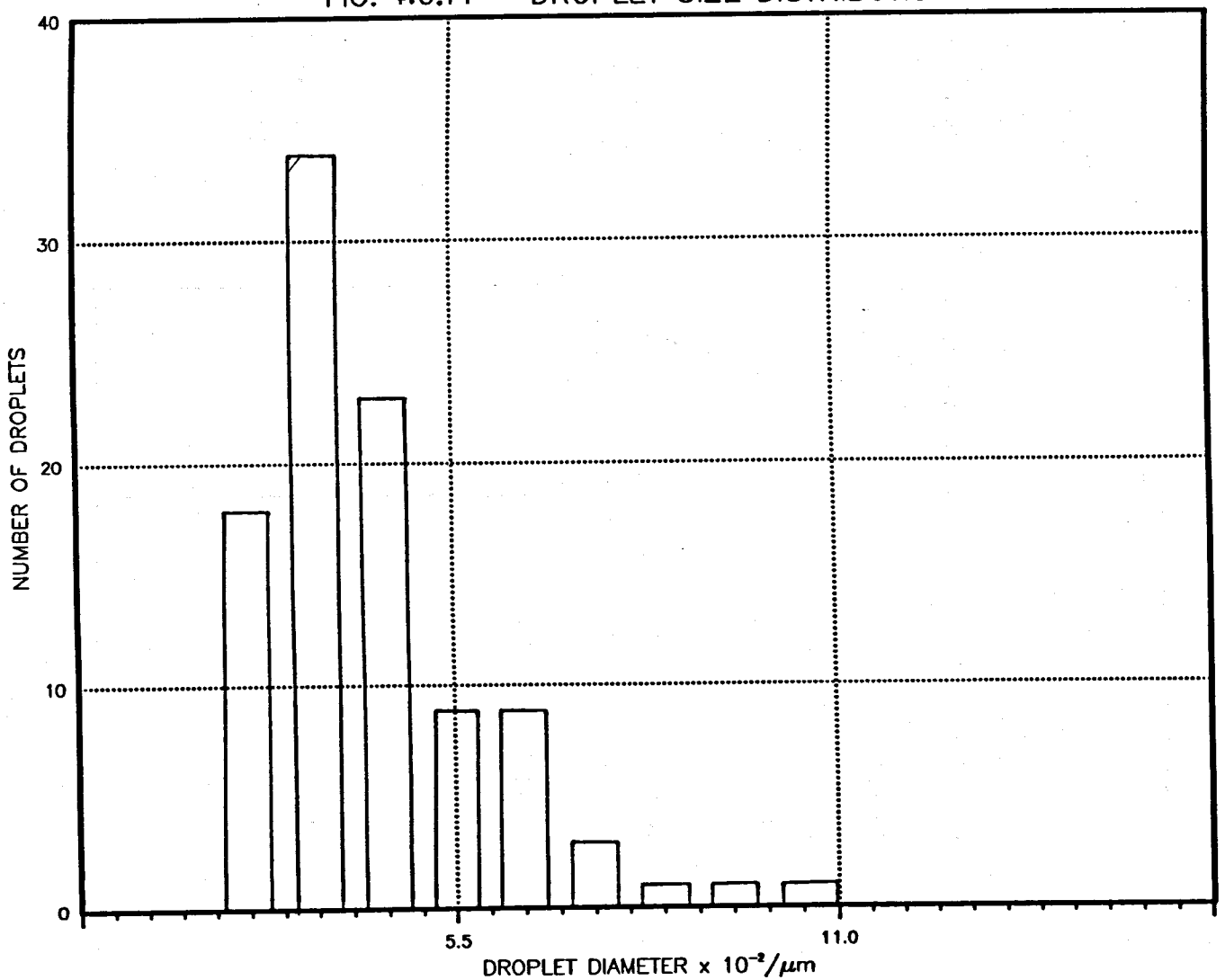

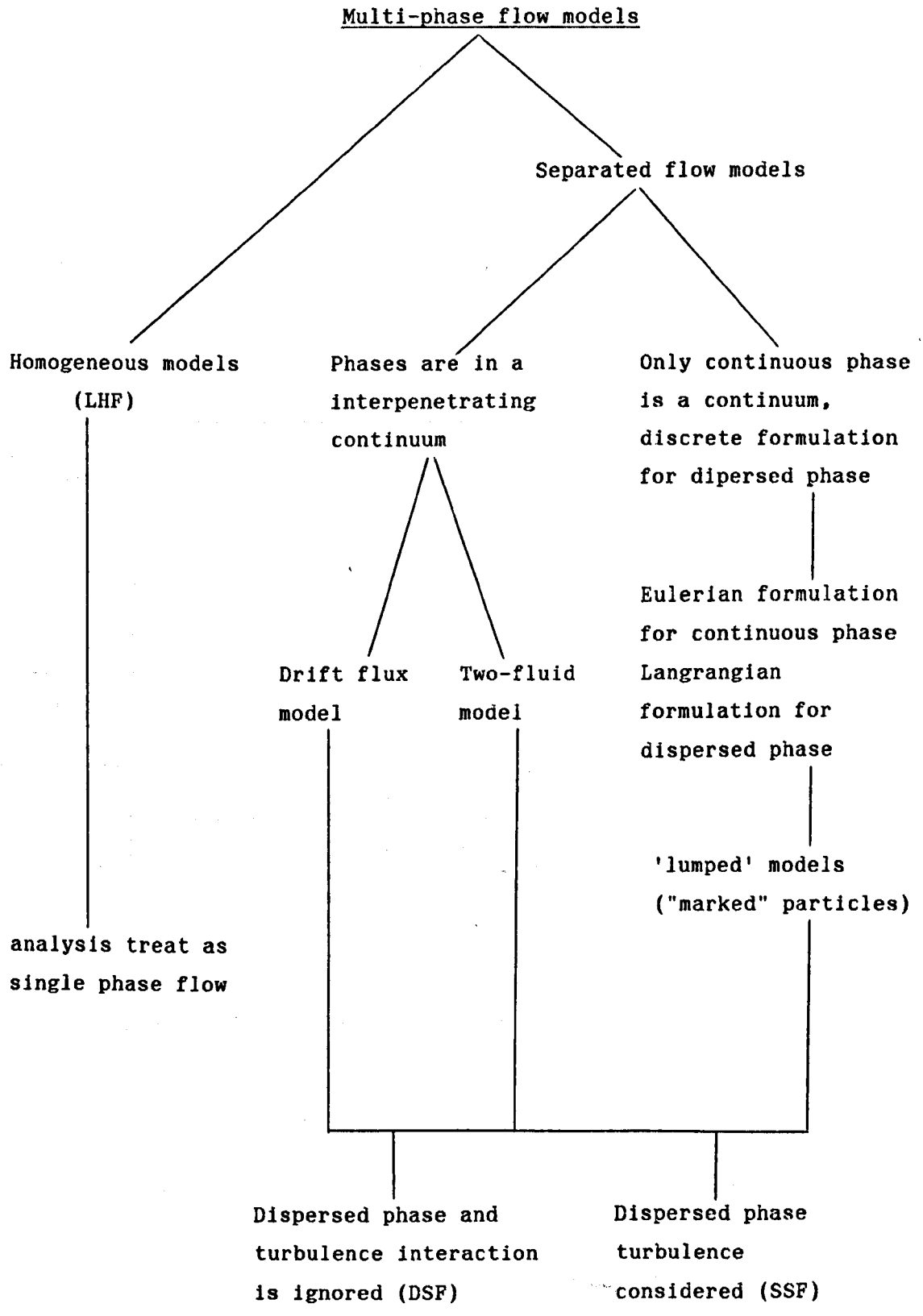

FIGURE 5.1.1 STRUCTURE OF TWO-PHASE MODELS

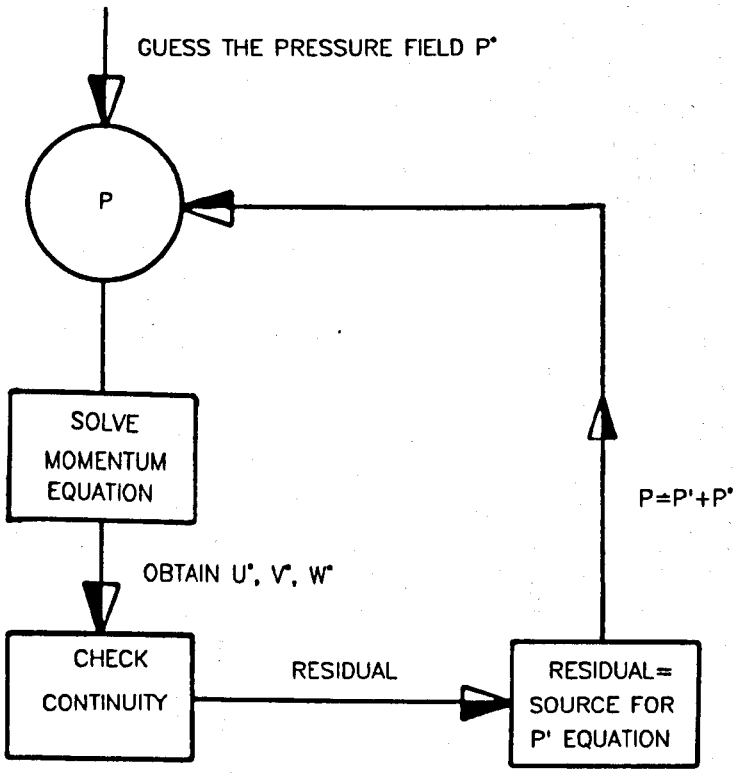

FIGURE 5.2.1 PRESSURE–VELOCITY COUPLING TREATMENT

EXPERIMENT OF MARUYAMA ET AL IS SIMULATED UNDER FOLLOWING CONDITIONS

FLUID:- AIR/AIR, VELOCITY RATIO= 4.6, PIPE VELOCITY= 2.0 m/s

JET TO PIPE DIAMETER RATIO= 0.255, PIPE LENGTH= 10 Metres

------ ≡ EXPERIMENTAL (MARUYAMA, 1981)

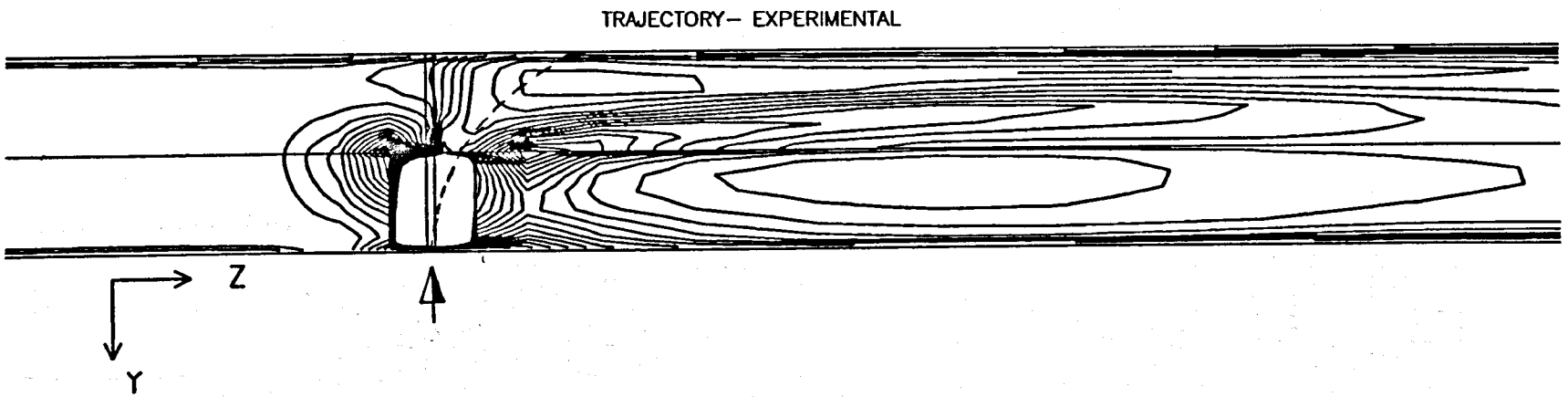

FIGURE 6.1.1 VELOCITY CONTOURS AT THE INJECTION PLANE

EXPERIMENT OF MARUYAMA ET AL(1981) WAS SIMULATED UNDER FOLLOWING CONDITIONS

FLUID:- AIR/AIR, VELOCITY RATIO= 2.0, PIPE VELOCITY= 1.0 m/s

JET TO PIPE DIAMETER RATIO= 0.255, PIPE LENGTH= 10 Metres

PIPE RADIUS= 255 mm

DISTANCE TO IMPINGEMENT POINT IS 7.34 DIAMETERS

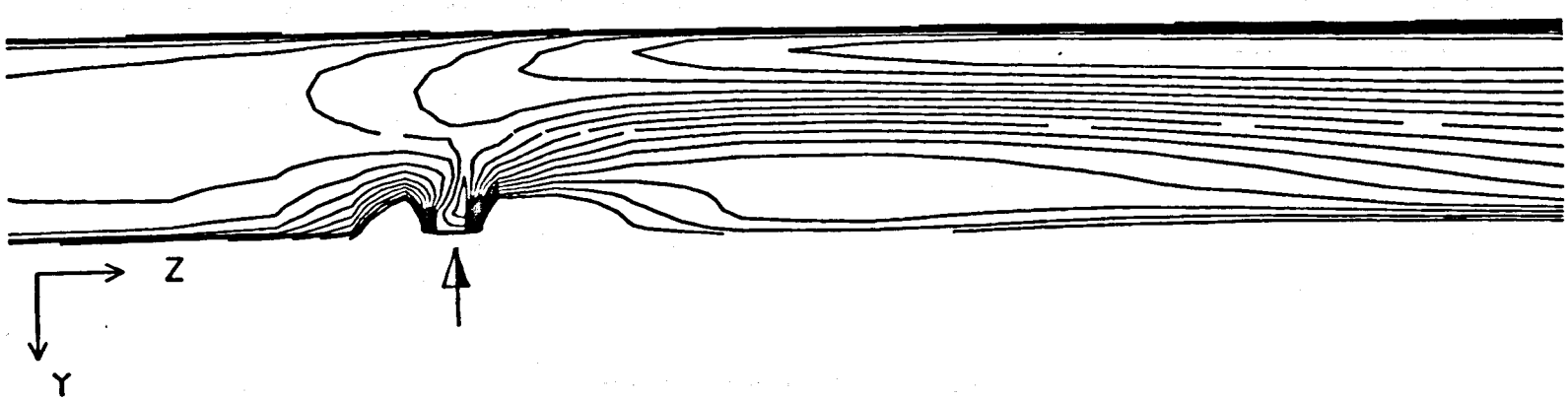

FIGURE 6.1.2 VELOCITY CONTOURS AT THE INJECTION PLANE

EXPERIMENT OF MARUYAMA ET AL(1981) WAS SIMULATED UNDER FOLLOWING CONDITIONS

FLUID:- AIR/AIR, VELOCITY RATIO= 3.1, PIPE VELOCITY= 1.0 m/s

JET TO PIPE DIAMETER RATIO= 0.255, PIPE LENGTH= 10 Metres

-------- ≡ EXPERIMENTAL

PIPE RADIUS= 255 mm

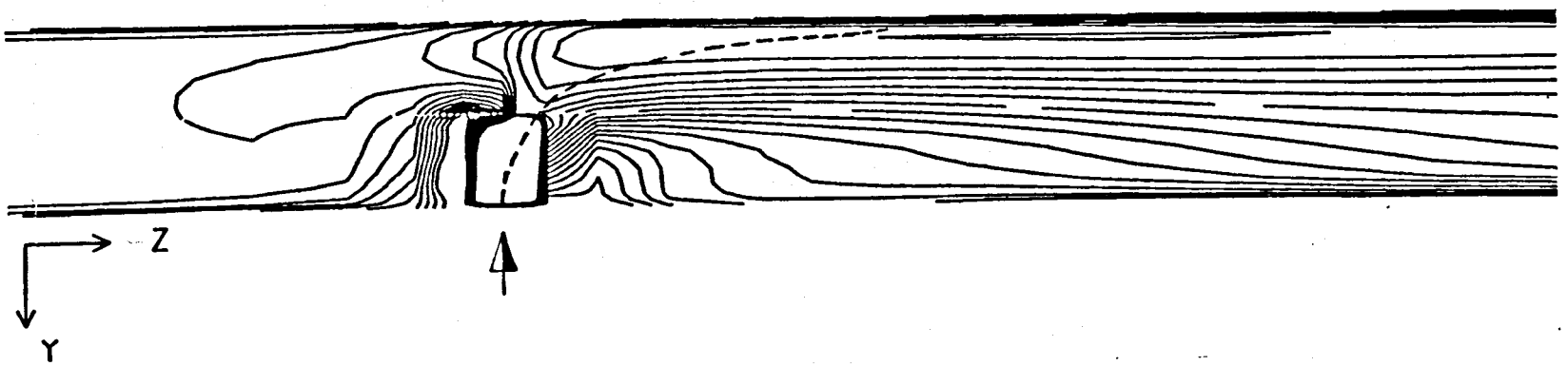

FIGURE 6.1.3 VELOCITY CONTOURS OF THE INJECTION PLANE

PIPE SECTION IS 0·5 DIAMETERS DOWNSTREAM FROM INJECTION PLANE

FLUID:– AIR/AIR, VELOCITY RATIO= 4.6, PIPE VELOCITY= 1.0 m/s

JET TO PIPE DIAMETER RATIO= 0.255, PIPE LENGTH= 10 Metres

PIPE RADIUS= 255 mm

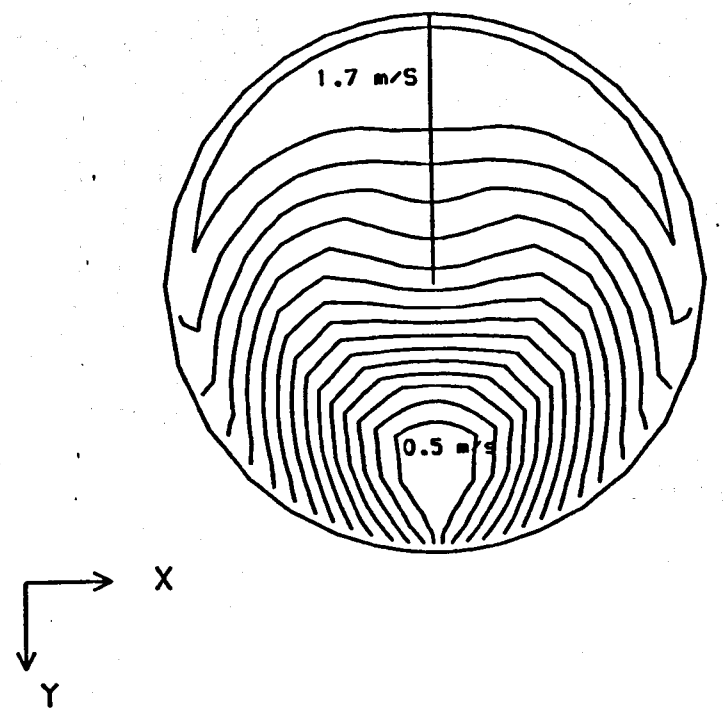

FIGURE 6.1.4 AXIAL VELOCITY CONTOURS AT A DOWNSTREAM SECTION

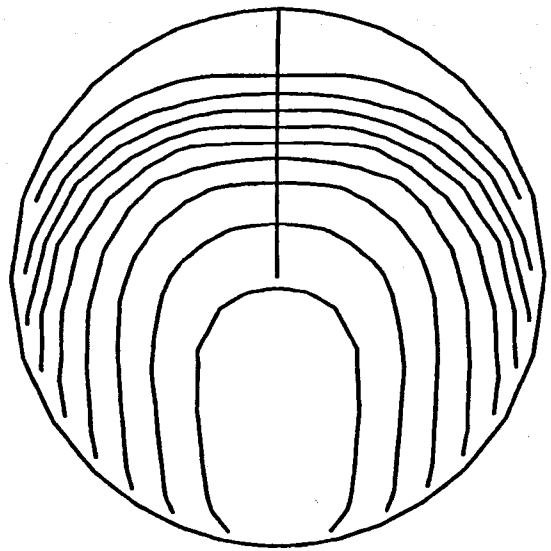

X

A). TEMPERATURE CONTOURS
PRESENT SIMULATION

JET TO PIPE DIAMETER RATIO= 0.255
VELOCITY RATIO =4.6 FLUID:– AIR/AIR,
PIPE RADIUS= 255 mm

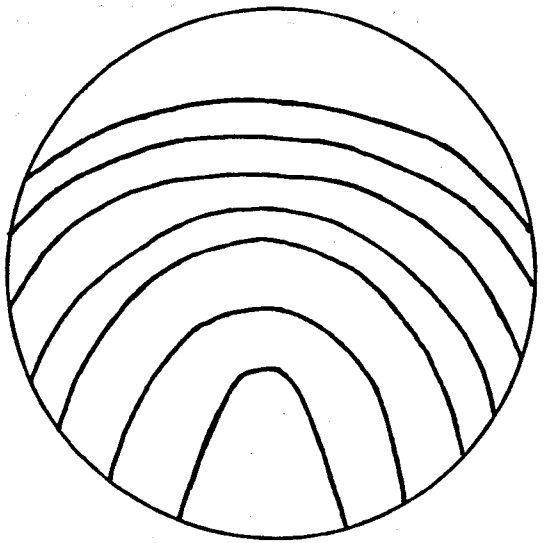

B). DIMENSIONLESS TEMPERATURE CONTOURS
EXPERIMENTALLY DETERMINED BY
MARUYAMA ET AL (1881)

FIGURE 6.1.5 TEMPERATURE CONTOURS AT 2 DIAMETERS DOWNSTREAM

EXPERIMENT OF MARUYAMA ET AL(1981) WAS SIMULATED UNDER FOLLOWING CONDITIONS

FLUID:- AIR/AIR, VELOCITY RATIO= 4·6, PIPE VELOCITY= 1.0 m/s

JET TO PIPE DIAMETER RATIO= 0.255, PIPE LENGTH= 10 Metres

PIPE RADIUS= 255 mm

------- ≡ EXPERIMENTAL

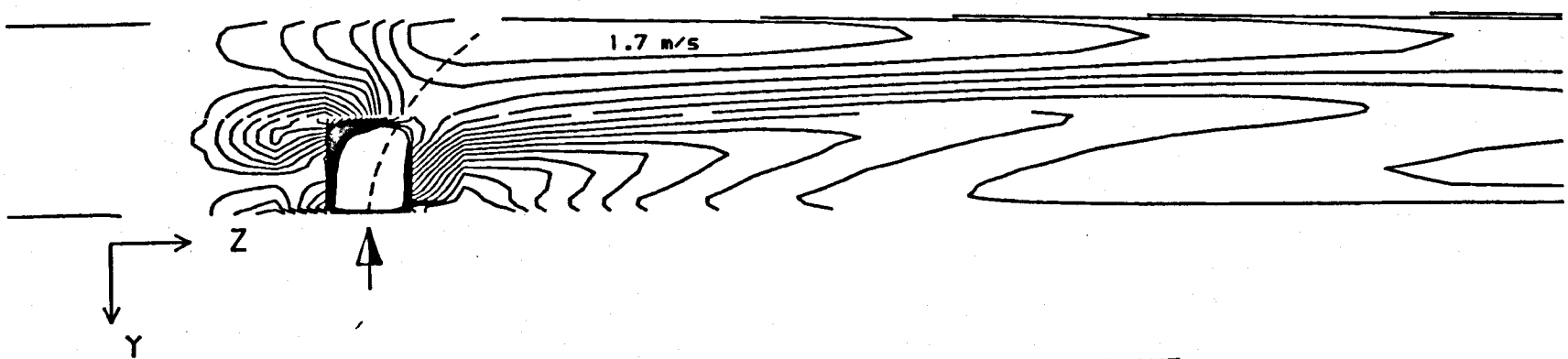

FIGURE 6.1.6 VELOCITY CONTOURS OF THE INJECTION PLANE

EXPERIMENT OF FITZGERALAD ET AL(1979) WAS SIMULATED FOR CONDITIONS BELOW

FLUID:- WATER/WATER, VELOCITY RATIO= 1222/220

PIPE VELOCITY= 220 mm/s, PIPE LENGTH= 4.0 Meters

PIPE DIAMETER= 152 mm, JET TO PIPE DIAMETER RATIO= 0.225

THE CONTOURS DEMONSTRATE THAT THE JET BENDS OVER AND APPROXIMATELY COINCIDES WITH PIPE AXIS AS SEEN EXPERIMENTALLY BY FITZGERALD ET AL(1979)

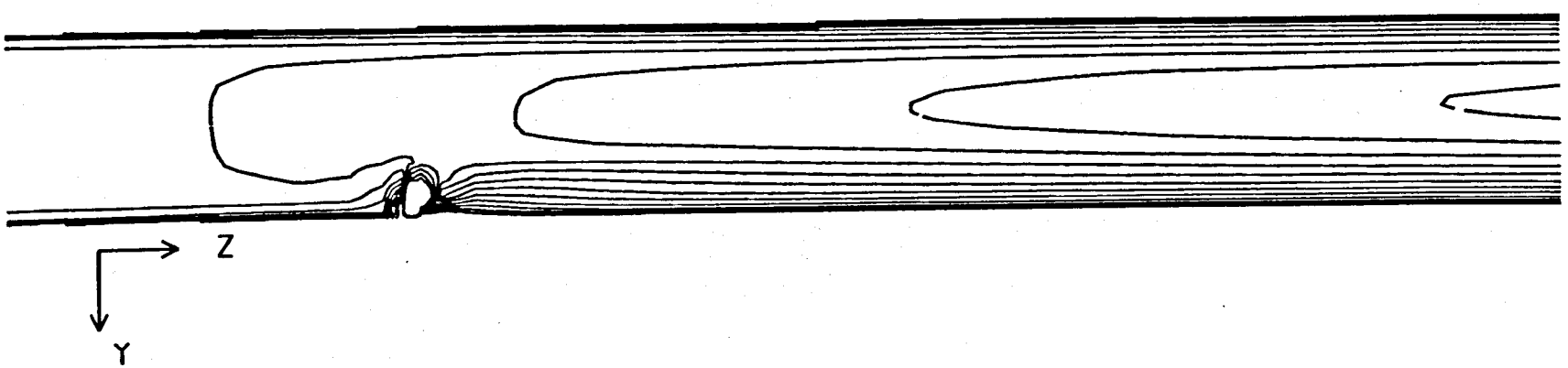

FIGURE 6.2.1 VELOCITY CONTOURS AT THE INJECTION PLANE

PIPE SECTION IS 1 DIAMETER DOWNSTREAM TO INJECTION PLANE
EXPERIMENT OF FITZGERALAD ET AL(1979) WAS SIMULATED FOR CONDITIONS BELOW

FLUID:- WATER/WATER, VELOCITY RATIO= 1222/220
PIPE VELOCITY= 220 mm/s, PIPE LENGTH= 4.0 Metres
PIPE DIAMETER= 152 mm, JET TO PIPE DIAMETER RATIO= 0.225

THESE CONTOURS DEMONSTRATE THAT THE JET IS CENTRED AT THE PIPE SECTION AS OBSERVED EXPERIMENTALLY BY FITZGERALD ET AL (1979).

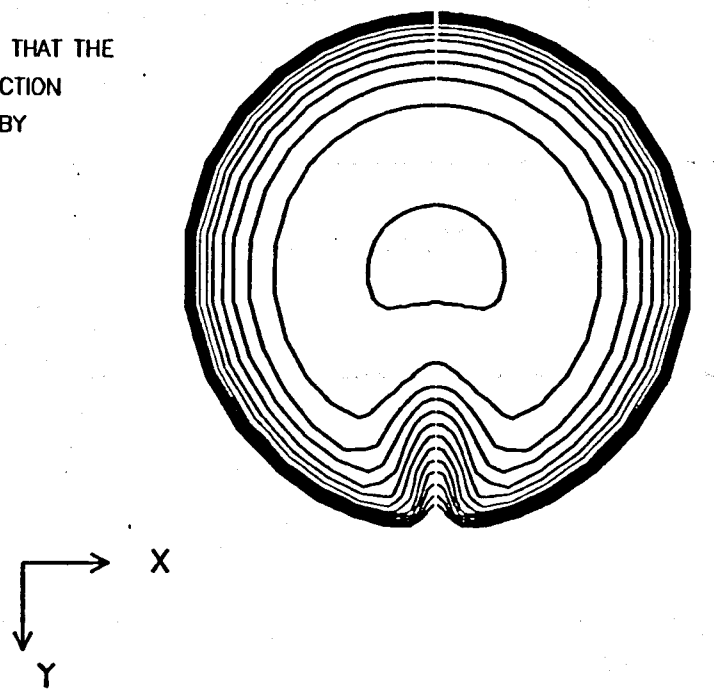

FIGURE 6.2.2 AXIAL VELOCITY CONTOURS AT A DOWNSTREAM SECTION

SIMULATION IS SAME AS IN FIGURE 6.2.1

RADIAL VELOCITY CONTOURS AT THE AXIS ARE APPROXIMATELY ZERO. HENCE, THE JET BENDS OVER AND COINCIDES WITH THE PIPE AXIS AS OBSERVED EXPERIMENTALY BY FITZGERALD ET AL (1979).

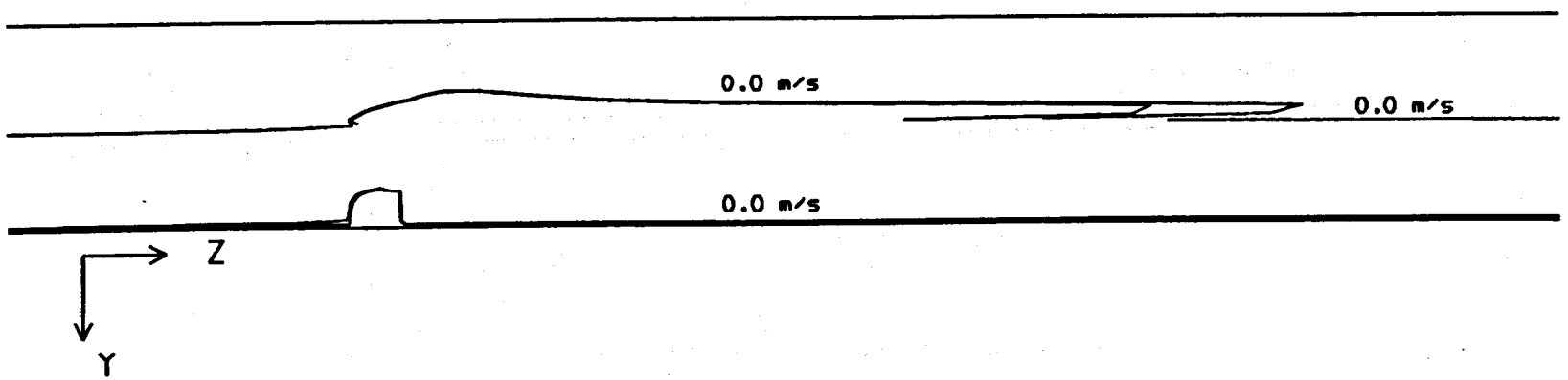

FIGURE 6.2.3 CONTOURS OF RADIAL VELOCITY AT THE INJECTION PLANE

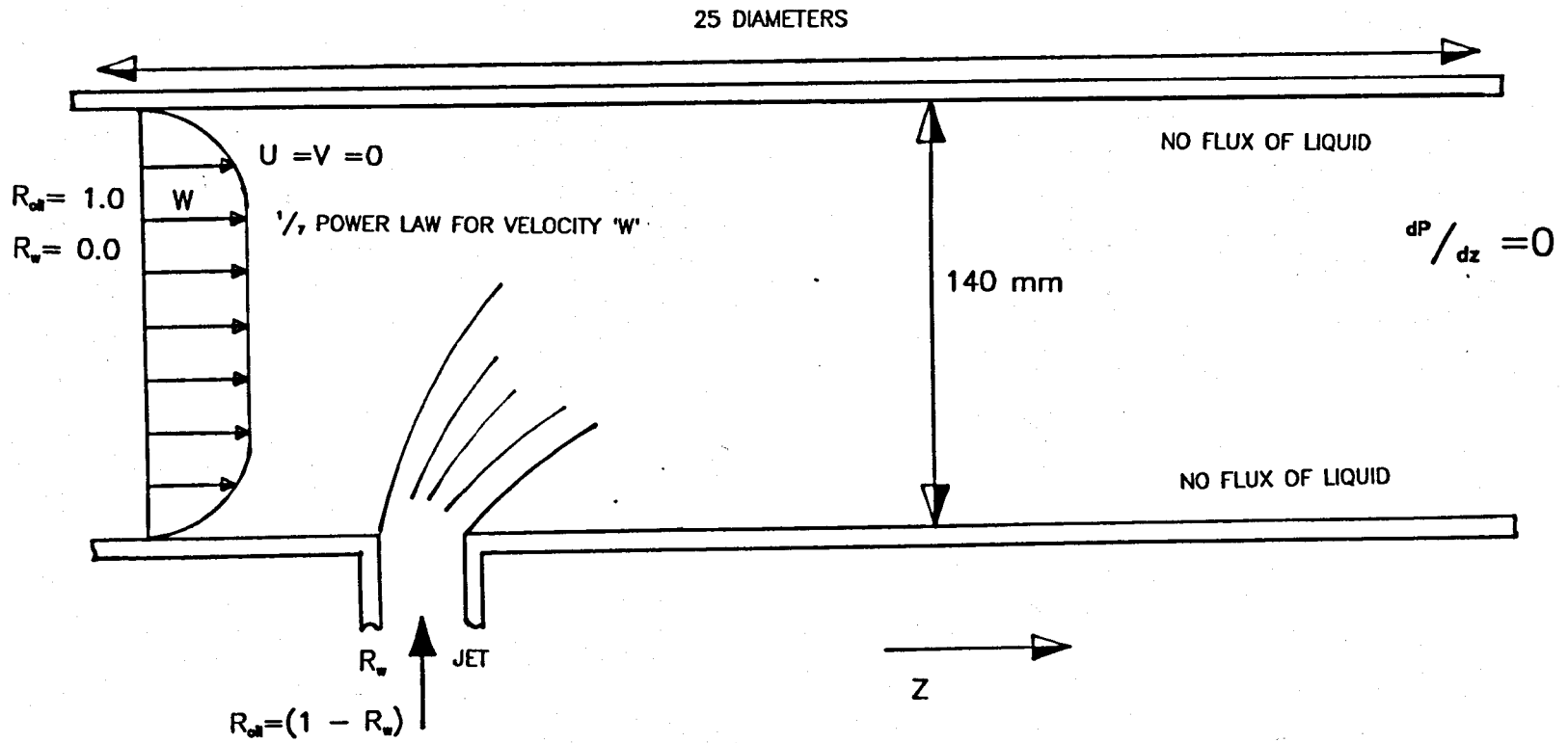

R_w= VOLUME FRACTION OF WATER (OBTAINED IN CHAPTER 4.0)

R_{oil}= VOLUME FRACTION OF OIL

FIGURE 6.2.4 THE SCHEMATIC DIAGRAM OF THE NUMERICAL SIMULATION

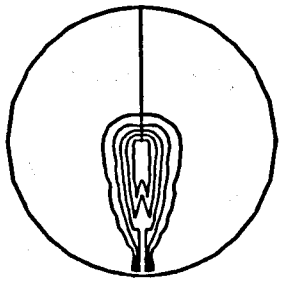

FIVE EQUALLY DIVIDED C1 CONTOURS
FROM 0.000 TO 0.042
0.09 DIAMETERS DOWNSTREAM FROM JE T

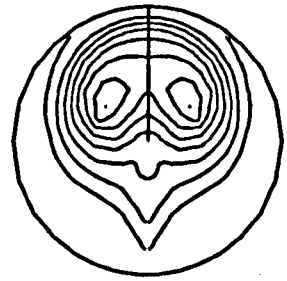

EIGHT EQUALLY SPACED CONTOURS
FROM 3E-4 TO 8E-3
9.1 DIAMETERS DOWNSTREAM FROM JE T

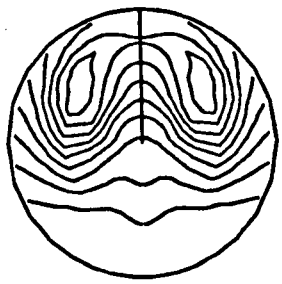

TEN EQUALLY SPACED C1 CONTOURS
FROM 2E-4 TO 5E-3
13.7 DIAMETERS DOWNSTREAM FROM JE T

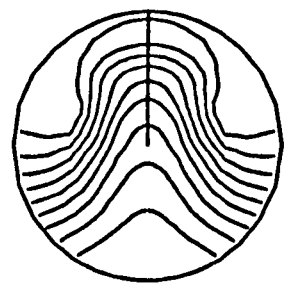

NINE EQUALLY SPACED C1 CONTOURS
FROM 8E-4 TO 2E- 3
22 DIAMETERS DOWNSTREAM FROM JE T

FIGURE 6.3.1 WATER CONCENTRATION (C1) CONTOURS FROM HOMOGENEOUS MODEL VELOCITY RATIO=11, PIPE DIAMETER=140MM, PIPE INLET VELOCITY=0.95M/S CONCENTRATION SOURCE AND DROPLETS SIZE WERE CALCULATED IN ACCORDANCE WITH EQUATIONS 4.4.24 AND 4.4.25, WHEN THE STRATIFIED WATER LAYER IS 10MM. $\mu_{oil}=1.15*10^{-3}Nsm^{-2}$, $\mu_{w}=1.0*10^{-3}Nsm^{-2}$, $\rho_{oil}=800Kg/m^3$, $\rho_{w}=1000Kg/m^3$ EQUIVALENT JET ORIFICE DIAMETER = 4.2mm

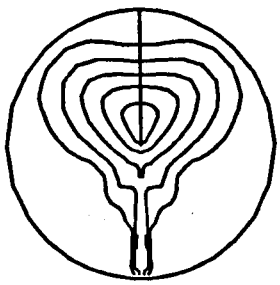

FIVE EQUALLY SPACED C1 CONTOURS
FROM 0 TO 0.037
0.09 DIAMETERS DOWNSTREAM FROM JET

TEN EQUALLY SPACED C1 CONTOURS
FROM 0.006 TO 0.009
9.1 DIAMETERS DOWNSTREAM FROM JET

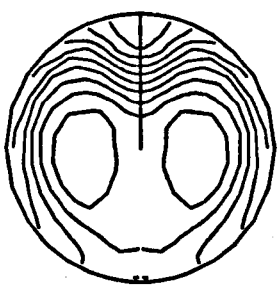

NINE EQUALLY SPACED C1 CONTOURS
FROM 0.007 TO 0.008
13.7 DIAMETERS DOWNSTREAM FROM JET

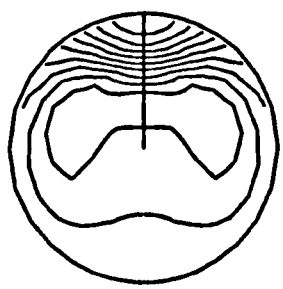

NINE EQUALLY SPACED CONTOURS
FROM .0072 TO .0079
22 DIAMETERS DOWNSTREAM FROM JET

FIGURE 6.4.1 WATER CONCENTRATION CONTOURS FROM HOMOGENEOUS MODEL VELOCITY RATIO=11, PIPE DIAMETER=140MM, PIPE INLET VELOCITY=0.95M/S CONCENTRATION SOURCE AND DROPLETS SIZE WERE CALCULATED IN ACCORDANCE WITH EQUATIONS 4.4.24 AND 4.4.25, WHEN THE STRATIFIED WATER LAYER IS 10MM. $\mu_{oil}=1.15*10^{-3}Nsm^{-2}$, $\mu_{w}=1.0*10^{-3}Nsm^{-2}$ $\rho_{oil}=800Kg/m^3$, $\rho_{w}=1000Kg/m^3$ EQUIVALENT JET ORIFICE DIAMETER = 6.7mm,

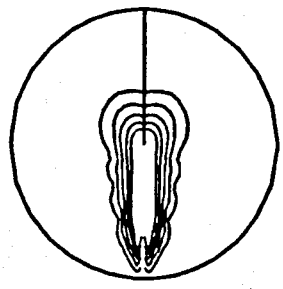

FIVE EQUALLY SPACED WATER VOLUME FRACTION CONTOURS FROM 0.0 TO 0.05

0.09DIAMETERS DOWNSTREAM FROM JET

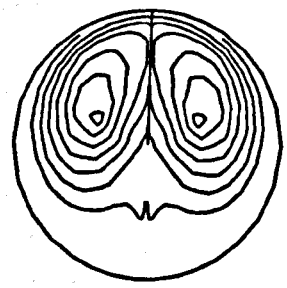

SEVEN EQUALLY SPACED WATER VOLUME FRACTION CONTOURS FROM 0.001 TO 0.018

9.1 DIAMETERS DOWNSTREAM FROM JET

TEN EQUALLY SPACED WATER VOLUME FRACTION CONTOURS FROM 4E-5 TO 9

13.7 DIAMETERS DOWNSTREAM FROM JET

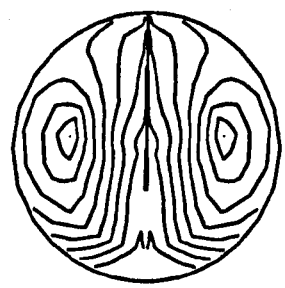

NINE EQUALLY SPACED WATER VOLUME FRACTION CONTOURS FROM 2E-4 TO 5E-3

22 DIAMETERS DOWNSTREAM FROM JET

FIGURE 6.5.1 WATER VOLUME FRACTION CONTOURS FROM TWO-FLUID MODEL INTER-FACIAL FRICTION AND GRAVITATIONAL EFFECTS ARE INCLUDED CONCENTRATION SOURCE AND DROPLETS SIZE WERE CALCULATED IN ACCORDANCE WITH EQUATIONS 4.4.24 AND 4.4.25, WHEN THE STRATIFIED WATER LAYER IS 10MM. $\mu_{oil}=1.15*10^{-3}Nsm^{-2}$, $\mu_{w}=1.0*10^{-3}Nsm^{-2}$ $\rho_{oil}=800Kg/m^3$, $\rho_{w}=1000Kg/m^3$ EQUIVALENT JET ORIFICE DIAMETER = 4.2mm

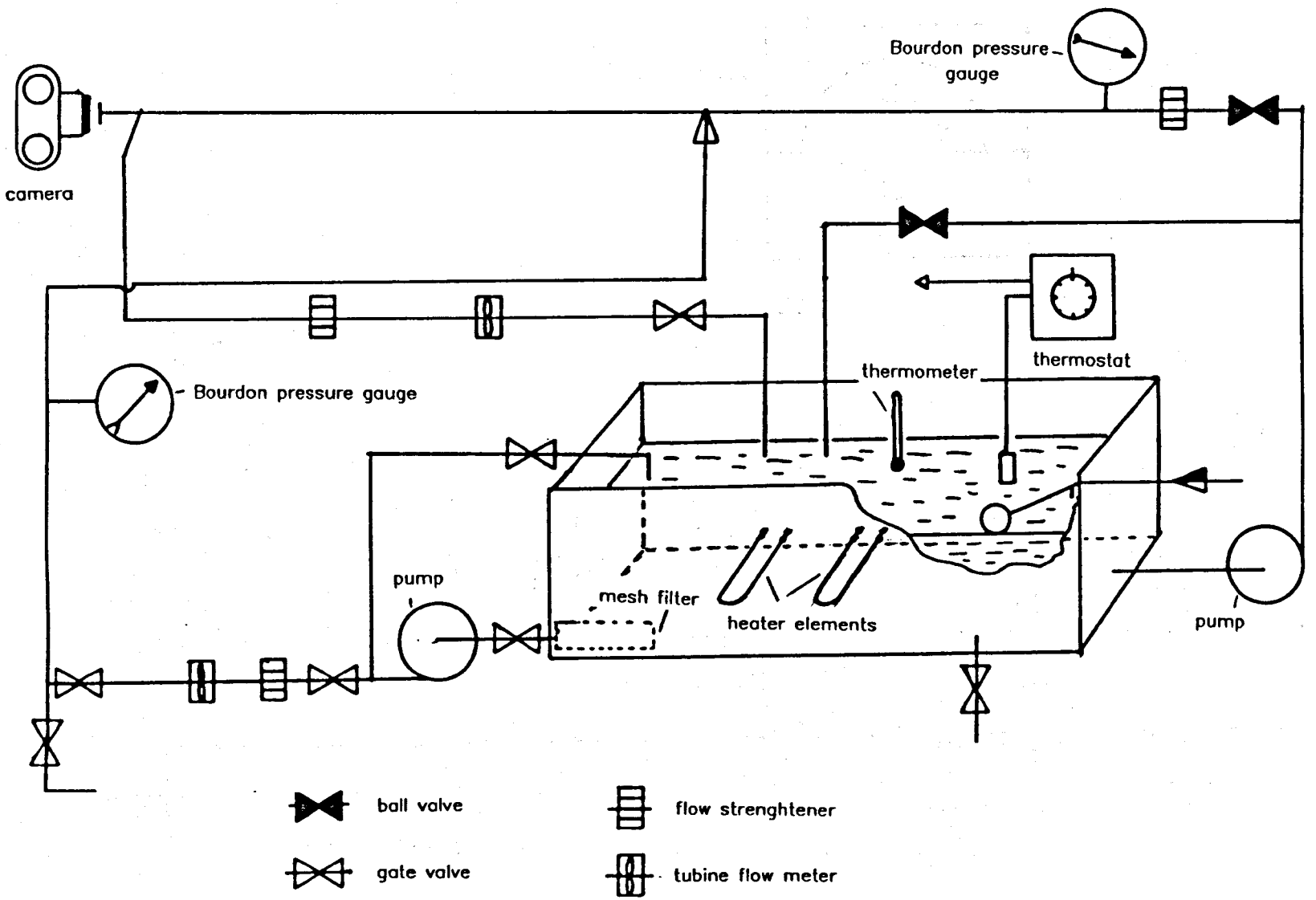

FIG. 7.1 GENERAL ARRANGEMENT OF THE EXPERIMENTAL RIG

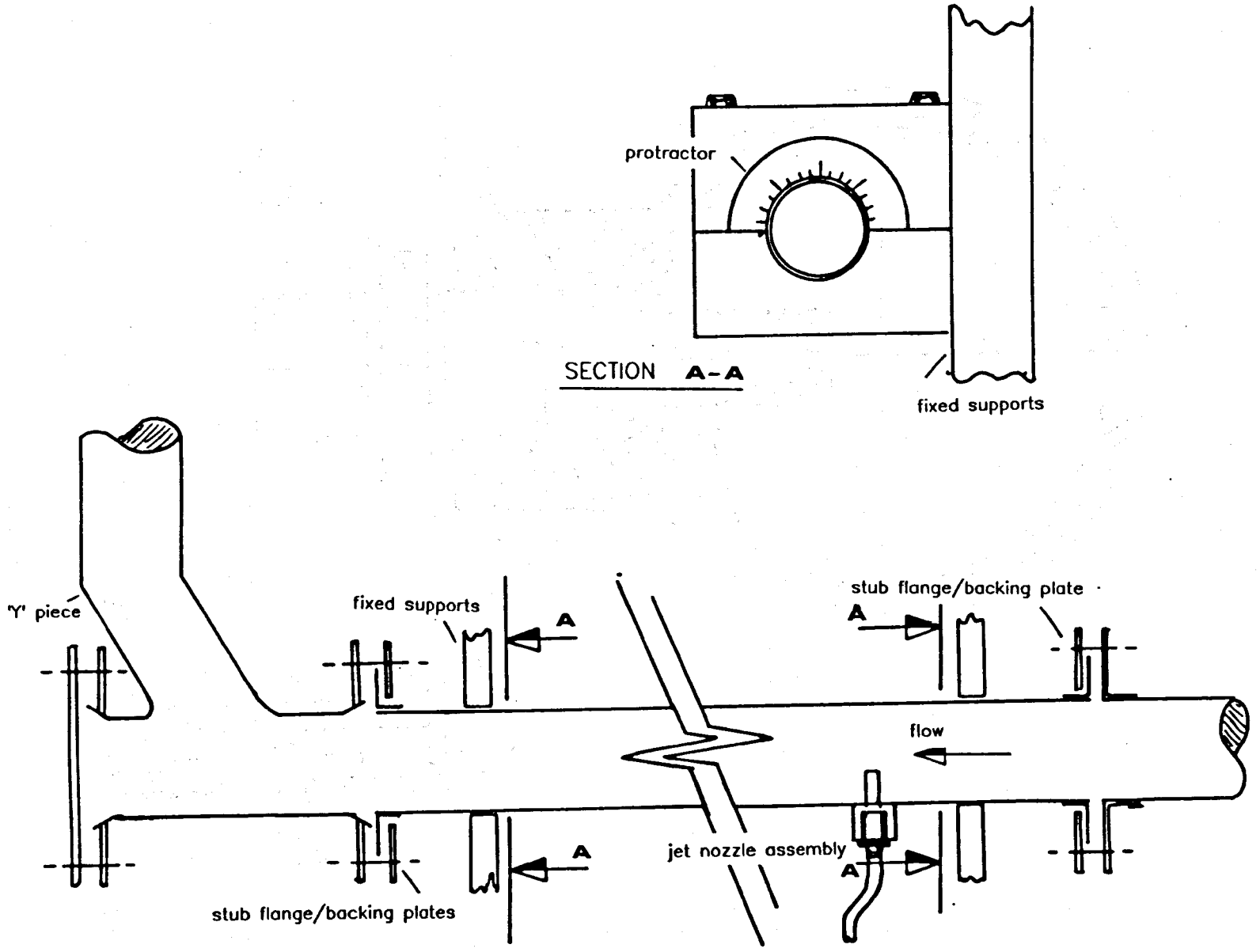

FIG. 7.2.1 GENERAL CONSTRUCTION AND DETAIL OF THE TEST SECTION

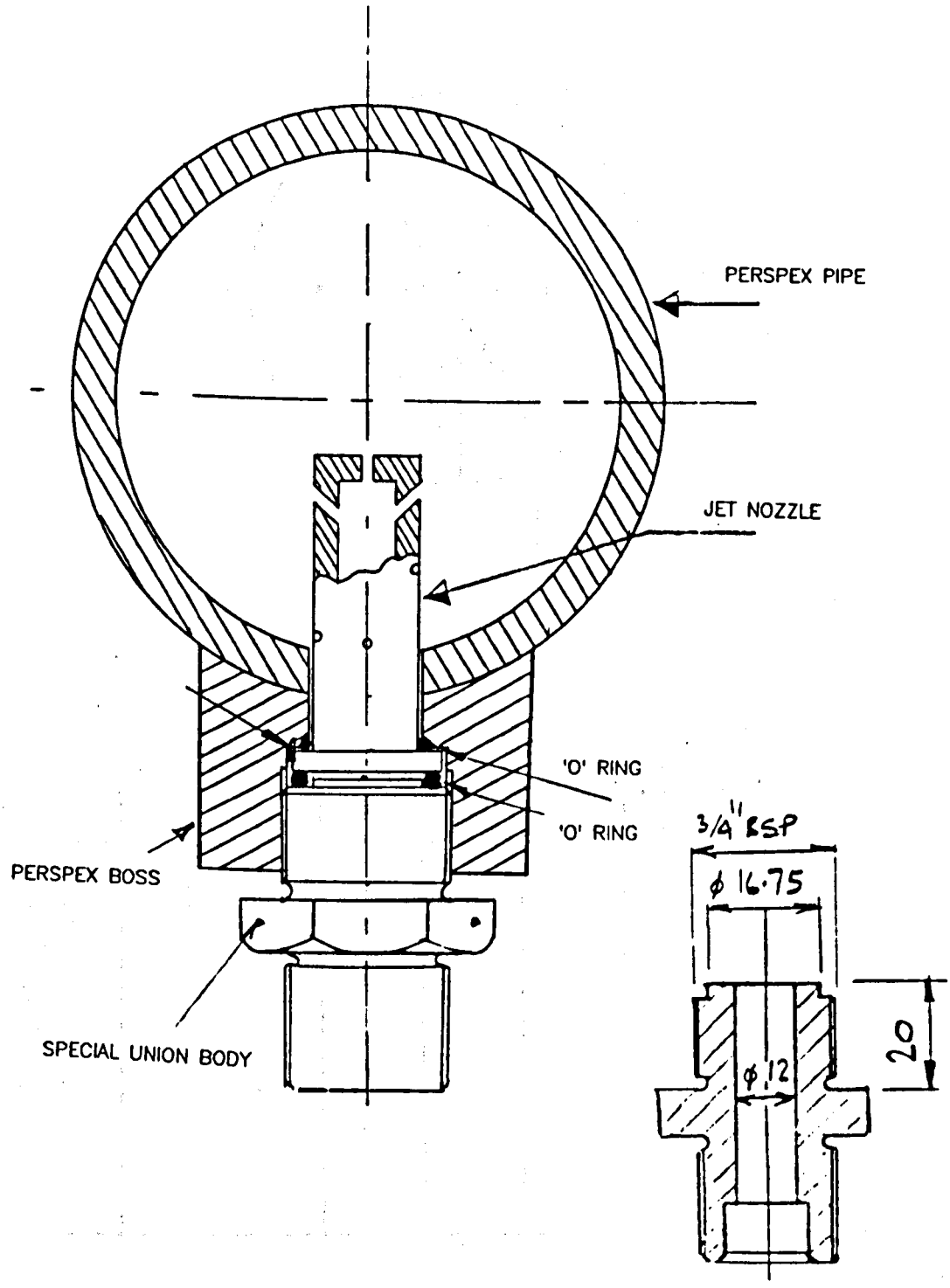

FIG. 7.2.2 JET NOZZLE ASSEMBLY AND BOSS

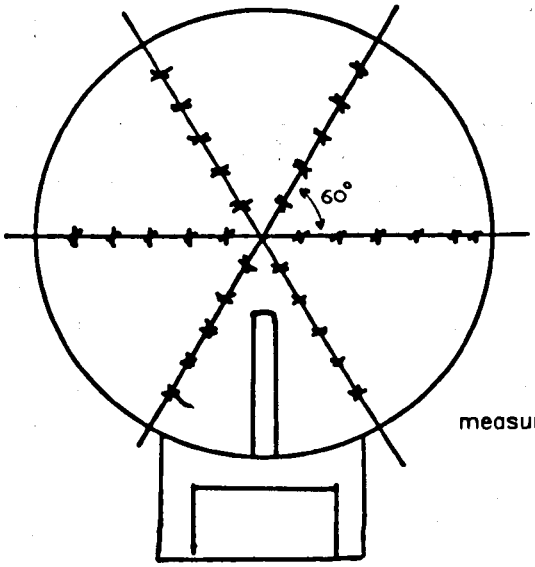

measuring points along diameters

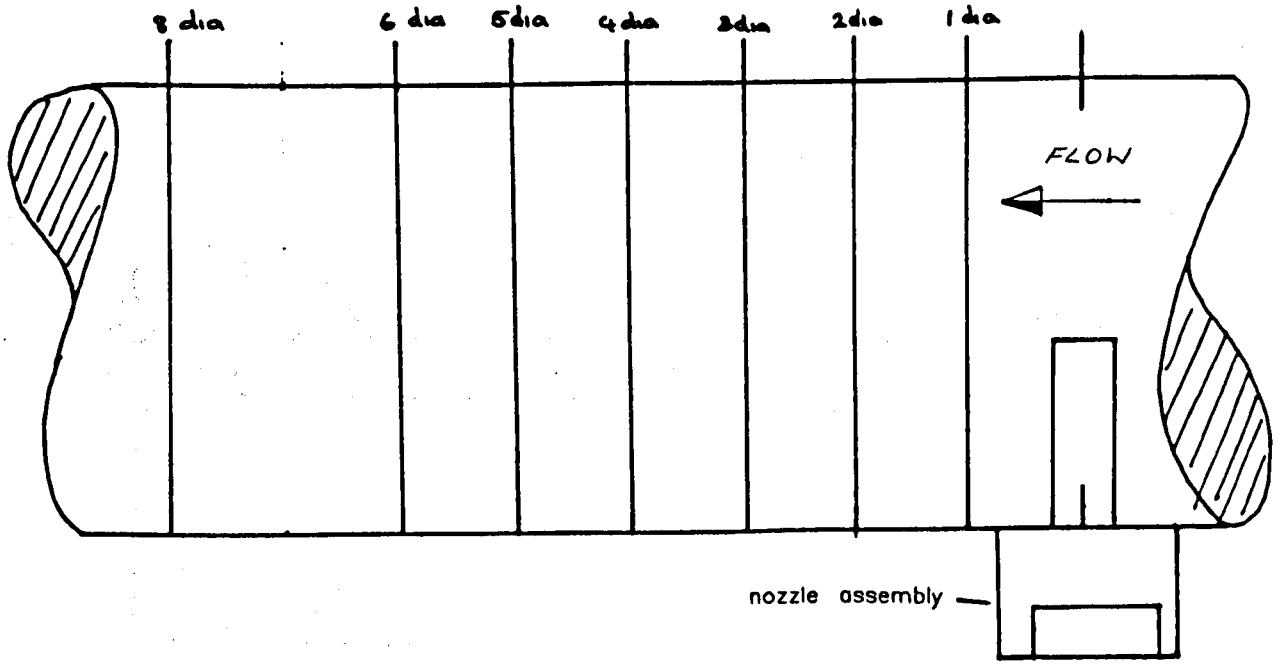

FIG. 7.3 LOCATIONS OF MEASURING POINTS AND SECTIONS

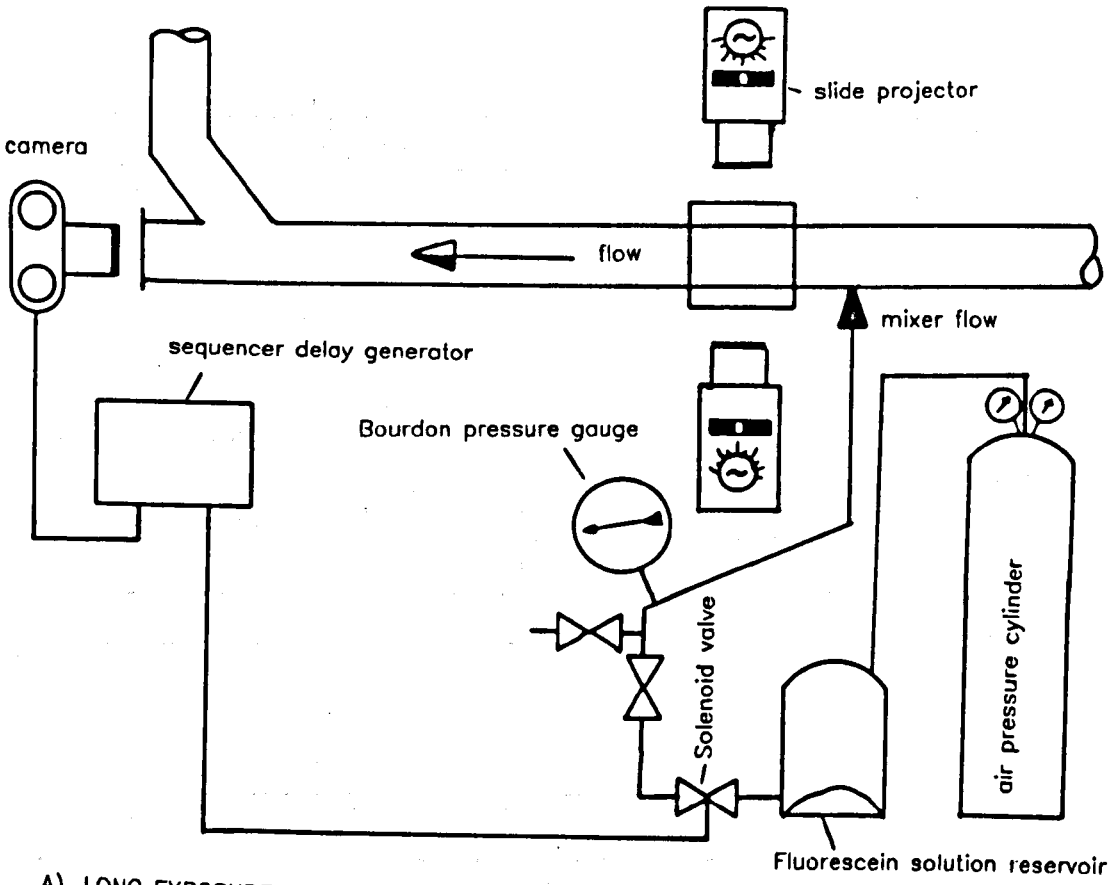

A). LONG EXPOSURE ARRANGEMENT

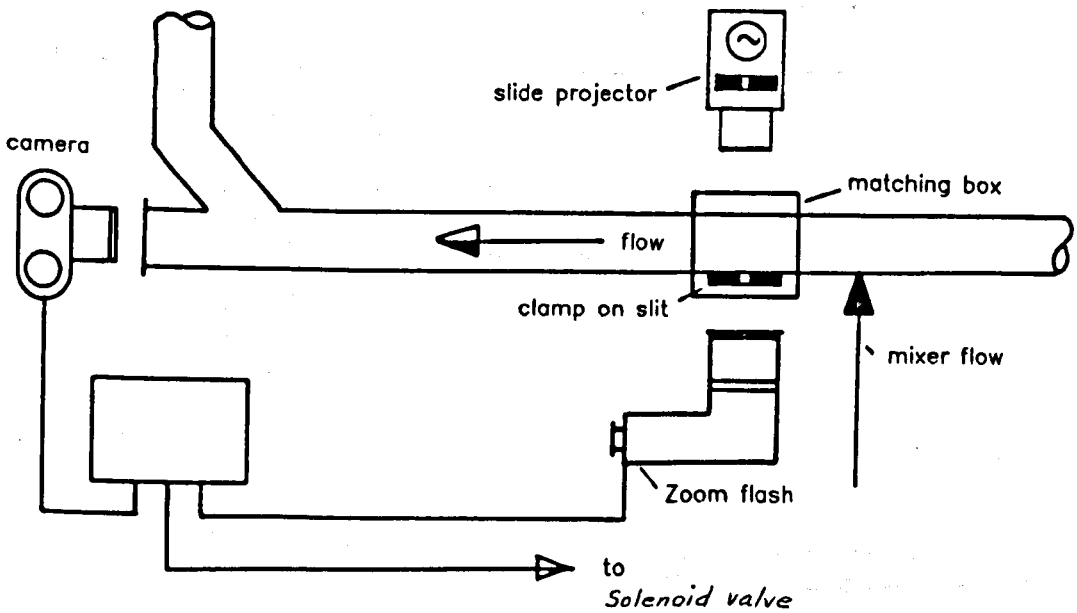

B) INSTANTANEOUS EXPOSURE ARRANGEMENT

FIG. 7.4 ARRANGEMENT OF THE TEST SECTION FOR FLOW VISUALISATION

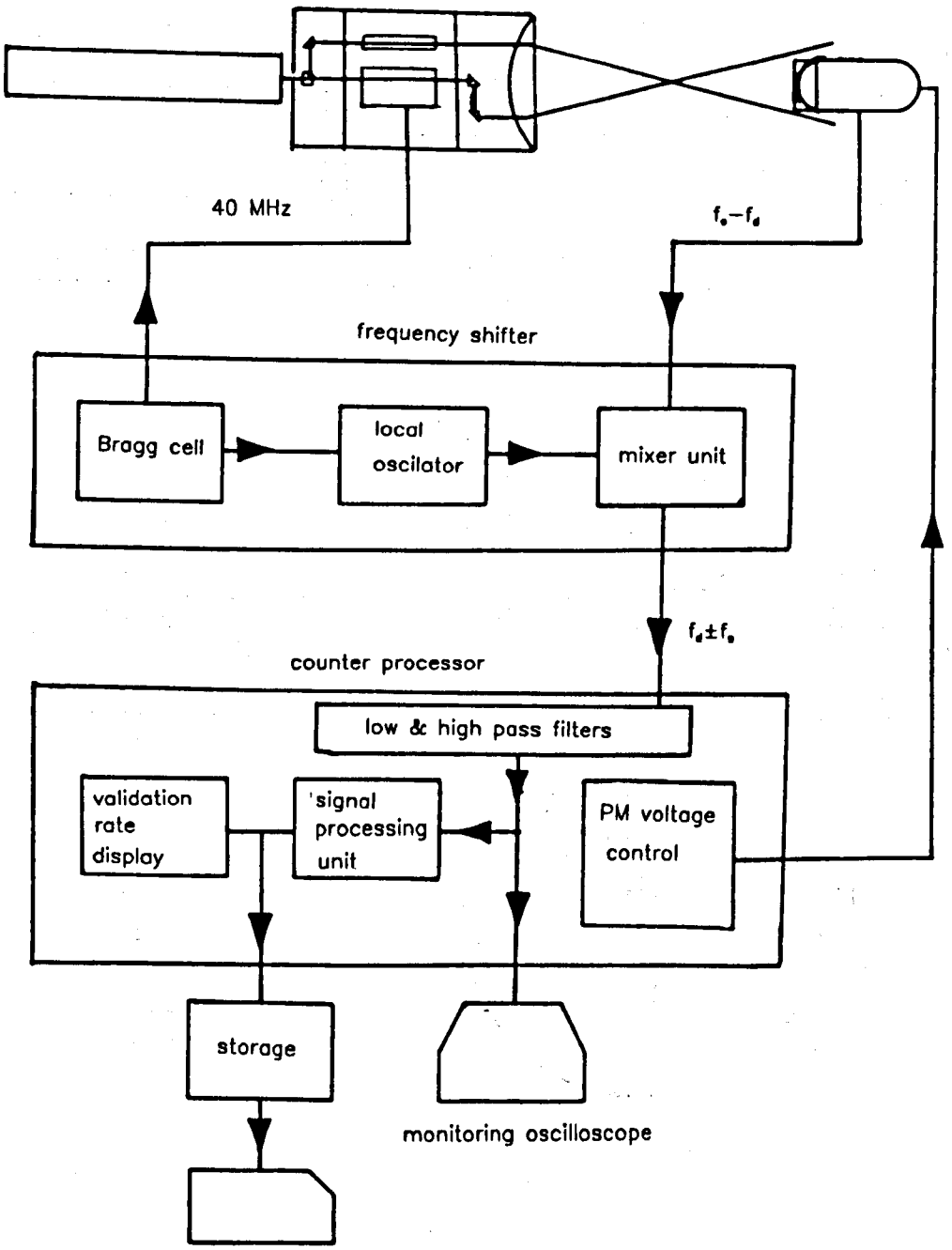

FIG. 7.5 SCHEMATIC DIAGRAM OF LDA SYSTEM

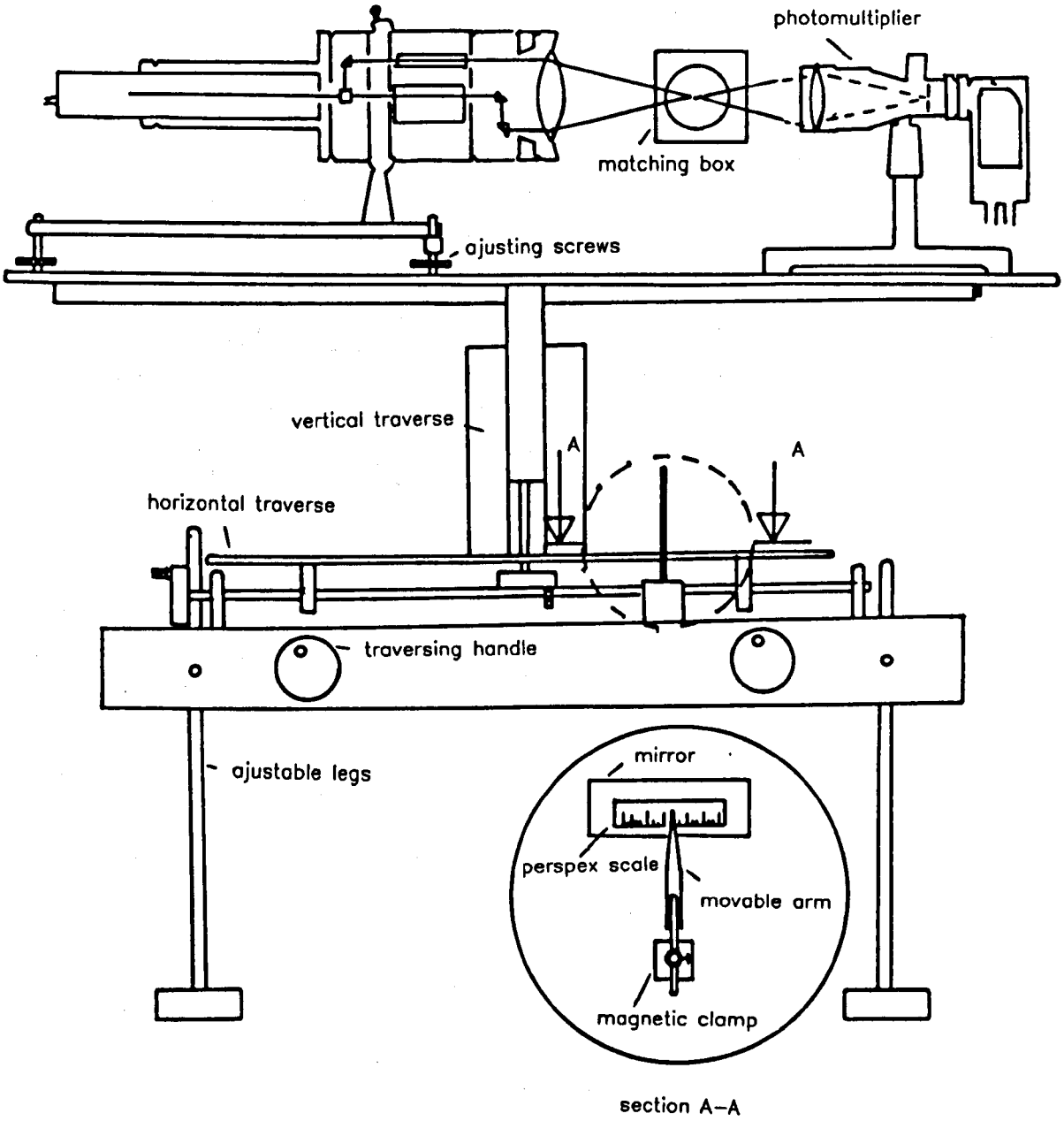

FIG. 7.6 ARRANGEMENT OF LDA OPTICS

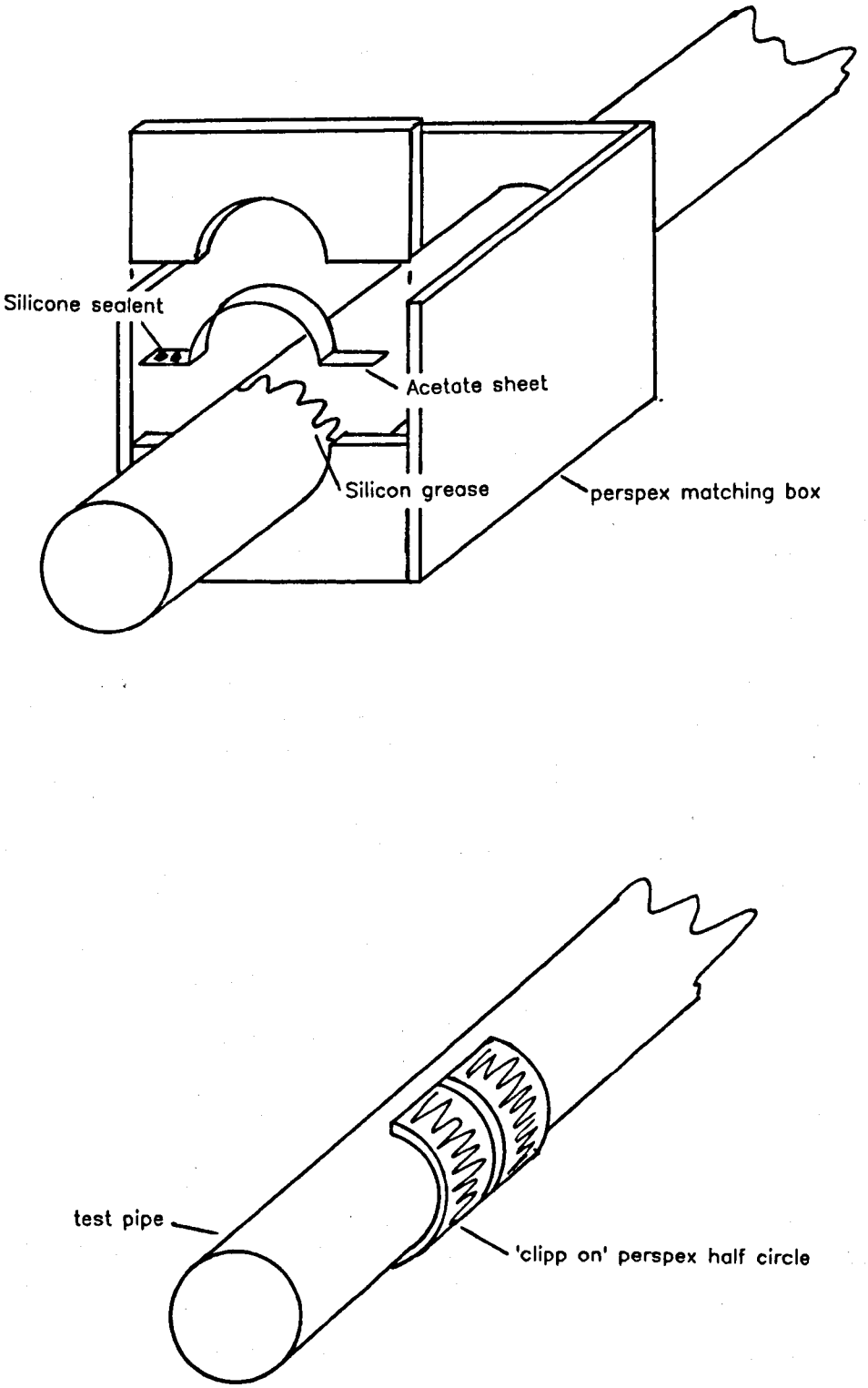

FIG. 7.7 MATCHING BOX MOUNTING DETAILS

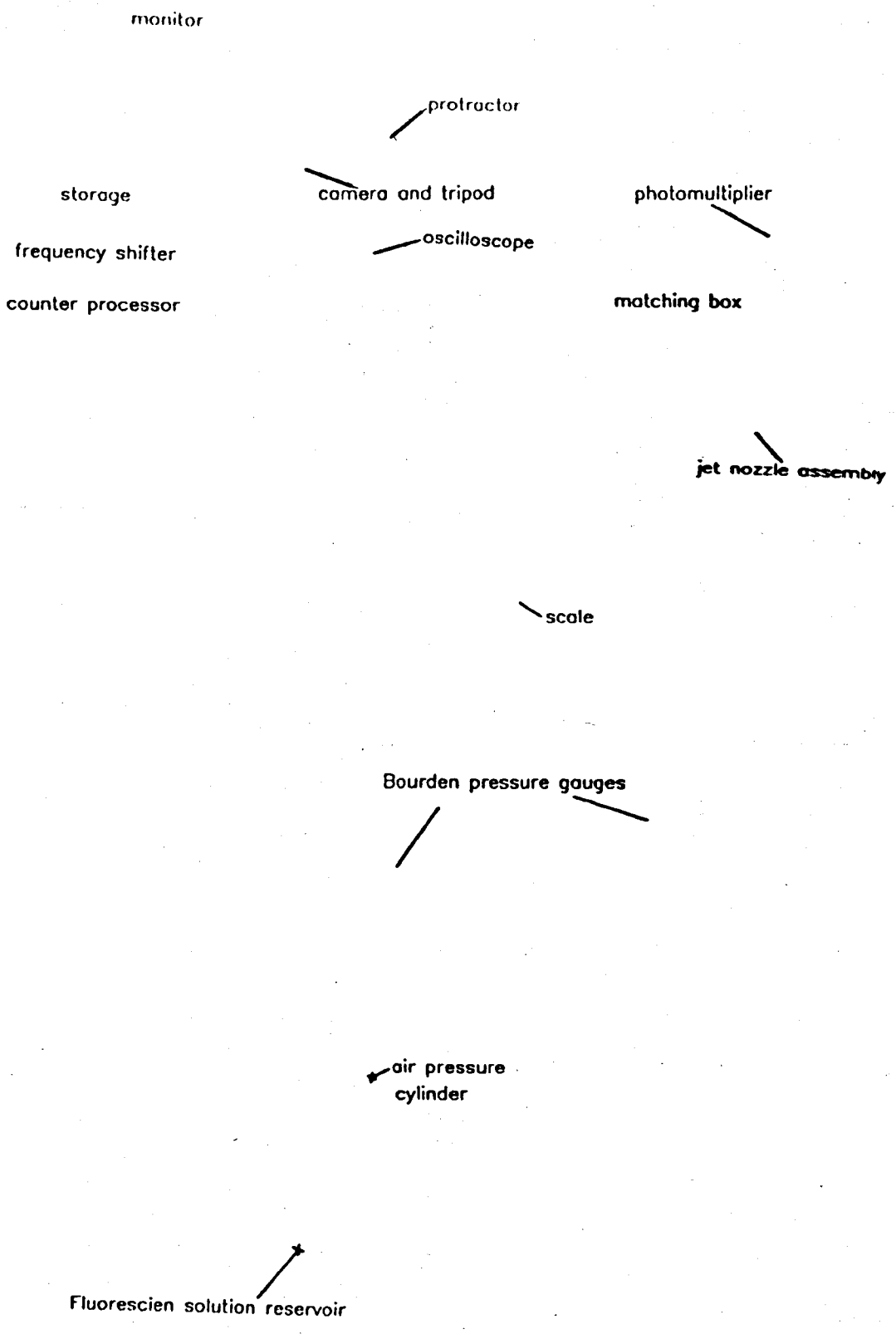
monitor
protractor
storage
camera and tripod
photomultiplier
oscilloscope
frequency shifter
counter processor
matching box
jet nozzle assembly
scale
Bourden pressure gauges
air pressure cylinder
Fluorescien solution reservoir

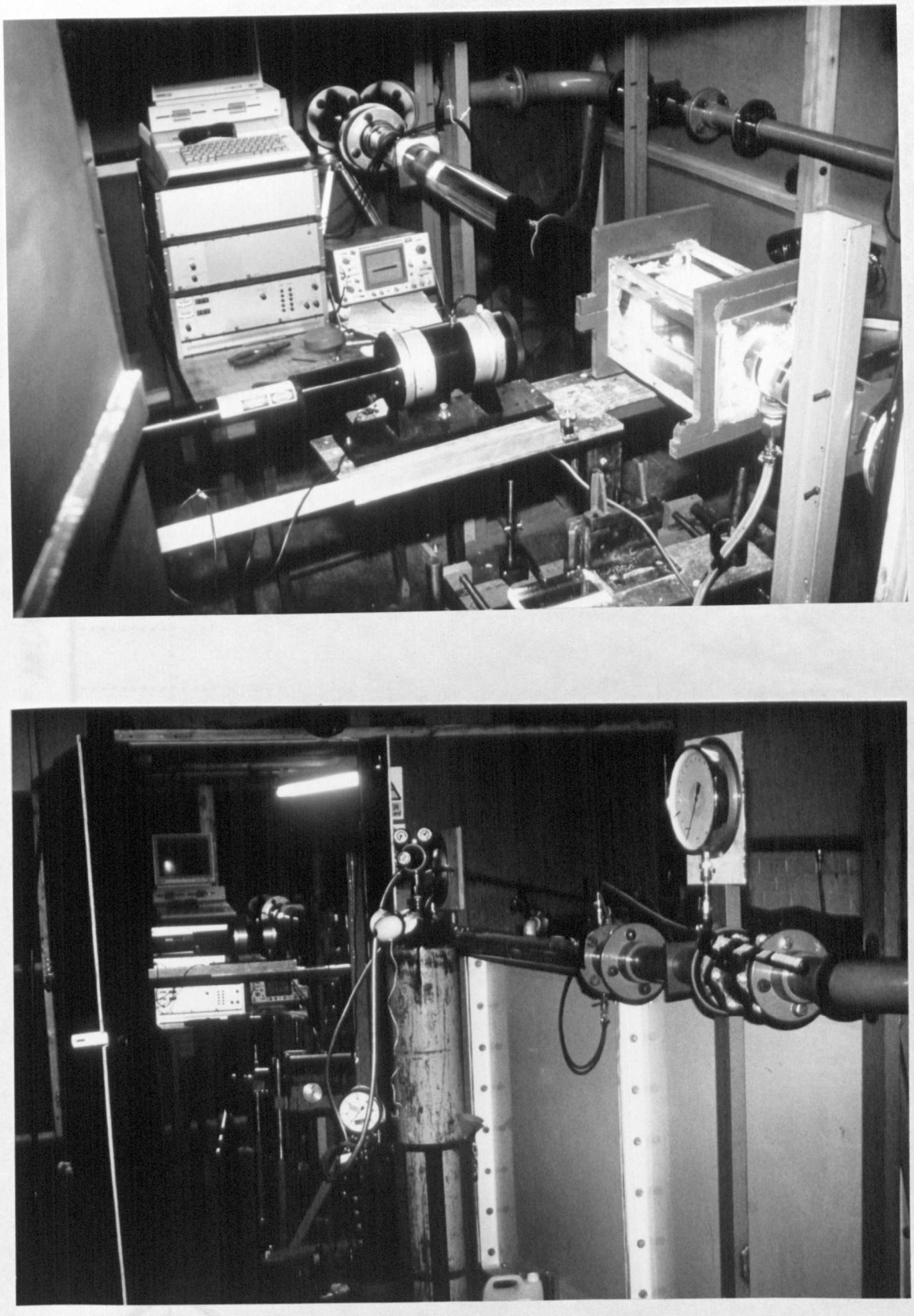

FIG. 7.8 LDA INSTRUMENTS AND THE RIG ARRANGEMENT

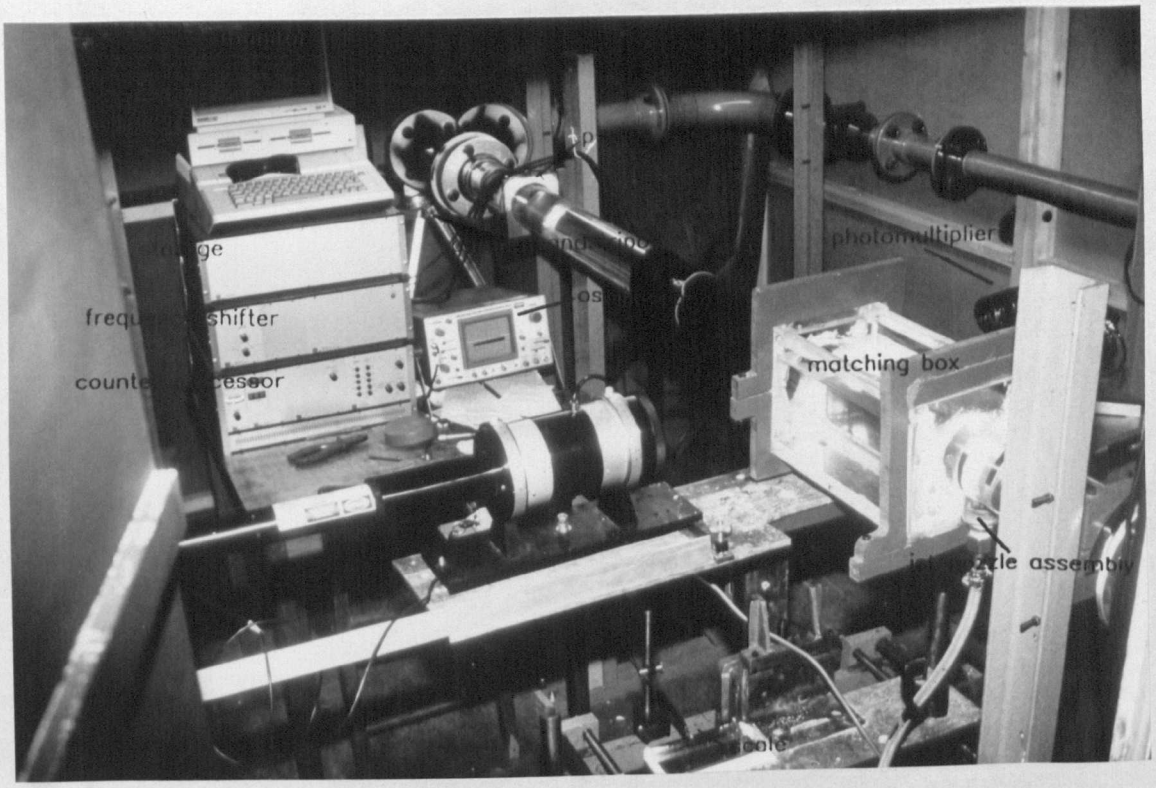

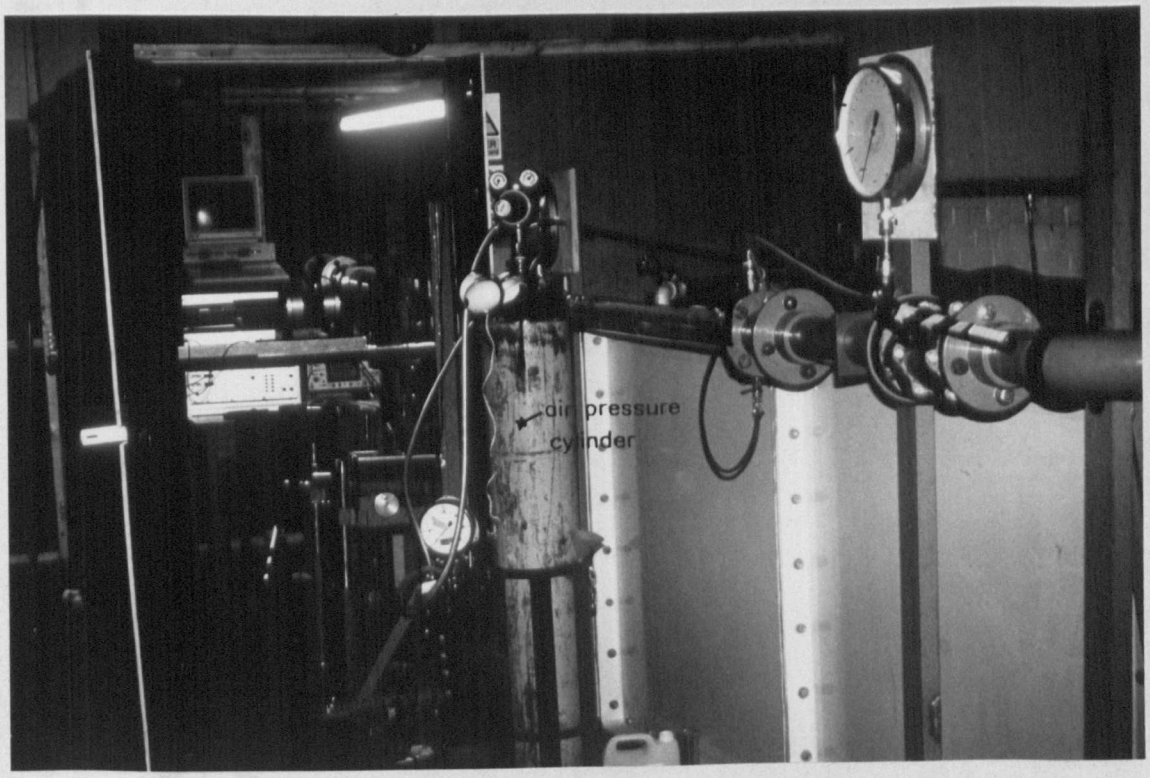

FIG. 7.8 LDA INSTRUMENTS AND THE RIG ARRANGEMENT

FIG. 7.9.1 AXIAL VELOCITY OF MULTI–NOZZLE

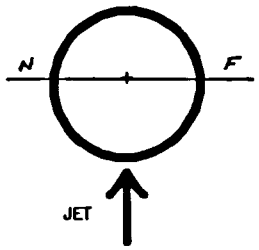

N ≡ NEAR WALL

F ≡ FAR WALL

○ 1 DIAMETER DOWNSTREAM

× 2 DIAMETERS DOWNSTREAM

✱ 3 DIAMETERS DOWNSTREAM

● 4 DIAMETERS DOWNSTREAM

△ 6 DIAMETERS DOWNSTREAM

Reynolds number = 27600

Velocity ratio = 57

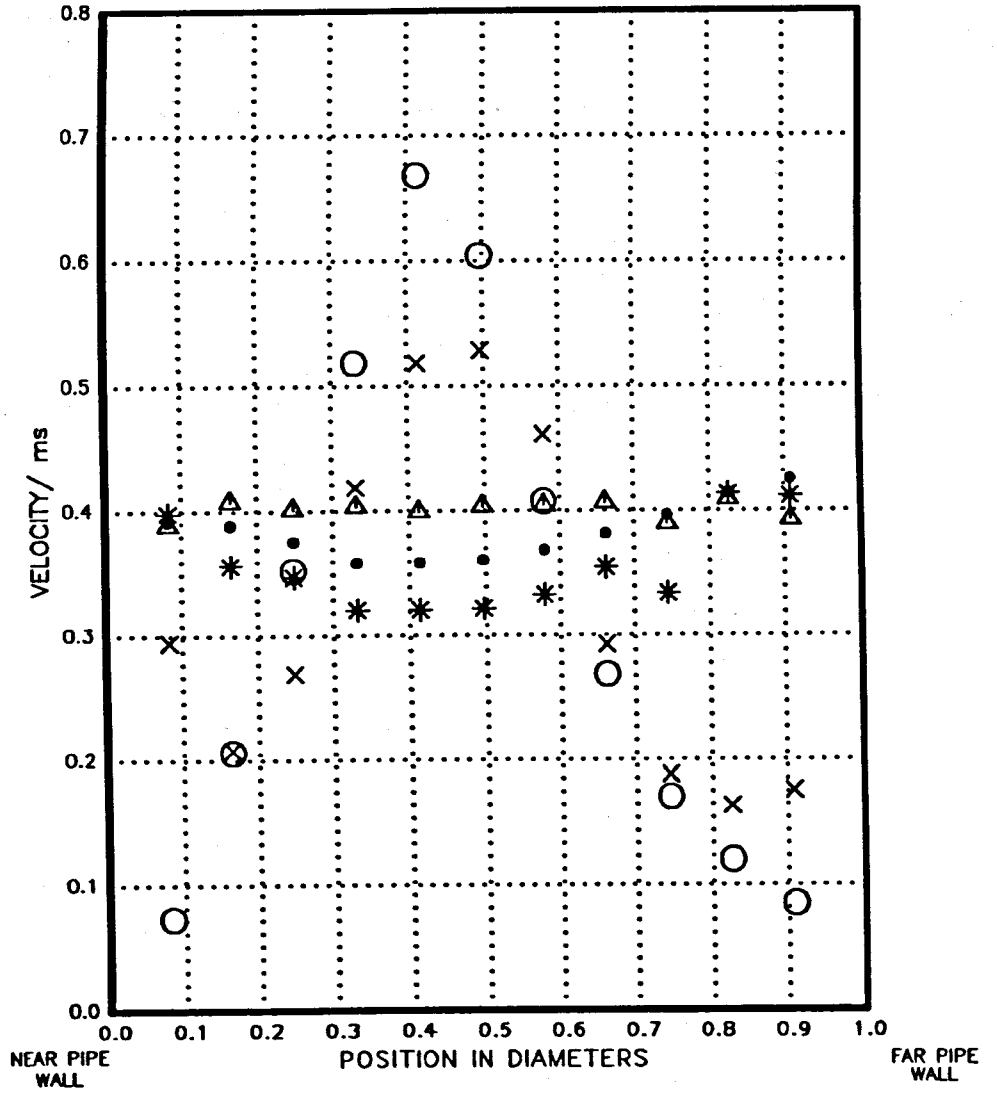

FIG. 7.9.2 AXIAL RMS VELOCITY OF MULTI–NOZZLE

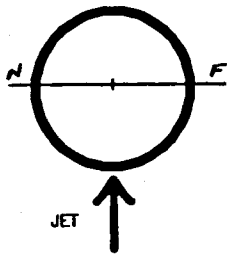

N ≡ NEAR WALL

F ≡ FAR WALL

- O 1 DIAMETER DOWNSTREAM
- × 2 DIAMETERS DOWNSTREAM
- ✱ 3 DIAMETERS DOWNSTREAM
- • 4 DIAMETERS DOWNSTREAM
- △ 6 DIAMETERS DOWNSTREAM

Reynolds number = 27600

Velocity ratio = 57

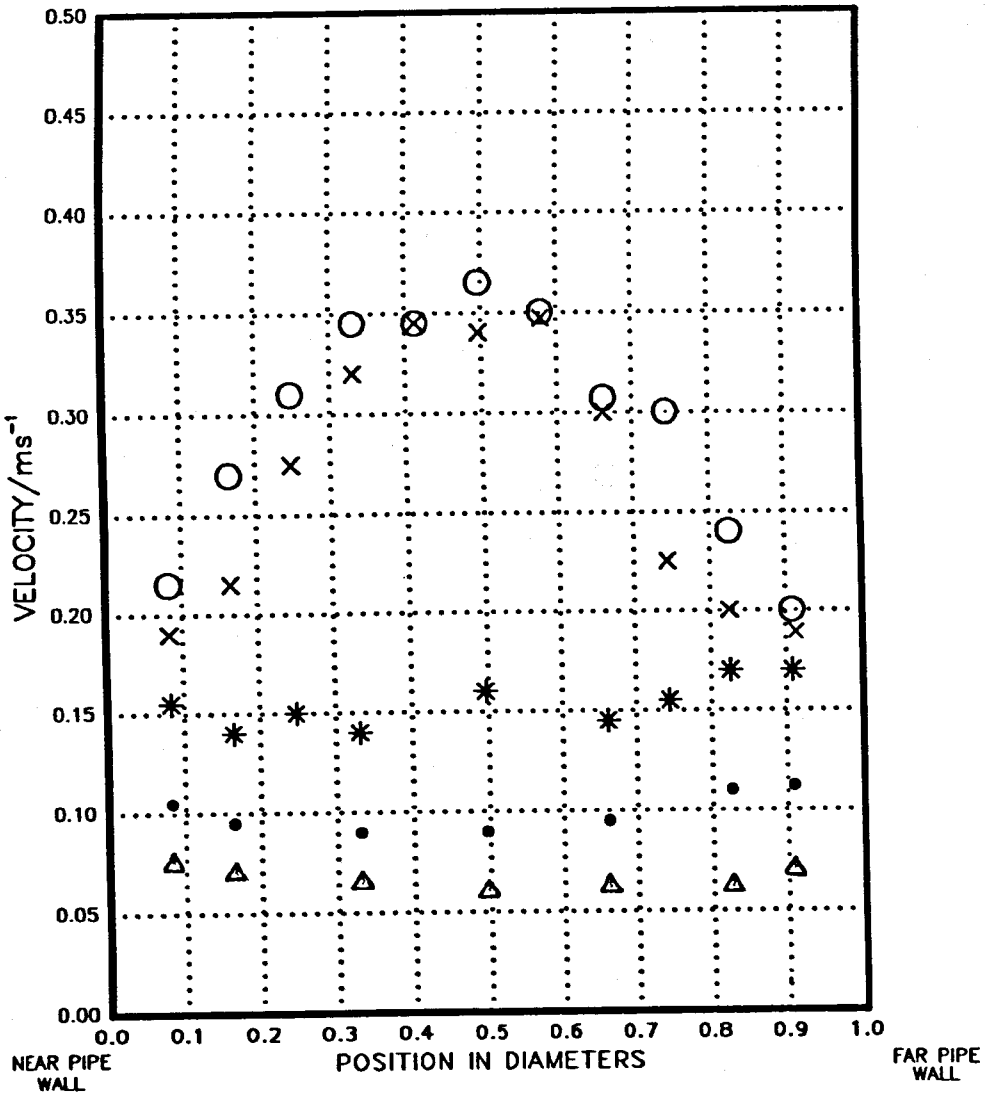

FIG. 7.9.3 TANGENTIAL VELOCITY OF MULTI–NOZZLE

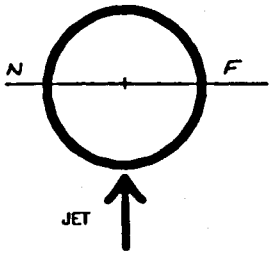

N ≡ NEAR WALL

F ≡ FAR WALL

O 1 DIAMETER DOWNSTREAM

× 2 DIAMETERS DOWNSTREAM

✱ 3 DIAMETERS DOWNSTREAM

● 4 DIAMETERS DOWNSTREAM

△ 6 DIAMETERS DOWNSTREAM

Reynolds number = 27600

Velocity ratio = 57

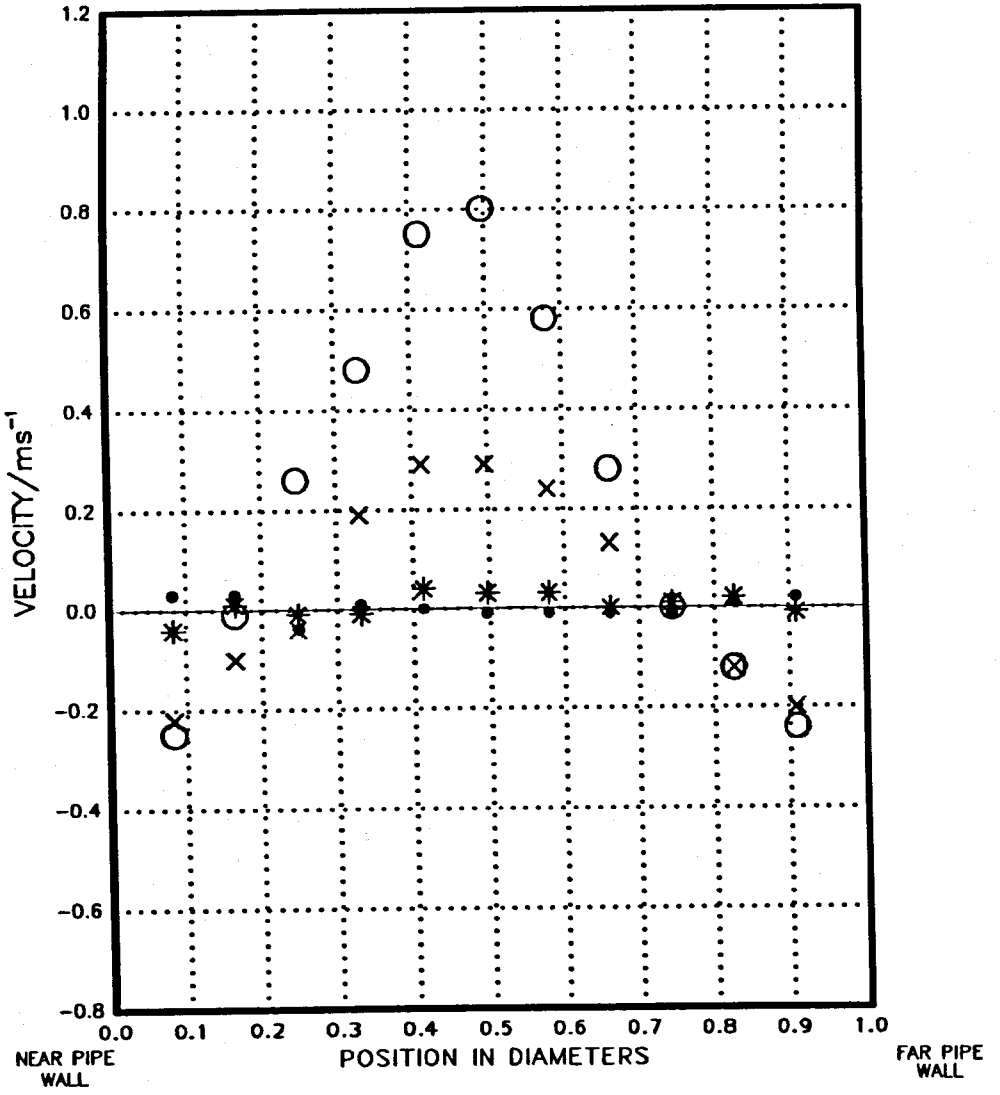

FIG. 7.9.4 TANGENTIAL RMS VELOCITY OF MULTI-NOZZLE

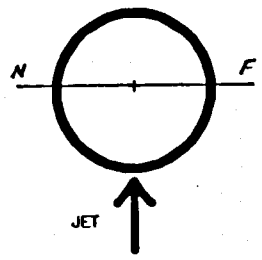

N ≡ NEAR WALL

F ≡ FAR WALL

O 1 DIAMETER DOWNSTREAM

× 2 DIAMETERS DOWNSTREAM

* 3 DIAMETERS DOWNSTREAM

• 4 DIAMETERS DOWNSTREAM

△ 6 DIAMETERS DOWNSTREAM

Reynolds number = 27600

Velocity ratio = 57

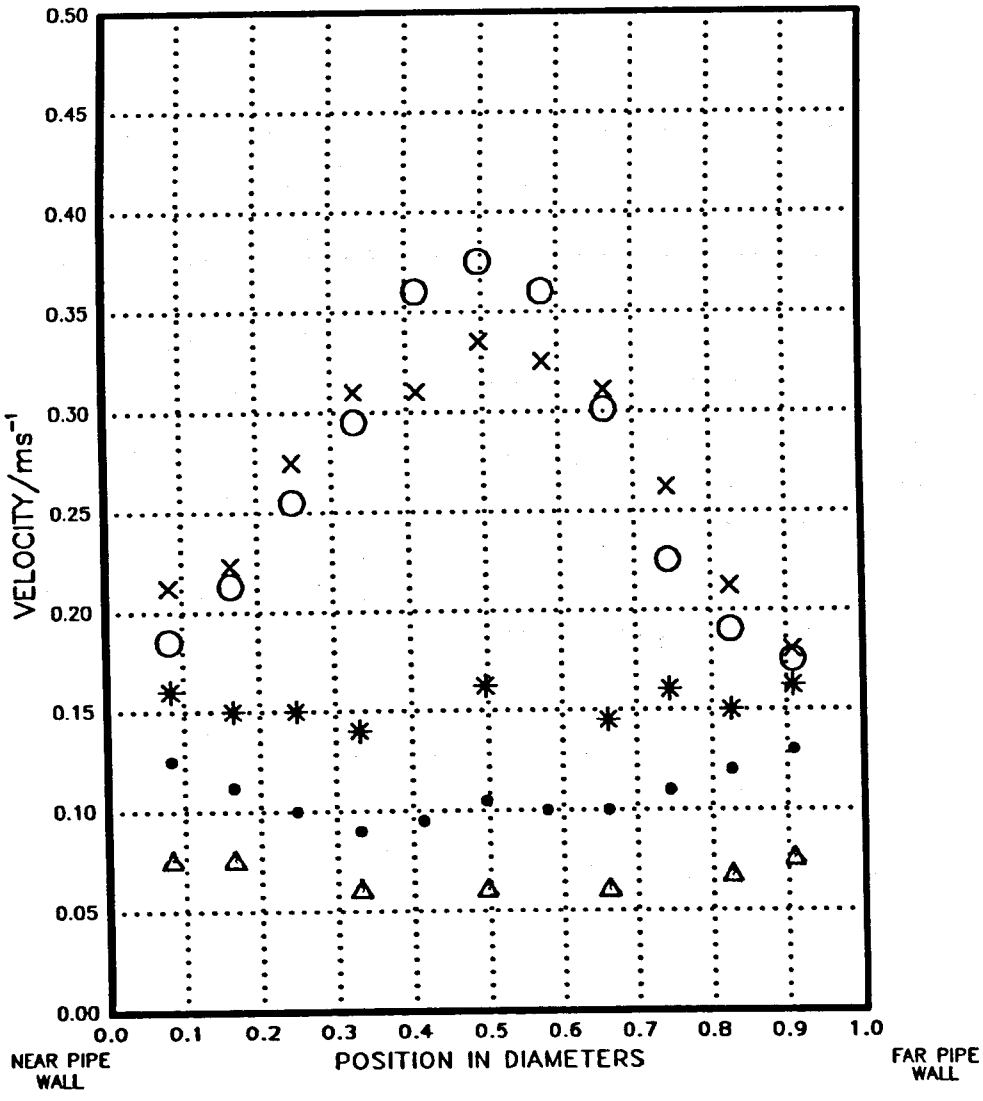

FIG. 7.9.5 AXIAL VELOCITY OF MULTI-NOZZLE

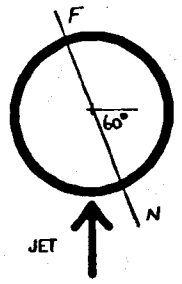

N ≡ NEAR WALL

F ≡ FAR WALL

O 1 DIAMETER DOWNSTREAM

× 2 DIAMETERS DOWNSTREAM

✱ 3 DIAMETERS DOWNSTREAM

● 4 DIAMETERS DOWNSTREAM

△ 6 DIAMETERS DOWNSTREAM

Reynolds number = 27600

Velocity ratio = 57

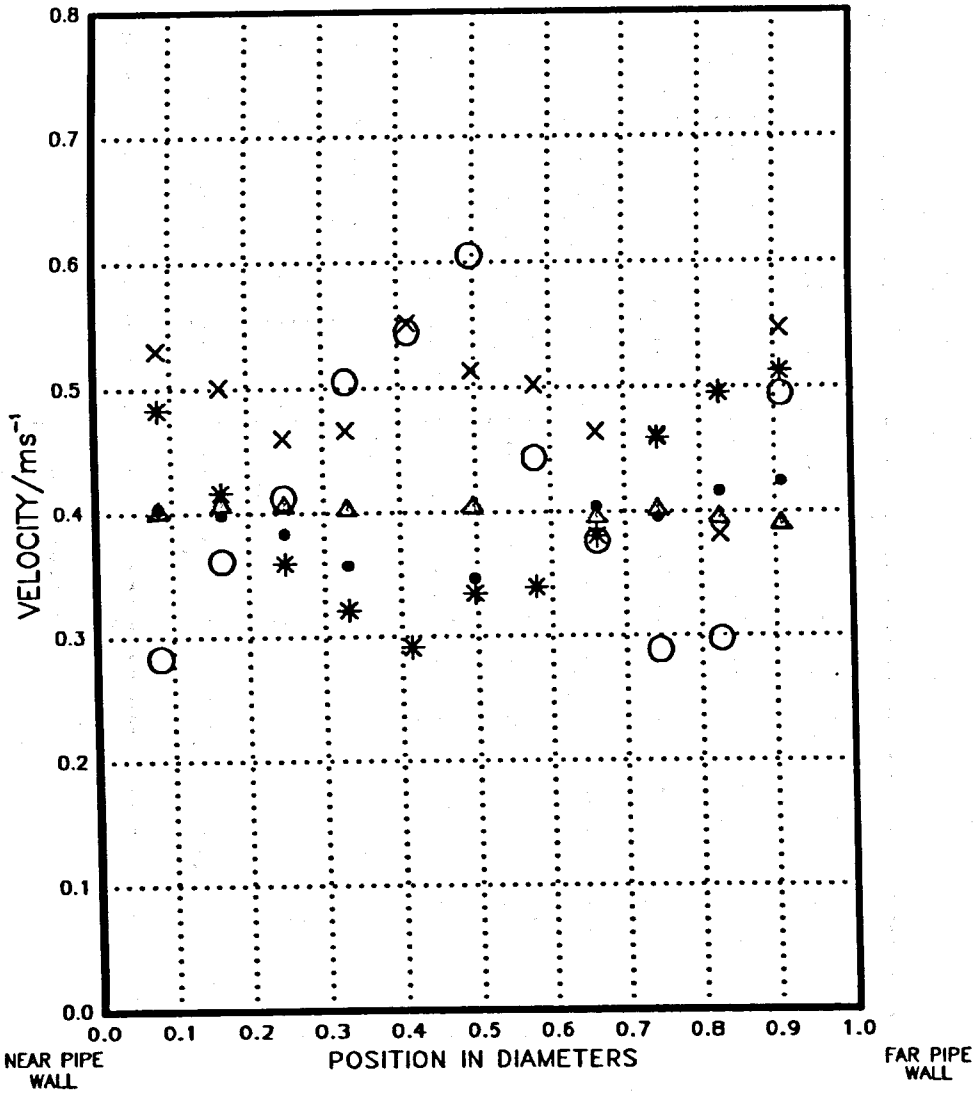

FIG. 7.9.6 AXIAL RMS VELOCITY OF MULTI NOZZLE

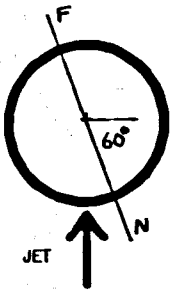

N ≡ NEAR WALL

F ≡ FAR WALL

○ 1 DIAMETER DOWNSTREAM

× 2 DIAMETERS DOWNSTREAM

✱ 3 DIAMETERS DOWNSTREAM

● 4 DIAMETERS DOWNSTREAM

△ 6 DIAMETERS DOWNSTREAM

Reynolds number = 27600

Velocity ratio = 57

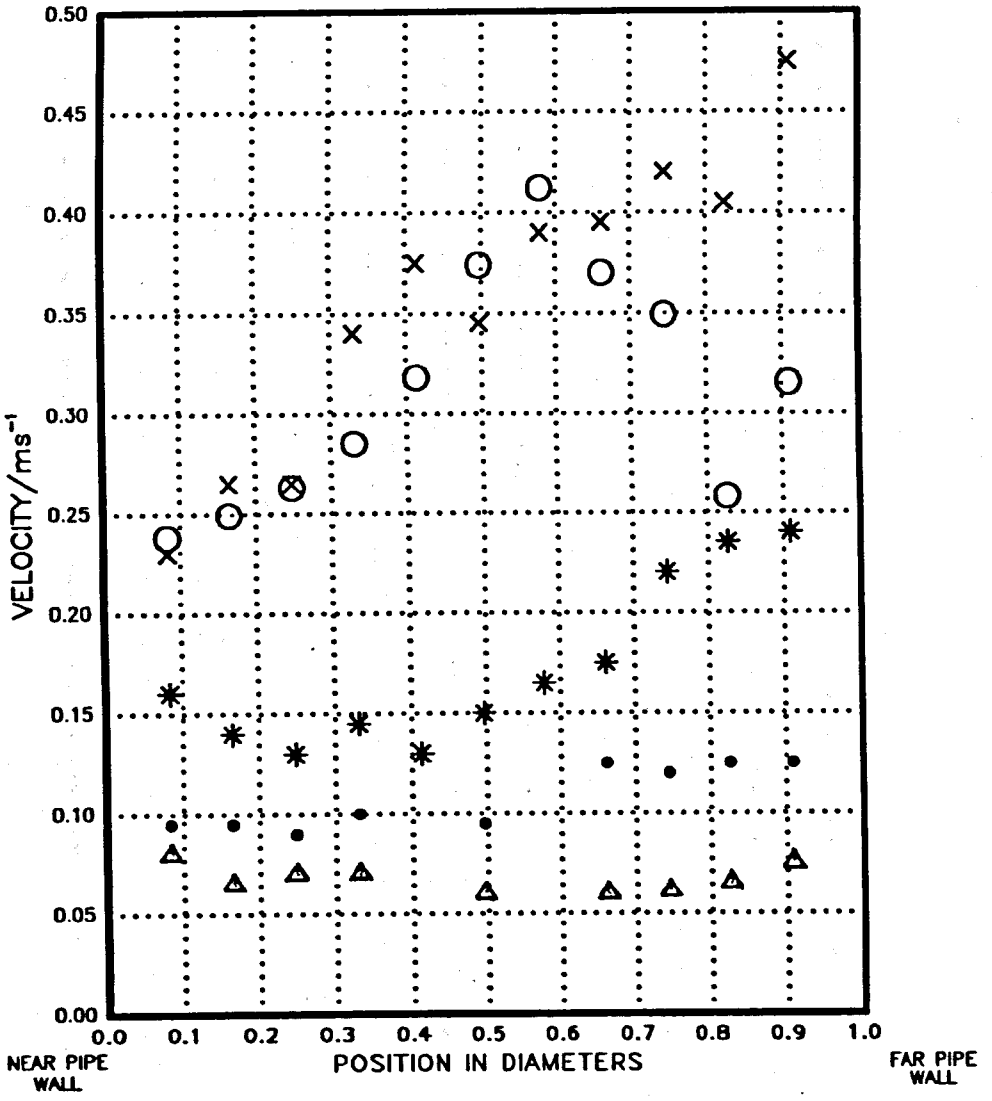

FIG. 7.9.7 TANGENTIAL VELOCITY OF MULTI–NOZZLE

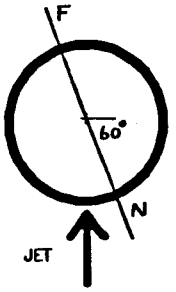

N ≡ NEAR WALL

F ≡ FAR WALL

O 1 DIAMETER DOWNSTREAM

× 2 DIAMETERS DOWNSTREAM

✱ 3 DIAMETERS DOWNSTREAM

• 4 DIAMETERS DOWNSTREAM

△ 6 DIAMETERS DOWNSTREAM

Reynolds number = 27600

Velocity ratio = 57

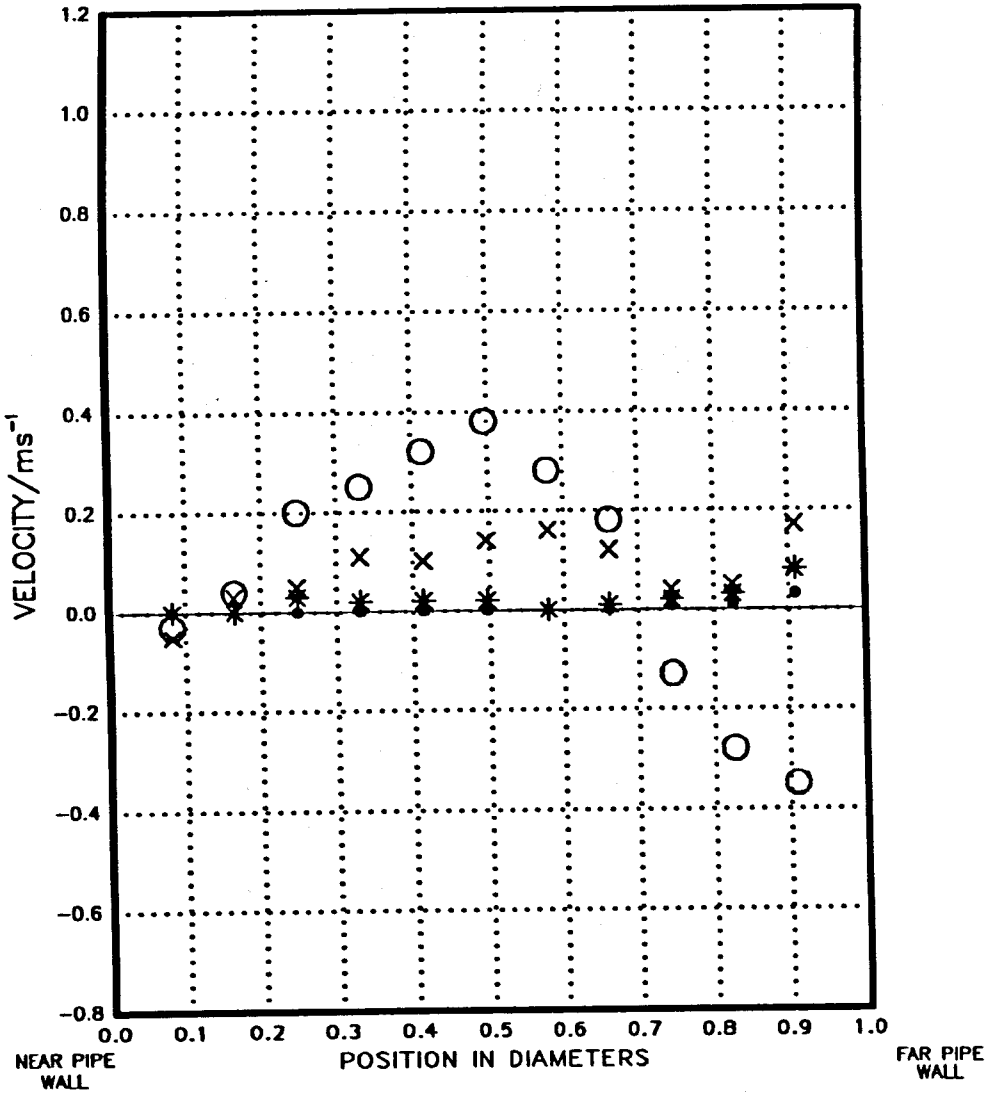

FIG. 7.9.8 TANGENTIAL RMS VELOCITY OF MULTI-NOZZLE

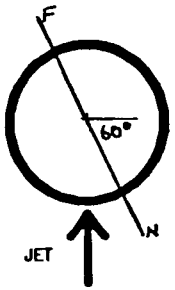

N ≡ NEAR WALL

F ≡ FAR WALL

O 1 DIAMETER DOWNSTREAM

× 2 DIAMETERS DOWNSTREAM

✱ 3 DIAMETERS DOWNSTREAM

● 4 DIAMETERS DOWNSTREAM

△ 6 DIAMETERS DOWNSTREAM

Reynolds number = 27600

Velocity ratio = 57

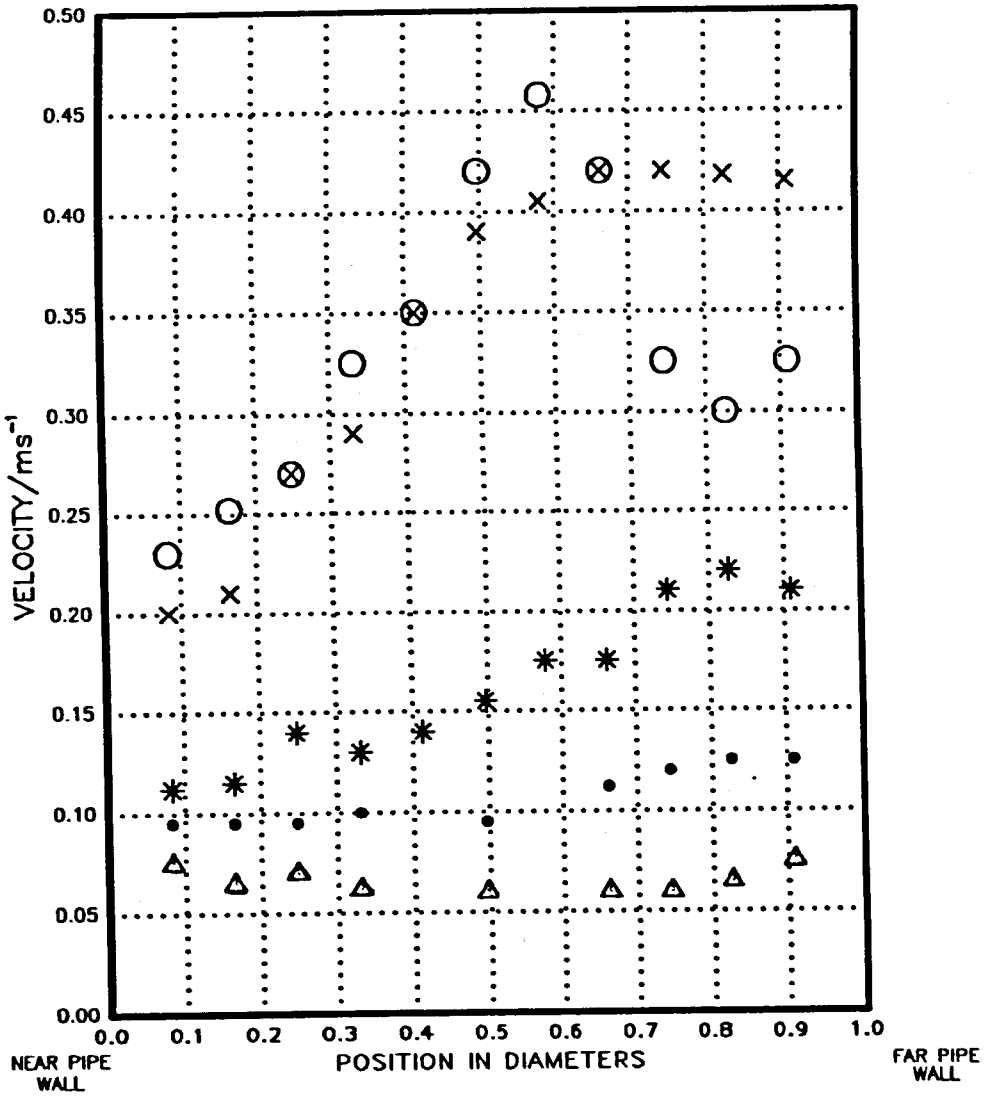

FIG. 7.9.9 AXIAL RMS VELOCITY OF MULTI-NOZZLE

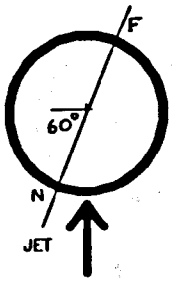

N ≡ NEAR WALL

F ≡ FAR WALL

O 1 DIAMETER DOWNSTREAM

× 2 DIAMETERS DOWNSTREAM

✱ 3 DIAMETERS DOWNSTREAM

● 4 DIAMETERS DOWNSTREAM

△ 6 DIAMETERS DOWNSTREAM

Reynolds number = 27600

Velocity ratio = 57

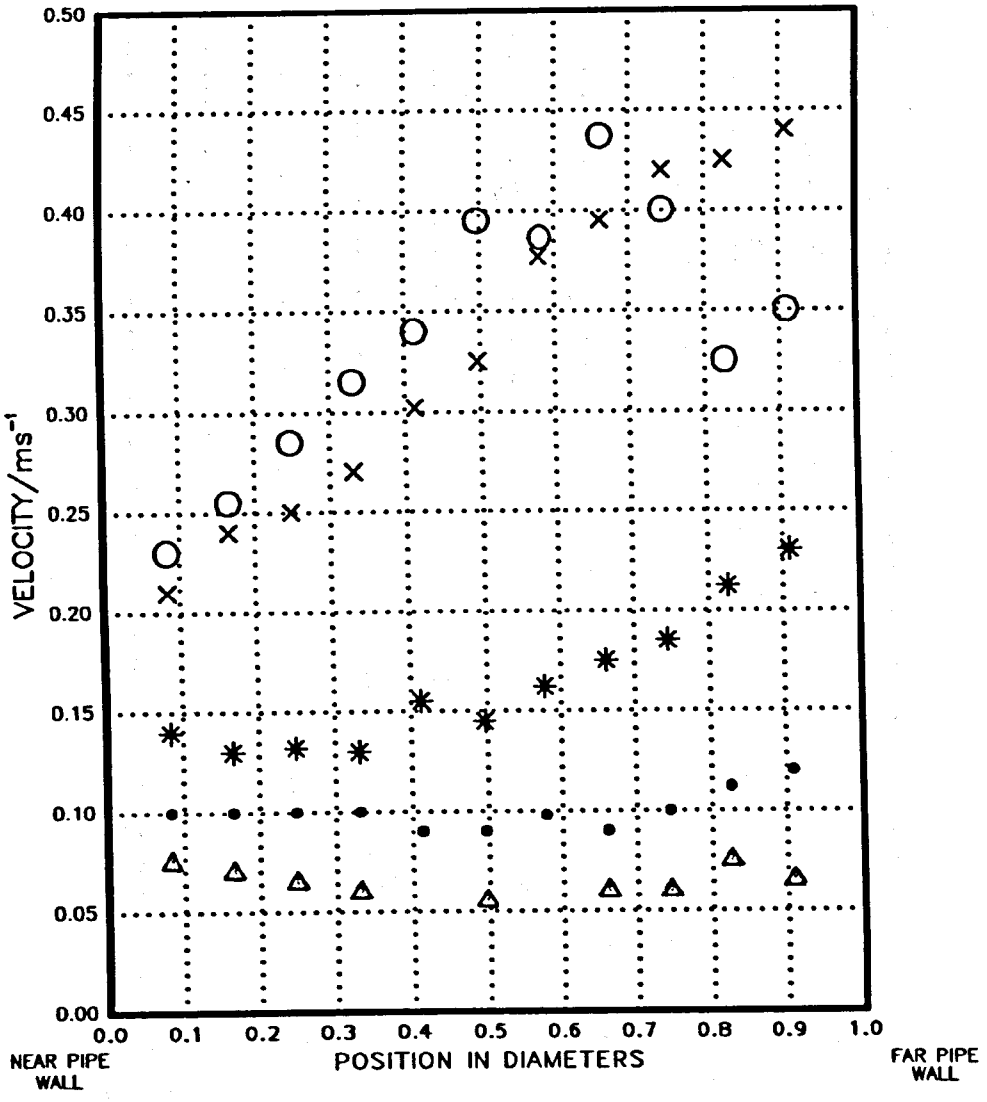

FIG. 7.9.10 TANGENTIAL RMS VELOCITY OF MULTI–NOZZLE

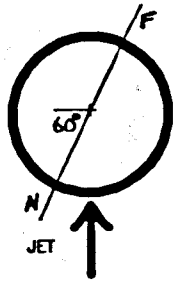

N ≡ NEAR WALL

F ≡ FAR WALL

O 1 DIAMETER DOWNSTREAM

× 2 DIAMETERS DOWNSTREAM

* 3 DIAMETERS DOWNSTREAM

• 4 DIAMETERS DOWNSTREAM

△ 6 DIAMETERS DOWNSTREAM

Reynolds number = 27600

Velocity ratio = 57

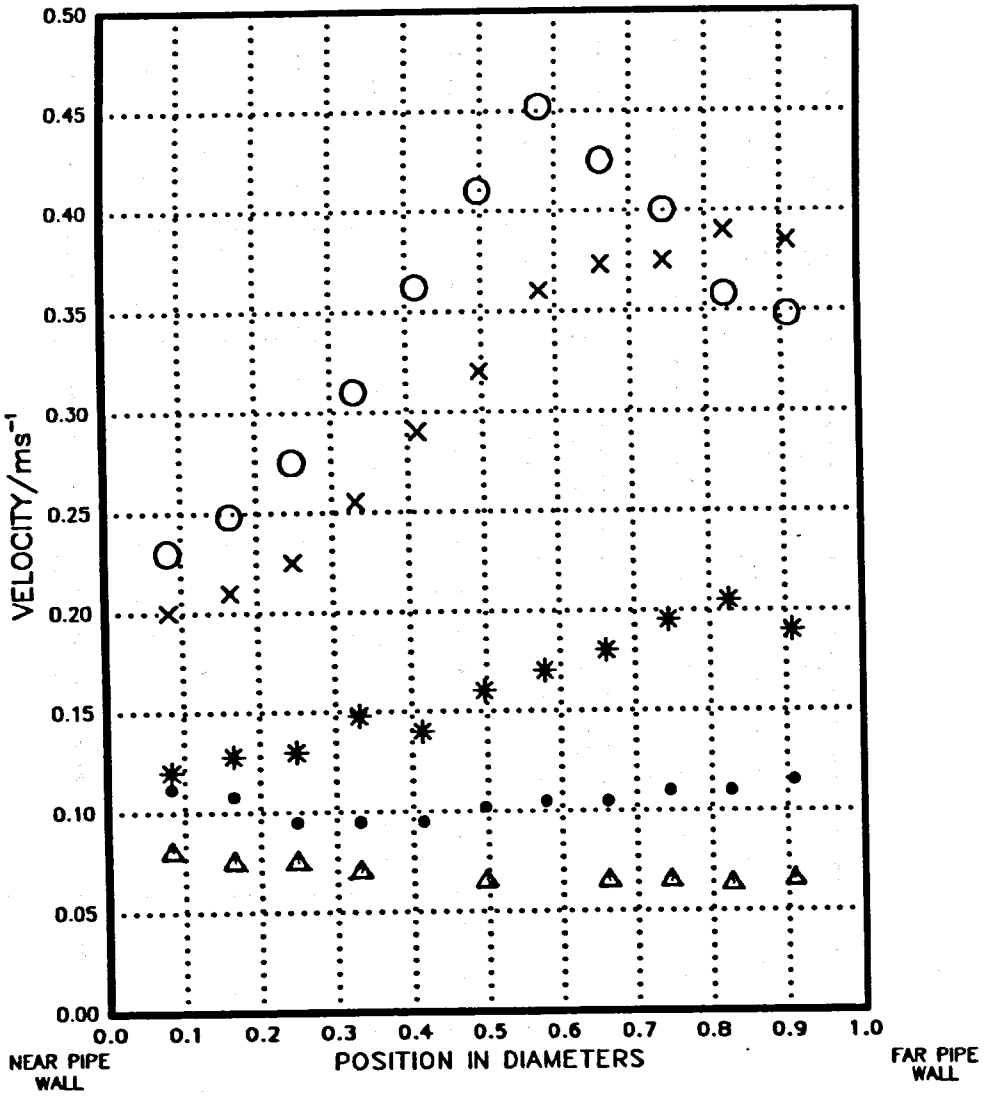

FIG. 7.9.11 AXIAL VELOCITY OF SINGLE NOZZLE

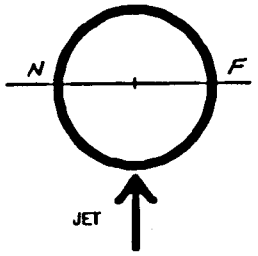

N ≡ NEAR WALL

F ≡ FAR WALL

O 1 DIAMETER DOWNSTREAM

× 2 DIAMETERS DOWNSTREAM

✱ 3 DIAMETERS DOWNSTREAM

• 4 DIAMETERS DOWNSTREAM

△ 6 DIAMETERS DOWNSTREAM

Reynolds number = 27600

Velocity ratio = 57

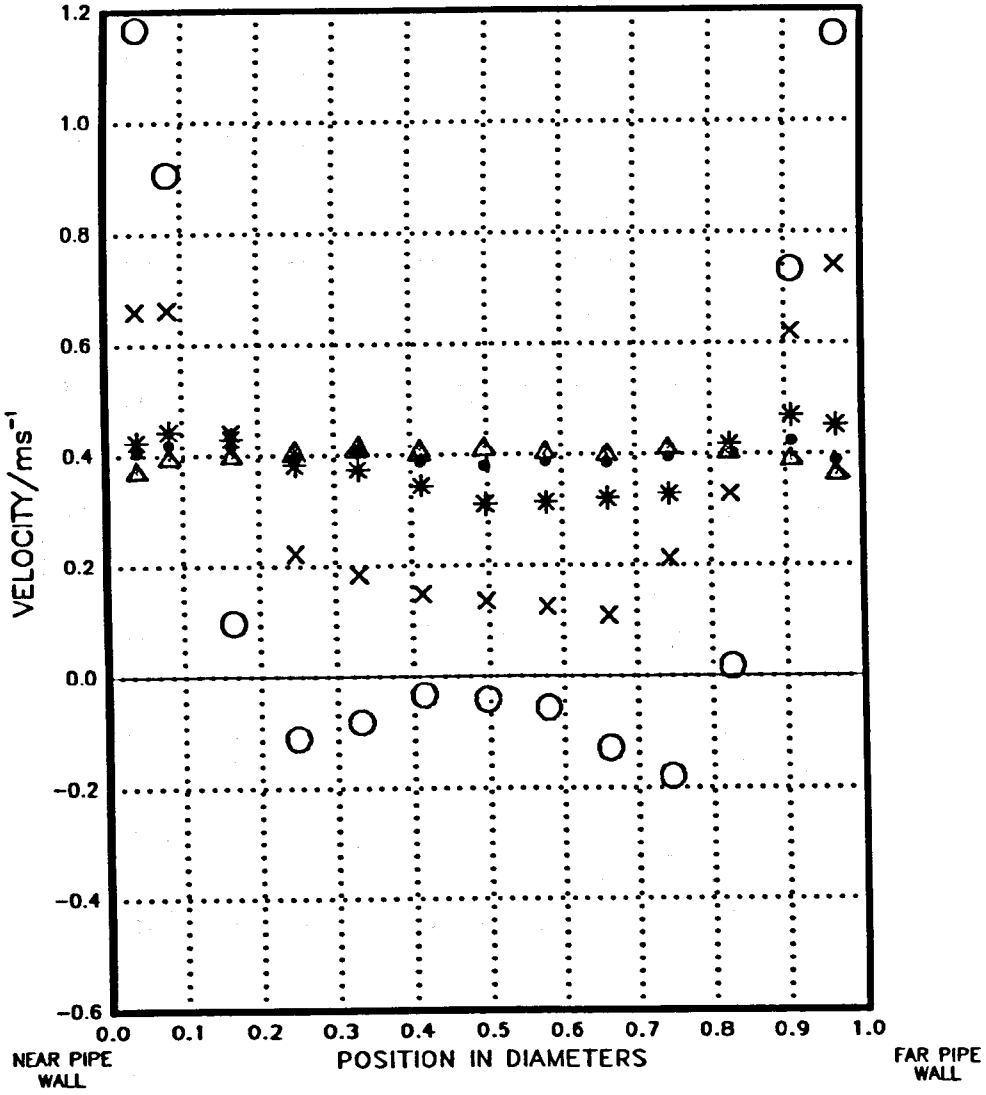

FIG. 7.9.12 AXIAL RMS VELOCITY OF SINGLE NOZZLE

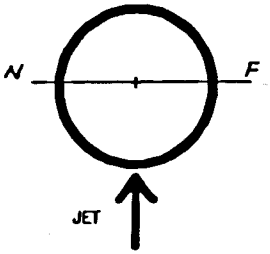

N = NEAR WALL

F = FAR WALL

O 1 DIAMETER DOWNSTREAM

× 2 DIAMETERS DOWNSTREAM

✱ 3 DIAMETERS DOWNSTREAM

• 4 DIAMETERS DOWNSTREAM

△ 6 DIAMETERS DOWNSTREAM

Reynolds number = 27600

Velocity ratio = 57

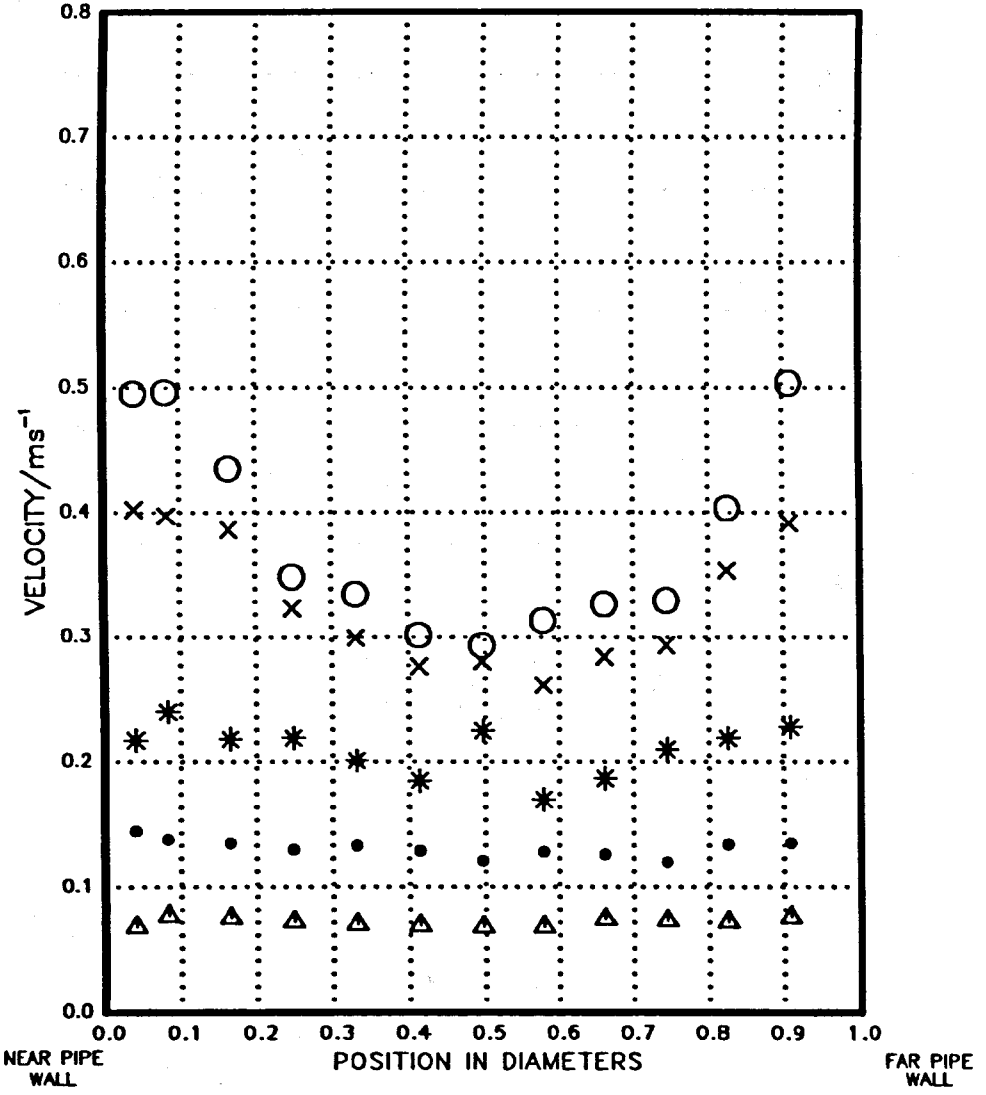

FIG. 7.9.13 TANGENTIAL VELOCITY OF SINGLE NOZZLE

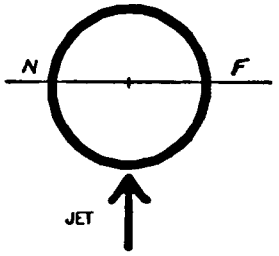

N ≡ NEAR WALL

F ≡ FAR WALL

O 1 DIAMETER DOWNSTREAM

× 2 DIAMETERS DOWNSTREAM

✱ 3 DIAMETERS DOWNSTREAM

● 4 DIAMETERS DOWNSTREAM

△ 6 DIAMETERS DOWNSTREAM

Reynolds number = 27600

Velocity ratio = 57

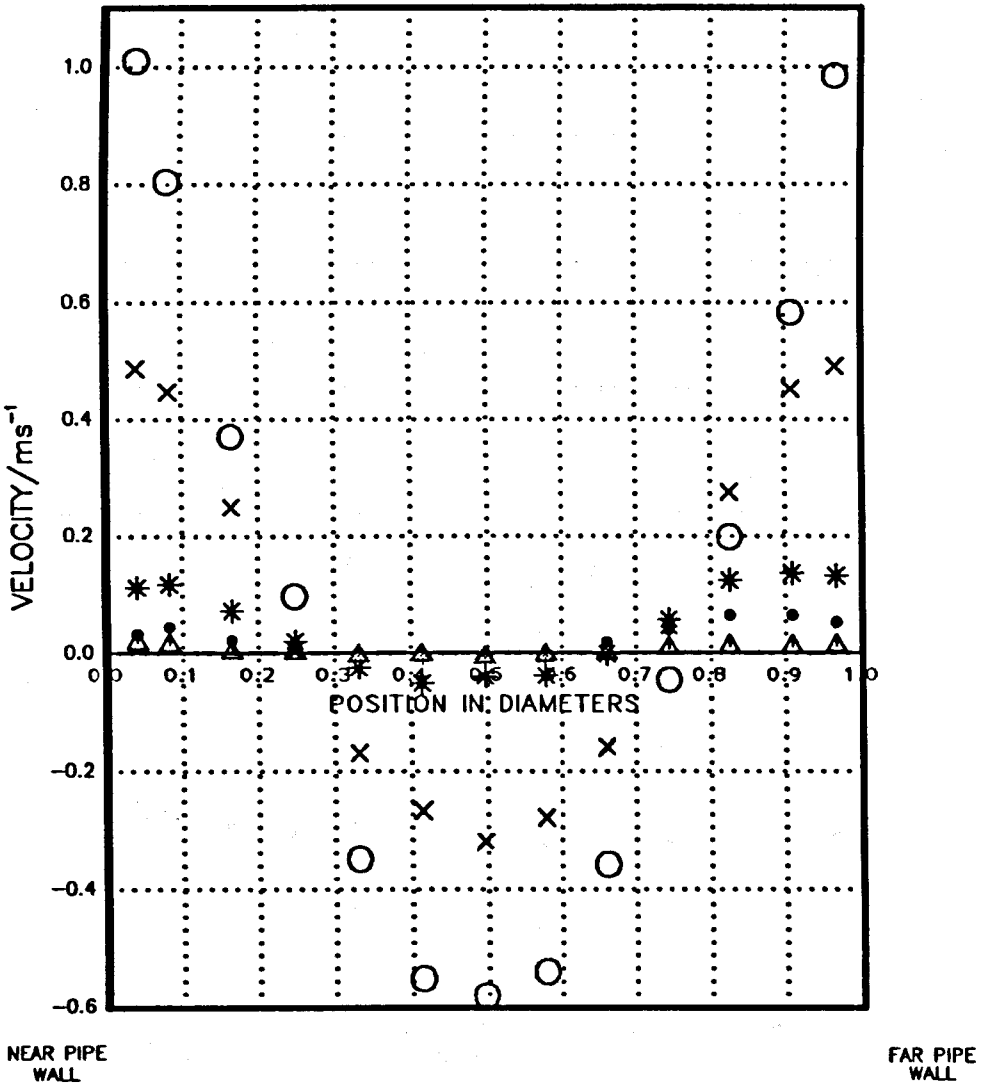

FIG. 7.9.14 TANGENTIAL RMS VELOCITY OF SINGLE NOZZLE

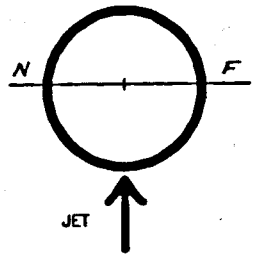

N ≡ NEAR WALL

F ≡ FAR WALL

○ 1 DIAMETER DOWNSTREAM

× 2 DIAMETERS DOWNSTREAM

✱ 3 DIAMETERS DOWNSTREAM

● 4 DIAMETERS DOWNSTREAM

△ 6 DIAMETERS DOWNSTREAM

Reynolds number = 27600

Velocity ratio = 57

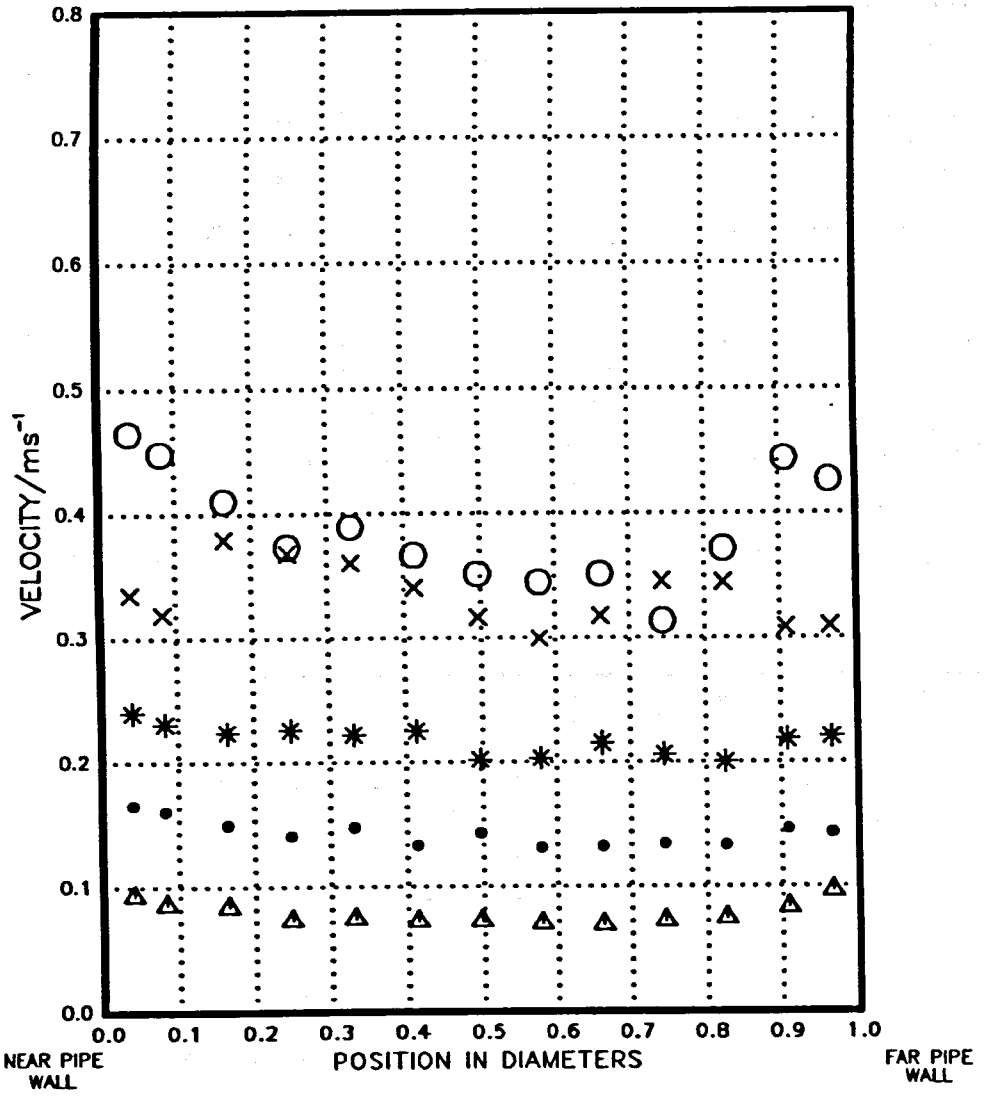

FIG. 7.9.15 AXIAL VELOCITY OF SINGLE NOZZLE

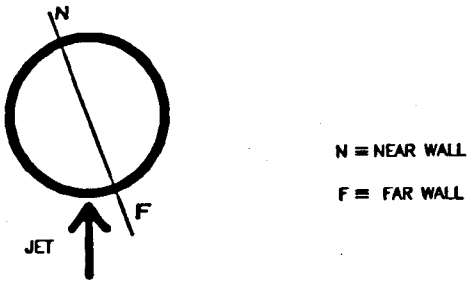

N ≡ NEAR WALL

F ≡ FAR WALL

O 1 DIAMETER DOWNSTREAM

× 2 DIAMETERS DOWNSTREAM

✱ 3 DIAMETERS DOWNSTREAM

● 4 DIAMETERS DOWNSTREAM

△ 6 DIAMETERS DOWNSTREAM

Reynolds number = 27600

Velocity ratio = 57

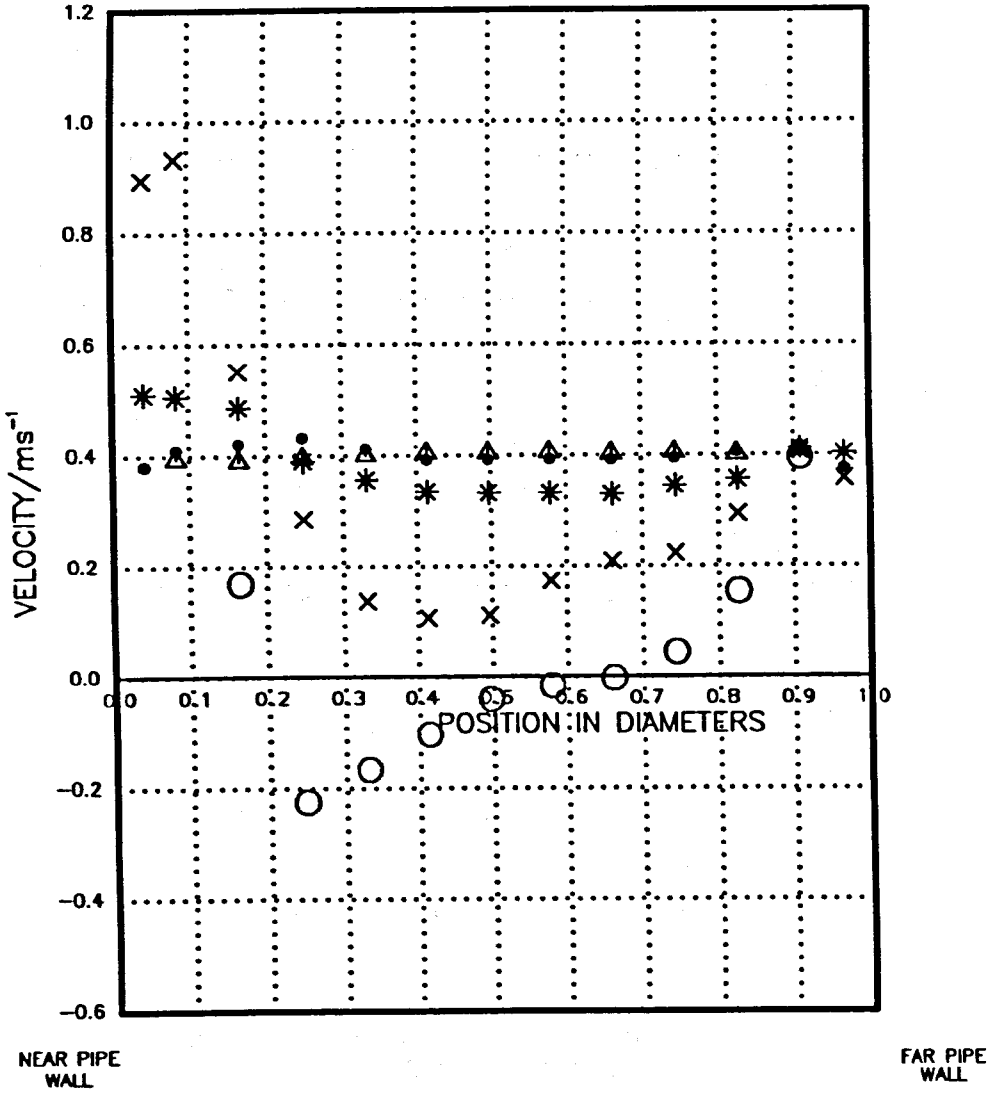

FIG. 7.9.16 AXIAL RMS VELOCITY OF SINGLE NOZZLE

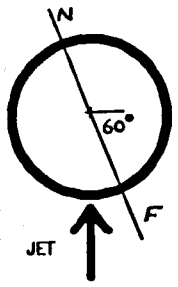

N ≡ NEAR WALL

F ≡ FAR WALL

O 1 DIAMETER DOWNSTREAM

× 2 DIAMETERS DOWNSTREAM

✱ 3 DIAMETERS DOWNSTREAM

● 4 DIAMETERS DOWNSTREAM

△ 6 DIAMETERS DOWNSTREAM

Reynolds number = 27600

Velocity ratio = 57

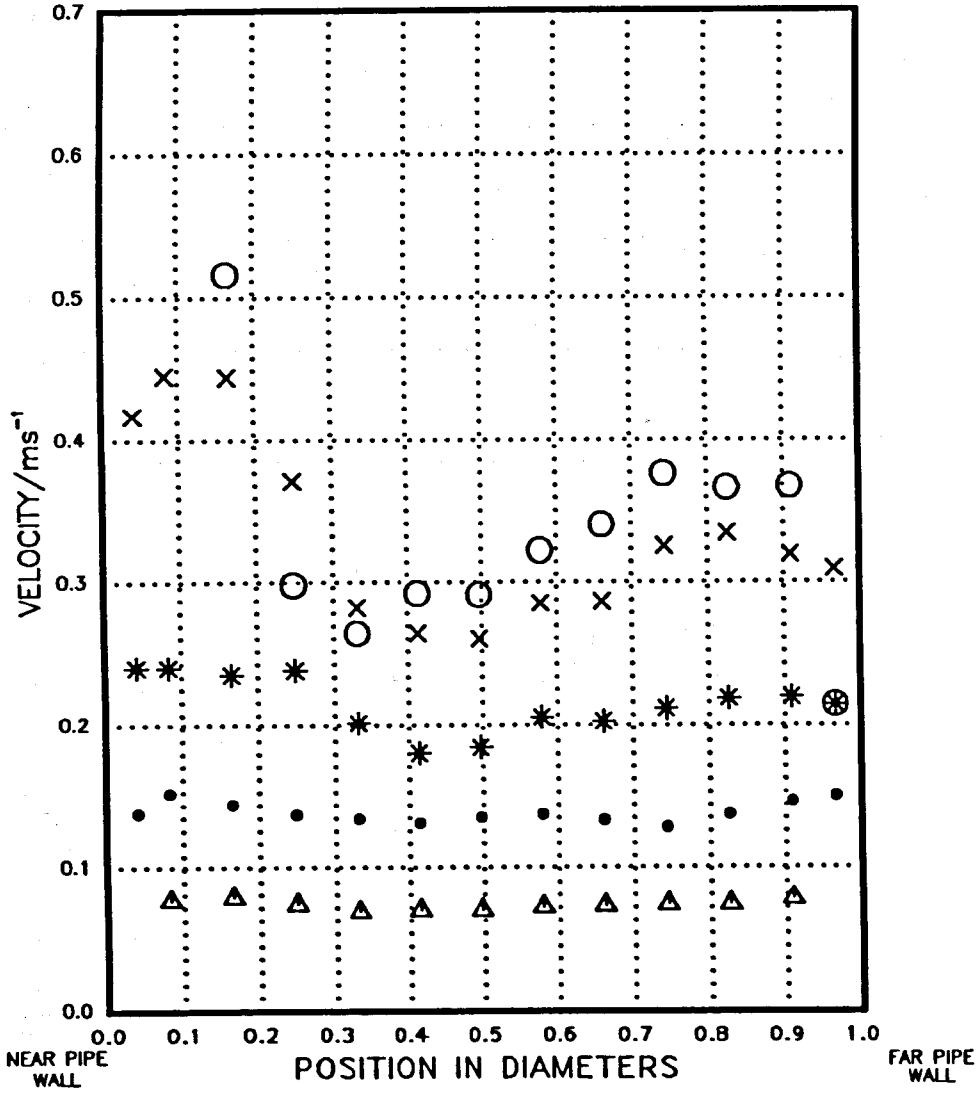

FIG. 7.9.17 TANGENTIAL VELOCITY OF SINGLE NOZZLE

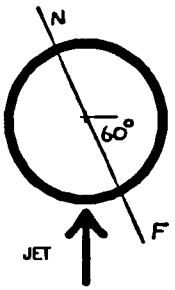

N ≡ NEAR WALL

F ≡ FAR WALL

O 1 DIAMETER DOWNSTREAM

× 2 DIAMETERS DOWNSTREAM

✱ 3 DIAMETERS DOWNSTREAM

● 4 DIAMETERS DOWNSTREAM

△ 6 DIAMETERS DOWNSTREAM

Reynolds number = 27600

Velocity ratio = 57

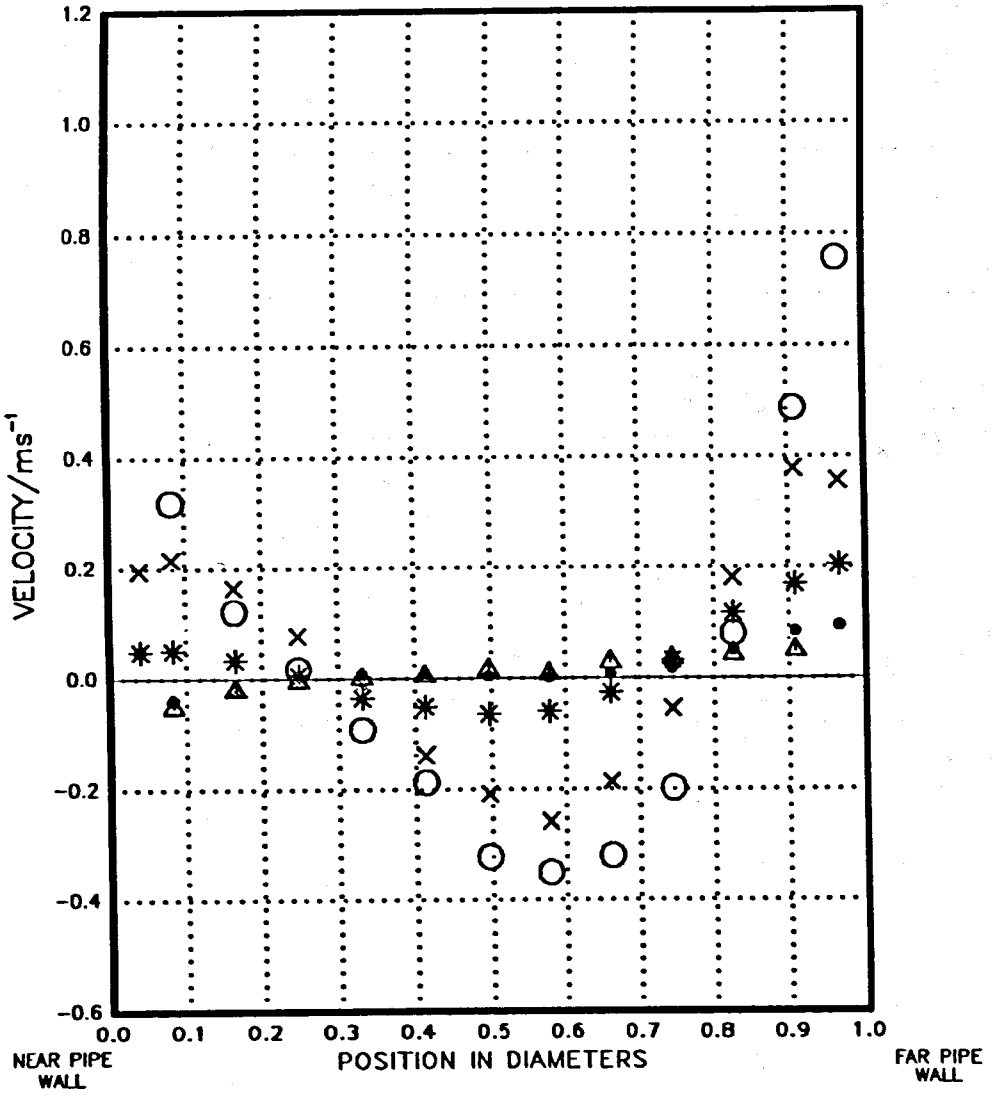

FIG. 7.9.18 TANGENTIAL RMS VELOCITY OF SINGLE NOZZLE

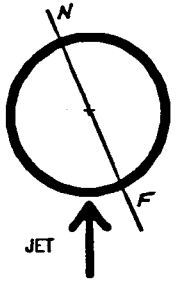

N ≡ NEAR WALL

F ≡ FAR WALL

O 1 DIAMETER DOWNSTREAM

× 2 DIAMETERS DOWNSTREAM

✱ 3 DIAMETERS DOWNSTREAM

● 4 DIAMETERS DOWNSTREAM

△ 6 DIAMETERS DOWNSTREAM

Reynolds number = 27600

Velocity ratio = 57

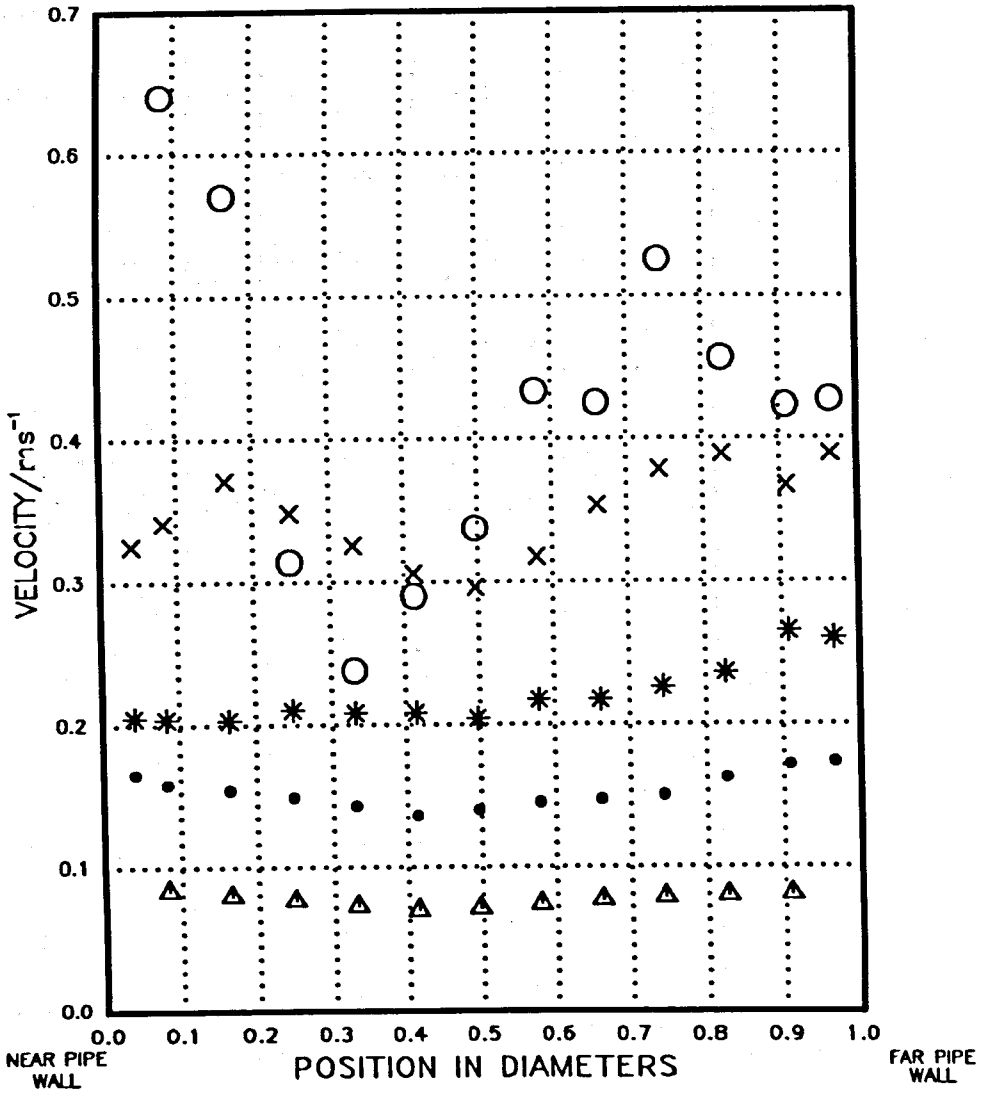

FIG. 7.10.1 AXIAL VELOCITY OF SINGLE NOZZLE

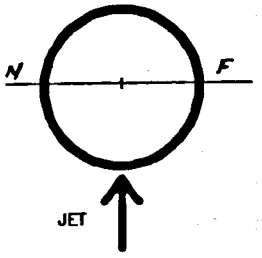

N ≡ NEAR WALL

F ≡ FAR WALL

O 1 DIAMETER DOWNSTREAM

× 2 DIAMETERS DOWNSTREAM

✱ 3 DIAMETERS DOWNSTREAM

• 4 DIAMETERS DOWNSTREAM

△ 6 DIAMETERS DOWNSTREAM

Reynolds number = 27600

Velocity ratio = 17

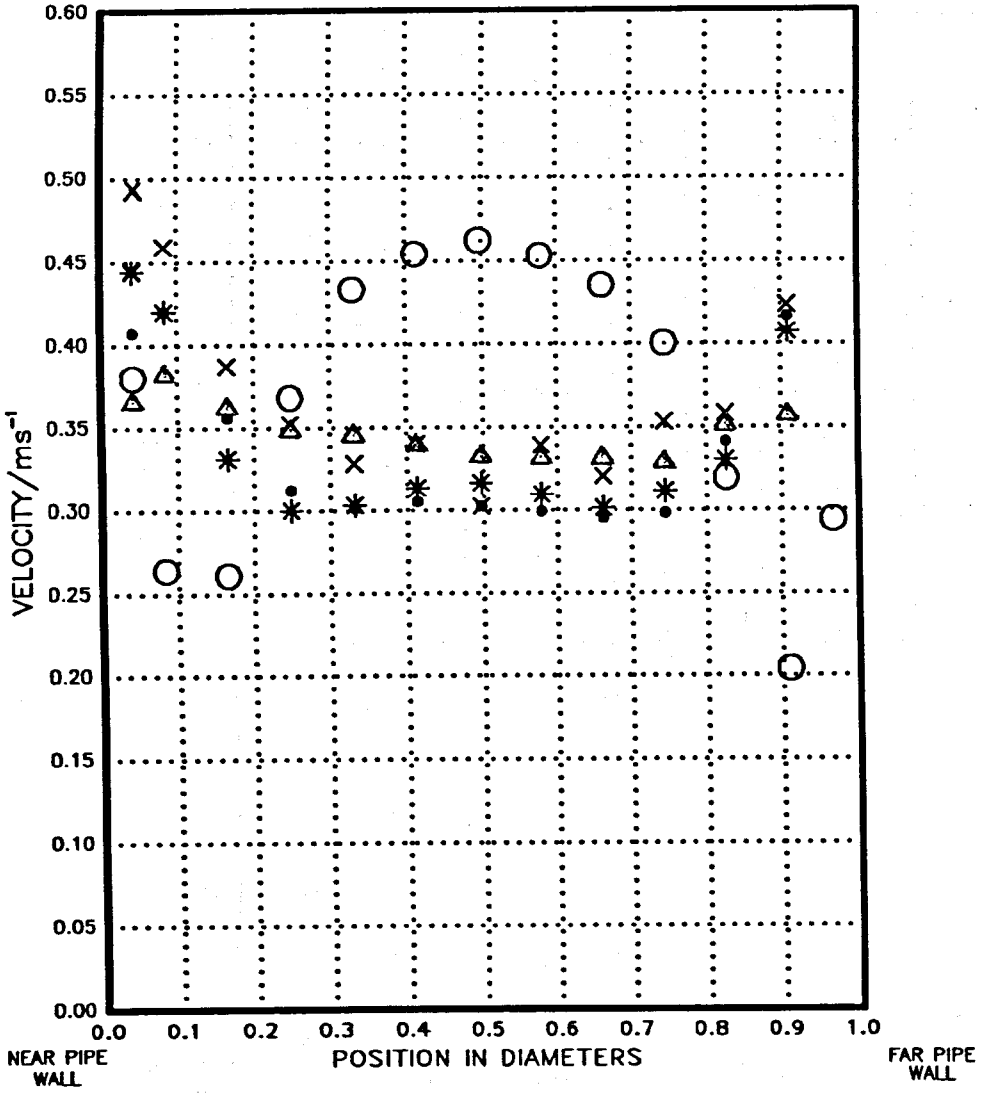

FIG. 7.10.2 AXIAL RMS VELOCITY OF SINGLE NOZZLE

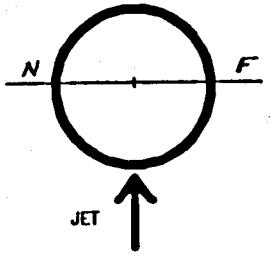

N = NEAR WALL

F = FAR WALL

O 1 DIAMETER DOWNSTREAM

× 2 DIAMETERS DOWNSTREAM

✱ 3 DIAMETERS DOWNSTREAM

● 4 DIAMETERS DOWNSTREAM

△ 6 DIAMETERS DOWNSTREAM

Reynolds number = 27600

Velocity ratio = 17

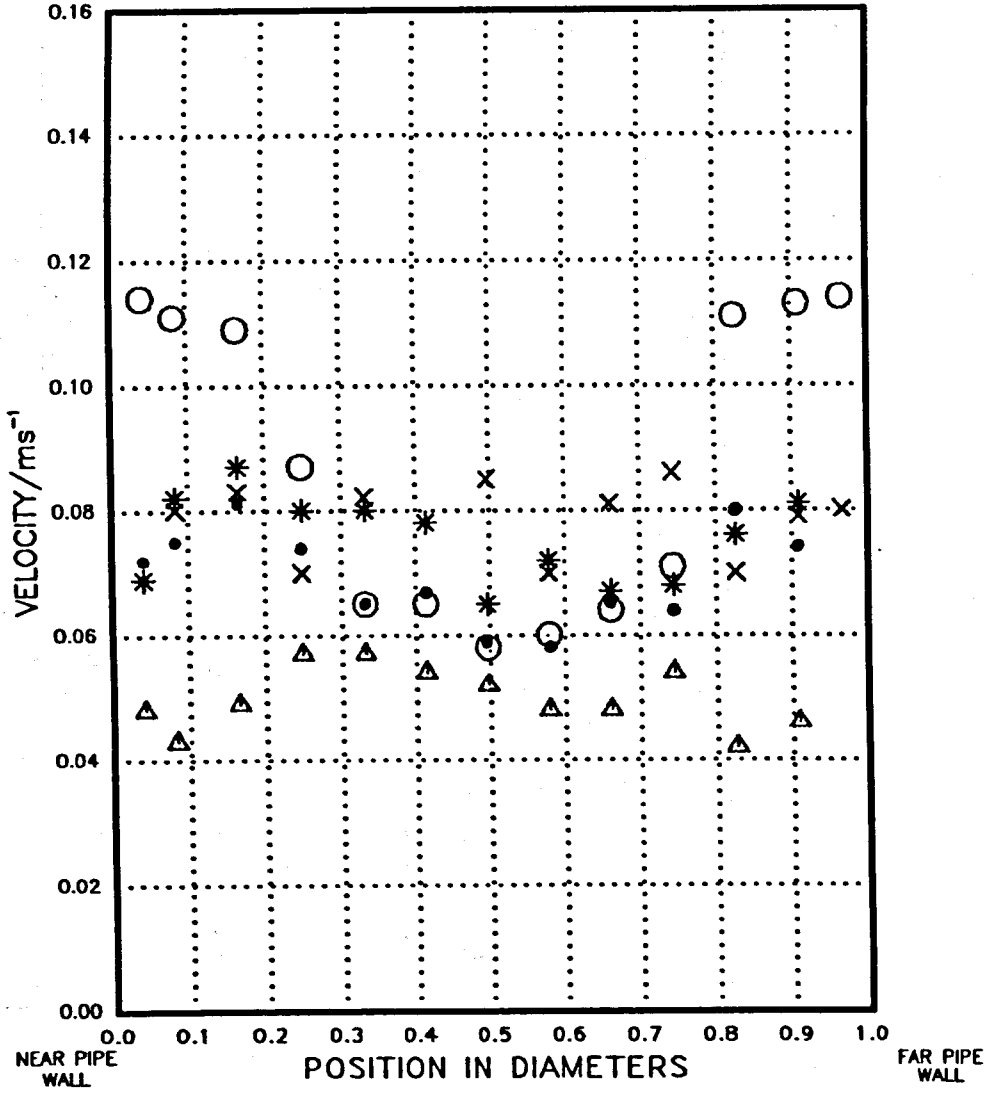

FIG. 7.10.3 *TANGENTIAL VELOCITY OF SINGLE NOZZLE*

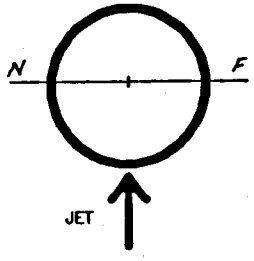

N ≡ NEAR WALL

F ≡ FAR WALL

O 1 DIAMETER DOWNSTREAM

× 2 DIAMETERS DOWNSTREAM

✱ 3 DIAMETERS DOWNSTREAM

● 4 DIAMETERS DOWNSTREAM

△ 6 DIAMETERS DOWNSTREAM

Reynolds number = 27600

Velocity ratio = 17

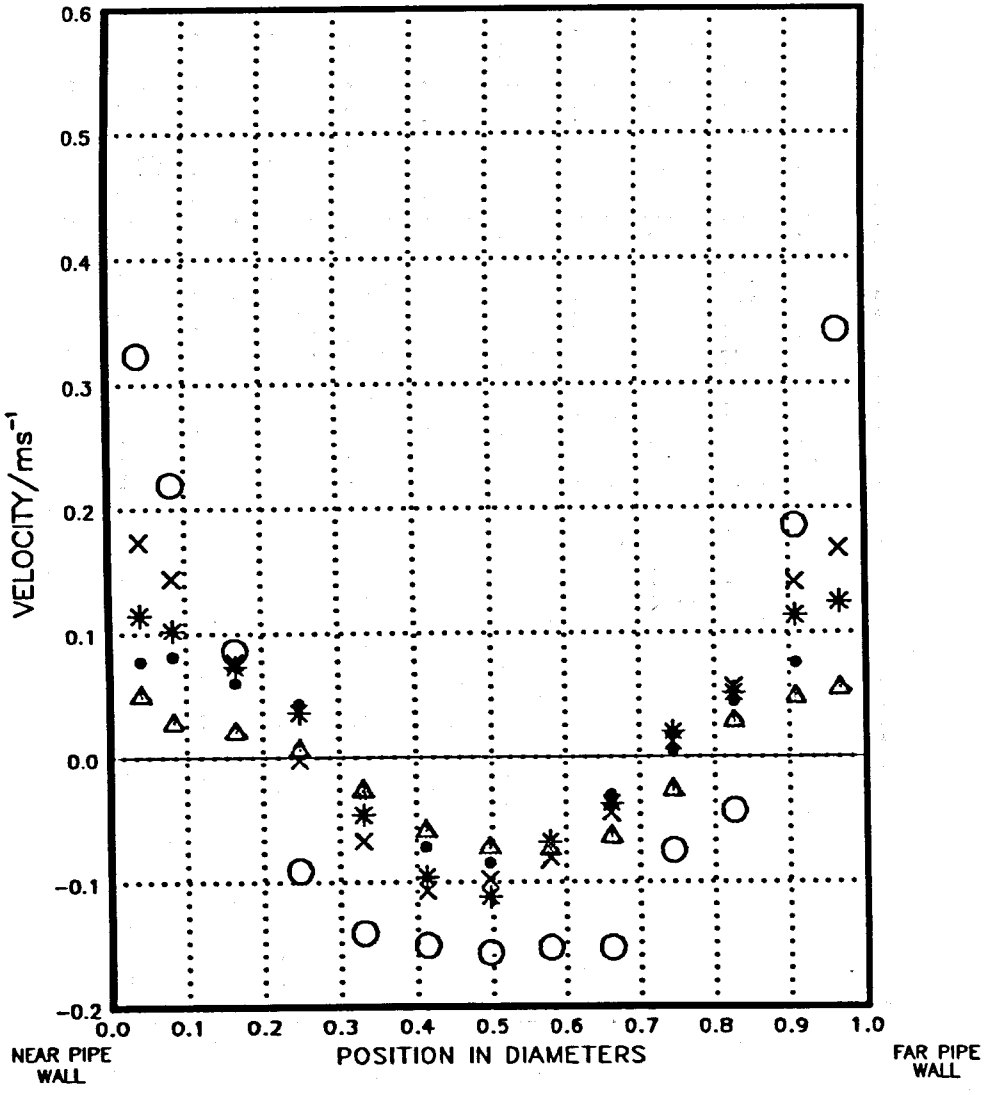

FIG. 7.10.4 TANGENTIAL RMS VELOCITY OF SINGLE NOZZLE

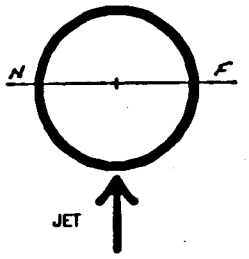

N ≡ NEAR WALL

F ≡ FAR WALL

O 1 DIAMETER DOWNSTREAM

× 2 DIAMETERS DOWNSTREAM

✱ 3 DIAMETERS DOWNSTREAM

• 4 DIAMETERS DOWNSTREAM

△ 6 DIAMETERS DOWNSTREAM

Reynolds number = 27600

Velocity ratio = 17

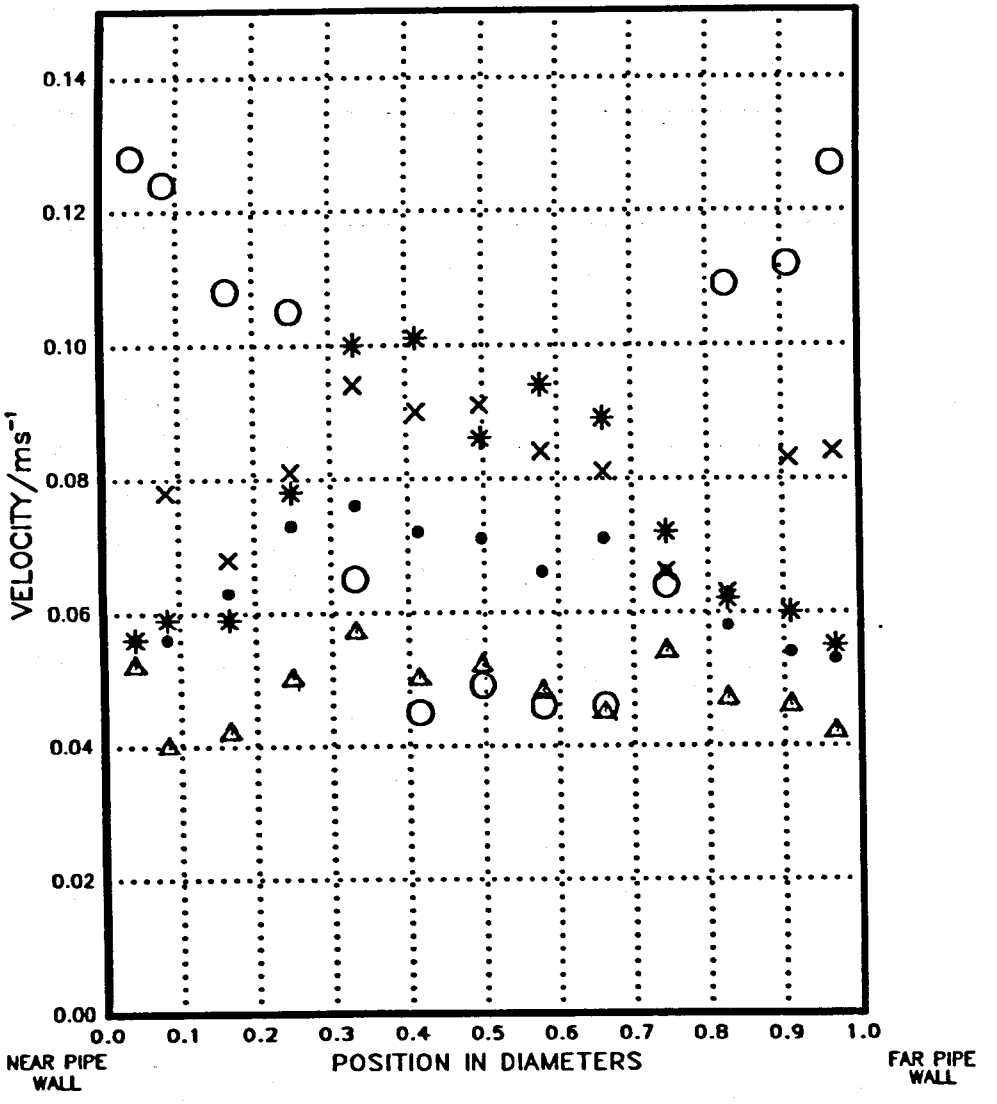

FIG. 7.10.5 *AXIAL VELOCITY OF SINGLE NOZZLE*

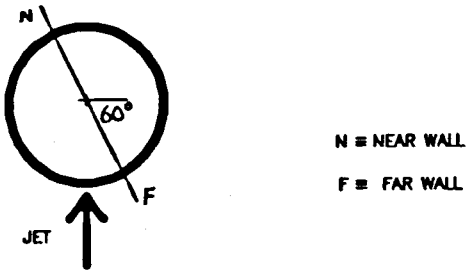

N ≡ NEAR WALL

F ≡ FAR WALL

O 1 DIAMETER DOWNSTREAM

× 2 DIAMETERS DOWNSTREAM

✱ 3 DIAMETERS DOWNSTREAM

● 4 DIAMETERS DOWNSTREAM

△ 6 DIAMETERS DOWNSTREAM

Reynolds number = 27600

Velocity ratio = 17

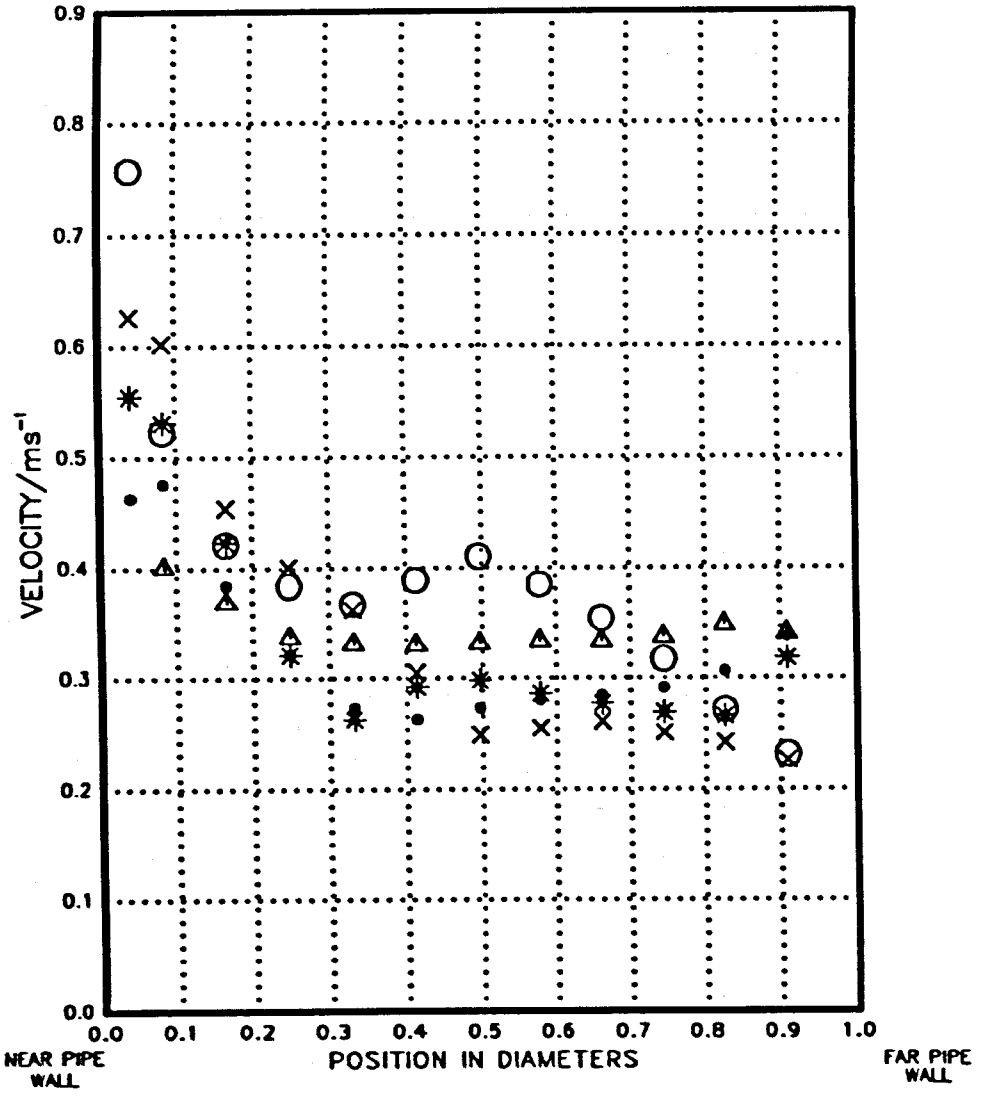

FIG. 7.10.6 AXIAL RMS VELOCITY OF SINGLE NOZZLE

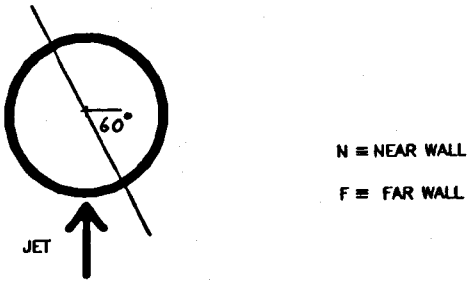

N ≡ NEAR WALL

F ≡ FAR WALL

O 1 DIAMETER DOWNSTREAM

× 2 DIAMETERS DOWNSTREAM

✳ 3 DIAMETERS DOWNSTREAM

• 4 DIAMETERS DOWNSTREAM

△ 6 DIAMETERS DOWNSTREAM

Reynolds number = 27600

Velocity ratio = 17

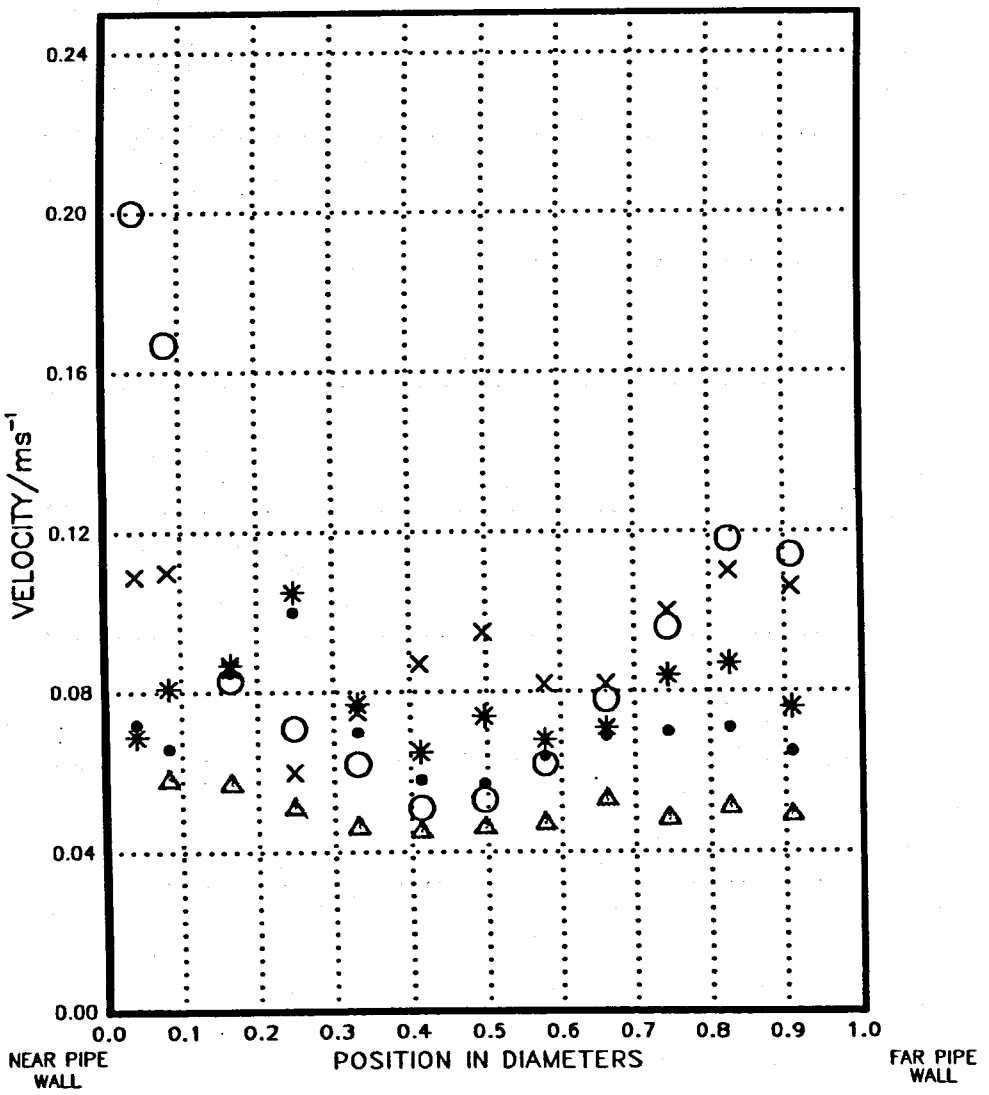

FIG. 7.10.7 *TANGENTIAL VELOCITY OF SINGLE NOZZLE*

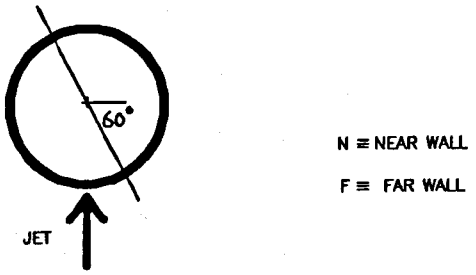

N ≡ NEAR WALL

F ≡ FAR WALL

O 1 DIAMETER DOWNSTREAM

× 2 DIAMETERS DOWNSTREAM

✱ 3 DIAMETERS DOWNSTREAM

● 4 DIAMETERS DOWNSTREAM

△ 6 DIAMETERS DOWNSTREAM

Reynolds number = 27600

Velocity ratio = 17

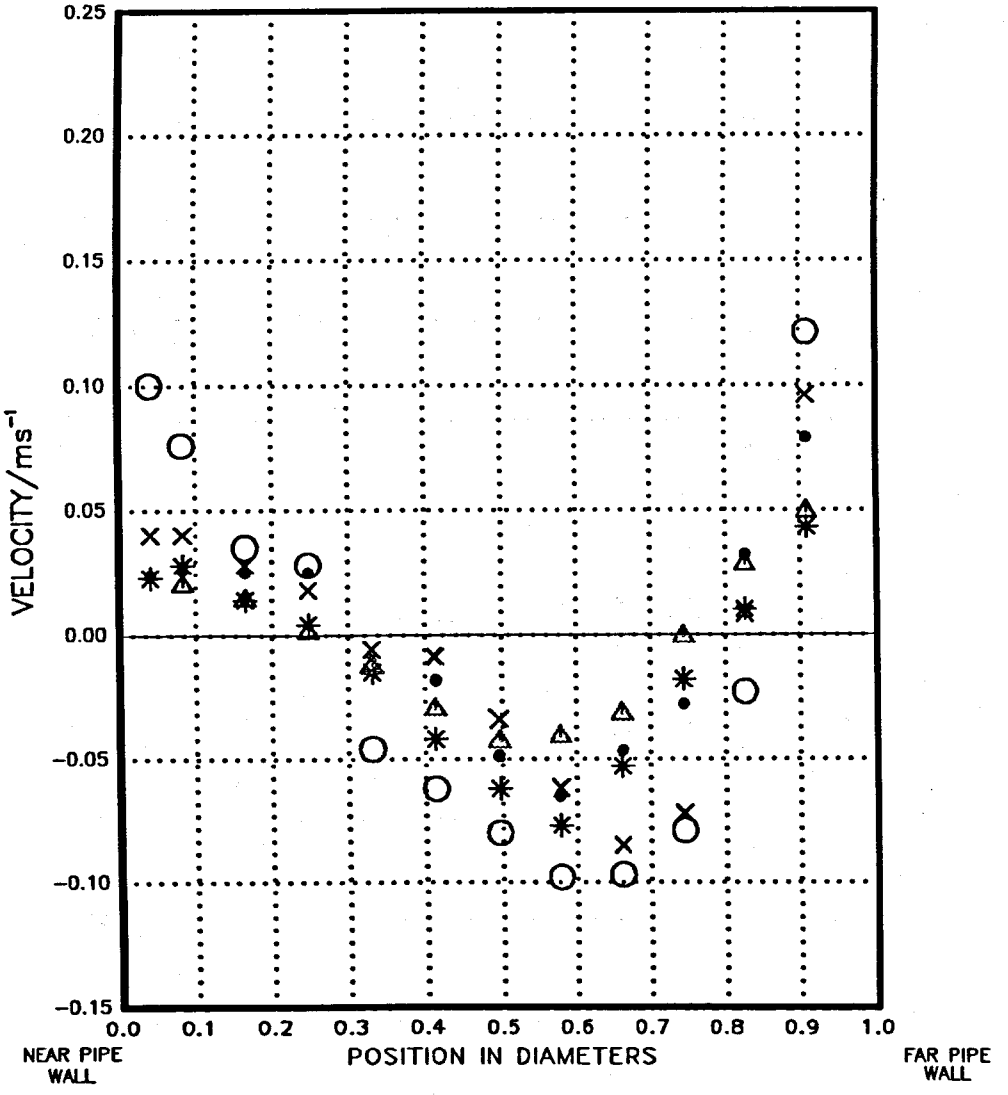

FIG. 7.10.8 TANGENTIAL RMS VELOCITY OF SINGLE NOZZLE

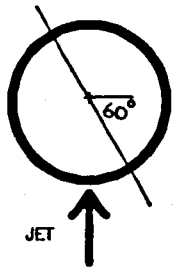

N ≡ NEAR WALL

F ≡ FAR WALL

O 1 DIAMETER DOWNSTREAM

× 2 DIAMETERS DOWNSTREAM

✳ 3 DIAMETERS DOWNSTREAM

• 4 DIAMETERS DOWNSTREAM

△ 6 DIAMETERS DOWNSTREAM

Reynolds number = 27600

Velocity ratio = 17

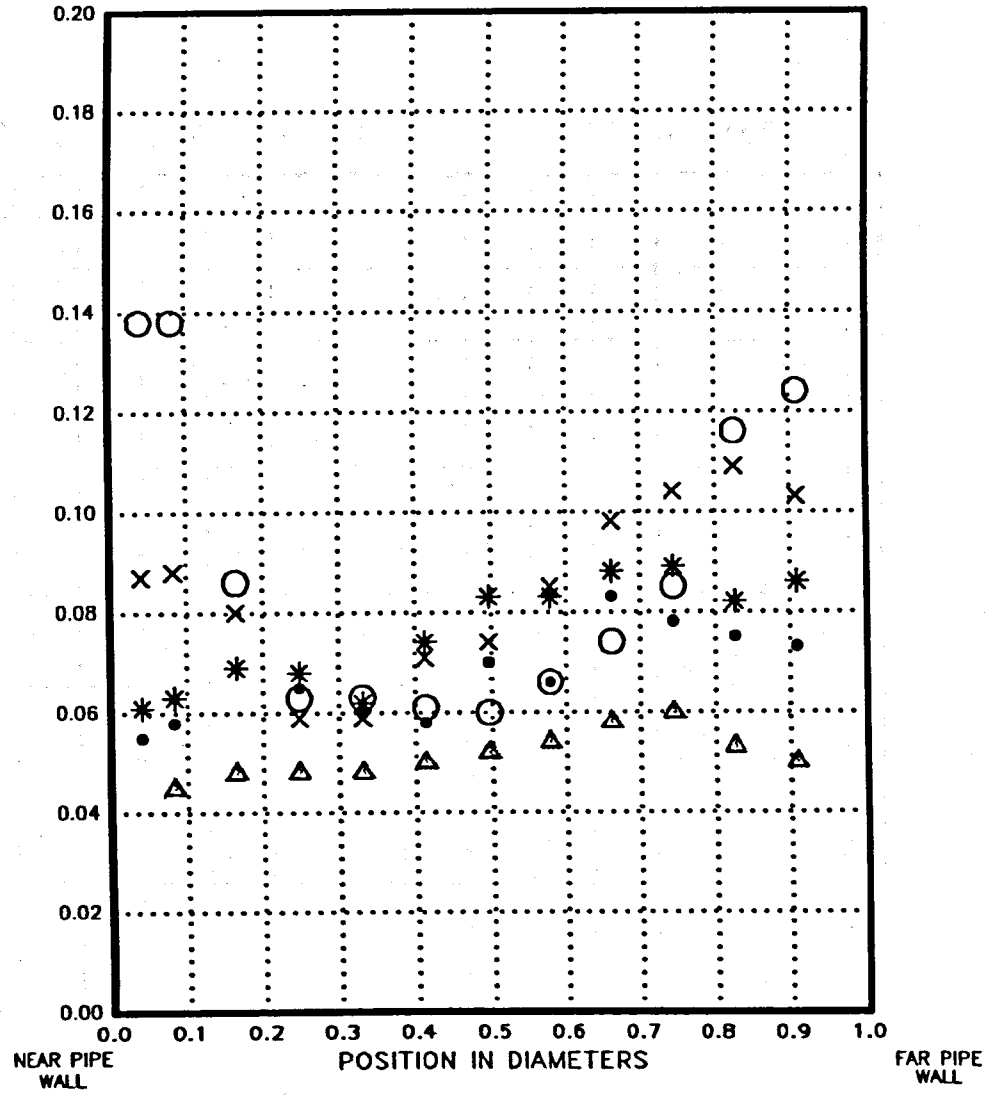

FIG. 7.11.1 TANGENTIAL VELOCITY (AT AXIS) DECAY OF MULTI-NOZZLE

Reynolds number = 27600

O VELOCITY RATIO 36

× VELOCITY RATIO 57

✱ VELOCITY RATIO 70

Reynolds number = 48400

● VELOCITY RATIO 36

Correlation

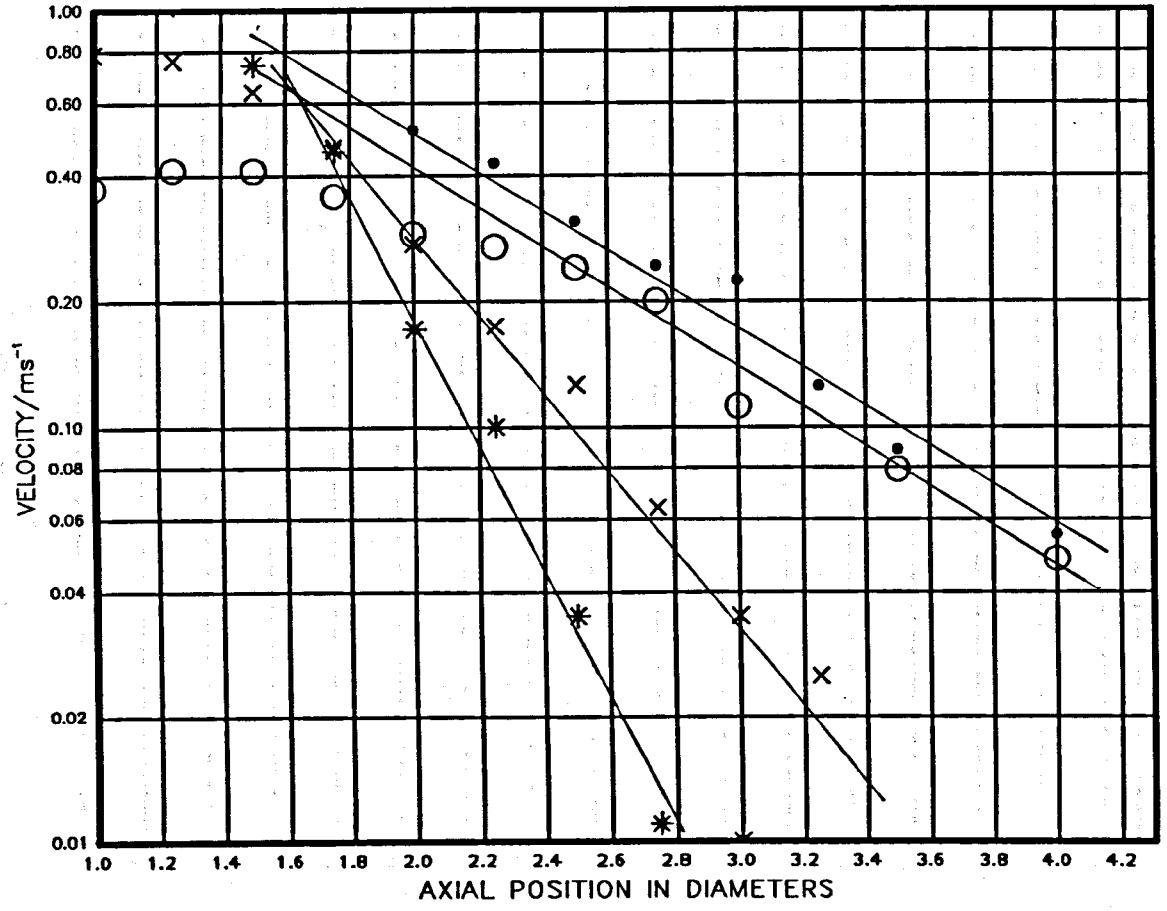

FIG. 7.11.2 TANGENTIAL VELOCITY (AT AXIS) DECAY OF SINGLE NOZZLE

Reynolds number = 27600

O VELOCITY RATIO 36

x VELOCITY RATIO 57

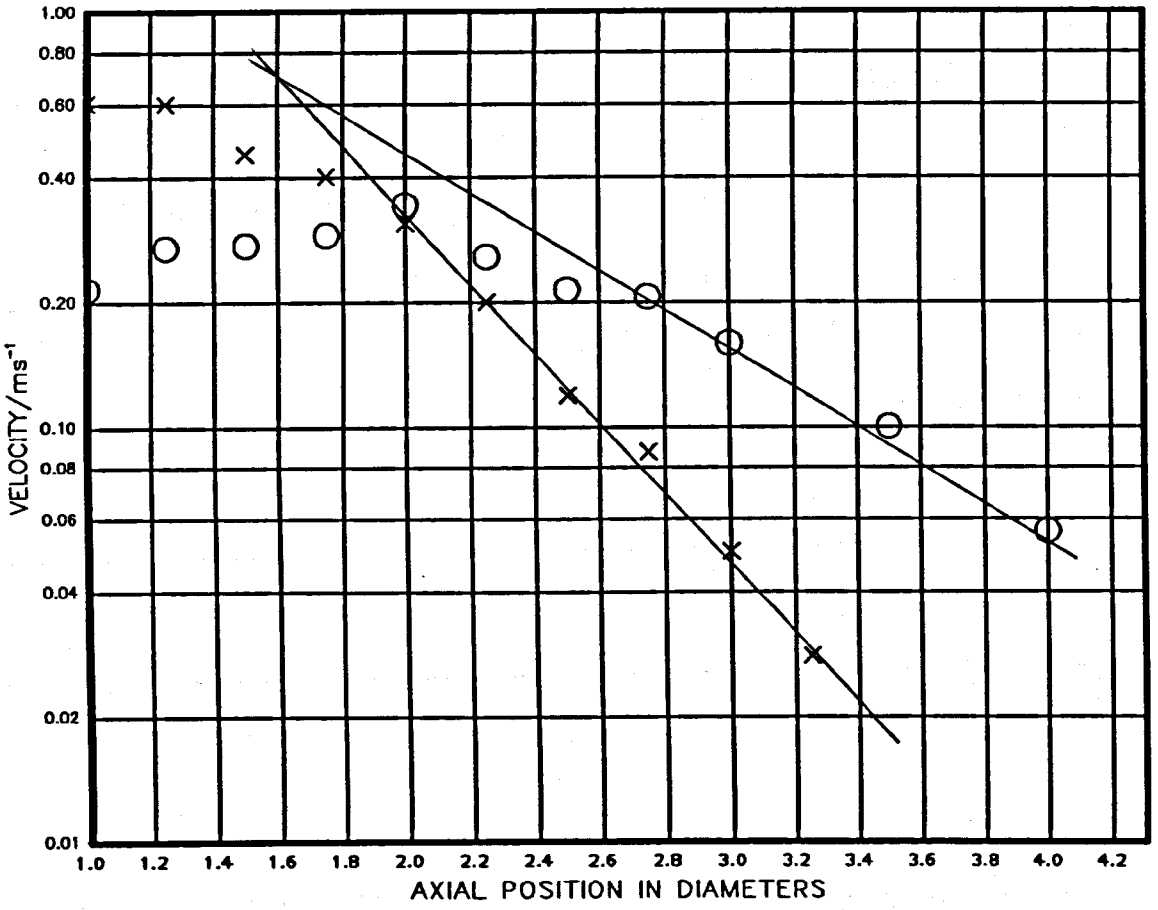

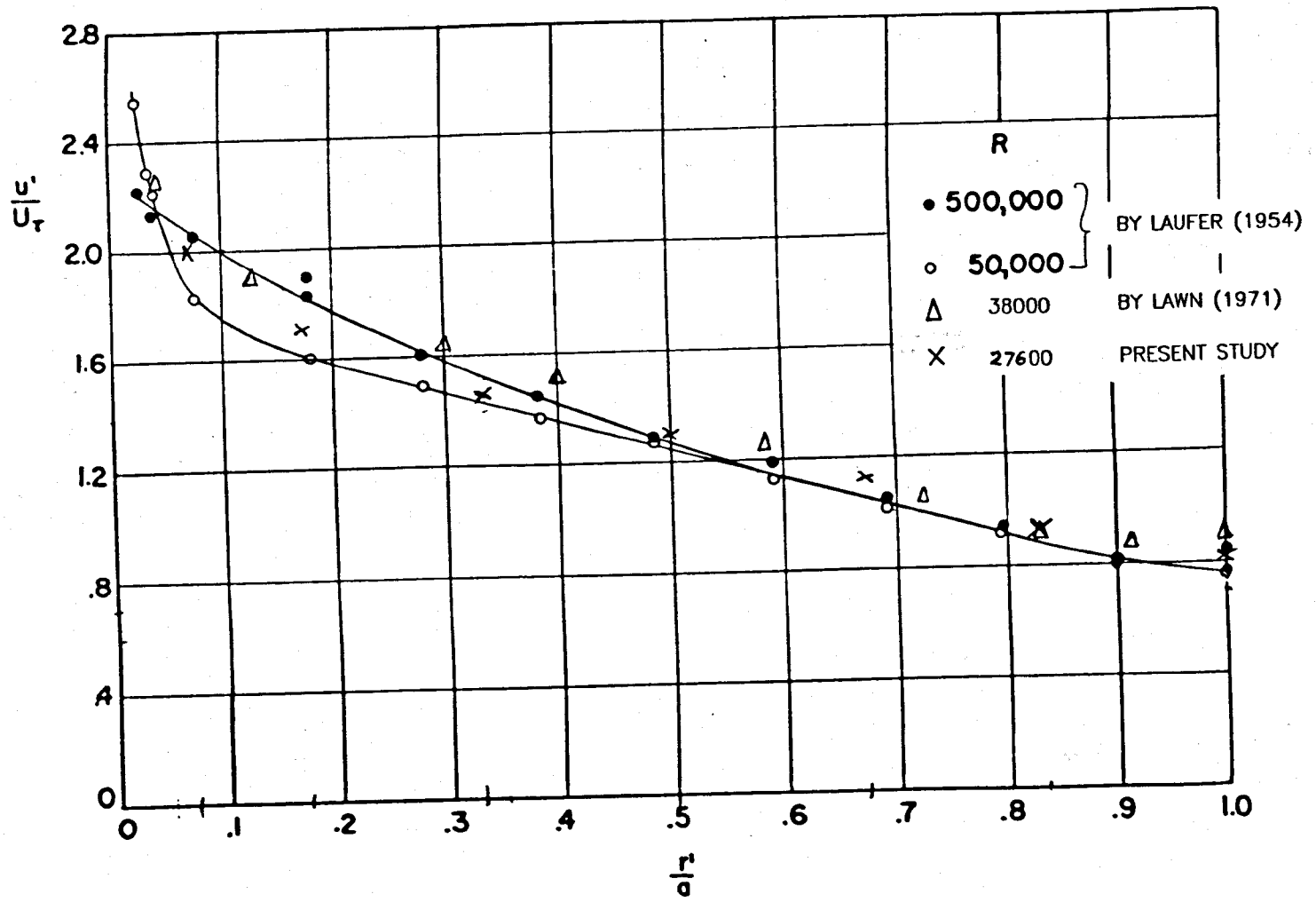

FIG. 7.12 COMPARISION OF u'(RMS VELOCITY) WITH PREVIOUS EXPERIMENTAL DATA

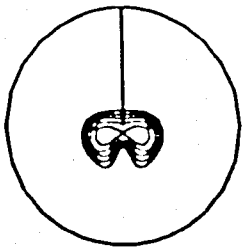

EQUALLY SPACED C1
CONTOURS FROM 0·01 TO 0·014
Velocity ratio= 12
0·5 Dia. downstream

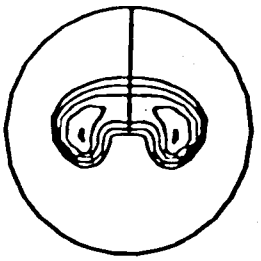

EQUALLY SPACED C1
CONTOURS FROM 0·005 TO 0·009
Velocity ratio= 12
1·0 Dia. downstream

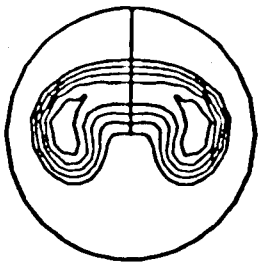

EQUALLY SPACED C1
CONTOURS FROM 0·003 TO 0·006
Velocity ratio= 12
2·0 Dia. downstream

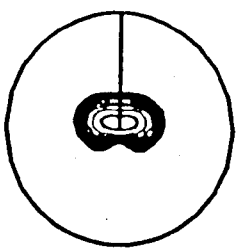

EQUALLY SPACED C1
CONTOURS FROM 0·01 TO 0·015
Velocity ratio= 14
0·5 Dia. downstream

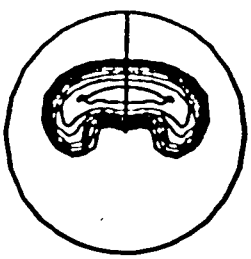

EQUALLY SPACED C1
CONTOURS FROM 0·005 TO 0·009
Velocity ratio= 14
1·0 Dia. downstream

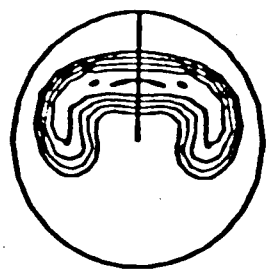

EQUALLY SPACED C1
CONTOURS FROM 0·004 TO 0·008
Velocity ratio= 14
2·0 Dia. downstream

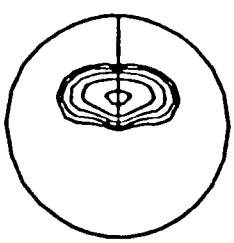

EQUALLY SPACED C1
CONTOURS FROM 0·01 TO 0·015
Velocity ratio= 17
0·5 Dia. downstream

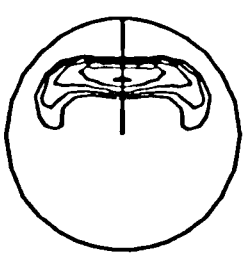

EQUALLY SPACED C1
CONTOURS FROM 0·007 TO 0·013
Velocity ratio= 17
1·0 Dia. downstream

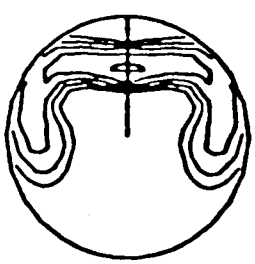

EQUALLY SPACED C1
CONTOURS FROM 0·005 TO 0·0085
Velocity ratio= 17
2·0 Dia. downstream

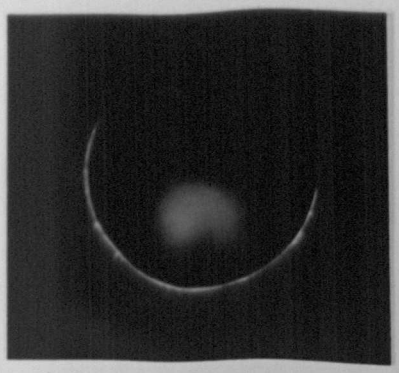

Long exposoure
Velocity ratio= 1/2
1/2 Dia. downstream

Long exposure
Velocity ratio= 1/2
1 Dia. downstream

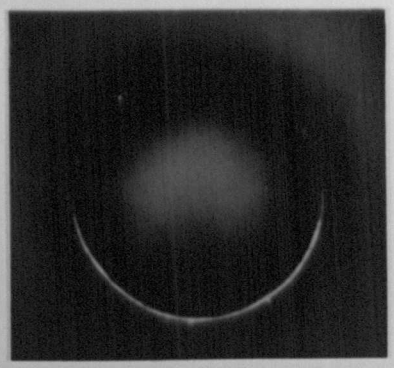

Long exposure
Velocity ratio= 1/2
2 Dia. downstream

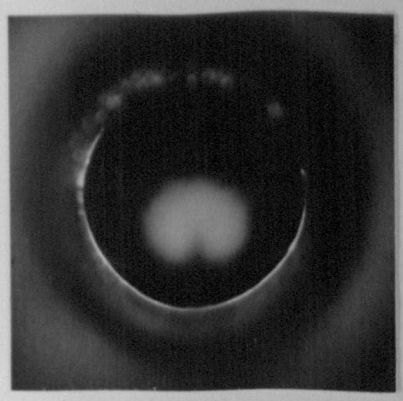

Long exposure
Velocity ratio= 1/4
1/2 Dia. downstream

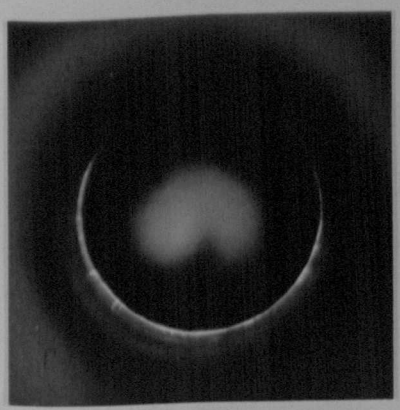

Long exposoure
Velocity ratio= 1/4
1 Dia. downstream

Long exposure
Velocity ratio= 1/4
2 Dia. downstream

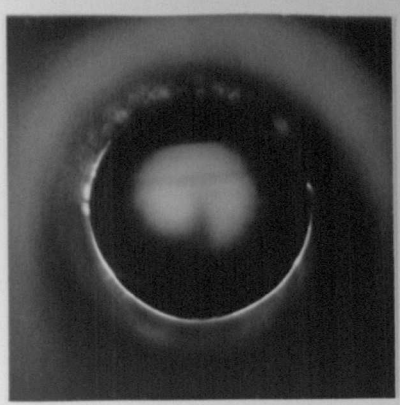

Long exposure
Velocity ratio= 1/7
1/2 Dia. downstream

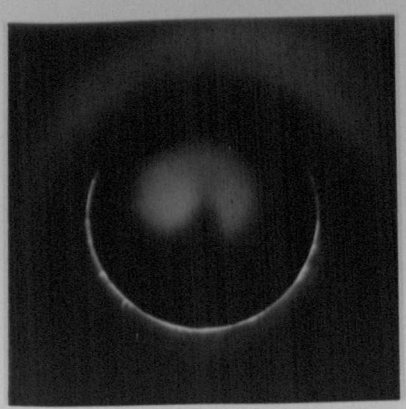

Long exposure
Velocity ratio= 1/7
1 Dia. downstream

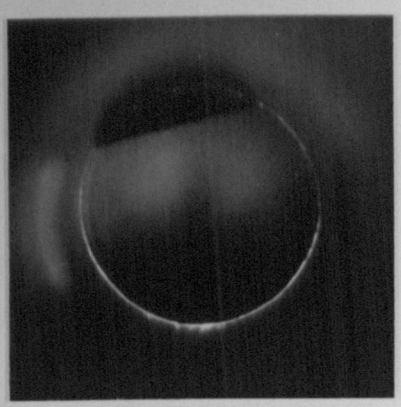

Long exposure
Velocity ratio= 1/7
2 Dia. downstream

FIG. 7.13.1 FLOW VISUALISATION – DISPERSION OF PASSIVE CONTAMINANT BY SINGLE JET IN PIPE CROSS FLOW

Pipe Re Number= 27600

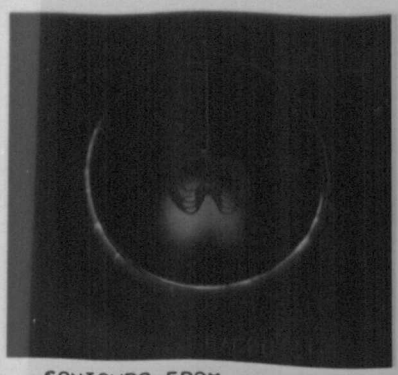

CONTOURS FROM 0·01 TO 0·014
Velocity ratio= 1·2
0·5 Dia. downstream

CONTOURS FROM 0·005 TO 0·009
Velocity ratio= 1·2
1·0 Dia. downstream

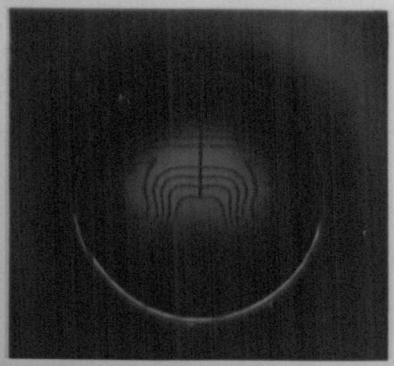

CONTOURS FROM 0·003 TO 0·006
Velocity ratio= 1·2
2·0 Dia. downstream

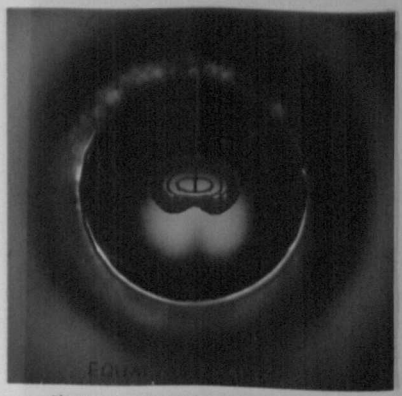

CONTOURS FROM 0·01 TO 0·015
Velocity ratio= 1·4
0·5 Dia. downstream

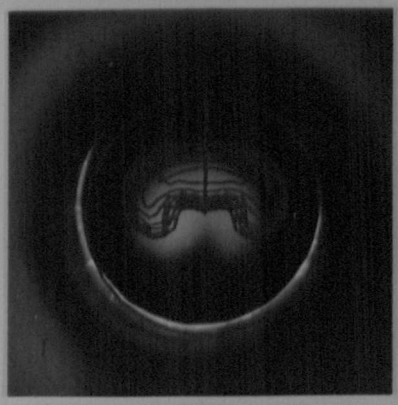

CONTOURS FROM 0·005 TO 0·009
Velocity ratio= 1·4
1·0 Dia. downstream

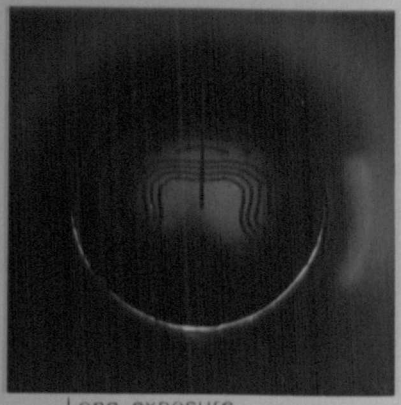

CONTOURS FROM 0·004 TO 0·008
Velocity ratio= 1·4
2·0 Dia. downstream

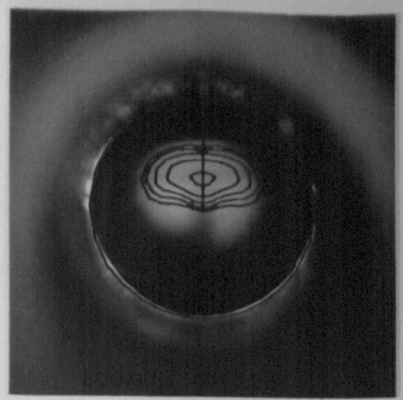

CONTOURS FROM 0·01 TO 0·015
Velocity ratio= 1·17
0·5 Dia. downstream

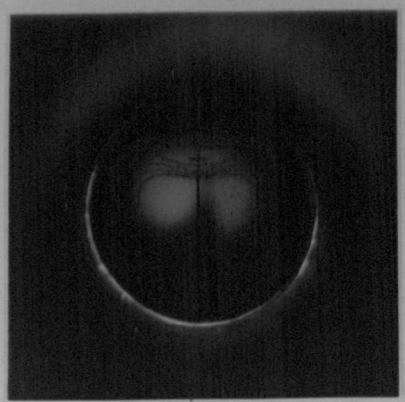

CONTOURS FROM 0·007 TO 0·013
Velocity ratio= 1·17
1·0 Dia. downstream

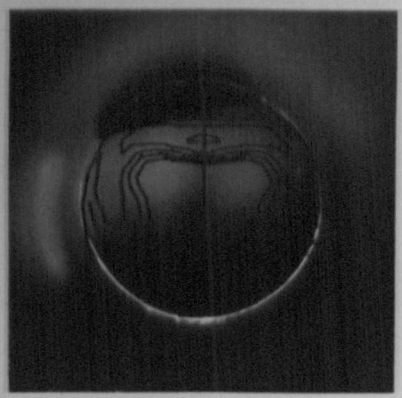

CONTOURS FROM 0·005 TO 0·0085
Velocity ratio= 1·17
2·0 Dia. downstream

FIG. 7.13.1 FLOW VISUALISATION – DISPERSION OF PASSIVE CONTAMINANT BY SINGLE JET IN PIPE CROSS FLOW
Pipe Re Number= 27600

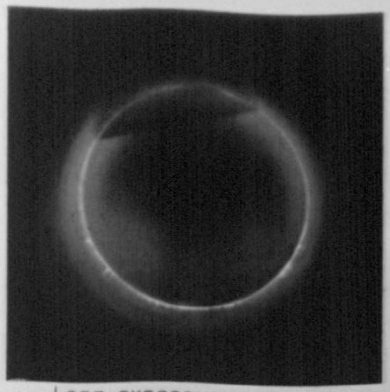

Long exposoure
Velocity ratio= 57
1·0 Dia. downstream

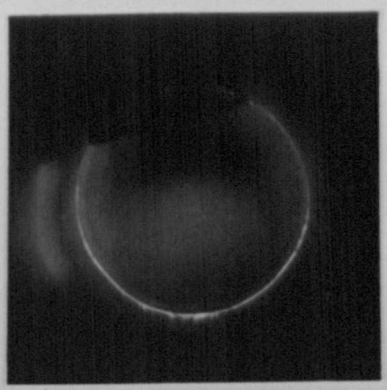

Long exposure
Velocity ratio= 57
2·0 Dia. downstream

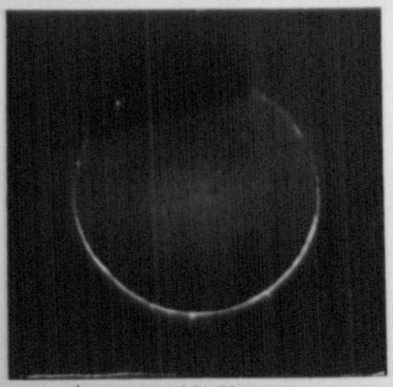

Long exposure
Velocity ratio= 57
3·0 Dia. downstream

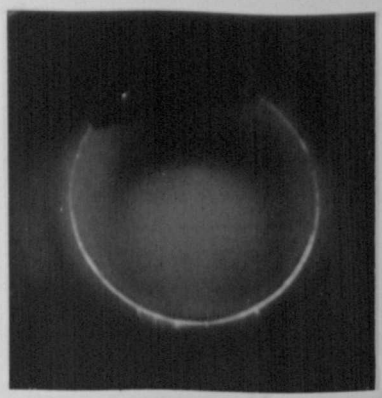

Long exposure
Velocity ratio= 40
3·0 Dia. downstream

Long exposure
Velocity ratio= 14
3·0 Dia. downstream

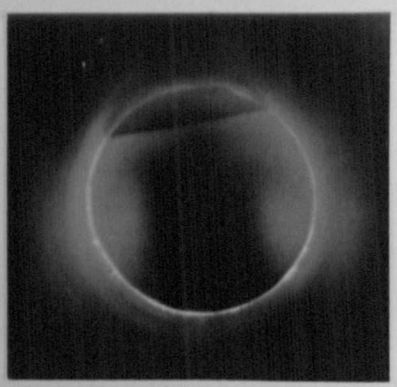

Long exposure
Velocity ratio= 40
1·0 Dia. downstream

Instantaneous exposure
Velocity ratio= 12
0·0 Dia. downstream

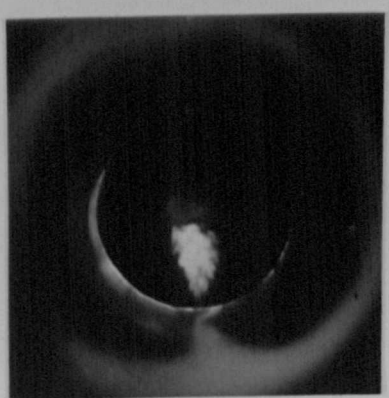

Instantaneous exposure
Velocity ratio= 17
0·0 Dia. downstream

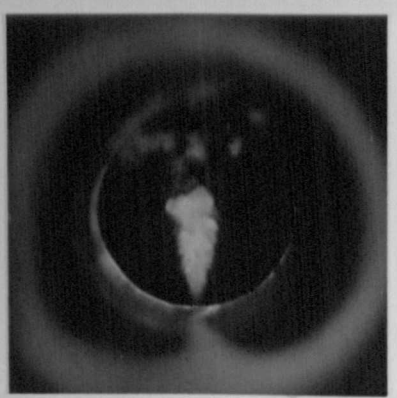

Instantaneous exposure
Velocity ratio= 40
0·0 Dia. downstream

FIG. 7.13.2 FLOW VISUALISATION – DISPERSION OF PASSIVE CONTAMINANT BY SINGLE JET IN PIPE CROSS FLOW

Pipe Re Number= 27600

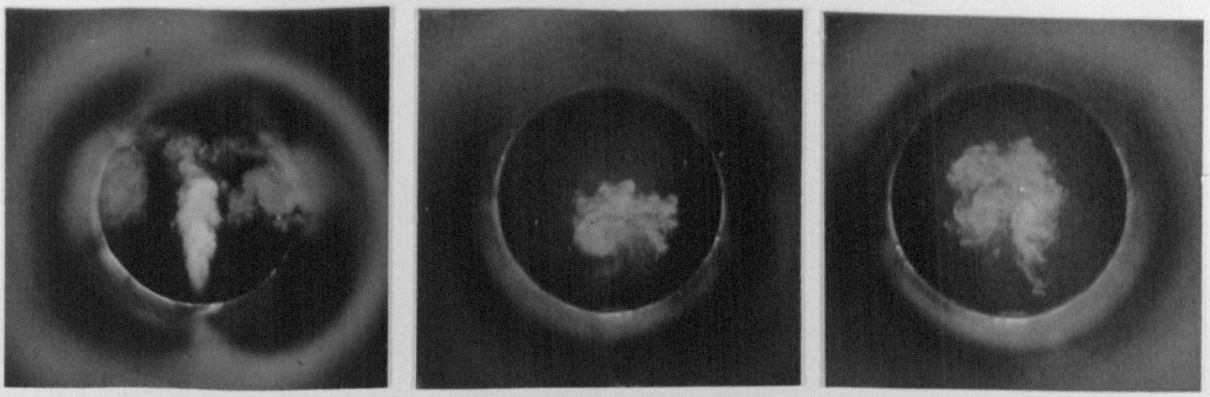

Instantaneous exposure
Velocity ratio= 57
0·0 Dia. downstream

Instantaneous exposure
Velocity ratio= 12
½ Dia. downstream

Instantaneous exposure
Velocity ratio= 14
1·0 Dia. downstream

FIG. 7.13.3 FLOW VISUALISATION – DISPERSION OF PASSIVE CONTAMINANT BY SINGLE JET IN PIPE CROSS FLOW
Pipe Re Number= 27600

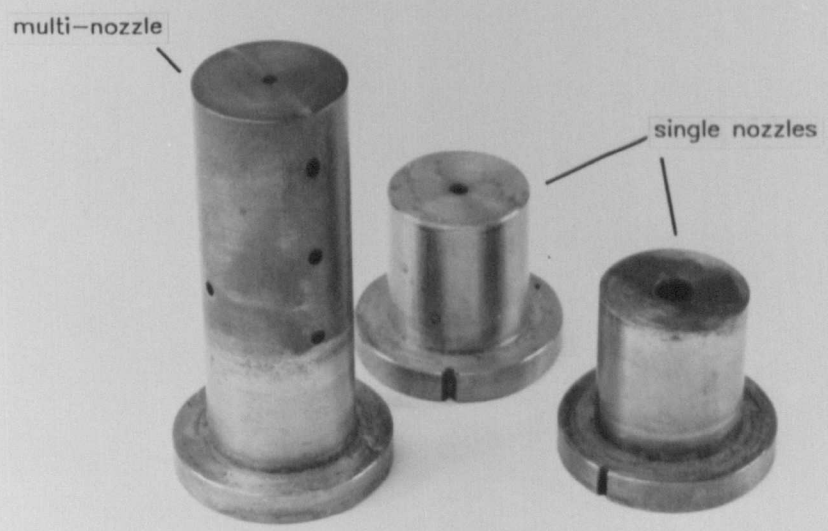

FIG. 7.13.4 JET MIX NOZZLES

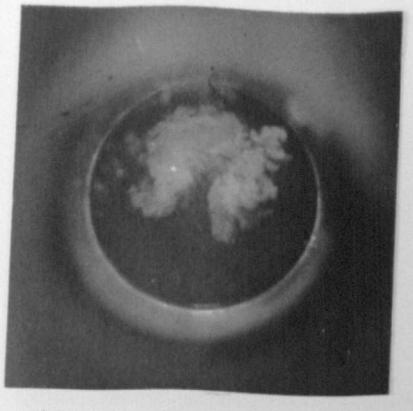

Instantaneous exposure
Velocity ratio= 17
1·0 Dia. downstream

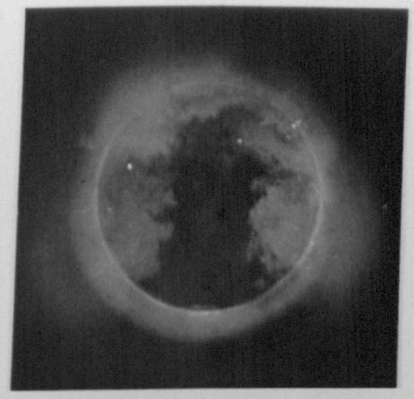

Instantaneous exposure
Velocity ratio= 40
1·0 Dia. downstream

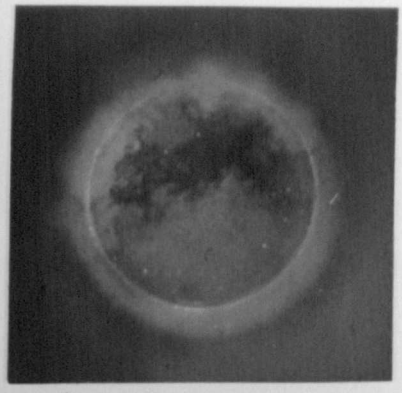

Instantaneous exposure
Velocity ratio= 57
1·0 Dia. downstream

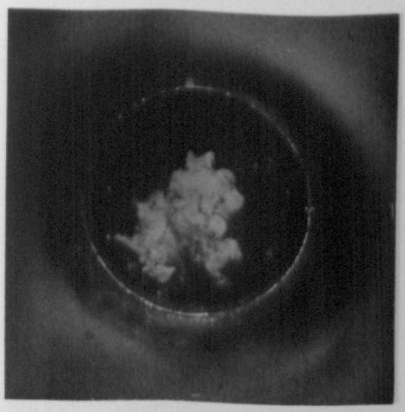

Instantaneous exposure
Velocity ratio= 12
1·0 Dia. downstream

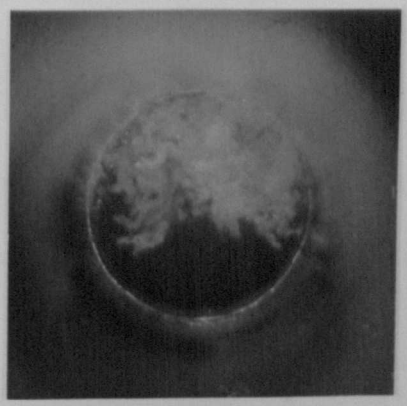

Instantaneous exposure
Velocity ratio= 17
2·0 Dia. downstream

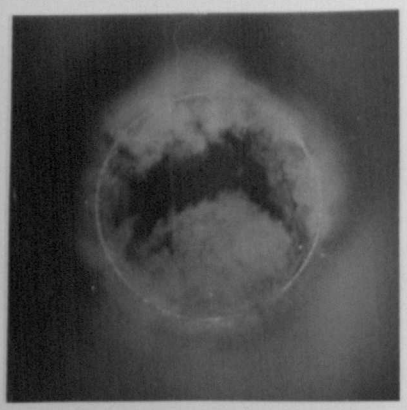

Instantaneous exposure
Velocity ratio= 40
2·0 Dia. downstream

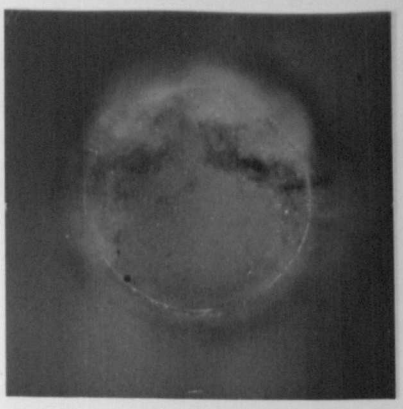

Instantaneous exposure
Velocity ratio= 57
2·0 Dia. downstream

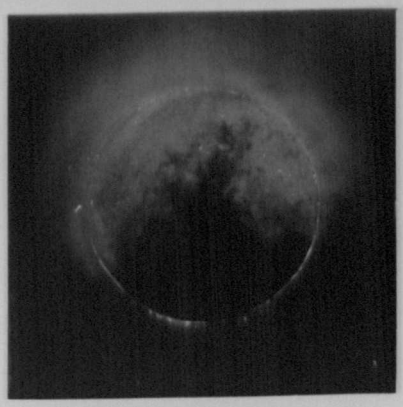

Instantaneous exposure
Velocity ratio= 17
3·0 Dia. downstream

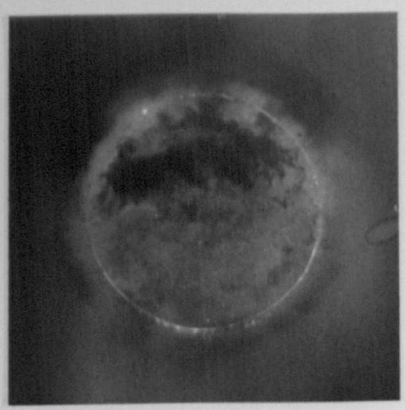

Instantaneous exposure
Velocity ratio= 40
3·0 Dia. downstream

FIG. 7.13.5 FLOW VISUALISATION – DISPERSION OF PASSIVE CONTAMINANT BY SINGLE JET IN PIPE CROSS FLOW
Pipe Re Number= 27600

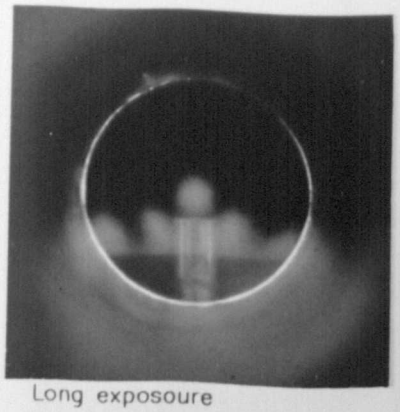

Long exposoure
Velocity ratio= 14
1·0 Dia. downstream

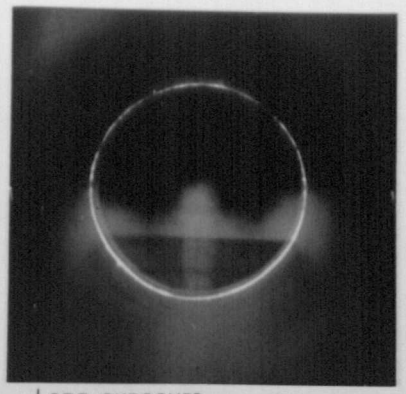

Long exposure
Velocity ratio= 14
2·0 Dia. downstream

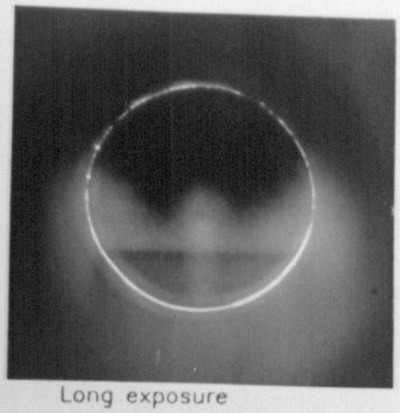

Long exposure
Velocity ratio= 14
3·0 Dia. downstream

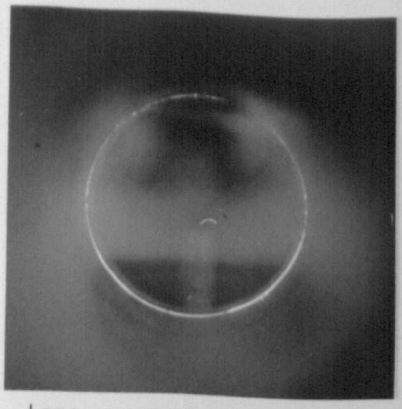

Long exposure
Velocity ratio= 57
1·0 Dia. downstream

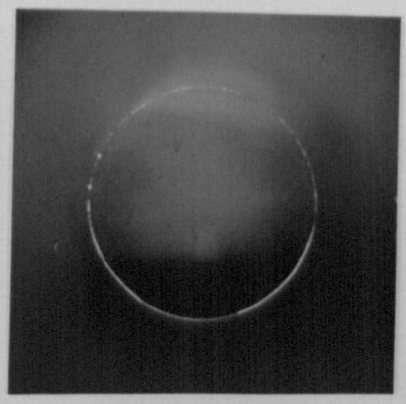

Long exposure
Velocity ratio= 57
3·0 Dia. downstream

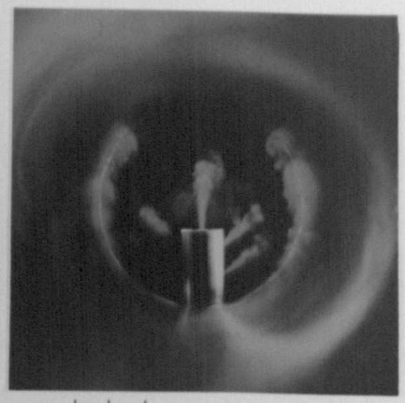

Instantaneous exposure
Velocity ratio= 57
0·0 Dia. downstream

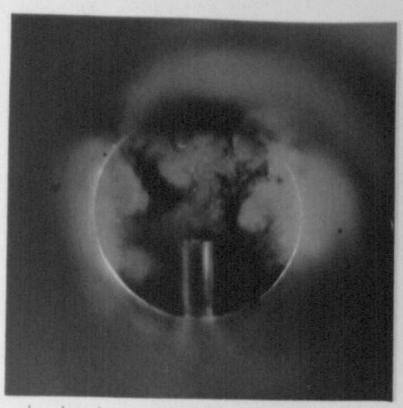

Instantaneous exposure
Velocity ratio= 57
1/2 Dia. downstream

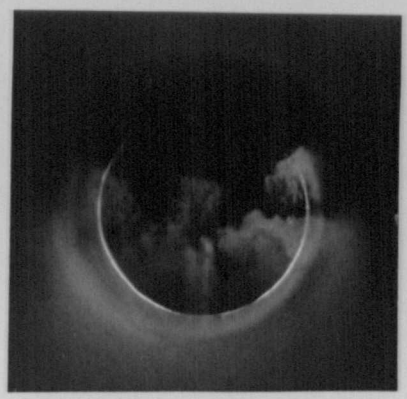

Instantaneous exposure
Velocity ratio= 17
1·0 Dia. downstream

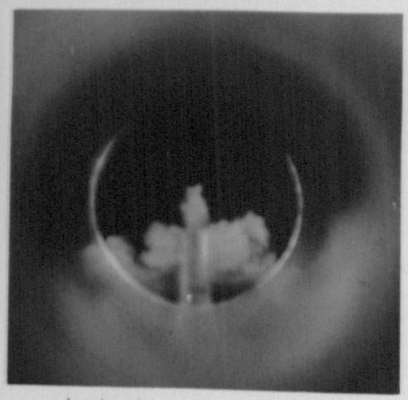

Instantaneous exposure
Velocity ratio= 14
1/2 Dia. downstream

FIG. 7.13.6 FLOW VISUALISATION – DISPERSION OF PASSIVE CONTAMINANT BY MULTI-JET IN PIPE CROSS FLOW

Pipe Re Number= 27600

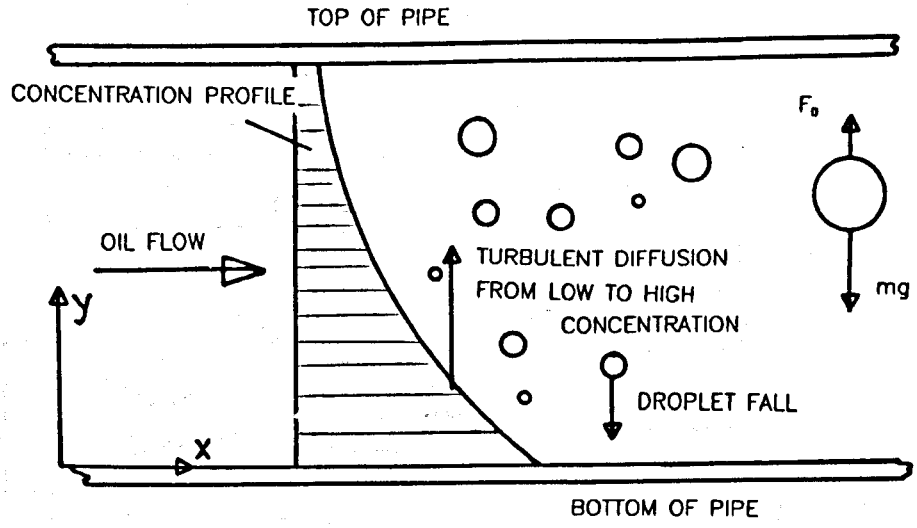

FIG. 8.1 DIAGRAM OF MIXING IN A PIPE

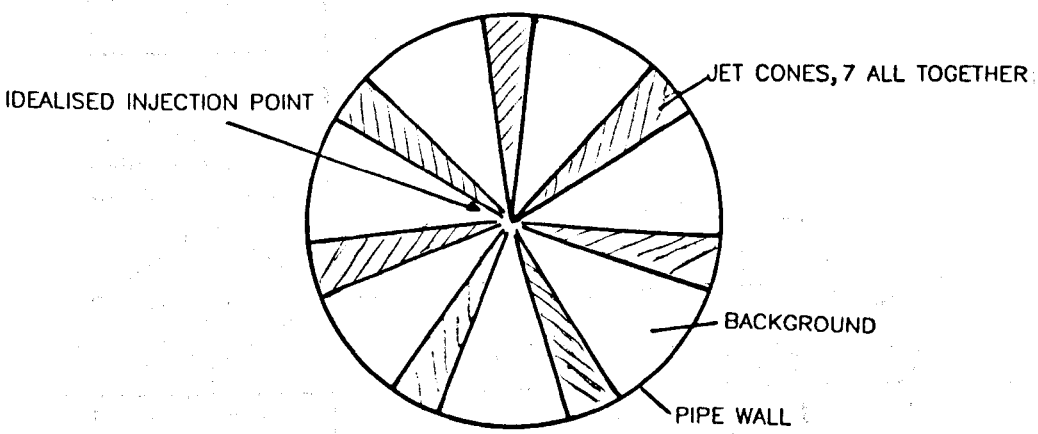

FIG. 8.2 IDEALISED JET GEOMETRY AT INJECTION POINT

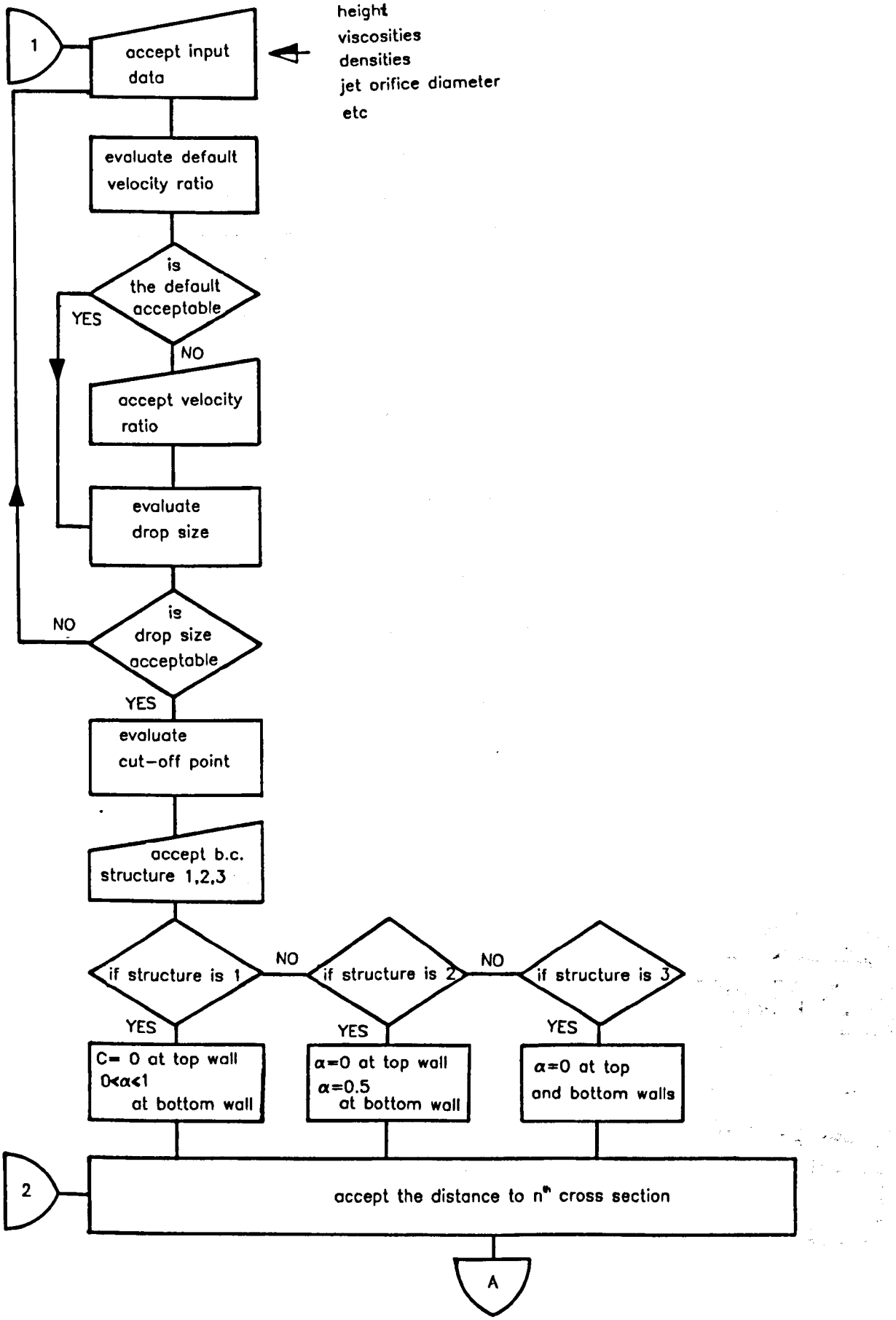

FIG. 8.3 FLOW CHART

FIG. 8.3 CONT.

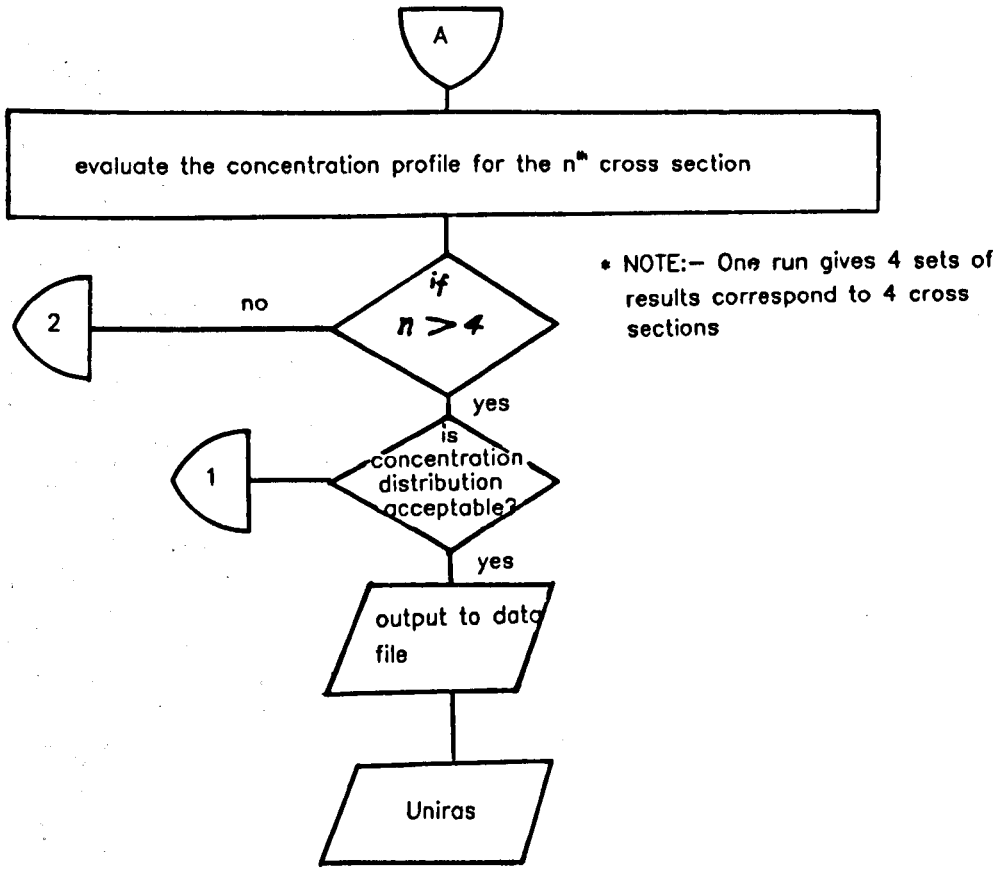
A
evaluate the concentration profile for the n^th cross section
if
n > 4
no
2
yes
is
concentration
distribution
acceptable?
1
yes
output to data
file
Uniras
* NOTE:- One run gives 4 sets of results correspond to 4 cross sections

GEOMETRICAL PARAMETERS

HEIGHT= 0.2 Metres

JET DIA./HEIGHT= 0.019

KINEMATIC PARAMETERS

REYNOLDS NUMBER= 21333

VELOCITY RATIO= 50

K. VISCOSITY OF OIL= 1.87 $\times 10^{-6}$ m^2/s

MAX. DROPLET DIAMETER= 0.58 mm

CUT-OFF POINT= 3.06 DIAS.

FIG. 8.4 MIXING BY MULTI-NOZZLE MIXER

STICKING PROBABILITY IS 0.0 AT TOP WALL

STICKING PROBABILITY IS 0.5 AT BOTTOM WALL

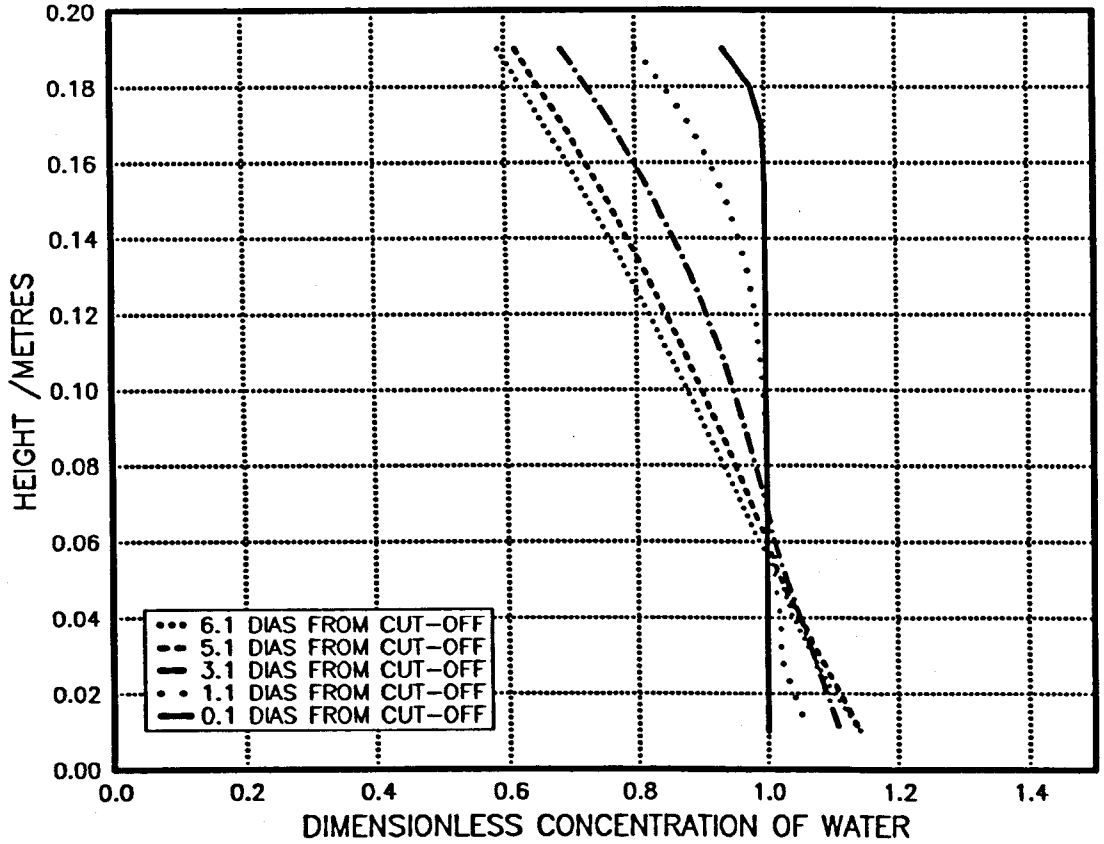

GEOMETRICAL PARAMETERS

HEIGHT= 0.2 Metres

JET DIA./HEIGHT= 0.019

KINEMATIC PARAMETERS

REYNOLDS NUMBER= 21333

VELOCITY RATIO= 50

K. VISCOSITY OF OIL= 1.87 $\times 10^{-6}$ m^2/s

MAX. DROPLET DIAMETER= 0.58 mm

CUT–OFF POINT= 3.06 DIAS.

FIG. 8.5 MIXING BY MULTI–NOZZLE MIXER

STICKING PROBABILITY IS 0.0 AT TOP WALL

STICKING PROBABILITY IS 0.0 AT BOTTOM WALL

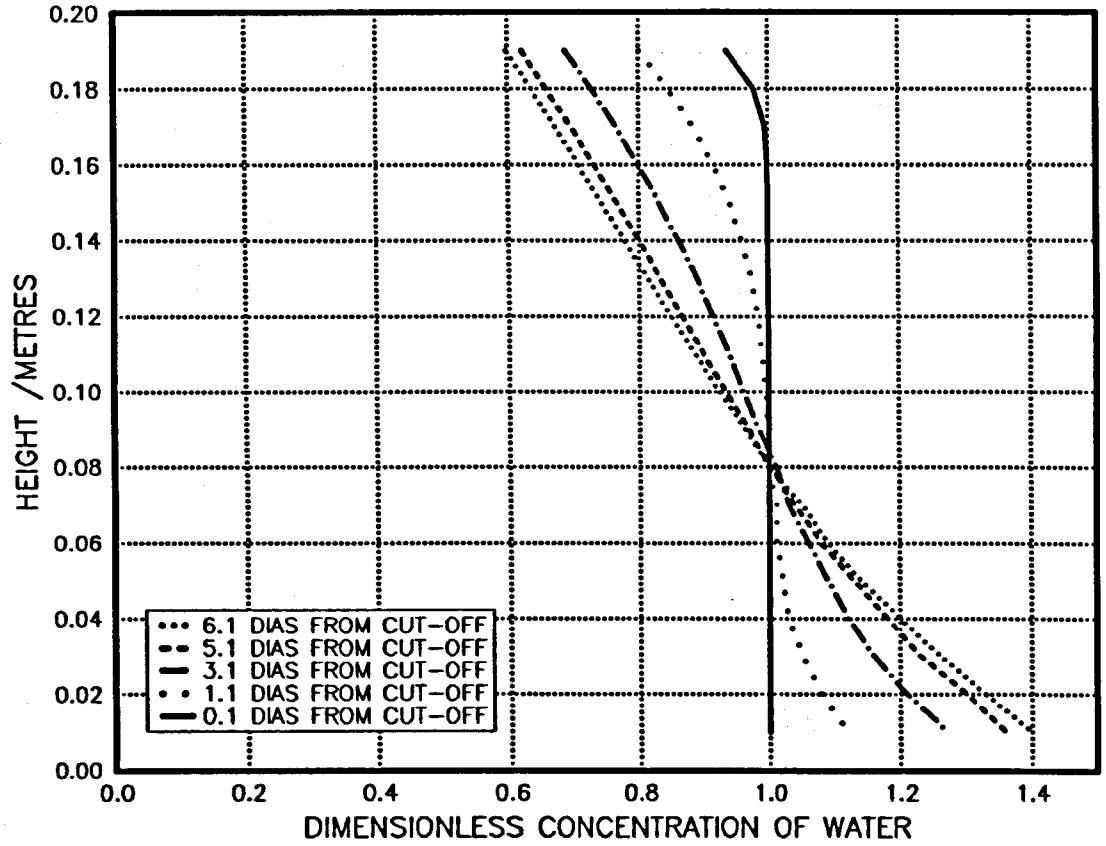

GEOMETRICAL PARAMETERS

HEIGHT= 0.2 Metres

JET DIA./HEIGHT= 0.019

KINEMATIC PARAMETERS

REYNOLDS NUMBER= 21333

VELOCITY RATIO= 60

K. VISCOSITY OF OIL= 1.87 $x10^{-6}$ m^2/s

MAX. DROPLET DIAMETER= 0.41 mm

CUT-OFF POINT= 2.75 DIAS.

FIG. 8.6 MIXING BY MULTI-NOZZLE MIXER

STICKING PROBABILITY IS 0.0 AT TOP WALL

STICKING PROBABILITY IS 0.5 AT BOTTOM WALL

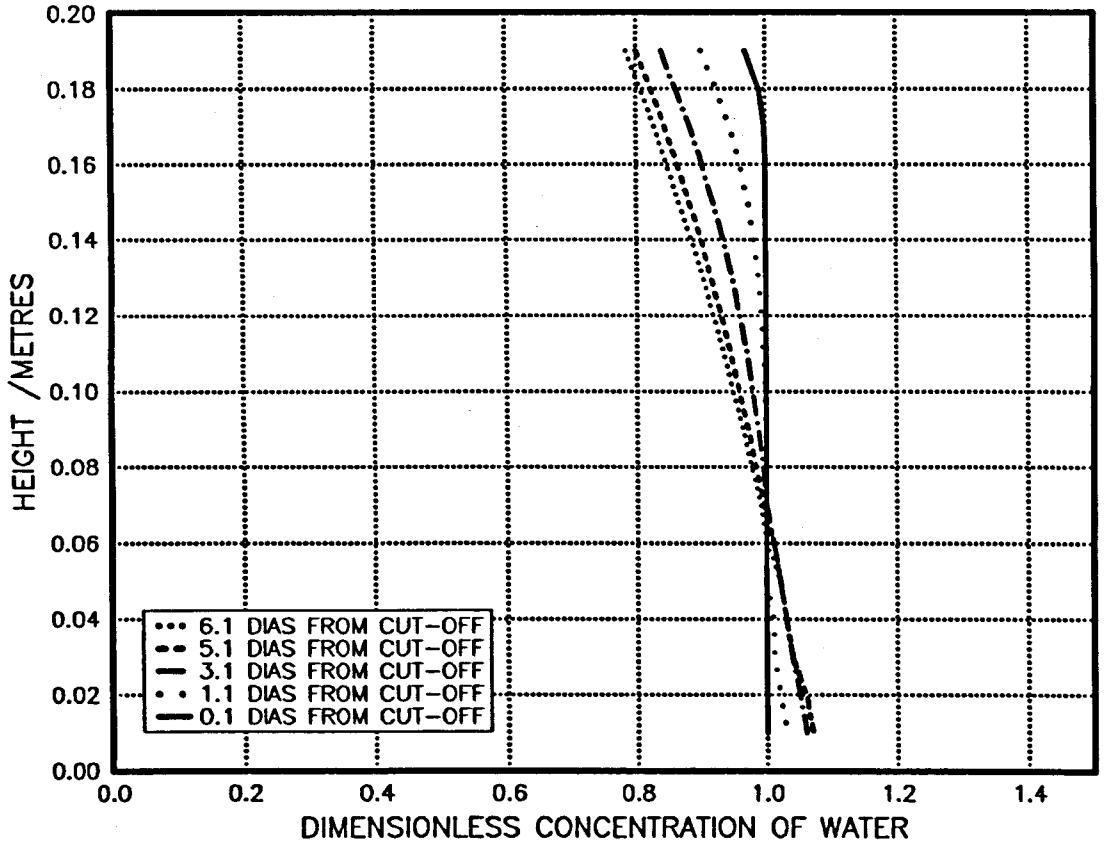

GEOMETRICAL PARAMETERS

HEIGHT= 0.2 Metres

JET DIA./HEIGHT= 0.019

KINEMATIC PARAMETERS

REYNOLDS NUMBER= 21333

VELOCITY RATIO= 60

K. VISCOSITY OF OIL= 1.87 x10^{-6} m^2/s

MAX. DROPLET DIAMETER= 0.46 mm

CUT–OFF POINT= 2.75 DIAS.

FIG. 8.7 MIXING BY MULTI–NOZZLE MIXER

STICKING PROBABILITY IS 0.0 AT TOP WALL

STICKING PROBABILITY IS 0.0 AT BOTTOM WALL

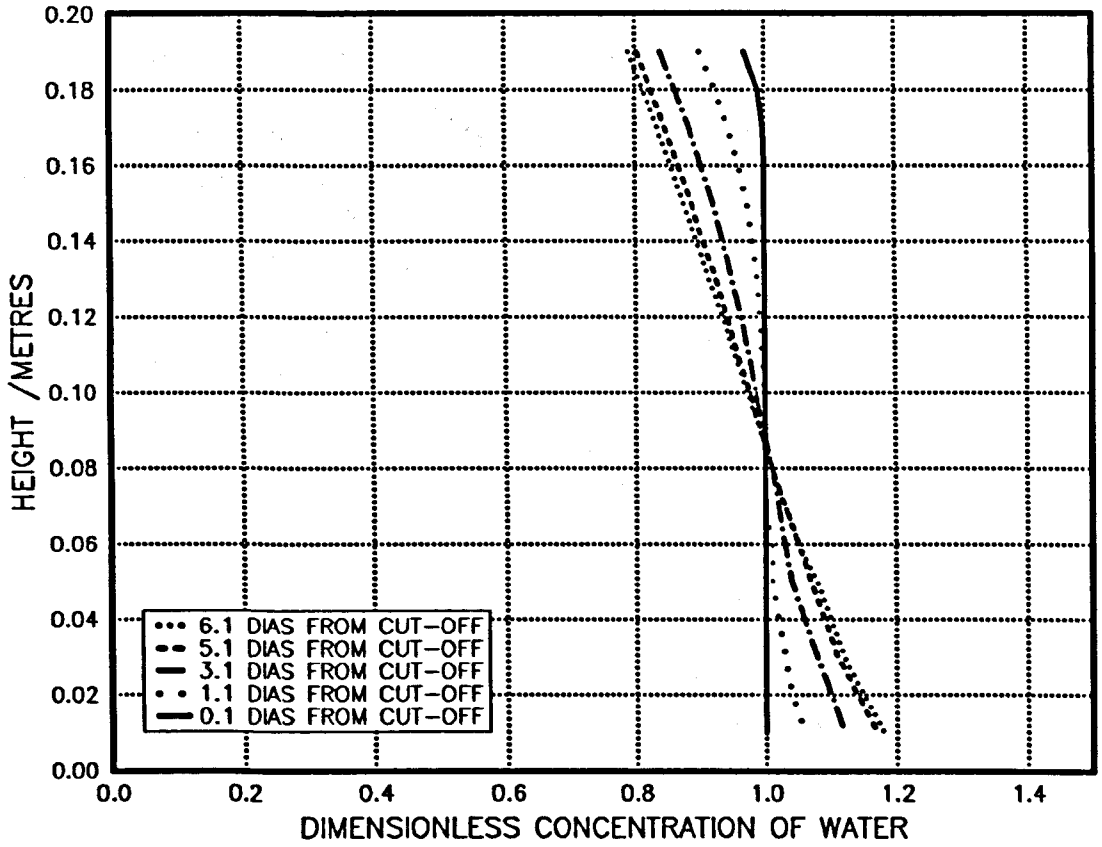

GEOMETRICAL PARAMETERS

HEIGHT= 0.2 Metres

JET DIA./HEIGHT= 0.019

KINEMATIC PARAMETERS

REYNOLDS NUMBER= 21333

VELOCITY RATIO= 35

K. VISCOSITY OF OIL= 1.87 $x10^{-6}$ m^2/s

MAX. DROPLET DIAMETER= 1.19 mm

CUT-OFF POINT= 3.88 DIAS.

FIG. 8.8 MIXING BY MULTI-NOZZLE MIXER

STICKING PROBABILITY IS 0.0 AT TOP WALL

STICKING PROBABILITY IS 0.5 AT BOTTOM WALL

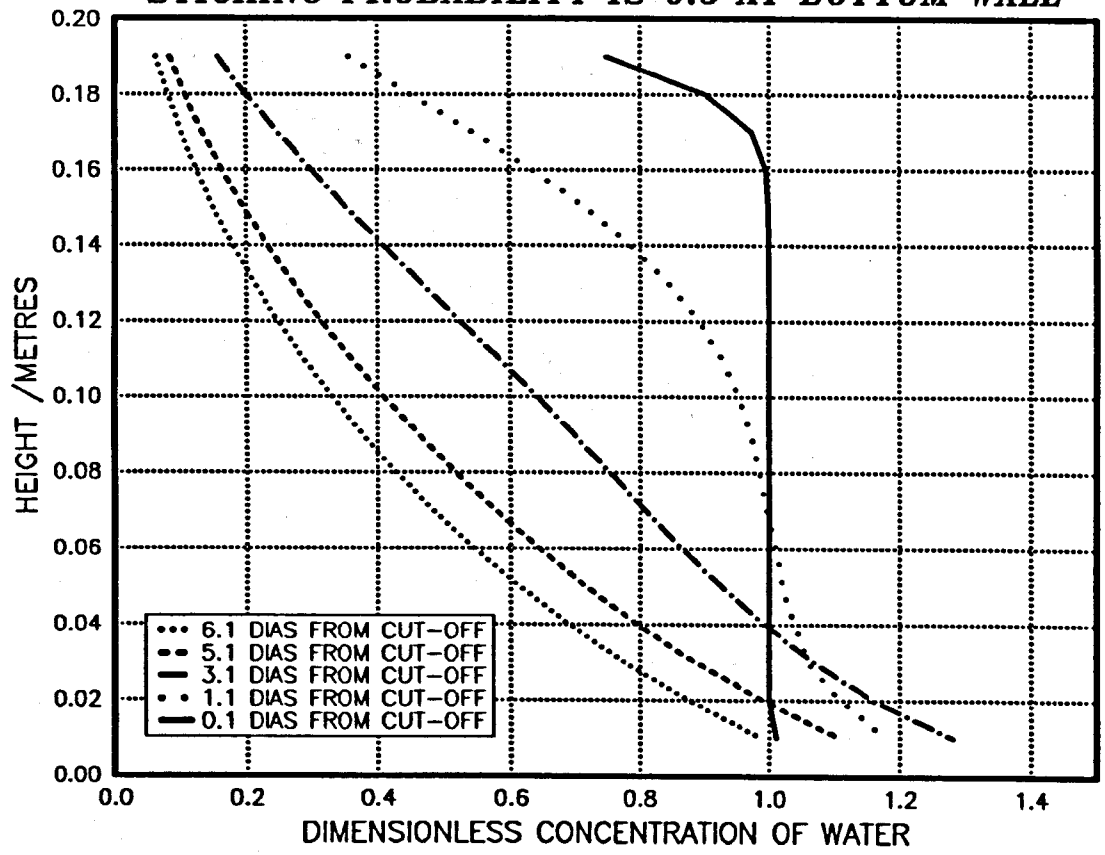

FIG.8.9 MIXING BY MULTI–NOZZLE MIXER (JMIX21)

STICKING PROBABILITY IS 0.4 AT BOTTOM WALL

CONCENTRATION IS ZERO AT TOP WALL

GEOMETRICAL PARAMETERS

HEIGHT= 0.2 Metres

JET DIA./HEIGHT= 0.019

KINEMATIC PARAMETERS

REYNOLDS NUMBER= 69444

VELOCITY RATIO= 20

K. VISCOSITY OF OIL= 1.87 x10^{-6} m^2/s

MAX. DROPLET DIAMETER= 0.15 mm

CUT–OFF POINT= 8.1 DIAS.

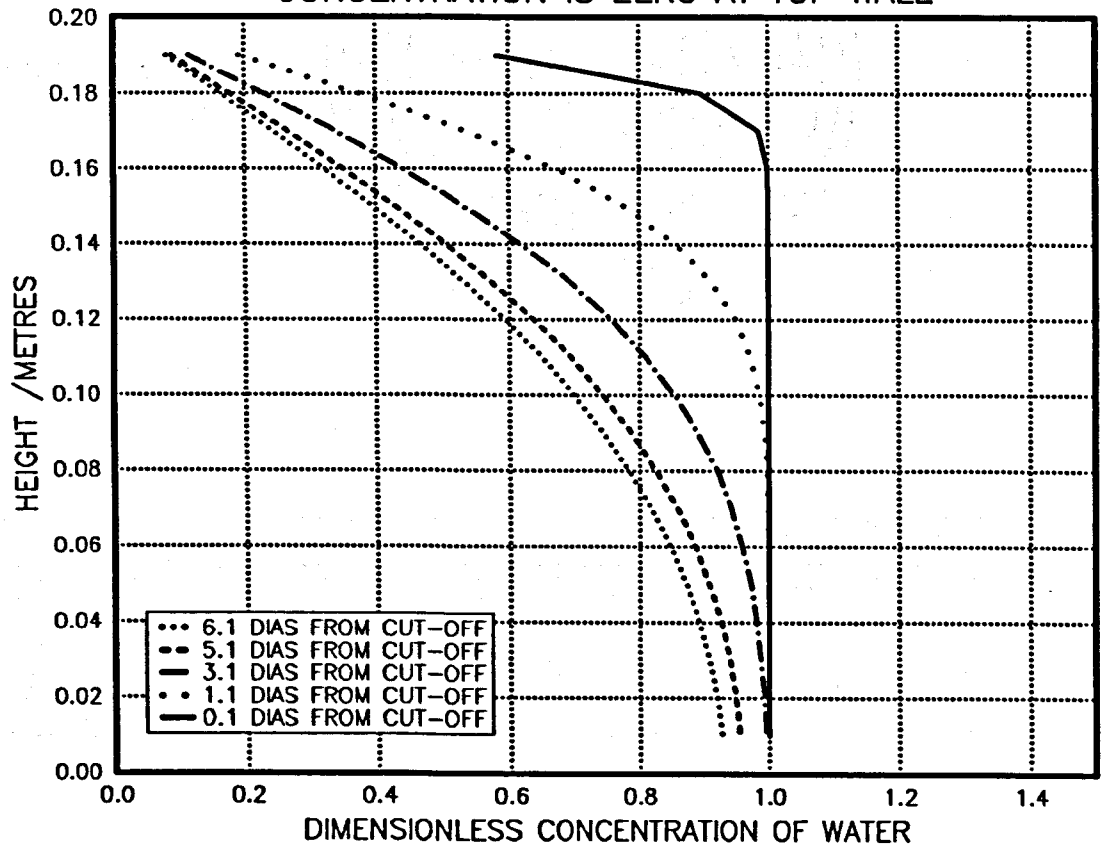

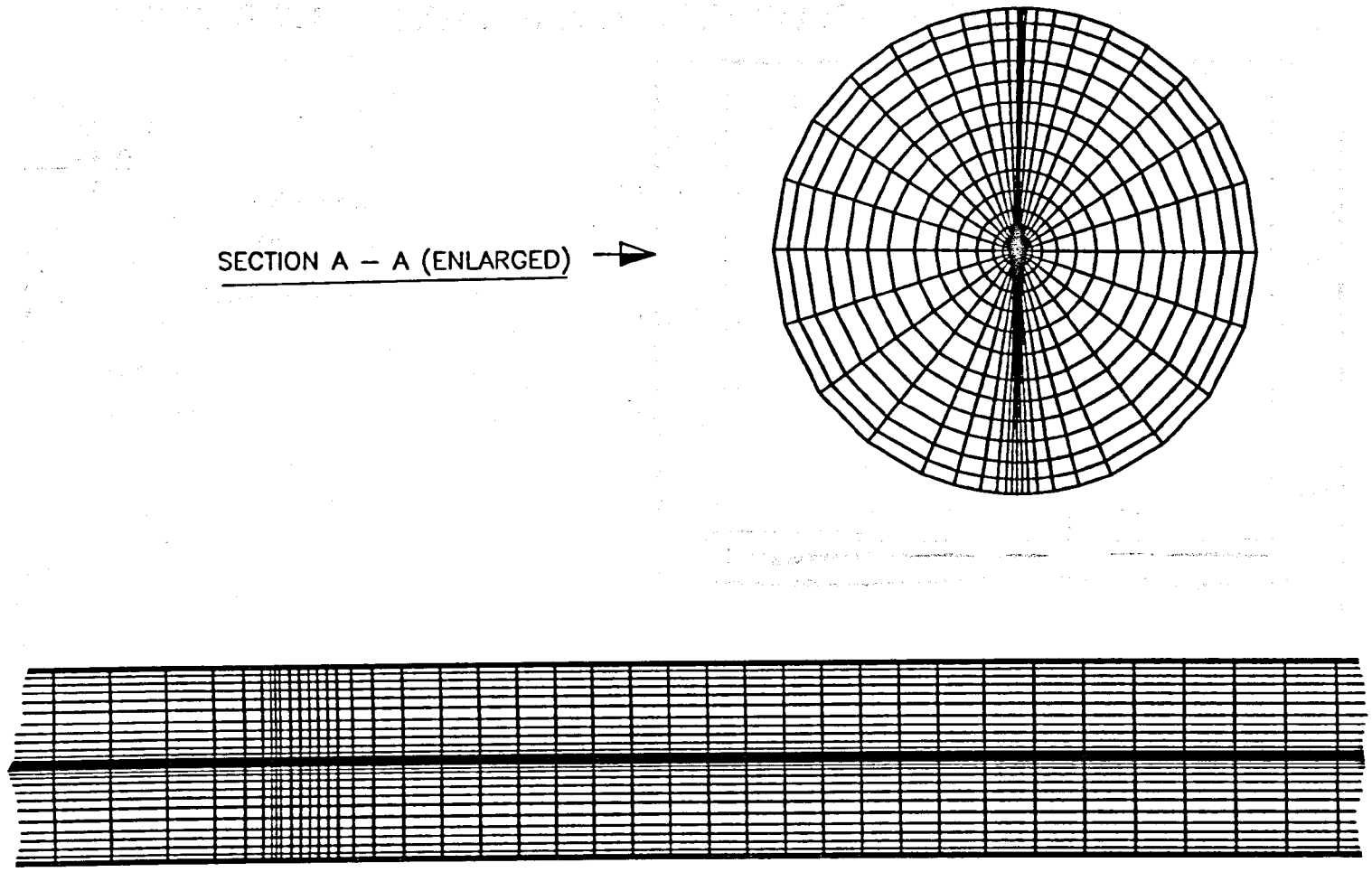

FIG. 9.1 DETAILS OF FINITE VOLUME GRIDS

FIG. 9.2.1 TANGENTIAL VELOCITY COMPARISION

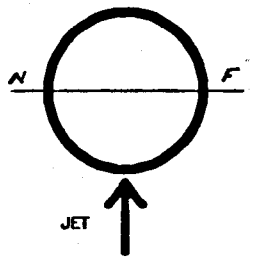

N ≡ NEAR WALL

F ≡ FAR WALL

O EXPERIMENTAL

× CALCULATED

Position= 1 diameter downstream from jet

Reynolds number = 27600

Velocity ratio = 17

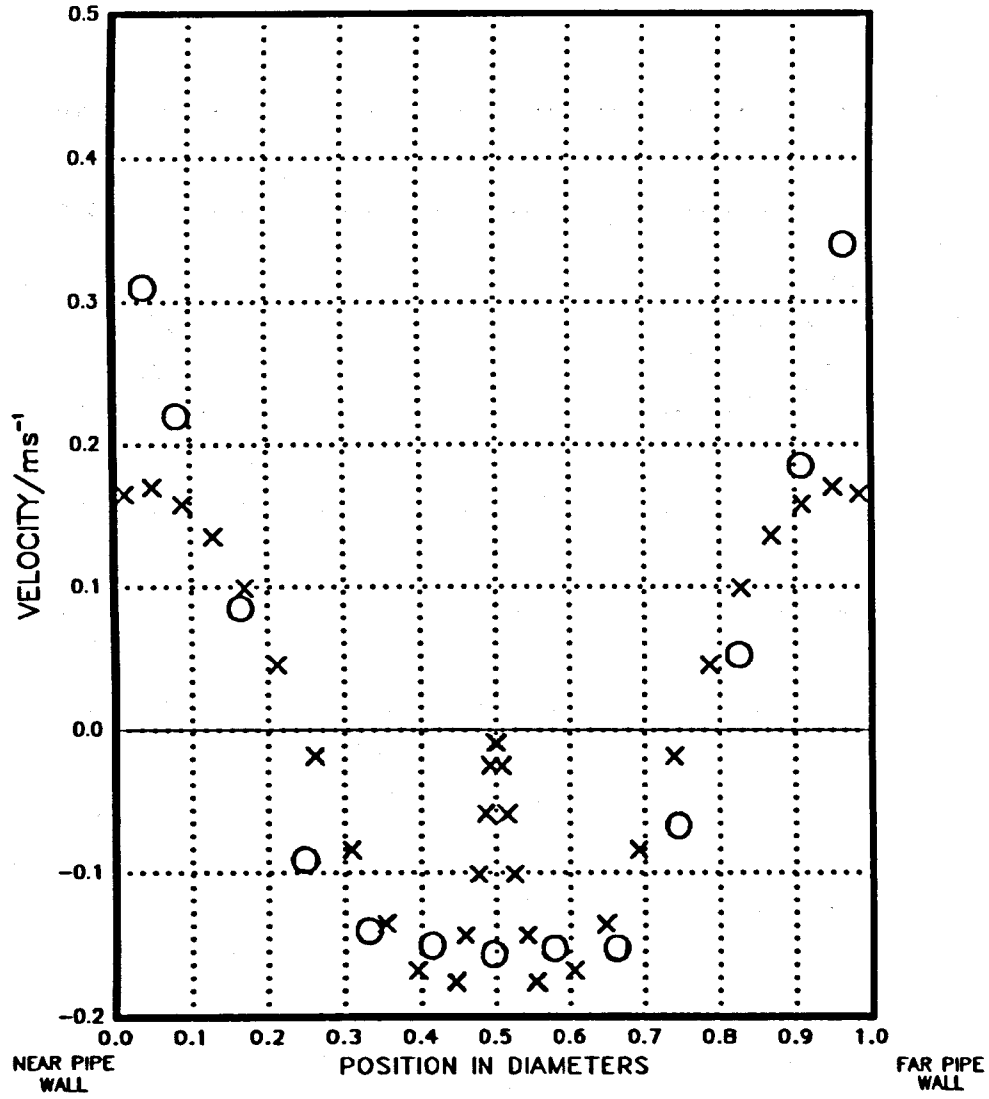

FIG. 9.2.2 TANGENTIAL VELOCITY COMPARISION

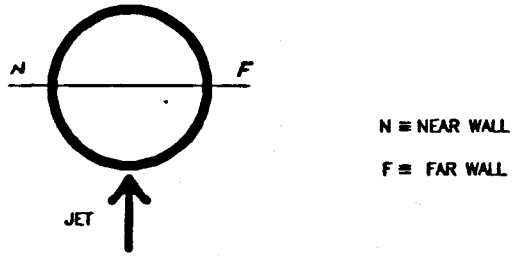

N ≡ NEAR WALL

F ≡ FAR WALL

O EXPERIMENTAL

× CALCULATED

Position= 2 diameters downstream from jet

Reynolds number = 27600

Velocity ratio = 17

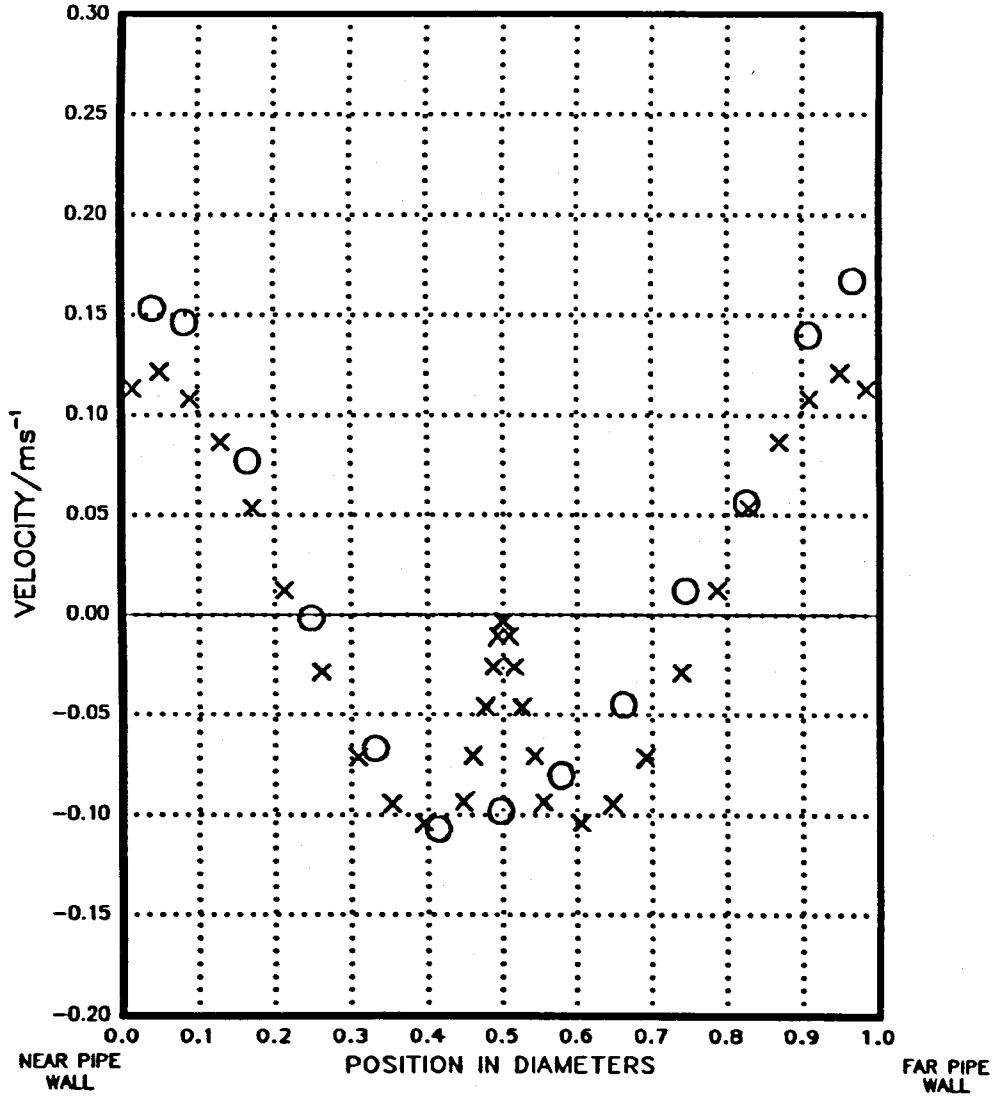

FIG. 9.2.3 TANGENTIAL VELOCITY COMPARISION

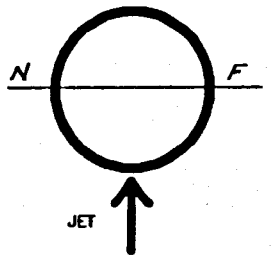

N ≡ NEAR WALL

F ≡ FAR WALL

O EXPERIMENTAL

× CALCULATED

Position= 3 diameters downstream from jet

Reynolds number = 27600

Velocity ratio = 17

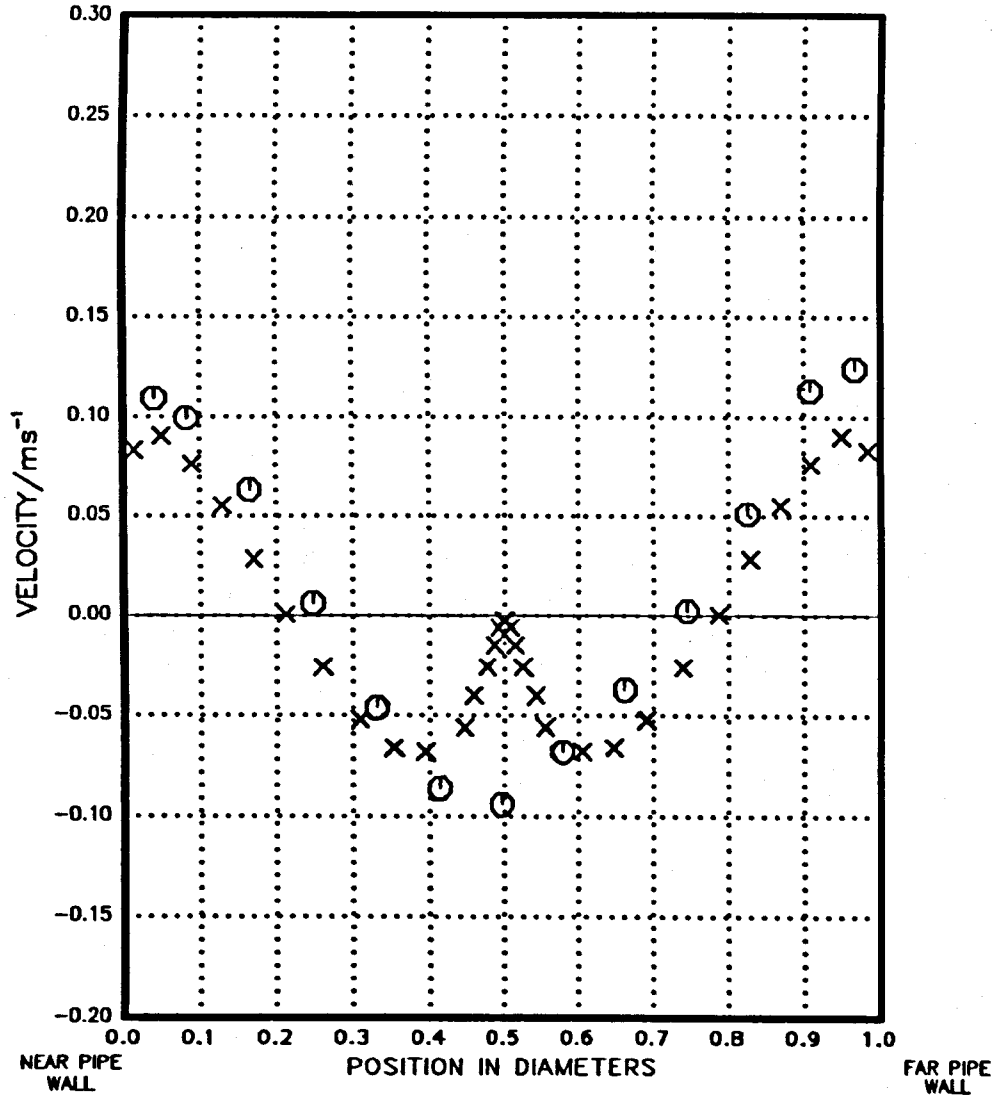

FIG. 9.2.4 TANGENTIAL VELOCITY COMPARISION

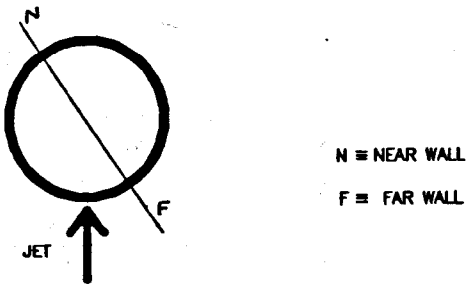

N ≡ NEAR WALL

F ≡ FAR WALL

O EXPERIMENTAL

× CALCULATED

Position= 1 diameter downstream from jet

Reynolds number = 27600

Velocity ratio = 17

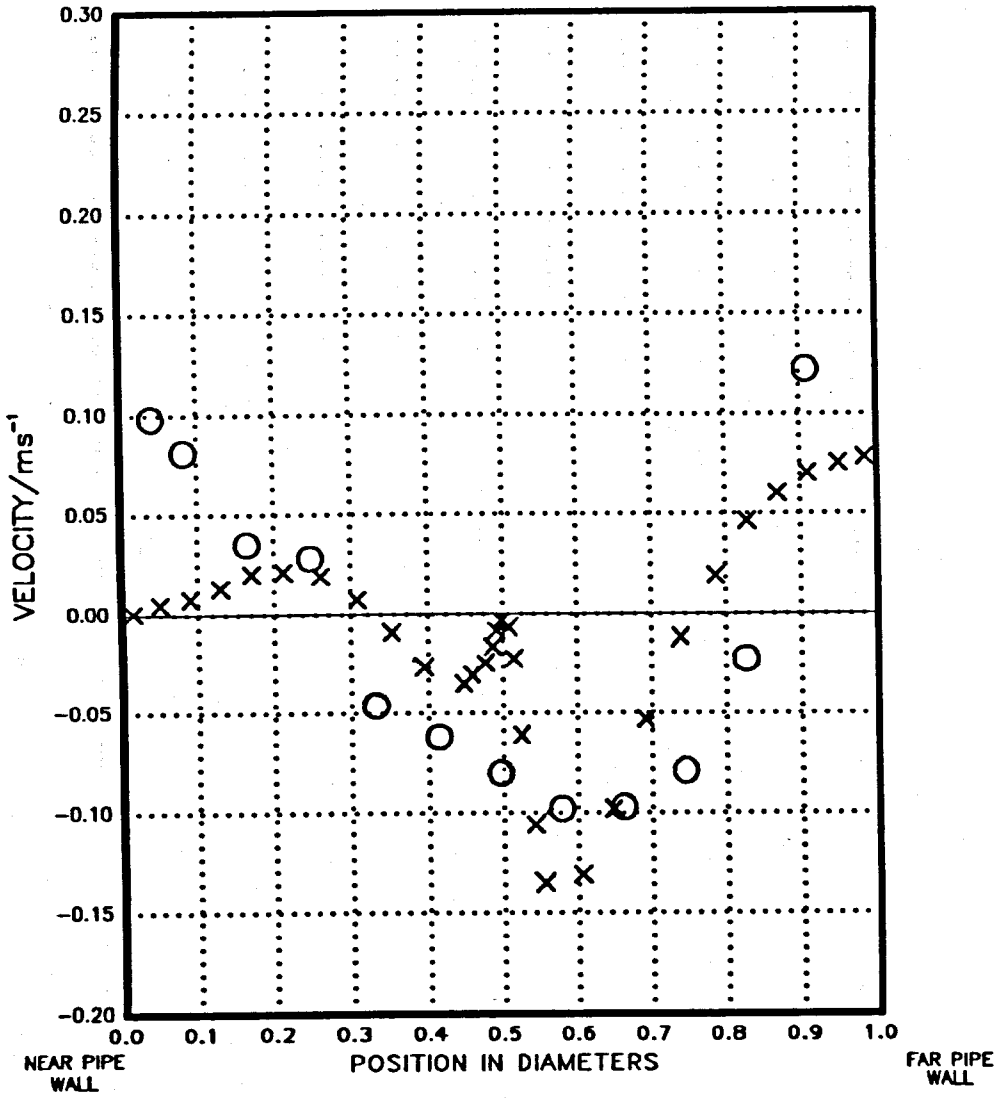

FIG. 9.2.5 TANGENTIAL VELOCITY COMPARISION

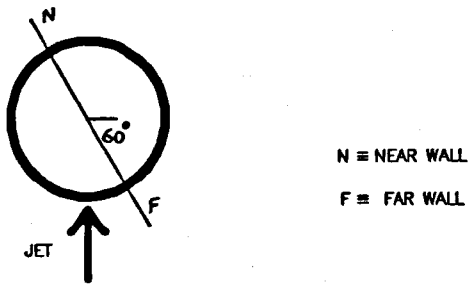

N ≡ NEAR WALL

F ≡ FAR WALL

O EXPERIMENTAL

× CALCULATED

Position= 2 diameters downstream from jet

Reynolds number = 27600

Velocity ratio = 17

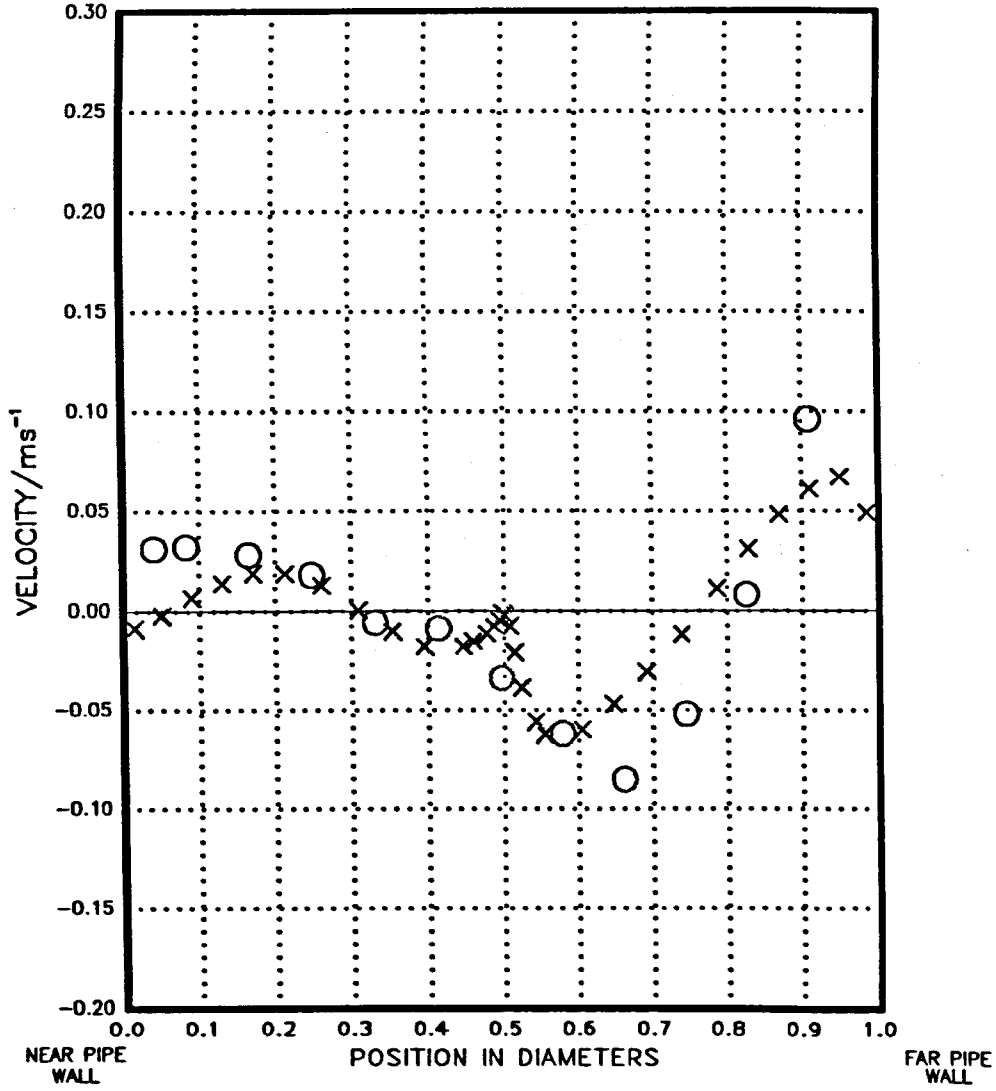

FIG. 9.2.6 *TANGENTIAL VELOCITY COMPARISION*

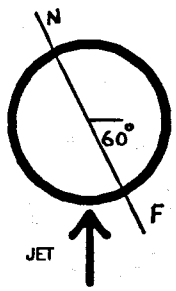

N ≡ NEAR WALL

F ≡ FAR WALL

O EXPERIMENTAL

× CALCULATED

Position= 3 diameters downstream from jet

Reynolds number = 27600

Velocity ratio = 17

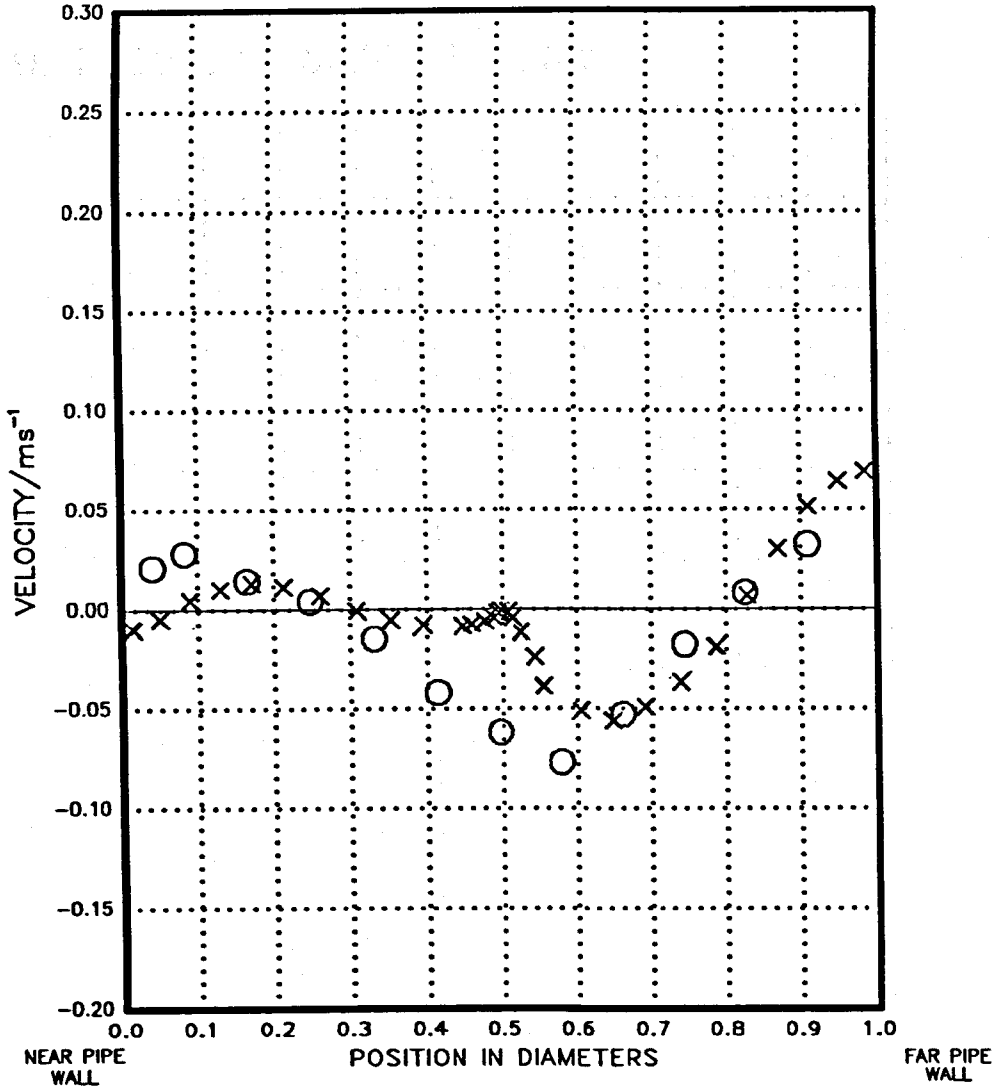

FIG. 9.3.1 AXIAL VELOCITY COMPARISION

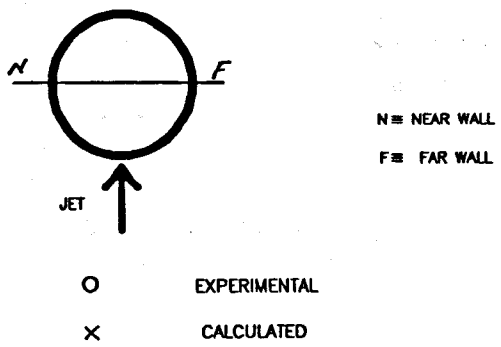

Position= 2 diameters downstream from jet

Reynolds number = 27600

Velocity ratio = 17

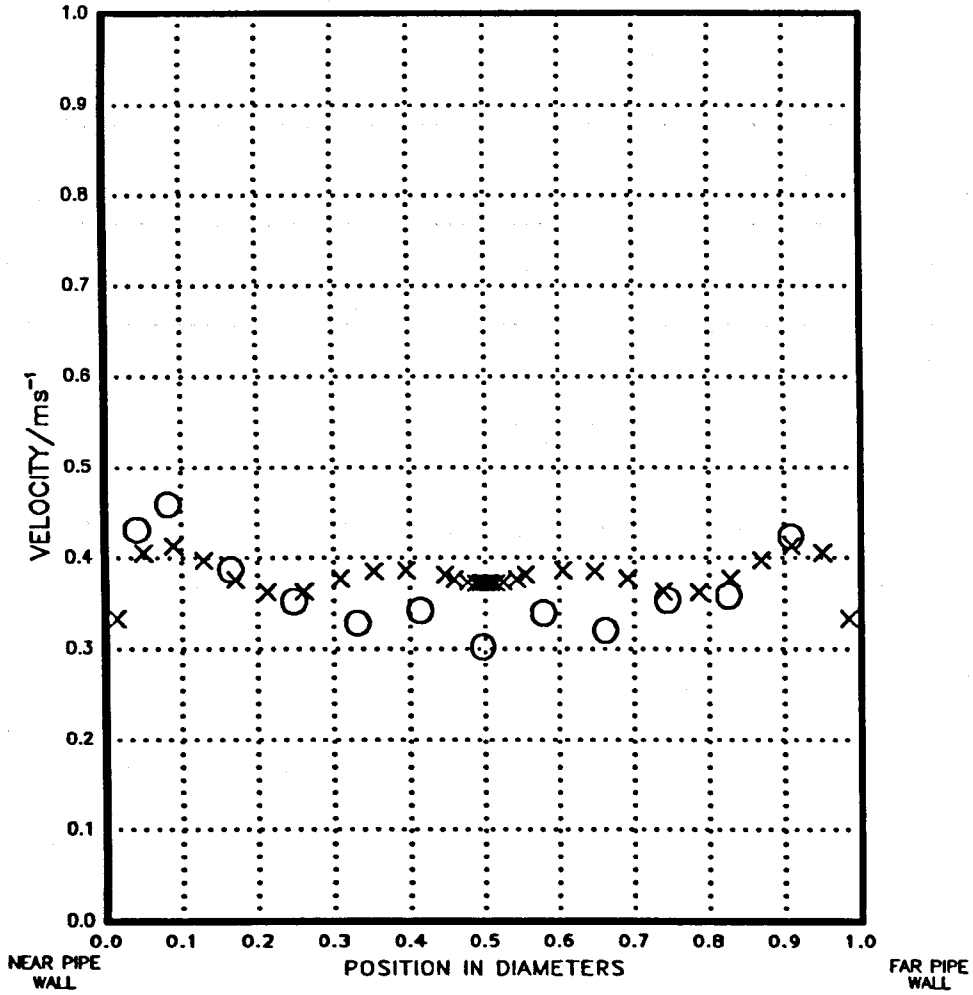

FIG. 9.3.2 AXIAL VELOCITY COMPARISION

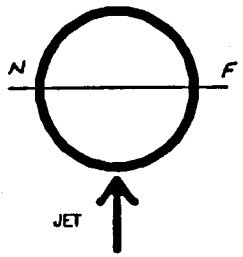

N ≡ NEAR WALL

F ≡ FAR WALL

O EXPERIMENTAL

× CALCULATED

Position= 3 diameters downstream from jet

Reynolds number = 27600

Velocity ratio = 17

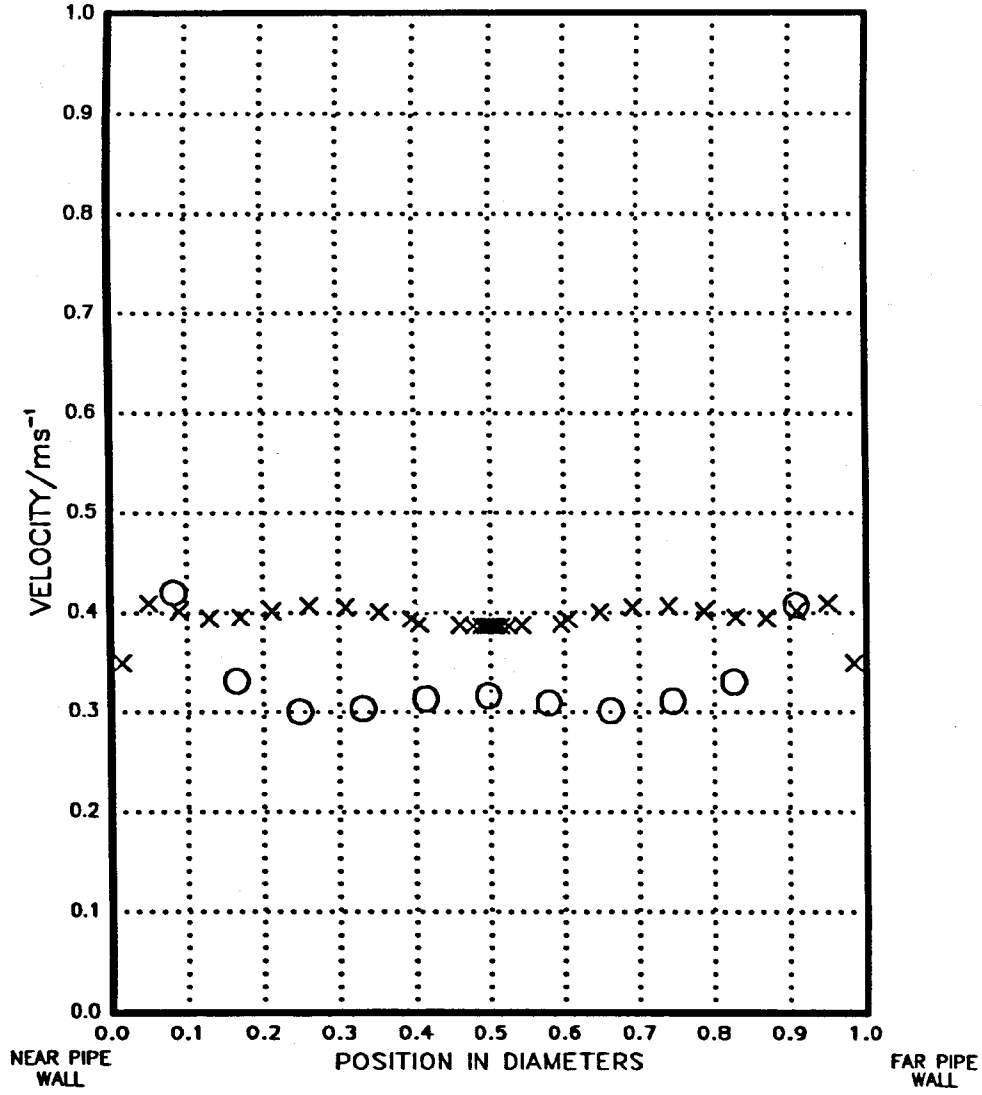

FIG. 9.3.3 AXIAL VELOCITY COMPARISION

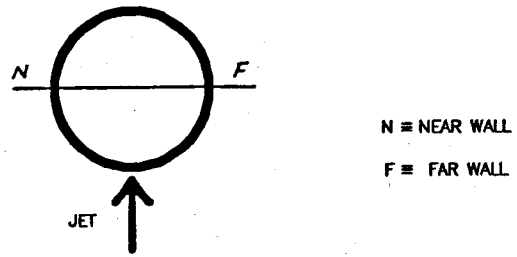

N ≡ NEAR WALL

F ≡ FAR WALL

O EXPERIMENTAL

× CALCULATED

Position= 4 diameters downstream from jet

Reynolds number = 27600

Velocity ratio = 17

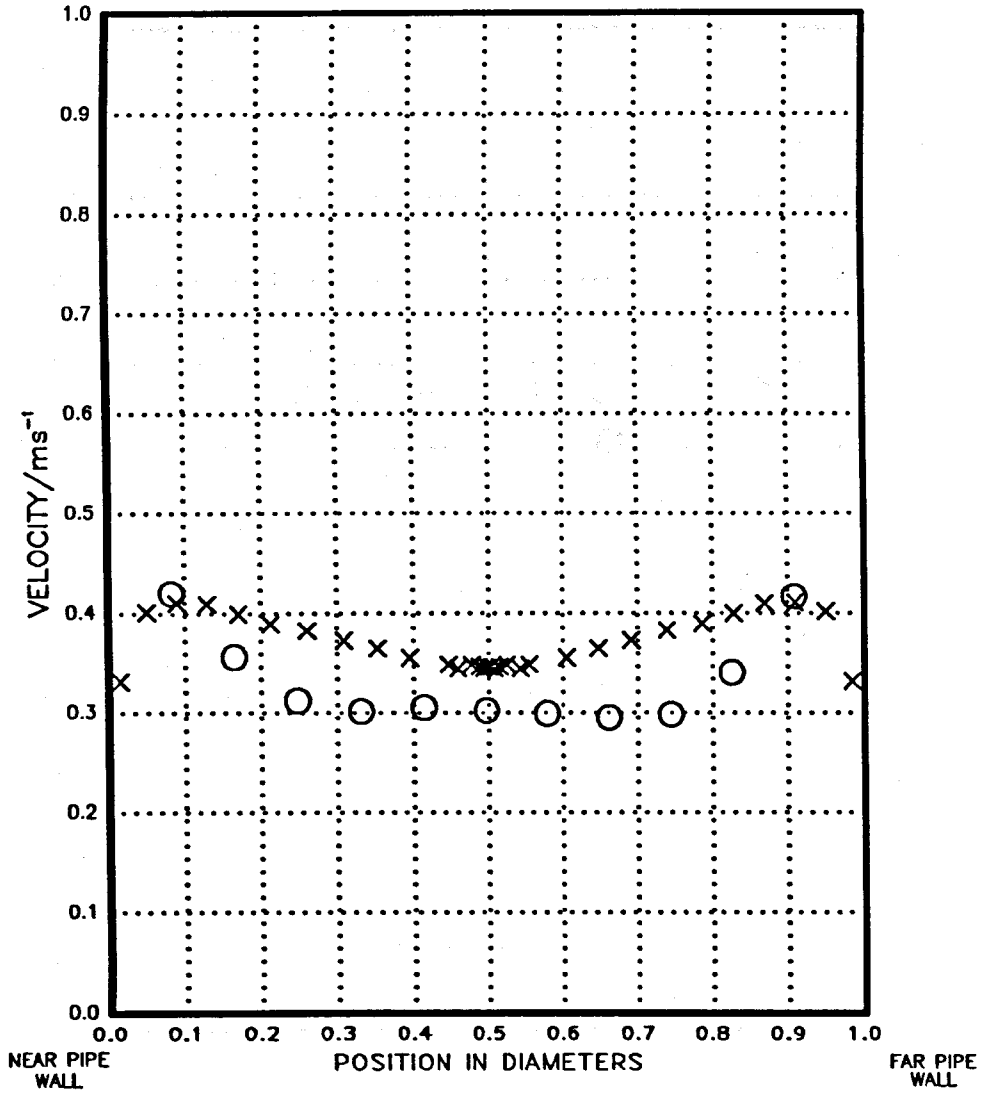

FIG. 9.3.4 AXIAL VELOCITY COMPARISION

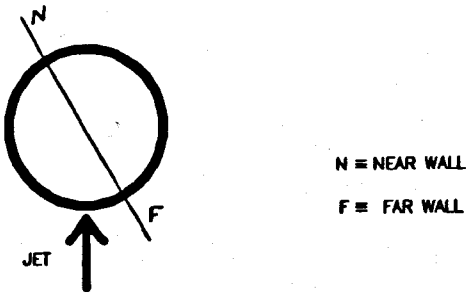

N ≡ NEAR WALL

F ≡ FAR WALL

O EXPERIMENTAL

× CALCULATED

Position= 1 diameter downstream from jet

Reynolds number = 27600

Velocity ratio = 17

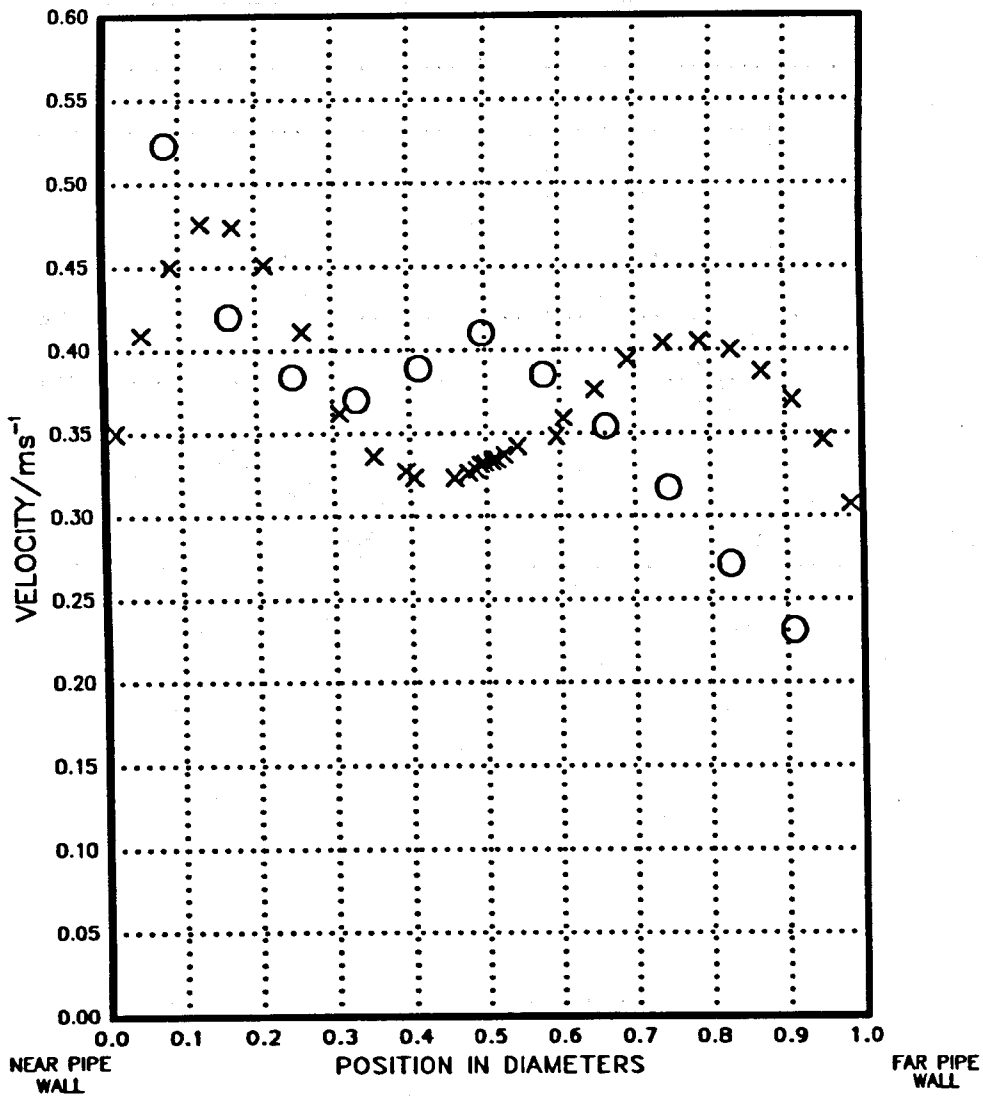

FIG. 9.3.5 AXIAL VELOCITY COMPARISION

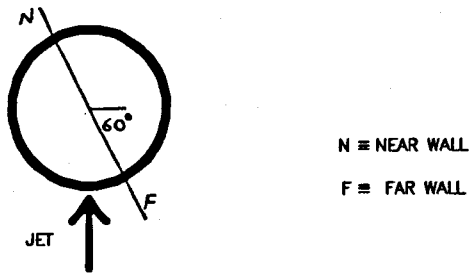

N ≡ NEAR WALL

F ≡ FAR WALL

O EXPERIMENTAL

× CALCULATED

Position= 2 diameters downstream from jet

Reynolds number = 27600

Velocity ratio = 17

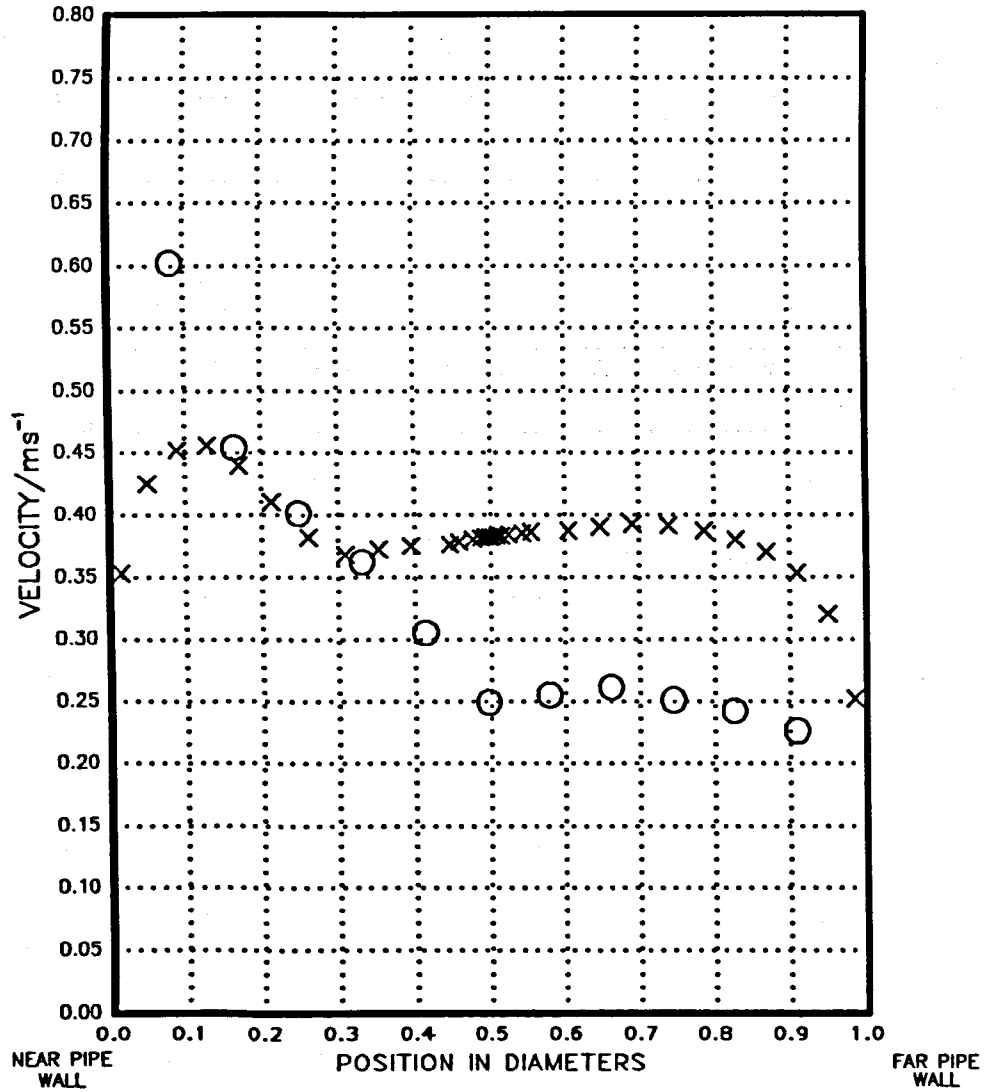

FIG. 9.3.6 AXIAL VELOCITY COMPARISION

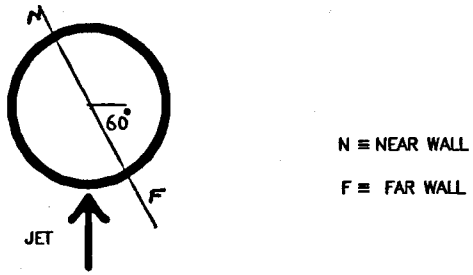

N ≡ NEAR WALL

F ≡ FAR WALL

O EXPERIMENTAL

× CALCULATED

Position= 3 diameters downstream from jet

Reynolds number = 27600

Velocity ratio = 17

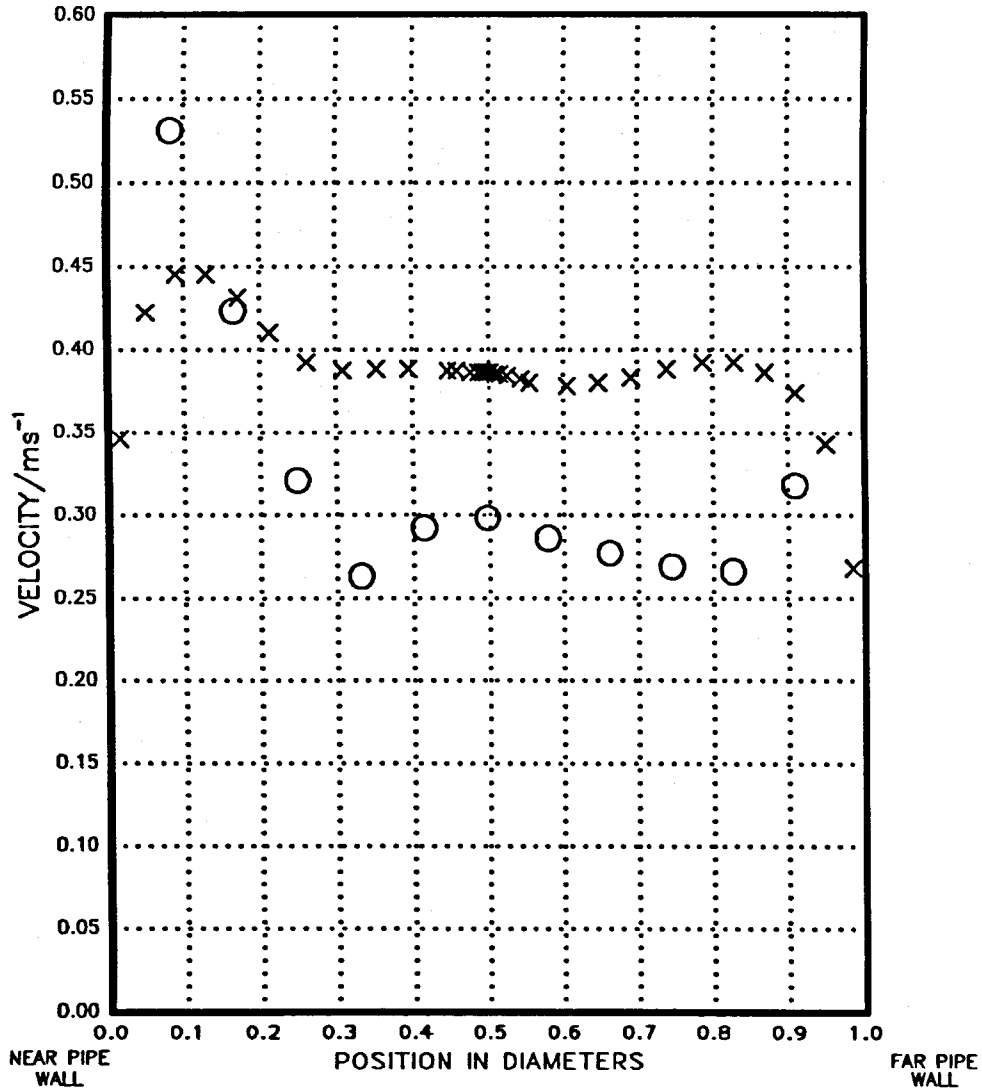

APPENDICES

APPENDIX A3

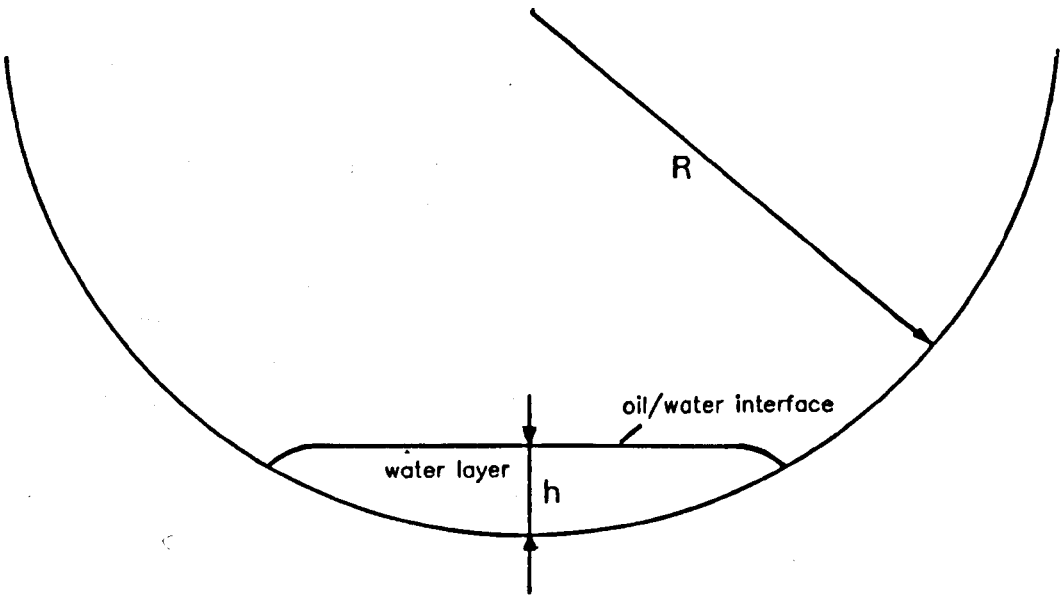

$$\frac{A_S}{\pi R^2} = \frac{1}{\pi}\left\{\cos^{-1}\left[\frac{R-h}{R}\right] - \frac{(R-h)(2Rh-H^2)^{\frac{1}{2}}}{R^2}\right\}$$

where A_S is cross sectional area of the water layer

h/mm	$A_S/\pi R^2$
5	0.0113
10	0.0318
15	0.0576

APPENDIX A4

A4.1) Displacement thickness on a smooth plate

Displacement thickness for turbulent flow 'δ' = $0.018Y/(VY/\nu)^{1/7}$
(Blevins, 1984)

if Y = 5mm; $\nu = 1.48\times10^{-6}$; V = 6 m/s

$$\delta = 0.018\times5\times10^{-3}/(6\times5\times10^{-3}/1.48\times10^{-6})^{1/7}$$
$$= \underline{0.022\times10^{-3}\ m.}$$

A4.2 Shape of a interface between two immiscible fluids

This shape is given as (Champion et al, 1961):-

$\sigma(1/R_1 + 1/R_2) - \rho gy$ = constant, where 'y' is the vertical distance from a reference point. (A.4.1)

R_1, R_2 = the principal radii of curvature
σ = interfacial surface tension
ρ = $\rho_2 - \rho_1$ = density difference of the two fluids.

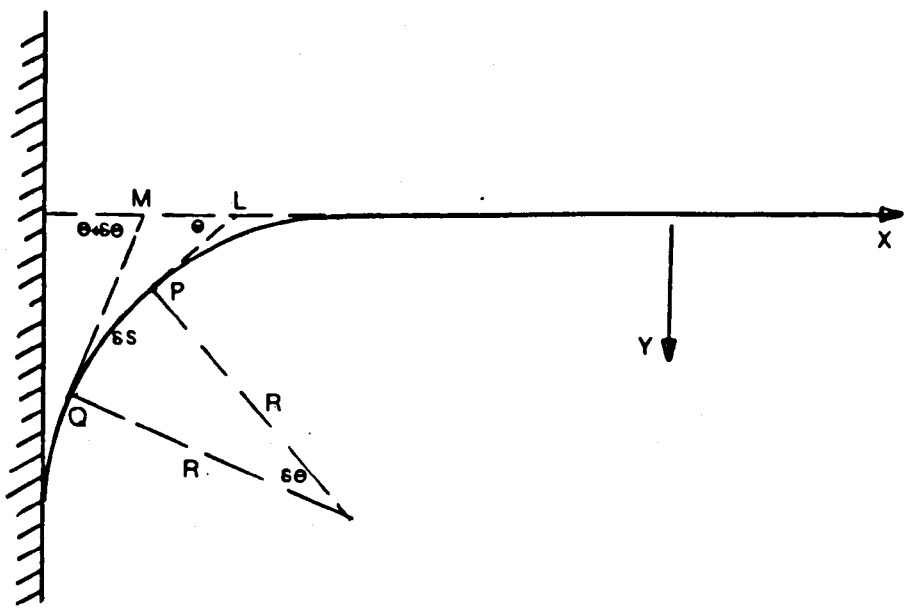

We take the origin from the upper-most point of the interface.

Therefore, the constant in the equation A.4.1 becomes zero. And if we also consider a two dimensional situation $R_2 \rightarrow \infty$.

Hence, the equation A.4.1 becomes:-

$\sigma/R = \rho g y$, where $R_1 = R$ (A.4.2)

Consider the tangents PL, QM and normal PS, QS drawn at P and Q two points on the curvature, between elementary distance 'δs'. Let the tangents make angles 'θ' and '$\theta+\delta\theta$' with axis 'OX'. The normal meet at S, the centre of curvature. The angle PSQ = $\delta\theta$, PS = QS = R and PQ = δs.

Hence, $\delta s = R\delta\theta \rightarrow 1/R = \delta\theta/\delta s$ and $\sigma/R = \sigma\delta\theta/\delta s = \rho g y$ (A.4.3)

Since $\delta y/\delta s = \text{Sin}\ \theta \rightarrow 1/\delta s = \text{Sin}\theta/\delta y$
Hence equation A.4.3 becomes:-
$\sigma(\delta\theta/\delta s)\delta y = \sigma\ \text{Sin}\theta\ \delta\theta = \rho g y\ \delta y$

On integrating we have:-

$-\sigma\ \text{Cos}\ \theta = \frac{1}{2}\rho g y^2 + \text{constant}$

When $y = 0$; $\theta = 0$; $\text{Cos}\theta = 1$; the constant = 2σ

Hence, $g(\rho_2 - \rho_1)y^2 = 2\sigma(1 - \text{Cos}\theta)$ (A.4.4)

A4.3 Calculation of interface area

For example i):-

h = 18mm

liquid/liquid system = pure kerosene and pure water

Hence, $\rho_{oil} = 800\ kg/m^3$

$\rho_w = 1000\ kg/m^3$

$\sigma = 0.033\ Nm^{-1}$

$\theta = 95^0$ (from photographs figs. 4.4.6 to 4.4.9)

R = 70mm

From equation 4.4.5:-

$$r = \{2\sigma/g(\rho_w - \rho_{oil})\}^{1/2} = 5.8\times10^{-3} \text{ m}$$

To find 'γ', from equation 4.4.6, first 'ψ' was taken as 180^0 and the corresponding 'γ' was calculated.

Equation 4.4.6 is:-

$$\text{Cos } \gamma = \{R + r[1 + \text{Cos}(\gamma+\psi)] - h\}/R$$

$$\text{Cos } (R + r) = R + r - h$$

Substituting the appropriate values gives, $\gamma = 40.3$. Now , when $\psi = 95$ estimate a value for 'γ' as 39^0. Substituting this value to right hand side of equation 4.4.6 gives a value of 0.768. Equating the left hand side to this value gives $\gamma = 39.8^0$.

When 'γ' is guessed for the second time as 39.9^0 and equating the right hand side of the equation 4.4.6 gives 0.767, which in fact correspond to Cos 39.9. Hence, 'γ' in this particular example is 39.9^0.

Interface area = $2(L_2 + L_1)$x depth (equation 4.4.4)

depth = 0.134 m.

From equation 4.4.2, $L_2 = [r(180-\gamma-\psi)/180]\pi$

$= \underline{4.565\times10^{-3} \text{ m}}$

From equation 4.4.3:-

$$L_1 = (R \text{ Sin}\gamma) - r \text{ Cos}(90-\gamma-\psi)$$

$$= 40.79\times10^{-3} \text{ m}$$

Therefore, interface area = $\underline{12.16\times10^{-3} \text{ m}}$

<u>Example ii):-</u>

Since equation for 'r' is changing with fluid properties, the interface area should also change with fluid properties. Therefore,

this example considers the other extreme of the value 'r' for the

fluid properties on test. Other extreme value of 'r' would be when the fluid properties are:-

ρ_{oil} = 813 kg/m^3

ρ_w = 1000 kg/m^3

σ = 0.023 Nm^{-1}

h = 18mm

R = 70 mm and the photographic prints shown that 'ψ' is still the same at 95°.

Therefore, $r = \{2\sigma/g(\rho_w - \rho_{oil})\}^{\frac{1}{2}} = 5.01 \times 10^{-3}$

As before by trail and error 'γ' was found to be 40.2°.

Therefore, $L_1 = \{r(180-\gamma-\psi)/180\}\pi = 3.9\times10^{-3}$ m.

$L_2 = (R \sin\gamma) - r \cos(90-\gamma-\psi) = 41.65\times10^{-3}$ m.

Therefore, interface area = $\underline{12.2\times10^{-3}\ m}$

Similarly, a plot drawn, as before, for interface area aginst height for these fluid properties almost coincides with the plot in fig. 4.5.1 with negligible difference. Therefore, this curve will be used in future for all fluid properties to obtain interface area as a function of a height.

A4.4 Sample calculation for entrainment

i). V_j = 7.6 m/s; h = 18 mm (for initial setting ie: t= 0.0)
Liquid/liquid system = pure kerosene and pure water

Results:- a plot of these results are shown in fig.4.5.3.

time/sec	0.4	0.5	0.6	0.7	0.8
interface drop/0.3705 mm					
position 1	3.05	3.825	4.6	5.375	6.8
position 3	2.85	4.275	5.3	6.125	6.6
average drop of position 1 & 3	2.95	4.05	4.95	5.75	6.7

From the least-square straight line fitting method:-

$$\bar{x} = 1/n \, \Sigma_{i=1}^{n} x_i = 0.6; \quad \bar{y} = 1/n \, \Sigma_{i=1}^{n} y_i = 4.88$$

If the line is given by $y = mx + c$

$$m = \Sigma(x_i-\bar{x})(y_i-\bar{y})/\Sigma(x_i-\bar{x}) = [\Sigma x_i y_i - n\bar{x}\bar{y}]/[\Sigma x_i^2 - n\bar{x}^2]$$
$$= [15.56 - 14.64]/[1.9 - 1.8]$$
$$= \underline{9.2}$$

Therefore, the interface drop rate = 9.2x0.3705 mm/sec
= $9.2 \times 0.3705 \times 10^{-3}$ m/s

Since the interface height has dropped from 18mm to a certain value in the range t= 0.4 to 0.8 seconds, it is not correct to assume that this drop rate corresponds to h = 18mm. Therefore, this drop rate was related to interface height at $\bar{x}$ (=0.6 sec.). Hence the interface height = 18 - $\bar{y}$x 0.3705) = <u>16.16 mm.</u>

The interface area corresponding to 16.16mm from fig. 4.5.1 is 11.55×10^{-3} m^2. Hence the interface volume drop rate = $(9.2 \times 0.3705 \times 10^{-3}) \times 11.55 \times 10^{-3}$ m^3/sec.

Since interface water mass drop rate = water entrainment rate

Water entrainment rate = <u>39.85×10^{-3} kg/sec</u>.

But when the velocity is changed between 4 m/s and 9 m/s (in the experiment corresponding to the plot in fig. 4.5.3) this effective interface height also change from a maximum to a minimum. They were, when calculated as above, (18 - 3.1x0.3705) = 16.85mm and (18 -

5.3x0.375) = 16mm respectively. Therefore, the effective interface height for this experimental range (4 m/s to 9 m/s) was taken as (16.8 + 16)/2 = 16.4 mm. Also note that the entrainment rate(E_w) corresponds to 4m/s and 9m/s are $25x10^{-3}$ and $43x10^{-3}$ kg/s respectively.

A4.5 Calculations related to drop size experiments

i). For the SMD against velocity experiment (fig. 4.6.9) the interface height was set 10.2mm at t=0.0 sec. The experiment was conducted for the velocity range 4.2 m/s to 9.0 m/s. As before (mentioned in A4.4 above), the water layer interface height is a function of time. The photographs were taken at t =0.6 sec. Therefore the SMD was related to the interface height at t= 0.6 sec. When the velocity was 4.2 m/s the level drop at position (2) and at 0.6 sec. was (2.15x 0.3705)mm. Therefore the SMD was related to height of {10.2 - [(2.15 + 5.4)/2]0.3705} = 8.8mm.

ii). Since entrainment is a weak function of interfacial surface tension and viscosity the level height at t= 0.6 sec was calculated, for the other two experiments of SMD against intefacial surface tension and oil viscosity (fig. 4.6.10 and 4.6.11), in correspond with μ_{oil}= 1.15 $x10^{-3}$ and σ= 0.033 Nm^{-1} and V_j = 5.8m/s. When the height was set h= 10.1 mm (at t=0 sec) the level drop at 0.6 sec. was (3.625x 0.3705)mm. Therefore the SMD was related to the level height at 0.6 sec, that is (10.1 - 3.625x 0.3705) = 8.76mm.

iii). The experiment of SMD against oil viscosity for the larger level height (fig. 4.6.11) the interface level at t=0.0 sec was set to 14.7 mm. For the conditions as in ii). the level drop at 0.6 sec was (3.2x 0.3705) mm. Therefore the SMD was related to the level height of (14.7- 3.2x 0.3705) mm = 13.51 mm.

A4.6 Image Data (ie. one example) From The Optomax V at ICAP

Sample Number 13/4/88 nos. 10 to 15
Center Position = 44 Field Pos. 1 =31 Field Pos. 2 = 51
1800 0
Calibration = 16.339869 Micron/pixel

Initial cursor position	Final cursor position	Difference	Size microns	Dia. square micron**2	Dia. Cube micron**3
1	22	-21	343.137	117743.1717	40402068.01
139	160	-21	343.137	117743.1717	40402068.01
159	187	-28	457.516	209321.1940	95767864.91
187	201	-14	228.758	52330.29851	11970983.11
216	255	-39	637.255	406093.7961	258785257.8
315	333	-18	294.118	86505.18734	25442701.72
387	416	-29	473.856	224539.6992	106399528.8
427	466	-39	637.255	406093.7961	258785257.8
432	478	-46	751.634	564953.6309	424638342.7
486	509	-23	375.817	141238.4077	53079792.84
528	552	-24	392.157	153786.9997	60308626.30
538	574	-36	588.235	346020.7493	203541613.8
570	586	-16	261.438	68349.77765	17869222.61
618	655	-37	604.575	365511.1156	220978938.7
644	674	-30	490.196	240292.1870	117790285.7
620	641	-21	343.137	117743.1717	40402068.01
483	508	-25	408.497	166869.5743	68165674.62
460	490	-30	490.196	240292.1890	117790285.7
528	551	-23	375.817	141238.4077	53079792.84
600	622	-22	359.477	129223.7984	46452998.61
629	652	-23	375.817	141238.4077	53079792.84
60	83	-23	357.817	141238.4077	53079792.84
104	147	-43	702.614	493666.9487	346857490.7
168	190	-22	359.477	129223.7984	46452998.61
168	190	-22	359.477	129223.7984	46452998.61
171	196	-25	408.497	166869.5743	68165674.62
195	218	-23	375.817	141238.4077	53079792.84
206	229	-23	375.817	141238.4077	53079792.84
260	281	-21	343.137	117743.1717	40402068.01
335	353	-18	294.118	86505.18734	25442701.72
396	414	-18	294.118	86505.18734	25442701.72
462	499	-37	604.575	365511.1156	220978938.7
501	518	-17	277.778	77160.49117	21433469.40
553	576	-23	375.817	141238.4077	53079792.84
559	584	-25	408.497	166869.5743	68165674.62
580	603	-23	375.817	141238.4077	53079792.84
626	650	-24	392.157	153786.9997	60308626.30
644	664	-20	326.797	106796.5276	34900825.40
81	105	-24	392.157	153786.9997	60308626.30
473	501	-28	457.516	209321.1940	95767864.91
507	525	-18	294.118	86505.18734	25442701.72
550	568	-18	294.118	86505.18734	25442701.72
179	236	-57	931.373	867454.7952	807923569.9
238	265	-27	441.176	194636.6715	85869118.30

253	283	-30	490.196	240292.1870	117790285.7
18	50	-32	522.876	273399.1106	142953780.9
529	573	-44	718.954	516895.1935	371623988.9
538	559	-21	343.137	117743.1717	40402068.01
600	616	-16	261.438	68349.77765	17869222.61
68	105	-37	604.575	365511.1156	220978938.7
129	143	-14	228.758	52330.29851	11970983.11
242	258	-16	261.438	68349.77765	17869222.61
270	285	-15	245.098	60073.04676	14723785.72
337	352	-15	245.098	60073.04676	14723785.72
397	452	-28	457.516	209321.1940	95767864.91
580	605	-25	408.497	166869.5743	68165674.62
584	624	-40	653.595	427186.1103	279206603.2
663	676	-13	212.418	45121.53290	9584639.177
682	702	-20	326.797	106796.5276	34900825.40
15	39	-24	392.157	153786.9997	60308626.30
33	51	-18	294.118	86505.18734	25442701.72
34	54	-20	326.797	106796.5276	34900825.40
98	125	-27	441.176	194636.6715	85869118.30
200	223	-23	375.817	141238.4077	53079792.84
217	234	-17	277.778	77160.49117	21433469.40
241	261	-20	326.797	106796.5276	34900825.40
244	267	-23	375.817	141238.4077	53079792.84
261	285	-24	392.157	153786.9997	60308626.30
270	292	-22	359.477	129223.7984	46452998.61
292	309	-17	277.778	77160.49117	21433469.40
351	376	-25	408.497	166869.5743	68165674.62
520	558	-38	620.915	385535.4645	239384761.5
59	89	-30	490.196	240292.1970	117790285.7
406	434	-28	457.516	209321.1940	95767864.91
540	564	-24	392.157	153786.9997	60308626.40
587	604	-17	277.778	77160.49117	21433469.40
568	599	-31	506.536	256578.6575	129966311.2
0	25	-25	408.497	166869.5743	68165674.62
4	39	-35	571.895	327064.3657	187046611.2
40	66	-26	424.837	180486.1316	76677113.41
24	79	-55	898.693	807648.7398	725828103.3
52	89	-37	604.575	365511.1156	220978938.7
82	107	-25	408.497	166869.5743	68165674.62
72	103	-31	506.536	256578.6575	129966311.2
128	148	-20	326.797	106796.5276	34900825.40
133	157	-24	392.157	153786.9997	60308626.30
138	163	-25	408.497	166869.5743	68165674.62
230	255	-25	408.497	166869.5743	68165674.62
328	363	-35	571.895	327064.3657	187046611.2
332	359	-27	441.176	194636.6715	85869118.30
367	389	-22	359.477	129223.7984	46452998.61
474	505	-31	506.536	256578.6575	129966311.2
489	551	-62	1013.072	1026314.630	1039730490.
507	526	-19	310.458	96383.86614	29923095.18
617	644	-27	441.176	194636.6715	85869118.30
	Total	=	43660.130	21117411.38	11548875081

Droplet Statistic

Total Number of Drops	= 101.000	
Sauter Mean Diameter	= 546.889	microns
Volume Mean Diameter	= 485.370	microns
Area Mean Diameter	= 457.256	microns
Mean Droplet Diameter	= 432.279	microns

APPENDIX A5

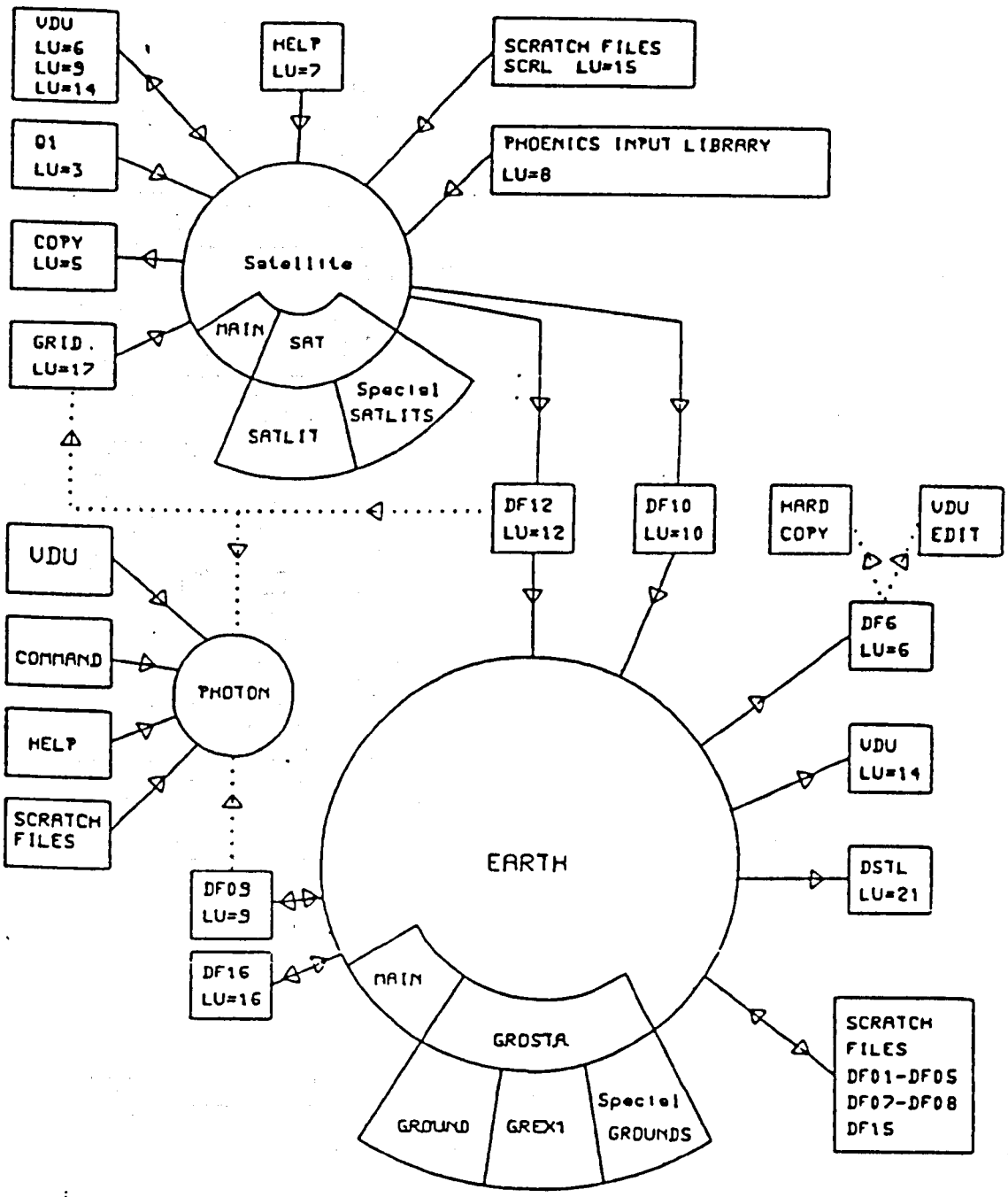

FIGURE A5.1 PHOENICS VERSION 1.3, FLOW CHART

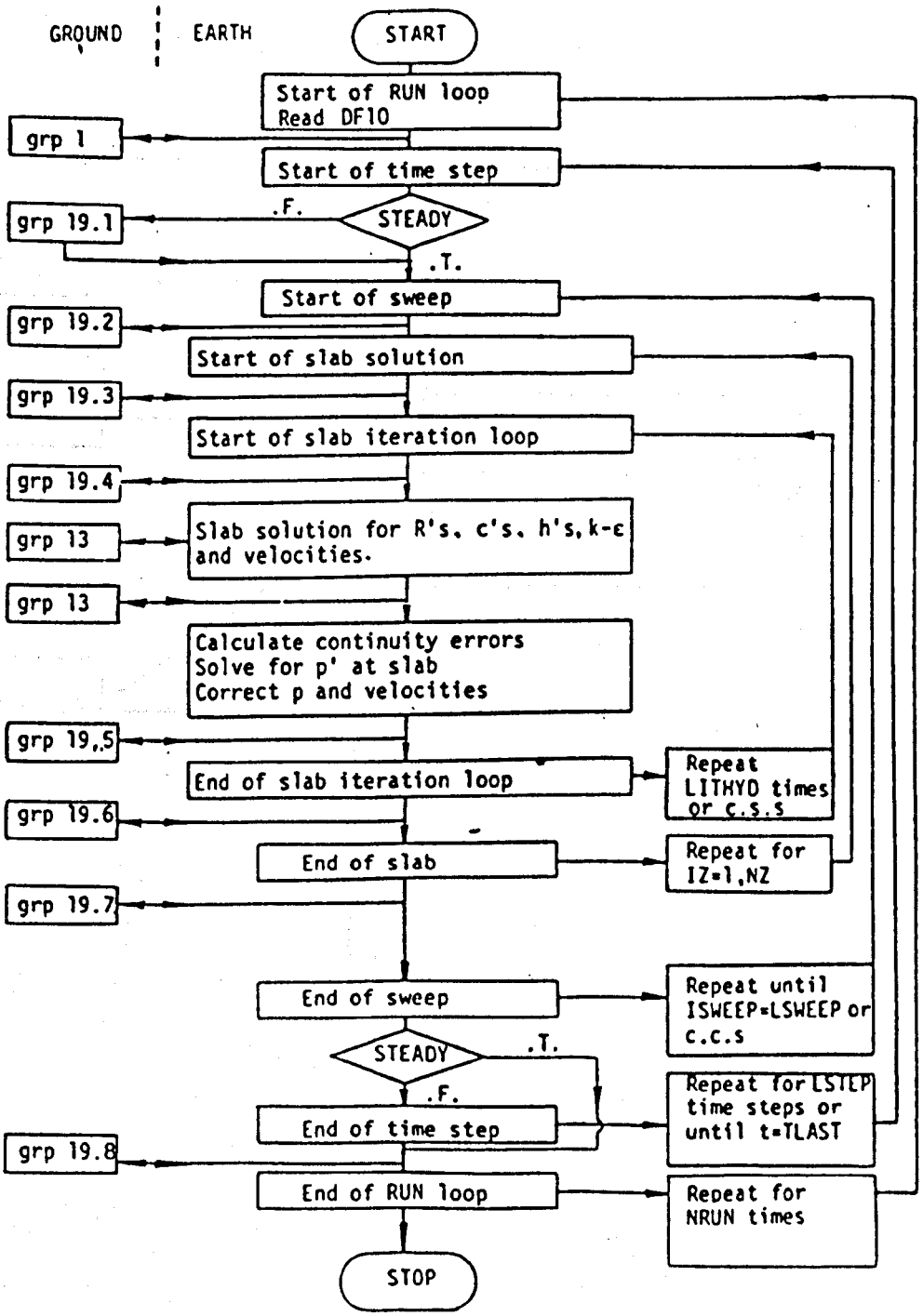

FIGURE A5.2 SOLUTION SEQUENCE FOR THE SLABWISE ELLIPTIC SOLVER

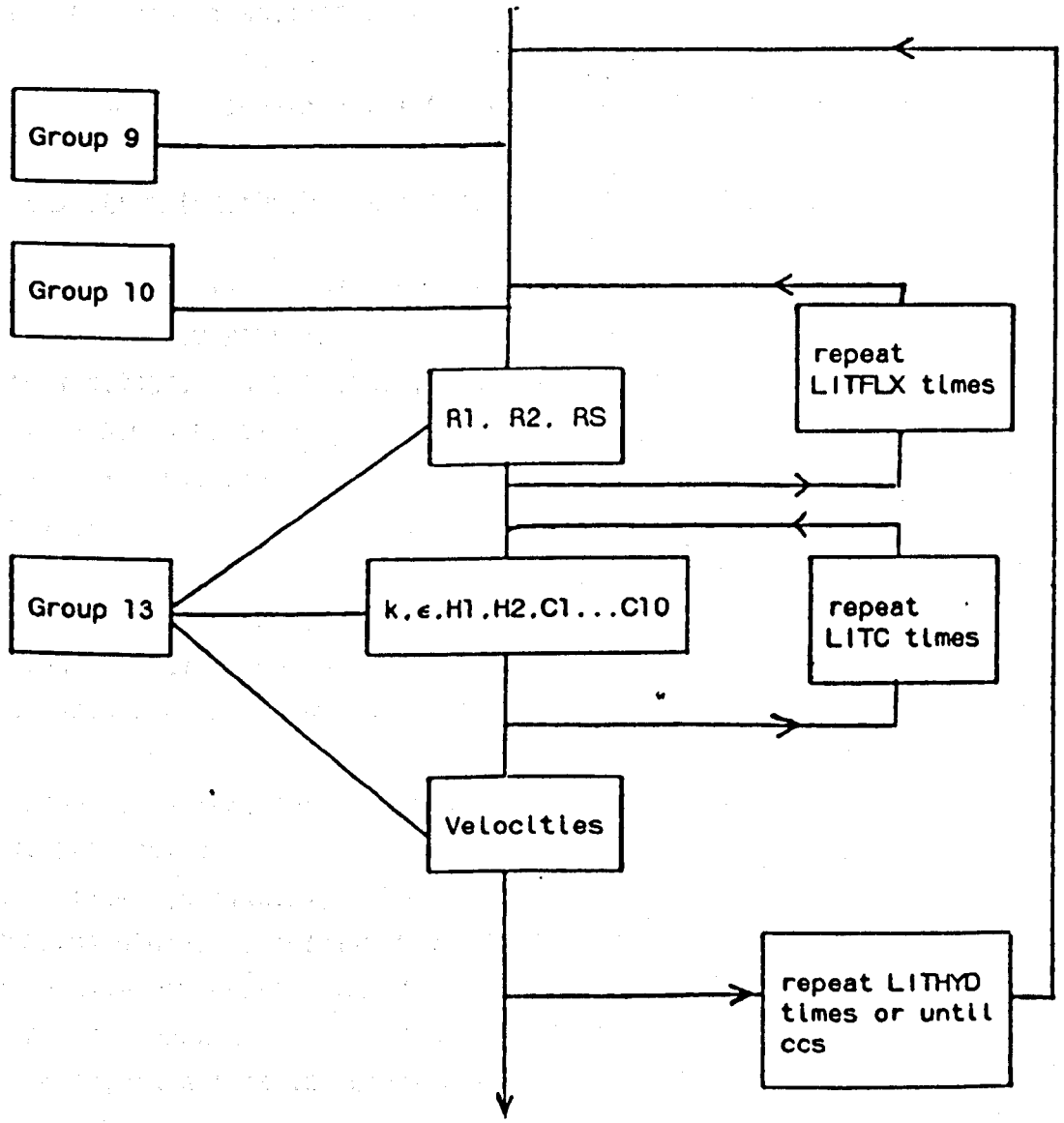

FIGURE A5.3 SOLUTION SEQUENCE FOR THE SLABWISE ELLIPTIC SOLVER

APPENDIX A6

Here we give briefly the main features that were used to simulate the problem in computer code PHOENICS. Therefore for more details, such as the specification of symbols, subroutines and function statements refer to CHAM (1986,1987).

Note:- that the length units for this simulation was taken as 'mm'.

A6.1 Q1 file for the Homogeneous model (written in language PIL)

GROUP 1. Run title and other preliminaries

TEXT(SINGLE JET MIXER)

REAL(WIN,VJET,ENIN,DSIN,DAVE,OLDEN,STENSI)

STENSI= 0.023;RHO1= 0.8*1E-6

Comments:- this simulation was carried out in 'mm' length units. RSG2= $(U^2+V^2)^{1/2}$

GROUP 2. Transience; time-step specification

Comments:- This group was set empty for steady flow simulation, since the default value of STEADY is T (True).

GROUP 3. X-direction grid specification

CARTES=F; NX=20

GRDPWR(X,-NX,3.1416,2)

XFRAC(3)=0.042; XFRAC(4)=0.072; XFRAC(5)=0.123

Comments:- CARTES=F indicates that cylinderical coordinate in use. NX=20 is number of spatial subdivision in the Z direction. GRDPWR(X,-NX,3.1416,.2) gives a symmetrical power-law grid which start from each edge and meet in the middle. X-direction coordinates of the east faces of the computational cell 3, 4, 5, were modified by using XFRAC(3)=0.042; XFRAC(4)=0.072; XFRAC(5)=0.123.

GROUP 4. Y-direction grid specification

NY=10; YVLAST=70.0

GRDPWR(Y,NY,YVLAST,2)

YFRAC(8)=0.88; YFRAC(9)=0.94

Comments:- YVLAST= 70 specify the radius of the pipe in mm. Other instructions are similar to GROUP 3 above.

GROUP 5. Z-direction grid specification

ZWLAST=4000; NZ=32

ZFRAC(1)=---

Comments:- All Z-direction grid specifications were set by using ZFRAC command.

GROUP 6. Body-fitted coordinates or grid distortion

Comments:- No entry was made, since the body-fitted coordinates were not used.

GROUP 7. Variables stored, solved and named

SOLVE(P1,U1,V1,W1); STORE(ENUT)

TURMOD(KEMODL); SOLVE(C1)

SOLUTION(P1,Y,Y,Y,N,N,N)

SOLVE(C1)

NAME(22)= RSG2; STORE(RSG2)

Comments:- SOLVE(P1,U1,V1,W1,C1) indicates pressure, three velocities and concentration of a species (water) are to be solved. TURMOD(KEMODL) commands k-ϵ turbulent model to be used. Command STORE(ENUT), asks to store turbulent kinematic viscosity. SOLUTION(P1,Y,Y,Y,N,N,N), commands P1 to be solved, by using whole-field solution method and then to be stored.

GROUP 8. Terms (in differential equations) and devices

TERMS(P1,Y,Y,Y,N,Y,N); TERMS(U1,Y,Y,Y,N,Y,N)

TERMS(V1,Y,Y,Y,N,Y,N); TERMS(W1,Y,Y,Y,N,Y,N)

TERMS(KE,N,Y,Y,N,Y,N); TERMS(EP,N,Y,Y,N,Y,N)

TERMS(C1,Y,Y,Y,N,Y,N)

Comments:- These indicate that the built-in-sources, convection and diffusion terms in equation 6.1.1 are active for variables P1,U1,V1,W1,C1. For variables KE and EP built-in-sources are inactive, and convection and diffusion terms are active. The Transient terms are inactive for all variables. All variables are belong to first phase, therefore interface transport terms are inactive.

GROUP 9. Properties of the medium (or media)

RHO1=8E-7; ENUL=1.15

PRNDTL(C1)=0.5, PRT(C1)=0.5

Comments:- RHO1=denisity of the first phase (oil). ENUL=the laminar kinematic viscosity. PRNDTL(C1)= laminar Schmidt Number (or Prandtl number). PRT(C1)= turbulent Schmidt Number (or Prandtl number).

GROUP 10. Inter-phase-transfer processes and properties

Comments:- No entry was made, since the simulation was in single phase.

GROUP 11. Initialisation of variables and porosity fields

WIN= 950; VJET=10000

ENIN=0.0325*WIN**2

DSIN=1.826*ENIN**1.5/YVLAST

FIINIT(P1)= 1E-10; FIINIT(V1)=1E-8; FIINIT(V1)= 1E-8

FIINIT(W1)= WIN; FIINIT(C1)= 0.0

FIINIT(KE) = ENIN; FIINIT(EP)= DSIN

FIINIT(VIST) = (0.09*RHO1*ENIN**2)/DSIN

FIINIT(C1)=0.0

Comments:- WIN = inlet velocity = 1000 mm/sec. VJET= velocity of the jet. ENIN= inlet specific kinetic energy, DSIN= inlet specific dissipation. The command FIINIT() initialise other variables.

GROUP 12. Convection and diffusion adjustments

Comments:- No ajustments were made to fluxes of convection and diffusion. WIN is the average velcity at pipe inlet.

GROUP 13. Boundary conditions and special sources

KELIN=2

1. In pipe domain

PATCH(KESOURCE, PHASEM, NX, 1,NY, 1, NZ, 1, !1)

COVAL(KESOURCE, KE, GRND4, GRND4)

COVAL(KESOURCE, EP, GRND4, GRND4)

Comments:- Here the k-ϵ model was activated. Type 'PHASEM' indicates per unit mass. KELIN=2 signify which linearization (out of 3) is to

be used for the source terms of the turbulence parameter k and ϵ. This selection should not alter the solution. The one used, proved to be useful in confined flows in which turbulence level otherwise increases without control.

2. Entry to pipe

```
PATCH(INLET, P1, FIXFLU, GRND)
COVAL(INLET, W1, ONLYMS, GRND)
COVAL(INLET, C1, ONLYMS, 0.0)
COVAL(INLET, KE, ONLYMS, ENIN)
COVAL(INLET, EP, ONLYMS, DSIN)
```

Comments:- Mass influx was set by using the 'FIXFLU and velocity distribution across the pipe was calculated according to the 1/7 power law. Sources flow in, was set by using "ONLYMS' which means source per mass flow rate.

3. Downstream boundary

```
PATCH(OUTLET, HIGH, 1, NX, 1, NY, NZ, NZ, 1, 1)
COVAL(OUTLET, P1, FIXVAL, 0.0)
```

Comment:- P1 is fixed at outlet (ie P1 =constant). FIXVAL has a numeric values of 1E10. More details of selection of outlet boundaries are given in Patankar (1980).

4. Pipe wall

```
PATCH(WALL1, NWALL, 1, NX, NY, NY, 1, 7, 1, 1)
COVAL(WALL1, U1, GRND2, 0.0)
COVAL(WALL1, W1,GRND2, 0.0)
COVAL(WALL1, KE, GRND2,GRND2)
COVAL(WALL1, EP, GRND2, GRND2)
```

Comments:- Log-law function methods were used for the wall boundary

```
PATCH(WALL2, NWALL, 1, NX, NY, NY, 9, NZ, 1, 1)
COVAL(WALL2, V1, GRND2, 0.0)
COVAL(WALL2, W1, GRND2, 0.0)
COVAL(WALL2, KE, GRND2, GRND2)
COVAL(WALL2, EP, GRND2, GRND2)
```

```
PATCH(WALL3, NWALL, 2, NX, NY, NY, 7, 9, 1, 1)
COVAL(WALL3, U1, GRND2, 0.0)
COVAL(WALL3, W1, GRND2, 0.0)
COVAL(WALL3, KE, GRND2, GRND2)
COVAL(WALL3, EP, GRND2, GRND2)
```

5. Side entry

```
PATCH(SIDEIN, NORTH, 1, 7, NY, NY, 8, 8, 1, 1)
COVAL(SIDEIN, P1, FIXFLU, RHO1*VJET)
COVAL(SIDEIN, V1, ONLYMS, -VJET)
COVAL(SIDEIN, KE, ONLYMS, ENIN*(VJET/WIN)**2)
COVAL(SIDEIN, EP, ONLYMS, DSIN*(VJET/WIN)**1.5)
```

Comments:- The above specifications ensure no transport of water across the walls. The water source at the jet was programmed and coded in SATLIT.FOR.

GROUP 14 Downstream pressure for PARAB=T

Comments:- No entry was made since the flow was not free parabolic.

GROUP 15. Termination of sweeps

```
LSWEEP=100
RESREF(P1)=1E4; RESREF(V1)= 10; RESREF(U1)=10
RESREF(W1)= 10; RESREF(KE)= 5E2; RESREF(EP)= 1E3
```

Comments:- 'RESREF' value for a particular variable is used as a termination criteria for sweeps. This is a reference value to monitor convergence. Residuals are divided by this value, where the RESREF indicates the maximum error for a particular variable as well as the application. This is sometimes called termination for outer iterations. Note that the resref of P1 refers to volume flow rate.

GROUP 16.

```
LITER(P1)= 10; LITER(U1)= 1; LITER(V1)= 1
LITER(W1)= 1; LITER(KE)= 1; LITER(EP)= 1
ENDIT(P1)= 1E-10; ENDIT(V1)= 1E-3; ENDIT(U1)= 1E-3
ENDIT(W1)= 1E-3; ENDIT(KE)= 1E-3; ENDIT(EP)= 1E-3
```

Comments:- LITER(), is a command to specify the maximum number of iterations of the inner solver for the variable indicated. This refers

to a particular slab (eg. in 3-D simulations). First iteration are incicated for an slab and then the number of sweeps performed downstream and upstream until convergence. ENDIT() command terminate the iterations of the linear equation solver, when the cell-average absolute change in the variable from one iteration to the next falls below the appropriate value given by ENDIT.

GROUP 17. Under relaxation devices

RELAX(P1, LINRLX, 0.1)

RELAX(U1, FALSDT, YVLAST/VJET)

RELAX(V1, FALSDT, YVLAST/VJET)

RELAX(W1, FALSDT, YVLAST/VJET)

RELAX(KE, FALSDT, 0.01)

RELAX(EP, FALSDT, 0.01)

Comments:- Here a false time step is used as an under-relaxation device. Although, the domain residence time was set for slack relaxation of velocities, these needed to be intervened during the solution process.

GROUP 18. Limits on variables or increments to them

VARMAX(U1)=3E4; VARMIN= -1E5

VARMAX(V1)= 3E4; VARMIN(V1)= -1E5

VARMAX(W1)= 3E4; VARMIN(W1)= -1E5

Comments:- This another tool used to achieve convergence faster. VARMAX and VARMIN provide the maximum and minimum values allowed for the variables.

GROUP 19. Data communicated by satellite to GROUND.

DUDY= T

RSG1= RAD

RSG3= WIN

RSG4= VJET

RSG5= YVLAST

RSG6= STENSI

RSG7=RHO1

Comments:- When the user intervenes with "GROUND" sometimes special data needs to set here. DUDY=T, activates a call to derivative

function FNDUDY in GREX1. WIN is the average velocity weighted by the cross sectional area.

GROUP 20. Preliminary print-out

ECHO= T

Comments:- Here preliminary printouts are controlled. ECHO= T, gives an EARTH 'echo' of the data provided by the SATELLITE.

GROUP 21 Print-out of variables

Printout of variables controlled by 'OUTPUT' statment.

OUTPUT(Variable index, Y or N for six times)

Comments:-The six questions answered by the 'Y's and 'N's are

1). Field printout?

2). Correction-equation monitor printout?

3). Slabwise-residual printout?

4). Whole-field resudual printout?

5). Spot value table and /or plot?

6). Residual table or plot?

GROUP 22. Monitor print-out

TSTSWP= 2

Comments:- The frequency, the residuals are written to LOG file.

GROUP 23. Field print-out and plot control of outputs to DF6 file

NUMCLS= 10

NXPRIN= NX/NX; NYPRIN= NY/NY; NZPRIN= NZ/NZ

IXPRL= NX; IYPRL= NY

ITABL= 3

Comments:- NUMCLS= 10, indicates the number of print columns are 10. NXPRIN gives the 'IX' interval in the tabulations of the variables. IXPRL= nx; IYPRL= ny says that the last X and Y grid that need printing are NX and NY. ITABL = 3, indicates how the tables and plot need tabulating.

A6.2 SUBROUTINE SATLIT FILE FOR MODEL 1 (Homogeneous model)

These are extracts from SATLIT.FOR, but not a complete listing of it.

```
      REAL WTDEN,OLDEN,OILVIS,STENSION,HIEG,DIA,VJET,OILMS,
     &WERE,FRCF,VENTR,ENTR

C   GROUP 13. Boundray conditions and special sources
    13 CONTINUE
C   Calculate the water concentration source (C1) for patch 'SIDEIN'
C   All length units are in 'mm'. WTDEN=Density of water
C   OLDEN=Density of oil, STENSION=Interfacial surface tension
C   HEIG= Height of the water layer, DIAJ= Diameter of jet inlet,
C   VJET=RSG4= Velocity of jet, OILMS= Oil mass flow rate,
C   OILV= Oil volume flow rate, WERE= We to Re number ratio ,
C   OILVIS= Dynamic viscosity of oil, FRCF= Skin friction coefficient,
C   ENTR= Water mass entrainment rate,
C   VENTR= Water volume entrainment rate,
C   SOUR= Water concentration source
      OLDEN= 8E-7
      OILVIS= 1.15E-6
      STENSION= 0.023
      WTDEN= 1E-6
      HEIG= 10.0
      DIAJ= 4.2
C   Since Dia. of the jet is 4.0mm, oil mass flow rate is:-
      OILMS= RSG4*OLDEN*3.14*4
      OILV= OILMS/OLDEN
      WERE= OILVIS*RSG4/STENSION
      FRCF= (3.48 +0.707*ALOG(6*1E3*WERE))**-2.5
C   Entrainment rate of water volume is:-
      WTV= (HEIG/DIA)*(3*FRCF**0.5)*I=OILV*OLDEN/WTDEN
C
C   Volume ratios of water and oil are:-
      WTRAT= WTV/(WTV+OILV)
      OLRAT= OILV/(WTV+OILV)
      WRITE(6,*) WTRAT
C   Let C1 be volume per mixture volume
```

```
      CALL PATCH('SIDEIN',NORTH,1,1,NY,NY,8,8,1,1)
      CALL COVAL('SIDEIN',C1,ONLYMS,WTRAT)
      RETURN
C   GROUP 14. Downstream pressure for PARAB= TRUE
```

A6.3 SUBROUTINE GROUND FILE FOR MODEL 1 (Homogeneous model)

These are extracts from GROUND.FOR, but not a complete listing of it.

```
2   User dimensions own arrays here:
      PARAMETER (MY=20, MX=20)
      PARAMETER (LX=20, LY=1)
      DIMENSION ARRAY(MY,MX),GVAL(LY,LX)
      DIMENSION CRRAY(MY,MX),ERRAY(MY,MX),DMAX(MY,MX),TOP(MY,MX)
     &,BOT(MY,MX),AREA(MY,MX)
      DIMENSION RATIO(1,1),GXCO(MY,MX),GYCO(MY,MX),GD1(MY,MX)
     &,GW1(MY,MX),GV1(MY,MX),GVW1(MY,MX)
.
C   GROUP 1. Run titles and other preliminaries
C
    1 GOTO (1001,1002),ISC
 1001 CONTINUE
      CALL MAKE(XG2D)
      CALL MAKE(YG2D)
      RETURN
 1002 CONTINUE

C   GROUP 13. Boundary conditions and special sources
C-------------------SECTION 12----------------------
C   Inlet velocity profile is assumed as that of power law
C   Average velocity at inlet cross section (WIN)=RSG3
C   Radius of the pipe (YVLAST) = RSG5
C   Using 1/7 power law it can be proved, CVEL= 60*WIN/49, where
C   CVEL is the axial velocity at the axis.
C
      CVEL= 60*RSG3/49
```

```
      IF(NPATCH.EQ.'INLET')THEN
      IF(INDVAR.EQ.P1)THEN
      CALL GETYX(YG2D,GR,MY,MX)
      DO 1351 IY = 1,NY
      DO 1351 IX = 1,NX
 1351 GVAL(IY,IX)=CVEL*RHO1*(RSG5-GR(IY,IX))**0.1429/(RSG5**0.1429)
      ELSE IF (INDVAR.EQ.W1) THEN
      CALL GETYX(YG2D,GR,MY,MX)
      DO 1361 IY = 1,NY
      DO 1361 IX = 1,NX
 1361 GVAL(IY,IX)=CVEL*(RSG5-GR(IY,IX))**0.1429/(RSG5**0.1429)


   GROUP 19 Special calls to GROUND from EARTH
C --------------------SECTION 6-------FINISH OF IZ SLAB.
C   Calculation of (V1**2+W1**2)**0.5=RSG2
      CALL GETYX(V1,GV1,MY,MX)
      CALL GETYX(W1,GW1,MY,MX)
      DO 1960 IX=1,NX
      DO 1960 IY=1,NY
      GVW1(IY,IX)=(GV1(IY,IX)**2+GW1(IY,IX)**2)**0.5
 1960 CONTINUE
      CALL SETYX(22,GVW1,MY,MX)
```

A6.4 Q1 FILE FOR TWO- FLUID MODEL

Following additions and modifications were made to Q1 file of the Homogeneous Model

```
  GROUP 7  Variables stored, solved and named
ONEPHS=F
NAME(9)=OIL; NAME(10)=WATER
SOLVE(U2,V2,W2,OIL,WATER)
```

Comments:— ONEPHS=F, inicates that the flow is not single phase, but two-phase. SOLVE(U2,V2,W2,OIL,WATER), indicates that the conservation equation of second phase momentum and conservation of oil and water

volume fractions are to be solved. Where oil and water taken as the two immiscible components.

GROUP 8 Terms (in differential equation)

```
TERMS(OIL,Y,Y,Y,N,Y,N)
TERMS(WATER,Y,Y,Y,N,Y,N)
TERMS(U2,Y,Y,N,N,N,Y)
TERMS(V2,Y,Y,N,N,N,Y)
TERMS(W2,Y,Y,N,N,N,Y)
```

Comments:- TERMS commands of Oil and water, indicates that convection, diffusive terms are active in their conservation equation, but the transient terms and interface transport terms are inactive. TERMS command of the 2^{nd} phase velocities indicate that the diffusion is inactive and the interface transport is active.

GROUP 9 Properties

```
RHO2=1E-6
```

Comments:- RHO2 is the density of second phase(water).

GROUP 10 Inter-phase- transport processes and properties

```
CFIPS=GRND
```

Comments:- The above command indicates that the interface friction force is evaluated in accordance with a user subroutine in GROUND.

GROUP 11 Initialization of variables or porosity fields

```
FIINIT(U2)=1E-8; FIINIT(V2)=1E-8
FIINIT(W2)=WIN
FIINIT(OIL)=1.0; FIINIT(WATER)=0.0
```

Comments:- Command FIINIT initializes the second phase velocities and the volume fractions of the two phases.

GROUP 13 Boundary conditions and special sources

1. Buoyancy force

```
PATCH(BUOY,PHASEM,1,NX,1,NY,1,NZ,1,1)
COVAL(BUOY,U2,FIXFLU,GRND)
COVAL(BUOY,V2,FIXFLU,GRND)
```

Comments:- The above commands introduce a negative buoyancy (gravity)

source to the second phase (water) momentum conservation equation. These sources are calculated by the user in subroutines coded in GROUND.

```
  GROUP 15 Termination of sweeps
RESREF(U2)=10; RESREF(V2)=10; RESREF(W2)=10
RESREF(OIL)=0.01; RESREF(WATER)=0.01

  GROUP 17 Under-relaxation devices
RELAX(U2,FALSDT,1E-2)
RELAX(V2,FALSDT,1E-3)
RELAX(W2,FALSDT,1E-3)

  GROUP 18 Limits on variables or increments to them
VARMAX(U2)=1E4; VARMIN(U2)=-1E5
VARMAX(V2)=1E4; VARMIN(V2)=-1E5
VARMAX(W2)=1E4; VARMIN(W2)=-1E5.
VARMAX(WATER)=1E10; VARMIN(WATER)=0.0
VARMAX(OIL)=1E10; VARMIN(OIL)=0.0

  GROUP 19 Special calls to GROUND from EARTH
RSG8=9800.0*(RHO1-RHO2)
```

A6.5 SUBROUTINE SATLIT FILE OF MODEL2 (TWO-FLUID)

The following additions and modifications were made to SATLITE file of Model 1(Homogeneous Model)

```
C GROUP 10 Inter-phase-transfer processes and properties
C Droplet size calculations; Droplet radius= RAD=RSG1
C
   10 CONTINUE
C Sauter mean dia. in 'mm' is =RSG1=RAD
      HEIG=10
      DIAJ=4.2
      OILVIS=1E-6
```

```
      WTVIS=1E-6
      STENSION=0.023
      RHO1=1E-6
      VJET=10000.0
      RLENTH=HEIG/DIAJ
      RVIS= (OILVIS/WTVIS)**0.31
      RAD= (133.6*STENSION/(2*RHO1*VJET**2))*RLENTH*RVIS
      RETURN
C
  GROUP 13 Boundary conditions and special sources
      CALL COVAL commands of model 1 was superseded by the following:-
      CALL COVAL('SIDEIN',P1,FIXFLU,OLRAT*RHO1*VJET)
      CALL COVAL('SIDEIN',P2,FIXFLU,WRAT*RHO2*VJET)
      CALL COVAL('SIDEIN',V1,ONLYMS,-VJET)
      CALL COVAL('SIDEIN',V2,ONLYMS,-VJET)
```

A6.6 SUBROUTINE GROUND OF MODEL 2 (TWO-FLUID)

Following additions and modifications were made to GROUND of model 1

```
C  GROUP 10 Inter-phase-transfer processes and properties
C
   10 GO TO (101,102,103,104),ISC
  101 CONTINUE
C   *------------------SECTION 1 ------------------------
C  For CFIPS.LE.GRND--- inter-phase friction coeff. AUX(INTFRC)
C  Calculation of inter-phase friction coefficient
C
C  Initialise all velocity components local to Ground to 0.0
c
      DO 1011 IX=1,NX
      DO 1011 IY=1,NY
        GU1(IY,IX)=0.0
        GU2(IY,IX)=0.0
        GV1(IY,IX)=0.0
        GV2(IY,IX)=0.0
```

```
        GW1(IY,IX)=0.0
        GW2(IY,IX)=0.0
 1011 CONTINUE
C
C  Get cell volume at current slab
      CALL GETYX(VOL,GVOL,MX,MY)
C  Get velocity components for phase 1
      IF(SOLVE(U1)) CALL GETYX(U1,GU1.MY.MX)
      IF(SOLVE(V1)) CALL GETYX(V1,GV1,MX,MY)
      IF(SOLVE(W1)) CALL GETYX(W1,GW1,MX,MY)
      IF(SOLVE(U2)) CALL GETYX(U2,GU2,MX,MY)
      IF(SOLVE(V2)) CALL GETYX(V2,GV2,MX,MY)
      IF(SOLVE(W2)) CALL GETYX(W2,GW2,MX,MY)
C
C  Get phase 1 density, and phase 2 vol. fraction
      CALL GETYX(R2,GR2,MY,MX)
C
C  Begining of DO-loop for interface friction
      DO 1012 IX=1,NX
      DO 1012 IY=1,NY
C  PHOENICS does not store velocities at boundaries so here the south
C  and west velocities are picked up
C
      IF(SOLVE(U1).AND.IX.EQ.NX) GU1(IY,IX)=GU1(IY,IX-1)
      IF(SOLVE(U2).AND.IX.EQ.NX) GU2(IY,IX)=GU2(IY,IX-1)
      IF(SOLVE(V1).AND.IY.EQ.NY) GV1(IY,IX)=GV1(IY-1,IX)
      IF(SOLVE(V2).AND.IY.EQ.NY) GV2(IY,IX)=GV2(IY-1,IX)
C
C  Calculate absolute slip velocity between phases
      GVSLIP(IY,IX) =SQRT((GU1(IY,IX)-GU2(IY,IX)**2+
     &                    (GV1(IY,IX)-GV2(IY,IX)**2+
     &                    (GW1(IY,IX)-GW2(IY,IX)**2)
C
C  Calculate local particle Reynolds number
      GVISC=ENUL
C  ENUL= Molecular kinematic viscosity. This is specified in Q1 file.
      REP=2.*RSG1*GVSLIP(IY,IX)/GVISC
```

```
      GREYNO(IY,IX)=REP
      IF(REP.LE.2.0) THEN
C
C  Laminar flow regime
      GCD(IY<IX)=24.0/REP
      ELSE IF (REP.GT.2.0.AND.REP.LE.2000.0)THEN
C
C  Transition Regime
      GCD(IY,IX)=17.0/(REP**0.48)
      ELSE IF (REP.GT.2000.0) THEN
C
C  Turbulent Regime
      GCD(IY,IX)=0.44
      ENDIF
C
C  Calculate the projected area of phase 2 particles in cell
      APROJ=0.75+GR2(IY,IX)*GVOL(IY,IX)/RADP
C
C  Calculate the inter-phase friction force per velocity difference
C  per cell.
      GVAL(IY,IX)=GCD(IY,IX)*APROJ*RHO1*GVSLIP(IY,IX)
 1012 CONTINUE
      CALL SETYX(AUX(INTFRC),GVAL,MY,MX)
C
C  To ensure that the friction is not 0.0
      CALL FN22(AUX(INTFRC),1.0E-10)
C
C  All the details of the subroutines called in the above programme
C  are given in Cham (1986, 1987).

* Following were incoporated in GROUP 13

 1311 CONTINUE
C---------------------- SECTION 12 ---------------------- value = GRND
C  Introduce the bouancy force (related to water)
      CALL ONLYIF(U2,V2,'BUOY')
      CALL GETYX (XG2D,GXCO,MX,MY)
```

```
      DO 1351 IX=1,NX
      DO 1351 IY=1,NY
      IF(INDVAR.EQ.U2)THEN
C  RSG8 is specified in Q1 file, and is equal to
C  deinsity difference*gravitational constant
      GVAL(IY,IX)=(-RSG8)*SIN(GXCO(IY,IX))
      ELSE IF (INDVAR.EQ.V2)THEN
      GVAL(IY,IX)=(RSG8)*COS(GXCO(IY,IX))
      ELSE
      ENDIF
 1351 CONTINUE
      SETYX(VAL,GVAL.MY.MX)
      RETURN
```

A6.7 GRID NODE LOCATIONS

When the grid, 20*16*60, was set as shown in fig 9.1, the distance to the axial direction nodes from the injection plane are as follows:-

ZSLAB(19) = NODE 19 = 0.5 dia.
ZSLAB(22) = NODE 22 = 1.04 dia.
ZSLAB(27) = NODE 27 = 2.0 dia.
ZSLAB(33) = NODE 33 = 3.07 dia.
ZSLAB(37) = NODE 37 = 4.0 dia.

A6.8 THE RELATIONSHIP BETWEEN THE PIPE CENTRE LINE VELOCITY AND THE AVERAGE VELOCITY

Let U_c the centre line velocity, R radius of the pipe, U_a average velocity, r the radial distance from the centre and U the axial velocity.

According to the 1/7 power law:-

$$\frac{U}{U_c} = \left[\frac{R - r}{R}\right]^{\frac{1}{7}}$$

Therefore the volume flow at the pipe cross section is:-

$$\pi R^2 U_a = \int_0^R 2\pi r\, U dr = \int_0^R 2\pi\, U_c\, r \left[\frac{R - r}{R}\right]^{\frac{1}{7}} dr \qquad (A6.1)$$

Let $y = (R - r)$, hence, $r = (R - y)$, $dr = -dy$ and at $r=R$ $y=o$, $r=0$ $y=R$

$$\pi R^2 U_a = -\int_R^0 2\pi\, U_c \left[\frac{y}{R}\right]^{1/7} (R - y)\, dy$$

$$= -2\pi\, U_c \left[\frac{7}{8} \frac{y^{8/7}}{R^{1/7}} R - \frac{7}{15} \frac{y^{15/7}}{R^{1/7}}\right]_R^0$$

$$= \frac{49}{60}\, \pi\, U_c\, R^2$$

A6.9 CALCULATION OF AVERAGE TURBULENT ENERGY IN FULLY DEVELOPED PIPE FLOW

Laufer's (1954) experimental results of $\bar{u}$ are approximated to a linear relationship of the form $\bar{u}/U^* = m(r/R) + c$.

Therefore

$$\bar{U}\pi\, R^2 \bar{u}_a^2 = \int_0^R 2\pi r \frac{U_c}{} \left[\frac{R - r}{R}\right]^{1/7} (M r + c)^2\, dr$$

where $M = m/r$, $\bar{u}_a$ = average RMS across the pipe section and by substituting $y = (R-r)$ as in appendix A6.8

$$\frac{\bar{U} R^2\, \bar{u}_a^2}{2U_c U^{*2}} = -\int_R^0 \left[\frac{y}{R}\right]^{1/7} \left\{M^2(R - y)(R^2 - 2Ry + y^2) + 2Mc(R^2 - 2Ry + y^2) + (R-y)c^2\right\} dy$$

$$\frac{\overline{U}R^2\ \overline{u}_a^2}{2U_c U^{*2}} = -\left[\frac{1}{R}\right]^{1/7}\left[\frac{7}{8}(M^2R^3+c^2R+2McR^2)y^{8/7}+\frac{7}{15}(-3M^2R^2-4RMc-c^2)y^{15/7}\right.$$

$$\left.+\frac{7}{22}(3M^2R+2Mc)y^{22/7}-\frac{7}{29}M^2\,y^{29/7}\right]_R^0$$

$$= 0.188\ m^2 + 0.408\ c^2 + 0.52\ mc$$

From Laufer (1954) experimental results m and c can be approximated to 1.22 and 0.78 respectively. And $U_c = (60/49)\ U_a$ (from appendix A6.8)

Hence, $\overline{u}_{ave} = 1.58\ U^*$

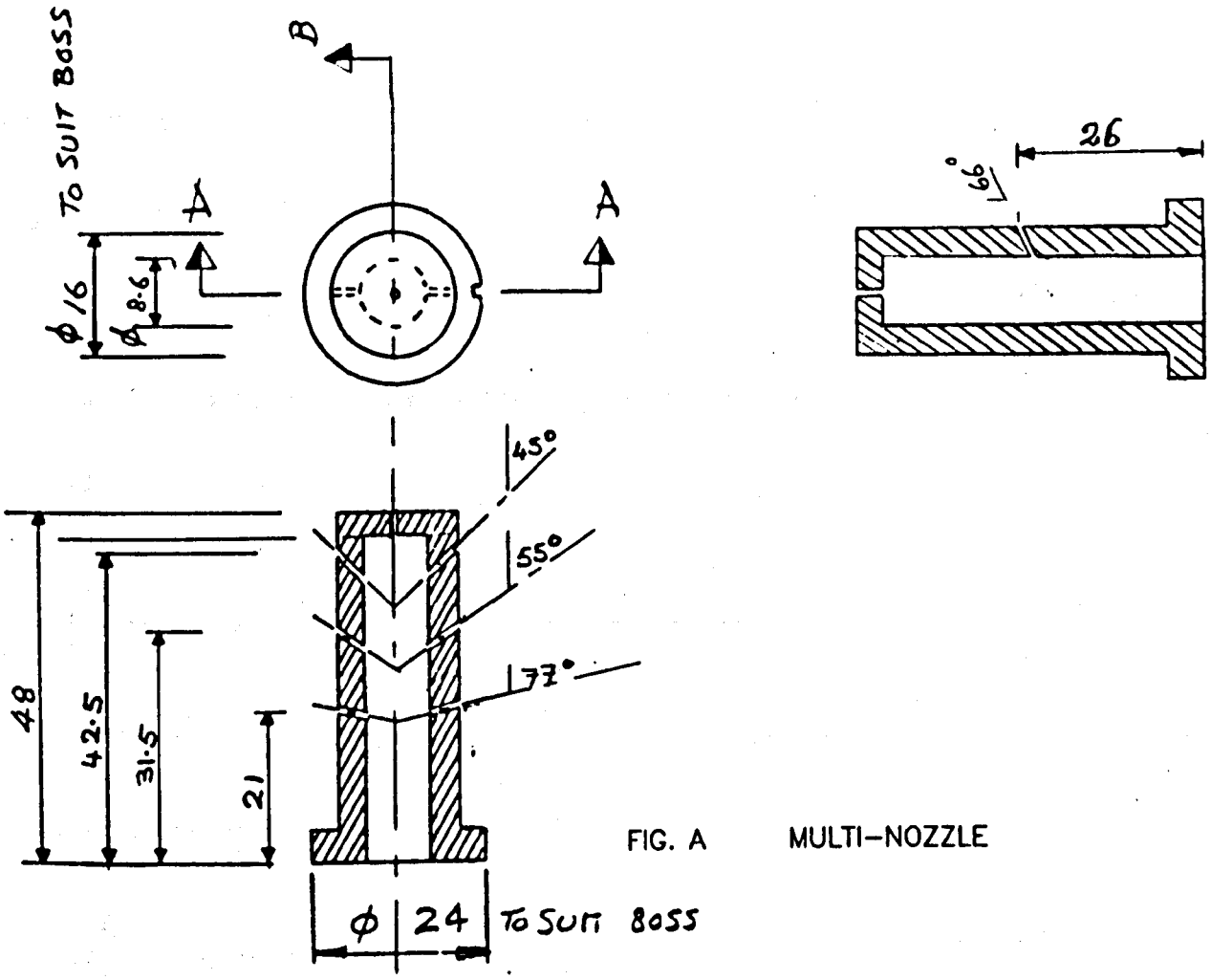

FIG. A MULTI–NOZZLE

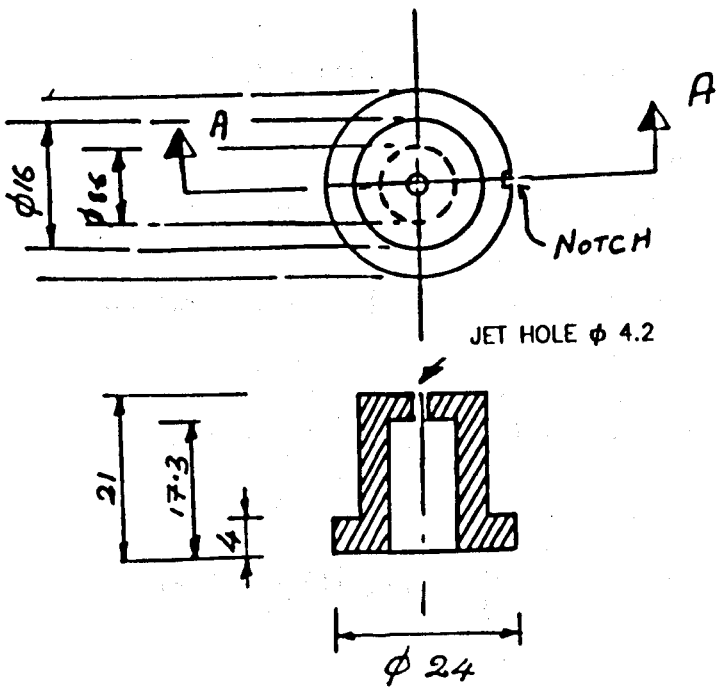

FIG. B SINGLE NOZZLE

FIG. A7.1 MULTI AND SINGLE NOZZLES CONSTRUCTION DRAWING

APPENDIX A8

APPENDIX A8.1

$$Y_n = \alpha_n \cos\alpha_n y + h_1 \sin\alpha_n y \qquad \text{(A8.1)}$$

Here we intend to prove the following two expressions:-

$$\int_0^{\ell} Y_m Y_n \, dy = 0 \quad \text{when } m \neq n \text{ and}$$

$$\int_0^{\ell} Y_n^2 \, dy = \frac{\{(\alpha_n^2 + h_1^2)[\ell(\alpha_n^2 + h_2^2) - h_2] + h_1(\alpha_n^2 + h_2^2)\}}{2(\alpha_n^2 + h_2^2)} \quad \text{when } m = n$$

i). Consider the case $m \neq n$:-

From equation A8.1

$$\frac{d^2Y_m}{dy^2} + \alpha_m^2 Y_m = 0 \qquad \text{(A8.2)}$$

$$\frac{d^2Y_n}{dy^2} + \alpha_n^2 Y_n = 0 \qquad \text{(A8.3)}$$

(A8.2 x Y_n) - (A8.3 x Y_m) gives :-

$$(\alpha_m^2 - \alpha_n^2) Y_m Y_n = Y_m \frac{d^2Y_n}{dy^2} - Y_n \frac{d^2Y_m}{dy^2} \qquad \text{(A8.4)}$$

Now integrate A8.4 with respect to 'y', hence

$$(\alpha_m^2 - \alpha_n^2) \int_0^{\ell} Y_m Y_n dy = \int_0^{\ell} \left[Y_m \frac{d^2Y_n}{dy^2} - Y_n \frac{d^2Y_m}{dy^2} \right] dy \qquad \text{(A8.5)}$$

$$(\alpha_m^2 - \alpha_n^2) \int_0^{\ell} Y_m Y_n dy = \left[Y_m \frac{dY_n}{dy} - Y_n \frac{dY_m}{dy} \right]_0^{\ell} \qquad \text{(A8.6)}$$

since,

$$\left.\begin{aligned} \frac{dY_r}{dy} + h_1 Y_r &= 0 \quad \text{at } y=0 \\ \frac{dY_r}{dy} + h_2 Y_r &= 0 \quad \text{at } y=\ell \end{aligned}\right\} \qquad (A8.7)$$

Equation A8.6 reduces to

$$(\alpha_m^2 - \alpha_n^2)\int_0^{\ell} Y_m Y_n dy = 0 \qquad (A.6)$$

Since the roots are not pure imaginary (see Appendix C)

$$\int_0^{\ell} Y_m Y_n dy = 0 \quad \text{when } m \neq n$$

ii). Consider the case where m= n:-

From equation A8.3,

$$\frac{d^2Y_n}{dy^2} = -\alpha_n^2 Y_n \qquad (A8.10)$$

Integrating with respect to 'y' gives:-

$$\alpha_n^2 \int_0^{\ell} Y_n^2 dy = \int_0^{\ell} \left[-Y_n \frac{d^2Y_n}{dy^2} \right] dy \qquad (A8.11)$$

$$\alpha_n^2 \int_0^{\ell} Y_n^2 dy = \left[-Y_n \frac{dY_n}{dy} \right]_0^{\ell} + \int_0^{\ell} \left[\frac{dY_n}{dy} \right]^2 dy \qquad (A8.11)$$

$$\int_0^{\ell} Y_n^2 dy = \frac{1}{\alpha_n^2} \left[-Y_n \frac{dY_n}{dy} \right]_0^{\ell} + \frac{1}{\alpha_n^2} \int_0^{\ell} \left[\frac{dY_n}{dy} \right]^2 dy \qquad (A8.12)$$

Differentiating A8.1 gives:-

$$\frac{1}{\alpha_n} \frac{dY_n}{dy} = \alpha_n \sin\alpha_n y + h_1 \cos\alpha_n y \qquad (A8.14)$$

$$Y_n^2 + \frac{1}{\alpha_n^2}\left[\frac{dY_n}{dy}\right]^2 = \alpha_n^2 + h_1^2 \qquad \text{(A8.15)}$$

Integrating with respect to 'y' gives:-

$$\int_0^{\ell}\left\{Y_n^2 + \frac{1}{\alpha_n^2}\left[\frac{dY_n}{dy}\right]^2\right\}dy = (\alpha_n^2 + h_1^2)\ell \qquad \text{(A8.16)}$$

A8.16 + A8.12 gives:-

$$2\int_0^{\ell} Y_n^2\, dy = (\alpha_n^2 + h_1^2)\ell - \frac{1}{\alpha_n^2}\left[Y_n\frac{dY_n}{dy}\right]_0^{\ell} \qquad \text{(A8.17)}$$

From A8.7

$$\left.\begin{aligned}\frac{dY_n}{dy} + h_1 Y_n &= 0 \quad \text{at } y=0\\ \frac{dY_n}{dy} + h_2 Y_n &= 0 \quad \text{at } y=\ell\end{aligned}\right\} \qquad \text{(A8.18)}$$

Substituting A8.7 to A8.15 gives:-

$$(\alpha_n Y_n)^2 + (h_1 Y_n)^2 = \alpha_n^2(\alpha_n^2 + h_1) \text{ for } y=0$$

Therefore, $Y_n^2 = \alpha_n^2$ for $y=0$, if $\alpha_n^2 + h_1 \neq 0$ (A8.19)

(note; $(\alpha_n^2 + h_1^2) \neq 0$ condition indicate, α_n has no pure imaginary root)

$$(\alpha_n Y_n)^2 + (h_2 Y_n)^2 = \alpha_n^2(\alpha_n^2 + h_1) \text{ for } y=\ell \qquad \text{(A8.20)}$$

(A8.18) multiplied by Y_n gives:-

$$Y_n\frac{dY_n}{dy} = h_1 Y_n^2 \text{ at } y=0$$

$$= h_1\alpha_n^2 \quad \text{from A8.19}$$

$$Y_n \frac{dY_n}{dy} = \frac{h_2 \alpha_n^2 (\alpha_n^2 + h_1^2)}{(\alpha_n^2 + h_2^2)} \qquad \text{from A8.19}$$

$$\left[Y_n \frac{dY_n}{dy} \right]_o^{\ell} = \frac{h_2 \alpha_n^2 (\alpha_n^2 + h_1^2)}{(\alpha_n^2 + h_2^2)} - h_1 \alpha_n^2$$

$$= \frac{\alpha_n^2 \{ (\alpha_n^2 + h_1^2) h_2 + h_1 (\alpha_n^2 + h_2^2) \}}{2(\alpha_n^2 + h_2^2)}$$

Substituting to A.17 gives:-

$$\int_o^{\ell} Y_n^2 \, dy = \frac{\{ (\alpha_n^2 + h_1^2) [\ell (\alpha_n^2 + h_2^2) - h_2] + h_1 (\alpha_n^2 + h_2^2) \}}{2(\alpha_n^2 + h_2^2)} \qquad \text{when } m=n$$

==========

Appendix A8.2 Evaluating Fourier coefficients for boundary condition-Type a

$$A_n = \frac{2}{\ell_o} \int^{\ell} c_o \exp \frac{Wy}{2D_f} \sin \alpha_n y \, dy$$

$$= \text{Im. pt.} \frac{2}{\ell_o} \int^{\ell} \left\{ c_o \exp \frac{Wy}{2D_f} \left[\cos \alpha_n y + i \sin \alpha_n y \right] \right\} dy$$

$$= \text{Im. pt.} \frac{2}{\ell_o} \int^{\ell} \left\{ c_o \exp \frac{Wy}{2D_f} \left[\exp i \alpha_n y \right] \right\} dy$$

$$= \text{Im. pt.} \frac{2}{\ell} \int^{\ell} \left\{ c_o \exp \left[\frac{Wy}{2D_f} + i \alpha_n y \right] \right\} dy$$

$$= \text{Im. pt.} \frac{2c_o}{\ell} \left\{ \frac{1}{(W/2D_f) + (i \alpha_n)} \exp \left[\frac{Wy}{2D_f} + i \alpha_n y \right] \right\}_o^{\ell}$$

$$= \text{Im. pt.}\ \frac{2c_o}{\ell}\left\{\frac{1}{(W/2D_f) + (i\alpha_n)}\left[\exp\left[\frac{W}{2D_f} + i\alpha_n\right]\ell - 1\right]\right\}$$

$$= \text{Im. pt.}\ \frac{2c_o}{\ell}\left\{\frac{(W/2D_f) - (i\alpha_n)}{(W/2D_f)^2 + (\alpha_n)^2}\left[\exp\left[\frac{W}{2D_f} + i\alpha_n\right]\ell - 1\right]\right\}$$

$$= \text{Im. pt.}\ \frac{2c_o}{\ell}\left\{\frac{(W/2D_f) - (i\alpha_n)}{(W/2D_f)^2 + (\alpha_n)^2}\left[\exp\left[\frac{W\ell}{2D_f}\right](\cos\alpha_n\ell + i\sin\alpha_n\ell) - 1\right]\right\}$$

$$= \frac{-2c_o}{\ell}\left\{\frac{(W/D_f)(\sin\alpha_n\ell) + \alpha_n(\cos\alpha_n\ell)}{(W/2D_f)^2 + (\alpha_n)^2}\right\}\exp\left[\frac{W\ell}{2D_f}\right]$$

$$+ \frac{2c_o}{\ell}\ \frac{\alpha_n}{(W/2D_f)^2 + \alpha_n^2}$$

Appendix A8.3 Evaluating Fourier coefficients for boundary condition-Type b

$$A_n = \frac{2}{\ell}\int_o^{\ell} c_o \exp\frac{Wy}{2D_f}\cos\alpha_n y\,dy, \quad \text{where } \alpha_n = n\pi/\ell \text{ (for type b)}$$

$$= \text{Re. pt.}\ \frac{2}{\ell}\int_o^{\ell}\left\{c_o\exp\frac{Wy}{2D_f}\left[\cos\alpha_n y + i\sin\alpha_n y\right]\right\}dy$$

$$= \text{Re. pt.}\ \frac{2}{\ell}\int_o^{\ell}\left\{c_o\exp\frac{Wy}{2D_f}\left[\exp i\alpha_n y\right]\right\}dy$$

$$= \text{Re. pt.}\ \frac{2}{\ell}\int_o^{\ell}\left\{c_o\exp\left[\frac{Wy}{2D_f} + i\alpha_n y\right]\right\}dy$$

$$= \text{Re. pt.} \frac{2c_o}{\ell}\left\{\frac{1}{(W/2D_f) + (\alpha_n^2)} \exp\left[\frac{Wy}{2D_f} + i\alpha_n y\right]\right\}_o^{\ell}$$

$$= \text{Re. pt.} \frac{2c_o}{\ell}\left\{\frac{1}{(W/2D_f) + (\alpha_n^2)} \left[\exp\left[\frac{W}{2D_f} + i\alpha_n\right]\ell - 1\right]\right\}$$

$$= \text{Re. pt.} \frac{2c_o}{\ell}\left\{\frac{(W/2D_f) - (i\alpha_n)}{(W/2D_f)^2 + (\alpha_n)^2} \left[\exp\left[\frac{W}{2D_f} + i\alpha_n\right]\ell - 1\right]\right\}$$

$$= \text{Re. pt.} \frac{2c_o}{\ell}\left\{\frac{(W/2D_f) - (i\alpha_n)}{(W/2D_f)^2 + (\alpha_n)^2} \left[\exp\left[\frac{W\ell}{2D_f}\right](\cos\alpha_n\ell + i\sin\alpha_n\ell) - \frac{W}{2D_f}\right]\right\}$$

Since $\alpha_n = n\pi/\ell$ (note:- if $\alpha_n \neq n\pi/\ell$, there would be another extra term)

$$= \frac{c_o}{(W/2D_f)^2 + (n\pi/\ell)^2} \cdot \frac{W}{D_f\ell}\left\{\exp\left[\frac{W\ell}{2D_f}\right]\cos n\pi - 1\right]\right\}$$

==========

Appendix A8.4 Evaluating Fourier coefficients for boundary condition-Type c

$$A_n = \frac{2\alpha_n^2}{\ell(\alpha_n^2 + h^2)} \int_o^{\ell} c_o \exp\left[\frac{Wy}{2D_f}\right] Y_n \, dy$$

where, $Y_n = \cos\alpha_n y + (h/\alpha_n)\sin\alpha_n y$, $\alpha_n = n\pi/\ell$ and $n = 1,2 \text{ ---}\infty$

Let

$$A_{n1} = \frac{2}{\ell}\int_o^{\ell} c_o \exp\frac{Wy}{2D_f} \cos\frac{n\pi y}{\ell} dy \quad \text{and}$$

$$A_{n2} = \frac{2}{\ell}\int_o^{\ell} c_o \exp\frac{Wy}{2D_f} \sin\frac{n\pi y}{\ell} dy$$

Therefore,

$$A_n = \frac{\alpha_n^2}{\ell(\alpha_n^2 + h^2)} \left[A_{n1} + \frac{h}{\alpha_n} A_{n2} \right]$$

Where A_{n1} is evaluated in appendix A8.3

A_{n2} is evaluated in appendix A8.2